



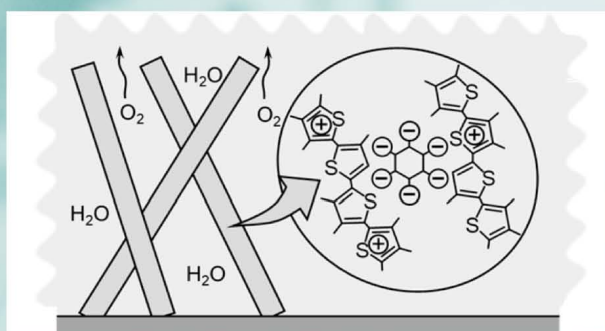
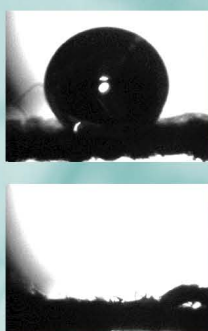
ISSN 2518-718X (Print)
ISSN 2663-4872 (Online)

BULLETIN OF THE KARAGANDA UNIVERSITY

Special Issue

Specialty Polymers in Oil Industry, Bio-, Nanotechnology and Medicine

Guest Editors: Prof. Sarkyt Kudaibergenov, Prof. Nurxat Nuraje



CHEMISTRY Series

№ 3(107)/2022

ISSN 2663-4872 (Online)
ISSN-L 2518-718X (Print)
Индексі 74617
Индекс 74617

**ҚАРАҒАНДЫ
УНИВЕРСИТЕТІНІҢ
ХАБАРШЫСЫ**

ВЕСТНИК
КАРАГАНДИНСКОГО
УНИВЕРСИТЕТА

BULLETIN
OF THE KARAGANDA
UNIVERSITY

ХИМИЯ сериясы

Серия **ХИМИЯ**

CHEMISTRY Series

№ 3(107)/2022

Арнайы шығарылым

**Мұнай өнеркәсібінде, био-, нанотехнологияда
және медицинада полимерлердің арнайы қолданылуы**

Специальный выпуск

**Полимеры специального назначения в нефтяной промышленности,
био-, нанотехнологиях и медицине**

Special Issue

Specialty Polymers in Oil Industry, Bio-, Nanotechnology and Medicine

Шілде–тамыз–қыркүйек
30 қыркүйек 2022 ж.

Июль–август–сентябрь
30 сентября 2022 г.

July–August–September
September, 30th, 2022

1996 жылдан бастап шығады
Жылына 4 рет шығады
Қарағанды, 2022

Издается с 1996 года
Выходит 4 раза в год
Қарағанда, 2022

Founded in 1996
Published 4 times a year
Karaganda, 2022

Guest Editors

S.E. Kudaibergenov, Full Professor, Doctor of Chemical Sciences,
Director of the Institute of Polymer Materials and Technology, Almaty (Kazakhstan);

Nurxat Nuraje, PhD, Associate Professor, Doctor of chemical sciences, Head of the Laboratory of Advanced Solar Energy Materials and Systems, National Laboratory Astana, Nazarbayev University, Nur-Sultan (Kazakhstan)

Editor-in-Chief

M.Zh. Burkeyev, Doctor of Chemical sciences

Executive secretary

I.A. Pustolaikina, Candidate of Chemical sciences

Editorial board

- Z.M. Muldakhmetov**, Academician of NAS RK, Doctor of chem. sciences, Institute of Organic Synthesis and Coal Chemistry of the Republic of Kazakhstan, Karaganda (Kazakhstan);
- S.M. Adekenov**, Academician of NAS RK, Doctor of chem. sciences, International Research and Production Holding “Phytochemistry”, Karaganda (Kazakhstan);
- V. Khutoryanskiy**, Professor, University of Reading, Reading (United Kingdom);
- Fengyun Ma**, Professor, Xinjiang University, Urumqi (PRC);
- Xintai Su**, Professor, South China University of Technology, Guangzhou (PRC);
- R.R. Rakhimov**, Doctor of chem. sciences, Norfolk State University, Norfolk (USA);
- M.B. Batkibekova**, Academician of the Engineering Academy of the Kyrgyz Republic, Doctor of chem. sciences, Kyrgyz State Technical University named after I. Razzakov, Bishkek (Kyrgyzstan);
- S.A. Beznosyuk**, Doctor of phys.-math. sciences, Altai State University, Barnaul (Russia);
- B.F. Minaev**, Doctor of chem. sciences, Bohdan Khmelnytsky National University of Cherkasy, Cherkasy (Ukraine);
- I.V. Kulakov**, Doctor of chem. sciences, University of Tyumen (Russia);
- R.P. Bhole**, PhD, Associate Professor, Dr. D.Y. Patil Institute of Pharmaceutical Sciences and Research, Sant Tukaram Nagar, Pimpri, Pune (India);
- A.M. Makasheva**, Doctor of techn. sciences, Zh. Abishev Chemical-Metallurgical Institute, Karaganda (Kazakhstan);
- M.I. Baikenov**, Doctor of chem. sciences, Karagandy University of the name of acad. E.A. Buketov (Kazakhstan);
- L.K. Salkeeva**, Doctor of chem. sciences, Karagandy University of the name of acad. E.A. Buketov (Kazakhstan);
- Ye.M. Tazhbaev**, Doctor of chem. sciences, Karagandy University of the name of acad. E.A. Buketov (Kazakhstan);
- O.G. Yaroshenko**, Doctor of Pedagogical Sciences, Academician of the National Academy of Pedagogical Sciences of Ukraine, Institute of Higher Education of the National Academy of Educational Sciences of Ukraine, Kyiv (Ukraine);
- V.N. Fomin**, Cand. of chemical science, Head of the laboratory of engineering profile “Physical and chemical research methods”, Karagandy University of the name of acad. E.A. Buketov (Kazakhstan)

Postal address: 28, University Str., Karaganda, 100024, Kazakhstan

Tel./fax: (7212) 34-19-40.

E-mail: chemistry.vestnik@ksu.kz; meyram.burkeyev@ksu.kz; irina.pustolaikina@ksu.kz

Web-site: <http://chemistry-vestnik.ksu.kz>

Editors Zh.T. Nurmukhanova, S.S. Balkeyeva, Z.E. Ramazanova

Computer layout V.V. Butyaikin

Bulletin of the Karaganda University. Chemistry series.

ISSN 2663-4872 (Online). ISSN-L 2518-718X (Print).

Proprietary: NLC “Karagandy University of the name of academician E.A. Buketov”.

Registered by the Ministry of Information and Social Development of the Republic of Kazakhstan.

Rediscount certificate No. KZ27VPY00027382 dated 30.09.2020.

Signed in print 29.09.2022. Format 60×84 1/8. Offset paper. Volume 36,5 p.sh. Circulation 200 copies.

Price upon request. Order № 108.

Printed in the Publishing house of NLC “Karagandy University of the name of acad. E.A. Buketov”.

28, University Str., Karaganda, 100024, Kazakhstan. Tel.: (7212) 35-63-16. E-mail: izd_kargu@mail.ru

Cover: The cover is selected from the article “Polymer Complexes for Electrocatalytic Oxygen Evolution” by Hiroyuki Nishide and Hiromi Shinohara.

CONTENTS

PREFACE

<i>Kudaibergenov S.E., Nuraje N.</i> Foreword by the Editors of the Special Issue.....	5
--	---

MEMORABLE DATES

<i>Kudaibergenov S.E.</i> The Contribution of Professor Esen Bekturov to Physical Chemistry of Polymers	9
---	---

SPECIALTY POLYMERS IN OIL INDUSTRY, BIO-, NANOTECHNOLOGY AND MEDICINE

<i>Bekturov E.A., Moustafine R.I., Kudaibergenov S.E., Khutoryanskiy V.V.</i> Interpolymer Complexes of Synthetic, Natural and Semi-Natural Polyampholytes: A Review.....	14
<i>Sagyndikov M.S., Kushekov R.M., Seright R.S.</i> Review of Important Aspects and Performances of Polymer Flooding versus ASP Flooding	35
<i>Kanabekova P., Martin A., Kemelbekova A., Kulsharova G.</i> Applications of Nanofiber Membranes in Microphysiological Systems	56
<i>Shinohara H., Nishide H.</i> Polymer Complexes for Electrocatalytic Oxygen Evolution	67
<i>Michurov D.A., Kolosova O.Yu., Lozinsky V.I.</i> Cryostructuring of Polymeric Systems. 61. Physico-chemical Properties of Poly(vinyl alcohol) Cryogels Prepared on the Basis of Urea-Containing DMSO-Solutions of the Polymer and Evaluation of the Resultant Gel Materials as Potential Drug Carriers.....	75
<i>Avazova O.B., Milusheva R.Yu., Nurgaliev I.N., Rashidova S.Sh.</i> Polymolecular Complexes of Chitosan with the <i>Bombyx Mori</i> Protein	87
<i>Mussabayeva B.Kh., Kassymova Zh.S., Orazzhanova L.K., Klivenko A.N., Sabitova A.N., Bayakhmetova B.B.</i> Interpolyelectrolyte Complex Chitosan – Alginate for Soil Structuring.....	102
<i>Du Juan, Xu Shimei.</i> Solvents Triggered Coil-to-Globule-to-Coil Transition of Dual Nanocomposite Hydrogels with Inorganic Hybrid Crosslinking.....	115
<i>Ayazbayeva A.Ye., Nauryzova S.Z., Aseyev V.O., Shakhvorostov A.V.</i> Immobilization of Methyl Orange and Methylene Blue within the Matrix of Charge-Imbalanced Amphoteric Nanogels and Study of Dye Release Kinetics as a Function of Temperature and Ionic Strength	127
<i>Mukhametgazy N., Gussenov I.Sh., Shakhvorostov A.V., Tenhu Heikki.</i> Oil Recovery at High Brine Salinity Conditions Using Amphoteric Terpolymer.....	141
<i>Zhubanov A.A., Bondaletov V.G., Kozhabekov S.S., Galymzhan A.Z.</i> Amidation of Polyethylene-Acrylic Acid Copolymer as Pour Point Depressants for Waxy Crude Oils	150
<i>Toktarbaiuly O., Kurbanova A., Ualibek O., Seralin A., Zhunussova T., Sugurbekova G., Nuraje N.</i> Fabrication of Superhydrophobic Self-Cleaning Coatings by Facile Method: Stable after Exposure to Low Temperatures and UV Light.....	158
<i>Wu C.Y., Ling W.Q., Yao Y.C., Guo M., Nuraje N.</i> Three-Dimensional Fingerprint Spectroscopy Study on the Biopolymer System of Polyphenol Oxidase Binding with Cumalic Acid	168
<i>Deberdeev T.R., Akhmetshina A.I., Karimova L.K., Grishin S.V., Kochemasova D.V.</i> Thermal Behavior of Novel Aromatic Oligoesters and Oligoesteramides	180
<i>Kazhmuratova A.T., Zhunissova M.S., Plocek Jiri, Fomin V.N., Sarsenbekova A.Zh., Khamitova T.O.</i> Influence of the RAFT Agent on the Reaction Direction of the Copolymerization of Polypropylene Glycol Maleate with Acrylic Acid	189
<i>Burkeyev M.Zh., Shibayeva S.R., Khamitova T.O., Plocek Jiri, Nurmaganbetova M.T., Kazhmuratova A.T., Zhumagalieva T.S.</i> Synthesis and Investigation of the Properties of Polymer-immobilized Silver- and Gold Nanoparticles.....	198

<i>Galiyeva A.R., Tazhbayev Ye.M., Zhumagaliyeva T.S., Daribay A.T.</i> Encapsulation of Isoniazid in Polylactide-Co-Glycolide Nanoparticles by Nanoprecipitation	208
<i>Nurgaliev I.N.</i> DFT Study of Chitosan Ascorbate Nanoparticles Structure	218
<i>Mashentseva A.A., Aimanova N.A., Parmanbek N., Altynbaeva L.Sh., Nurpeisova D.T.</i> Application of the Cu@PET Composite Track-Etched Membranes for Catalytic Removal of Cr(VI) Ions	227
<i>Zhinzhilo V.A., Litvinova A.Yu., Lyamina V.M., Dzhardimalieva G.I., Uflyand I.E.</i> Coordinating Polymers Based on Nickel(II) and Cobalt(II) Trimesinates as Promising Adsorbents of Organic Dyes	239
<i>Houbi A., Zharmenov A.A., Atassi Y., Bagasharova Z.T., Mirzalieva S., Karibayev B.A.</i> Synthesis and Microwave Absorption Properties of Ni _{0.5} Zn _{0.5} Fe ₂ O ₄ /CI Composite Coated with Polyaniline within Paraffin Wax Matrix.....	254
<i>Mamytbekov G.K., Beksultanov Zh.I., Bannykh V.I., Dan'ko I.V.</i> Synthesis, Structure and Properties of Hybrid Composite Bentonite-Based Materials.....	267
<i>Berdinazarov Q.N., Khakberdiev E.O., Normurodov N.F., Ashurov N.R.</i> Mechanical and Thermal Degradation Properties of Isotactic Polypropylene Composites with Cloisite15A and Cloisite20A	283

PREFACE

Received: 17 July 2022 | Published online: 01 August 2022

<https://doi.org/10.31489/2022Ch3/3-22-00>

S.E. Kudaibergenov¹, N. Nuraje²

¹*Institute of Polymer Materials and Technology, Almaty, Kazakhstan;*

²*National Laboratory Astana, Nazarbayev University, Nur-Sultan, Kazakhstan*

Foreword by the Editors of the Special Issue

The editors, guest editors, and advisory board members of *Bulletin of Karaganda University, Chemistry Series* decided to dedicate this Special Issue to the 90th anniversary of Doctor of chemical sciences, Professor, Academician of the National Academy of Sciences Esen Abikenovich Bekturov who has made an outstanding contribution to physical chemistry of polymers. In the frame of the Special Issue entitled: “**Specialty Polymers in Oil Industry, Bio-, Nanotechnology and Medicine**” colleagues from China, Czech Republic, Finland, Japan, Kazakhstan, Russia, Syria, UK, USA, and Uzbekistan share their research with readers of the journal.

The contribution of Professor Esen Bekturov to the Physical Chemistry of Polymers is outlined in the essay by Prof. **Sarkyt Kudaibergenov** (*Institute of Polymer Materials and Technology, Kazakhstan*). The essay briefly describes the life path, scientific and pedagogical activities of Professor Esen Bekturov together with his prominent contribution to R&D, role in the transfer of knowledge, and training of highly qualified specialists.

A review by Prof. **Vitaliy Khutoryanskiy** from the *University of Reading (UK)* and coauthors considers the state of the art in synthetic, natural, and semi-natural polyampholytes, as well as their interpolymer complexes with polyelectrolytes, proteins, DNA, non-ionic polymers including applications of these systems. Historical background on polyampholytes and interpolymer complexes provides comprehensive information on the current state of this subject.

A review by **Marat Sagyndikov** (*Satbayev University, KazMunaiGas Engineering LLP, Kazakhstan*) and Prof. **Randall Seright** (*New Mexico Institute of Mining and Technology, USA*) describes important aspects and performances of polymer flooding based on a survey of recent projects combined with the Kalamkas field experience. A comprehensive literature review allows optimizing the applicability of polymer flooding technology in temperature, brine salinity, water source selection, oil properties, formation type, and permeability.

The mini-review by **Perizat Kanabekova** and coauthors (*Nazarbayev University, Kazakhstan*) is focused on the use of electrospun nanofiber membranes for the development of lung-on-a-chip platforms. The authors briefly introduce microfluidic and lung-on-chip devices, microphysiological systems and demonstrate the perspectives of nanofiber membranes as a material for mimicking the basement membrane in the lung tissue.

Prof. **Hiroyuki Nishide** and coauthors (*Waseda University, Japan*) highlight the polymer complexes for electrocatalytic oxygen evolution. The paper discusses the prerequisites, characteristics, advantages and emerging challenges of π -conjugated polymers as electrochemical catalysts to modify anodic current collectors for water oxidation. It is demonstrated that the polymer complex of poly(ethylenedioxythiophene) and phytic acid supported by a hydrophilic poly(2-hydroxyethyl methacrylate) efficiently generates oxygen through anodic water oxidation.

Continuation of a series of articles presented by Prof. **Vladimir Lozinsky** and coauthors (*A.N. Nesmeyanov Institute of Organoelement Compounds, Russian Academy of Sciences*) is poly(vinyl alcohol) (PVA) cryogels derived from the urea-containing DMSO-solutions that can be applied as potential drug delivery system. Using a chaotropic additive like urea the authors were able to fabricate the PVA cryogels with high mechanical strength and thermal resistance. The release kinetics of model drug — ϵ -amino caproic acid from the drug-loaded PVA cryogels was evaluated. The suggested the concept of authors may open a possibility for biomedical applications of PVA-based cryogels.

Polymolecular complexes of natural polysaccharide — chitosan with *Bombyx mori* protein in aqueous solutions was studied by Prof. **Sayera Rashidova** and coauthors (*Institute of Chemistry and Physics of Polymers of the Academy of Sciences of the Republic of Uzbekistan*) with the help of FTIR spectroscopy. The density functional theory (DFT) method was also used for analysis and evaluation of complexes formed between chitosan and amino acids (asparagine, threonine, serine, glutamine, alanine, tyrosine, histidine, and lysine) isolated from the pupae of the silkworm *Bombyx mori*.

Researchers from the *Shakarim University of Semey* and *Astana International University, Kazakhstan* (Prof. **Binur Mussabayeva** and Dr. **Alexey Klivenko**) presented the application of interpolyelectrolyte complexes (IPEC) derived from chitosan and alginic acid for soil structuring. Treatment of soil by IPEC improves wind resistance, humidity and decreases the water permeability. The results of vegetation and field experiments in tillage treatment by IPEC showed a positive effect on the growth of radish of the Rubin variety.

The article by Prof. **Shimei Xu** and coauthors (*Sichuan University, Xinjiang University, P.R. China*) is focused on the reentrant phase transition of dual nanocomposite hydrogel composed of poly-*N*-isopropylacrylamide/Laponite/SiO₂ (PNIPAM/Laponite/SiO₂) upon shrinkage/reswelling process. The reentrant “coil-globule-coil” conformational and phase transitions of PNIPAM/Laponite/SiO₂ were attributed to competitive hydrogen bonds between water and polar solvents. The obtained results are promising in many applications for “on-off” switches, artificial organs and actuators in liquid environments.

Young Kazakh researchers in collaboration with Prof. **Vladimir Aseyev** (*Department of Chemistry, University of Helsinki, Finland*) investigated the immobilization of ionic dyes — methyl orange and methylene blue — within the matrix of charge-imbanced amphoteric nanogels consisting of non-ionogenic (*N*-isopropylacrylamide), negatively charged (sodium salt of 2-acrylamido-2-methylpropanesulfonate) and positively charged (3-acrylamidopropyltrimethylammonium chloride) monomers and studied the dye release kinetics as a function of temperature and ionic strength of solution. A delivery system developed in this study may be a promising therapeutic platform for applications in pharmaceuticals.

Oil displacement by amphoteric terpolymer consisting of acrylamide (AAM), 2-acrylamido-2-methylpropanesulfonic acid sodium salt (AMPS) and (3-acrylamidopropyl) trimethylammonium chloride (APTAC) was demonstrated in the article of **Nurbatyr Mukhametgazy** (*Satbayev University, Kazakhstan*) and Prof. **Heikki Tenhu** (*Department of Chemistry, University of Helsinki, Finland*). The advantage of amphoteric terpolymer AAM-AMPS-APTAC over hydrolyzed poly(acrylamide), that is traditionally used in enhanced oil recovery, was shown at high salinity of oil reservoir.

Amidation of polyethylene-*co*-acrylic acid copolymer (PE-*co*-AA) by alkylamines and further application as pour point depressants for waxy crude oils is reported by Dr. **Serik Kozhabekov** and coauthors (*Kazakh-British Technical University, Kazakhstan*). The efficiency of the modified PE-*co*-AA copolymers as a pour point depressant was tested with respect to highly wax crude oil from the Akshabulak field. The obtained results expand our fundamental knowledge of polymer additives with respect to the highly paraffinic oils of Kazakhstan.

Prof. **Nurxat Nuraje** and coauthors (*National Laboratory Astana, Nazarbayev University, Kazakhstan*) prepared superhydrophobic self-cleaning coatings by a simple, facile and cheap method using easily available materials such as poly(dimethylsiloxane) and TiO₂ nanoparticles. The wettability, particle size, and electrokinetic potential of superhydrophobic materials were studied. These materials can potentially be used in concrete fabrication as anti-ice paving slabs, building facades, roofs and waterproofing of buildings.

The molecular mechanism of binding of coumaric acid (CA) with polyphenol oxidase (PPO) was explored by Dr. **Ming Guo** and coauthors (*Zhejiang Agriculture and Forestry University, China*) by combination of spectroscopic and molecular modeling methods. According to the thermodynamic parameters, the CA-PPO complex is predominantly stabilized by hydrophobic interactions and hydrogen bonds between the interacting components.

Dr. **Alsu Akhmetshina** and coauthors (*Kazan National Research Technological University, Kazan, Russian Federation*) synthesized and characterized a series of aromatic oligoesters and oligoesteramides possessing liquid crystalline properties *via* high-temperature polycondensation of aromatic dicarboxylic acids with 4-hydroxybenzoic acid (or 4-aminobenzoic acid) and 1,5-naphthalene diol. As a result, high thermally stable polymeric materials in the range of 372–378 °C were obtained. The application area of liquid crystalline polymer covers the aerospace needs of today; they are an excellent candidate for printed circuit boards, fiber optic strength members, and conductor reinforcements.

The team of authors led by Dr. **Akerke Kazhmuratova** (*Karaganda Buketov University, Kazakhstan*) and Dr. **Jiri Plocek** (*Institute of Inorganic Chemistry of the Czech Academy of Sciences, Czech Republic*) reported the facile synthesis of novel hydrogels based on unsaturated polyester and acrylic acid by reversible addition-fragmentation chain transfer (RAFT) polymerization in dioxane. The structure, composition and morphology of obtained polymers were evaluated by FTIR, NMR spectroscopy and SEM.

Prof. **Meyram Burkeyev** and coauthors from *Karaganda Buketov University, Kazakhstan* and the *Institute of Inorganic Chemistry of the Czech Academy of Sciences, Czech Republic* stabilized the gold and silver nanoparticles by the copolymers of polypropylene glycol maleate phthalate with acrylic acid. The obtained nanocomposites in the range of 35–50 nm exhibited antimicrobial activity with respect to gram-positive and gram-negative bacteria.

Research team headed by Prof. **Erkeblan Tazhbayev** from *Karaganda Buketov University, Kazakhstan* prepared polymeric nanoparticles based on polylactide-*co*-glycolide and anti-tuberculosis drug – isoniazid by nanoprecipitation. The average size of nanoparticles varied from 93 to 869 nm. Incorporation of isoniazid into the polymer matrix was confirmed by TGA and DSC. The degradation of polymer matrix followed by drug release was evaluated at different pHs.

Theoretical approach, in particular the DFT method, was used by Dr. **Ilmar Nurgaliev** (*Institute of Polymer Chemistry and Physics, Tashkent, Uzbekistan*) to study the interaction between chitosan dimer with ascorbic acid (AA) and sodium tripolyphosphate for fabrication of chitosan-ascorbate nanostructures. The obtained results show that the complexation of chitosan dimer with AA proceeds through donor-acceptor interaction, which is energetically favorable among all kinds of considered interactions. The applied model can be used to control the size of the resulting nanoparticles of chitosan derivatives with organic acids, including AA, and further develop the drug delivery system.

Dr. **Anastassiya Mashentseva** and coauthors (*Institute of Nuclear Physics, L.N. Gumilyov Eurasian National University, Kazakhstan*) fabricated the composite track-etched PET-based membranes on copper microtubes using various compositions of precipitation solution and various types of reducing agents such as formaldehyde, dimethylamine borane, and glyoxylic acid. They were used as efficient catalysts for reduction of Cr(VI) present in wastewater to Cr(III) with a high yield of 95–97 %.

Metalloorganic framework (MOF) structures based on nickel and cobalt trimesinates were used for adsorption of organic dyes, in particular, Congo red (CR) and methylene blue (MB) by Prof. **Igor Uflyand** and Prof. **Gulzhan Dzhardimalieva** from *Southern Federal University, Rostov-Don* and *Institute for Problems of Chemical Physics RAS (Russia)*. Temperature-dependent adsorption degree of CR and MB was equal to 97 and 83 %, respectively. The adsorption mechanism of dyes was analyzed by empirical models of Temkin and Freundlich, of which the Freundlich model was optimal. The calculated thermodynamic parameters reveal that the process is spontaneous and has an insignificant endothermic character.

Researchers from the *Institute of Complex Processing of Mineral Raw Materials, Kazakhstan* (Prof. **Abdurassul Zharmenov** and **Anas Houbi**) in collaboration with the Higher Institute for Applied Science and Technology, Damascus, Syria (Dr. **Yomen Atassi**) considered the ternary composite materials obtained from poly(aniline), NiZn ferrite ($\text{Ni}_{0.5}\text{Zn}_{0.5}\text{Fe}_2\text{O}_4$) and carbonyl iron using the sol-gel method and in situ polymerization technique. The composite materials were characterized by FTIR spectroscopy, XRD and SEM. In addition, the electromagnetic interference shielding and microwave absorption properties were measured in the frequency region of 8.8–12 GHz.

Prof. **Galymzhan Mamytbekov** and coauthors (*Institute of Nuclear Physics, Kazakhstan*) developed hybrid composite materials based on poly-N-vinylpyrrolidone and agar-agar in the presence of plasticizers (PEG-400, glycerin) and mineral filler bentonite by electron irradiation method. The structure of resulted hybrid composites is defined as an interpenetrating network within which the mineral component is distributed as intercalated particles. The swelling and mechanical properties of composite hydrogels were studied. It is expected that the hybrid composite hydrogels can be applied for tissue engineering and anti-burn hydrogel dressings with a wound healing effect and high bactericidal activity.

A group of researchers led by Prof. **Nigmat Ashurov** from the *Institute of Polymer Chemistry and Physics (Uzbekistan)* presented the properties of nanomaterials derived from the modified by maleic anhydride isotactic polypropylene and two kinds of clay minerals – montmorillonite that differs in the interlayer space. As a result, the formation of both intercalated and exfoliated nanocomposite structures was detected. The physicochemical and mechanical properties of nanocomposites were evaluated by XRD, TGA, DSC, and mechanical testing. The nanocomposites possess increased thermal stability and elastic modulus that are interesting from the practical point of view.

The Guest Editors of this Special Issue would be extremely happy if the compiled articles reached their goal and delivered a positive reader experience.

Information about Guest Editors*

Kudaibergenov, Sarkyt Elekenovich — Full Professor, Doctor of Chemical Sciences, Director of the Institute of Polymer Materials and Technology, Atyrau-1, 3/1, 050019, Almaty, Kazakhstan; e-mail: skudai@mail.ru; <https://orcid.org/0000-0002-1166-7826>;

Nuraje, Nurxat — Associate Professor, Doctor of Chemical Sciences, Head of the Laboratory of Advanced Solar Energy Materials and Systems, National Laboratory Astana, Nazarbayev University, Kabanbay batyr avenue, 53, 010000, Nur-Sultan, Kazakhstan; e-mail: nurxat.nuraje@nu.edu.kz; <https://orcid.org/0000-0003-4751-2719>

*The editor's name is presented in the order: *Last Name, First and Middle Names*

MEMORABLE DATES

Essay

Received: 18 March 2022 | Published online: 13 July 2022

UDC 541.64+678.744

<https://doi.org/10.31489/2022Ch3/3-22-0>

S.E. Kudaibergenov*

Institute of Polymer Materials and Technology, Almaty, Kazakhstan
(*Corresponding author's e-mail: skudai@mail.ru)

The Contribution of Professor Esen Bekturov to Physical Chemistry of Polymers

The article is dedicated to the 90th anniversary of Academician Esen Abikenovich Bekturov, a prominent Kazakhstani chemist who has made an outstanding world contribution to the physical chemistry of polymers. His scientific interests focused on the study of water-soluble and water-swelling polymers, interpolymer and polymer-metal complexes, polymeric catalysts and associates, polymeric hydrogels, molecular complexes of polymers, nanomaterials and nanotechnology are summarized in numerous monographs published in Japan, Germany, Poland, and Kazakhstan. The essay briefly reflects the life path, creativity, scientific and pedagogical activity of Professor Esen Bekturov, as well as the most important and prominent publications. His role in the transfer of knowledge, training of high-qualified specialists, his contribution to Research and Development (R&D), recognized by numerous International and Republican awards and participation at International Conferences and Symposiums, are highlighted.



We shall not cease from exploration
And the end of all our exploring
Will be to arrive where we started
And know the place for the first time

“Four Quartets”
T.S. Eliot, Nobel Laureate

The Kazakh proverb says: “The deep river flows noiselessly”. The life and scientific philosophy of the Doctor of chemical sciences, Professor, Academician of the Kazakh National Academy of Sciences, Laureate of Kazakh State Prize, and Honored science worker of the Republic of Kazakhstan Esen Bekturov fully corresponds to this truth. Professor Esen Bekturov is a well-known specialist in the field of physical chemistry of polymers in the scientific community of Kazakhstan and abroad, an extremely modest and cultured person who sets high moral standards for himself and others, enjoys great authority in his family, among friends, colleagues and disciples. On December 14, 2021, he celebrated his 90th birthday. The winged and sarcastic phrase of the famous physicist, Nobel Prize winner P.L. Kapitsa: “... a scientist after 75 years is idolized, to whom everyone prays”, is an exception for Professor Esen Bekturov, who is still active, works for the benefit of his beloved science, generates and distributes fresh ideas, prepares and guides the younger generation for independent Kazakhstan and leads an active lifestyle. Esen Bekturov was born in 1931 in the family of Abiken Bekturov, who later became one of the first founders and academicians of the Kazakh SSR Academy of Sciences and for 20 years was the first director of the Institute of Chemical Sciences (named after A.B. Bekturov in 1991), and followed his father's footsteps.

After graduating from the Faculty of Chemistry of the Kazakh State University in 1954, Esen Bekturov became an aspirant and in 1958 defended his candidate dissertation. His scientific advisor was the Academician of the Kazakh Academy of Sciences, Professor M.I. Usanovich, one of the founders of the acid-base theory.

Esen Bekturov spent his postdoctoral period at the Moscow State University and Institute of Elementoorganic Compounds under the patronage of Academician of the Academy of Sciences of the USSR, Professor V.A. Kargin and Corresponding Member of the Academy of Sciences of the USSR, Professor S.R. Rafikov. Preliminary, Esen Bekturov headed the group, and then in 1966, the laboratory of physical chemistry of polymers at the Institute of Chemical Sciences was organized under the auspice of the founder of the Kazakh school of polymer chemists, Academician of the Kazakh Academy of Sciences, Professor S.R. Rafikov.

The subject of E. Bekturov's doctoral thesis, which he defended in 1972, was devoted to the study of hydrodynamic, conformational and molecular characteristics of amphiphilic polymers in solutions. He summarized these results in the monographs "Ternary Polymeric Systems in Solutions", "Synthetic Water-Soluble Polymers in Solutions", "Catalysis by Polymers", and "Cationic Polymers" published in Kazakhstan, Germany, and Poland [1–7].

In early 1970s, Professor Bekturov's laboratory simultaneously with the research teams of the Moscow State University and Waseda University (Japan) began to develop the still promising scientific direction of the so-called interpolymer complexes as the products of interactions of two complementary macromolecules stabilized by cooperative hydrogen bonds. As a logical continuation of such studies, the complexation reactions of functional polymers with various low- and high-molecular-weight compounds (metal ions, surfactants, dyes, drugs, polyelectrolytes, proteins) were initiated to create effective metal sorbents, metal-supported polymeric catalysts, ion-conductive polymers, composite materials, ultrathin films. Investigations in the field of polymer-polymer and polymer-metal complexes, molecular complexes of polymers, catalysis by polymers and metal-supported catalysts have been published in the books and review articles by Springer-Verlag, Huttig & Wepf in Germany [8–13]. The review article of Professors E. Bekturov and L. Bimendina on Interpolymer Complexes, published in 1981 in the book "Advances in Polymer Science" (Springer), was cited 580 times [3].

In 1986, Professor E. Bekturov and coworkers were awarded by Kazakh State Prize in the field of Science and Technology for the cycle of monographs and books published on water-soluble polymers and their complexes.

At present, the research topics of Professor E. Bekturov cover the stimuli-responsive gels and networks of natural and synthetic polyelectrolytes, polymers for biotechnology, biomedicine, nanotechnology, and environmental protection [14–19].

In Soviet times, despite the existing "Iron Curtain", Professor E. Bekturov took the courage to break "the window to Europe". Due to his deep knowledge of English, he gave plenary and invited lectures at leading scientific Centers and Universities in Japan, Turkey, Germany, Switzerland, Italy, Iran, Canada, and the Czech Republic. Owing to his promotion of the achievements of Kazakh polymer chemists, the Laboratory of Physical Chemistry of Polymers became a "Mecca" for scientists from various regions of Kazakhstan and former Soviet Union countries and was recognized by foreign scientists.

For sixty-five years of scientific activity, Professor E. Bekturov has published about 950 articles and reviews, including more than 100 papers published in English in peer-reviewed journals. He is the author and co-author of 35 books published in Kazakhstan, Russia, Poland, Germany, and Japan, and 20 copyright certificates for patents of the USSR and Kazakhstan.

The transfer of knowledge and experience is one of the Life Credo of Professor E. Bekturov. He trained more than two dozen candidates of sciences and nine doctors of sciences for the Universities, Research Institutes and Industries of Kazakhstan. During 2010–2021 Professor Esen Bekturov gave the lecture courses on "Modern problems of polymer science" and "Physical chemistry of polymers" in English for Master and PhD students of the Abai Kazakh National Pedagogical University [20, 21].

Professor E. Bekturov always pays attention to scientific organizations. For example, he was a permanent member of the International Advisory Board of IUPAC Symposium on Macromolecule-Metal Complexes, the International Symposium on Specialty Polymers. Esen Bekturov's achievements in fundamental science have been recognized by numerous awards and certificates of honor, including the Al-Khorezmi International science and technique festival, the N. Bohr UNESCO gold medal (1997), the Kazakh State stipend for outstanding scientists who contributed to the development of science and technique (2000), Nation-

al Independent Prize “Tarlan” in the nomination of science, K.I. Satpayev Prize for the development of specialty polymers for application in petrochemistry and nanotechnology (2019). According to the Web of Science International Information and Analytical Platform, in 2019, Esen Bekturov, as a professor of the Abai Kazakh National Pedagogical University, was awarded the title “Leader in publishing activities in the Web of Science Core Collection over the past 5 years among pedagogical universities of the Republic of Kazakhstan”. He is Honorary Director of the Institute of Polymer Materials and Technology (1999), Honorary Professor of the Pavlodar State University (2001) and Semey Shakarim University (2005). For his contribution to the development of science in Kazakhstan, he was awarded the Medals “For Labor’s Heroism”, “Labor’s Veteran” and “10 Years of the Constitution of the Republic of Kazakhstan”. In 2018, Al-Farabi Kazakh National University published the book entitled “Өнегелі өмір” (“Exemplary Life”), dedicated to the life and creative activity of Professor Esen Bekturov [22].

The Polymer Society of Kazakhstan, former students, colleagues and friends congratulate Professor Esen Bekturov on his 90th birthday and wish him all the best in his scientific and personal life.

This is an updated version of Essay published previously in *Macromol. Chem. Phys.*, 2006, Vol. 207, P. 2165–2166. DOI: 10.1002/macp.200600320 [23].

References

- 1 Бектуров Е.А. Тройные полимерные системы в растворах / Е. А. Бектуров; отв. ред. Б.А. Жубанов; ИХН АН КазССР. — Алма-Ата: Наука, 1975. — 252 с.
- 2 Бектуров Е.А. Интерполимерные комплексы / Е.А. Бектуров, Л.А. Бимендина. — Алма-Ата: Наука, 1977. — 264 с.
- 3 Bekturov E.A. Interpolymer complexes / E.A. Bekturov, L.A. Bimendina // *Advances in Polymer Science*. — 1981. — Vol. 41. — P. 99–147.
- 4 Бектуров Е.А. Синтетические водорастворимые полимеры в растворах / Е.А. Бектуров, З.Х. Бакауова. — Алма-Ата: Наука, 1981. — 248 с.
- 5 Bekturov E.A. Synthetic Water-Soluble Polymers in Solution. Basel / Е.А. Bekturov, Z. Kh. Bakauova. — Heidelberg. — New York, Huethig & Wepf, 1986. — 241 p.
- 6 Бектуров Е.А. Катионные полимеры / Е.А. Бектуров, С.Е. Кудайбергенов, Р.Э. Хамзамулина. — Алма-Ата: Наука, 1986. — 160 с.
- 7 Bekturov E.A. Polimery kationowe / Е.А. Bekturov, S.E. Kudaibergenov, R.E. Khamzamulina. — Warsaw: Panstwowe Wydawnictwo Naukowe, 1991. — 162 p.
- 8 Бектуров Е.А. Полимерные комплексы и катализаторы / Е.А. Бектуров, Л.А. Бимендина, С.Е. Кудайбергенов. — Алма-Ата: Наука, 1982. — 192 с.
- 9 Бектуров Е.А. Ассоциация полимеров с малыми молекулами / Е.А. Бектуров, Р.Е. Легкунец. — Алма-Ата: Наука, 1983. — 208 с.
- 10 Bekturov E.A. Nonionic association of macromolecules / Е.А. Bekturov // In: *Intermacromolecular complexes. Characteristics and applications*. — 1983. — Tokyo, Japan.
- 11 Бектуров Е.А. Молекулярные комплексы полимеров / Е. А. Бектуров, Р.Э. Хамзамулина, З.Х. Бакауова и др.; отв. ред. Б.А. Жубанов; ИХН АН КазССР. — Алма-Ата: Наука, 1988. — 174 с. ISBN 5-628-00039-6
- 12 Бектуров Е.А. Катализ полимерами / Е. А. Бектуров, С.Е. Кудайбергенов; отв. ред. Б. А. Жубанов; ИХН АН КазССР. — Алма-Ата: Наука, 1988. — 184 с.
- 13 Bekturov E.A. Catalysis by Polymers / Е.А. Bekturov, S.E. Kudaibergenov. — Heidelberg: Huthig and Wepf Verlag Zug., 1996. — 153 p.
- 14 Бектуров Е.А. Полимерные электролиты, гидрогели, комплексы и катализаторы / Е.А. Бектуров. — Алматы: ТОО «Print-S», 2007. — 241 с.
- 15 Bekturov E.A. Polyelectrolytes (Chain Models of Polyions) / Е.А. Bekturov, L.A. Bimendina, S.E. Kudaibergenov // *Concise Polymeric Materials Encyclopedia*. — Boca Raton: CRC Press. — 1996. — P. 5141–5146.
- 16 Бектуров Е.А. Полимеры в нанотехнологии / Е.А. Бектуров, С.Е. Кудайбергенов, Ж.Е. Ибраева. — Алматы: Типография «Центр оперативной полиграфии», 2019. — 388 с.
- 17 Ибраева Ж.Е. Стабилизация наночастиц металлов гидрофильными полимерами / Ж.Е. Ибраева, С.Е. Кудайбергенов, Е.А. Бектуров. Saarbrücken: Lap Lambert, 2013. — 367 с. ISBN: 978-3-659-47956-4.
- 18 Бектуров Е.А. Полимер-протектированные наночастицы металлов / Е.А. Бектуров, С.Е. Кудайбергенов, А.К. Жармагамбетова, Р.М. Исаков, Ж.Е. Ибраева, С.Н. Шмаков. — Алматы, 2010. — 273 с.
- 19 Кудайбергенов С.Е. Композиционные гидрогелевые материалы / С.Е. Кудайбергенов, Ж.Е. Ибраева, М.Г. Яшкарлова, Е.А. Бектуров. — Семей, 2011. — 146 с.
- 20 Кудайбергенов С.Е. Физическая химия растворов полимеров / С.Е. Кудайбергенов, Е.А. Бектуров, Ш. Шаяхметов. — Алматы: Санат, 1995. — 248 с.

21 Бектуров Е.А. Краткий курс физико-химии полимеров / Е.А. Бектуров, С.Е. Кудайбергенов. — Алматы: Изд. «Ұлағат» КазНПУ имени Абая, 2017. — 223 с.

22 Бектуров Е. / Под ред. Г.М. Мутанова. Серия «Өнегелі өмір». — Алматы: Қазақ университеті, 2018. Вып. 142. — 298 с. ISBN978-601-04-3345-8.

23 Kudaibergenov S.E. On the Occasion of Esen Bekturov's 75th Birthday / S.E. Kudaibergenov // *Macromolecular Chemistry and Physics*. — 2006. — Vol. 207, Iss. 23. — P. 2165–2166.

С.Е. Құдайбергенов

Профессор Есен Бектұровтың полимерлердің физикалық химиясына қосқан үлесі

Мақала полимерлердің физикалық химиясына әлемдік үлес қосқан көрнекті қазақстандық химик, академик Есен Әбікенұлы Бектұровтың туғанына 90 жыл толуына арналған. Оның суда еритін және суда ісінетін полимерлерге, интерполимер және полимер-металл кешендеріне, полимер катализаторлары мен ассоциацияларына, полимер гидрогельдеріне, полимерлердің молекулалық кешендеріне негізделген, наноматериалдар мен нанотехнологияларды зерттеуге бағытталған ғылыми ізденістері Жапония, Германия, Польша және Қазақстанда жарық көрген ғылыми еңбектерде және монографияларда жарияланған. Сонымен қатар, мақалада профессор Есен Бектұровтың өмір жолы, шығармашылығы, ғылыми-педагогикалық қызметі, маңызды жарияланымдары да қысқаша берілген. Ғалымның білім берудегі, жоғары білікті мамандарды даярлаудағы ролі, ғылыми-зерттеу және тәжірибелік-конструкторлық жұмыстарға (ҒЗТҚЖ) қосқан үлесі туралы айтылған, бірнеше халықаралық және республикалық марапаттары, халықаралық конференциялар мен симпозиумдарға қатысқаны атап өтілген.

С.Е. Кудайбергенов

Вклад профессора Есена Бектурова в физическую химию полимеров

Статья посвящена 90-летию со дня рождения академика Есена Абикиновича Бектурова, выдающегося казахстанского химика, внесшего выдающийся мировой вклад в физическую химию полимеров. Его научные интересы, сосредоточенные на изучении водорастворимых и водонабухающих полимеров, интерполимерных и полимерно-металлических комплексов, полимерных катализаторов и ассоциатов, полимерных гидрогелей, молекулярных комплексов полимеров, наноматериалов и нанотехнологий, обобщены в многочисленных монографиях, изданных в Японии, Германии, Польше и Казахстане. В очерке кратко отражены жизненный путь, творчество, научная и педагогическая деятельность профессора Есена Бектурова, а также наиболее важные и значительные публикации. Показаны его роль в передаче знаний, подготовке высококвалифицированных специалистов, вклад в научно-исследовательские и опытно-конструкторские работы (НИОКР), отмеченные многочисленными международными и республиканскими наградами, участием в международных конференциях и симпозиумах.

References

- 1 Bekturov, E.A. (1975). *Troinye polimernye sistemy v rastvorakh [Ternary polymer systems in solutions]* B.A. Zhubanov (Ed.). *Institut khimicheskikh nauk akademii nauk Kazakhskoi SSR — Institute of Chemistry Sciences of Academy of Sciences of Kazakh SSR*. Alma-Ata: Nauka [in Russian].
- 2 Bekturov, E.A., & Bimendina, L.A. (1977). *Interpolimernye komplekсы [Interpolymer complexes]*. Alma-Ata: Nauka [in Russian].
- 3 Bekturov, E.A., & Bimendina, L.A. (1981). Interpolymer complexes. In: *Speciality Polymers. Advances in Polymer Science*, Vol. 41. Springer, Berlin, Heidelberg. https://doi.org/10.1007/3-540-10554-9_11
- 4 Bekturov, E.A., & Bakauova, Z.Kh. (1981). *Sinteticheskie vodorastvorimye polimery v rastvorakh [Synthetic water-soluble polymers in solutions]*. Alma-Ata: Nauka [in Russian].
- 5 Bekturov, E.A., & Bakauova, Z.Kh. (1986). *Synthetic water-soluble polymers in solutions*. Basel: Huethig & Wepf Verlag, Germany. ISBN 3-857-110-3
- 6 Bekturov, E.A., Kudaibergenov, S.E., & Khamzamalina, R.E. (1986). *Kationnyye polimery [Cationic polymers]*. Alma-Ata: Nauka [in Russian].

- 7 Bekturov, E.A., Kudaibergenov, S.E., & Khamzamalina, R.E. (1991). *Polimery kationowe*. Warsaw: Panstwowe Wydawnictwo Naukowe.
- 8 Bekturov, E.A., Kudaibergenov, S.E., & Bimendina, L.A. (1982). *Polimernye komplekxy i katalizatory [Polymer complexes and catalysts]*. Alma-Ata: Nauka [in Russian].
- 9 Bekturov, E.A., & Legkumetz, R.E. (1983). *Assotsiatsiia polimerov s malymi molekulami [Association of polymers with small molecules]*. Alma-Ata: Nauka [in Russian].
- 10 Bekturov, E.A. (1983). Nonionic association of macromolecules. In: *Intermacromolecular complexes. Characteristics and applications*. Tokyo. Japan.
- 11 Bekturov, E.A., Khamzulina, R.E., Bakauova, Z.Kh. et al. (1988). *Molekuliarnye komplekxy polimerov [Molecular complexes of polymers]*. B.A. Zhubanov (Ed.). *Institut khimicheskikh nauk akademii nauk Kazakhskoi SSR — Institute of Chemistry Sciences of Academy of Sciences of Kazakh SSR*. Alma-Ata: Nauka [in Russian].
- 12 Bekturov, E.A., & Kudaibergenov, S.E. (1988). *Kataliz polimerami [Catalysis by polymers]*. Alma-Ata: Nauka [in Russian].
- 13 Bekturov, E.A., & Kudaibergenov, S.E. (1996). *Catalysis by polymers*. Basel: Huethig & Wepf Verlag. Germany.
- 14 Bekturov, E.A. (2007). *Polimernye elektrolity, gidrogeli, komplekxy i katalizatory [Polymer electrolytes, hydrogels, complexes and catalysts]*. Almaty: Print-S [in Russian].
- 15 Bekturov, E.A., Bimendina, L.A., & Kudaibergenov, S.E. (1996) Polyelectrolytes (Chain Models of Polyions). *Concise Polymeric Materials Encyclopedia*. Boca Raton: CRC Press. p. 5141–5146.
- 16 Bekturov, E.A., Kudaibergenov, S.E., & Ibraeva, Zh.E. (2019). *Polimery v nanotekhnologii [Polymers in nanotechnology]*. Almaty: Tsentr operativnoi poligrafii [in Russian].
- 17 Ibraeva, Zh.E., Kudaibergenov, S.E., & Bekturov, E.A. (2013). *Stabilizatsiia nanochastits metallov gidrofilnymi polimerami [Stabilization of metal nanoparticles by hydrophilic polymers]*. Saarbrücken: Lambert Academic Publishing. Germany [in Russian].
- 18 Bekturov, E.A., Kudaibergenov, S.E., Zharmagambetova, A.K., Iskakov, R.M., Ibraeva Zh.E., & Shmakov S.N. (2010). *Polimer-protektirovannye nanochastitsy metallov [Polymer-protected metal nanoparticles]*. Almaty [in Russian].
- 19 Kudaibergenov, S.E., Ibraeva Zh.E., Yashkarova, M.G., & Bekturov, E.A. (2011). *Kompozitsionnye gidrogelevye materialy [Composite hydrogel materials]*. Semey [in Russian].
- 20 Kudaibergenov, S.E., Bekturov, E.A., & Shayakhmetov, Sh.Sh. (1995). *Fizicheskaya khimiya rastvorov polimerov [Physical chemistry of polymer solutions]*. Almaty: Sanat [in Russian].
- 21 Bekturov, E.A., & Kudaibergenov, S.E. (2017). *Kratkii kurs fiziko-khimii polimerov [Concise course of physical chemistry of polymers]*. Almaty: Ulagat [in Russian].
- 22 Mutanova, G.M. (Ed.). (2018). E. Bekturov. Seriya “Onegeli omir” [Series “Exemplary life”]. Almaty: Qazaq universiteti [in Russian].
- 23 Kudaibergenov, S.E. (2006). *On the occasion of Esen Bekturov’s 75th Birthday. Macromolecular Chemistry and Physics*. 207, 2165–2166. <https://doi.org/10.1002/macp.200600320>.

Information about addressee and author *

Bekturov, Esen Abikenovich — Full Professor, Doctor of Chemical Sciences, Academician of Kazakh National Academy of Sciences, Abai Kazakh National Pedagogical University, Almaty, Kazakhstan; Dostyk ave., 13, 050010; Institute of Polymer Materials and Technology, Almaty, Kazakhstan; Atyrau-1, 3/1, 050019. e-mail: ebekturov@mail.ru; <https://orcid.org/0000-0002-6198-4432>;

Kudaibergenov, Sarkyt Elekenovich — Full Professor, Doctor of Chemical Sciences, Director, Institute of Polymer Materials and Technology, Almaty, Kazakhstan; Atyrau-1, 3/1, 050019. e-mail: skudai@mail.ru; <https://orcid.org/0000-0002-1166-7826>

*The author’s name is presented in the order: *Last Name, First and Middle Names*

SPECIALTY POLYMERS IN OIL INDUSTRY, BIO-, NANOTECHNOLOGY AND MEDICINE

Review

Received: 24 May 2022 | Revised: 15 June 2022 | Accepted: 1 July 2022 | Published online: 18 July 2022

UDC 541.64+678.744

<https://doi.org/10.31489/2022Ch3/3-22-9>

E.A. Bekturov¹, R.I. Moustafine², S.E. Kudaibergenov³, V.V. Khutoryanskiy^{4*}

¹*Abay Kazakh National Pedagogical University, Almaty, Kazakhstan;*

²*Institute of Pharmacy, Kazan State Medical University, Kazan, Russia;*

³*Institute of Polymer Materials and Technology, Almaty, Kazakhstan;*

⁴*University of Reading, Reading, UK*

(*Corresponding author's e-mail: v.khutoryanskiy@reading.ac.uk <mailto:ayazbayeva.aigerim@gmail.com>)

Interpolymer Complexes of Synthetic, Natural and Semi-Natural Polyampholytes: A Review

This review is focused on synthetic, natural and semi-natural polyampholytes and their ability to form interpolymer complexes with other polyelectrolytes and non-ionic polymers. It provides definition, classification and overview of physicochemical properties of polyampholytes. The conformation and phase behaviour of intrinsically disordered proteins and semi-natural polyampholytes derived from aminoacids is discussed. The ability of synthetic, natural and semi-natural polyampholytes to form interpolymer complexes with water-soluble polymers is considered. Most of the research in this area is focused on interpolyelectrolyte complexes of polyampholytes with oppositely charged polyelectrolytes; however, there are also studies demonstrating the formation of hydrogen-bonded complexes. The nature of the complexation is often affected by solution pH and also isoelectric point of polyampholytes. The complexation between polyampholytes and other polymers may lead to formation of colloidal dispersions (nano- and microparticles), liquid-liquid phase separation (called complex coacervation), fully soluble polycomplexes or physically cross-linked gels. A substantial body of studies in this area was focused on the complexes formed by proteins. Application of interpolymer complexes formed by polyampholytes in biotechnology, medicine, encapsulation technologies, separation science, biocatalysis, food science and pharmaceuticals is discussed.

Keywords: polyampholytes, polypeptides, proteins, intrinsically disordered proteins (IDPs), intra-macromolecular complexes (intra-MMC), inter-macromolecular complexes (inter-MMC), interpolyelectrolyte complexes, drug delivery, complex coacervation, gelatin.

Content

List of abbreviations

Review Plan

Introduction

1 Synthetic, natural and semi-natural polyampholytes

2 Interpolymer complexes of synthetic and natural polyampholytes

3 Applications of interpolymer complexes derived from synthetic, natural and semi-natural polyampholytes

Conclusions

Acknowledgements

References



Esen Bekturov is an outstanding Kazakh polymer scientist, Doctor of chemical sciences, Professor, Academician of the Kazakh National Academy of Sciences, Laureate of Kazakh State Prize, and Honored science worker of the Republic of Kazakhstan. His achievements in polymer science

have been recognized by numerous awards and honors, including the Al-Khorezmi International science and technique festival, the N. Bohr UNESCO gold medal, National Independent Prize “Tarlán” in the nomination of science, K.I. Satpayev Prize for the development of specialty polymers for application in petrochemistry and nanotechnology. Prof. Esen Bekturov has about 950 papers and reviews, including more than 100 papers published in English in peer reviewed journals. He is author and coauthor of 35 books published in Kazakhstan, Russia, Poland, Germany, and Japan. For the contribution to development of science in Kazakhstan he was awarded by the Medals “For Labor’s Heroism”, “Labor’s Veteran”, and “10 Years of the Constitution of the Republic of Kazakhstan”.



Rouslan Moustafine is an Associate Professor of Pharmacy at Kazan State Medical University, Tatarstan, Russian Federation. He was the Head of Department of Pharmaceutical, Analytical and Toxicological Chemistry from 2003 to 2018, the Dean of Faculty of Pharmaceutical Sciences from 2009 to 2018 and now is the Director of the Institute of Pharmacy and Head of the Laboratory of Drug Delivery Systems. He received his PhD in Pharmaceutical Technology from I. Sechenov’s Moscow State Medical University in 1991 and his PhD project was focused on the application of interpolymer complexes in oral drug delivery. His area of specialization is the development of interpolyelectrolyte complexes with Eudragits® and other pharmaceutical polymers and their application in the design of novel drug delivery systems. In 2009, Dr. Moustafine was the recipient of the prestigious annual national award “Professions” — to the best Russian scientists in the medical and pharmaceutical field. Dr. Moustafine has published over 55 peer-reviewed papers, reviews, and two book chapters.



Sarkyt Kudaibergenov is a prominent Kazakh polymer scientist, Doctor of chemical sciences, Professor, laureate of Kazakh State Prize, laureate of the “Parasat” award for being the most published and internationally cited Kazakhstani author abroad, winner of a medal “For merits in the development of science in the Republic of Kazakhstan”, laureate of the Satpayev Prize for the development of specialty polymers for application in petrochemistry and nanotechnology. He has co-authored 18 monographs and textbooks, published in Russian, Polish and English, as well as over 400 research articles and reviews, more than 145 of which have appeared in international peer-reviewed journals. His research subject is related to the development and implementation of specialty polymers in oil industry, petrochemistry, catalysis, biotechnology, nanotechnology, medicine and environmental protection.

to the development and implementation of specialty polymers in oil industry, petrochemistry, catalysis, biotechnology, nanotechnology, medicine and environmental protection.



Vitaliy Khutoryanskiy is a Professor of Formulation Science at Reading School of Pharmacy, University of Reading (UK). Prof Khutoryanskiy has researched broadly in the area of new polymers, nanomaterials and biomaterials for pharmaceutical, biomedical, agrochemical and food applications, with a particular emphasis on transmucosal drug delivery, mucoadhesive and mucus-penetrating nanocarriers and hydrogels. He was the recipient of the 2012 McBain Medal from the Society of Chemical Industry and Royal Society of Chemistry (UK), was elected as a Fellow of the Royal Society of Chemistry in 2015, received Sentinel of Science Award from Publons in 2016, was selected as a PhD supervisor of the Year by FindAPhD in 2020, and was chosen to deliver Innovative Science Award Lecture by the Academy of Pharmaceutical Sciences (UK) in 2022. He has published >200 original research articles and reviews, indexed by Scopus, edited 5 books and filed 3 patent applications.

List of abbreviations

- BPA: blockpolyampholyte
- BSA: bovine serum albumin
- CS: chitosan sulfate
- DAA: diallylamine
- DNA: deoxyribonucleic acid
- IA: itaconic acid
- LPEI: linear poly(ethyleneimine)
- MA: maleic acid
- 2M5VPy-AA: 2-methyl-5-vinylpyridine-acrylic acid
- MDAA-MA: N-methyldiallylamine-maleic acid

MIP: Molecularly-imprinted polyampholyte
 NaPSS: poly(styrene sulfonate sodium salt)
 NIPAM: N-isopropylacrylamide
 PAA: poly(acrylic acid)
 PDMDAAC: poly(N, N-dimethyl-N, N-diallylammonium chloride)
 PDMAPS: poly[3-dimethyl(methacryloyloxyethyl ammonium propane sulfonate)]
 PMPC: poly(2-(methacryloyloxy)ethylphosphorylcholine
 PAMPS: poly(2-acrylamido-2-methyl propane sulfonic acid)
 PDMAAA-Q: poly(3-acrylamidopropyltrimethyl ammonium chloride)
 PEG: poly(ethylene glycol)
 PVBTMAC: poly(vinylbenzyltrimethylammonium chloride)
 VI: N-vinylimidazole
 VCL: N-vinylcaprolactame

Review Plan

Inclusion and Exclusion Criteria: The present review is devoted to interpolymer complexes of synthetic, natural and semi-natural polyampholytes with polyelectrolytes, proteins, DNA, and non-ionic polymers.

The review data mostly cover the publications from 1949 to 2022. However, some old literature sources dated on 1896, 1929, 1934 are also cited. In addition to a survey of the prevalent literature, most attention is paid to the authors' own research into the field of polyampholytes and interpolymer complexes since 1981. Articles in the relevant area were searched and analysed from the databases like Scopus, Web of Science, PubMed etc. along with other online scientific search engines (Google Scholar). The keywords used for the search were: "polyampholytes", "polypeptides", "proteins", "intrinsically disordered proteins", "DNA", "polyelectrolyte complexes", "intra- and inter-macromolecular complexes". No statistical methods were used in this review.

Introduction

The analysis of literature published over the past half century shows that the number of publications on polyampholytes generally continues to increase each year, starting from 1970. Figure 1 presents the data on the number of publications and citations in this area.

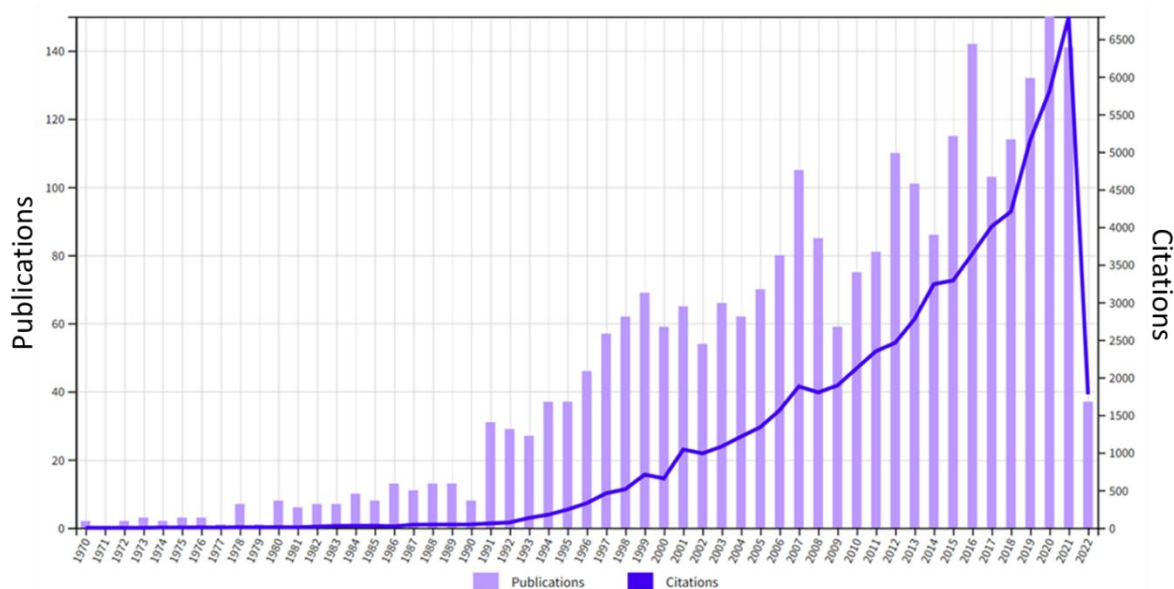


Figure 1. Progress of publications and citations on polyampholytes according to the data of Web of Knowledge, generated using the keywords "polyampholyte*" or "amphoteric polymer*".

This review aims to present the analysis of literature on synthetic, natural and semi-natural polyampholytes, focusing on their ability to form complexes with various water-soluble polymers of ionic

and non-ionic nature. Examples of applications of these complexes in different areas are also presented and briefly discussed.

1 Synthetic, natural and semi-natural polyampholytes

According to IUPAC terminology [1], ampholytic polymer is defined as a polyelectrolyte consisting of macromolecules that contain both cationic and anionic groups, or corresponding ionizable groups. An ampholytic polymer (synonym is polyampholyte) in which ionic groups of opposite signs are incorporated into the same pendant groups is called, depending on the structure of the pendant groups, a zwitterionic polymer, polymeric inner salt, or polybetaine.

The intensive development of research on polyampholytes since 1950s included the pioneering studies of Alfrey, Morawetz, Fuoss [2–4], Katchalsky [5–7], Ehrlich, Doty [8]. The interest to this type of polymeric materials was due to several reasons. One of the reasons is the similarity of the hierarchical structure of amphoteric macromolecules to structural organization of proteins [9, 10]. Second is the possibility of modeling protein folding using synthetic polyampholytes [11]. Third is the advances in the synthesis of amphoteric polypeptides [12–17] based on amino acids. Fourth is the possibility of preparing semi-natural polyampholytes by modification of natural building blocks [18, 19].

Proteins are amphoteric biopolymers, which from polymer science point of view, represent copolymers consisting of aminoacid (peptide) sequences ($-\text{NH}-\text{CHR}-\text{CO}-$), where their side groups (pendant groups) have acidic, basic, hydrophilic or hydrophobic moieties while the terminal groups are capped with carboxylic and amine groups. However, proteins have unique structure, properties and functions that can only be achieved in a living organism [20]. The number of possible conformations of globular proteins is exponentially dependent on the number of aminoacid residues in their chain. Some specific functions of these biopolymers can be successfully modeled using synthetic polyampholytes.

In the last years, mimicking the behavior of biopolymers through amphoteric macromolecules became the subject of numerous discussions [21–24]. Among the natural polyampholytes the intrinsically disordered proteins (IDPs) (also known as intrinsically unstructured proteins) attracted a great interest [25–29]. The IDPs can adopt random coil, pre-molten globule, molten globule, and folded conformations in aqueous solutions that can also exhibit transitions between each other [22]. The stimuli-responsive phase behavior of IDPs is governed by relationships between the information encoded in their aminoacid sequences and ensembles of conformations [30]. Synthetic polypeptides derived from aminoacids belong to semi-natural polyampholytes. Insertion of amino acids into the structure of synthetic polymers is an effective tool for the design of different non-biological bio-mimetic polyampholytes with unique physicochemical properties [12–19].

Synthetic amphoteric macromolecules comprise combinations of weak acid-weak base, strong acid-strong base, strong acid-weak base or weak acid-strong base monomers. Conditionally they can be classified as annealed, quenched, and betainic (or zwitterionic) types [31–40]. Annealed polyampholytes have acid-base monomers that are ionized depending on pH, while quenched polyampholytes with strongly charged cationic and anionic monomers retain their charges independently on pH. The “semi-annealed” or “semi-quenched” polyampholytes are amphoteric macromolecules formed with weak acid/cationic or weak base/anionic monomeric units. Betainic (or zwitterionic) polyampholytes are macromolecules with identical number of acid-base (or fully charged anionic-cationic) species in the same monomer units. Polybetaines may be grouped into polycarboxyl-, polysulfo-, and polyphosphobetaines [35, 36]. The macromolecules formed with the compensation of the cationic-anionic monomer pairs without counterions also belong to zwitterionic polymers [37] or polyampholytic ionic liquids [41, 42]. In the current literature the terms “zwitterionic polyampholytes”, “polybetaines”, “zwitterionic polyelectrolytes”, “polyzwitterions” are also widely used. Figure 2 illustrates the examples of synthetic polyampholytes with different chemical structures.

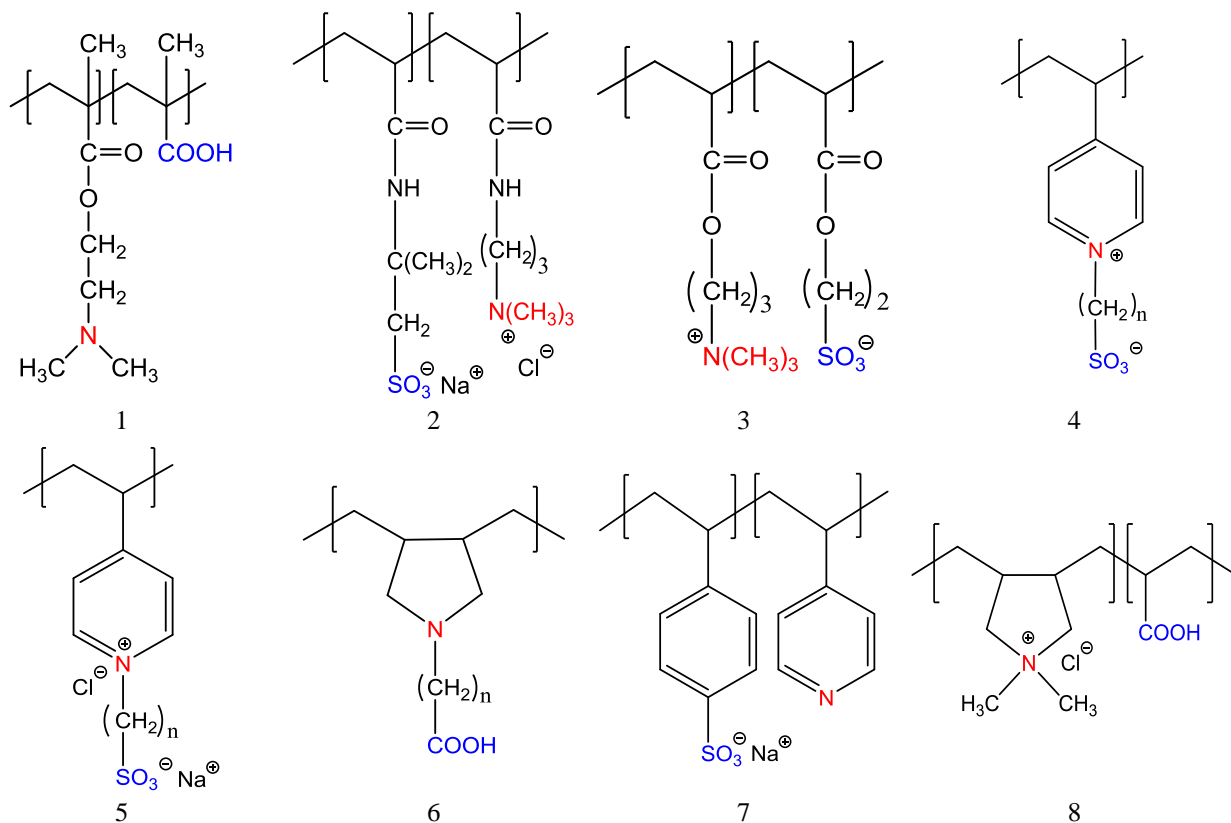


Figure 2. Repeating units of annealed (1), quenched (2), zwitterionic (3, 4), quenched betainic (5), annealed betainic (6) and self-annealed (or self-quenched) (7, 8) polyampholytes

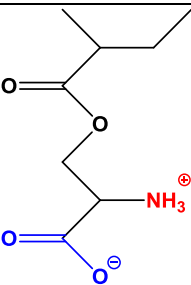
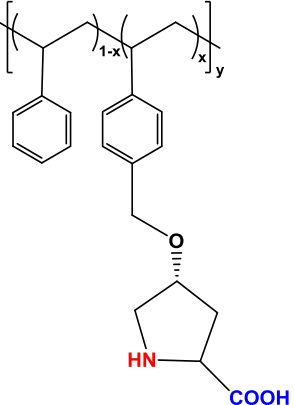
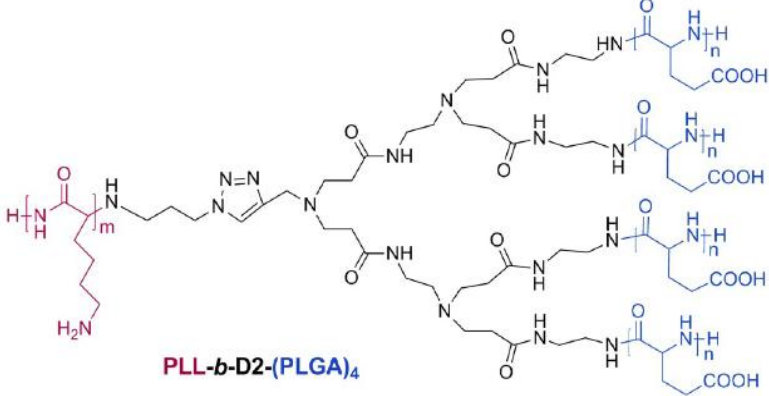
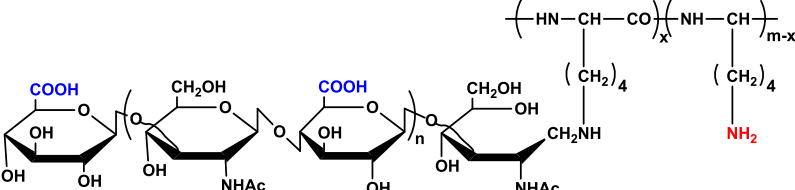
Table 1 provides some examples of amphoteric polypeptides based on L-lysine, L-serine, L-proline, and L-glutamic acid.

Table 1

Examples of amphoteric polypeptides

No.	Structural units of polypeptide-based polyampholytes	Name	Refs
1		Alternating amphoteric polypeptide obtained via the Ugi reaction	[43]
2		Triblock amphoteric copolymer derived from PEO ₄₂ -PLLys ₆₁ -PLGlu ₆₂	[44]

Continuation of Table 1

1	2	3	4
3		Poly(L-serinyl acrylate)	[45]
4		Styrene copolymers containing L-proline functionality	[15]
5		Linear-dendron-like polyampholyte, poly-(L-lysine)- <i>b</i> -D2-poly(L-glutamic acid) [PLL- <i>b</i> -D2-(PLGA) ₄], where D2 is the second generation of poly(amido amine)	[46]
6		Comb-type amphoteric copolymers composed of a poly(L-lysine) backbone and hyaluronic acid side chains	[47]

Semi-natural polyampholytes can be prepared by modification of natural polysaccharides, such as chitosan, cellulose, starch, gellan, alginic acid, by introducing either carboxylic (sulfo) or amine (ammonium) groups or both into their macromolecules [48–58]. For instance, to introduce sulfonate or carboxylic groups into chitosan chain it was modified by 1,3-propane sultone, 5-formyl-2-furansulfonic acid sodium salt, 2-formyl benzene sulfonic acid sodium salt, 4-formyl-1,3-benzene disulfonic acid disodium salts [58] or sodium alginate [18]. An amine derivative of gellan gum, exhibiting polyampholyte character, was obtained by functionalizing the polysaccharide backbone with pendant ethylenediamine moieties [59]. The physicochemical properties of amphoteric macromolecules were characterized by spectroscopy, colorimetry, chromatography, and rheological methods. Quaternized gellan derivatives were prepared by grafting N-(3-chloro-2-hydroxypropyl)-trimethyl ammonium chloride onto gellan's hydroxyl groups under alkali conditions at different gellan/N-(3-chloro-2-hydroxypropyl)-trimethyl ammonium chloride molar ratios [57].

2 Interpolymer complexes of synthetic and natural polyampholytes

In early 1970th, V.A. Kabanov et al. [59], E. Tsuchida et al. [60] and E.A. Bekturov et al. [61] started a new scientific direction, so-called interpolymer complexes (IPCs). IPCs are the products of interactions of two complementary macromolecules stabilized by cooperative ionic and/or hydrogen bonds. The specific interactions between macromolecules are important in biological systems and these assemblies are controlled by intra- and inter-macromolecular (intra-MMC and inter-MMC) complexation [60]. The latest developments in the area of interpolymer complexation via hydrogen bonding are presented in the book entitled "Hydrogen-bonded interpolymer complexes. Formation, structure and applications", representing a collection of original and review articles written by recognized experts from Germany, Greece, Kazakhstan, Poland, Romania, Russia, UK, Ukraine, and the USA [62]. This book highlights many important applications of interpolymer complexes in stabilization of colloidal systems, ecology, biotechnology, nanotechnology, medicine, and pharmaceuticals.

Formation of intra-MMC and inter-MMC complexes with participation of synthetic polyampholytes was reviewed in [63]. The complexation between statistical polyampholyte derived from copolymer of 2-methyl-5-vinylpyridine-acrylic acid (2M5VPy-AA) and poly(acrylic acid) (PAA), was first studied by V.A. Kabanov et al. [64]. It was found that the common cooperative system with ionic and hydrogen bonds between the 2M5VPy-AA and PAA is responsible for inter-MMC formation (Fig. 3).

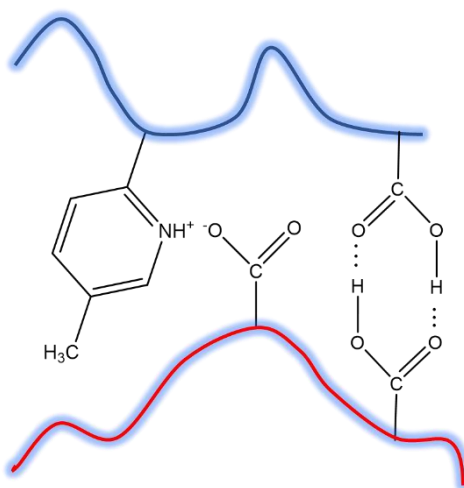


Figure 3. Schematic representation of formation of inter-MMC between copolymer of 2M5VPy-AA and PAA

The competition between the intra-MMC and inter-MMC was established in the mixture of N-methyl-diallylamine-maleic acid (MDAA-MA) and poly(N,N-dimethyl-N,N-diallylammonium chloride) (PDMDAAC) at pH = 3.9 corresponding to the isoelectric point (pH_{IEP}) of alternative polyampholyte [65]. As revealed from ^{13}C NMR and Raman spectra, some parts of carboxylate anions of MDAA-MA are involved in the formation of intra-MMC while some other parts form inter-MMC between carboxylate anions of MDAA-MA and quaternary nitrogen atoms of PDMDAAC.

Alternating copolymers of N, N-dimethyldiallylammonium and alkyl (or aryl) derivatives of maleamic acids were used to form complexes with PAA and poly(styrene sodium sulfonate) (NaPSS) [66]. It was found that the polyelectrolyte-polyampholyte complexes form compact core-shell particles and preserved in aqueous solution as a result of liberated edges from the carboxylic groups of polyampholyte.

The complexation of amphoteric dendrimers with linear and crosslinked anionic and cationic polyelectrolytes was studied by Zansokhova et al. [67, 68]. The efficiency of binding of polyampholyte dendrimers by oppositely charged linear or crosslinked polyelectrolytes was determined by the competition between intra-dendrimeric zwitterions and interionic salt bonds of functional groups of dendrimers and polyelectrolytes.

Formation of both intra-MMC and inter-MMC stabilized by cooperative ionic bonds is mostly specific for block polyampholytes [69–72]. It was found that the phase diagram of BPA-cationic polyelectrolyte system is dependent on the inter-MMC concentration and pH and may result in the formation of solution, gel or precipitate (Fig. 4).

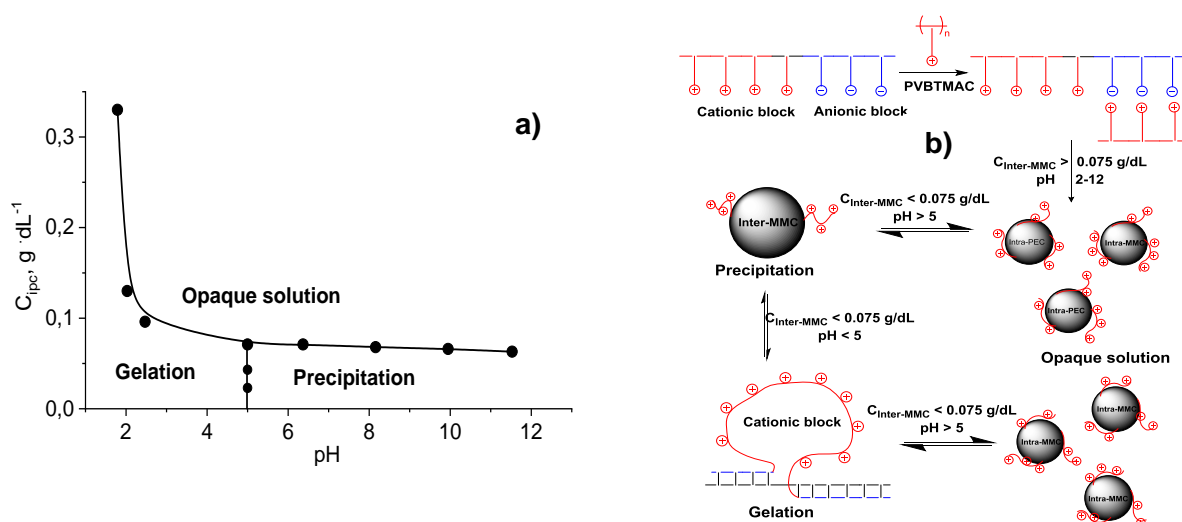


Figure 4. Phase diagram of inter-MMC composed of BPA and cationic polyelectrolyte — poly(vinylbenzyltrimethylammonium chloride) (PVBTMAC) (a) and schematic representation of phase transitions in dependence of inter-MMC concentration and solution pH (b). Reprinted from [64]

The complexation of polyampholyte gels with linear polyelectrolytes and/or between polyelectrolyte gels and linear polyampholytes is a less studied subject [74]. It is expected that the mechanism of sorption of polyelectrolytes by amphoteric gel is similar to the diffusion of linear polyelectrolytes within the oppositely charged polymer networks. Penetration of macromolecules into the hydrogel proceeds via “race-relay ion transport” (or “ion-hopping transportation”) mechanism leading to a gel deswelling. The swelling-deswelling behavior of amphoteric gel made of maleic acid (MA), *N,N'*-dimethyldiallylammonium chloride (DMDAAC) and diallylamine (DAA) was studied in the absence and presence of NaPSS [67]. The pristine amphoteric gel MA-DMDAAC-DAA shrinks at $pH_{IEP} \approx 4.6$ while the swelling degree of the inter-MMC composed of amphoteric gel MA-DMDAAC-DAA and linear NaPSS is minimal in a wide pH range between 3.5 and 8.5 (Fig. 5). It increases significantly in the strongly acidic and alkaline regions. The complex of MA-DMDAAC-DAA with NaPSS contracts over a wide range of pH because NaPSS present in the network acts as an additional physical crosslinker.

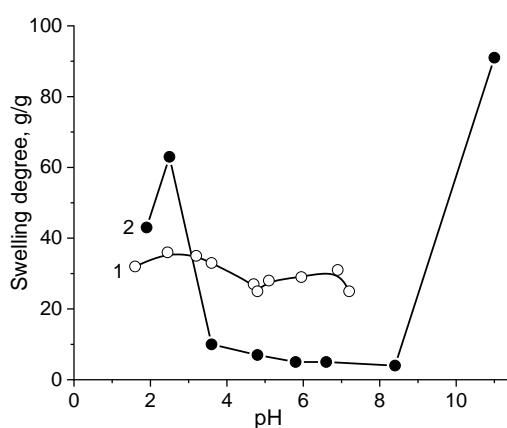


Figure 5. pH dependent swelling of amphoteric gel MA-DMDAAC-DAA (1) and inter-MMC formed between MA-DMDAAC-DAA and NaPSS (2) in pure water. Reprinted from [64]

Chen et al. [75] studied the complexes formed by poly(zwitterion) — poly[3-dimethyl(methacryloyloxyethyl ammonium propane sulfonate)] (PDMAPS) with polymeric anion: poly(2-acrylamido-2-methyl propane sulfonic acid) (PAMPS) or polymeric cations: poly(3-acrylamidopropyltrimethyl ammonium chloride) (PDMAPAA-Q) and *x,y*-ionene bromides ($x = 3,6$; $y = 3,4$). They found that the complexation of PDMAPS with PAMPS substantially increases the viscosity to form a network and decreases the upper criti-

cal solution temperature (UCST) while PDMAPS-PDMAPAA-Q complexes first decrease the UCST and then increase without formation of the network.

The formation of inter-MMC between anionic diblock (AMPSNa-APTAC)₉₁-(AMPS)₆₇ (denoted as P(SA)₉₁S₆₇) and cationic diblock (AMPSNa-APTAC)₉₁-(APTAC)₈₈ (denoted as P(SA)₉₁A₈₈) polyampholytes was studied by Yusa et al. [76]. They form stoichiometric inter-MMC micelles in aqueous solution (Fig. 6).

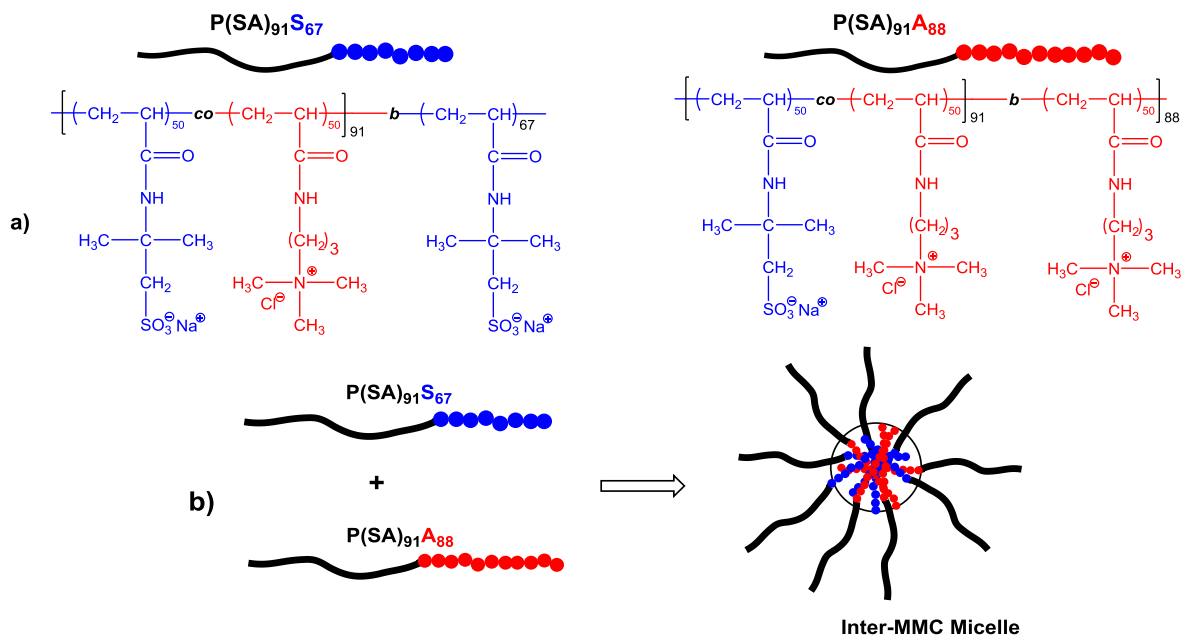


Figure 6. Structure of random copolymers of 2-acrylamido-2-methyl-1-propanesulfonic acid sodium salt-*co*-(3-acrylamidopropyl)trimethylammonium chloride-*block*-2-acrylamido-2-methyl-1-propanesulfonic acid sodium salt (AMPSNa-*co*-APTAC-*b*-AMPSNa) and 2-acrylamido-2-methyl-1-propanesulfonic acid sodium salt-*co*-(3-acrylamidopropyl)trimethylammonium chloride-*block*-(3-acrylamidopropyl)trimethylammonium chloride (AMPSNa-*co*-APTAC-*b*-APTAC) (a) and formation of inter-MMC micelle (b). Adapted and redrawn from Ref. [76]

The inter-MMC vesicles were also prepared from mixtures of aqueous solutions of diblock copolymers with a hydrophilic poly(2-(methacryloyloxy)ethylphosphorylcholine) (PMPC) block and either a cationic (APTAC) or anionic (AMPSNa) blocks [77]. Both inter-MMC micelles and vesicles may be considered as suitable carriers for pharmacologically-active compounds and used as drug delivery systems.

The presence of charged groups in natural and semi-natural polyampholytes, including proteins, results in a possibility of their involvement in specific interactions with oppositely charged polyelectrolytes of either synthetic or natural origin in solutions. If a solution of polyampholyte is mixed with solution containing oppositely charged polyelectrolyte this will often lead to the formation of interpolyelectrolyte complexes (IPEC). These IPECs depending on the nature of interacting species, their concentration in solutions, component ratio and environmental factors (pH and ionic strength of solution, solvent nature and temperature) will be formed as fully soluble associates, colloidal dispersions (nano- or micro-particles) or physically-cross-linked gels. In some cases, these interactions may also cause liquid-liquid phase separation called complex coacervation. The studies of these interactions date back to 1896, when Kossel reported the first observations of precipitation of egg albumin with addition of oppositely charged protamine [78]. In 1920–1930, Bungenberg de Jong et al. [79, 80] published several studies on the interactions between gelatin and gum arabic and observed liquid-liquid phase separation and formation of complex coacervates. The research of IPECs formed by natural and semi-natural polyampholytes has substantially progressed since these early studies with numerous reviews and monographs published [81–84].

The main driving force for the formation of these IPECs is electrostatic attraction; therefore, polyelectrolytes would not interact with proteins of the same net charge unless they have non-uniform charge distribution [83]. The electrostatic attraction between proteins and polyelectrolytes could potentially be completely suppressed in solutions with high ionic strength. For example, titration of 0.5 g/L solution of bovine serum albumin (BSA) with 0.5 g/L solution of strong cationic polyelectrolyte poly[2-methacryloyloxyethyl]trimethyl ammonium chloride (PMADQUAT) result in formation of cloudy mixtures in the ab-

sence of inorganic salt (Fig. 7); however, the maximum turbidity in this mixture is lower when the ionic strength of solution is increased to 0.05 [85]. When the ionic strength of solutions increased to 0.2 and 1, mixing BSA and PMADQUAT does not result in appearance of turbidity. This could be either because the complexation is completely suppressed in this system or the polycomplex formed is fully soluble.

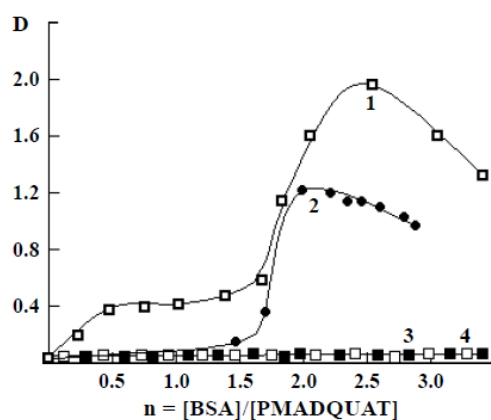


Figure 7. Turbidimetric titration curves of 0.5 g/L PMADQUAT solutions by 0.5 g/L BSA with different ionic strength: 0 (1), 0.05 (2), 0.2 (3), and 1 (4). Reprinted from [85]

The appearance of turbidity in protein-polyelectrolyte solution mixtures indicates the presence of the complexation but it does not show whether this interaction leads to formation of solid colloidal particles (precipitation) or liquid droplets (complex coacervation). Complex coacervation is a special case of this interaction, resulting in formation of two phases; one of those is dense and rich in protein and polyelectrolyte, whereas another one is dilute and contains an equilibrium mixture of protein and polyelectrolyte [82]. A centrifugation of the mixture and visual observation can be used to distinguish between precipitation and coacervation.

Polyampholyte-protein interaction of random- and block polyampholytes based on N,N-dimethylaminoethylmethacrylate-*co*-methacrylic acid-*co*-methylmethacrylate (DMAEM-MAA-MMA) with soybean trypsin inhibitor (STI), ovalbumin, ribonuclease and lysozyme was comprehensively studied [86]. The most favorable region of interaction of polyampholyte and protein is between their isoelectric points. An increase in the salt concentration suppresses polyampholyte-protein interactions confirming that the main driving force of self-aggregation is electrostatic [87]. The study of the supernatant and precipitate has shown that only about 10 % of the protein precipitates with the random polyampholyte DMAEM-MAA-MMA, while 90 % of the protein remains in the equilibrium liquid. While block polyampholyte DMAEM-MAA-MMA gives the opposite trend with 90 % of precipitation of protein [88]. Separation of protein mixture using random triblock polyampholyte DMAEM₈MMA₁₂MAA₁₆ was reported in [89–91]. In this method proposed for protein separation by precipitation, a polyampholyte should be added to a mixture of two proteins to be separated, one of which should have a net negative charge and the other one should be with a net positive charge. A prerequisite in the process is that the two oppositely charged proteins do not interact strongly with each other. Depending on the net charge of the polyampholyte used, one of the proteins will form a complex with the polyampholyte, resulting in precipitation, while the other one will remain in a supernatant phase. The protein-polyampholyte precipitate formed can be isolated and redissolved at a different pH. Then, protein and polyampholyte can be separated from each other by precipitating the polyampholyte at the pH_{IEP} . The separation of protein mixture can be also performed at the pH_{IEP} of block polyampholytes. Through this method, one of the blocks of the polyampholyte will interact with the oppositely charged groups of the protein, while the main chain (or other block) — with another protein charge as shown in Figure 8 [64]. In both cases protein release will occur at the pH_{IEP} of BPA due to the formation intra-MMC between anionic and cationic blocks within one macromolecular chain.

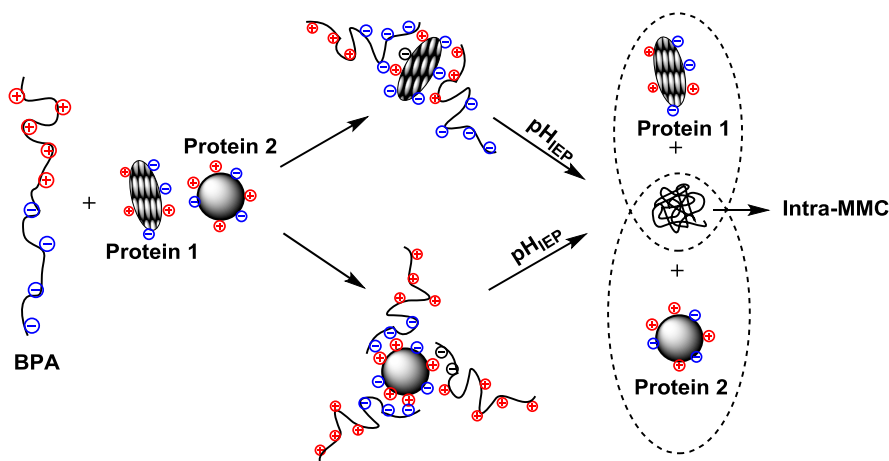


Figure 8. Separation of protein mixture at the pH_{IEP} of BPA. Reprinted from [64]

Uptake/release of cytochrome C by random and “core-shell” polyampholyte microgels consisting of N-vinylcaprolactame (VCL), itaconic acid (IA) (VCL-IA “core” part) and N-isopropylacrylamide (NIPAM), N-vinylimidazole (VI) (NIPAM-VI “shell” part) [91] and sorption/desorption of NaPSS by “core-shell” polyampholyte microgels composed of anionic — an itaconic acid monomethyl ether (NIPAM-*co*-MIA) “shell” and cationic — N-(3-aminopropyl)methacrylamide hydrochloride (NIPAM-*co*-APMH) “core” was carried out in [92]. The isoelectric points pH_{IEP} of random and “core-shell” polyampholyte microgels (VCL-IA/NIPAM-VI) were replaced near of $pH \sim 6.0$. Random and “core-shell” polyampholyte microgels were loaded with cytochrome C at $pH 8.0$. The pH triggered protein release results show that cytochrome C releases at the pH_{IEP} ($pH \sim 6.0$) much faster for both polyampholyte system due to formation of intra-MMC between oppositely charged groups of amphoteric macromolecules. The uptake and release of NaPSS by “core-shell” amphoteric microgels was observed at $pH 2.0$ and 11.0 , respectively. Strong binding of NaPSS with cationic fragment of APMH in “core” of NIPAM-*co*-APMH requires high $pH 10$ for full deprotonation of APMH groups to dissociate the amphoteric microgel-NaPSS complexes.

The complexation of zwitterionic monolithic column derived from crosslinked N,N-dimethyl-N-methacryloxyethyl-N-(3-sulfopropyl)ammonium betaine with proteins (lysozyme, ovalbumin, conalbumine, cytochrome C, and myoglobin) leads to efficient separation of lysozyme by changing the pH of mobile phase [94].

Molecularly-imprinted polyampholyte (MIP) hydrogels based on nonionic acrylamide, anionic AMPS and cationic APTAC were used for selective separation of bovine serum albumin (BSA) and lysozyme [95]. It was established that the best sample for sorption of BSA is amphoteric hydrogel with excess of APTAC while for sorption of lysozyme the polyampholyte gel with excess of AMPS is more suitable. The sorption capacity of amphoteric hydrogels with respect to BSA and lysozyme is 305.7 and 64.1-74.8 mg per 1 g of hydrogel, respectively. Desorption of BSA and lysozyme from MIP template conducted in 1M aqueous NaCl was found to be 82–88 %. The separation of BSA and lysozyme from their mixture was performed using MIP templates. The study of adsorption-desorption of polyampholyte hydrogels adjusted to either BSA or lysozyme shows that the mixture of BSA and lysozyme can be efficiently separated using MIP hydrogels.

Polyampholytes are able to bind polynucleotides and oligonucleotides, such as siRNA, or DNA, and deliver to mammalian cells for the treatment of genetic-based diseases [96]. The literature analysis indicates that synthetic polyampholytes are less studied with respect to gene delivery compared to cationic polyelectrolytes (Fig. 9) [48]. Several types of BPA, especially highly charged BPA composed of linear poly(ethyleneimine) (LPEI) and poly(methacrylic acid) and low charge BPA composed of LPEI and poly(glutamic acid) [97], multi-stimuli-responsive chiral-achiral amino acid-based block copolymers composed of poly(N-acryloyl amino acid) and poly(vinyl amine) [98] and comb-type polyampholyte consisting of a poly(L-lysine) backbone and hyaluronic acid side chains [99] were tested with respect to DNA delivery. It was found that the efficiency of DNA delivery is increased and toxicity is reduced relative to complexes formed between polycations and DNA (or siRNA). The delivered DNA (or siRNA) is effective in inhibiting specific gene expression in cells. In the context of DNA delivery, the release mechanism of DNA from inter-MMC is shown in Figure 10 [100]. The resulting BPA-DNA may aggregate with the formation of “core-shell” structure where the “core” part is the inter-MMC formed between cationic block of BPA and

anionic DNA, while the “shell” part consisting of the anionic block preserves the solubility of BPA-DNA complexes in water and simultaneously prevents interaction with proteins. The cooperative intra-ionic contacts between anionic and cationic blocks prevail over the inter-ionic contacts between cationic block and DNA at or near the isoelectric point (pH_{IEP}). As a result, anionic and cationic blocks of BPA form intra-MMC themselves and DNA releases. If intra-chain interaction between anionic and cationic blocks of BPA (intra-MMC) dominates over inter-chain interaction between BPA and DNA (inter-MMC) the latter can be detached from BPA-DNA complex and released at the pH_{IEP} of BPA.

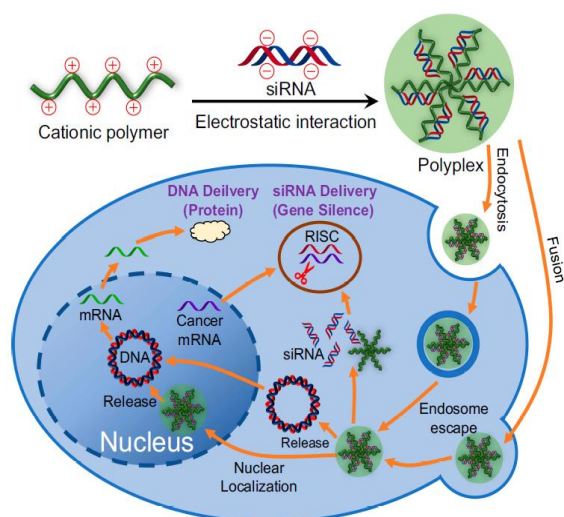


Figure 9. Gene delivery mechanism into the cell by polycomplex formed between cationic polymer and siRNA. Reproduced from [48] with permission from Dove Medical Press Ltd

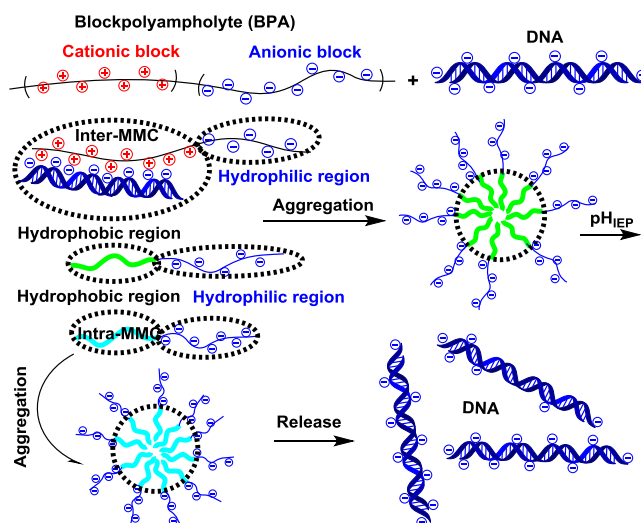


Figure 10. Schematic routes of BPA-DNA complex formation and proposed release mechanism of DNA at the pH_{IEP} of BPA. Adapted and modified from [100]

Skorikova et al. [101] studied the formation of inter-MMC between sulfated chitosan, a polyampholyte with amine and sulfo groups, and 2,5-ionene bromide. The turbidimetric titration of 2,5-ionene bromide with chitosan sulfate (CS) at $pH = 2.5$ and 11.5 indicates that the composition of MMC is different in acidic and alkaline regions. At acidic pH only a half of sulfate groups participate in the formation of nonstoichiometric complex because the rest exists in the form of intra-MMC. At alkali pH the composition of polyelectrolyte complexes is stoichiometric because all sulfate groups are involved in formation of inter-MMC. Formation of inter-MMC between cellulose-based polyampholyte and PDMDAAC was studied by Elschner et al. [102]. The inter-MMC exhibited pH -responsive character, was switchable in a physiologically relevant pH range and is a promising nanocarrier in the field of drug delivery.

Protein-polyelectrolyte complexes with participation of proteins (insulin and glucose oxidase), antimicrobial peptide (LL-37), polysaccharides (heparin and alginate), and synthetic polyelectrolytes (NaPSS and poly(allylamine hydrochloride)) were assembled by layer-by-layer (LbL) technique [103]. It was shown that the adsorption behavior and the multilayer growth are strongly dependent on the nature of the protein and polyelectrolyte used. Integrating proteins in LbL thin films is sometimes challenging due to their amphoteric nature and is beneficial for surface modification with hard-to-immobilize proteins and peptides.

In addition to interpolyelectrolyte complexes formed by natural and semi-natural polyampholytes with oppositely charged polyelectrolytes, there are also reports on the complexes stabilised by hydrogen bonding. One of the early reports of the complexation via hydrogen bonding is the study on the interactions between pepsin and poly(ethylene glycol) (PEG) by Kokufuta and Nishimura [104]. They established that addition of PEG to pepsin leads to the increase of reduced viscosity of enzyme solution, when the solutions had a pH of 3; however, this increase in viscosity was not observed at pH 4.5. The authors interpreted these observations as a formation of water-soluble complexes, in which ether groups of PEG bind to carboxylic groups of the enzyme via hydrogen bonding. Later, Xia, Dubin and Kokufuta [105] reported the use of quasi-elastic light scattering measurements to confirm the complexation between pepsin and non-ionic polyethylene glycol via hydrogen bonding. Subsequently, Azegami et al. [106] reported the formation of complexes between human serum albumin (HSA) and PEG, in which several HSA macromolecules are bound to PEG chain at pH 2.

Based on these studies of complexation between proteins and PEG the following structural organisation for these complexes was proposed (Fig. 11).

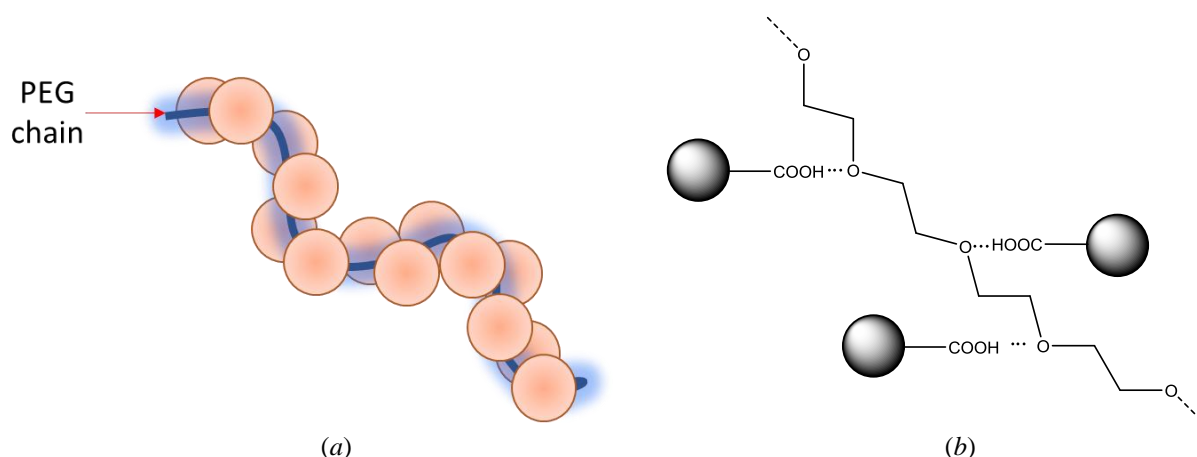


Figure 11. Structural organisation of protein — PEG complexes (a) and mechanism of hydrogen bonding between proteins and PEG under acidic conditions (b). Protein molecules are shown as spheres in these images

Later, Matsunami et al. [107] also reported the complex formation between various proteins (HSA, ovalbumin and lysozyme) and non-ionic poly(N-isopropylacrylamide). They established that hydrophobic interactions play an important role in the formation of these complexes.

3 Application of interpolymer complexes derived from synthetic, natural and semi-natural polyampholytes

Multifunctional nature of polyampholytes and their diverse physicochemical properties open numerous opportunities for applications, including the use of materials resulting from their complexes with other polymers. One of the most widely industrially used polyampholytes is gelatin, which is a product of partial hydrolysis of collagen, present in bones, cartilage and skin of slaughter animals. It is industrially one of the most important semi-natural polyampholyte with unique set of physicochemical properties. The properties of gelatin depend on the method of its production either through acid or alkaline-based processes. The gelatin prepared using the alkaline process exhibits the isoelectric point in the region of 4.8–5.2 (gelatin B), whereas gelatin A, manufactured via the acid process, will have the isoelectric point at 7–9 [108, 109]. The unique ability of gelatin to form concentrated (up to 40 w/v %) and relatively non-viscous aqueous solutions at 50 °C and their quick gelation upon cooling is one of the main reasons for its wide application in pharmaceutical and food industry (Fig. 12).

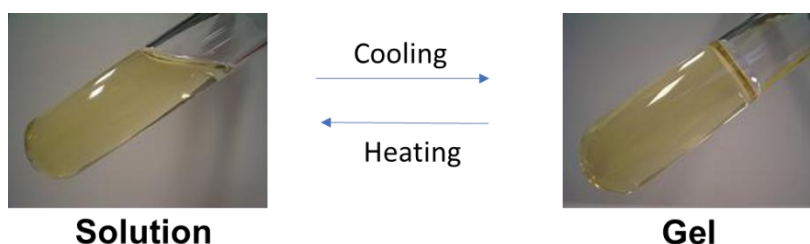


Figure 12. Reversible gelation in 40 w/v % solutions of gelatin upon changes in temperature

The complexation of gelatin with oppositely charged synthetic and natural polyelectrolytes received a lot of attention since the pioneering studies by Bungenberg de Jong et al. [79, 80]. The classical gelatin – Arabic gum system forming complex coacervates received a lot of interest for the preparation of microcapsules delivery of drugs and other active ingredients. For example, Chang et al. [110] reported encapsulation of camphor oil together with polystyrene into gelatin-gum Arabic microcapsules. Shaddel et al. [111] reported microencapsulation of black raspberry water extracts by double emulsion technique prior to complex coacervation to stabilise anthocyanins under harsh processing and storage conditions. Complexes of gelatin

with gum arabic are also promising for applications as food additives, stabilisation of dairy products, for increasing water retention capacity in meat products, and as emulsifiers in ice creams [112].

Interpolyelectrolyte complexes formed by gelatin and oppositely charged polyelectrolytes can also be used in the design of solid dosage forms for drug delivery. For example, Moustafine [113] studied the complexation between gelatin and weakly cross-linked poly(acrylic acid) in aqueous solutions. These complexes were then isolated in solid state and compressed into tablets with and without a model drug (diclofenac sodium). The studies of swelling of these tablets in phosphate buffer (pH 7.5) demonstrated that the swelling degree of the matrices decreases with increase in the polyampholyte content in the dosage form. When the behaviour of these tablets was studied in acidic media (pH 1.2), imitating the environment in the stomach, these dosage forms undergo erosion. The release of the drug from these tablets was also found to correlate with gelatin/poly(acrylic acid) ratio in the dosage form.

Complexes of polyampholytes with other polymers are also found interest as nano-vehicles for drug delivery. For example, an interesting application of protein — polyelectrolyte complexation was reported by Al-Saadi et al. [114]. They studied an alternate deposition of bovine serum albumin (BSA) and glycol chitosan on the surface of magnetic iron oxide nanoparticles, forming a multi-layered coating. Using circular dichroism technique, it was demonstrated that the secondary structure of BSA present in the formed multi-layer coating remains unaltered and the protein was capable of binding small drug molecules such as diazepam, ibuprofen and warfarin. The drug binding constants (K) measured for BSA deposited on the magnetic nanoparticle surface are almost identical to the K values typical for native protein. The authors considered the application of layer-by-layer deposition of protein — polyelectrolyte complexes as a method promising for developing magnetically-driven drug delivery systems, which may be used for protein delivery. Lomova et al. [115] utilised the complexation between bovine serum albumin and tannic acid to prepare biodegradable capsules using a layer-by-layer deposition approach. Hydrogen bonding was proposed to be the main driving force for the complexation between BSA and tannic acid. These capsules were prepared using CaCO_3 microparticles as a sacrificial template. Calcium carbonate microparticles were prepared by the reaction between CaCl_2 and Na_2CO_3 in the presence of fluorescently labelled BSA as a model drug. Then a multi-layered coating with 6 bilayers was formed on the surface of these microparticles using the layer-by-layer complexation between BSA and tannic acid. Subsequently, these particles were treated with ethylenediamine tetraacetate to extract CaCO_3 . These microcapsules were discussed as a promising vehicle for applications in drug delivery and cosmetics.

The complexation of proteins with polyelectrolytes and selective phase separation in these systems can be successfully used to isolate specific proteins from their mixture. For example, Wang et al. [116] studied the efficiency of separation in the mixtures containing proteins bovine serum albumin, β -lactoglobulin, γ -globulin, and ribonuclease A using their complexation with poly(diallyldimethylammonium chloride). They established that the selectivity of separation depends on pH and increases with molecular weight of cationic polyelectrolyte and reduction in solution ionic strength.

Other applications of polyampholyte-polymer complexes include systems with immobilised enzymes, where complexation with polyelectrolytes can boost their catalytic performance. This could potentially be of importance for enzymes used in complex multicomponent formulations, such as laundry, food, pharmaceutical or cosmetic applications. For example, Thiele et al. [117] reported the observation of the enhancement effects in catalytic activity of a nonspecific subtilisin protease upon its complexation with poly(acrylic acid) and poly(L- γ -glutamic acid).

Conclusions

It is expected that understanding of the fundamental relationships between the microstructure and property of synthetic, natural and semi-natural polyampholytes can expand our knowledge and cause the renewed interest of both theorists and experimentalists in advanced experimental and theoretical investigations. Future possibilities regarding polyampholytes may be related to semi-natural polyampholytes that can be prepared through modification of such natural polysaccharides as chitosan, cellulose, starch, gellan, and alginic acid, among others, through introduction of either carboxylic (sulfo) or amine (ammonium) groups, or both, into the macromolecular chains. A further potential development in polyampholytes in our mind will include intrinsically disordered proteins (IDPs), which belong to strong polyampholytes, polypeptide-based polyampholytes and polyampholytic ionic liquids. Inter-macromolecular complexes of polyampholytes are the products of complexation between linear and crosslinked synthetic polyampholytes, of random, regular, graft, block and dendritic microstructures, with polyelectrolytes, proteins and polynucleotides. The applica-

tions of interpolymer complexes formed by various polyampholytes are currently growing, with particular interest in microencapsulation technologies, food and pharmaceutical industries, protein separation and formulation of enzymes.

Acknowledgements

R.I. Moustafine and V.V. Khutoryanskiy gratefully acknowledge Russian Science Foundation–RSF (project no. 20-65-46007) for partial financial support of work on this review.

References

- Hess, M., Jones, R.G., Kahovec, J., Kitayama, T., Kratochvíl, P., Kubisa, P., Mormann, W., Stepto, R.F.T., Tabak, D., Vohlídal, J., & Wilks, E.S. (2006). Terminology of polymers containing ionizable or ionic groups and of polymers containing ions (IUPAC Recommendations 2006). *Pure and Applied Chemistry*, 78(11), 2067–2074. <https://doi.org/10.1351/pac200678112067>
- Alfrey, T., Morawetz, H., Fitzgerald, E.B., & Fuoss, R.M. (1950). Synthetic electrical analog of proteins. *Journal of the American Chemical Society*, 72(4), 1864. <https://doi.org/10.1021/ja01160a532>
- Alfrey, T., & Morawetz, H. (1952). Amphoteric polyelectrolytes. I. 2-vinylpyridine—methacrylic acid copolymers1, 2. *Journal of the American Chemical Society*, 74(2), 436–438. <https://doi.org/10.1021/ja01122a046>
- Alfrey, T., Fuoss, R.M., Morawetz, H., & Pinner, H. (1952). Amphoteric polyelectrolytes. II. Copolymers of methacrylic acid and diethylaminoethyl methacrylate1. *Journal of the American Chemical Society*, 74(2), 438–441. <https://doi.org/10.1021/ja01122a047>
- Katchalsky, A., & Gillis, J. (1949). Potentiometric behavior of polyampholytes. Copolymers of 2-vinylpyridine-acrylic acid. *Recl Trav Chim-Pays Bas*, 68, 871–877.
- Katchalsky, A., & Miller, I.R. (1954). Polyampholytes. *J Polym Sci*, 13, 57–68. <https://doi.org/10.1002/pol.1954.120136805>
- Mazur, J., Silberberg, A., & Katchalsky, A. (1959). Potentiometric behavior of polyampholytes. *J Polym Sci*, 35, 43–70. <https://doi.org/10.1002/pol.1959.1203512805>
- Ehrlich, G., & Doty, P. (1954). Macro-ions. III. The solution behavior of a polymeric ampholyte1. *Journal of the American Chemical Society*, 76(14), 3764–3777. <https://doi.org/10.1021/ja01643a053>
- Ciferri, A., & Kudaibergenov, S. (2007). Natural and synthetic polyampholytes, 1. *Macromolecular Rapid Communications*, 28(20), 1953–1968. <https://doi.org/10.1002/marc.200700162>
- Kudaibergenov, S.E., & Ciferri, A. (2007). Natural and synthetic polyampholytes, 2. Functions and applications. *Macromolecular Rapid Communications*, 28(20), 1969–1986. <https://doi.org/10.1002/marc.200700197>
- Edwards, S.F., King, P.R., & Pincus, P. (1980). Phase changes in polyampholytes. *Ferroelectrics*, 30(1), 3–6. <https://doi.org/10.1080/00150198008209479>
- Roy, S.G., & De, P. (2014). pH responsive polymers with amino acids in the side chains and their potential applications. *Journal of Applied Polymer Science*, 131(20). <https://doi.org/10.1002/app.41084>
- Mori, H., & Endo, T. (2012). Amino-acid-based block copolymers by RAFT polymerization. *Macromolecular Rapid Communications*, 33(13), 1090–1107. <https://doi.org/10.1002/marc.201100887>
- Kruse, J.-H., Biehl, P., & Schacher, F.H. (2019). Different routes to ampholytic polydehydroalanine: orthogonal versus simultaneous deprotection. *Macromolecular Rapid Communications*, 1800857. <https://doi.org/10.1002/marc.201800857>
- Evans A.C., Skey, J., Wright, M., Qu, W., Ondeck, C., Longbottom, D.A., & O'Reilly R.K. (2009). Functional and tunable amino acid polymers prepared by RAFT polymerization. *J Polym Sci Part A: Polym Chem*, 47, 6814–6826. <https://doi.org/10.1002/pola.23721>
- Shirbin, S.J., Lam, S.J., Chan, N.J.-A., Ozmen, M.M., Fu, Q., O'Brien-Simpson, N., Reynolds, E.C., & Qiao, G.G. (2016). Polypeptide-based macroporous cryogels with inherent antimicrobial properties: the importance of a macroporous structure. *ACS Macro Letters*, 5(5), 552–557. <https://doi.org/10.1021/acsmacrolett.6b00174>
- Tao, Y., Wang, S., Zhang, X., Wang, Z., Tao, Y., & Wang, X. (2018). Synthesis and properties of alternating polypeptoids and polyampholytes as protein-resistant polymers. *Biomacromolecules*, 19(3), 936–942. <https://doi.org/10.1021/acs.biomac.7b01719>
- Janciauskaite, U., Visnevskij, C., Radzevicius, K., & Makuska, R. (2009). Polyampholytes from natural building blocks: synthesis and properties of chitosan-O-alginate copolymers. *Chemija*, 20, 128–135.
- Lin, M., Liu, H., Deng, J., An, R., Shen, M., Li, Y., & Zhang, X. (2019). Carboxymethyl chitosan as a polyampholyte mediating intrafibrillar mineralization of collagen via collagen/ACP self-assembly. *Journal of Materials Science & Technology*, 35, 1894–1905. <https://doi.org/10.1016/j.jmst.2019.05.010>
- Cohn, E.J., & Edsall, J.T. (1943). Proteins, amino acids and peptides as ions and dipolar ions. New York: Reinhold Publishing Corporation.
- Laschewsky, A., Marsat, J.N., Skrabania, K., Berlepsch, H., & Böttcher, C. (2009). Bioinspired block copolymers: translating structural features from proteins to synthetic polymers. *Macromol Chem Phys*, 211, 215–221.
- Sackmann, E. (1994). Intra- and extracellular macromolecular networks: physics and biological function. *Macromol Chem Phys*, 195, 7–28.

- 23 Gunliffe, D., Pennadam, S., & Alexander, C. (2004). Synthetic polymers—merging the interface. *Eur Polym J*, *40*, 5–25.
- 24 Grinberg, V.Y., Burova, T.V., Grinberg, N.V., Alvarez-Lorenzo, C., & Khokhlov, A.R. (2019). Protein-like energetics of conformational transitions in a polyampholyte hydrogel. *Polymer*, *179*, 121617. <https://doi.org/10.1016/j.polymer.2019.121617>
- 25 Bright, J.N., Woolf, T.B., & Hoh, J.H. (2001). Predicting properties of intrinsically unstructured proteins. *Progress in Biophysics and Molecular Biology*, *76*(3), 131–173. [https://doi.org/10.1016/s0079-6107\(01\)00012-8](https://doi.org/10.1016/s0079-6107(01)00012-8)
- 26 Uversky, V.N. (2019). Intrinsically disordered proteins and their “mysterious” (meta)physics. *Frontiers in Physics*, *7*. <https://doi.org/10.3389/fphy.2019.00010>
- 27 Van der Lee, R., Buljan, M., Lang, B., Weatheritt, R.J., Daughdrill, G.W., Dunker, A.K., Fuxreiter, M., Gough, J., Gsponer, J., Jones, D.T., Kim, P.M., Kriwacki, R.W., Oldfield, C.J., Pappu, R.V., Tompa, P., Uversky, V.N., Wright, P.E., & Babu, M.M. (2014). Classification of intrinsically disordered regions and proteins. *Chemical Reviews*, *114*(13), 6589–6631. <https://doi.org/10.1021/cr400525m>
- 28 Wright, P.E., & Dyson, H.J. (2015). Intrinsically disordered proteins in cellular signalling and regulation. *Nature Reviews Molecular Cell Biology*, *16*(1), 18–29. <https://doi.org/10.1038/nrm3920>
- 29 Oldfield, C.J., & Dunker, A.K. (2014). Intrinsically disordered proteins and intrinsically disordered protein regions. *Annual Review of Biochemistry*, *83*(1), 553–584. <https://doi.org/10.1146/annurev-biochem-072711-164947>
- 30 Das, R.K., & Pappu, R.V. (2013). Conformations of intrinsically disordered proteins are influenced by linear sequence distributions of oppositely charged residues. *Proceedings of the National Academy of Sciences*, *110*(33), 13392–13397. <https://doi.org/10.1073/pnas.1304749110>
- 31 Kudaibergenov, S.E. (2002). Polyampholytes: Synthesis, Characterization and Application. New York: Kluwer Academic/Plenum Publishers, 220. <https://doi.org/10.1007/978-1-4615-0627-0>
- 32 Lowe, A.B., & McCormick, C.L. (2002). Synthesis and solution properties of zwitterionic polymers. *Chemical Reviews*, *102*(11), 4177–4190. <https://doi.org/10.1021/cr020371t>
- 33 Kudaibergenov, S.E. (1999). Recent advances in studying of synthetic polyampholytes in solutions. *Adv Polym Sci*, *144*, 115–197.
- 34 Kudaibergenov, S.E. (2008). Polyampholytes. In *Encyc Polym Sci Technol. John Wiley Interscience: Hoboken, NJ, USA*, 1–30.
- 35 Kudaibergenov, S., Jaeger, W., & Laschewsky, A. (2006). Polymeric Betaines: Synthesis, Characterization, and Application. *Advances in Polymer Science*, *157*–224. https://doi.org/10.1007/12_078
- 36 Laschewsky, A. (2014). Structures and synthesis of zwitterionic polymers. *Polymers*, *6*(5), 1544–1601. <https://doi.org/10.3390/polym6051544>
- 37 Singh, P.K., Singh, V.K., & Singh, M. (2007). Zwitterionic Polyelectrolytes: A Review. *e-Polymers*, *7*(1). <https://doi.org/10.1515/epoly.2007.7.1.335>
- 38 He, X.Y., Zhou, W.R., Xu, X.J., & Yang, W. (2013). Preparation and application of zwitterionic polymers. *Prog in Chem*, *25*(6), 1023–1030. <https://doi.org/10.7536/PC121106>
- 39 Bernards, M., & He, Y. (2014). Polyampholyte polymers as a versatile zwitterionic biomaterial platform. *Journal of Biomaterials Science, Polymer Edition*, *25*(14-15), 1479–1488. <https://doi.org/10.1080/09205063.2014.938976>
- 40 Liu, H., & Zhou, J. (2012). Biological applications of zwitterionic polymers. *Prog in Chem*, *24*(11), 2187–2197.
- 41 Ohno, H., Yoshizawa-Fujita, M., & Ogihara, W. (2011). Electrochemical Aspects of Ionic Liquids. New Jersey: John Wiley & Sons, Inc., Hoboken, 433–439.
- 42 Fouillet, C.C.J., Greaves, T.L., Quinn, J.F., Davis, T.P., Adamcik, T., Sani, M.A., Separovic, F., Drummond, C.J., & Mezzenga, R. (2017). Copolyampholytes produced from RAFT polymerization of protic ionic liquids. *Macromolecules*, *50*, 8965. <https://doi.org/10.1021/acs.macromol.7b01768>
- 43 Tao, Y., Wang, S., Zhang, X., Wang, Z., Tao, Y., & Wang, X. (2018). Synthesis and properties of alternating polypeptoids and polyampholytes as protein-resistant polymers. *Biomacromolecules*, *19*(3), 936–942. <https://doi.org/10.1021/acs.biomac.7b01719>
- 44 Sun, J., Černoch, P., Völkel, A., Wei, Y., Ruokolainen, J., & Schlaad, H. (2016). Aqueous self-assembly of a protein-mimetic ampholytic block copolypeptide. *Macromolecules*, *49*(15), 5494–5501. <https://doi.org/10.1021/acs.macromol.6b00817>
- 45 Maji, T., Banerjee, S., Biswas, Y., & Mandal, T.K. (2015). Dual-stimuli-responsive L-serine-based UCST-type polymer with tunable thermosensitivity. *Macromolecules*, *48*(14), 4957–4966. <https://doi.org/10.1021/acs.macromol.5b01099>
- 46 Chen, L., Chen, T., Fang, W., Wen, Y., Lin, S., Lin, J., & Cai, C. (2013). Synthesis and pH-responsive “Schizophrenic” aggregation of a linear-dendron-like polyampholyte based on oppositely charged polypeptides. *Biomacromolecules*, *14*(12), 4320–4330. <https://doi.org/10.1021/bm401215w>
- 47 Asayama, S., Nogawa, M., Takei, Y., Akaike, T., & Maruyama, A. (1998). Synthesis of novel polyampholyte comb-type copolymers consisting of a poly(L-lysine) backbone and hyaluronic acid side chains for a DNA carrier. *Bioconjugate Chemistry*, *9*(4), 476–481. <https://doi.org/10.1021/bc970213m>
- 48 Chen, L., Tian, Z., & Du, Y. (2004). Synthesis and pH sensitivity of carboxymethyl chitosan-based polyampholyte hydrogels for protein carrier matrices. *Biomaterials*, *25*(17), 3725–3732. <https://doi.org/10.1016/j.biomaterials.2003.09.100>
- 49 Ouerghemmi, S., Dimassi, S., Tabary, N., Leclercq, L., Degoutin, S., Chai, F., Pierlota, C., Cazauxa, F., Ungd, A., Staelensa, J.-N., Blanchemain, N., & Martel, B. (2018). Synthesis and characterization of polyampholytic aryl-sulfonated chitosans and their in vitro anticoagulant activity. *Carbohydrate Polymers*, *196*, 8–17. <https://doi.org/10.1016/j.carbpol.2018.05.025>

- 50 Meng, P.R., & Li, L.B. (2014). Study on the preparation of starch-based polyampholyte and slow release performance. *Materials Science Forum*, 809–810, 302–307. <https://doi.org/10.4028/www.scientific.net/msf.809-810.302>
- 51 Yin, Q., Zhou, G., Liu, Y.-Y., Yin, Q.-J., Luo, J.-H., & Jiang, B. (2010). Molecular dynamic simulation of carboxyethyl chitosan: effect of temperature, salt concentration and pH. *Journal of Theoretical and Computational Chemistry*, 09(supp01), 167–176. <https://doi.org/10.1142/s0219633610005487>
- 52 Yu, C., Liu, Y.-F., Tang, H.-L., & Tan, H.-M. (2010). Study of carboxymethyl chitosan-based polyampholyte superabsorbent polymer (Part II): Investigating the state of water in CMCTS-g-(PAA-co-PTMAAC) hydrogel. *Iranian Polym J.*, 19, 417–425.
- 53 Yu, C., Liu, Y.-F., Tang, H.-L., & Tan, H.-M. (2010). Study of carboxymethyl chitosan based polyampholyte superabsorbent polymer. Optimization of synthesis conditions and pH sensitive property study of carboxymethyl chitosan-g-poly(acrylic acid-co-dimethyldiallylammonium chloride) superabsorbent polymer. *Carbohydrate Polymers*, 81, 365–371. <https://doi.org/10.1016/j.carbpol.2010.02.007>
- 54 Dhar, N., Akhlaghi, S.P., & Tam, K.C. (2012). Biodegradable and biocompatible polyampholyte microgels derived from chitosan, carboxymethyl cellulose and modified methyl cellulose. *Carbohydrate Polymers*, 87(1), 101–109. <https://doi.org/10.1016/j.carbpol.2011.07.022>
- 55 Cheng, B., Pei, B., Wang, Z., & Hu, Q. (2017). *Advances in chitosan-based superabsorbent hydrogels*. *RSC Advances*, 7(67), 42036–42046. <https://doi.org/10.1039/c7ra07104c>
- 56 Kono, H., Oeda, I., & Nakamura, T. (2013). The preparation, swelling characteristics, and albumin adsorption and release behaviors of a novel chitosan-based polyampholyte hydrogel. *Reactive and Functional Polymers*, 73(1), 97–107. <https://doi.org/10.1016/j.reactfunctpolym.2012.08.016>
- 57 Novac, O., Lisa, G., Profire, L., Tuchilus, C., & Popa, M.I. (2014). Antibacterial quaternized gellan gum based particles for controlled release of ciprofloxacin with potential dermal applications. *Materials Science and Engineering: C*, 35, 291–299. <https://doi.org/10.1016/j.msec.2013.11.016>
- 58 Dimassi, S., Tabary, N., Chai, F., Blanchemain, N., & Martel, B. (2018). Sulfonated and sulfated chitosan derivatives for biomedical applications: a review. *Carbohydrate Polymers*, 202, 382–396. <https://doi.org/10.1016/j.carbpol.2018.09.011>
- 59 Fiorica, C., Pitarresi, G., Palumbo, F.S., Mauro, N., Federico, S., Giammona, G. (2020). Production and physicochemical characterization of a new amine derivative of gellan gum and rheological study of derived hydrogels. *Carbohydrate Polymers*, 236, 116033. <https://doi.org/10.1016/j.carbpol.2020.116033>
- 60 Kabanov, V.A., & Zezin, A.B. (1984). Soluble interpolymeric complexes as a new class of synthetic polyelectrolytes. *Pure and Applied Chemistry*, 56(3), 343–354. <https://doi.org/10.1351/pac198456030343>
- 61 Tsuchida, E., & Abe, K. (1982). Interactions between macromolecules in solution and intermacromolecular complexes. *Advances in Polymer Science*, 1–119. <https://doi.org/10.1007/bfb0017549>
- 62 Bekturov, E.A., & Bimendina, L.A. (1981). Interpolymer complexes. *Advances in Polymer Science*, 99–147. https://doi.org/10.1007/3-540-10554-9_11
- 63 Khutoryanskiy, V.V., & Staikos, G. (2009). Hydrogen-bonded interpolymer complexes: formation, structure and applications. Singapore: World Scientific Pub. Co., 366. ISBN 978-981-270-977-6
- 64 Kudaibergenov, S., & Nuraje, N. (2018). Intra- and interpolyelectrolyte complexes of polyampholytes. *Polymers*, 10(10), 1146. <https://doi.org/10.3390/polym10101146>
- 65 Savinova, I.V., Fedoseeva, N.A., Evdakov, V.P., & Kabanov, V.A. (1976). Polymer-polymer complexes with participation of synthetic polyampholytes. *Vysokomol. Soedin. Ser. A*, 18, 2050–2057.
- 66 Kudaibergenov, S.E., Sigitov, V.B., Bekturov, E.A., Koetz, J., & Philipp, B. (1989). Studing of novel polyampholytes based on allylamines and maleic acid by ¹³C NMR and Raman spectroscopy. *Vysokomol. Soedin. Ser. B*, 31, 132–136.
- 67 Ibraeva, Z. E., Hahn, M., Jaeger, W., Bimendina, L.A., & Kudaibergenov, S.E. (2004). Solution properties and complexation of polyampholytes based on N, N-dimethyldiallylammonium chloride and maleic acid or alkyl (aryl) derivatives of maleamic acids. *Macromolecular Chemistry and Physics*, 205(18), 2464–2472. <https://doi.org/10.1002/macp.200400242>
- 68 Zansokhova, M.F., Rogacheva, V.B., Gulyaeva, Z.G., Zezin, A.B., Joosten, J., & Brackman, J. (2008). Interaction of ampholyte dendrimers with linear polyelectrolytes. *Polymer Science Series A*, 50(6), 656–664. <https://doi.org/10.1134/s0965545x08060096>
- 69 Rogacheva, V.B., Panova, T.V., Bykova, E.V., Zezin, A.B., Joosten, J., & Brackman, J. (2009). Interaction of ampholyte dendrimers with network polycations and polyanions. *Polymer Science Series A*, 51(3), 242–249. <https://doi.org/10.1134/s0965545x0903002x>
- 70 Bekturov, E.A., Kudaibergenov, S.E., Frolova, V.A., Schultz, R.S., & Zoller, J. (1990). Conformational and complex formation ability of poly(methacrylic acid)-block-poly(1-methyl-4-vinylpyridinium chloride). *Makromol. Chem.*, 191, 1329–1333. <https://doi.org/10.1002/macp.1990.021910220>
- 71 Bekturov, E.A., Kudaibergenov, S.E., Khamzamalina, R.E., Frolova, V.A., Nurgaliev, D.E., Schulz, R.C., & Zöller, J. (1992). Phase behavior of block-polyampholytes based on poly(methacrylic acid)-block-poly(1-methyl-4-vinylpyridinium chloride) in aqueous salt solutions. *Makromol. Chem., Rapid Commun.*, 13, 225–229. <https://doi.org/10.1002/marc.1992.030130407>
- 72 Kudaibergenov, S.E., Frolova, V.A., Bekturov, E.A., & Rafikov, S.R. (1990). Interpolymer reactions with participation of blockpolyampholyte poly(1-methyl-4-vinylpyridinium chloride)-poly(methacrylic acid). *Proceedings of Academy of Sciences of USSR*, 311, 396–398.

- 73 Bekturov, E.A., Kudaibergenov, S.E., Frolova, V.A., Khamzamalina, R.E., Schulz, R.C., & Zoller, J. (1990). Conformational and complex formation ability of poly(methacrylic acid)-block-poly(1-methyl-4-vinylpyridinium chloride) in aqueous solution, *Makromol. Chem.*, *191*, 457–463.
- 74 Kabanov, V.A. (2005) Polyelectrolyte complexes in solution and in the condensed phase. *Uspekhi Khimii*, *74*, 5–23. [in Russian].
- 75 Chen, L., Honma, Y., Mizutani, T., Liaw, D.-J., Gong, J.P., & Osada, Y. (2000). Effect of polyelectrolyte complexation on the UCST of zwitterionic polymer. *Polymer*, *41*, 141–147. [https://doi.org/10.1016/S0032-3861\(99\)00161-5](https://doi.org/10.1016/S0032-3861(99)00161-5)
- 76 Nakahata, R., & Yusa, S. (2018). Preparation of water-soluble polyion complex (PIC) micelles covered with amphoteric random copolymer shells with pendant sulfonate and quaternary amino groups. *Polymers*, *10*(2), 205. <https://doi.org/10.3390/polym10020205>
- 77 Nakai, K., Ishihara, K., Kappl, M., Fujii, S., Nakamura, Y., & Yusa, S. (2017). Polyion complex vesicles with solvated phosphobetaine shells formed from oppositely charged diblock copolymers. *Polymers*, *9*, 49. <https://doi.org/10.3390/polym9020049>
- 78 Kossel, A. (1896). Über die basischen Stoffen des Zellkerns (The basic substances of the cell nucleus). *Z. Physiol. Chem.*, *22*, 178.
- 79 Bungenberg de Jong, H.G. (1934). Complex relationships in lyophilic colloidal systems. I. General introduction. *Recl. Trav. Chim. Pays-Bas*, *53*, 163–170. <https://doi.org/10.1002/recl.19340530207>
- 80 Bungenberg de Jong, H.G. & Kruyt, H.R. (1929). Coacervation (Partial miscibility in colloid systems). *Proc. KNAW*, *32*, 849–856.
- 81 Xia, J. Protein-polyelectrolyte complexes / J. Xia, P. Dubin, J. Bock, R. Davis, D.N. Schulz, C. Thies. — Berlin, Heidelberg: Macromolecular Complexes in Chemistry and Biology. Springer, 1994.
- 82 Cooper, C. L., Dubin, P. L., Kayitmazer, A. B., & Turksen, S. (2005). Polyelectrolyte–protein complexes. *Current Opinion in Colloid & Interface Science*, *10*(1-2), 52–78. <https://doi.org/10.1016/j.cocis.2005.05.007>
- 83 Kayitmazer, A.B., Seeman, D., Minsky, B.B., Dubin, P.L., & Xu, Y. (2013). Protein–polyelectrolyte interactions. *Soft Matter*, *9*(9), 2553. <https://doi.org/10.1039/c2sm27002a>
- 84 Gao, S., Holkar, A., & Srivastava, S. (2019). Protein–polyelectrolyte complexes and micellar assemblies. *Polymers*, *11*(7), 1097. <https://doi.org/10.3390/polym11071097>
- 85 Khutoryanskiy, V.V., Nurkeeva, Z.S., Mun, G.A., Rebenchuk, N.L., Ivaschenko, A.T., & Rosiak, J.M. (2002). Polycomplexes of bovine serum albumin with poly[2-methacryloyloxy) ethyl]trimethyl ammonium chloride. *Euras. Chem. Tech. J.*, *4*, 195–198. <https://doi.org/10.18321/ectj534>
- 86 Patrickios, C.S., Jang, C.J., Hertler, W.R. & Hatton, T.A. (1993). Protein interactions with acrylic polyampholytes, *Polym.Prepr.*, *34*(1), 954–955. <https://doi.org/10.1002/bit.260440903>
- 87 Viklund, C. & Irgum, K. (2000). Synthesis of porous zwitterionic sulfobetaine monoliths and characterization of their interaction with proteins, *Macromolecules*, *33*, 2539–2544. <https://doi.org/10.1021/ma991965>
- 88 Patrickios, C. S., Sharma, L. R., Armes, S. P., & Billingham, N. C. (1999). Precipitation of a water-soluble ABC triblock methacrylic polyampholyte: effects of time, pH, polymer concentration, salt type and concentration, and presence of a protein. *Langmuir*, *15*(5), 1613–1620. <https://doi.org/10.1021/la970662a>
- 89 Nath, S., Patrickios, C.S., & Hatton, T. A. (1995). Turbidimetric Titration Study of the Interaction of Proteins with Acrylic Polyampholytes. *Biotechnol.Prog.* *11*(1), 99–103. <https://doi.org/10.1021/bp00031a014>
- 90 Nath, S. (1995). Complexation behavior of proteins with polyelectrolytes and random acrylic polyampholytes using turbidimetric titration. *J.Chem.Tech.Biotech.*, *62*(3), 295–300. <https://doi.org/10.1002/jctb.280620313>
- 91 Patrickios, C.S., Hertler, W.R. & Hatton, T.A. (1994). Protein complexation with acrylic polyampholytes. *Biotechnol.Bioeng.*, *44*, 1031–1039. <https://doi.org/10.1002/bit.260440903>
- 92 Xu, W., Rudov, A. A., Schröder, R., Portnov, I. V., Richtering, W., Potemkin, I. I., & Pich, A. (2019). Distribution of ionizable groups in polyampholyte microgels controls interactions with captured proteins: from blockade and “levitation” to accelerated release. *Biomacromolecules*. *20* (4), 1578–1591. <https://doi.org/10.1021/acs.biomac.8b01775>
- 93 Gelissen, A.P.H., Scotti, A., Turnhoff S.K., Janssen C., Radulescu, A., Pich, A., Rudov, A.A., Potemkin, I.I., Richtering, W. An anionic shell shields a cationic core allowing for uptake and release of polyelectrolytes within core-shell responsive microgels. *Soft Matter*, 2018, vol. 14, p.4287. <https://doi.org/10.1039/C8SM00397A>
- 94 Gao, W., Liu, X.-L., Li, J.-Y., Lian, H., & Mao, L. (2019). One-pot preparation of zwitterionic sulfoalkylbetaine monolith for rapid and efficient separation of lysozyme from egg white. *Journal of Pharmaceutical and Biomedical Analysis*, *175*, 112761. <https://doi.org/10.1016/j.jpba.2019.07.009>
- 95 Shakhvorostov, A.V., & Kudaibergenov, S.E. (2021). Molecular imprinting of bovine serum albumin and lysozyme within the matrix of polyampholyte hydrogels based on acrylamide, sodium salt of 2-acrylamido-2-methyl-1-propanesulfonic acid and (3-acrylamidopropyl)trimethyl ammonium chloride. *Chemical Bulletin of Kazakh National University*, *100*(1), 4–11. <https://doi.org/https://doi.org/10.15328/cb1182>
- 96 US Patent 6383811. Polyampholytes for delivering polyions to a cell / Wolff J.A., Hagstrom J.E., Budker V.G., Trubetskoy V.S.
- 97 US Patent 2004/0162235 A1. Delivery of siRNA to cells using polyampholytes / Trubetskoy V.S., Rozema D.B., Mo-nahan S.D., Budker V.G., Hagstrom J.E., Wolf J.A.

- 98 Koseki, T., Kanto, R., Yonenuma, R., Nakabayashi, K., Furusawa, H., Yano, S., & Mori, H. (2020). Multi-stimuli-responsive chiral-achiral ampholytic block copolymers composed of poly(N-acryloyl amino acid) and poly(vinyl amine). *Reactive and Functional Polymers*, 104540. <https://doi.org/10.1016/j.reactfuncpolym.2020.104540>
- 99 Asayama, S., Nogawa, M., Takei, Y., Akaike, T., & Maruyama, A. (1998). Synthesis of novel polyampholyte comb-type copolymers consisting of a poly(L-lysine) backbone and hyaluronic acid side chains for a DNA carrier. *Bioconjugate Chemistry*, 9(4), 476–481. <https://doi.org/10.1021/bc970213m>
- 100 Kudaibergenov, S.E. (2020). Advances in synthetic polyampholytes for biotechnology and medicine. *Rev. J. Chem.*, 10(1–2), 12–39. <https://doi.org/10.1134/S2079978020010021>
- 101 Skorikova, Y.Y., Vikhoreva, G.A., Kalyuzhnaya, R.I., Zezin, A.B., Gal'braikh, L.S., & Kabanov, V. A. (1988). Polyelectrolyte complexes based on chitosan. *Polymer Science U.S.S.R.*, 30(1), 49–55. [https://doi.org/10.1016/0032-3950\(88\)90253-5](https://doi.org/10.1016/0032-3950(88)90253-5)
- 102 Elschner, T., & Heinze, T. (2014). A promising cellulose-based polyzwitterion with pH-sensitive charges. *Beilstein Journal of Organic Chemistry*, 10, 1549–1556. <https://doi.org/10.3762/bjoc.10.159>
- 103 Vranckx, C., Lambricht, L., Pr at, V., Cornu, O., Dupont-Gillain, C., & vander Straeten. A. (2022). Layer-by-layer nanoarchitectonics using protein–polyelectrolyte complexes toward a generalizable tool for protein surface immobilization. *Langmuir*, 38(18), 5579–5589. <https://doi.org/10.1021/acs.langmuir.2c00191>
- 104 Kokufuta, E., & Nishimura, H. (1991). Complexation of pepsin poly(ethylene glycol). *Polymer Bulletin*, 26, 277–282. <https://doi.org/10.1007/BF00587970>
- 105 Xia, J., Dubin, P.L., & Kokufuta E. (1993). Dynamic and electrophoretic light scattering of a water-soluble complex formed between pepsin and polyethylene glycol. *Macromolecules*, 26, 6688–6690. <https://doi.org/10.1021/ma00076a066>
- 106 Azegami, S., Tsuboi, A., Izumi, T., Hirata, M., Dubin, P.L., Wang, B., & Kokufuta E. (1999). Formation of an Intrapolymer Complex from Human Serum Albumin and Poly(ethylene glycol). *Langmuir*, 15, 940–947. <https://doi.org/10.1021/la9809269>
- 107 Matsunami, H., Fujita, C., Ogawa, K., & Kokufuta, E. (2007). Static light scattering study of complex formation between protein and neutral water-soluble polymer. *Colloids and Surfaces B: Biointerfaces*, 56(1–2), 149–154. <https://doi.org/10.1016/j.colsurfb.2006.10.01>
- 108 Gullapalli, R. P. (2010). Soft gelatin capsules (softgels). *Journal of Pharmaceutical Sciences*, 99(10), 4107–4148. <https://doi.org/10.1002/jps.22151>
- 109 Alipal, J., Mohd Pu'ad, N. A. S., Lee, T. C., Nayan, N.H., Sahari, N., Basri, H., Abdullah, H. Z. (2021). A review of gelatin: properties, sources, process, applications, and commercialisation. *Materials Today: Proceedings*, 42, 240–250. <https://doi.org/10.1016/j.matpr.2020.12.922>
- 110 Chang, C.-P., Leung, T.-K., Lin, S.-M., & Hsu, C.-C. (2006). Release properties on gelatin-gum arabic microcapsules containing camphor oil with added polystyrene. *Colloids and Surfaces B: Biointerfaces*, 50(2), 136–140. <https://doi.org/10.1016/j.colsurfb.2006.04.008>
- 111 Shaddel, R., Hesari, J., Azadmard-Damirchi, S., Hamishehkar, H., Fathi-Achachlouei, B., & Huang, Q. (2018). Use of gelatin and gum Arabic for encapsulation of black raspberry anthocyanins by complex coacervation. *International Journal of Biological Macromolecules*, 107, 1800–1810. <https://doi.org/10.1016/j.ijbiomac.2017.10.044>
- 112 de Oliveira, L.C., Barbosa, J.R., da Concei o Amaral Ribeiro, C., Mar al de Vasconcelos, M.A., de Aguiar, B.A., da Silva Pereira, J.V., Albuquerque, G.A., da Silva, F.N.L., Crizel, R.L., Campelo, P.H., & de F tima Henriques Louren o, L. (2019). Improvement of the characteristics of fish gelatin — gum arabic through the formation of the polyelectrolyte complex. *Carbohydrate Polymers*, 223, 115068. <https://doi.org/10.1016/j.carbpol.2019.115068>
- 113 Moustafine R.I. (1991). Development and studies of prolonged release dosage forms based on interpolymer complexes. PhD thesis, I.I. Sechenov Moscow Medical Academy, Moscow.
- 114 Al-Saadi, A., Yu, C.H., Khutoryanskiy, V.V., Shih, S.-J., Crossley, A., & Tsang, S.C. (2009). Layer-by-layer electrostatic entrapment of protein molecules on superparamagnetic nanoparticle: a new strategy to enhance adsorption capacity and maintain biological activity. *The Journal of Physical Chemistry C*, 113(34), 15260–15265. <https://doi.org/10.1021/jp903100j>
- 115 Lomova, M.V., Brichkina, A.I., Kiryukhin, M.V., Vasina, E.N., Pavlov, A.M., Gorin, D.A., Sukhorukov, G.B., Antipina, M.N. (2015). Multilayer Capsules of Bovine Serum Albumin and Tannic Acid for Controlled Release by Enzymatic Degradation. *ACS Appl. Mater. Interfaces*, 7, 11732–11740. <https://doi.org/10.1021/acsami.5b03263>
- 116 Wang, Y.-F., Gao, J.Y., & Dubin, P.L. (1996). Protein separation via polyelectrolyte coacervation: selectivity and efficiency. *Biotechnol. Prog.*, 12, 356–362. <https://doi.org/10.1021/bp960013+>
- 117 Thiele, M.J., Davari, M.D., K nig, M., Hofmann, I., Junker, N.O., Garakani, T.M., Vojcic, L., Fitter, J., Schwaneberg, U. (2018). Enzyme–polyelectrolyte complexes boost the catalytic performance of enzymes. *ACS Catal.*, 8, 10876–10887. <https://doi.org/10.1021/acscatal.8b02935>

Е.А. Бектұров, Р.И. Мұстафин, С.Е. Құдайбергенов, В.В. Хуторянский
**Жасанды, табиғи және жартылай табиғи полиамфолиттердің
интерполимерлі кешендері: Шолу**

Бұл шолу жасанды, табиғи және жартылай табиғи полиамфолиттерге, олардың басқа полиэлектролиттермен және иондық емес полимерлермен кешен түзу қабілетіне арналған. Полиамфолиттердің анықтамасы мен классификациясы беріліп, олардың физика-химиялық қасиеттеріне қысқаша шолу жасалған. Амин қышқылдарынан алынған ішкі ретсіз ақуыздар мен жартылай табиғи полиамфолиттердің конформациялық және фазалық сипаттамалары берілген. Шолудың негізгі бөлімі полиамфолиттері бар полимерлі кешендердің түзілуіне арналған. Осы саладағы зерттеулердің көпшілігі қарама-қарсы зарядталған полиэлектролиттері бар полиамфолиттердің полиэлектролиттік кешендерімен ұсынылған; алайда, әдебиеттерде сутегі байланыстарымен тұрақтанған комплекстердің түзілуі туралы мәліметтер де бар. Бұл жағдайда кешендер түзілу табиғаты көбінесе ерітіндінің рН-мен полиамфолиттердің изоэлектрлік нүктесімен анықталады. Полиамфолиттер мен басқа полимерлер арасындағы кешендердің түзілуі коллоидтық дисперсиялардың (нано- және микробөлшектердің) түзілуіне, сұйық-сұйық типі бойынша фазаның бөлінуіне (кешенді коацервация деп аталады), толық ерітін кешендердің, сондай-ақ физикалық тігілген гельдердің пайда болуына әкелуі мүмкін. Бұл саладағы зерттеулердің едәуір бөлігі ақуыздар түзетін кешендерге арналған. Полиамфолиттердің интерполимерлі кешендерін биотехнологияда, медицинада, инкапсуляция технологиясында, әртүрлі қоспаларды бөлу ғылымында, биокатализде, тамақ ғылымында және фармацевтикада қолданылуы талқыланған.

Кілт сөздер: полиамфолиттер, полипептидтер, ішкі ретсіз белоктар (ІРБ), ішкі-макромолекулалар аралық кешендер (ішкі-МАК), макромолекулалық аралық кешендер (МАК), интерполиэлектролиттік кешендер, дәрілік заттарды жеткізу, кешенді коацервация, желатин.

Е.А. Бектұров, Р.И. Мұстафин, С.Е. Құдайбергенов, В.В. Хуторянский
**Интерполимерные комплексы синтетических,
природных и полуприродных полиамфолитов
Обзор**

Данный обзор посвящен синтетическим, природным и полуприродным полиамфолитам и их способности к образованию комплексов с другими полиэлектролитами и неионными полимерами. Даны определение и классификация полиамфолитов, приведен краткий обзор их физико-химических свойств. Описано конформационное и фазовое поведение внутренне разупорядоченных белков и полуприродных полиамфолитов, полученных из аминокислот. Основная часть этого обзора посвящена образованию полимерных комплексов с полиамфолитами. Большинство исследований в этой области представлено полиэлектролитными комплексами полиамфолитов с противоположно заряженными полиэлектролитами; однако в литературе имеются и сведения об образовании комплексов, стабилизированных водородными связями. Природа комплексообразования в данном случае часто определяется рН раствора, а также изоэлектрической точкой полиамфолитов. Комплексообразование между полиамфолитами и другими полимерами может приводить к формированию коллоидных дисперсий (нано- и микрочастицы), фазовому разделению по типу жидкость–жидкость (называемому комплексной коацервацией), образованию полностью растворимых комплексов, а также физически сшитых гелей. Значительная часть исследований в этой области посвящена комплексам, образованным белками. Обсуждено применение интерполимерных комплексов полиамфолитов в биотехнологии, медицине, технологиях инкапсулирования, науке о разделении различных смесей, биокатализе, пищевой науке и фармацевтике.

Ключевые слова: полиамфолиты, полипептиды, внутренне разупорядоченные белки, внутримакромолекулярные комплексы, межмакромолекулярные комплексы, интерполиэлектролитные комплексы, доставка лекарств, комплексная коацервация, желатин.

Information about authors*

Bekturov, Esen Abikenovich — Full Professor, Doctor of Chemical Sciences, Academician of Kazakh National Academy of Sciences, Abai Kazakh National Pedagogical University, Dostyk ave., 13, 050010; Almaty, Kazakhstan; e-mail: ebekturov@mail.ru; <https://orcid.org/0000-0002-6198-4432>;

Moustafine, Rouslan Ibragimovich — Associate Professor, Candidate of Chemical Sciences, Institute of Pharmacy, Kazan State Medical University, Butlerova Street, 49, 420012, Kazan, Russia; e-mail: rouslan.moustafin@gmail.com; <https://orcid.org/0000-0002-0916-2853>;

Kudaibergenov, Sarkyt Elekenovich — Full Professor, Doctor of Chemical Sciences, Director of Institute of Polymer Materials and Technology, Atyrau-1, 3/1, 050019, Almaty, Kazakhstan; e-mail: skudai@mail.ru; <https://orcid.org/0000-0002-1166-7826>;

Khutoryanskiy, Vitaliy Victorovich (*corresponding author*) — Full Professor, Candidate of Chemical Sciences, University of Reading, RG6 6AB, Reading, UK; e-mail: v.khutoryanskiy@reading.ac.uk; <https://orcid.org/0000-0002-7221-2630>

*The author's name is presented in the order: *Last Name, First and Middle Names*

M.S. Sagyndikov^{1,2}, R.M. Kushekov², R.S. Seright³

¹Satbayev University, Almaty, Kazakhstan;

²KMG Engineering LLP, Aktau, Kazakhstan;

³New Mexico Institute of Mining and Technology, New Mexico, USA

(*Corresponding author's e-mail: Sagyndikov.marat.s@gmail.com)

Review of Important Aspects and Performances of Polymer Flooding versus ASP Flooding

Polymer flooding is a promising and effective chemical Enhanced Oil Recovery (cEOR) technology. Polymer flooding is especially cost-effective, whereas other chemical flooding methods, such as Alkaline Surfactant Polymer (ASP), are not profitable and cause serious on-site problems (scaling, uptime decrease, injectivity issue, hard-breaking emulsions). Recent papers in the literature mention ~30 field polymer floods. Most of them reported technical success. Although, polymer flooding has been applied ~60 years and it still requires further investigation to provide improvements. Thus, this paper describes important aspects and performances during polymer flooding based on a review of recent projects, combined with the Kalamkas field experience. A comprehensive literature review examines the applicability range in temperature, brine salinity, water source selection, oil properties, formation type, and permeability. Water source selection has an essential role during pilot/field project design and is one of the most responsible technical and economic success decisions. Polymer slug design has been extensively analyzed especially for the high viscosity oil fields; the selected oil/polymer viscosity ratio was usually much less than one. We placed significant emphasis on clarifying observed high polymer injectivities. We conducted feasibility studies of some reported ASP floods to clarify that this technology is not profitable at current oil prices. Also, we performed TAN analysis of three Kazakhstan oil fields for screening of ASP flood.

Keywords: polyacrylamide, polymer flood, chemical enhanced oil recovery (EOR), alkaline surfactant polymer (ASP), feasibility study.



Marat Sagyndikov heads Enhanced Oil Recovery service at the KMG Engineering LLP. His research interests include a special core analysis, reservoir modeling, and oil recovery improvement using polymers and gels. He has extensive experience in Polymer flood, dealing with all stages from R&D to engineering and field implementation. He holds a B.S. degree in Petroleum Engineering

from the China University of Petroleum and an M.S. degree in Reservoir Engineering from Heriot-Watt University. Furthermore, He is doing a PhD degree in Petroleum Engineering at Satbayev University.



Randall Seright heads the Reservoir Sweep Improvement group at the Petroleum Recovery Research Center of New Mexico Tech. His research focuses on developing methods to prevent fluid channeling through

reservoirs and to reduce excess water and gas production during oil recovery, especially using polymers and gels. He has extensive interest and experience in improving sweep efficiency during water flooding and chemical flooding. He holds a B.S. degree in Chemical Engineering from Montana State University (Bozeman) and a PhD degree in Chemical Engineering from the University of Wisconsin (Madison). He worked for Exxon Production Research Company for eight years before joining the PRRC. He is a life member of the Society of Petroleum Engineers. He has provided short courses on Polymer Flooding and Water Shutoff in 18 countries. He received the SPE/DOE IOR Pioneer award in 2008 for his work on using polymer and gels to improve oil recovery.



Ruslan Kushekov is an engineer specializing in Enhanced Oil Recovery techniques at KMG Engineering LLP. He holds a B.Sc degree in Oil and Gas Business from Kazakh-British Technical University and M.Sc degree in Petroleum Engineering from Nazarbayev University. He has defended a master's thesis on "Polyacrylamides adsorption in sandstone reservoirs" and has experience in maintenance and supervising Polymer Flooding projects in Kazakhstani oil-fields.

Content

List of abbreviations
Review Plan
Introduction
1 Polymer Flood Implemented Reservoir Conditions
2 Polymers and Injection Parameters
3 Chemical (ASP) flood risks and feasibility assessment
Conclusions & Observations
Acknowledgements
References

List of abbreviations

ASP: alkaline surfactant polymer
ATBS: Acrylamide-Tertiary-Butyl Sulfonate
bbl: barrels of oil
Ca²⁺: calcium
CO₂: carbon dioxide
cp: centiPoise
Da: Daltons
EOR: enhanced oil recovery
ESP: electrical submersible pumps
HEC: hydroxyethylcellulose
HPAM: hydrolyzed polyacrylamide
IFT: interfacial tension
kg: kilograms
km²: kilometers square
m: meters
m³/d: cubic meters per day
md: milliDarcy
mg KOH/g: milligrams of potassium hydroxide per gram of oil
Mg²⁺: magnesium
MW: molecular weight
N₂: nitrogen
NVP: N-Vinyl-Pyrrolidone
OOIP: original oil in place
PCP: progressing-cavity pumps
PF: polymer flooding
ppb: parts per billion
ppm: parts per million
PV: pore volume
RF: recovery factor
SP: surfactant polymer
STOIP: stock tank oil initially in place
TAN: total acid number
TDS: total dissolved salts

Review Plan

Inclusion and Exclusion Criteria: The present review is focused on polyacrylamides and biopolymers used in oil and gas industry as a displacement agent to enhance oil recovery from the reservoirs.

The review data mostly cover the technical papers and publications with the current polymer flooding experience. Thus, over the 50 papers were investigated to collect the main data from the polymer field projects. Most of them were taken from the leading oil and gas resource OnePetro. A lot of scientific journals from sources such as Scopus and Web of Science were also cited. The keywords used for the search were ‘chemical EOR’, ‘polymer flooding’, ‘polyacrylamides’, ‘polymer injectivity’, ‘chemical stability of polymers’, ‘thermal stability of polymers’, ‘polymer flooding field results’ etc. No statistical methods were used in this review.

Introduction

Only 3–5 % of global oil production can be attributed to enhanced oil recovery (EOR) [1]. This fraction is expected to grow, even for reservoirs with harsh conditions that do not allow for efficient oil production [2]. There are commonly several directions of EOR [3]: gas (CO₂, N₂, hydrocarbon, immiscible), thermal (steam, hot water, in-situ combustion, SAGD), chemical (polymer (P), surfactant polymer (SP), alkaline surfactant polymer (ASP) floods) and others (microbiological). Gas injection is used as an agent for a pressure maintenance system, and usually starts near the beginning of the field production (secondary recovery). Also, a central aspect is the availability of a gas source. For example, most EOR gas projects in the USA, Canada, and China are neighboring huge CO₂ reservoirs/fields [4, 5]. Some operators inject gas for utilization purposes and mask it as an EOR technique [6–8]. Thermal EOR is generally effectively applicable for heavy oil fields, where viscosity ranges from 100–10 000 cp or even higher. However, implementation of thermal methods is mainly limited by heat losses [9–11]. Heat losses can occur due to the initial reservoir condition (high thermal conductivity of the upper and/or lower impermeable layers, reservoir depth), development stage (high formation water saturation near injection wells), and infrastructure (well construction type, completion, tubing). Also another critical issue is the obtainability of the freshwater source. In contrast, chemical EOR does not have the limitations mentioned above. Hence it has been widely used in sandstone fields, especially at the late development stage. Furthermore, polymer flooding (PF) is often the most feasible chemical EOR technology. Especially, polymer flooding has prominence, where ASP/SP flooding is not profitable and causes serious on-site problems (scaling, uptime decrease, injectivity issue, hard-to-break emulsions) [12–15]. In addition, this paper describes the economic viability of ASP flooding based on some field case studies from the literature.

The principle of polymer flooding is to increase the viscosity of injected water and thereby develop a more favorable mobility ratio between displacing water and oil in place [16]. This approach reduces or avoids water fingering caused by geologic heterogeneities [17]. The favorable conditions for effective implementation of polymer flooding have been changed and improved by the augmented understanding of its mechanism over the last 60 years. The aim of this paper is to understand how the range of these conditions has changed and the current stage of development. The paper reviews some parameters such as oil viscosity, reservoir temperature, permeability, water ion composition, salinity, polymer concentrations, and injected volumes. Observations on required injection volumes have been described based on the Kalamkas oilfield experience. Water source selection has an essential role during pilot/field project design and is one of the most responsible technical and economic success decisions. Polymer slug design has been extensively analyzed, and it has been shown that achieving a unit oil-polymer viscosity ratio is not required, especially for high viscosity oil fields. Nevertheless, achieving a unit mobility ratio is desirable (to minimize viscous fingering), although it is not always practical because of injectivity constraints. Therefore, we placed significant emphasis on clarifying observed high polymer injectivities. Also, we performed a total acid number (TAN) analysis of three Kazakhstan oil fields for screening for ASP flood.

1 Polymer Flood Implemented Reservoir Conditions

Reservoir Depth, Temperature, and Salinity. Table 1 summarizes the main reservoir characteristics of many recent field projects. It can be seen that the majority of polymer flood projects are conducted in relatively shallow reservoirs with a depth of 1 600 m (except the Abu Dhabi case of 2 650 m). The reason is that shallow reservoirs have lower temperatures, which promotes polymer stability. Polymer degradation can be substantial at high temperatures (over 70 °C according to [18]). Thermal degradation of partially hydrolyzed polyacryl amides usually involves increased hydrolysis of HPAM amide groups, leading to precipitation with divalent cations (Ca²⁺, Mg²⁺). Incidentally, salinity and hardness often exhibit a linear relationship, which was obtained by analysis of several projects shown in Figure 1. Data were taken from fields such as West Koyot, Pelican Lake, Buracica, Bohai bay, Kalamkas, and others. Moreover, the interactions of hydrolyzed polymers with divalent cations lead to the reduction of polymer coil size. As a result, a decrease in solution viscosity or even polymer precipitation occurs [19, 20]. However, the inclusion of copolymers/monomers such as ATBS (Acrylamide-Tertiary-Butyl Sulfonate) and/or NVP (N-Vinyl-Pyrrolidone) enhances the thermal stability substantially [21–23] and allows polymers to be tolerant up to 120 °C. According to the table, many polymer flooding projects, especially in Kazakhstan, are conducted using monomer-modified polymers and show promising results even at high salinities [24–28].

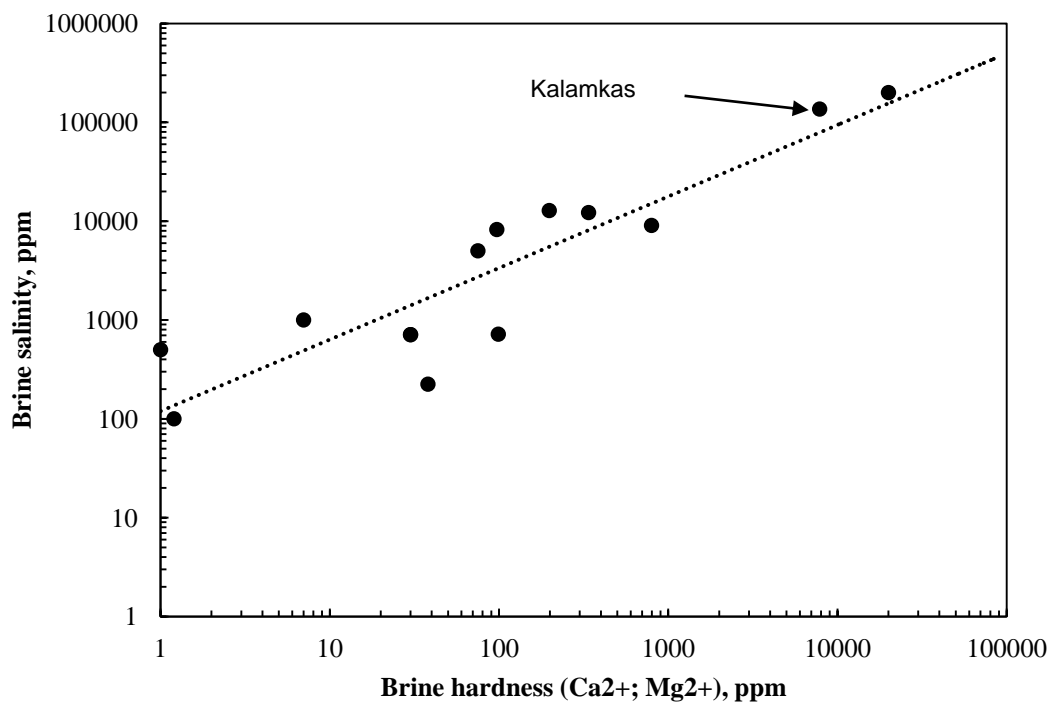


Figure 1. Relationship of water hardness to water salinity from different polymer flood projects

Formation Permeability. The permeability of reservoirs affects the molecular weight (MW) of polymers used. The weight and size of polymer molecules are critical since larger polymer molecules tend to plug in relatively small pore throats, reducing the permeability and solution concentration. This process is called mechanical entrapment, which negatively affects the propagation of polymer in the reservoir [2, 17, 29]. Theoretically, less retention is expected as permeability increases. Therefore, experience-supported recommendations for polymer selection depending on polymer weight have been made by Wang et al. [30]. The minimum permeability required for successful polymer flooding is in the range of 100–300 md, and MW should generally be not greater than 17–25 million Daltons. This statement is supported by Table 1, where the permeability is mostly greater than 100 md, while the average permeability is around 2 000 md.

Oil viscosity. Recent years in the history of polymer flooding (especially in Canada) have made it clear that achieving a favorable mobility ratio close to 1 or less is not always the primary goal, but to reduce it as much as possible. As many field experiences show, injecting the same or close viscosity to live oil may be unnecessary. The fact that end-point relative permeability to water is usually much less than that to oil is often used to justify why the injected polymer viscosity can be less than oil viscosity. This approach has been applied to Canadian fields, where oil viscosity reaches 15 000 cP, and a “favorable” mobility ratio cannot even be achieved. Nevertheless, the experience of oilfields such as Pelican Lake, Seal, Mooney, East Bodo, etc. shows that polymer flooding can effectively produce more oil even if the oil is heavy. Many of these fields experienced an unsuccessful thermal injection, which becomes non-profitable in deep and/or thin reservoirs and requires a lot of energy [31]. Besides that, the design of the injected polymer viscosity is commonly based on the optimum economic output (i.e., net present value) according to reservoir modeling and feasibility studies. Some of these concepts are presented in literature sources [28, 32, 33].

Table 1

Polymer flooding conditions in world projects

#	Field	Status	Depth, m	Formation thickness, m	Temperature, °C	Porosity, %	Permeability, md	Brine salinity, ppm	Live oil viscosity, cp
1	2	3	4	5	6	7	8	9	10
1	Marmul, Oman [34–36]	Field scale (Al Khalata)	550–675	–	46	25–30	100–2 000	4 600	90
2	Milne Point, Alaska, USA [37–39]	Pilot (J-Pad)	1 082	3–5.5	21.7	32	500–5 000	27 500	300

Continuation of Table 1

#	Field	Status	Depth, m	Formation thickness, m	Temperature, °C	Porosity, %	Permeability, md	Brine salinity, ppm	Live oil viscosity, cp
1	2	3	4	5	6	7	8	9	10
3	Captain (offshore), UK [40–42]	Pilot (SUCS)	914	<36.6	30.5	31	5 000	N/A	80
4	Dalia/Camelia (offshore), Angola [43, 44]	Pilot (DAL-710, 713, 729)	800–1 000	6–10	45–56	–	>1 000	117 700	1–11
5	Daqing, China [32, 45]	Field scale	1 000	6.1	45	25	1 100	3 000–7 000	9
6	Shengli, China [46]	Field scale	1 230	7.9–30.5	71	33.5	1 800	3 900	50–150
7	Shuanghe, China [47]	Pilot (Dong-Gudao)	1 460	25.2	72	20	422	4 356	7.8
8	Bohai bay, China [48]	Pilot (Layer II)	1 300–1 600	15–25	65	31	2 000	9 374	24–452
9	Tambaredjo, Suriname [49]	Pilot (Block-X)	375–425	13.7	36	33	3 000–10 000	10 000	300–1 100
10	East-Messoyahskoe, Russia [50]	Pilot (T1-sand)	800	15–50	16	28–30	50–5 000	N/A	111
11	Matzen, Austria [51–53]	Pilot (PK1-3)	1 150	20	50	20–30	500	25 000	19
12	Carmopolis, Brazil [54, 55]	Pilot (8 TH)	700	50	50	12–22	100	20 000	70–120
13	Canto do Amaro, Brazil [54, 55]	Pilot	500	8	55	22	204	500	7
14	Buracica, Brazil [54, 55]	Pilot (Pilot-1)	305	20–40	60	20	150–400	33 000	11
15	Diadema, Argentina [56, 57]	Pilot (Pilot-1)	900	4–12	50	30	500	16 000	100
16	El Corcobo, Argentina [58, 59]	Pilot	650	0.5–18	38	27–33	500–4 000	46 000	160–300
17	Bockstedt, Germany [60]	Pilot	1 200	15	54	24–30	2 000	186 000	11–29
18	East Bodo, Canada [9]	Pilot	794	3.2	27	30	1 000	25 000–29 000	600–2 000
19	Mooney, Canada [61, 62]	Pilot (11-14 pattern)	875–925	3–5	29	26	1 500	N/A	300–600
20	Seal, Canada [10, 62]	Pilot	600–650	8.5	20	27–33	3 000–5 800	N/A	3 000–7 000
21	Caen, Canada [10, 63]	Pilot	930	2.9	21	26.5	500–2 000	13 509	69.5–99
22	Wainwright, Canada [64]	Pilot (Suffield area)	650	–	–	30	300	72 000	100–200
23	Pelican Lake, Canada [11, 65]	Pilot (B pool)	300–450	1–9	12–17	28–32	300–5 000	N/A	1 650–15 000
24	Mangala, India [66–68]	Pilot (NE-5)	600	24–40	<62	21–28	5 000	7 140	9–22
25	Abu Dhabi [69]	Single well injection test	2 650	20	>93	20–30	10–1 000	>200 000	1
26	Nuraly	Pilot	1 550	10	81	19	368	57 000	0.91
27	East-Moldabek, Kazakhstan [25]	Pilot scale	250	10	25	35	1 500	140 000	400
28	Zaburunje, Kazakhstan [25]	Pilot (FM1)	875	10	38	30	230–1 000	145 000	20
29	Kalamkas, Kazakhstan [24, 27, 28]	Industrial pilot scale	746	10–20	39	28	946	136 211	16

Note – all 29 fields are sandstone reservoirs except the Abu Dhabi (carbonate-limestone) oil field.

Figure 2 shows a radar diagram of the major screening parameters for polymer flooding, showing the polymer flooding applicability range. Wide ranges are associated with most parameters, and the ranges have been expanded due to the growth in the understanding of the technology and its refinement during the past 60 years. However, temperature and depth of formation remain the weakest side of polymer flooding. Even if new monomer-modified co- and terpolymers are showing promising laboratory results [22, 23, 70–72], there

are no real field implementations where the formation temperature is greater than 109 °C [73]. Nevertheless, the radar chart provides an excellent visual representation of observations made previously in this work.

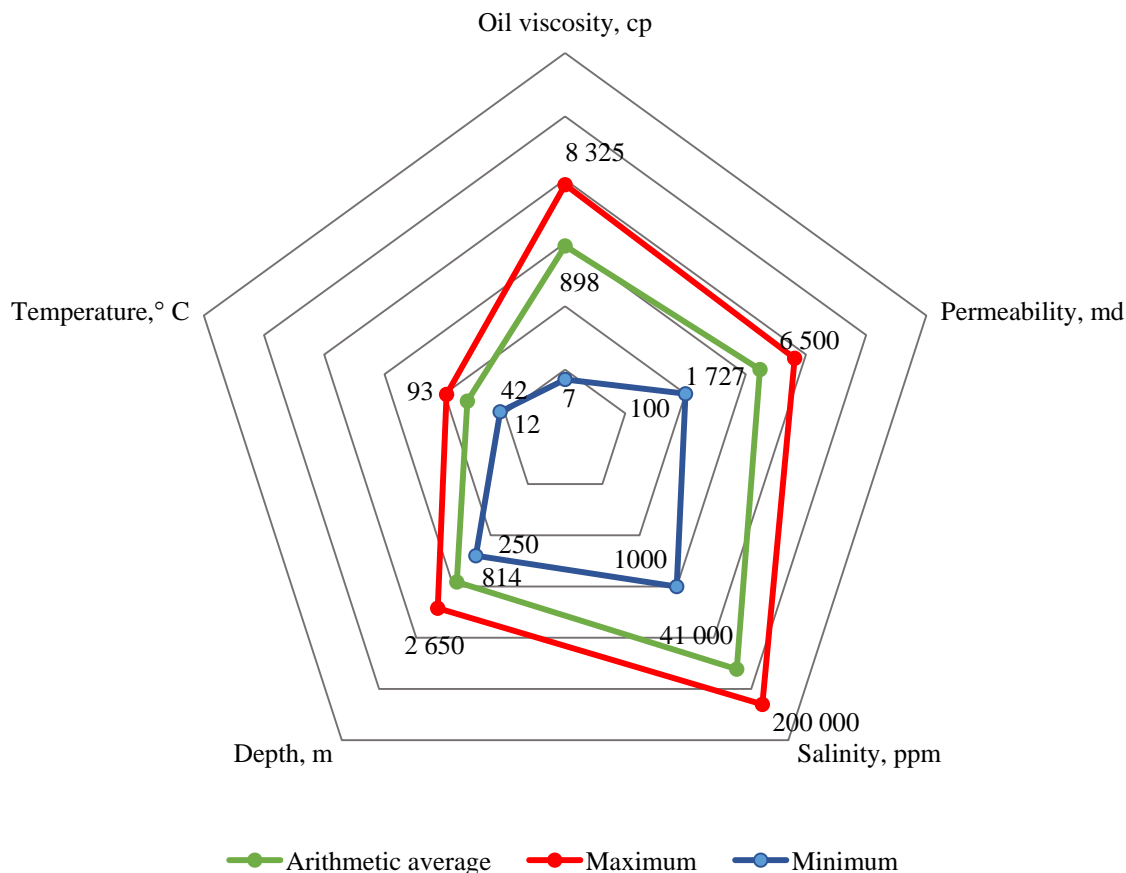


Figure 2. Main screening parameters for polymer flood according Table 1

2 Polymers and Injection Parameters

Polymers used in EOR. Table 2 summarizes the main injection parameters during the polymer flooding. According to many authors [2, 16, 17, 74], there are two main types of polymers in terms of their origin: synthetic polymers or polyacrylamides (PAM) used in paper production and biopolymers used in the food industry as a thickener. In early polymer flood applications, polyacrylamides were used much more frequently than biopolymers due to their efficient manufacturing environment and commercial availability. This tendency continues till these days because over 95 % of polymer floods are based on polyacrylamides. Also, it is essential to highlight that polyacrylamide is mainly used in its partially hydrolyzed form (HPAM). The main representative of biopolymers is xanthan gum (derivation of micro-organism *Xanthomonas campestris*) [75, 76], which is characterized by semi-rigid molecules, whereas the structure of polyacrylamide molecules is flexible long chains [77]. Understanding the structure of molecules and microscale studies reveals each polymer type’s key features. Thus, the primary polymer parameters, such as stability to temperature, high water salinity, mechanical degradation, biodegradation, dissolvability, viscosifying characteristics, adsorption to the rock surface, etc., are noted.

There are many laboratory and simulation studies [78–81] that confirm HPAM benefits in viscosifying characteristics, biodegradation, and injectivity over biopolymers. Alagic et al. [80] states that biopolymers are often sensitive to biodegradation, and it is important to protect them against potential microbial degradation. On the other hand, Al-Murayri et al. [82] indicated that biopolymers are more stable in the presence of oxygen and H₂S in any concentration, while high concentrations limit stability for HPAM. Seright and Skjevraak [83] suggest that HPAM degradation can be mitigated by keeping dissolved oxygen at an undetectable or acceptable level (as close to zero as practical). For this reason, modern polymer injection units pro-

vide nitrogen blanketing in the polymer preparation system to prevent air contact with the solution [26]. Specialized equipment for HPAM solutions was also mentioned in many works [37, 44, 84]. For example, Abbas et al. [84] argue that specialized equipment is essential in the field conditions to overcome problems with dissolving HPAMs (e.g. fish-eyes and gels). In contrast, such dissolution problems are not observed for hydroxyethylcellulose (HEC) biopolymers. Seright et al. [85] confirmed that xanthan solution is more resistant to mechanical degradation showing pseudoplastic behaviour during coreflooding experiments. In addition, synthetic HPAMs lack thermal and brine hardness stability, as will be discussed below. However, the main conclusion for the polymer's limitations is made by Ryles [18] who observed that the main challenge lies with high temperature rather than high salinity. Despite these disadvantages, HPAM is still the most widely used polymer in the world. An internet search suggests that $\sim 4 \times 10^9$ lbs of HPAM/PAM is produced each year, whereas only $\sim 4 \times 10^7$ lbs of xanthan is produced. Thus, HPAM production (and availability) is roughly 100 times greater than xanthan (the most extensively produced biopolymer). The price of xanthan (per weight) is 3–6 times greater than that of HPAM. This information is from a combination of internet and confidential sources.

A major factor that aids the application of polymer flooding is the current price for large HPAM purchases ($\sim \$2$ – $2.5/\text{kg}$) is actually less than that in 1980 ($\sim \$4$ – $5/\text{kg}$). This fact is remarkable because the Consumer Price Index in the USA (the average cost of goods and services) has more than tripled since 1980. Much of the credit for keeping HPAM prices must go to the HPAM manufacturers. However, some credit must also be given to several large-scale polymer floods (Daqing, Mangala, Pelican Lake) that played a significant role in providing the market and promoting low-cost polymers. Interestingly, the primary justification (used by big oil companies) for eliminating EOR in 1986 was that the “cost of chemicals would always rise in direct proportion to the price of oil”. The reality of HPAM price history emphasizes that technical and economic advances can upend conventional wisdom at a particular time.

Polymer Injection Design. A literature review reveals that polymer concentrations were in a wide range of 300–2 750 ppm and, on average, was 1 570 ppm, as shown in Fig. 3. Furthermore, the viscosity range was 3–300 cp and in average was 41 cp. Only a minority of field projects used polymer viscosity higher than 40 cp. On the other hand, some projects used relatively low polymer concentrations and achieved considerable viscosity because low-salinity (or fresh) water was used [86–88] (#26 line in Table 2). The selection of the process water source is paramount and should satisfy the following concepts: 1) compatibility with reservoir rock & fluids (no clay swelling/migration) should occur; 2) low cost and existing infrastructure; 3) high potential production capacity; 4) salinity (especially divalent cations) as lower as practical; 5) chemical stability; 6) dissolved iron, oxygen, TDS, oil contents as low as possible (absence is an ideal case); 7) if dissolved iron exists in the process water dissolved oxygen level should be controlled as low as possible (at a maximum <200 ppb based on [83] and <46 ppb based [89]).

Polymer Injectivity. Injectivity issues are important and of high current interest in polymer flooding technology. Besides creating a high-pressure displacement front *in-situ*, providing a sufficient injection rate is also essential. Moreover, in unfractured vertical injection wells, simple Darcy-law calculations reveal that polymer injectivity relative to water should be reduced by at least 80% [85]. In contrast, most field projects summarized in Table 2 reported relatively high polymer injectivity. Furthermore, the Kalamkas field case [24] demonstrated that polymer injectivity was roughly 4 times greater than water injectivity. Previous work has shown that the viscoelastic (or shear-thickening) behavior of HPAM polymers occurs at high fluxes, and as a consequence induces a fracture to form and extend in the well [90]. The presence of fractures during the polymer flood is consistent with the fact that most of the worldwide polymer flood projects inject into vertical wells above the formation parting pressure [33, 85, 87, 91–93]. In contrast, if fractures or fracture-like features are not present during polymer injection, achieving a favorable economical injection rate and acceptable voidage replacement ratio (e.g., the same as during a waterflood) are not practical. Also, Sagyndikov et al. [27] have demonstrated that these induced fractures reduce polymer mechanical degradation to a level that mitigates this degradation concern in a field setting.

Thomas et al. [94] have investigated injectivity prediction difficulties by reviewing some polymer field projects. The authors conclude that improving injectivity prediction is needed as pessimistic predictions are often obtained and can lead to the evaluation of polymer volumes that can be injected. The paper suggests further investigations using simulation processes, especially in reconsidering reservoir properties such as near-wellbore fractures and modeling polymer rheology and its features. Table 2 represents a modified summary of the polymer projects injectivity data presented by Thomas et al. [94].

Polymer formulation and injectivity of PF projects

#	Field	Polymer type	Mw, million Da	Polymer concentration, ppm	Polymer viscosity, cP	Porcess water salinity, ppm	Injection rate, m ³ /d	Injectivity issues
1	2	3	4	5	6	7	8	9
1	Marmul, Oman	HPAM	18–20	–	15	4 500	250–750*	No (fractures)
2	Milne Point, Alaska, USA	HPAM	N/A	1 600–1 800	45	2 500	350 and 95*	Initially no (decreased after 7 months)
3	Captain (offshore), UK	HPAM	18	~2 000	20	–	4 710 then 2 041*	No
4	Dalia/Camelia (offshore), Angola	HPAM	12–16	900	2.9	25 000–52 000	2 385*	No
5	Daqing, China	HPAM	N/A	2 000–2 500	40–300	700	0.14–0.2 PV/yr**	Mostly no (hydraulic fracturing applied if needed)
6	Shengli, China	HPAM	17	2 000	25–35	3 900	–	–
7	Shuanghe, China	HPAM (S625+S525)	N/A	1 090	93 at 3 rpm	fresh water	–	–
8	Bohai bay, China	Associative polymer	20	1 750	77.6–131	–	–	–
9	Tambaredjo, Suriname	HPAM Flopaam 3630S	N/A	<2 500	45 then 125	500	150–450*	No (fractures)
10	East-Messoyakhskoe, Russia	HPAM	20	1 830	30 at 7.34 s–1 80 at res. cond.	–	150*	No
11	Matzen, Austria	HPAM Flopaam 3630S	5–10	800	1.6–4.6 at res. cond.	23 000	400*	No (fractures)
12	Carmopolis, Brazil	HPAM	5–10	1 000	30	500	165*	No
13	Canto do Amaro, Brazil	HPAM	5–10	750	10	–	200–300**	No
14	Buracica, Brazil	HPAM	20	500	40	100	60–120**	No
15	Diadema, Argentina	HPAM Flopaam 3630S	N/A	1 500–3 000	70	16 000	1 000**	No
16	El Corcobo, Argentina	HPAM	N/A	500	20–25	1 044	1 000**	No
17	Bockstedt, Germany	Biopolymer Schizophyllan	18–20	300	25	–	135**	No (after reperforation and acidizing)
18	East Bodo, Canada	HPAM	20–25	1 500	50–60	–	200*	No (horizontal wells)
19	Mooney, Canada	HPAM	20	1 500	20–30	–	–	No (horizontal wells)
20	Seal, Canada	HPAM Flopaam 3630S	20	1 000–1 500	25–45	2 500–11 000	–	No (horizontal wells)
21	Caen, Canada	HPAM Flopaam 3630S	N/A	1 300	32	15 287	800*	No

Continuation of Table 2

#	Field	Polymer type	Mw, million Da	Polymer concentration, ppm	Polymer viscosity, cP	Porcess water salinity, ppm	Injection rate, m ³ /d	Injectivity issues
1	2	3	4	5	6	7	8	9
22	Wainwright, Canada	HPAM	20	2 100–3 000	25	72 000	–	No (after installing booster pumps)
23	Pelican Lake, Canada (2006-...)	HPAM Flopaam 3630S	20	600–3 000	13–25	–	–	No
24	Mangala, India (2014-...)	HPAM Flopaam 3630S	18–20	2 500–3 000	15–20	5 400	~740*	No
25	Abu Dhabi	HPAM (ATBS)	N/A	500–2 400	1.2–5.5	>200 000	144*	No
26	Nuraly (2014-2019)	HPAM Flopaam 5115 VHM AL-777	14	500	6	1 300	80–220*	No
27	East-Moldabek, Kazakhstan (2019-...)	HPAM Flopaam 1630S	N/A	2 400	23	140 000	50*	No
28	Zaburunje, Kazakhstan (2014-...)	HPAM	N/A	1 950	15	135 000	740**	No
29	Kalamkas, Kazakhstan (2014-...)	HPAM R-1 and Superpushe r K129	14	2 000	24	98 722–108 914	300*	No (fractures)

Note: * — injection rate for 1 well; ** — full field injection rate.

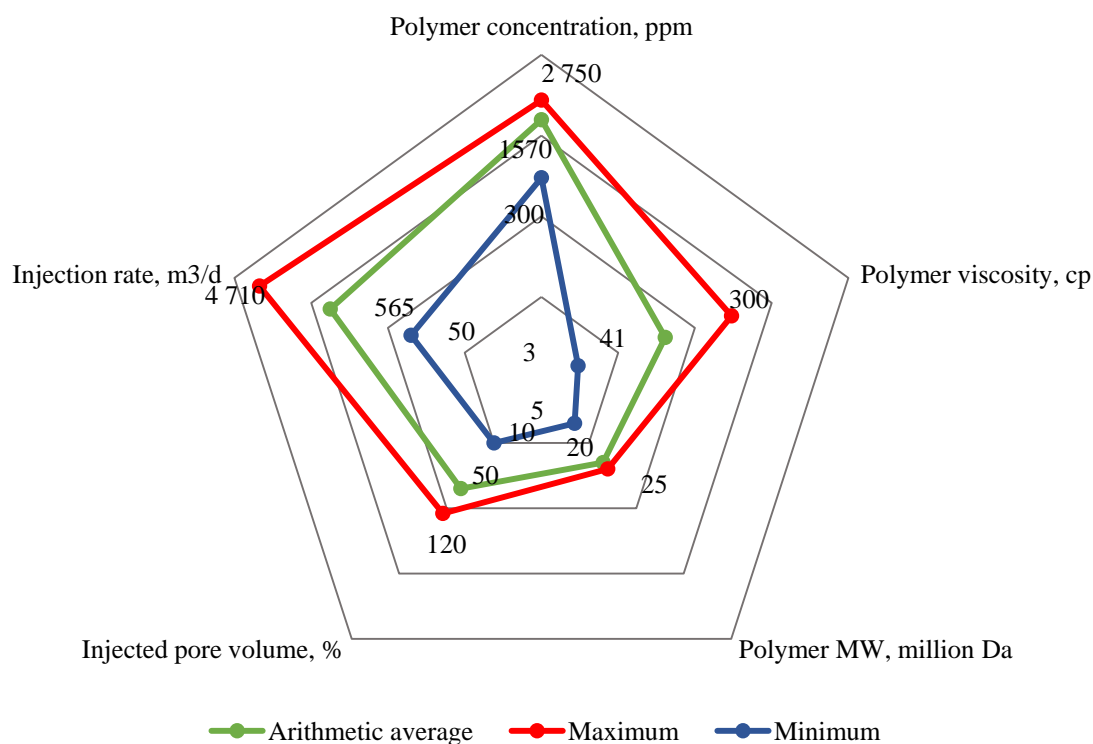


Figure 3. Polymer injection parameters for polymer flood according to Table 2

Polymer viscosity and slug design. Determining the desired viscosity of the polymer solution is a key objective of designing the polymer flooding project since it strictly affects project feasibility. A simple method to estimate desired viscosity has been developed by Sorbie and Seright [95]. As the authors say, the base-case method helps to determine the target polymer viscosity by simply multiplying waterflood end-point mobility ratio times the permeability contrast (highest permeability divided by the lowest permeability). Thus, the measurement of water and oil relative permeabilities is a key for the polymer flood design.

Table 3 summarizes the main reservoir development parameters (mobility ratio & permeability contrast) in the comparison of PF design (viscosity, slug size), implemented conditions (number of injectors & producer, watercut) and an achieved result (incremental recovery factor — RF).

As the polymer solution is a shear-thinning (non-Newtonian) agent, it is strongly recommended to consider its apparent viscosity (dependent on the shear rate). Typically, polymer viscosities are evaluated at a shear rate of 7.34 s^{-1} which has been accepted as the industry standard (corresponds to 6 rpm of UL adapter on Brookfield viscosimeter). In fact, typical shear rates in reservoir conditions (deep from well perforations) can be lower (depending on permeability, well spacing, and injection rate), so the apparent viscosity could be higher. In addition, reservoir temperature should be considered while measuring the polymer solution viscosity since the higher the temperature, the lower the viscosity is expected.

Sheng [96] and Seright [33] show that over the 60-year history of polymer flooding, the concentration and volume of polymer injection have increased over time. Whereas the slug volume in the 1960–1980 period was around 5–17 % of the pore volume, in the last 20 years the volume has reached 120% (Daqing field, PRC). The increase in volume is due to the absence of a residual resistance factor effect, i.e., the absence of a post-effect when polymer wells are converted to water injection. Testing on physical reservoir models has shown that the viscous fingering of the polymer bank has occurred in the high permeable zone, thereby not involving the low-permeable zone. This phenomenon has been clearly demonstrated by a field example from the Kalamkas field [27].

Horizontal wells for polymer flooding. Up to the mid 1990s, before the widespread use of horizontal wells, accepted screening criteria [97] advocated that 150 cp was the upper limit of oil viscosity for polymer flooding applicability. The introduction of horizontal wells has allowed polymer flood applications with much higher oil viscosities [11, 33, 87, 98]. In particular, horizontal wells considerably increase injectivity, reservoir access, and sweep efficiency, relative to vertical wells.

Table 3

Reservoir development parameters accepted for polymer flooding projects

#	Field	End Mobility Ratio	Perm. Contrast	Polymer viscosity, cP	Injected Volume, PV	I/P*	Water Cut before PF, %	Incremental RF, %
1	2	3	4	5	6	7	8	9
1	Marmul, Oman (2010-...)	~40	10:1	15	–	27/–	~90	~10 expected
2	Milne Point, Alaska, USA (2018-...)	>20	10:1	45	–	2/2 (horizontal)	~65	~10 expected
3	Captain (offshore), UK (2011-2013)	31	–	20	–	1/1 (horizontal)	85	~16
4	Dalia/Camelina (offshore), Angola (2010-...)	–	10:1	2.9	0.5 expected	3/– (deviated)	>40	3–7 expected
5	Daqing, China (2008-...)	9,4	4:1	40–300	0.4–1.2	–	95	15–18
6	Shengli, China (2008-2013)	–	–	25–35	>0.4	55/84	95	3.7
7	Shuanghe, China (1994-1999)	–	4:1	93 at 3 rpm	0.4	–	91	10.4
8	Bohai bay, China (2005-...)	–	4:1	77.6–131	0.31	10/35	>80	7.1
9	Tambaredjo, Suriname (2008-2015)	–	12:1	45 then 125	0.65	3/9	80	11
10	East-Messoyakhskoe, Russia (2017-2019)	30	–	30 at 7.34 s^{-1} 80 at res. cond.	0.1	2/4 (horizontal)	>90	–
11	Matzen, Austria (2011-...)	–	–	1.6–4.6 at res. cond.	–	2/6	~90	~10 expected

Continuation of Table 3

#	Field	End Mobility Ratio	Perm. Contrast	Polymer viscosity, cP	Injected Volume, PV	I/P*	Water Cut before PF, %	Incremental RF, %
1	2	3	4	5	6	7	8	9
12	Carmopolis, Brazil (1997-2003)	12	–	30	0.1	4/21	10	–
13	Canto do Amaro, Brazil (2001-2008)	2–5	–	10	0.16	2/6	6	–
14	Buracica, Brazil (1999-2003)	3	–	40	0.73	2/7	8	–
15	Diadema, Argentina (2007-...)	80	9:1	70	0.8	5/19	96	6–8 expected
16	El Corcobo, Argentina (2012-...)	–	–	20–25	–	6/22	~85	6–10 expected
17	Bockstedt, Germany (2013-...)	–	3:1	25	–	–/4	>90	–
18	East Bodo, Canada (2006-...)	42	–	50–60	–	1/12	95	20 expected
19	Mooney, Canada (2008-2010)	–	–	20–30	–	2/3 (horizontal)	90	18
20	Seal, Canada (2010-...)	–	–	25–45	–	3/4 (horizontal)	~18	8.8
21	Caen, Canada (2010-...)	44–64	4:1	32	0.6	2/10 (horizontal)	96	7–12 expected
22	Wainwright, Canada (2009-...)	–	–	25	0.5	13/24	–	–
23	Pelican Lake, Canada (2006-...)	165	4:1	13–25	–	–	90	25 expected
24	Mangala, India (2014-...)	28	10:1	15–20	~0.7	86/–	77	23
25	Abu Dhabi (2021-2022)	1.8	10:1	5.5	N/A	1/–	N/A	N/A
26	Nuraly (2014-2019)	0.7	30	6	0.153	4/22	81	
27	East-Moldabek, Kazakhstan (2019-...)	–	–	30	0.035	2/17	~85	5.7–7.7
28	Zaburunje, Kazakhstan (2014-...)	–	–	19	0.17	4/63	~90	2.3
29	Kalamkas, Kazakhstan (2014-...)	7	4:1	24	0.075	2/23	~90	9 (expected)

3 Chemical (ASP) flood risks and feasibility assessment

The alkali/surfactant/polymer injection was first invented in 1983 by Krumrin and Falcone in the laboratory to achieve the synergetic effect of the chemicals. After 10 years, in 1993, the first field-scale implementation was conducted in the West Kiehl Field, Wyoming, USA, reported by Clark et al. [99]. The pilot test was successful, leading to the production of 26 % of original oil in place (OOIP) in 2.5 years. Later, other countries such as Canada, India, and Russia implemented field pilot tests. Finally, the largest field-scale implementations were started in China in 2014. According to Wang et al. [100], the widespread use of polymers in Chinese fields provided solid foundations for ASP flooding. This point of view was also supported by laboratory experiments conducted by Aitkulov et al. [101], which indicated more enhanced oil recovery of ASP after polymer flooding rather than after waterflooding.

The synergetic effect of ASP flooding is based on mechanisms induced by each of three chemicals: polymers, which create a stable piston-like displacement front; surfactants, which decrease interfacial tension (IFT) between oil and water; and alkalis, which mitigate surfactant adsorption and create in-situ soaps to decrease IFT. These three mechanisms improve the ability of the oil to flow in porous media involving untouched zones of reservoir.

To better understand the effect of ASP on oil production growth, especially the mechanism underlying the surfactant-oil interaction it is necessary to examine the main studies on microemulsion types [3, 102,

103]. There are three types of microemulsions formed when oil and surfactant come into contact in the reservoir, based on Windsor's [104] terminology. Thus, Type II (-), Type III, and Type II (+) have been detected depending on brine salinity level. These Windsor types can be well described by ternary diagrams. Type II (-) means a two-phase environment at low salinities where only water and oil are presented. Then, it moves to the Type III microemulsion at medium salinity where three phases exist in equilibrium: water, oil, and microemulsion (middle phase). Type III is the transitional stage from Type II (-) to Type II (+) or vice versa, where Type II (+) also has two phases, but at high salinity: water and microemulsion. Type II (-) and Type II (+) can coexist in the Type III environment since Nelson and Pope [103] did not observe type-to-type behaviour in EOR processes. In general, Type III is the most favorable condition for effective oil displacement in porous media since the pure oil phase and lowest IFT are achieved. Based on this theory and these processes, the evaluation of ASP formulation (phase behaviour tests) is conducted to reach successful ASP flooding projects. If the formulation fits reservoir conditions, over 20 % of incremental oil recovery can be accomplished, which is almost two times greater than polymer flooding.

Although ASP flooding seems promising in the laboratory as a tertiary recovery method, field experience has revealed several complicating features of the technology. Thus, it has been observed that the main problems while ASP flooding is related to operational arrays [12–15]. The scaling problem is the most common among ASP flood projects, and it creates the need to redesign surface facilities from ASP solution preparation units to production and processing units. Experience in China has shown that frequent pump failures have greatly shortened pump-checking time to tens of days [105]. Figure 4 represents some pictures of scaling accumulated on stators of progressing-cavity pumps (PCP) in the Daqing oilfield. ASP flooding in the Mangala field led to impairment of the artificial lifting system. As a result, jet pumps were accepted as suitable instead of electrical submersible pumps (ESP) [106]. The simple explanation for scale formation in the tubes is the significantly high pH level of the injected water, caused by the large amounts of alkali added [107]. Apart from reconsidering the artificial lift systems, it is also required to implement chemical techniques such as scale inhibitors and chemical-feeding systems [15], which certainly increase project operational costs.



Figure 4. Scaling PCP rotors in Daqing ASP flooding area [105]

Another complicating feature during production can be viscous hard-to-break emulsions, as was observed in several pilots in China. Guo et al. [15] reported that the maximum emulsion viscosity of the produced fluid reached 487 cp during strong alkali injection (NaOH). Some cases demonstrate great emulsion viscosities which are 10 times greater than injected ASP solution. The authors acknowledge that the phenomenon is not well understood, but the presence of emulsions and their problems remain a fact. The main associated problem is the loss of production. Therefore, potential emulsification issues should be envisaged preliminary as it was done in the Bhagyam field having additional demulsifier injection wells near producers [12]. Also, Finol et al. [13] have reported preliminary laboratory experiments on identifying cost-effective demulsifiers in the designing stage of the Al Khalata pilot test.

Feasibility study on ASP flooding projects. According to Dean et al. [108], the development of ASP formulations and their implementation in the field/pilot units has two main objectives: 1) academic applications aiming at a better understanding of the mechanism, and 2) practical applications pursuing economic benefits through the production of incremental oil. Based on a number of publications that are describing any ASP technology implementation at a pilot scale, it is observed that the authors refrain from providing the economic performance of any given project. This is the main reason for the difficulty in determining the real purpose of ASP projects. Moreover, some projects were evaluated without considering capital and/or operating expenditures, i.e., only the benefit from incremental oil was estimated, and the project's profitability was

not adequately assessed. Such cases can misrepresent the understanding of the economic feasibility of ASP flooding, which is critical due to its complexity and use of expensive chemicals.

This section focuses on the economic evaluation of ASP flooding projects conducted on Daqing (China) and Mangala (India) oilfields. It is worth noting that the economics of the projects have been evaluated based only on the data presented in the scientific articles of Gao et al. [109] and Pandey et al. [106]. Both projects were successful, providing additive oil recovery. Nevertheless, the economics behind them were not properly assessed. Therefore, the main question to answer is: does the extra oil produced by ASP flooding pay for itself?

Gao et al. [109] presented an ASP flooding project, which involved 16 injection and 25 production wells. Injection of the main ASP slug started in 2014 and by 2019 the accumulated oil increment was 0.647 million barrels which refers to 7.89% of the incremental recovery. Considering the size of the pilot area and the number of wells involved, the complications of water treatment and production that are common in ASP projects, it can be assumed that the project does not achieve economic benefit. In evidence, the simplified feasibility study considering only the costs of chemicals as the main part of operational expenditures is presented in this section. The consumption of chemicals has been pre-compiled based on the given injected pore volumes and the slug formulations, and chemical prices have been taken as industry average prices. Thus, the following assumptions over prices were accepted (Table 4):

Table 4

Chemical prices according to industry averages

Chemicals	USD/kg
Alkaline	0.65
Surfactant	7
Polymer	3.5

ASP project was held on the N3D block with an area of 0.49 km² and a pore volume of 1 798 200 m³, which is located on the East side of the Daqing oilfield. According to Guo et al. [15], the chemical formulations of ASP floods in China were analyzed. The authors presented data on 27 ASP flooding projects with slug concentrations. From the data, the average concentrations of each slug were identified and fitted to the injection volumes of the N3D block (Table 5). Combining all this available information and correct calculations makes it easy for us to imagine the costs of this project. It is estimated that around \$41 million was spent on chemicals only to provide such slug volumes (Table 6). The author states that the economic benefit of performed ASP project is \$32.35 million (calculated at \$50/bbl), which is about \$10 million more than the chemical cost. It is important to note that apart from the cost of chemicals, nothing else has been taken into account, i.e. the actual cost of the project could be times higher with capital and other operating costs caused by different challenges.

Table 5

Assumed design of Daqing ASP flooding [15; 109]

1 st year		2 nd -4 th years		5 th year		6 th year		Total injected
Pre-Slug (polymer)		ASP Main Slug		ASP Vice Slug		Post-Slug (polymer)		
PV	Concentration, %	PV	Concentration, %	PV	Concentration, %	PV	Concentration, %	PV
0,2	0.14	0.505	0.3%S + 1%A + + 0.18%P	0.21	0.1%S + 1.2%A + + 0.16%P	0.18	0.12	1.0924

A similar approach was applied to evaluate an Indian ASP experience performed in the Mangala oilfield in 2014 [106]. The critical reason for evaluating its economic efficiency is the involved well locations. According to the authors, the ASP pilot project was carried out on a 5-spot pattern block with 4 injection wells and 1 production well, and an area of 10 000 m². The main reason to investigate this case is the well locations that lead to injected volume loss 3/4. It suggests that the crucial part of injected volume abandons outside of the well grid. Therefore, the economic effect is questionable, as the cost of chemicals for effective sweeping increases by a factor of 4.

Table 6

Cost of chemicals used in Daqing ASP pilot

Slug consequence	Chemicals	Injected weight, tonnes	Cost for chemicals, USD	Cost for chemicals over the pilot period, USD
Pre-Slug (polymer)	A	0	0	1 762 236
	S	0	0	
	P	503.50	1 762 236	
ASP Main Slug	A	9 080.91	5 902 592	30 693 476
	S	2 724.27	19 069 911	
	P	1 634.56	5 720 973	
ASP Vice Slug	A	4 479.68	2 911 789	7 615 449
	S	373.31	2 613 144	
	P	597.29	2 090 515	
Post-Slug (polymer)	A	0	0	1 357 929
	S	0	0	
	P	387.98	1 357 929	
Total				41 429 089

As reported by Pandey et al. [110] at the design stage of the ASP pilot, the thickness of the pilot formation is 70 m with a net-to-gross of 40 %. Considering the area of 10 000 m² and average porosity, the volume of pores is 70 000 m³. Later, after a technically successful pilot, the slug formulations were presented in 2016 (Table 7).

Table 8 presents chemical cost estimation for each stage of ASP flooding at Mangala. Since the incremental oil reached 23 000 bbl, which the authors describe, the project will not be appropriate for returning investments spent even if the oil cost is 90 \$/bbl. It should be noted that there was polymer flooding at the same pilot area for 3 years before the ASP flooding. The polymer slugs were graded, and the pilot performed well generating incremental oil, referring to 10–15% of STOIP compared to waterflood [66]. Despite this fact, ASP flooding was technically justified, giving extra-incremental oil from the pilot area, but proved to be uneconomical.

Table 7

Chemical slug compositions prepared in Mangala ASP pilot [106]

ASP Main Slug		Polymer Drive-1		Polymer Drive-2		Chase Water Drive	
PV	Concentration, %	PV	Concentration, %	PV	Concentration, %	PV	Concentration, %
0.5	0.3%S+3%A+0.25%P	0.3	1.5%A+0.23%P	0.2	1%A+0.2%P	0.1	1%A

Table 8

Cost of chemicals used in Mangala ASP pilot

Slug consequence	Chemicals	Injected weight, tonnes	Cost for chemicals, USD	Cost for chemicals over the pilot period, USD
ASP Main Slug	A	1 050	682 500	1 638 000
	S	105	735 000	
	P	63	220 500	
Polymer Drive-1	A	315	204 750	373 800
	S	0	0	
	P	48.3	169 050	
Polymer Drive-2	A	140	91 000	189 000
	S	0	0	
	P	28	98 000	
Chase Water Drive	A	70	45 500	45 500
	S	0	0	
	P	0	0	
Total				2 246 300

ASP applicability studies on Kazakhstani fields. The previous section described the economic issues attributed to ASP flooding. Apart from this, the other critical property oil total acid number (TAN) for ASP applicability was studied. The high acidic constituents react with alkaline solutions to create in-situ surfactants [17]. Surfactants, for their part, obtain ultralow interfacial tension (IFT) between displacing agent and crude oil. Thus, several mechanisms are in place to enhance oil recovery. In the case of low TAN, alkalines may mitigate surfactant retention, which improves chemical consumption volumes.

In this regard, the TAN analysis of several Kazakhstan oilfields was carried out. The TAN analysis of the Mangistau (West Kazakhstan) oilfields, combined with actual ASP feasibility studies from other companies, argues that ASP is not a promising cEOR method for extending the life of brownfields (Table 9). According to Guo et al. [15], in 1987 the threshold value of the acid number for the effective reaction was considered 0.20 mg KOH/g, but then this number was reduced by several times, which can be noted in Table 9. Nevertheless, underestimating the importance of oil TAN, using highly reactive surfactants, is too risky because of production issues, such as scaling and hard-to-break emulsions. These problems, coupled with the expensive surfactant cost, only complicate and worsen the economics of projects.

Table 9

TAN analysis of Mangistau oilfields in comparison

Oilfields	Oil TAN, mg KOH/g	ASP flood conducted	Incremental RF, %	Complications
Bhagyam, India [12]	2.00	Yes	20	Emulsion, scaling, corrosion
Al Khalata, Oman [13]	0.78	Yes	–	Emulsion, scaling
Karazhanbas, Kazakhstan	0.251	No	–	–
Kalamkas, Kazakhstan	0.132	No	–	–
Uzen, Kazakhstan	0.048	No	–	–
West Salym, Russia [14]	0.040	Yes	16	Scaling
Daqing, China [15]	0.020	Yes	>20	Emulsion, scaling, repairment of surface equipment

Conclusions & Observations

The goal of this paper was to review important aspects and performances during polymer flooding. These aspects include reservoir conditions for effective implementation, polymer injection, and reservoir development parameters. The growing large-scale application polymer flooding demonstrates that it is the most feasible chemical EOR technology. In contrast, ASP/SP flood is not profitable and causes severe on-site problems. The primary novel finding from this review and analysis of field projects is to cast doubt on the economic feasibility of ASP flooding — especially in Kazakhstan. This work also provides a perspective on the TAN (total acid number) for Kazakhstan oilfields, especially for applicability to ASP flooding. Many insights into applicability of polymer flooding were also noted. In particular, the fact that HPAM prices are lower now than they were 40 years ago has greatly aided the ability for polymer flooding to be applied on a large scale today. The development of horizontal wells has greatly enhanced polymer injectivity and allowed the upper limit of oil viscosity for polymer flooding to be increased from ~150 cp to over 3000 cp. Controlled injection above the formation parting pressure has also played a major role in this regard. Until recently, commercially available EOR polymers were not sufficiently stable in reservoirs with temperatures exceeding ~70 °C. However, the recent availability of an ATBS polymer has the potential to allow feasible polymer flooding in reservoirs at temperatures up to 120 °C. A major difference from waterflooding is that the dissolved oxygen level as close to zero as practical—certainly less than 200 parts per billion. Above 60 °C, dissolved oxygen levels must be much closer to zero. In theory, polymer flooding can be applied in formations with any water salinity. However, practical considerations favor using the least saline water that is available. Field experience, as well as laboratory and theory, consistently reveal that the polymer bank size should be as large as practical (typically ~1 pore volume). Once injection is switched from polymer back to water injection, water cuts will quickly rise to high values. The vast majority of polymer floods have been applied in moderate-to-high permeability reservoirs (>100 md). This fact is due first to the need for high polymer injectivity and second because high-MW polymers exhibit difficulty in penetrating into less-permeability rock.

Acknowledgments

The authors express their gratitude to LLP “KMG Engineering” for providing the opportunity to publish the results of this study. Thanks also to Serik Sagyndikov for greatly appreciated guidance and help.

References

- 1 Alvarado, V., & Manrique, E. (2010). *Enhanced Oil Recovery: Field Planning and Development Strategies* (1st ed.). Gulf Professional Publishing.
- 2 Sheng, J. (2010). *Modern Chemical Enhanced Oil Recovery: Theory and Practice* (1st ed.). Gulf Professional Publishing.
- 3 Lake, L. W. (1989). *Enhanced Oil Recovery*. Englewood Cliffs, New Jersey: Prentice-Hall Inc.
- 4 Kirkpatrick, R., Flanders, W., & DePauw, R. (1985). *Performance of the Twofreds CO₂ Injection Project*. *SPE Annual Technical Conference and Exhibition*, Las Vegas, Nevada, USA. SPE-14439-MS. <https://doi.org/10.2118/14439-MS>
- 5 Pooladi-Darvish, M., Hong, H., Theys, S. O. P., Stocker, R., Bachu, S., & Dashtgard, S. (2008). CO₂ Injection for Enhanced Gas Recovery and Geological Storage of CO₂ in the Long Coulee Glauconite F Pool, Alberta. *SPE Annual Technical Conference and Exhibition*, Denver, Colorado, USA. SPE-115789-MS. <https://doi.org/10.2118/115789-MS>.
- 6 Abou-Sayed, A. S., Zaki, K. S., & Sarfare, M. D. (2005). An Assessment of Engineering, Economical and Environmental Drivers of Sour Gas Management by Injection. *SPE International Improved Oil Recovery Conference in Asia Pacific*, Kuala Lumpur, Malaysia. SPE-97628-MS. <https://doi.org/10.2118/97628-MS>.
- 7 Wilson, A. (2015). Tengiz Field Sector Model for IOR/EOR Process Evaluation. *Journal of Petroleum Technology* 67(01): 81–83. SPE-0115-0081-JPT. <https://doi.org/10.2118/0115-0081-jpt>.
- 8 Hao, H., Hou, J., Zhao, F., Huang, H., Wang, Z., & Liu, H. (2019). Feasibility Study of Gas-EOR Using CO₂ and N₂ Mixture in a Heavy Oil Reservoir: Experiments and Pilot Test. *Carbon Management Technology Conference*, Houston, Texas, USA. CMTC-552521-MS. <https://doi.org/10.7122/cmte-552521-MS>.
- 9 Wassmuth, F., Green, K., Arnold, W., & Cameron, N. (2009). Polymer Flood Application to Improve Heavy Oil Recovery at East Bodo. *Journal of Canadian Petroleum Technology* 48(02): 55–61. PETSOC-09-02-55. <https://doi.org/10.2118/09-02-55>.
- 10 Delamaide, E., Bazin, B., Rousseau, D., & Degre, G. (2014a). Chemical EOR for Heavy Oil: The Canadian Experience. *SPE EOR Conference at Oil and Gas West Asia*, Muscat, Oman. SPE-169715-MS. <https://doi.org/10.2118/169715-MS>.
- 11 Delamaide, E., Zaitoun, A., Renard, G., & Tabary, R. (2014b). Pelican Lake Field: First Successful Application of Polymer Flooding In a Heavy-Oil Reservoir. *SPE Reservoir Evaluation & Engineering* 17(03): 340–354. SPE-165234-PA. <https://doi.org/10.2118/165234-PA>.
- 12 Jain, S., Prasad, D., Pandey, A., Koduru, N., & Raj, R. (2020). Bhagyam ASP Pilot: Successful Formulation Development to Pilot Design and Planning. *SPE Improved Oil Recovery Conference*, Virtual. SPE-200408-MS. <https://doi.org/10.2118/200408-MS>.
- 13 Finol, J., Al-Harthi, S., Jaspers, H., Batrani, A., Al-Hadhrani, H., van Wunnik, J., Stoll, M., Faber, R., & de Kruijf, A. (2012). Alkali-Surfactant-Polymer Flooding Pilot Test in Southern Oman. *SPE EOR Conference at Oil and Gas West Asia*, Muscat, Oman. SPE-155403-MS. <https://doi.org/10.2118/155403-MS>.
- 14 Volokitin, Y., Shuster, M., Karpan, V., Mikhaylenko, E., Koltsov, I., Rakitin, A., Tkachev, I., & Salym, M. P. (2017). West Salym ASP Pilot: Surveillance Results and Operational Challenges. *SPE Russian Petroleum Technology Conference*, Moscow, Russia. SPE-187838-MS. <https://doi.org/10.2118/187838-MS>.
- 15 Guo, H., Li, Y., Li, Y., Kong, D., Li, B., & Wang, F. (2017). Lessons Learned From ASP Flooding Tests in China. *SPE Reservoir Characterisation and Simulation Conference and Exhibition*, Abu Dhabi, UAE. SPE-186036-MS. <https://doi.org/10.2118/186036-MS>.
- 16 Sorbie, K. S. (1991). *Polymer-Improved Oil Recovery* (1991st ed.). Springer.
- 17 Willhite, P., & Green, D. (2020). *Enhanced Oil Recovery*, Second Edition. Society of Petroleum Engineers.
- 18 Ryles, R.G. (1988). Chemical Stability Limits of Water-Soluble Polymers Used in Oil Recovery Processes. *SPE Reservoir Engineering* 3(01): 23–34. SPE-13585-PA. <https://doi.org/10.2118/13585-PA>.
- 19 Moradi-Araghi, A., & Doe, P.H. (1987). Hydrolysis and Precipitation of Polyacrylamides in Hard Brines at Elevated Temperatures. *SPE Reservoir Engineering* 2(02): 189–198. SPE-13033-PA. <https://doi.org/10.2118/13033-PA>.
- 20 Levitt, D., & Pope, G. A. (2008). Selection and Screening of Polymers for Enhanced-Oil Recovery. *SPE Symposium on Improved Oil Recovery*, Tulsa, Oklahoma, USA. SPE-113845-MS. <https://doi.org/10.2118/113845-MS>.
- 21 Diab, W.N., & Al-Shalabi, E.W. (2019). Recent Developments in Polymer Flooding for Carbonate Reservoirs under Harsh Conditions. *Offshore Technology Conference Brasil*, Rio de Janeiro, Brazil. OTC-29739-MS. <https://doi.org/10.4043/29739-MS>.
- 22 Gaillard, N., Giovannetti, B., Leblanc, T., Thomas, A., Braun, O., & Favero, C. (2015). Selection of Customized Polymers to Enhance Oil Recovery from High Temperature Reservoirs. *SPE Latin American and Caribbean Petroleum Engineering Conference*, Quito, Ecuador. SPE-177073-MS. <https://doi.org/10.2118/177073-MS>.
- 23 Seright, R.S., Wavrik, K.E., Zhang, G., & AlSofi, A.M. (2021). Stability and Behavior in Carbonate Cores for New EOR Polymers at Elevated Temperatures in Hard Saline Brines. *SPE Reservoir Evaluation & Engineering* 24(1): 1–18. SPE-200324-PA. <https://doi.org/10.2118/200324-PA>.

- 24 Sagyndikov, M., Mukhambetov, B., Orynbasar, Y., Nurbulatov, A., & Aidarbayev, S. (2018). Evaluation of Polymer Flooding Efficiency at Brownfield Development Stage of Giant Kalamkas Oilfield, Western Kazakhstan. *SPE Annual Caspian Technical Conference and Exhibition*, Astana, Kazakhstan. SPE-192555-MS. <https://doi.org/10.2118/192555-MS>.
- 25 Ispanbetov, T. (2019). *Polymer flooding in Zaburunje and Moldabek fields*, Kazakhstan. Proceedings of the International scientific conference "Modern oil production methods for unconventional reservoirs", Atyrau, Kazakhstan (in Russian).
- 26 Sagyndikov, M.S., Salimgarayev, I.I., Ogay, E.K., Seright, R.S., & Kudaibergenov, S.E. (2022a). Assessing polyacrylamide solution chemical stability during a polymer flood in the Kalamkas field, Western Kazakhstan. *Bulletin of the University of Karaganda — Chemistry*, 105(1), 99–112. <https://doi.org/10.31489/2022Ch1/99-112>.
- 27 Sagyndikov, M., Seright, R., Kudaibergenov, S., & Ogay, E. (2022b). Field Demonstration of the Impact of Fractures on Hydrolyzed Polyacrylamide Injectivity, Propagation, and Degradation. *SPE Journal* 27(02): 999–1016. SPE-208611-PA. <https://doi.org/10.2118/208611-PA>.
- 28 Sagyndikov, M., Seright, R., & Tuyakov, N. (2022c). An Unconventional Approach to Model a Polymer Flood in the Kalamkas Oilfield. *SPE Improved Oil Recovery Conference*, Virtual. SPE-209355-MS. <https://doi.org/10.2118/209355-MS>.
- 29 Chauveteau, G., & Kohler, N. (1974). Polymer Flooding: The Essential Elements for Laboratory Evaluation. *SPE Improved Oil Recovery Symposium*, Tulsa, Oklahoma. SPE-4745-MS. <https://doi.org/10.2118/4745-MS>.
- 30 Wang, D., Dong, H., Lv, C., Fu, X., & Nie, J. (2009). Review of Practical Experience by Polymer Flooding at Daqing. *SPE Reservoir Evaluation & Engineering* 12(03): 470–476. SPE-114342-PA. <https://doi.org/10.2118/114342-PA>.
- 31 Telkov, V. (2016). A new vision of polymer flooding as method of high-viscous oil displacement. *International scientific conference "Geopetrol 2016"*, Krakow, Poland.
- 32 Wang, D., Seright, R. S., Shao, Z., & Wang, J. (2008). Key Aspects of Project Design for Polymer Flooding at the Daqing Oilfield. *SPE Reservoir Evaluation & Engineering* 11(06): 1117–1124. SPE-109682-PA. <https://doi.org/10.2118/109682-PA>.
- 33 Seright, R.S. (2017). How Much Polymer Should Be Injected During a Polymer Flood? Review of Previous and Current Practices. *SPE Journal* 22(01): 1–18. SPE-179543-PA. <https://doi.org/10.2118/179543-PA>.
- 34 Thakuria, C., Al-Amri, M. S., Al-Saqri, K. A., Jaspers, H. F., Al-Hashmi, K. H., & Zuhaimi, K. (2013). Performance Review of Polymer Flooding in a Major Brown Oil Field of Sultanate of Oman. *SPE Enhanced Oil Recovery Conference*, Kuala Lumpur, Malaysia. SPE-165262-MS. <https://doi.org/10.2118/165262-MS>.
- 35 Guntupalli, S., Kechichian, J., Al-Yaarubi, A., Al-Amri, A., Al-Amri, M., Al-Hinai, G., Al-Shuaili, K., Svec, Y., & al Habsi, Y. (2018). A Successful ASP Sweep Evaluation in a Field Pilot. *SPE EOR Conference at Oil and Gas West Asia*, Muscat, Oman. SPE-190462-MS. <https://doi.org/10.2118/190462-MS>.
- 36 Choudhuri, B., Thakuria, C., Belushi, A. A., Nurzaman, Z., Hashmi, K. A., & Batycky, R. (2015). Optimization of a Large Polymer Flood With Full-Field Streamline Simulation. *SPE Reservoir Evaluation & Engineering* 18(03): 318–328. SPE-169746-PA. <https://doi.org/10.2118/169746-PA>.
- 37 Ning, S., Barnes, J., Edwards, R., Dunford, K., Eastham, K., Dandekar, A., Zhang, Y., Cercone, D., & Ciferno, J. (2019). First Ever Polymer Flood Field Pilot to Enhance the Recovery of Heavy Oils on Alaska's North Slope—Polymer Injection Performance. *SPE/AAPG/SEG Unconventional Resources Technology Conference*, Denver, Colorado, USA. URTEC-2019-643-MS. <https://doi.org/10.15530/urtec-2019-643>.
- 38 Dandekar, A., Bai, B., Barnes, J., Cercone, D., Ciferno, J., Ning, S., Seright, R., Sheets, B., Wang, D., & Zhang, Y. (2019). First Ever Polymer Flood Field Pilot — A Game Changer to Enhance the Recovery of Heavy Oils on Alaska's North Slope. *SPE Western Regional Meeting*, San Jose, California, USA. SPE-195257-MS. <https://doi.org/10.2118/195257-MS>.
- 39 Zhao, Y., Yin, S., Seright, R. S., Ning, S., Zhang, Y., & Bai, B. (2020). Performance of Low Salinity Polymer Flood in Enhancing Heavy Oil Recovery on the Alaska North Slope. *SPE/AAPG/SEG Unconventional Resources Technology Conference*, Virtual. URTEC-2020-1082-MS. <https://doi.org/10.15530/urtec-2020-1082>.
- 40 Poulsen, A., Shook, G. M., Jackson, A., Ruby, N., Charvin, K., Dwarakanath, V., Thach, S., & Ellis, M. (2018). Results of the UK Captain Field Interwell EOR Pilot. *SPE Improved Oil Recovery Conference*, Tulsa, Oklahoma, USA. SPE-190175-MS. <https://doi.org/10.2118/190175-MS>.
- 41 Jones, C., Ross, M., Getliff, J., Fuller, M., Hiscox, I., & Mandracchia, F. (2015). Captain Field Injector Performance, Historical Perspective and Recent Improvements. *SPE European Formation Damage Conference and Exhibition*, Budapest, Hungary. SPE-174183-MS. <https://doi.org/10.2118/174183-MS>.
- 42 Jackson, A. C., Dean, R. M., Lyon, J., Dwarakanath, V., Alexis, D., Poulsen, A., & Espinosa, D. (2019). Surfactant Stimulation Results in Captain Field to Improve Polymer Injectivity for EOR. *SPE Offshore Europe Conference and Exhibition*, Aberdeen, UK. SPE-195747-MS. <https://doi.org/10.2118/195747-MS>.
- 43 Morel, D. C., Jouenne, S., VERT, M., & Nahas, E. (2008). Polymer Injection in Deep Offshore Field: The Dalia Angola Case. *SPE Annual Technical Conference and Exhibition*, Denver, Colorado, USA. SPE-116672-MS. <https://doi.org/10.2118/116672-MS>.
- 44 Morel, D. C., Vert, M., Jouenne, S., Gauchet, R., & Bouger, Y. (2012). First Polymer Injection in Deep Offshore Field Angola: Recent Advances in the Dalia/Camelia Field Case. *Oil and Gas Facilities* 1(02): 43–52. SPE-135735-PA. <https://doi.org/10.2118/135735-PA>.
- 45 Demin, W., Gang, W., & Huifen, X. (2011). Large Scale High Viscous-Elastic Fluid Flooding in the Field Achieves High Recoveries. *SPE Enhanced Oil Recovery Conference*, Kuala Lumpur, Malaysia. SPE-144294-MS. <https://doi.org/10.2118/144294-MS>.

- 46 Gao, C.H. (2014). Experiences of Polymer Flooding Projects at Shengli Oilfield. *SPE EOR Conference at Oil and Gas West Asia*, Muscat, Oman. SPE-169652-MS. <https://doi.org/10.2118/169652-MS>
- 47 He, J., Song, Z., Qiu, L., Xie, F., Tan, Z., Yue, Q., & Li, X. (1998). High Temperature Polymer Flooding in Thick Reservoir in ShuangHe Oilfield. *SPE International Oil and Gas Conference and Exhibition in China*, Beijing, China. SPE-50933-MS. <https://doi.org/10.2118/50933-MS>.
- 48 Guo, Y., Zhang, J., Liu, Y., Liu, G., Xue, X., Luo, P., Ye, Z., Zhang, X., & Liang, Y. (2020). Successful Scale Application of Associative Polymer Flooding for Offshore Heavy Oilfield in Bohai Bay of China. *SPE/IATMI Asia Pacific Oil & Gas Conference and Exhibition*, Bali, Indonesia. SPE-196467-MS. <https://doi.org/10.2118/196467-MS>.
- 49 Delamaide, E., Soe Let, K. M., Bhoendie, K., Jong-A-Pin, S., & Paidin, W. R. (2016). Results of a Polymer Flooding Pilot in the Tambaredjo Heavy Oil Field, Suriname. *SPE Canada Heavy Oil Technical Conference*, Calgary, Alberta, Canada. SPE-180739-MS. <https://doi.org/10.2118/180739-MS>.
- 50 Ilyasov, I., Gudz, A., Podkorytov, A., Komarov, V., & Glushchenko, N. (2020). Results of the First Polymer Flooding Pilot at East-Messoyakhskoe Oil Field. *SPE Russian Petroleum Technology Conference*, Virtual. SPE-201822-MS. <https://doi.org/10.2118/201822-MS>.
- 51 Clemens, T., Deckers, M., Kornberger, M., Gumpenberger, T., & Zechner, M. (2013). Polymer Solution Injection — Near Wellbore Dynamics and Displacement Efficiency, Pilot Test Results, Matzen Field, Austria. *EAGE Annual Conference & Exhibition incorporating SPE Europec*, London, UK. SPE-164904-MS. <https://doi.org/10.2118/164904-MS>
- 52 Lüftenegger, M., Kadnar, R., Puls, C., & Clemens, T. (2015). Operational Challenges and Monitoring of a Polymer Pilot, Matzen Field, Austria. *EUROPEC 2015*, Madrid, Spain. SPE-174350-MS. <https://doi.org/10.2118/174350-MS>
- 53 Chiotoroiu, M. M., Peisker, J., Clemens, T., & Thiele, M. R. (2017). Forecasting Incremental Oil Production of a Polymer-Pilot Extension in the Matzen Field Including Quantitative Uncertainty Assessment. *SPE Reservoir Evaluation & Engineering* 20(04): 0894–0905. SPE-179546-PA. <https://doi.org/10.2118/179546-PA>
- 54 Melo, M.A., Lins, A.G., & Silva, I.P. (2017). Lessons Learned From Polymer Flooding Pilots in Brazil. *SPE Latin America and Caribbean Mature Fields Symposium*, Salvador, Bahia, Brazil. SPE-184941-MS. <https://doi.org/10.2118/184941-MS>.
- 55 Melo, M.A., Holleben, C.R., Silva, I.G., de Barros Correia, A., Silva, G.A., Rosa, A.J., Lins, A.G., & de Lima, J.C. (2005). Evaluation of Polymer-Injection Projects in Brazil. *SPE Latin American and Caribbean Petroleum Engineering Conference*, Rio de Janeiro, Brazil. SPE-94898-MS. <https://doi.org/10.2118/94898-MS>
- 56 Buciak, J., Fondevila Sancet, G., & del Pozo, L. (2014). Polymer-Flooding-Pilot Learning Curve: Five-Plus Years' Experience To Reduce Cost per Incremental Barrel of Oil. *SPE Reservoir Evaluation & Engineering* 18(01): 11–19. SPE-166255-PA. <https://doi.org/10.2118/166255-PA>.
- 57 Pozo, L. D., Daparo, W. D., Fernandez, G., & Carbonetti, J. (2018). Implementing a Field Pilot Project for Selective Polymer Injection in Different Reservoirs. *SPE Improved Oil Recovery Conference*, Tulsa, Oklahoma, USA. SPE-190205-MS. <https://doi.org/10.2118/190205-MS>.
- 58 Hryc, A., Hochenfellner, F., Best, R. O., Maler, S., & Freedman, P. (2018). Development of a Field Scale Polymer Project in Argentina. *SPE Improved Oil Recovery Conference*, Tulsa, Oklahoma, USA. SPE-190326-MS. <https://doi.org/10.2118/190326-MS>.
- 59 Hryc, A., Hochenfellner, F., Best, R. O., Maler, S., & Puliti, R. (2016). Evaluation of a Polymer Injection Pilot in Argentina. *SPE Latin America and Caribbean Heavy and Extra Heavy Oil Conference*, Lima, Peru. SPE-181210-MS. <https://doi.org/10.2118/181210-MS>.
- 60 Ogezi, O., Strobel, J., Egbuniwe, D., & Leonhardt, B. (2014). Operational Aspects of a Biopolymer Flood in a Mature Oilfield. *SPE Improved Oil Recovery Symposium*, Tulsa, Oklahoma, USA. SPE-169158-MS. <https://doi.org/10.2118/169158-MS>.
- 61 Watson, A., Trahan, G. A., & Sorensen, W. (2014). An Interim Case Study of an Alkaline-Surfactant-Polymer Flood in the Mooney Field, Alberta, Canada. *SPE Improved Oil Recovery Symposium*, Tulsa, Oklahoma, USA. SPE-169154-MS. <https://doi.org/10.2118/169154-MS>.
- 62 Saboorian-Jooybari, H., Dejam, M., & Chen, Z. (2015). Half-Century of Heavy Oil Polymer Flooding from Laboratory Core Floods to Pilot Tests and Field Applications. *SPE Canada Heavy Oil Technical Conference*, Calgary, Alberta, Canada. SPE-174402-MS. <https://doi.org/10.2118/174402-MS>.
- 63 Liu, J. Z., Adegbesan, K., & Bai, J. J. (2012). Suffield Area, Alberta, Canada – Caen Polymer Flood Pilot Project. *SPE Heavy Oil Conference Canada*, Calgary, Alberta, Canada. SPE-157796-MS. <https://doi.org/10.2118/157796-MS>.
- 64 Irvine, R., Davidson, J., Edwards, S., Kingsbury, J., Hui-June, P., & Tardiff, C. (2012). Case Study of Polymer Flood Pilot in a Low Permeability Mannville Sand of the Western Canadian Sedimentary Basin Using Produced Water for Blending. *SPE Improved Oil Recovery Symposium*, Tulsa, Oklahoma, USA. SPE-154050-MS. <https://doi.org/10.2118/154050-MS>.
- 65 Delaplace, P., Delamaide, E., Roggero, F., & Renard, G. (2013). History Matching of a Successful Polymer Flood Pilot in the Pelican Lake Heavy Oil Field, Canada. *SPE Annual Technical Conference and Exhibition*, New Orleans, Louisiana, USA. SPE-166256-MS. <https://doi.org/10.2118/166256-MS>.
- 66 Prasad, D., Pandey, A., Kumar, M. S., & Koduru, N. (2014). Pilot to Full-Field Polymer Application in One of the Largest Onshore Field in India. *SPE Improved Oil Recovery Symposium*, Tulsa, Oklahoma, USA. SPE-169146-MS. <https://doi.org/10.2118/169146-MS>.
- 67 Kumar, M. S., Pandey, A., & Jha, M. K. (2012). Polymer Injectivity Test in Mangala Field - A Significant Step towards Field Wide Implementation. *SPE Oil and Gas India Conference and Exhibition*, Mumbai, India. SPE-155162-MS. <https://doi.org/10.2118/155162-MS>.

- 68 Kumar, P., Raj, R., Koduru, N., Kumar, S., & Pandey, A. (2016). Field Implementation of Mangala Polymer Flood: Initial Challenges, Mitigation and Management. *SPE EOR Conference at Oil and Gas West Asia*, Muscat, Oman. SPE-179820-MS. <https://doi.org/10.2118/179820-MS>.
- 69 Baloch, S., Leon, J., Masalmeh, S., Chappell, D., Brodie, J., Romero, C., al Mazrouei, S., al Tenaiji, A., al Balooshi, M., Igogo, A., Azam, M., Maheshwar, Y., & Dupuis, G. (2021). Expanding Polymer Injectivity Tests on a Second Giant Carbonate UAE Oil Reservoir at High Salinity & High Temperature Conditions. *Abu Dhabi International Petroleum Exhibition & Conference*, Abu Dhabi, UAE. SPE-207498-MS. <https://doi.org/10.2118/207498-MS>.
- 70 Gaillard, N., Giovannetti, B., & Favero, C. (2010). Improved Oil Recovery using Thermally and Chemically Protected Compositions Based on co- and ter-polymers Containing Acrylamide. *SPE Improved Oil Recovery Symposium*, Tulsa, Oklahoma, USA. SPE-129756-MS. <https://doi.org/10.2118/129756-MS>.
- 71 Vermolen, E. C., van Haasterecht, M. J., Masalmeh, S. K., Faber, M. J., Boersma, D. M., & Gruenenfelder, M. (2011). Pushing the Envelope for Polymer Flooding Towards High-temperature and High-salinity Reservoirs with Polyacrylamide Based Ter-polymers. *SPE Middle East Oil and Gas Show and Conference*, Manama, Bahrain. SPE-141497-MS. <https://doi.org/10.2118/141497-MS>.
- 72 Rodriguez, L., Antignard, S., Giovannetti, B., Dupuis, G., Gaillard, N., Jouenne, S., Bourdarot, G., Morel, D., Zaitoun, A., & Grassl, B. (2018). A New Thermally Stable Synthetic Polymer for Harsh Conditions of Middle East Reservoirs: Part II. NMR and Size Exclusion Chromatography to Assess Chemical and Structural Changes During Thermal Stability Tests. *SPE Improved Oil Recovery Conference*, Tulsa, Oklahoma, USA. SPE-190200-MS. <https://doi.org/10.2118/190200-MS>.
- 73 Moore, J. K. (1969). Reservoir Barrier and Polymer Waterflood: Northeast Hallsville Crane Unit. *J. Pet. Tech.*: 1130-1136.
- 74 Szabo, M. (1975). Laboratory Investigations of Factors Influencing Polymer Flood Performance. *Society of Petroleum Engineers Journal* 15(04): 338-346. SPE-4669-PA. <https://doi.org/10.2118/4669-PA>.
- 75 Jeanes, A., Pittsley, J. E., & Senti, F. R. (1961). *J. Appl. Polym. Sci.*, 5: 519-526.
- 76 Lipton, D. (1974). Improved Injectability of Biopolymer Solutions. *Fall Meeting of the Society of Petroleum Engineers of AIME*, Houston, Texas. SPE-5099-MS. <https://doi.org/10.2118/5099-MS>.
- 77 Dominguez, J., & Willhite, G. (1977). Retention and Flow Characteristics of Polymer Solutions in Porous Media. *Society of Petroleum Engineers Journal* 17(02): 111-121. SPE-5835-PA. <https://doi.org/10.2118/5835-PA>.
- 78 Yang, F., Wang, D., Yang, X., Sui, X., Chen, Q., & Zhang, L. (2004). High Concentration Polymer Flooding is Successful. *SPE Asia Pacific Oil and Gas Conference and Exhibition*, Perth, Australia. SPE-88454-MS. <https://doi.org/10.2118/88454-MS>.
- 79 Clarke, A., Howe, A. M., Mitchell, J., Staniland, J., & Hawkes, L. A. (2015). How Viscoelastic Polymer Flooding Enhances Displacement Efficiency. *SPE Asia Pacific Enhanced Oil Recovery Conference*, Kuala Lumpur, Malaysia. SPE-174654-MS. <https://doi.org/10.2118/174654-MS>.
- 80 Alagic, E., Dopffel, N., Bødtker, G., Hovland, B., Mukherjee, S., Kumar, P., & Dillen, M. (2020). Biodegradation Mitigation and Protection Strategies for the Biopolymer Schizophyllan. *SPE Europec*, Virtual. SPE-200562-MS. <https://doi.org/10.2118/200562-MS>.
- 81 Elhossary, D. A., Sebastian, A., Alameri, W., & Al-Shalabi, E. W. (2021). Bulk Rheology and Injectivity Assessments of Potential Biopolymer and Synthetic Polymer for Applications in Carbonates Under Harsh Conditions. *Abu Dhabi International Petroleum Exhibition & Conference*, Abu Dhabi, UAE. SPE-208105-MS. <https://doi.org/10.2118/208105-MS>.
- 82 Al-Murayri, M. T., Kamal, D. S., Garcia, J. G., Al-Tameemi, N., Driver, J., Hernandez, R., Fortenberry, R., & Britton, C. (2018). Stability of Biopolymer and Partially Hydrolyzed Polyacrylamide in Presence of H₂S and Oxygen. *SPE Annual Technical Conference and Exhibition*, Dallas, Texas, USA. SPE-191581-MS. <https://doi.org/10.2118/191581-MS>.
- 83 Seright, R. S., & Skjevra, I. (2015). Effect of Dissolved Iron and Oxygen on Stability of Hydrolyzed Polyacrylamide Polymers. *SPE Journal* 20(03): 433-441. SPE-169030-PA. <https://doi.org/10.2118/169030-PA>.
- 84 Abbas, S., Sanders, A. W., & Donovan, J. C. (2013). Applicability of Hydroxyethylcellulose Polymers for Chemical EOR. *SPE Enhanced Oil Recovery Conference*, Kuala Lumpur, Malaysia. SPE-165311-MS. <https://doi.org/10.2118/165311-MS>.
- 85 Seright, R. S., Seheult, M., & Talashek, T. (2009). Injectivity Characteristics of EOR Polymers. *SPE Reservoir Evaluation & Engineering* 12(05): 783-792. SPE-115142-PA. <https://doi.org/10.2118/115142-PA>.
- 86 Wang, Z., Zhang, J., & Jiang, Y. (1988). Evaluation Of Polymer Flooding In Daqing Oil Field And Analysis Of Its Favourable Conditions. *International Meeting on Petroleum Engineering*, Tianjin, China. SPE-17848-MS. <https://doi.org/10.2118/17848-MS>.
- 87 Manichand, R. N., Moe Soe Let, K. P., Gil, L., Quillien, B., & Seright, R. S. (2013). Effective Propagation of HPAM Solutions Through the Tambaredjo Reservoir During a Polymer Flood. *SPE International Symposium on Oilfield Chemistry*, The Woodlands, Texas, USA. SPE-164121-MS. <https://doi.org/10.2118/164121-MS>.
- 88 Zhao, Y., Yin, S.Z., Seright, R.S., Ning, S., Zhang, Y., & Bai, B.J. (2020). Enhancing Heavy-Oil-Recovery Efficiency by Combining Low-Salinity-Water and Polymer Flooding. *SPE J.* 26 (3): 1535-1551. SPE-204220-PA. <https://doi.org/10.2118/204220-PA>.
- 89 Jouenne, S., Klimenko, A., & Levitt, D. (2016). Polymer Flooding: Establishing Specifications for Dissolved Oxygen and Iron in Injection Water. *SPE J.* 22(2): 438-446. SPE-179614-PA. <https://doi.org/10.2118/179614-PA>.
- 90 Ma, Y., & McClure, M. W. (2016). The Effect of Polymer Rheology and Induced Fracturing on Injectivity and Pressure-Transient Behavior. *SPE Reservoir Evaluation & Engineering* 20(02): 394-402. SPE-184389-PA. <https://doi.org/10.2118/184389-PA>.

- 91 Khodaverdian, M. F., Sorop, T., Postif, S. J., & van den Hoek, P. J. (2009). Polymer Flooding in Unconsolidated Sand Formations: Fracturing and Geomechanical Considerations. *EUROPEC/EAGE Conference and Exhibition*, Amsterdam, The Netherlands. SPE-121840-MS. <https://doi.org/10.2118/121840-MS>.
- 92 van den Hoek, P. J., Al-Masfry, R. A., Zwartz, D., Jansen, J. D., Hustedt, B., & van Schijndel, L. (2009). Optimizing Recovery for Waterflooding Under Dynamic Induced Fracturing Conditions. *SPE Reservoir Evaluation & Engineering* 12(05): 671–682. SPE-110379-PA. <https://doi.org/10.2118/110379-PA>.
- 93 van den Hoek, P. J., Mahani, H., Sorop, T. G., Brooks, A. D., Zwaan, M., Sen, S., Shuaili, K., & Saadi, F. (2012). Application of Injection Fall-Off Analysis in Polymer flooding. *SPE Europec/EAGE Annual Conference*, Copenhagen, Denmark. SPE-154376-MS. <https://doi.org/10.2118/154376-MS>.
- 94 Thomas, A., Giddins, M., & Wilton, R. (2019). Why is it so Difficult to Predict Polymer Injectivity in Chemical Oil Recovery Processes? *IOR 2019 – 20th European Symposium on Improved Oil Recovery*. <https://doi.org/10.3997/2214-4609.201900114>.
- 95 Sorbie, K., & Seright, R. (1992). Gel Placement in Heterogeneous Systems With Crossflow. *SPE/DOE Enhanced Oil Recovery Symposium*, Tulsa, Oklahoma. SPE-24192-MS. <https://doi.org/10.2118/24192-MS>.
- 96 Sheng, J. J., Leonhardt, B., & Azri, N. (2015). Status of Polymer-Flooding Technology. *Journal of Canadian Petroleum Technology* 54(02): 116–126. SPE-174541-PA. <https://doi.org/10.2118/174541-PA>.
- 97 Taber, J., Martin, F., & Seright, R. (1997). EOR Screening Criteria Revisited Part 1: Introduction to Screening Criteria and Enhanced Recovery Field Projects. *SPE Res Eng* 12(3): 189–198. SPE-35385-PA. <https://doi.org/10.2118/35385-PA>.
- 98 Seright, R.S., Campbell, A.R., Mozley, P.S., & Han, P. (2010). Stability of Partially Hydrolyzed Polyacrylamides at Elevated Temperatures in the Absence of Divalent Cations. *SPE Journal* 15(02): 341–348. <https://doi.org/10.2118/121460-PA>.
- 99 Clark, S.R., Pitts, M.J., & Smith, S.M. (1993). Design and Application of an Alkaline-Surfactant-Polymer Recovery System for the West Kiehl Field. *SPE Advanced Technology Series* 1(01): 172–179. SPE-17538-PA. <https://doi.org/10.2118/17538-PA>.
- 100 Wang, Z., Pang, R., Le, X., Peng, Z., Hu, Z., & Wang, X. (2013). Survey on injection–production status and optimized surface process of ASP flooding in industrial pilot area. *Journal of Petroleum Science and Engineering* 111: 178–183. <https://doi.org/10.1016/j.petrol.2013.09.010>.
- 101 Aitkulov, A., Dao, E., & Mohanty, K. K. (2018). ASP Flood After a Polymer Flood vs. ASP Flood After a Water Flood. *SPE Improved Oil Recovery Conference*, Tulsa, Oklahoma, USA. SPE-190271-MS. <https://doi.org/10.2118/190271-MS>.
- 102 Healy, R., Reed, R., & Stenmark, D. (1976). Multiphase Microemulsion Systems. *Society of Petroleum Engineers Journal* 16(03): 147–160. SPE-5565-PA. <https://doi.org/10.2118/5565-PA>.
- 103 Nelson, R., & Pope, G. (1978). Phase Relationships in Chemical Flooding. *Society of Petroleum Engineers Journal* 18(05): 325–338. SPE-6773-PA. <https://doi.org/10.2118/6773-PA>.
- 104 Winsor, P. A. (1954). Solvent Properties of Amphiphilic Compounds. London: Butterworth Scientific Publication.
- 105 He, L., Gang, C., & Guochen, S. (2007). Technical Breakthrough in PCPs' Scaling Issue of ASP Flooding in Daqing Oilfield. *SPE Annual Technical Conference and Exhibition*, Anaheim, California, USA. SPE-109165-MS. <https://doi.org/10.2118/109165-MS>.
- 106 Pandey, A., Koduru, N., Stanley, M., Pope, G. A., & Weerasooriya, U. P. (2016). Results of ASP Pilot in Mangala Field: A Success Story. *SPE Improved Oil Recovery Conference*, Tulsa, Oklahoma, USA. SPE-179700-MS. <https://doi.org/10.2118/179700-MS>.
- 107 Jiecheng, C., Wanfu, Z., Qingguo, W., Gang, C., Wenguang, B., Changming, Z., & Meie, L. (2014). Technical Breakthrough in Production Engineering Ensures Economic Development of ASP Flooding in Daqing Oilfield. *SPE Asia Pacific Oil & Gas Conference and Exhibition*, Adelaide, Australia. SPE-171506-MS. <https://doi.org/10.2118/171506-MS>.
- 108 Dean, E., Pitts, M., Wyatt, K., James, D., Mills, K., Al-Murayri, M., & Al-Kharji, A. (2020). Practical Chemical Formulation Design – Time to Break Away from Micellar Polymer Floods, Again. *SPE Improved Oil Recovery Conference*, Virtual. SPE-200385-MS. <https://doi.org/10.2118/200385-MS>.
- 109 Gao, S., He, Y., Zhu, Y., Han, P., Peng, S., & Liu, X. (2020). Associated Polymer ASP Flooding Scheme Optimization Design and Field Test after Polymer Flooding in Daqing Oilfield. *SPE Improved Oil Recovery Conference*, Virtual. SPE-200443-MS. <https://doi.org/10.2118/200443-MS>.
- 110 Pandey, A., Beliveau, D., Corbishley, D. W., & Suresh Kumar, M. (2008). Design of an ASP Pilot for the Mangala Field: Laboratory Evaluations and Simulation Studies. *SPE Indian Oil and Gas Technical Conference and Exhibition*, Mumbai, India. SPE-113131-MS. <https://doi.org/10.2118/113131-MS>.

М.С. Сагындиқов, Р.М. Кушеков, Р.С. Серайт

ASP суландырумен салыстырғандағы полимерлерлі суландыруының маңызды аспектілері мен нәтижелеріне шолу

Полимерлі суландыру — бұл мұнай өндіруді арттырудың болашағы зор және тиімді химиялық әдіс. Полимерлі суландыру әсіресе сілтілі/беттік-белсенді зат/полимерлі суландыру (ASP) тиімсіз болған кезде және кен орнында күрделі проблемалар туындаған кезде тиімді (тұзды тұндыру, жөндеу кезеңінің төмендеуі, ұңғыманың қабылдау проблемалары, бұзылуы қиын эмульсиялар). Соңғы

Әдебиет дереккөздерінде полимерлі суландырудың 30-ға жуық далалық сынақтары туралы айтылады. Олардың көпшілігі техникалық жетістіктер туралы мәлімет береді. Полимерлі суландыру 60 жыл бойы қолданылғанымен, оны жақсарту үшін әлі де қосымша зерттеулер қажет. Мақалада Қаламқас кен орнының тәжірибесімен біріктірілген соңғы жобаларды шолу негізінде полимерлік суландырудың маңызды аспектілері мен сипаттамалары берілген. Әдебиеттердің кең шолуында температура, су қабатының минералдануы, су көзін таңдау, мұнай қасиеттері, қабат типі және өткізгіштігі тұрғысынан қолдану диапазоны қарастырылған. Су көзін таңдау пилоттық/өндірістік жобаны әзірлеу кезінде маңызды рөл атқарады және ең маңызды техникалық және экономикалық шешімдердің бірі болып табылады. Полимер қойыртпағының дизайны, әсіресе мұнай және полимердің тұтқырлықтарының арақатынасы бірден әлдеқайда аз болатын тұтқырлығы жоғары мұнай кен орындары үшін егжей-тегжейлі талданған. Полимерлердің жоғары қабылдағыштығын түсіндіруге ерекше көңіл бөлінген. Ағымдағы мұнай бағасы бойынша технологияның тиімсіздігін растау кезінде кейбір танымал ASP жобалары үшін техникалық-экономикалық негіздеме жүргізілген. Сонымен қатар, ASP суландыру скринингі үшін үш қазақстандық мұнай кен орындарындағы мұнайдың қышқыл мөлшеріне сандық талдау жасалған.

Кілт сөздер: полиакриламид, полимерлік суландыру, мұнай беруді ұлғайтудың химиялық әдістері, сілті/беттік белсенді зат/полимер (ASP) суландыру, техникалық-экономикалық негіздеме.

М.С. Сагындиқов, Р.М. Кушеков, Р.С. Серайт

Обзор важных аспектов и характеристик полимерного заводнения в сравнении с ASP заводнением

Полимерное заводнение является многообещающим и эффективным химическим методом увеличения нефтеотдачи (xМУН). Полимерное заводнение особенно эффективно, когда щелочь/ПАВ/полимерное заводнение (ASP) нерентабельно и вызывает серьезные проблемы на месторождении (солеотложения, снижение межремонтного периода, проблемы с приемистостью, трудноразрушаемые эмульсии). В последних литературных источниках упоминается о ~30 полевых испытаний полимерного заводнения. В большинстве из них сообщается о техническом успехе. Несмотря на то, что полимерное заводнение применяется уже ~60 лет, оно все еще требует дальнейших исследований для совершенствования. В данной статье описаны важные аспекты и характеристики полимерного заводнения на основе обзора последних проектов в сочетании с опытом месторождения «Каламқас». В обширном литературном обзоре рассмотрен диапазон применимости по температуре, минерализации пластовой воды, отбору источника воды, свойствам нефти, типу пласта и проницаемости. Выбор источника воды играет важную роль при разработке пилотного/коммерческого проекта и является одним из наиболее ответственных технико-экономических решений. Дизайн полимерных оторочек был подробно проанализирован, особенно для месторождений высоковязкой нефти, где выбранное соотношение вязкости нефти и полимера намного меньше единицы. Особое внимание уделено разъяснению наблюдаемой высокой приемистости полимеров. Проведена технико-экономическая оценка по некоторым известным ASP проектам для подтверждения нерентабельности технологии при текущих ценах на нефть. Кроме того, авторами статьи проведен анализ кислотного числа нефти трех казахстанских нефтяных месторождений для скрининга ASP заводнения.

Ключевые слова: полиакриламид, полимерное заводнение, химический метод увеличения нефтеотдачи, щелочь/ПАВ/полимерное заводнение, технико-экономическое обоснование.

Information about authors *

Sagyndikov, Marat Serikovich (*corresponding author*) — PhD student, Satbayev University, Satpayev str., 22, 050013, Almaty, Kazakhstan; e-mail: Sagyndikov.marat.s@gmail.com; <https://orcid.org/0000-0003-0086-723X>;

Kushekov, Ruslan Maratovich — Engineer at Enhanced Oil Recovery Service, LLP “KMG Engineering” “KazNIPImunaygas”, 35 mcr. b. 6/1, 130000, Aktau, Kazakhstan; e-mail: ruslan.kushekov@gmail.com; <https://orcid.org/0000-0001-9922-0158>;

Seright, Randall Scott — Senior Engineer and Associate Director of the New Mexico Petroleum Recovery Research Center, PhD degree in Chemical Engineering from the University of Wisconsin (Madison): Adjunct Professor at New Mexico Tech’s Petroleum Engineering Department, Socorro, 801 Leroy Place, 87801, New Mexico, USA; e-mail: randy.seright@nmt.edu; <https://orcid.org/0000-0003-1734-5155>

*The author’s name is presented in the order: *Last Name, First and Middle Names*

P. Kanabekova¹, A. Martin¹, A. Kemelbekova², G. Kulsharova^{1*}

¹Nazarbayev University, Nur-Sultan, Kazakhstan;

²Institute of Physics and Technology, Satbayev University, Almaty, Kazakhstan

(*Corresponding author's e-mail: gulsim.kulsharova@nu.edu.kz)

Applications of Nanofiber Membranes in Microphysiological Systems

Microfluidic organs-on-chips or microphysiological systems (MPS) are promising tools that can potentially replace animal testing in drug development. MPS are platforms with microchannels seeded with certain organ cells used to emulate in vivo environments in laboratory conditions. Among them, platforms seeded with lung cells called lung-on-chip devices can evaluate the influence of toxic particles, gases, and chemicals on lung tissue in vitro. Lung-on-chip devices allow the mimicry of healthy lung conditions and a wide range of diseases (asthma, cancer, autoimmune, infections). This review focuses on the use of electrospun nanofiber membranes as a functional basement membrane which plays a central role in the development of lung-on-a-chip platforms. Here, we briefly introduce microfluidic devices, MPS, and lung-on-chip devices. Existing basement membrane models, such as thin-film and gel-based membranes, and their challenges/disadvantages are discussed. Next, the concepts of electrospinning and nanofiber membranes are introduced. Finally, the nanofiber membranes used in lung-on-chip devices are reviewed. Implementation of different polymer materials used to synthesize the nanofiber membranes and different methods for incorporation of the membrane inside the device are discussed. Electrospun nanofiber membranes provide good mechanical properties, allow transmigration of the immune cells, and withstand the physiological strain without affecting the cell viability.

Keywords: microfluidics, microphysiological, nanofiber, basement membrane, electrospinning, lung-on-chip, polycaprolactone, adherent junction.



Alma Martin received her PhD degree in Pharmaceutical Sciences from the University of Copenhagen. Her research interests are focused on the development of a variety of biomaterials including hydrogels, films, cryogels, nanofibrous membranes and nanoparticles for the biomedical and regenerative medicine field. She has been

awarded The Best Manuscript Award from the Journal of Wound Ostomy and Continence Nursing for a review paper that became a basis for CE nursing test in the USA. She was also awarded The Biotechnology Prize for the most outstanding performance from the University of Essex, and won a few of travel grants for research-oriented activities.



Gulsim Kulsharova is an Assistant Professor at the Department of Electrical and Computer Engineering and a Principal Investigator of Microfluidics Laboratory in NU. She received her B.S. in Engineering Physics, M.S. in Electrical and Computer Engineering from University of Illinois, USA in 2012 and a PhD from University College London in the UK under Marie Sklodowska-Curie fellowship. During her studies, she expanded her research interests at the University of Oulu in Finland.

Gulsim joined Nazarbayev University as a postdoctoral scholar in 2019 and is currently a member of IEEE and EUROOC societies. She has been working on fabrication and development of microfluidic devices for organ-on-a-chip technology, sensors, and nanobiomaterials.



Perizat Kanabekova is a researcher in Nazarbayev University. She has completed MD degree and Bs in Biological Sciences in Nazarbayev University. Her research interests are focused on the development of nanofibrous membrane for lung-on-chip basement membrane.



Kemelbekova Ainagul is a PhD candidate of materials science. Currently, she is an assistant at the K.I. Satpayev Kazakh National Technical University and a junior researcher at the Institute of Physics and Technology. Her research interests cover nanofiber membranes in micro physiological systems, solar cells. She is actively engaged in scientific research and is working on a dissertation.

Content

Introduction

- 1 Lung-on-chip microfluidic device
 - 2 Existing lung-on-chip basement membranes
 - 3 Nanofibers in microfluidic systems
 - 4 Nanofibers in organ-on-chip models
 - 5 Nanofibers in lung-on-chip models
- Conclusions

Review Plan

Inclusion and Exclusion Criteria: The present review is focused on use of nanofiber membranes as basement membrane in lung-on-chip microfluidic devices.

The review is limited to publications done on lung-on-chip devices in English language. Only articles in microfluidic area were analyzed from sources like Google Scholar, Scopus. The keywords listed above were used in a search of relevant papers. The resultant articles were included to the review. No statistical or correlational analysis was used.

Introduction

Microfluidics can be represented by controlled fluid flow through microstructures or microchannels etched or molded into different material substrates (glass, polymer, silicon). There are various applications of microfluidic devices including material synthesis, molecular analysis, cell studies, drug toxicity, etc. These applications make microfluidics a rapidly developing and promising area in research [1]. One of the applications of microfluidics, organ-on-chip technology, allows mimicry of physiological systems through miniaturized and microscale designs. The mimicry is achieved by designing channels repeating structures within the organs and controlling the significant parameters within the device. Among the parameters, the concentration gradient within the fluid, diversity of cells and their patterning, interactions, fluid, shear forces, and others can be adapted to affect the functionality and characteristics of the device [2]. Conventional 2D cell culture techniques cannot replicate the microphysiological patterns because of their flat nature. Additionally, animal testing does not fully replicate human tissue and raises an ethical issue. Therefore, organ-on-chip platforms have great potential in drug development and toxicology [2].

Currently, a wide range of organ-on-chips for mimicking respiratory, kidney, cardiovascular, pancreatic, gastrointestinal, and neural tissues exist. The concept of ‘body-on-chip’ combining multiple organs is being introduced to develop a system for the complex evaluation of pharmacokinetics and pharmacodynamics of drugs [3]. Within the scope of this review, lung-on-chip models are reviewed. Lung-on-chip devices can be designed to represent healthy and diseased tissues. The design of lung tissue focuses on creating a device that would replicate a mechanically active alveolar-capillary interface with a functional basement membrane (BM) [4–6]. Among the diseases designed on-chip are pneumonia [7, 8], chronic obstructive pulmonary disease (COPD) [9], asthma [10, 11], tuberculosis (TB) [12], lung cancer [13–19], and cystic fibrosis [20, 21]. To simulate a diseased state, ‘healthy’ tissues are treated with chemicals and/or particles that induce pathological changes.

As in many other organ-on-chip devices, the lung-on-chip platforms can use the primary cells, stem cells, and human cell lines. Human cell lines are alveolar epithelial cells, which carry the transport of gases and nutrients. For example, adenocarcinomic cells such as A549 are commonly used [22]. They are easy to use and can be manipulated to induce mutations related to disease conditions such as cystic fibrosis. However, the main limitation is their transformation to immortalize, which is a principal difference from healthy airway cells [23]. The possibility to use primary human cells makes lung-on-chip devices an excellent tool in personalized medicine for drug sensitivity studies. However, the main limitation of using primary cells is their limited proliferative capacity [22]. In turn, preparing lung cells from stem cells is more difficult, which requires different growth and differentiation factors, but they are excellent in replicating human tissue because controlled differentiation induces the expression of proteins and structures as in desired one [24]. Lung tissue besides epithelial and vascular cells includes a wide variety of cells, such as mesenchymal, immune, and smooth muscle cells essential for breathing action, and neurons that control breathing [25]. Combination and diversity of cells, a complicated morphology, and relation to other organ systems make it difficult to replicate lung tissue using conventional cell culture techniques, therefore microfluidic devices might aid in overcoming the challenges related to recapitulating microstructures.

1 Lung-on-chip microfluidic device

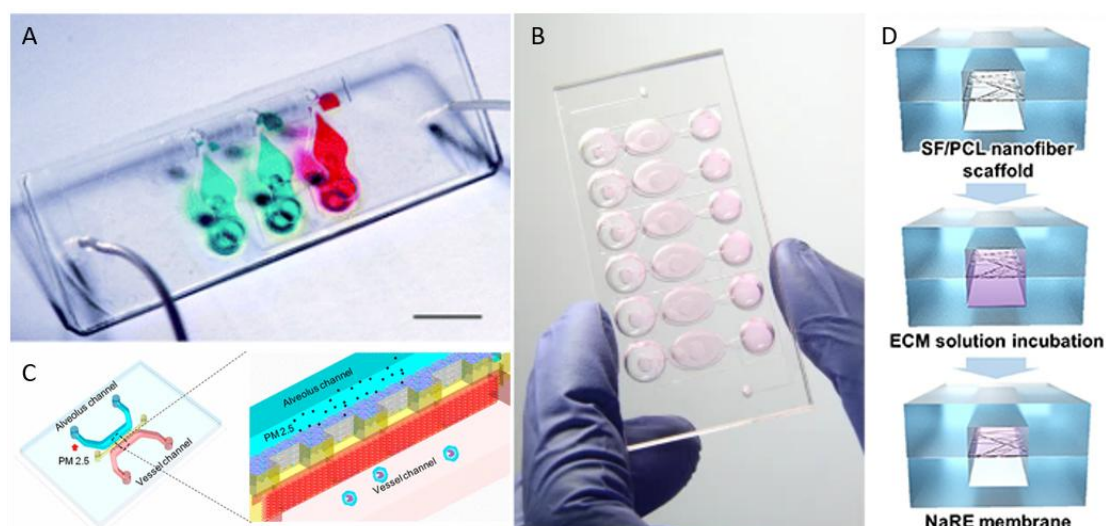
The lung-on-chip devices mimic the basic functional unit of the lung, an alveoli-capillary barrier. Thin layer of pneumocytes and endothelial vascular cells separated and connected by basement membrane is the place where the oxygen/carbon dioxide exchange takes place. In the design of lung-on-chip, scientists rely on the very first lung-on-chip device suggested by Huh in 2010 [4]. It was a two-chamber system, separated by polydimethylsiloxane (PDMS) thin layer. Each chamber represented air and blood compartments respectively, while PDMS functioned as basement membrane [4]. In designing the microphysiological devices, repeating the biomechanical signaling and forces within platform is crucial. For example, the elastic modulus in alveoli tissue is approximately 5 kPa and the expansion of alveoli during the calm breathing reaches only 4% of primary length with alternations of those values in diseased conditions [26]. The strain reaches 12% during deep inspiration, but it is important to note that alveolar distension is not uniform, so strain in some areas can increase to 30%. Besides, other parameters are also important, for example during the breathing the lung tissue stretches and recoils approximately 12 times per minute [27]. Therefore, devices that incorporate the flow are known to be more representative of organ structure than static models [28]. These characteristics are crucial in functionality, timely metabolic exchange and support of the lung tissue itself.

Basement membrane (BM) is a type of extracellular matrix that can be found around many tissues. In lungs, it lies between the epithelial lung and vascular cells. BM is specific for different tissues and has different roles, in alveolar tissues it maintains epithelial cells, facilitates gas exchange, and is involved in immune response [29]. The main components of the BM are proteins that provide elastic/plastic properties and strength: collagen, elastin, proteoglycans [26]. The changes in composition of the basement membrane are common in a wide range of diseases including autoimmune conditions, cancers and inflammatory diseases [30]. Collagen is one of the most abundant proteins, which forms the network of fibrils, aiding in resisting forces and providing tensile strength. In turn, elastin is responsible for elastic properties and stretchability of the BM [27]. Those proteins undergo remodeling in disease conditions, resulting in misbalance and dysregulations in functioning of the BM. In mimicking the BM for lung-on-chip the mechanical characteristics described above are important along with chemical properties of the material such as hydrophobicity, biocompatibility and physical structure that ensure its functionality.

2 Existing lung-on-chip basement membranes

A thin layer of PDMS separating the air and fluid compartment, which was prepared by the microstructuring-lamination process, was cyclically stretched in a breathing manner in a lung-on-chip device developed by Stucki as shown in Figure 1A [31]. The integrity of protein meshwork and thus permeability of BM was not disrupted during 'breathing' and the stretch increased the metabolic activity of the cells, enhancing the gas exchange function [31]. Later, the authors suggested a new PDMS-membrane-based device, shown in Figure 1B, which maintained cells for 3 weeks without an external perfusion system [32]. Although PDMS is elastic, not toxic for cells, has pores for the transport in between layers, and was frequently used as BM in lung-on-chip, some disadvantages make it not an ideal candidate. Most of the recent research mentions the ability of PDMS to absorb small molecules, which affect the biochemical microenvironment within the microfluidic device [33]. Other examples of porous membranes that are used to separate air and fluid compartments are polycarbonate (PC) and polyethylene terephthalate (PET). However, the authors mention the main disadvantage of using these membranes as the recreation of a 2D flat surface, which does not fully recapitulate the curvature of alveoli [6]. As a result, a microcurved 3D microfluidic device was designed to conserve the spatial configuration of the lung functional unit. Although the epithelial and endothelial cells were maintained within the device for 2 weeks with features and topography similar to real lung tissues, the mimicry of breathing movement was impossible due to the lack of elastic properties [6].

The BM can be 'synthesized' by preparing layer of 'gel', which would accommodate cells and mediate the signaling and communication between them. For example, Huang et al. [5] synthesized hydrogel from gelatin methacryloyl (GelMA), while Xu et al. used commercial Matrigel sandwiched between PDMS layer as shown in Figure 1C [34]. In both experiments, the BM maintained its barrier function and some cell experiments were conducted to evaluate the functionality of the devices. The gel-based BMs enhanced recapitulation of microphysiological structures due to its primary 3D nature, so cells maintained the characteristics such as adherent junctions in accordance with histological features of lung tissue. However, the disadvantage of working with hydrogels is the inability to mimic stretchable properties and strain as in 'breathing' [33].



A — PDMS based lung-on-chip with thin PDMS basement membrane [31];
 B — PDMS based lung-on-chip with PDMS based BM without external perfusion system [32];
 C — PDMS based lung-on-chip with Matrigel BM [34];
 D — PMMA based lung-on-chip with Nanofiber-Reinforced membrane [35]

Figure 1. Lung-on-chip device models

Another example of the BM mimicry was formed by drop-casting the solution of collagen and elastin on golden mesh in PDMS based microfluidic device, which revealed significantly less absorption of small molecules, with mechanical properties close to physiological 4 kPa elasticity modulus and cause 10 % mechanical strain [33]. Moreover, authors mention that golden mesh structure recapitulates the geometric structure, while the collagen and elastin are natural and biodegradable. Next, BM can be recapitulated using the nanofiber membranes sandwiched in device between polymethyl methacrylate (PMMA) layers as shown in Figure 1D [35]. Nanofiber membranes as a focus of this review will be explained in the next section.

3 Nanofibers in microfluidic systems

Nanofiber membranes show the potential in becoming a better alternative to the conventional membranes in microfluidic systems. Electrospun nanofiber membranes possess a high surface area, a highly porous and interconnected structure that is closer to resembling the basement membrane and extracellular matrix (ECM) of tissues [35, 36]. These unique properties support and facilitate the attachment and migration of cells on the scaffold [37]. The high porosity of the nanofibrous membrane allows more efficient nutrient and waste exchange that further contributes to improved cell proliferation [38]. Even though a simple coating of the conventional membranes with ECM proteins improves cytocompatibility, it is unable to create a 3D topography of the cellular microenvironment [39]. In comparison, during the electrospinning of the nanofibers, proteins can be integrated within the polymer solution reducing fabrication steps and allowing a more homogeneous distribution of proteins throughout the scaffold enhancing its resemblance to the native ECM in tissues [37].

The electrospinning technique is a relatively straightforward process. Electrospinning utilizes high voltage applied to a polymer solution to generate fibers that are deposited on a grounded collector plate. High voltage is required to overcome the surface tension of the polymer solution and induce its transformation into a jet. This facilitates stretching of the polymer chains and evaporation of the solvent, which allows the collection of dry nanofibers. The electrospinning process involves multiple variables that may influence the quality of the nanofibers assessed by their interfiber porosity, fiber morphology, and topography. These variables include conductivity, dielectric constant and surface tension of the solution, molecular weight and structure of the polymer, compatibility of the polymer and solvent, solvent evaporation rate, and solution viscosity. In addition, process settings, such as voltage, flow rate, distance from the needle tip to collector, temperature, and humidity also play an essential role in the suitability of the final solution to be electrospun into dry and homogeneous fibers [40–42].

In microfluidic systems, nanofibrous membranes can be used as bioanalytical systems and organ-on-chip models [43]. Their high surface area enhances the sensitivity of bioanalytical systems through increased

surface functionalization. Examples of such systems include the immobilization of antigens or antibodies for developing immunoassays similar to ELISA assay [44]. In such a system, PLGA and PLA nanofibers showed superior properties to PDMS membrane in immobilizing proteins due to the presence of carboxyl groups on their surface [45]. Moreover, nanofibrous microfluidic systems are also researched for detection of *Escherichia coli* [46], HIV [47], metalloproteinase-9 [48], opium alkaloids [49], cancer biomarkers [50], and circulating tumor cells [51, 52]. These nanofibrous microfluidic systems also hold great potential in molecular diagnostics and screening for therapeutic agents [53].

4 Nanofibers in organ-on-chip models

The unique resemblance of nanofibrous membranes to the native tissue ECM allows their use in organ-on-a-chip models [54]. Electrospun nanofibrous membranes may allow the use of exceptionally thin thickness close to that of a basement membrane in tissues. However, in comparison to conventional membranes such as PDMS, electrospun fibrous membranes may exhibit lower tensile strength and may be too fragile. During sealing procedure of the microfluidic chip, the roughness of the nanofibrous membrane surface may reduce the bonding efficiency and the membrane may get deformed in the process [37, 43], eventually leading to leakage. Nevertheless, due to the previously mentioned limitations of the conventional PDMS membranes, developing electrospun nanofibers are actively researched as an option to mimic the native cellular microenvironment in tissues [55].

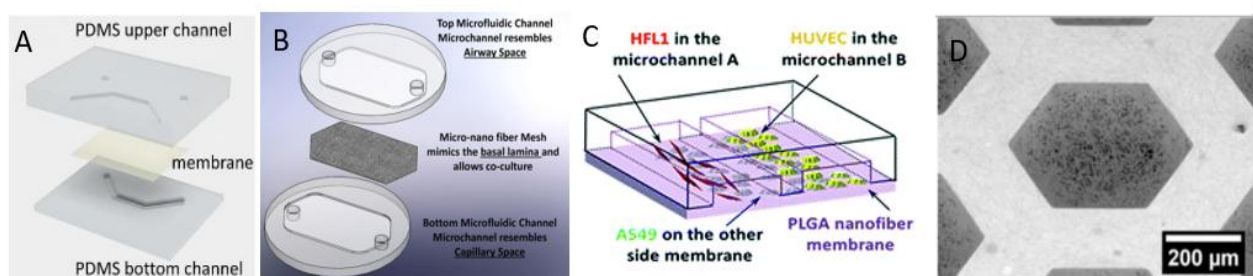
One of the initial *in vitro* models with electrospun membranes studied mimicry of cellular microenvironment using nanofibrous membranes in a microfluidic system [56]. For this purpose, polyurethane in dimethylformamide and tetrahydrofuran mixture was electrospun onto an aluminum foil. The hydrophobic surface of the membrane was treated with acrylic acid to introduce carboxyl and carbonyl group for better cell adhesion and proliferation. This treatment led to lower contact angles and reduced hydrophobicity of the material. In comparison to untreated controls, seeded human mesenchymal stem cells demonstrated better proliferation on the acid-treated membranes. However, this method did not compare nanofibrous membranes to PDMS membranes and the surface treatment of the nanofibrous membrane introduced additional fabrication step.

Later, liver-on-chip models using electrospun nanofibrous membrane were developed from PCL dissolved in chloroform [57]. This membrane was placed on the bottom of the microfluidic chamber. The hepatic carcinoma cells HepG2 were cultured on top of the membrane and showed excellent viability for 14 days. Here, they demonstrated real-time measurements of albumin and alpha-fetoprotein using an ELISA assay. This model utilized nanofibrous membranes collected on the aluminum foil and was not directly electrospun onto the chip.

In comparison, Chuchuy, Rogal [37] demonstrated a proof-of-concept study with the possibility of the electrospun polymer solution of PLA and PLA with GelMA in hexafluoroisopropanol (HFIP) directly onto the microfluidic chip. To create more oriented nanofibers, aluminum foil was placed on the opposite sides of the microfluidic chip. To ensure electrospinning of the nanofibers only to the chip surface, the area around it was sealed with a non-conductive tape. The deposited membrane was then cut to shape using a solvent-wetted scalpel. The comparison between pure PLA and GelMA-PLA fibers demonstrated that during the process of thermal fusion bonding, the membranes exhibited deformation on the edges, changes in fiber diameter, and reduction in membrane size. In contrast, GelMA-PLA nanofibrous membranes were more heat-resistant and remained flat during bonding, but showed slight sagging. Additionally, endothelial and epithelial cells performed better on the gelatin-containing PLA nanofibrous membranes due to the innate cell-recognizing motifs in gelatin, whereas pure PLA membranes required a time-consuming coating process to improve cell adhesion and proliferation.

5 Nanofibers in lung-on-a-chip models

Several studies used PCL-based nanofibrous membranes for lung-on-chip models [39, 58, 59]. A study by Tas, Rehnberg [39] used a commercially available PCL membrane to simulate clinical ventilator-induced lung injury by applying 25 % of mechanical strain on the cell-seeded membrane (Figure 2A). Here, PCL nanofibrous membrane was selected for its good mechanical properties that withstand higher mechanical strain in comparison to natural polymers such as collagen.



- A — PCL nanofibrous membranes for simulating ventilator-induced lung injury [39];
 B — Gelatin-containing PCL nanofibrous membrane for simulating alveolar-capillary barrier [58];
 C — PLGA nanofibrous membrane for simulating alveolar respiratory membrane [62];
 D — Gelatin nanofibrous membranes for simulating alveolar air-tissue interface [63].

Figure 2. Incorporation of nanofibrous membranes into microfluidic device for lung-on-chip models

A couple of other studies simulated an alveolar-capillary barrier using electrospun PCL nanofibrous membranes [58, 59]. Different ratios of PCL and gelatin in HFIP solution were used to electrospun nanofibrous membranes that were bound to the layers of the microfluidic system *via* oxygen plasma treatment (Figure 2B). A higher ratio of gelatin to PCL in the nanofibers led to an increase in fiber diameter size and distribution, altered fiber morphology from tubular to flat and reduced elasticity of the membrane. Airway re-opening was mimicked by introducing air bubbles over the seeded layer of A549. The endothelial layer in this system was presented by the human umbilical vein endothelial cells (HUVEC). The cellular responses in this system were measured through the distribution of actin filaments and the formation of tight junctions in epithelial and endothelial cells. The comparison of different ratios of PCL and gelatin in the nanofibrous membranes demonstrated that epithelial and endothelial cells respond differently to the mechanical properties of the membranes. Thus, A549 cells formed less tight junctions and spread more on the less dense and softer nanofibrous membranes, whereas HUVEC cells formed more actin filaments. Moreover, A549 cells showed more susceptibility to cell injury when cultured on rigid membranes [58].

Another study reported a PCL-based nanofibrous membrane that was able to support the growth of endothelial and epithelial cells for 21 days [59]. To mimic the alveolar-capillary barrier, human pulmonary endothelial cells (HPMEC) and lung epithelial cells (NCI-H441) were seeded on the membrane. To simulate inflammation during lung diseases, nanofibrous membranes were exposed to pro-inflammatory cytokines TNF- α and IL-8 to induce inflammation response through reduction of tight junction between epithelial cells that was measured by the amount of secreted intercellular adhesion molecule 1 (sICAM). The level of sICAM was higher in the apical layer compared to the basal layer. Additionally, these PCL nanofibrous membranes allowed the migration of neutrophils from the apical to the basal side of the membrane despite almost twice the smaller pore size in comparison to the 3 μ m pore sizes in the control PET membranes. This demonstrates that despite smaller pore size, nanofibrous PCL membranes were able to mimic inflammatory response by allowing transmigration of neutrophils through the simulated alveolar-capillary barrier.

In general, PCL-based nanofibrous membranes demonstrated a good resemblance to the native ECM and basement membrane. The Young's Modulus of pre-wetted PCL membranes was 7.2 MPa [58] and 9.7 MPa for dry PCL membranes [59], which was close to the native alveolar basement membrane [62, 63]. Additionally, in comparison to the control PET membrane, high production of collagen on PCL nanofibrous membranes was observed [59].

A biodegradable and biocompatible PLGA polymer was solubilized in trifluoroethanol (TFE) to fabricate nanofibers for a lung-on-chip system [60]. To simulate the tumor microenvironment in alveoli, two or three types of cells were seeded: A549, fetal lung cancer cells (HFL1), and HUVEC cells. For a two-cell system, A549 was seeded on the outer side of the nanofibrous membrane, whereas HFL1 cells were seeded on the inner side of the membrane facing the microchannel. For a three-cell type system, the distribution of cells on the membrane was similar to the two-cell system, only there was a second microchannel, where the HUVEC cells were seeded on the membrane facing it (Figure 2C). Additionally, anti-cancer drug gefitinib was tested in the two-cell system. The addition of the drug leads to a significant reduction in viability of A549 cells, demonstrating the efficiency of the drug in inducing apoptosis of cancer cells. In the three-cell system, A549 cells induced apoptosis of HUVEC cells and migrated through the membrane onto the other

side. This multi-cellular microfluidic system simulated the tumor microenvironment by mimicking tumor invasion.

A simulation of the alveolar air-tissue interface was demonstrated using gelatin nanofibers [61]. Gelatin is a degradation product of collagen, which is commonly found in the basement membrane and ECM. To electrospin the nanofibers, gelatin from porcine skin was solubilized in the mixture of acetic acid, ethyl acetate, and water. Due to the high hydrolytic degradation rate of gelatin in water, the fabricated nanofibers were crosslinked with N-(3-dimethylaminopropyl)-N'-ethylcarbodiimide hydrochloride and N-hydroxy-succinimide. The nanofibers were directly electrospun on a hexagonally-shaped honeycomb PDMS microframe (Figure 2D). However, SEM images demonstrated the loss of fiber integrity that resulted in a microporous structure of the membrane. A549 cells were seeded on the membrane and were supported with a culture media flow in the basal channel. An airwave was applied on the apical side of the membrane to introduce mechanical strain on the grown cell layer. The introduced mechanical strain simulating a 5% physiological strain did not affect the viability and proliferation of the cells. However, periodically applied strain reduced cell attachment to the nanofibers, which resulted in a better and more homogenous redistribution of A549 cells on the membrane.

Conclusions

The advances in micromachine fabrication led to the development of lung-on-chip models that combine anatomy, material science, and physical properties to explore the lung microstructure. Development of functional basement membrane remains challenging as existing models have drawbacks such as properties to absorb small molecules in case of PDMS or the inability to mimic mechanical parameters as in hydrogels. In comparison, electrospun nanofiber membranes might be optimized by parameters such as thickness, porosity, fiber morphology, and others. Despite being more fragile, they are gaining attention in the microfluidics area. Nanofiber-based membranes in lung-on-chip devices demonstrated good properties in cell transmigration, mimicking the disease conditions, and succeeded in its barrier function. All the studies demonstrate nanofiber membranes as a promising candidate for mimicry of basement membrane in lung tissue.

Acknowledgments

This research was funded by the Ministry of Education and Science of the Republic of Kazakhstan Grant for young scientists: AP09058308, the Nazarbayev University Faculty-development research grant: 080420FD1910 and the social policy grant awarded to Gulsim Kulsharova.

References:

- 1 Fallahi, H., Zhang, J., Phan, H.P., & Nguyen, N.T. (2019). Flexible Microfluidics: Fundamentals, Recent Developments, and Applications. *Micromachines (Basel)*, 10(12). <https://doi.org/10.3390/mi10120830>
- 2 Wu, Q., Liu, J., Wang, X., Feng, L., Wu, J., Zhu, X., Wen, W., & Gong, X. (2020). Organ-on-a-chip: recent breakthroughs and future prospects. *Biomed Eng Online*, 19(1), 9. <https://doi.org/10.1186/s12938-020-0752-0>.
- 3 Ma, C., Peng, Y., Li, H., & Chen, W. (2021). Organ-on-a-Chip: A New Paradigm for Drug Development. *Trends Pharmacol Sci*, 42(2), 119-133. <https://doi.org/10.1016/j.tips.2020.11.009>.
- 4 Huh, D., Matthews, B., Mammoto, A., Montoya-Zavala, M., Hsin, H., & Ingber, D. (2010). Reconstituting Organ-Level Lung Functions on a Chip. *Science*, 328(5986), 1662-1668. <https://doi.org/10.1126/science.1188302>
- 5 Huang, D., Liu, T., Liao, J., Maharjan, S., Xie, X., Perez, M., Anaya, I., Wang, S., Tirado Mayer, A., King, Z., Kong, W., Mainardi, V.L., Garciamendez-Mijares, C.E., Garcia Martinez, G., Moretti, M., Zhang, W., Gu, Z., Ghaemmaghami, A.M., & Zhang, Y.S. (2021). Reversed-engineered human alveolar lung-on-a-chip model. *Proc Natl Acad Sci U S A*, 118(19). <https://doi.org/10.1073/pnas.2016146118>.
- 6 Baptista, D., Moreira Teixeira, L., Barata, D., Tahmasebi Birgani, Z., King, J., van Riet, S., Pasman, T., Poot, A.A., Stamatiadis, D., Rottier, R.J., Hiemstra, P.S., Carlier, A., van Blitterswijk, C., Habibović, P., Giselbrecht, S., & Truckenmuller, R. (2022). 3D Lung-on-Chip Model Based on Biomimetically Microcurved Culture Membranes. *ACS Biomater Sci Eng*. <https://doi.org/10.1021/acsbiomaterials.1c01463>
- 7 Cao, T., Shao, C., Yu, X., Xie, R., Yang, C., Sun, Y., ... Ye, F. (2022). Biomimetic Alveolus-on-a-Chip for SARS-CoV-2 Infection Recapitulation. *Research (Wash D C)*, 2022, 9819154. <https://doi.org/10.34133/2022/9819154>
- 8 Huang, G., Huang, Q., Xie, L., Xiang, G., Wang, L., Xu, H., Ma, L., Luo, X., Xin, J., Zhou, X., Jin, X., & Zhang, L. (2017). A rapid, low-cost, and microfluidic chip-based system for parallel identification of multiple pathogens related to clinical pneumonia. *Sci Rep*, 7(1), 6441. <https://doi.org/10.1038/s41598-017-06739-2>

- 9 Benam, K.H., Villenave, R., Lucchesi, C., Varone, A., Hubeau, C., Lee, H.H., Alves, S.E., Salmon, M., Ferrante, T.C., Weaver, J.C., Bahinski, A., Hamilton, G.A., & Ingber, D.E. (2016). Small airway-on-a-chip enables analysis of human lung inflammation and drug responses *in vitro*. *Nat Methods*, *13*(2), 151–157. <https://doi.org/10.1038/nmeth.3697>
- 10 Nawroth, J.C., Lucchesi, C., Cheng, D., Shukla, A., Ngyuen, J., Shroff, T., Varone, A., Karalis, K., Lee, H.H., Alves, S., Hamilton, G.A., Salmon, M., & Villenave, R. (2020). A Microengineered Airway Lung Chip Models Key Features of Viral-induced Exacerbation of Asthma. *American journal of respiratory cell molecular biology*, *63*(5), 591–600. <https://doi.org/10.1165/rcmb.2020-0010MA>
- 11 Villenave, R., Lucchesi, C., Lee, H., Nguyen, J., Varone, A., Karalis, K., Alves, S.E., Salmon, M.D., & Hamilton, G.A. (2017). Severe Asthma on-Chip: a novel platform enables study of viral-induced exacerbations in asthma and drug response *In Vitro*. *European Respiratory Journal*. <https://doi.org/10.1183/1393003.congress-2017.PA4136>
- 12 Thacker, V.V., Dhar, N., Sharma, K., Barrile, R., Karalis, K., & McKinney, J. D. (2020). A lung-on-chip model of early Mycobacterium tuberculosis infection reveals an essential role for alveolar epithelial cells in controlling bacterial growth. *Elife*, *9*. <https://doi.org/10.7554/eLife.59961>
- 13 Hassell, B. A., Goyal, G., Lee, E., Sontheimer-Phelps, A., Levy, O., Chen, C. S., & Ingber, D. E. (2018). Human Organ Chip Models Recapitulate Orthotopic Lung Cancer Growth, Therapeutic Responses, and Tumor Dormancy *In Vitro*. *Cell Rep*, *23*(12), 3698. <https://doi.org/10.1016/j.celrep.2017.09.043>
- 14 Khalid, M. A. U., Kim, Y. S., Ali, M., Lee, B. G., Cho, Y.-J., & Choi, K. H. (2020). A lung cancer-on-chip platform with integrated biosensors for physiological monitoring and toxicity assessment. *Biochemical Engineering Journal*, *155*. <https://doi.org/10.1016/j.bej.2019.107469>
- 15 Park, S., Kim, T.H., Kim, S. H., You, S., & Jung, Y. (2021). Three-Dimensional Vascularized Lung Cancer-on-a-Chip with Lung Extracellular Matrix Hydrogels for *In Vitro* Screening. *Cancers (Basel)*, *13*(16). <https://doi.org/10.3390/cancers13163930>
- 16 Liao, H.-J., Chieh, J.-A., Chen, Y.-C., Lee, K.-Y., Chan, Y.-F., Ho, S.-C., Sun, W.-L., Wang, Y.-S., Huang, W.-C., Chang, W.-C., & Liu, C.-H. (2021). *Lung Cancer On Chip for Testing Immunotherapy*. In *21st International Conference on Solid-State Sensors, Actuators and Microsystems, TRANSDUCERS 2021* (pp. 1032-1035). (21st International Conference on Solid-State Sensors, Actuators and Microsystems, TRANSDUCERS 2021). Institute of Electrical and Electronics Engineers Inc.. <https://doi.org/10.1109/Transducers50396.2021.9495530>
- 17 Imparato, G., Urciuolo, F., & Netti, P.A. (2022). Organ on Chip Technology to Model Cancer Growth and Metastasis. *Bioengineering (Basel)*, *9*(1). <https://doi.org/10.3390/bioengineering9010028>
- 18 Xu, M., Wang, Y., Duan, W., Xia, S., Wei, S., Liu, W., & Wang, Q. (2020). Proteomic Reveals Reasons for Acquired Drug Resistance in Lung Cancer Derived Brain Metastasis Based on a Newly Established Multi-Organ Microfluidic Chip Model. *Front Bioeng Biotechnol*, *8*, 612091. <https://doi.org/10.3389/fbioe.2020.612091>
- 19 Jung, D. J., Shin, T. H., Kim, M., Sung, C.O., Jang, S. J., & Jeong, G.S. (2019). A one-stop microfluidic-based lung cancer organoid culture platform for testing drug sensitivity. *Lab Chip*, *19*(17), 2854–2865. <https://doi.org/10.1039/C9LC00496C>
- 20 Ogden, H. L., Kim, H., Wikenheiser-Brokamp, K. A., Naren, A.P., & Mun, K.S. (2021). Cystic Fibrosis Human Organs-on-a-Chip. *Micromachines (Basel)*, *12*(7). <https://doi.org/10.3390/mi12070747>
- 21 Plebani, R., Potla, R., Soong, M., Bai, H., Izadifar, Z., Jiang, A., Travis, R.N., Belgur, C., Dinis, A., Cartwright, M.J., Prantil-Baun, R., Jolly, P., Gilpin, S.E., Romano, M., & Ingber, D.E. (2022). Modeling pulmonary cystic fibrosis in a human lung airway-on-a-chip: Cystic fibrosis airway chip. *J Cyst Fibros*. <https://doi.org/10.1016/j.jcf.2021.10.004>
- 22 Campillo, N., Oliveira, V.R., & da Palma, R.K. (2021). Alveolus Lung-on-a-Chip Platform: A Proposal. *Chemosensors*, *9*(9). <https://doi.org/10.3390/chemosensors9090248>
- 23 Miller, A.J., & Spence, J.R. (2017). *In Vitro* Models to Study Human Lung Development, Disease and Homeostasis. *Physiology (Bethesda)*, *32*(3), 246–260. <https://doi.org/10.1152/physiol.00041.2016>
- 24 Nawroth, J.C., Barrile, R., Conegliano, D., van Riet, S., Hiemstra, P.S., & Villenave, R. (2019). Stem cell-based Lung-on-Chips: The best of both worlds? *Adv Drug Deliv Rev*, *140*, 12–32. <https://doi.org/10.1016/j.addr.2018.07.005>
- 25 Basil, M.C., Katzen, J., Engler, A.E., Guo, M., Herriges, M.J., Kathiriya, J.J., Windmueller, R., Ysasi, A.B., Zacharias, W.J., Chapman, H.A., Kotton, D.N., Rock, J.R., Snoeck, H.W., Vunjak-Novskovic, G., Whitsett, J.A., & Morrissey, E.E. (2020). The Cellular and Physiological Basis for Lung Repair and Regeneration: Past, Present, and Future. *Cell Stem Cell*, *26*(4), 482–502. <https://doi.org/10.1016%2Fj.stem.2020.03.009>
- 26 Roan, E., & Waters, C.M. (2011). What do we know about mechanical strain in lung alveoli? *Am J Physiol Lung Cell Mol Physiol*, *301*(5), L625–L635. <https://doi.org/10.1152/ajplung.00105.2011>
- 27 Waters, C.M., Roan, E., & Navajas, D. (2012). Mechanobiology in lung epithelial cells: measurements, perturbations, and responses. *Compr Physiol*, *2*(1), 1–29. <https://doi.org/10.1002%2Ffcphy.c100090>
- 28 Bennet, T. J., Randhawa, A., Hua, J., & Cheung, K.C. (2021). Airway-On-A-Chip: Designs and Applications for Lung Repair and Disease. *Cells*, *10*(7). <https://doi.org/10.3390/cells10071602>
- 29 Zhou, Y., Horowitz, J. C., Naba, A., Ambalavanan, N., Atabai, K., Balestrini, J., ... Thannickal, V. J. (2018). Extracellular matrix in lung development, homeostasis and disease. *Matrix Biol*, *73*, 77–104. <https://doi.org/10.1016/j.matbio.2018.03.005>
- 30 Chakraborty, A., & de Jesus Perez, V.A. (2020). Hiding in Plain Sight: The Basement Membrane in Pulmonary Vascular Remodeling. *Am J Respir Cell Mol Biol*, *63*(1), 13–14. <https://doi.org/10.1165/rcmb.2020-0100ED>
- 31 Stucki, A.O., Stucki, J.D., Hall, S.R., Felder, M., Mermoud, Y., Schmid, R.A., Geiser, T., & Guenat, O.T. (2015). A lung-on-a-chip array with an integrated bio-inspired respiration mechanism. *Lab Chip*, *15*(5), 1302–1310. <https://doi.org/10.1039/C4LC01252F>

- 32 Stucki, J., Hobi, N., Galimov, A., Stucki, A., Schneider-Daum, N., Lehr, C., Huwer, H., Frick, M., Funke-Chambour, M., Geiser, T., & Guenat, O. (2018). Medium throughput breathing human primary cell alveolus-on-chip model. *Scientific Reports*, *8*(1). <https://doi.org/10.1038/s41598-018-32523-x>
- 33 Zamprogno, P., Wuthrich, S., Achenbach, S., Thoma, G., Stucki, J. D., Hobi, N., Schneider-Daum, N., Lehr, C., Huwer, H., Geiser, T., Schmid, R. A., & Guenat, O. T. (2021). Second-generation lung-on-a-chip with an array of stretchable alveoli made with a biological membrane. *Commun Biol*, *4*(1), 168. <https://doi.org/10.1038/s42003-021-01695-0>
- 34 Xu, C., Zhang, M., Chen, W., Jiang, L., Chen, C., & Qin, J. (2020). Assessment of Air Pollutant PM2.5 Pulmonary Exposure Using a 3D Lung-on-Chip Model. *ACS Biomater Sci Eng*, *6*(5), 3081–3090. <https://doi.org/10.1021/acsbomaterials.0c00221>
- 35 Youn, J., Hong, H., Shin, W., Kim, D., Kim, H. J., & Kim, D. S. (2022). Thin and stretchable extracellular matrix (ECM) membrane reinforced by nanofiber scaffolds for developing in vitro barrier models. *Biofabrication*, *14*(2). <https://doi.org/10.1088/1758-5090/ac4dd7>
- 36 Nemati, S., Kim, S. J., Shin, Y. M., & Shin, H. (2019). Current progress in application of polymeric nanofibers to tissue engineering. *Nano Convergence*, *6*(1). <https://doi.org/10.1186/s40580-019-0209-y>
- 37 Chuchuy, J., Rogal, J., Ngo, T., Stadelmann, K., Antkowiak, L., Achberger, K., Liebau, S., Schenke-Layland, K., & Loskill, P. (2021). Integration of Electrospun Membranes into Low-Absorption Thermoplastic Organ-on-Chip. *Acs Biomaterials Science & Engineering*, *7*(7), 3006–3017. <https://doi.org/10.1021/acsbomaterials.0c01062>
- 38 Osorio, L. A., Silva, E., & Mackay, R. E. (2021). A Review of Biomaterials and Scaffold Fabrication for Organ-on-a-Chip (OOAC) Systems. *Bioengineering-Basel*, *8*(8). <https://doi.org/10.3390/bioengineering8080113>
- 39 Tas, S., Rehnberg, E., Bölükbas, D. A., Beech, J. P., Kazado, L. N., Svenningsson, I., ... Wagner, D. E. (2021). 3D printed lung on a chip device with a stretchable nanofibrous membrane for modeling ventilator induced lung injury. *bioRxiv*. <https://doi.org/10.1101/2021.07.02.450873>
- 40 Ibrahim, H. M., & Klingner, A. (2020). A review on electrospun polymeric nanofibers: Production parameters and potential applications. *Polymer Testing*, *90*. <https://doi.org/10.1016/j.polymertesting.2020.106647>
- 41 Reddy, V. S., Tian, Y. L., Zhang, C. Q., Ye, Z., Roy, K., Chinnappan, A., Ramakrishna, S., Liu, W., & Ghosh, R. (2021). A Review on Electrospun Nanofibers Based Advanced Applications: From Health Care to Energy Devices. *Polymers*, *13*(21). <https://doi.org/10.3390/polym13213746>
- 42 Xue, J. J., Wu, T., Dai, Y. Q., & Xia, Y. N. (2019). Electrospinning and Electrospun Nanofibers: Methods, Materials, and Applications. *Chemical Reviews*, *119*(8), 5298–5415. <https://doi.org/10.1021/acs.chemrev.8b00593>
- 43 Giannitelli, S. M., Costantini, M., Basoli, F., Trombetta, M., & Rainer, A. (2018). 8 - Electrospinning and microfluidics: An integrated approach for tissue engineering and cancer. In V. Guarino & L. Ambrosio (Eds.), *Electrofluidodynamic Technologies (EFDTs) for Biomaterials and Medical Devices* (pp. 139-155): Woodhead Publishing. <https://doi.org/10.1016%2FB978-0-08-101745-6.00008-6>
- 44 Rezaei, Z., & Mahmoudifard, M. (2019). Pivotal role of electrospun nanofibers in microfluidic diagnostic systems - a review. *Journal of Materials Chemistry B*, *7*(30), 4602–4619. <https://doi.org/10.1039/C9TB00682F>
- 45 Mahmoudifard, M., Vossoughi, M., & Soleimani, M. (2019). Different types of electrospun nanofibers and their effect on microfluidic-based immunoassay. *Polymers for Advanced Technologies*, *30*(4), 973-982. <https://doi.org/10.1002/pat.4531>
- 46 Matlock-Colangelo, L., Coon, B., Pitner, C. L., Frey, M. W., & Baeumner, A. J. (2016). Functionalized electrospun poly(vinyl alcohol) nanofibers for on-chip concentration of E. coli cells. *Anal Bioanal Chem*, *408*(5), 1327–1334. <https://doi.org/10.1007/s00216-015-9112-5>
- 47 Yang, D., Niu, X., Liu, Y., Wang, Y., Gu, X., Song, L., Zhao, R., Ma, L., Shao, Y., & Jiang, X. (2008). Electrospun Nanofibrous Membranes: A Novel Solid Substrate for Microfluidic Immunoassays for HIV. *Advanced Materials*, *20*(24), 4770–4775. <https://doi.org/10.1002/adma.200801302>
- 48 Han, S. W., & Koh, W. G. (2016). Hydrogel-Framed Nanofiber Matrix Integrated with a Microfluidic Device for Fluorescence Detection of Matrix Metalloproteinases-9. *Analytical Chemistry*, *88*(12), 6247–6253. <https://doi.org/10.1021/acs.analchem.5b04867>
- 49 Farahani, A., & Sereshti, H. (2020). An integrated microfluidic device for solid-phase extraction and spectrophotometric detection of opium alkaloids in urine samples. *Anal Bioanal Chem*, *412*(1), 129–138. <https://doi.org/10.1007/s00216-019-02214-1>
- 50 Zhang, Z., & Negrath, S. (2013). Microfluidics and cancer: are we there yet? *Biomed Microdevices*, *15*(4), 595-609. <https://doi.org/10.1007/s10544-012-9734-8>
- 51 Hou, S., Zhao, L., Shen, Q., Yu, J., Ng, C., Kong, X., ... Tseng, H. R. (2013). Polymer nanofiber-embedded microchips for detection, isolation, and molecular analysis of single circulating melanoma cells. *Angew Chem Int Ed Engl*, *52*(12), 3379-3383. <https://doi.org/10.1002/anie.201208452>
- 52 Wang, S., Liu, K., Liu, J., Yu, Z. T.-F., Xu, X., Zhao, L., ... Tseng, H.-R. (2011). Highly Efficient Capture of Circulating Tumor Cells by Using Nanostructured Silicon Substrates with Integrated Chaotic Micromixers. *Angewandte Chemie International Edition*, *50*(13), 3084-3088. <https://doi.org/10.1002/anie.2011005853>
- 53 Giannitelli, S. M., Costantini, M., Basoli, F., Trombetta, M., & Rainer, A. (2018). Electrospinning and microfluidics *Electrofluidodynamic Technologies (EFDTs) for Biomaterials and Medical Devices* (pp. 139-155). <https://doi.org/10.1016%2FB978-0-08-101745-6.00008-6>
- 54 Pasma, T., Grijpma, D., Stamatialis, D., & Poot, A. (2018). Flat and microstructured polymeric membranes in organs-on-chips. *Journal of The Royal Society Interface*, *15*(144), 20180351. <https://doi.org/10.1098/rsif.2018.0351>

- 55 Moghadas, H., Saidi, M. S., Kashaninejad, N., & Nguyen, N. T. (2018). A high-performance polydimethylsiloxane electrospun membrane for cell culture in lab-on-a-chip. *Biomicrofluidics*, 12(2). <https://doi.org/10.1063/1.5021002>
- 56 Lee, K. H., Kwon, G. H., Shin, S. J., Baek, J. Y., Han, D. K., Park, Y., & Lee, S. H. (2009). Hydrophilic electrospun polyurethane nanofiber matrices for hMSC culture in a microfluidic cell chip. *Journal of Biomedical Materials Research Part A*, 90a(2), 619-628. <https://doi.org/10.1002/jbm.a.32059>.
- 57 Kim, J. H., Park, J. Y., Jin, S., Yoon, S., Kwak, J. Y., & Jeong, Y. H. (2019). A Microfluidic Chip Embracing a Nanofiber Scaffold for 3D Cell Culture and Real-Time Monitoring. *Nanomaterials*, 9(4). <https://doi.org/10.3390/2Fnano9040588>
- 58 Higueta-Castro, N., Nelson, M. T., Shukla, V., Agudelo-Garcia, P. A., Zhang, W., Duarte-Sanmiguel, S. M., Englert, J.A., Lannuti, J.J., Hansford, D.J., & Ghadiali, S. N. (2017). Using a Novel Microfabricated Model of the Alveolar-Capillary Barrier to Investigate the Effect of Matrix Structure on Atelectrauma. *Scientific Reports*, 7. <https://doi.org/10.1038/s41598-017-12044-9>
- 59 Jain, P., Nishiguchi, A., Linz, G., Wessling, M., Ludwig, A., Rossaint, R., Möller, M., & Singh, S. (2021). Reconstruction of Ultra-thin Alveolar-capillary Basement Membrane Mimics. *Advanced Biology*, 5(8). <https://doi.org/10.1002/adbi.202000427>
- 60 Welling, L. W., Zupka, M. T., & Welling, D. J. (1995). Mechanical-Properties of Basement-Membrane. *News in Physiological Sciences*, 10, 30-35. <https://doi.org/10.1152/physiologyonline.1995.10.1.30>
- 61 Doryab, A., Taskin, M. B., Stahlhut, P., Schroppel, A., Wagner, D. E., Groll, J., & Schmid, O. (2020). A Biomimetic, Copolymeric Membrane for Cell-Stretch Experiments with Pulmonary Epithelial Cells at the Air-Liquid Interface (Vol. 31, 2004707, 2020). *Advanced Functional Materials*, 32(20). <https://doi.org/10.1002/adfm.202004707>
- 62 Yang, X. Y., Li, K. Y., Zhang, X., Liu, C., Guo, B. K., Wen, W. J., & Gao, X. H. (2018). Nanofiber membrane supported lung-on-a-chip microdevice for anti-cancer drug testing. *Lab on a Chip*, 18(3), 486-495. <https://doi.org/10.1039/C7LC01224A>
- 63 Radiom, M., He, Y., Peng-Wang, J., Baeza-Squiban, A., Berret, J. F., & Chen, Y. (2020). Alveolar mimics with periodic strain and its effect on the cell layer formation. *Biotechnology and Bioengineering*, 117(9), 2827-2841. <https://doi.org/10.1002/bit.27458>

П. Канабекова, А. Мартин, А. Кемелбекова, Г. Кульшарова

Наноталшықты мембраналарды микрофизиологиялық жүйелерде қолдану

«Ағзадағы-чип» микрофлюидті құрылғысы дәрі-дәрмектің ұйымшылдығын зерттеуде жануарларды сынауды алмастыра алатын перспективалы құрал болып табылады. «Өкпедегі-чип» құрылғысы бөлшектердің, газдардың және өкпе тініндегі химиялық заттардың ұйымшылдығын бағалау үшін, сондай-ақ ауырған жағдайда дәрілердің тиімділігі мен ұйымшылдығын зерттеу үшін қолданылады. Сонымен қатар, «өкпедегі-чип» құрылғысы денсаулықтың жағдайын, демікпе, қатерлі ісік, аутоиммунды және жұқпалы аурулар сияқты аурулардың кең ауқымын анықтауға мүмкіндік береді. Мақала микрофизиологиялық платформа шеңберінде функционалды базалды мембрана ретінде электрірілген наноталшықты мембраналарды қолдануға арналған. Мұнда микрофлюидті құрылғылар және «өкпедегі-чип» құрылғыларының тұжырымдамасы қысқаша берілген, базалды мембрананың маңыздылығы сипатталған. ПДМС, ПК сияқты қолданыстағы базалды мембрана үлгілері, гель негізіндегі мембраналар, оның ішінде оларды пайдалану барысында туындайтын қиындықтар мен кемшіліктер сипатталған. Электрірінді және наноталшықты мембраналар туралы түсініктеме берілген. «Өкпедегі-чип» құрылғысында қолданылатын наноталшықты мембраналар қарастырылған. Наноталшықты мембраналарды синтездеу үшін әртүрлі полимерлі материалдарды қолдану және мембрананы құрылғыға енгізудің әртүрлі әдістері сипатталған. Осылайша, электрірілген әдісімен алынған наноталшықты мембраналар жақсы механикалық қасиеттерді көрсетеді, иммундық жасушаларды тасымалдауға мүмкіндік береді және жасуша өміршеңдігі мен пролиферациясына әсер етпестен физиологиялық керілуді қамтамасыз етеді.

Кілт сөздер: микрофлюидтер, микрофизиологиялық, наноталшық, базалды мембрана, электроспиннинг, өкпедегі-чип, поликапролактон, жабысатын қоспа.

П. Канабекова, А. Мартин, А. Кемелбекова, Г. Кульшарова

Применение нановолоконных мембран в микрофизиологических системах

Микрофлюидные устройства «орган-на-чипе» — многообещающие платформы, которые потенциально могут заменить испытания на животных в исследованиях токсичности лекарств. Устройства «легкие-на-чипе» используются для оценки токсичности частиц, газов и химических веществ на ткани легких, а также для изучения эффективности и токсичности лекарств при заболеваниях. Устройства «легкие-на-чипе» позволяют имитировать здоровое состояние, а также широкий спектр заболеваний,

таких как астма, рак, аутоиммунные и инфекционные заболевания. Этот обзор посвящен использованию электропряденных нановолоконных мембран в качестве функциональной базальной мембраны в рамках микрофизиологической платформы. Здесь кратко представлена концепция микрофлюидных устройств и устройств «легкие-на-чипе», описана важность базальной мембраны. Затем изучены существующие модели базальной мембраны, такие как ПДМС, РК, мембраны на основе геля, включая проблемы и недостатки, связанные с их использованием. Затем вводится понятие электропрядения и нановолоконных мембран. Наконец, рассмотрены мембраны из нановолокна, применяемые в устройствах «легкие-на-чипе». Описано использование различных полимерных материалов для синтеза мембран из нановолокна и различные методы включения мембраны внутрь устройства. Таким образом, мембраны из нановолокна, полученные методом электропрядения, проявляют хорошие механические свойства, позволяют трансмигрировать иммунных клеток и обеспечивают физиологическое натяжение, не влияя на жизнеспособность и пролиферацию клеток.

Ключевые слова: микрофлюидика, микрофизиологический, нановолокно, базальная мембрана, электроспиннинг, легкие-на-чипе, поликапролактон, слипчивое соединение.

Information about authors*

Kanabekova, Perizat - MD, Researcher, Nazarbayev University, Kabanbay Batyr 53, 010000, Nur Sultan, Kazakhstan; e-mail: perizat.kanabekova@nu.edu.kz; <https://orcid.org/0000-0001-5753-4271>;

Martin, Alma - PhD, Instructor, Nazarbayev University, Kabanbay Batyr 53, 010000, Nur Sultan, Kazakhstan; e-mail: alma.martin@nu.edu.kz; <https://orcid.org/0000-0002-5592-8872>;

Kemelbekova, Ainagul - Assistant, Institute of Physics and Technology, Satbayev University, Satpaev str. 22, 050013, Almaty, Kazakhstan; e-mail: a.kemelbekova@satbayev.university; <https://orcid.org/0000-0003-4813-8490>;

Kulsharova, Gulsim - PhD, Assistant Professor, Nazarbayev University, Kabanbay Batyr 53, 010000, Nur Sultan, Kazakhstan; e-mail: gulsim.kulsharova@nu.edu.kz; <https://orcid.org/0000-0003-0642-5512>

*The author's name is presented in the order: *Last Name, First and Middle Names*

H. Shinohara¹, H. Nishide^{1*}

¹Research Institute for Science and Engineering, Waseda University, Tokyo, Japan

(*Corresponding author's e-mail: nishide@waseda.jp)

Polymer Complexes for Electrocatalytic Oxygen Evolution

Electrocatalytic water oxidation for oxygen gas evolution has been widely studied from the perspective of sustainable technology. However, the use of organic polymers as catalyst layers for this reaction remains undeveloped. We discuss, here, the prerequisites, characteristics, and advantages of π -conjugated polymers as electrochemical catalysts to modify anodic current collectors for water oxidation, including some examples by citing the previous works in literature. In section 3, we present our latest results, the use of an organic polymer complex of poly(ethylenedioxythiophene) and phytic acid supported by a hydrophilic poly(hydroxyethyl methacrylate) platform, which efficiently generates oxygen gas through anodic water oxidation.

Keywords: polymer complex, π -conjugated polymer, electrocatalyst, water oxidation, oxygen evolution, hydrophilic polymer, polythiophene, phytic acid.

Introduction

Water-splitting reaction to produce hydrogen and oxygen gases is one of the pinnacles of sustainable chemistry, and numerous efforts have focused on the electrocatalytic production of hydrogen and oxygen from water reduction and oxidation, respectively [1–7]. In addition to hydrogen production, the reductive process can follow other pathways, such as the reduction of nitrogen and carbon dioxide to produce ammonia, ethylene, ethanol, and propanol. Although the final targets are clean hydrogen and feedstock production for applications in sustainable energy and chemical industries, respectively, it is equally important to oxidize water into oxygen to balance and proceed with the counter-reductive reactions. The product of this reaction, oxygen, is the top three commodities and essential chemicals that are widely used in key oxidation reactions in chemical manufacturing, facilitated combustion, medical and respiratory care, wastewater treatment, and fish farming [8].

To generate oxygen from water, the catalysts for the electrochemical anodes have been extensively studied using molecular metal complexes, precious metal oxides, transition metal oxides, sulfides, and phosphides, as well as carbon and doped carbon materials [2, 9]. Catalysts that are used in catalytic processes with water at the polymer interface coated on a current-collecting anode substrate are of great interest; however, they remain at the early stage of development at present. These catalysts are advantageous for molecular engineering of organic polymers because they can modulate the electronic π -conjugated structure and the high hydrophilic surface area at the reaction front with water. Polymer-based catalysts are also attractive in film-forming processability, unlimited resources, non-toxicity, and chemical stability in acid/alkaline conditions.

The requirements for polymers with electrocatalytic water-oxidation capability involve the following: (i) a catalytic site for the water-oxidation reaction, (ii) an electrically conducting, three-dimensional network from the anodic substrate toward the reaction front, and (iii) a hydrophilic micro- and nanostructured scaffold for the pathways of reactant water molecules and product oxygen (microbubbles). A quick and effective method for examining such catalytic platforms is to use polymer complexes because they have been known to produce micro- and nanostructured functional polymers with hydrophilic/hydrophobic controlled properties. Bekturov et al. discussed a wide variety of polymer complexes approximately a half-century ago and summarized their findings [10, 11] with those of related fields [12, 13]. Some of these have prompted the practical application of polymer complexes in biomedical and nanomaterial fields [14–16]. For example, Kudaibergenov et al. successfully studied polymer complexation in oil engineering processes [17]. Furthermore, polyelectrolyte complexes and organic π -conjugated molecules have been extensively studied for dye fixation [18, 19]. Conductive hydrogels have been intensively studied for use in sensors and biomedical devices because fibrous assemblies of conjugated polymers create conducting network within hydrophilic scaffolds [20–22]. The application of conducting hydrophilic polymer complexes as electrocatalysts for water oxidation is expected to attract considerable interest.

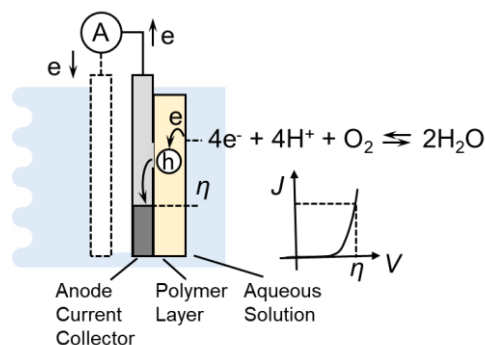


Figure 1. Energy-level diagram for the polymer-modified anode and water oxidation/oxygen evolution reaction and current density (J) curve for the oxygen evolution reaction; η is the overpotential to achieve the J

This article describes the theoretical background and chemical design of the electrochemical water oxidation to evolve oxygen gas in Section 1, as well as the characteristics of a series of electrocatalysts. In Section 2, we discuss the advantages and unsolved issues of organic (metal-free) π -conjugated polymers to modify the anodes for water oxidation by referring to recent works. Then in Section 3, our latest study on an electrocatalytic polymer is presented by using the polymer complex system composed of a conjugated polymer, a multivalent acid, and a hydrophilic polymer for efficient water oxidation. Finally, the perspectives are given for the emerging subject of facile water oxidation for on-site oxygen gas evolution.

1. Electrocatalytic water oxidation for oxygen gas production

Electrocatalysts play a key role in anodic water oxidation to generate oxygen and have been extensively studied in water electrolysis processes. While the cathodic reduction of protons or water to produce hydrogen involves a two-electron reaction, anodic water oxidation follows a four-electron/proton-coupled reaction (Fig. 1) and is more sluggish with a higher overpotential to overcome the kinetic barrier of the reaction than cathodic reductive reactions [9]. The oxygen evolution reaction is regarded as the rate-determining step or bottleneck for water-splitting reaction and reductive conversion to produce important feedstocks, which is hampered without an efficient oxygen-evolution catalyst. RuO_2 and IrO_2 exhibit excellent activity for water oxidation; however, both catalysts are made of precious metals and are chemically unstable during anodic operation and degraded into their per-oxidized forms [23]. Sustainable research has been devoted to developing electrocatalysts, with appropriate activity, composed of low-cost and widely available transition metal oxides such as MnO_x [24]. Attention has also been paid to carbon materials, including nanostructured carbons such as graphene and nanotubes. Heteroatom-doped carbon materials, such as N-, O-, and P-doped carbons, have recently emerged as promising electrocatalysts; however, their preparation is energy-consuming [25]. It is worth noting that these carbon materials might be unstable and oxidized to carbon dioxide at > 0.9 V vs. reversible hydrogen electrode (RHE).

Few studies have been reported on metal-free, organic-based electrocatalysis for oxygen evolution reactions, presumably because of their poor chemical stabilities under critical positive potential applications or oxidative conditions. Figure 1 shows the energy-level diagram of the polymer-modified anode for the oxidative reaction of water. Under the application of an anodic bias with a current collector, electrons are removed from the polymer layer to form a partially oxidized (doped) derivative (or hole formation), which successively extracts electrons from water molecule to oxidatively produce oxygen gas. The polymer catalytically mediates electron transfer from the water molecules to the anodic current collector; thus, it is more mediation-active, and the smaller bias or overpotential, η , (vs. the reaction equilibrium potential) promotes oxygen production.

2. Water oxidation using the polymer-modified anodes

Polyimides are thermo- and chemically stable and mechanically tough engineering plastics. Polyimide modification as a durable organic polymer-modified anode for efficient water oxidation to produce oxygen was reported by Li et al. [26]. They prepared poly(*p*-phenylene pyromellitic diimide) (PPPI, **1** in Figure 2) with a large and rough surface via in situ condensation after coating a solvent-soluble precursor polymer on carbon cloth (CC). Electrical impedance analysis indicated appropriate conductivity of the polyimide layer up to a thickness of 200 nm. Scanning electron microscopy (SEM) images and X-ray photoelectron spectroscopy revealed the metal-free and porous features of the polyimide layer coated on the substrate (the porous surface was attributed to the removal of water during polycondensation). The polyimide/CC worked as a du-

rable and effective anode over a wide pH range, with an anodic current density (J) of 10 mA/cm^2 at a potential of 1.7 V vs. RHE , which was only 110 mV higher than the working potential of the benchmark IrO_2/CC electrode (Figure 3(a)). A large J was obtained in an alkaline pH 13 solution with 99 % of Faraday efficiency. The smaller Tafel slope of 75 mV/dec , compared to that of IrO_2 (87 mV/dec , Figure 3(b)), indicated favorable reaction kinetics (CC as an effective current collector and imide group as a potential catalytic site). The Tafel slope ($\log J$ vs. the given potential) reflects the activity of the electrode material or the activation energy of the redox reaction at the electrode-solution interface, in which smaller slopes indicate better reaction kinetics. In addition, the polyimide/CC can be processed into a desired shape for practical use, including as a mechanically-tough flexible electrode.

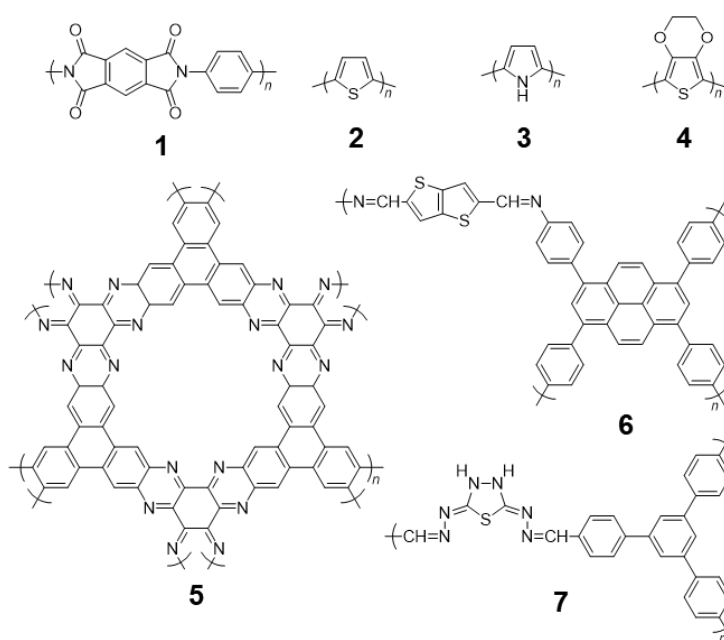


Figure 2. Chemical structures of π -conjugated polymers used to modify the anodic current collector

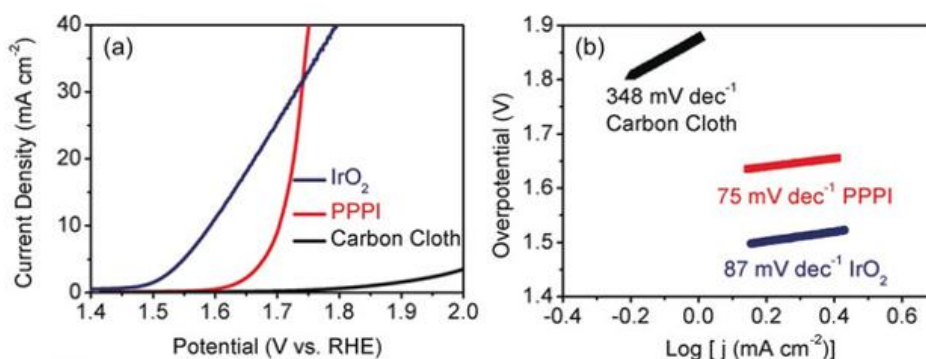


Figure 3. Water oxidation performance: (a) the anodic J and (b) Tafel slope of the poly(phenylene pyromellitic diimide) (PPPI)/CC and the benchmark IrO_2 (Copyright from Wiley-VCH 2018: Ref. 26))

Li et al. also prepared polythiophene (**2** in Figure 2) on an O-doped CC via electro-polymerization of thiophene [27]. The tough polythiophene layer with a thickness of 26 nm strongly adhered to carbon without detachment during the subsequent oxidative process. The polythiophene/O-doped CC anode worked as water oxidation catalysts to evolve oxygen. Its J reach up to 24 mA/cm^2 at 1.7 V vs. RHE in pH 13, which was twice that of the benchmark IrO_2 catalyst. The low overpotential and small Tafel slope of 61 mV/dec indicate the catalytic capability of the polythiophene/O-doped CC. The S 2p X-ray photoemission spectroscopy results suggested efficient redox catalysis of the thiophene, presumably involving a redox reaction between the sulfur and sulfone groups, which were strongly coupled with the O-doped carbon surface.

Zhang et al. designed a two-dimensional (2D) covalent organic framework composed of highly conjugated structures with appropriate carbon and nitrogen stoichiometry through DFT calculations [28]. Thermal

condensation of triphenylenehexamine and hexaketocyclohexane yielded a phenazine-linked basal plane framework with a C₄N composition (**5** in Figure 2). The crystalline-like framework was nanoporous, chemically robust, and exhibited water oxidation activity in an alkaline solution, with a J of 10 mA/cm² and a Tafel slope of 64 mV/dec. Carbon sites around nitrogen atoms in the conjugated structure are presumed to be the catalytic sites for the oxygen evolution reaction.

To achieve a current density of 10 mA/cm² and a Tafel slope of <100 mV/dec, Chen et al. wrapped a carbon nanotube with a conjugated 2D thiophene polymer connected to pyrene (**6** in Figure 2), which acted as an electrochemical water oxidation catalyst to evolve oxygen in an alkaline solution [29]. Jena et al. reported a covalent organic 3D framework that was prepared with a π -conjugated network of thiadiazole and triphenylbenzene (**7** in Figure 2) on a glassy carbon substrate. This exhibited electrocatalytic oxygen evolution activity with an onset of 250 mV and a J of 10 mA/cm² in an alkaline solution [30]. The low Tafel slope of 40 mV/dec and Faraday efficiency of 98 % were attributed to the oxidation pathway of four-electron oxidation. The π -conjugated network with a porous structure allows for fast charge and reactant transfer processes, and the catalytic activity per mass can reach up to 286 mA/mg.

He et al. prepared polypyrrole (**3** in Figure 2) doped with phytic acid (or inositol hexaphosphoric acid) on CC as a conductive hydrogel with efficient water oxidation electrocatalytic activity [31]. Pyrrole was oxidatively polymerized in situ on the CC in the presence of phytic acid. SEM images showed the formation of nanoparticles with a diameter of ca. 15 nm, which were interconnected to form a fibrous network on the carbon substrate. Spectroscopic analyses revealed the partial oxidation and homogeneous complexation of polypyrrole or doping with phytic acid with an optimum molar ratio of six. The contact angle of the water droplet was almost zero, indicating a super hydrophilic nature of the polymer complex. The polypyrrole-phytic acid/CC displayed water oxidation activity in an alkaline pH 10 solution with a high J and a low onset potential of 1.51 V vs. RHE, whereas both the polypyrrole without phytic acid and the CC substrate itself were negligible. A large J of 110 mA/cm² (for the cloth) was observed with a small Tafel slope of 55 mV/dec. Through DFT calculations, the phytic acid complexed with the doped polypyrrole was found to be involved with positively charged cyclohexane carbons, which are presumed to be the catalytic active sites. The doped polypyrrole was electrically conductive, forming a fast charge transfer network during water oxidation. The authors summarized a new direction for molecular/polymer-complex-based electrocatalysts formed on carbon substrates with high surface areas.

3. PEDOT–Phytic acid complex and its water oxidation activity

Poly(3,4-ethylenedioxythiophene) (PEDOT, **4** in Figure 2) is a representative conjugated polymer that is doped or oxidized with four (or more) thiophene units in the conjugated backbone to stabilize or store one hole or positive charge (doping level of ca. 25 %) accompanied by one counter anion compensation [32]. One of the typical counter acids (or anions) to complex with the positive charge of PEDOT is poly(styrene sulfonic acid) (PSS), forming a polyelectrolyte complex of PEDOT-PSS, which are commercially available as aqueous suspensions [33]. A variety of small-molecule acids can also be used as counter acids, including toluene sulfonic acid, perchloric acid, tetrafluoroboric acid, and trifluoroacetic acid. Among them, phytic acid (PA), six phosphonic acid-substituted cyclohexane, is a multivalent acid derivative that acts as a strong cation chelator that can suppress metal absorption into the human body [34]. In addition, PA was used in a polyaniline complex to produce a conductive hydrogel [35]. Meanwhile, poly(2-hydroxyethyl methacrylate) (pHEMA) is a hydrophilic polymer that adheres well to any substrate and is widely used as a platform for biomedical applications [35].

Herein, we focus on the combination of PEDOT, PA, and pHEMA, as a conducting polymer, chelating or complexing agent, and hydrophilic scaffold, respectively, to study its properties as an organic-based water oxidation electrocatalyst.

PEDOT-PSS water dispersion (Heraeus, CLEVIOSTM P VP Al 4083) and an ethanol solution of pHEMA (Sigma-Aldrich, average molecular weight: 3×10^5) were dropped on CC (Toyo Co., EC-CC1-060) as a current-collecting substrate and annealed for several hours at 120 °C to yield the conducting PEDOT coating. Without pHEMA, the PEDOT was directly delaminated from the CC substrate. pHEMA also caused a significant decrease in the surface hydrophilicity and contact angle of the PEDOT/pHEMA-modified CC (lower of Figure 4b). The thickness of the polymer layers was 300 nm. The obtained hydrophilic PEDOT/pHEMA/CC substrate was then immersed in an aqueous solution of PA (TCI). During this process, some PSS was eluted from the aqueous solution, which was confirmed by absorption spectroscopy. PA was irrigated into PEDOT-PSS and PSS was removed to form an effective PEDOT-PA complex through multivalent ionic interactions.

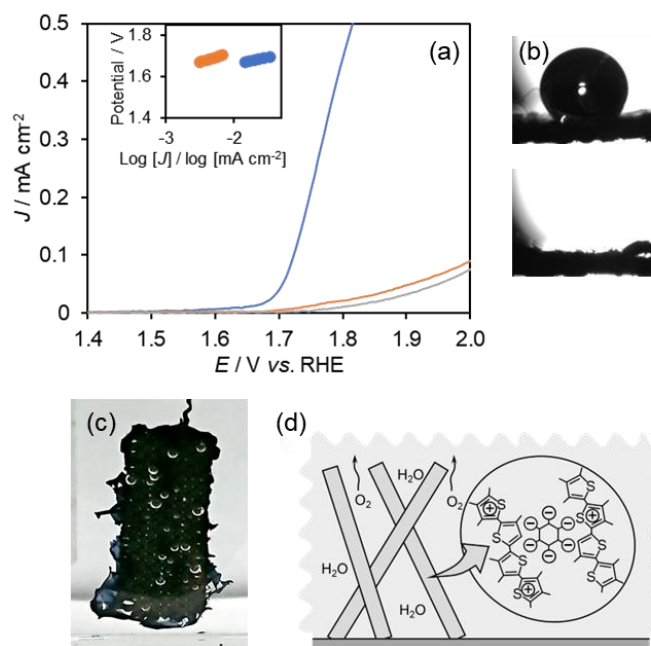


Figure 4. Water oxidation performance: (a) the anodic J and (inset) Tafel slope of the PEDOT-PA/pHEMA complex (blue), and PEDOT/pHEMA (red), and CC (gray), (b) Contact angle of (upper) CC substrate and (lower) PEDOT-PA/pHEMA-modified CC, (c) the PEDOT-PA/pHEMA complex during the anodic operation, and (d) Schematic image of the PEDOT-PA/pHEMA complex

The electrocatalytic performance of PEDOT-PA/pHEMA/CC was studied in an aqueous solution (pH 12) by linear sweep voltammetry using a potentiostat/galvanostat (Hokuto Denko, HZ-7000). Under anodic potential application, J for the PEDOT-PA/pHEMA complex can reach up to approximately 0.5 mA/cm^2 (Figure 4a), with an onset oxidation potential of 1.7 V vs. RHE. The anodic current corresponds to an oxidative reaction or water oxidation, and oxygen bubbles were continuously observed at the anode (Figure 4c). The J values for the PEDOT/pHEMA and CC substrate remained low, and the activity of the CC substrate immersed in the PA solution was also small, as in the control experiments. A small Tafel potential slope of 69 mV/dec was observed for the PEDOT-PA/pHEMA complex (inset of Figure 4a) in comparison with that for PEDOT/pHEMA. These results demonstrate the high activity of the PEDOT-PA/pHEMA complex layer for water oxidation to generate oxygen from water.

Figure 4d illustrates the PEDOT-PA/pHEMA polymer complex as a water oxidation electrocatalyst. The multivalent acidic PA ionically interacted with PEDOT to provide a partially doped (positively charged) PEDOT-fibrous pathway for electric conduction and to form a catalytic site. pHEMA immobilized the PEDOT-PA complex on the current collector and provided a hydrophilic platform for the water oxidation/oxygen evolution reaction. Overall, a simple complexation of the well-known PEDOT, PA, and pHEMA as a conductive polymer, chelating reagent, and hydrophilic polymer, respectively, successfully yielded an organic-based electrocatalyst for water oxidation to generate oxygen gas.

Conclusions

π -Conjugated polymers contain positive charges (holes) upon complexation with counter anions (doping). These holes are characterized by long lifetimes and tunable energy levels, which could mediate water oxidation in anodic potential applications. Organic-based polymer complexes composed of electrically conducting networks of conjugated polymers in the hydrophilic polymer platform for the reactant/product (water molecule/oxygen gas) pathway are possible metal-free, sustainable electrocatalyst candidates for facile water oxidation to generate oxygen in any decentralized location.

Acknowledgments

This work was partially supported by a Grand-in-Aid for Scientific Research No. 21H02018 from MEXT, Japan.

References

- 1 Armstrong, R.C., Wolfram, C.D., de Jong, K.P., Gross, R., Lewis, N. S., Boardman, B., Ragauskas, A. J., Ehrhardt-Martinez, K., Crabtree, G., & Ramana, M.V. (2016). The Frontiers of Energy. *Nature Energy*, 1(1), 15020. <https://doi.org/10.1038/nenergy.2015.20>
- 2 Ma, J. (2022). *Photo- And Electro-Catalytic Processes: Water Splitting, N₂ Fixing, CO₂ Reduction*. Wiley-VCH. <https://doi.org/10.1002/9783527830084>
- 3 Kim, J.H., Hansora, D., Sharma, P., Jang, J., & Lee, J.S. (2019). Toward Practical Solar Hydrogen Production — An Artificial Photosynthetic Leaf-to-Farm Challenge. *Chemical Society Reviews*, 48(7), 198–1971. <https://doi.org/10.1039/c8cs00699g>
- 4 Oka, K., Winther-Jensen, B., & Nishide, H. (2021). Organic π -Conjugated Polymers as Photocathode Materials for Visible-Light-Enhanced Hydrogen and Hydrogen Peroxide Production from Water. *Advanced Energy Materials*, 11(43), 2003724-n/a. <https://doi.org/10.1002/aenm.202003724>
- 5 Oka, K., Nishide, H., & Winther-Jensen, B. (2021). Completely Solar-Driven Photoelectrochemical Water Splitting Using a Neat Polythiophene Film. *Cell Reports Physical Science*, 2(1), 100306. <https://doi.org/10.1016/j.xcrp.2020.100306>
- 6 Nishide, H. (2022). Organic Redox Polymers as Electrochemical Energy Materials. *Green Chemistry*, 24, 4650–4679. <https://doi.org/10.1039/D2GC00981A>
- 7 Otep, S., Michinobu, T., & Zhang, Q. (2020). Pure Organic Semiconductor-Based Photoelectrodes for Water Splitting. *Solar RRL*, 4(8), 1900395-n/a. <https://doi.org/10.1002/solr.201900395>
- 8 Kirschner, M.J., Alekseev, A., Dowy, S., Grahl, M., Jansson, L., Keil, P., Lauermaun, G., Meilinger, M., Schmehl, W., Weckler, H., & Windmeier, C. (2000). Oxygen. *Ullmann's Encyclopedia of Industrial Chemistry*, 1–32. https://doi.org/10.1002/14356007.a18_329.pub2
- 9 Suen, N., Hung, S., Quan, Q., Zhang, N., Xu, Y., & Chen, H.M. (2017). Electrocatalysis for the Oxygen Evolution Reaction: Recent Development and Future Perspectives. *Chemical Society Reviews*, 46(2), 337–365. <https://doi.org/10.1039/c6cs00328a>
- 10 Bekturov, E.A., & Bimendina, L.A. (2005). Interpolymer Complexes. *Speciality Polymers* (pp. 99–147). Springer Berlin Heidelberg. https://doi.org/10.1007/3-540-10554-9_11
- 11 Bimendina, L.A., Kudaibergenov, S. E., & Bekturov, E.A. (2003). Polymer Complexes at Interfaces. *Journal of Macromolecular Science, Part C*, 43(1), 27–44. <https://doi.org/10.1081/MC-120018020>
- 12 Tsuchida, E., & Abe, K. (1982). *Interactions between Macromolecules in Solution and Intermacromolecular Complexes*. Springer Berlin Heidelberg. <https://doi.org/10.1007/BFb0017548>
- 13 Tsuchida, E., & Nishide, H. (2005). Polymer-Metal Complexes and their Catalytic Activity. *Molecular Properties* (pp. 1–87). Springer Berlin Heidelberg. https://doi.org/10.1007/3-540-08124-0_1
- 14 Geckeler, K. E., & Nishide, H. (2021). *Advanced Nanomaterials*. Wiley Subscription Services, Inc. <https://doi.org/10.1002/9783527628940>
- 15 Shinohara, H., Arai, T., & Nishide, H. (2002). Oxygen-Binding to Simple Cobaltporphyrins Combined with Polyvinylimidazole. *Macromolecular Symposia*, 186(1), 135–139. [https://doi.org/10.1002/1521-3900\(200208\)186:1<135::AID-MASY135>3.0.CO;2-R](https://doi.org/10.1002/1521-3900(200208)186:1<135::AID-MASY135>3.0.CO;2-R)
- 16 Preethi, N., Shinohara, H., & Nishide, H. (2006). Reversible Oxygen-Binding and Facilitated Oxygen Transport in Membranes of Polyvinylimidazole Complexed with Cobalt-Phthalocyanine. *Reactive & Functional Polymers*, 66(8), 851–855. <https://doi.org/10.1016/j.reactfunctpolym.2005.11.013>
- 17 Kudaibergenov, S. E., Tatykhanova, G. S., Sigitov, V. B., Nurakhmetova, Z. A., Blagikh, E. V., Gussenov, I. S., & Seilkhanov, T. M. (2016). Physico-Chemical and Rheological Properties of Gellan in Aqueous-Salt Solutions and Oilfield Saline Water. *Macromolecular Symposia*, 363(1), 20–35. <https://doi.org/10.1002/masy.201500139>
- 18 Moreno-Villoslada, I., Torres, C., González, F., Shibue, T., & Nishide, H. (2009). Binding of Methylene Blue to Polyelectrolytes Containing Sulfonate Groups. *Macromolecular Chemistry and Physics*, 210(13–14), 1167–1175. <https://doi.org/10.1002/macp.200900042>
- 19 Moreno-Villoslada, I., Torres-Gallegos, C., Araya-Hermosilla, R., & Nishide, H. (2010). Influence of the Linear Aromatic Density on Methylene Blue Aggregation around Polyanions Containing Sulfonate Groups. *The Journal of Physical Chemistry. B*, 114(12), 4151–4158. <https://doi.org/10.1021/jp909105r>
- 20 Guiseppi-Elie, A. (2009). Electroconductive Hydrogels: Synthesis, Characterization and Biomedical Applications. *Biomaterials*, 31(10), 2701–2716. <https://doi.org/10.1016/j.biomaterials.2009.12.052>
- 21 Kudaibergenov, S.E., & Okay, O. (2021). Behaviors of Quenched Polyampholytes in Solution and Gel State. *Polymers for Advanced Technologies*, 32(7), 2639–2654. <https://doi.org/10.1002/pat.5112>
- 22 Kudaibergenov, S.E. (2020). Macromolecular Complexes of Polyampholytes. *Pure and Applied Chemistry*, 92(6), 839–857. <https://doi.org/10.1515/pac-2019-1104>
- 23 Chalupczok, S., Kurzweil, P., Hartmann, H., & Schell, C. (2018). The Redox Chemistry of Ruthenium Dioxide: A Cyclic Voltammetry Study—Review and Revision. *International Journal of Electrochemistry*, 2018, e1273768. <https://doi.org/10.1155/2018/1273768>
- 24 Zhou, F., Izgorodin, A., Hocking, R.K., Spiccia, L., & MacFarlane, D.R. (2012). Electrodeposited MnO_x Films from Ionic Liquid for Electrocatalytic Water Oxidation. *Advanced Energy Materials*, 2(8), 1013–1021. <https://doi.org/10.1002/aenm.201100783>

- 25 Zhai, Q., Pan, Y., & Dai, L. (2021). Carbon-Based Metal-Free Electrocatalysts: Past, Present, and Future. *Accounts of Materials Research*, 2(12), 1239–1250. <https://doi.org/10.1021/accountsmr.1c00190>
- 26 Lin, Y., Feng, W., Zhang, J., Xue, Z., Zhao, T., Su, H., Hirano, S., Li, X., & Chen, J. (2018). A Polyimide Nanolayer as a Metal-Free and Durable Organic Electrode Toward Highly Efficient Oxygen Evolution. *Angewandte Chemie (International Ed.)*, 57(38), 12563–12566. <https://doi.org/10.1002/anie.201808036>
- 27 Zhang, S., Xue, Z., Lin, X., Lin, Y., Su, H., Hirano, S., Li, X., & Chen, J. (2020). Autoxidation of Polythiophene Tethered to Carbon Cloth Boosts its Electrocatalytic Activity towards Durable Water Oxidation. *Journal of Materials Chemistry. A, Materials for Energy and Sustainability*, 8(38), 19793–19798. <https://doi.org/10.1039/d0ta06368a>
- 28 Yang, C., Yang, Z., Dong, H., Sun, N., Lu, Y., Zhang, F., & Zhang, G. (2019). Theory-Driven Design and Targeting Synthesis of a Highly-Conjugated Basal-Plane 2D Covalent Organic Framework for Metal-Free Electrocatalytic OER. *ACS Energy Letters*, 4(9), 2251–2258. <https://doi.org/10.1021/acseenergylett.9b01691>
- 29 Liu, C., Liu, F., Li, H., Chen, J., Fei, J., Yu, Z., Yuan, Z., Wang, C., Zheng, H., Liu, Z., Xu, M., Henkelman, G., Wei, L., & Chen, Y. (2021). One-Dimensional van der Waals Heterostructures as Efficient Metal-Free Oxygen Electrocatalysts. *ACS Nano*, 15(2), 3309–3319. <https://doi.org/10.1021/acsnano.0c10242>
- 30 Mondal, S., Mohanty, B., Nurhuda, M., Dalapati, S., Jana, R., Addicoat, M., Datta, A., Jena, B. K., & Bhaumik, A. (2020). A Thiadiazole-Based Covalent Organic Framework: A Metal-Free Electrocatalyst toward Oxygen Evolution Reaction. *ACS Catalysis*, 10(10), 5623–5630. <https://doi.org/10.1021/acscatal.9b05470>
- 31 Hu, Q., Li, G., Liu, X., Zhu, B., Chai, X., Zhang, Q., Liu, J., & He, C. (2019). Superhydrophilic Phytic-Acid-Doped Conductive Hydrogels as Metal-Free and Binder-Free Electrocatalysts for Efficient Water Oxidation. *Angewandte Chemie (International Ed.)*, 58(13), 4318–4322. <https://doi.org/10.1002/anie.201900109>
- 32 Elschner, A., Kirchmeyer, S., Lovenich, W., Merker, U., & Reuter, K. (2010). *PEDOT*. CRC Press. <https://doi.org/10.1201/b10318>
- 33 Piro, B., Mattana, G., Zrig, S., Anquetin, G., Battaglini, N., Captao, D., Maurin, A., & Reisberg, S. (2018). Fabrication and Use of Organic Electrochemical Transistors for Sensing of Metabolites in Aqueous Media. *Applied Sciences*, 8(6), 928. <https://doi.org/10.3390/app8060928>
- 34 NCBI (n.d.). Phytic Acid. *National Library of Medicine*. <https://www.ncbi.nlm.nih.gov/mesh/68010833>
- 35 Pan, L., Yu, G., Zhai, D., Lee, H.R., Zhao, W., Liu, N., Wang, H., Tee, B.C., Shi, Y., Cui, Y., & Bao, Z. (2012). Hierarchical Nanostructured Conducting Polymer Hydrogel with High Electrochemical Activity. *Proceedings of the National Academy of Sciences – PNAS*, 109(24), 9287–9292. <https://doi.org/10.1073/pnas.1202636109>

Х. Шиохара, Х. Нишиде

Оттегінің электрокаталитикалық бөлінуіне арналған полимерлік комплекстер

Оттегі газын шығару үшін судың электрокаталитикалық тотығуы тұрақты технологиялар тұрғысынан кеңінен зерттелген. Дегенмен, бұл реакция үшін катализатор қабаттары ретінде органикалық полимерлерді пайдалану әлі дамымаған. Мақалада π -түйіндес полимерлерді судың тотығуында анодтық тоқалғышты модификациялау үшін электрохимиялық катализатор ретінде пайдаланудың негізі, сипаттамалары және артықшылықтары, соның ішінде алдыңғы жұмысқа сілтемелері бар кейбір мысалдар қарастырылған. Үшінші бөлімде судың анодты тотығуы арқылы газ тәрізді оттегін тиімді генерациялайтын гидрофильді поли(гидроксиэтилметакрилат) платформасымен қамтамасыз етілген поли(этилендиокситиофен) және фитин қышқылының органикалық полимер кешенін қолдану бойынша авторлардың соңғы зерттеулерінің нәтижелері берілген.

Кілт сөздер: полимер кешені, π -түйіндес полимер, электрокатализатор, судың тотығуы, оттегінің бөлінуі, гидрофильді полимер, политиофен, фитин қышқылы.

Х. Шиохара, Х. Нишиде

Полимерные комплексы для электрокаталитического выделения кислорода

Электрокаталитическое окисление воды с целью выделения газообразного кислорода широко изучено с точки зрения устойчивых технологий. Однако использование органических полимеров в качестве каталитических слоев для этой реакции остается неразработанным. В данной статье обсуждены предпосылки, характеристики и преимущества применения π -сопряженных полимеров в качестве электрохимических катализаторов для модификации анодных токосъемников при окислении воды, включая некоторые примеры с литературными ссылками на предыдущие работы. В разделе 3 представлены ре-

зультаты последних исследований авторов по использованию органического полимерного комплекса поли(этилендиокситиофена) и фитиновой кислоты, поддерживаемого гидрофильной поли(гидроксиэтилметакрилатной) платформой, который эффективно генерирует газообразный кислород посредством анодного окисления воды.

Ключевые слова: полимерный комплекс, π -сопряженный полимер, электрокатализатор, окисление воды, выделение кислорода, гидрофильный полимер, политиофен, фитиновая кислота.

Information about authors *

Shinohara, Hiromi — Senior Researcher, Research Institute for Science and Engineering, Waseda University, 3-4-1 Okubo, Shinjuku, Tokyo 169-8555, Japan; e-mail: hiromi.shinohara@aoni.waseda.jp; <https://orcid.org/0000-0003-2089-3435>;

Nishide, Hiroyuki (*corresponding author*) — Research Professor, Research Institute for Science and Engineering; Professor Emeritus, Waseda University, 3-4-1 Okubo, Shinjuku, Tokyo 169-8555, Japan; e-mail: nishide@waseda.jp; <https://orcid.org/0000-0002-4036-4840>

*The author's name is presented in the order: *Last Name, First and Middle Names*

D.A. Michurov, O.Yu. Kolosova, V.I. Lozinsky*

A.N. Nesmeyanov Institute of Organoelement Compounds of RAS, Moscow, Russia

(*Corresponding author's e-mail: loz@ineos.ac.ru)

Cryostructuring of Polymeric Systems.

61. Physicochemical Properties of Poly(vinyl alcohol) Cryogels Prepared on the Basis of Urea-Containing DMSO-Solutions of the Polymer and Evaluation of the Resultant Gel Materials as Potential Drug Carriers

Macroporous physical poly(vinyl alcohol)-based (PVA) cryogels were prepared originating from the dimethylsulfoxide solutions of the polymer that contained urea additives. The variables of the cryotropic gel-formation process were its temperature and the concentration of the added urea, which caused the increase in the rigidity and heat endurance of the resultant cryogels, as well as promoted widening of the macropores in the gel matter. Subsequent rinsing of the DMSO-swollen cryogels with the water excess resulted in the water-swollen PVA cryogels with simultaneous further increase in their rigidity. These gel matrices were tested with respect of their potential to operate as the polymeric carriers in the drug delivery systems. Loading of such water-swollen cryogels with a model drug, ϵ -amino caproic acid, and then studies of its release kinetics revealed that urea content in the initial PVA solutions used for the freeze-thaw-induced formation of the DMSO-swollen cryogels played the key role for the release characteristics of the drug-loaded water-swollen gel carrier. Namely, PVA cryogels prepared in the presence of a higher concentration of urea possessed the larger pores and, as a result, the drug release occurred somewhat faster.

Keywords: poly(vinyl alcohol) cryogels, dimethylsulfoxide polymer solutions, urea additives, cryogenic processing temperature, drug delivery cryogel carriers.

Introduction

Polymeric cryogels are the macroporous gel materials formed as a result of cryogenic processing (freezing — incubation in a frozen state — defrosting) of the molecular or colloidal solutions that contain certain low-molecular or high-molecular precursors [1–8]. Various polymeric cryogels are of both significant scientific and intensively developing applied interests. In particular, the latter assertion concerns the biomedical areas, where the use of different biocompatible cryogels has already revealed promising prospects [1, 7, 9–16]. One of the important types of these materials is the so-called drug delivery systems, e.g. the drug-carrying covers on wound and burns, and the respective cryogels are tested in details for such biomedical applications. Specific morphology of cryogels with the system of interconnected macropores allows loading the polymeric matrix with the drugs of a diverse chemical structure, aggregate state (soluble, solid and gaseous) and size (from the low-molecular weight substances to the polymeric ones and even nano/microparticles). Therefore, these gel materials are well-suitable for the drug delivery aims [1, 2, 9, 12–24]. With that, the polymeric matrix of similar delivery systems must be non-toxic, biocompatible and, if required, must be biodegradable. As regards the non-degradable (by the human organisms) cryogenically-structured polymeric carriers used in this field, the poly(vinyl alcohol)-based cryogels (PVACGs) [1, 4, 25–33] are of gross interest. Similar non-covalent macroporous gel materials [1, 4, 27, 34–41] are formed by the mechanism of interchain cross-linking via H-bonding. These cryogels possess excellent physico-mechanical properties, high heat endurance, and biocompatibility [1, 26–30, 39, 41]. Such combination of their useful characteristics opens wide possibilities for the biomedical applications of PVACGs [1, 14, 20, 27, 28, 33, 41–46].

The fabrication of PVACGs is a rather simple procedure, which includes the preparation of aqueous solution of this polymer, the addition, when it is required, soluble or insoluble (disperse filler) additives, then freezing the resultant feed liquid system at desired minus temperature for certain time period and subsequent thawing of frozen samples [1, 2, 35–30, 34–39]. The properties of thus prepared PVACGs depend on the molecular-weight characteristics of the initial polymer, its deacylation degree and chain tacticity, type and con-

centration of additives, when those are used, as well as on the regimes of all stages of the cryogenic processing and the number of freeze-thaw cycles [1, 2, 19, 20, 24–30, 36–40].

Apart from the PVACGs prepared from the aqueous solution of this gelling polymer, PVACGs are known to be formed based on its dimethylsulfoxide (DMSO) solutions [27, 34, 47–49]. In this case, it is found that some low-molecular solutes influenced on the physico-chemical properties of the resultant cryogels oppositely in comparison to the effects observed in aqueous media [50, 51]. Thus, it is revealed that such well-known chaotropes as urea or guanidine hydrochloride, the additives of which cause marked decrease in the gel strength and heat endurance of the PVACGs prepared from the aqueous polymer solutions [52, 53], in the DMSO media exhibit the antichaotropic (so-called *kosmotropic*) influence on the respective cryogels causing the considerable increase in their rigidity and fusion temperatures [51]. The studies of such phenomenon show that its main reason consisted in the urea-induced decrease in the solvation ability of DMSO with respect to PVA. As a result, this effect is the key factor responsible for strengthening of the structure formation upon the freeze-thaw gelation of this polymer in DMSO additionally containing additives like urea, which is capable of competing with PVA for the solvent. After the exhaustive rinsing of such PVACGs with water, i.e. after the removal of soluble additives and replacement of DMSO for H₂O, the elastic modulus and fusion temperature values of thus treated cryogels turned out to be higher significantly as compared to the PVACGs formed in the medium of pure water. In other words, it was possible to fabricate “aqueous” PVACGs possessing increased mechanical and thermal properties.

Considering these effects, we decided to use such preparation scheme, i.e. to fabricate “primary” PVACGs in the DMSO medium with urea additives, further to rinse thus formed gel systems by an excess of water, load the resultant “secondary” PVACGs with a model drug (ϵ -amino caproic acid (ϵ -ACA) in this case), and evaluate the release kinetics of this known hemostatic agent [54] from the cryogel carriers.

Therefore, the tasks of this study are as follows:

- (i) to reveal the influence of the concentration of added urea and the temperature of the cryotropic gel-formation on the physico-chemical characteristics of final cryogels;
- (ii) to trace how the same preparation parameters are reflected on the drug release behavior.

Experimental

2.1 Materials

The following substances were used: poly(vinyl alcohol) (molecular weight of ca. 86 kDa, the deacetylation degree of 100 %; Acros Organics, USA), urea (“ultra pure” grade) and ϵ -amino caproic acid (>99.5 %) (both Sigma, USA). Dimethyl sulfoxide (>99 %; Komponent-Reaktiv, Russian Federation) was additionally purified by the freeze-out procedure.

2.2. Methods

2.2.1. Preparation of PVA cryogels

The preparation of the feed PVA solutions and then their cryogenic processing were carried out as described previously [51]. Briefly, a known amount of dry polymer was dispersed in a calculated volume of DMSO to reach a PVA concentration of 100 g/L. The mixture was incubated for 18 h at room temperature for swelling of the polymer, followed by the system heating for 1 h on a boiling water bath under stirring until the completion of PVA dissolution. Subsequently, the required amount of dry urea was added and dissolved in this liquid system after its cooling to room temperature.

Preparation of the “primary” PVACGs for the physico-mechanical tests was performed in the sectional duralumin moulds (inner diameter 15 mm, height 10 mm). The gel samples of the same composition for the measurements of their fusion temperatures (T_f) were formed in transparent polyethylene test tubes (inner diameter 10 mm), the 3-mL portions of the polymer solution were poured, and a stainless steel ball (diameter 3.5 mm, weight 0.275 ± 0.005 g) was placed on the bottom of each tube. The containers and the tubes were put into the chamber of an FP 45 HP precision programmable cryostat (Julabo, Germany), where the samples were frozen and incubated for 12 h at the preset minus temperature. Then, the temperature was raised to 20 °C at a rate of 0.03 °C/min controlled by the cryostat microprocessor. Onwards, each cylindrical gel sample prepared in the duralumin moulds was subjected to the physico-mechanical tests (section 2.2.2) followed by immersing the sample in the vessel with 100 mL of pure water, where the cryogel was incubated with periodical stirring for 24 h. Such rinsing procedure was repeated 6 times to extract solutes from the samples and replace DMSO for water inside the gel bulk thus resulting in the transformation of the “primary” PVACGs to the “secondary” ones.

2.2.2. Physico-mechanical measurements

The compression Young's modulus (E) of the PVACG samples was determined from the linear portion of the stress–strain dependence using a TA-Plus automatic texture analyzer (Lloyd Instruments, UK) at a loading rate of 0.3 mm/min. Upon these experiments the applied load was automatically increased from 0 to 5 N. The tests were performed until reaching a 30 % of deformation. The measurements were performed for both “primary” and “secondary” PVACGs. The E values were measured for three parallel samples; the samples were examined in three to five independent experiments. The obtained results were averaged.

2.2.3. Heat endurance of PVA cryogels

Fusion temperatures (T_f) of the “primary” PVACGs were measured in accordance with the earlier reported procedure [29, 30, 50–52] by placing upside down the tightly corked polyethylene tube containing cryogel with the stainless steel ball (3.5 mm in diameter and 0.275 ± 0.005 g in weight) at the bottom into the water bath. The bath temperature was increased at a rate of 0.4 ± 0.1 °C/min. The gel fusion point was detected as the temperature when the ball fell down onto the stopper of the test tube after passing through the fused gel. The T_f values were measured for three parallel samples; the samples were examined in three independent experiments. The obtained results were averaged.

2.2.4. Optical microscopy studies

Macroporous morphology of the PVACG samples was investigated as described earlier [51] with use of an Eclipse 55i optical microscope (Nikon, Japan) equipped with an MMC-50C-M system (MMCSOft, Russian Federation) for digital image recording. In the as-prepared “primary” cryogels, DMSO was replaced by pure water, and the resultant “secondary” cryogels were cut for the 10- μ m thick sections orthogonally to the axis of cylindrical samples using a SM-1900 cryomicrotome (Leica, Germany). Each section was placed on the microscope glass, which was then immersed into a 1 % aqueous solution of Congo red (the standard dye used for painting PVA-based materials [61], including the PVA cryogels [19, 24, 29, 30, 35, 36, 50–53]) for staining for 10 s, and then rinsed with pure water. The excess of liquid was removed with a filter paper. Then, the section was poured with a drop of fixing solution (solution of 1 g of gelatin in 12 mL of 50 % aqueous glycerol and 0.2 g of phenol as a bacteriostatic agent) and sealed with a cover glass. Prior to the studies, the samples were stored in a closed vessel at 4 °C.

2.2.5. Loading of PVACGs with a model drug substance and its release from the gel carrier

The volumes of the cylindrical samples of “secondary” PVACGs (V_{sec}) were measured. Each sample was immersed into a vial with aqueous ϵ -ACA solution of necessary volume ($V_{\epsilon\text{-ACA}}$) so that the sum volume ‘cryogel+liquid’ turned out to be equal to 4 mL. Since the V_{sec} values depended on the urea concentration in the feed PVA solutions, the ϵ -ACA concentrations in the loading solutions were prepared with the intention to reach after the equilibration approximately the same ϵ -ACA amount (m_{eq}) being entrapped in these gel carriers (Table).

The release of ϵ -ACA from the amino-acid-loaded PVACGs was registered using the conductometry technique (a F30 conductometer, Mettler-Toledo, Switzerland). Each sample of the ϵ -ACA-saturated cryogel was placed into a beaker with 30 mL of pure water, and the values of electrical conductivity were measured under the instructions given in the manual for this instrument. The concentration of the amino acid in the respective solutions was found from the preliminary obtained calibration plot.

T a b l e

Composition of the systems used in the loading-release experiments

Urea concentration in the feed PVA solution, mol/L	V_{sec} , mL	$V_{\epsilon\text{-ACA}}$, mL	ϵ -ACA concentration in the loading solution, mg/L	m_{eq}^a , mg
0	1.29	2.71	23.3	29.9
2	1.01	2.99	30.0	30.0
4	0.79	3.21	37.9	29.9

^{a)} After the equilibration of the ‘cryogel+liquid’ system

Results and Discussion

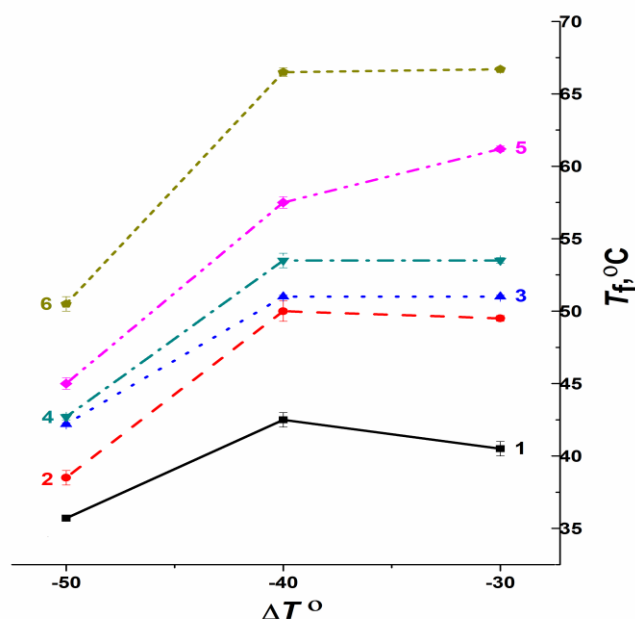
3.1. Preparation of “primary” and “secondary” PVACGs

As indicated in the ‘Introduction’, the subjects of this study are the PVA cryogels possessing both the increased durability and the potential ability to operate as the efficient biocompatible carriers for the drug

delivery systems like the covers on wounds or burns. To achieve the former goal, we selected the approach based on the earlier found kosmotropic influence of urea introduced in the feed DMSO solutions of PVA to be gelled cryogenically [51]. The respective PVACGs were prepared (section 2.2.1) starting from the urea-free (reference samples) and the urea-containing DMSO solutions of the polymer. Its concentration was 100 g/L in all the cases, and the content of urea was one of the following series: 0, 1.0, 1.5, 2.0, 3.0 or 4.0 mol/L. Such solutions were cryogenically solidified at the desired freezing temperature (T_{fr}): either -11.6 °C, or -21.6 °C, or -31.6 °C. Since the DMSO crystallization point (T_0) is $+18.4$ °C [55], in terms of the ΔT values equal to the $T_{fr}-T_0$ [50, 51], this parameter had the following moduli: $\Delta T = -30^\circ$, -40° and -50° , respectively. Such ΔT values testify that feed polymeric solutions were frozen at the temperatures 30, 40 or 50 degrees lower than the crystallization point of a neat DMSO. After storing frozen and then thawing the “primary” PVACGs were obtained (section 2.2.1). Subsequent measurement of their characteristics allowed us tracing the influence of such varying parameters as the urea concentration and the freezing temperature on the physico-chemical properties of these DMSO-swollen cryogels. Further change of DMSO for water resulted in the target “secondary” water-swollen PVACGs, which were then loaded with a model drug (ϵ -ACA), and its release kinetics was evaluated.

3.2. Thermal and physico-mechanical properties of the PVACGs under study

Since PVACGs are physical gel materials, the spatial network of which is maintained by the thermo-dissociating interchain H-bonds between the OH-groups of neighboring chains, the fusion temperature of PVACGs is the indicator of both the amount of such non-covalent bonds and their cooperativity within the microcrystallinity zones performing as the knots of the supramolecular polymeric network [25–30, 37]. In this respect, the elevation of the fusion temperature values (T_f) of PVACGs formed in the DMSO medium with increasing concentration of added urea (Fig. 1) points to some increase in the total amount of interchain H-bonds responsible for the heat endurance of the physical gels, in general [56], and of the PVA cryogels under consideration in the present study, in particular. In other words, the data of Fig. 1 confirm the earlier observed the antichaotropic influence [51] of urea on the freeze-thaw gelation of PVA in the DMSO medium.



Urea concentration: 0 (curve 1), 1.0 (curve 2), 1.5 (curve 3), 2.0 (curve 4), 2.0 (curve 5) and 4.0 (curve 6) mol/L

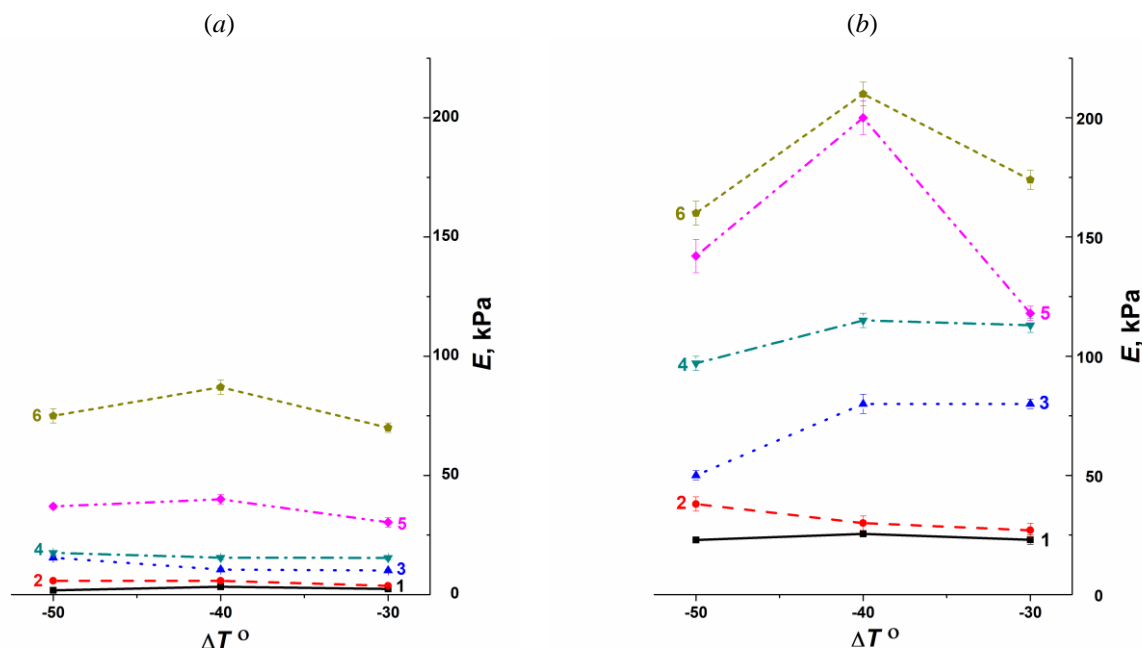
Figure 1. The values of the gel fusion temperature (T_f) of the “primary” PVA cryogels prepared on the basis of the urea-free and the urea-containing DMSO solutions of the polymer as dependent on the temperature of the cryotropic gelation process

The dependences in Fig. 1 demonstrate that both the urea-free and the urea-containing PVACGs prepared at the cryogenic processing temperatures $\Delta T = -30^\circ$ and -40° possessed higher heat endurance in comparison with the cryogels prepared at $\Delta T = -50^\circ$, thus indicating the decreased gel-formation efficiency with lowering the freezing temperature. Such a trend is known to be inherent in the PVA cryotropic gelation of

the urea-free aqueous solutions [27, 29], i.e., similar effect is common for the freeze-thaw gel-formation of this polymer in both the aqueous and the organic media.

In turn, the graphs in Figure 2 (plots *a* and *b*) combine the experimental data on the rigidity (in the terms of Young's modulus — E) of the “primary” and the “secondary” PVACGs. Thus, it is possible to compare their physico-mechanical properties depending on the ΔT values for the samples that contained various amount of urea in the composition of initial DMSO solutions of the PVA, as well as to demonstrate pictorially a paramount increase in the gel strength caused by the transition from the DMSO-containing “primary” cryogels to the aqueous “secondary” ones. The analysis of these results revealed the following trends with the respect of the factors capable of exerting major effects on the elasticity of the cryogels under discussion.

First, this work confirms previous study [51] on kosmotropic-like “action” of urea additives on the PVA cryotropic gel-formation in the DMSO medium. If in the case of the formation of cryogels via the freeze-thaw processing of the aqueous urea-containing PVA solutions, the increase in the urea concentration gave rise to the crucial decrease in the gel strength because of the urea-induced inhibition of the interchain PVA-PVA H-bonding [52, 53] while in the DMSO medium the effects were opposite. This result is stipulated by the competition of urea with PVA for the solvent, since the urea forms rather stable H-bonds with DMSO thus promoting the partial change of the PVA-DMSO solvate interactions for the additional interchain PVA-PVA H-bonding [51]. In particular, with increasing the initial urea concentration from 0 to 4 mol/L the E values of the respective “primary” PVACGs grew from 1.8–3.3 kPa up to 70–87 kPa, i.e. more than about 30-fold (Fig. 2*a*). Also, Figure 2*b* illustrates that this trend was retained for the “secondary” cryogels.



Urea concentration: 0 (curve 1), 1.0 (curve 2), 1.5 (curve 3), 2.0 (curve 4), 2.0 (curve 5) and 4.0 (curve 6) mol/L

Figure 2. The values of the elastic modulus of the “primary” (*a*) and the “secondary” (*b*) PVA cryogels prepared on the basis of the urea-free and the urea-containing DMSO solutions of the polymer as dependent on the temperature of the cryotropic gelation process

Second, the influence of the cryogenic stages temperature (i.e. ΔT values) within its range from -30° to -50° on the rigidity of the resultant “primary” PVACGs (Fig. 2*a*) had a weakly expressed bell-like character being more evidently pronounced with an increase in the urea concentration in the initial DMSO solutions of PVA (Fig. 2*a*). For the PVACGs prepared in the urea-free aqueous media such bell-like temperature dependences are well-known (e.g., see [29]). The reason is the competition of different factors that influence on the characteristics of the resultant PVACGs. Thus, at the same polymer concentration in an initial solution, the lower is the temperature of frozen system the higher is the PVA concentration in the unfrozen liquid microphase [57–59]. This effect promotes the polymer–polymer interactions and the formation of cryogels. However, a regular increase in viscosity and the retardation of the thermal mobility of chains and their seg-

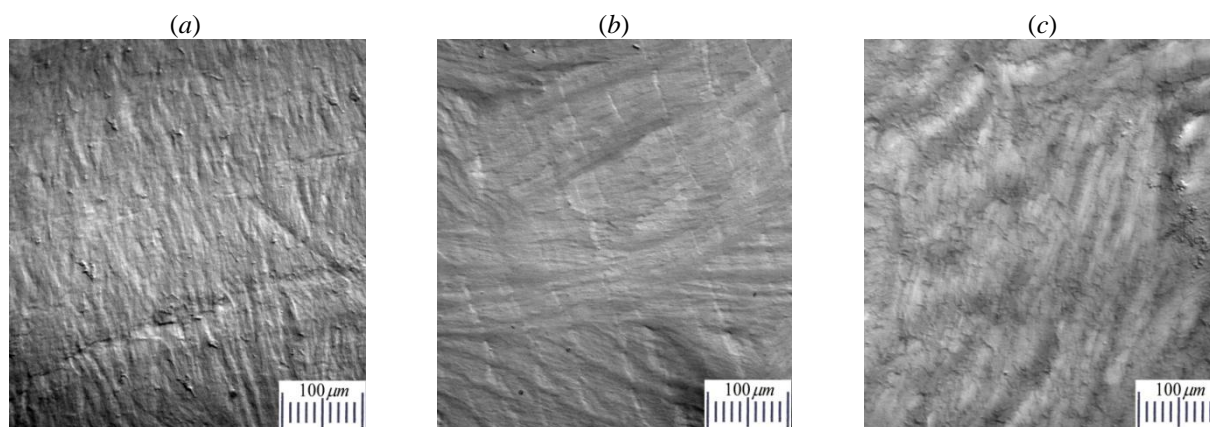
ments with a decrease in the temperature act as factors that inhibit gelation. As a result, the bell-like dependence of the physicochemical characteristics for such cryogels on the temperature of freezing–storage of the cryogenically-structuring polymer system is observed.

Third, the transformation of the “primary” PVACGs to the respective “secondary” ones resulted in the significant growth of the gel strength. For example, if the values of the elastic modulus for the urea-free “primary” PVACGs varied within the range from 1.8 to 3.3 kPa (curve 1, Fig. 2a), for the “secondary” cryogels these values grew up to the range of 23–26 kPa (curve 1, Fig. 2b), i.e. almost 10-fold. For the urea-containing “primary” PVACGs their E values, depending on the urea concentration and the temperature of cryogenic processing, were over the range of 4–87 kPa (curves 2–5, Fig. 2a), whereas after the samples transformation to the respective “secondary” aqueous cryogels their elastic moduli increased by many times and reached the level of 27–210 kPa (curves 2–5, Fig. 2b). Such reinforcement effects were found [51] to be induced by the replacement of the DMSO medium, which was a thermodynamically better solvent for PVA, by a poorer solvent — water [60]. As a consequence of such medium change, some fraction of the polymer-solvent interactions was replaced by the polymer-polymer ones, thus leading to the increase in the density and the rigidity of the 3D supramolecular network of the “secondary” PVACGs as compared with the “primary” ones.

3.3. Microstructure of the PVACGs under study

Since the PVACGs are the heterophase macroporous gel matrices [1, 4, 25–33], their integral physico-mechanical properties are stipulated not only by the rigidity of the polymeric phase (the walls of macropores) but also by the macroporous morphology of these gel materials. On the other hand, it is significant to compare the drug release characteristics of the drug-loaded “secondary” PVACGs fabricated from the DMSO-swollen “primary” cryogels that, in turn, were prepared in the presence of different amount of urea additives.

The first stage of such comparison was the microstructural study of the respective cryogels (section 2.2.4). The results of these experiments are illustrated by the optical microphotographs in Fig. 3, where the macroporous morphology is shown for the thin sections of the “secondary” PVACGs prepared originating from the initial polymer solutions, either the urea-free one (a), or those containing urea at the concentration of 2.0 (b) and 4.0 mol/L (c). The dark areas in these black-and-white images are the elements of the polymeric phase (the pore walls stained with the ‘Congo red’ dye), and the light areas are the macropores filled with water. The “secondary” water-swollen cryogels rather than the “primary” DMSO-swollen samples were investigated since the polymeric walls of macropores in the ‘primary’ cryogels were almost transparent, so the peculiarities of their texture in the thin sections were in fact indiscernible with an optical microscope. In addition, it turned out that the DMSO-swollen PVACGs were practically not stained with Congo red dye usually employed to contrast the thin sections of the water-swollen PVA cryogels [19, 24, 27, 29, 30, 53].



Urea concentration: 0 (a), 2.0 (b), and 4.0 (c) mol/L

Figure 3. Optical images of the microstructure registered for the Congo-red-stained thin sections of the “secondary” PVACGs derived from the respective “primary” samples prepared on the basis of the urea-free and the urea-containing DMSO solutions of the polymer by their cryotropic gelation at $\Delta T = -40^\circ$

Qualitatively, Figure 3 demonstrates clear differences between the character of macroporous morphology of the cryogels prepared from the urea-free (a) and the urea-containing (b, c) feed PVA solutions. If the PVACG formed by the freeze-thaw gelation of the urea-free PVA solution had the pores of an anisometric

shape and no more than $\sim 10 \mu\text{m}$ in cross-section, the presence of the urea additives in the initial PVA solutions caused a noticeable increase in the diversity of the pore shapes and sizes, especially with the urea concentration increase. With that the lamellar structures (up to $10\text{--}20 \mu\text{m}$ in the cross-section) of pore walls were arisen in the PVACG formed in the presence of 2.0 mol/L content of urea (Fig. 3*b*), and in the case of cryogel prepared with 4.0 mol/L of urea the porous texture of the matrix became more diffuse with widening of the pore size to the level of about $20\text{--}35 \mu\text{m}$ (Fig. 3*c*). It turns, the polymeric phase of such PVACG were stained stronger in the comparison to the image (b), thus indicating to the increased density of the polymeric network within the pore walls of this sample.

In general, the data of Figure 3 testified that the cross-section of the macropores in the PVACGs is increased with the growth of urea concentration in the DMSO solutions of PVA to be freeze-thaw structured. Therefore, such an effect should be manifested in the drug-release behavior of the soluble substances preliminary loaded in the PVACG-based drug carrier.

3.4. Loading and release of ϵ -ACA in and from the PVACGs

There are two principle options to insert some soluble substance to the polymer gel matrix intended for the use as a potential drug delivery system [17]. The first one is the introduction of the substance of interest in the mixture of precursors prior to the system gelation, thus resulting in the substance entrapment in the gel matrix after the completion of its formation. The main disadvantage of such approach is the lack of real possibility to rinse the resultant gel from the sol-fraction (e.g., the residues of precursor components that did not embed in the 3D polymeric network), since the entrapped target solute will be simultaneously washed-away. The second option includes the preliminary preparation of the gel matrix, its rinsing to remove the sol-fraction, and only then the loading of thus treated polymeric carrier with the solute of interest. In this study, we implemented the latter approach as the model drug compound the ϵ -amino caproic acid was used (section 2.2.5). Since for the microstructure of prepared in the present study PVACGs, the concentration of urea in the feed solutions to be structured cryogenically was more significant factor than the freezing temperature (Fig. 3). the ϵ -ACA loading/release experiments were carried out using “secondary” PVA cryogels derived from the corresponding “primary” gel samples formed under the identical thermal conditions, namely at $\Delta T = -40^\circ$. Thus, the feed DMSO solutions of PVA either did not contain the urea (reference system), or its concentrations were 2.0 or 4.0 mol/L .

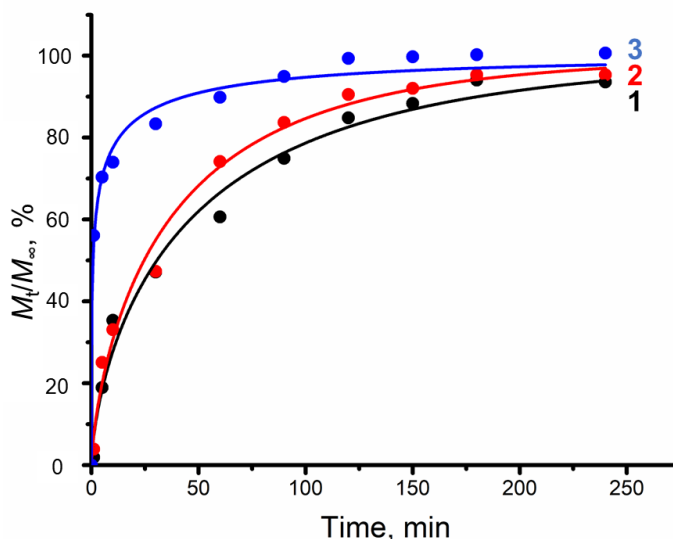
During these experiments the release kinetics was analyzed in terms of the Weibull's function [61] depicted as the solid lines of the plot in Fig. 4:

$$M_t/M_\infty = 1 - \exp(-a \times t^b),$$

where M_t is the amount of the released substance at time t ; M_∞ is the solute amount entrapped in the gel carrier (in our case this value is equal to that of m_{eq} in Table); M_t/M_∞ is the solute fraction (in per cent) released from the matrix for time t ; the parameters a and b are some constants. The latter ones are calculated automatically by the ORIGIN PRO software (OriginLab Corp., Northampton, USA) after uploading the Weibull's equation and the experimental data in this computer program.

Such kind of the kinetic data presentation is known to be a useful variant for the analysis of the drug release mechanism from various polymeric matrices [62]. In the case of ϵ -ACA release from the “secondary” PVACGs, this approach showed good correlation of the experimental values (round symbols in Fig. 4) with the Weibull's approximation. In addition, on a qualitative level, the obtained data turned out to be in a sufficient accordance with the microstructural features of the respective cryogel drug carriers. Namely, the larger was the size of gross pores inside the gel matrix (i.e. the larger was the PVA-free space of the pores within the macroporous cryogel), the faster was the drug release. Most likely, this trend was stipulated by the significant widening of the macropores in the resultant cryogels upon the increase in the urea concentration in the initial PVA solution (Fig. 3).

Thus, the late stage ($>60\%$) of the ϵ -ACA release in the case of drug carrier with the largest pores (PVACG formed originating from the feed solution with urea concentration of 4.0 mol/L ; curve 3 in Fig. 4) reached for $5\text{--}10$ min after start of release experiments. For the drug carrier based on the cryogel formed from the feed PVA solution with urea concentration of 2.0 mol/L (curve 2 in Fig. 4) this time period elongated up to $50\text{--}60$ min, and for the drug carrier formed in the urea-free system this was already about 1.5 h (curve 1 in Fig. 4). These data evidently demonstrate that urea content in the initial PVA solutions, which is used for the freeze-thaw-induced formation of “primary” cryogels, plays a key role for the release characteristics of the drug-loaded “secondary” PVACGs.



Urea concentration: 0 (curve 1), 2.0 (curve 2) and 4.0 (curve 3) mol/L

Figure 4. Kinetic profiles of ϵ -ACA release from the drug-loaded “secondary” PVACGs transformed from the “primary” cryogels prepared by the cryotropic gel-formation at $\Delta T = -40^\circ$ of the urea-free and the urea-containing DMSO solutions of the polymer

Conclusions

Urea is a well-known chaotropic agent capable of efficiently inhibiting the formation of H-bonds in aqueous media. Since the H-bonding processes are the main ones responsible for the gel-formation in the frozen water-PVA systems, the urea additives introduced in the feed aqueous PVA solutions cause significant deteriorative effects with respect of the rigidity and heat endurance of the resultant cryogels [52, 53]. On contrast, in such organic solvent, as dimethylsulfoxide, the additives of this chaotropes exhibit the opposite (i.e. the kosmotropic-like) influence causing the increase in the elastic modulus and fusion temperature of the resultant PVACGs [51]. Exactly the latter phenomenon was used in the present study to prepare the PVACGs possessing high mechanical strength and thermal resistance, following by the evaluation of such polymeric materials as potential carriers for the drug delivery systems.

The urea concentration on the feed DMSO solutions of PVA and the temperature of the cryogenic processing were the variables during the performed systematic studies. As a result, it was shown that the amount of urea introduced in the initial polymer solution to be freeze-thaw-gelled had exerted the crucial influence on the physico-chemical characteristics and macroporous morphology of both the DMSO-swollen “primary” PVACGs and, after replacement of the organic liquid by water, the water-swollen “secondary” cryogels. Subsequently, the latter ones were examined as potential drug vehicles in the ϵ -ACA loading/release experiments. The obtained data allowed to draw conclusion that by the variation of the initial urea concentration in the DMSO/PVA solutions used for the preparation of “primary” PVACGs it is possible to influence on the rigidity, heat endurance, and macroporous morphology of the resultant cryogels, and to govern the release behavior of the drugs uploaded in the bulk of the “secondary” PVA-cryogel-based delivery carriers.

Acknowledgements

The authors acknowledge Ministry of Science and Higher Education of Russian Federation for support (Contract No. 075-00697-22-00).

Conflicts of Interest

The authors declare no conflict of interest.

References

- 1 Lozinsky, V.I. (2002). Cryogels on the basis of natural and synthetic polymers: preparation, properties and application. *Russian Chemical Reviews*, 71(6), 489–511. <https://doi.org/10.1070/RC2002V071N06ABEH000720>
- 2 Gun'ko, V.M., Savina, I.N., & Mikhailovsky, S.V. (2013). Cryogels: Morphological, structural and adsorption characterisation. *Advances in Colloid and Interface Science*, 187–188, 1–46. <https://doi.org/10.1016/j.cis.2012.11.001>
- 3 Okay, O. (Eds.). (2014). *Polymeric Cryogels: Macroporous Gels with Remarkable Properties*; Springer: Cham, Switzerland, 330 p. ISBN 978-3-319-05845-0
- 4 Lozinsky, V.I. (2014). A brief history of polymeric cryogels. *Advances in Polymer Science*, 263, 1–48. https://doi.org/10.1007/978-3-319-05846-7_1
- 5 Reichelt, S. (2015). Introduction to macroporous cryogels. *Methods in Molecular Biology*, 1286, 173–181. https://doi.org/10.1007/978-1-4939-2447-9_14
- 6 Lozinsky, V.I. (2018). Cryostructuring of Polymeric Systems. 50⁺. Cryogels and Cryotropic Gel-Formation: Terms and Definitions. *Gels*, 4(3), 77. <https://doi.org/10.3390/gels4030077>
- 7 Tripathi, A., & Melo, J.S. (2019). Cryostructurization of polymeric systems for developing macroporous cryogel as a foundational framework in bioengineering applications. *Journal of Chemical Science*, 131(92). <https://doi.org/10.1007/s12039-019-1670-1>
- 8 Gutiérrez, M.C., Ferrer, M.L., & del Monte, F. (2008). Ice-templated materials: Sophisticated structures exhibiting enhanced functionalities obtained after unidirectional freezing and ice-segregation-induced self-assembly. *Chemistry of Materials*, 20(3), 634–648. <https://doi.org/10.1021/cm702028z>
- 9 Kumar, A. (Ed.). (2016). *Supermacroporous Cryogels: Biomedical and Biotechnological Applications* (1st ed.). CRC Press: Boca Raton, FL, USA; Taylor & Francis Group: Abingdon, UK, 480 p. ISBN 978-1-4822-281-6.
- 10 Lazzeri, L. (1996). Progress in bioartificial polymeric materials. *Trends in Polymer Science* 4(8), 249–252. ISSN 0966-4793.
- 11 Hixon, K.R., Lu, T., & Sell, S.A. (2017). A comprehensive review of cryogels and their roles in tissue engineering applications. *Acta Biomaterialia*, 62(1), 29–41. <https://doi.org/10.1016/j.actbio.2017.08.033>
- 12 Saylan, S., & Denizli, A. (2019). Supermacroporous composite cryogels in biomedical applications. *Gels* 5(1), Article 20. <https://doi.org/10.3390/gels5020020>
- 13 Eggermont, L.J., Rogers, Z.J., Colombani, T., Memic, A., & Bencherif, S.A. (2020). Injectable cryogels for biomedical applications. *Trends in Biotechnology*, 38(4), 418–431. <https://doi.org/10.1016/j.tibtech.2019.09.008>
- 14 Klivenko, A.N., Mussabayeva, B.Kh., Gaisina, B.S., & Sabitova, A.N. (2021). Biocompatible cryogels: preparation and application. *Bulletin of the University of Karaganda — Chemistry*, 103(1), 4–20. <https://doi.org/10.31489/2021Ch3/4-20>
- 15 Eigel, D., Werner, C., & Newland, B. (2021). Cryogel biomaterials for neuroscience applications. *Neurochemistry International*, 147(1), Article 105012. <https://doi.org/10.1016/j.neuint.2021.105012>
- 16 Tyshkunova, I.V., Poshina, D.N., & Skorik, Y.A. (2022). Cellulose cryogels as promising materials for biomedical applications. *International Journal of Molecular Science*, 23(4), 2037. <https://doi.org/10.3390/ijms23042037>
- 17 Langer, R., & Peppas, N.A. (2003). Advances in biomaterials, drug delivery, and bionanotechnology. *AIChE Journal*, 49(12), 2990–3006. <https://doi.org/10.1002/aic.690491202>
- 18 Komarova, G.A., Starodubtsev, S.G., Lozinsky, V.I., Kalinina, E.V., Landfester, K., & Khokhlov, A.R. (2008). Intelligent gels and cryogels with entrapped emulsions. *Langmuir*, 24(9), 4467–4469. <https://doi.org/10.1021/la703983v>
- 19 Podorozhko, E.A., Korlyukov, A.A., & Lozinsky, V.I. (2010). Cryostructuring of polymer systems. 30. Poly(vinyl alcohol)-based composite cryogels filled with small disperse oil droplets: A gel system capable of mechanically-induced releasing of the lipophilic constituents. *Journal of Applied Polymer Science*, 117(3), 1332–1349. <https://doi.org/10.1002/app.32028>
- 20 Timofejeva, A., D'Este, M., & Loca, D. (2017). Calcium phosphate/polyvinyl alcohol composite hydrogels: A review on the freeze-thaw synthesis approach and applications in regenerative medicine. *European Polymer Journal*, 95(1), 547–565. <https://doi.org/10.1016/j.eurpolymj.2017.08.048>
- 21 Hixon, K.R., Bogner, S.J., Ronning-Arnesen, G., Janowiak, B.E., & Sell, S.A. (2019). Investigating manuka honey antibacterial properties when incorporated into cryogel, hydrogel, and electrospun tissue engineering scaffolds. *Gels*, 5(1), Article 21. <https://doi.org/10.3390/gels5020021>
- 22 Auriemma, G., Russo, P., Del Gaudio, P., Garcia-Gonzalez, C.A., Landin, M., & Aquino, R.P. (2020). Technologies and formulation design of polysaccharide-based hydrogels for drug delivery. *Molecules*, 25(14), Article 3156. <https://doi.org/10.3390/molecules25143156>
- 23 Raschip, I.E., Fifere, N., Varganici, C.-D., & Dinu, M.V. (2020). Development of antioxidant and antimicrobial xanthan-based cryogels with turned porous morphology and controlled swelling features. *International Journal of Biological Macromolecules*, 156(1), 608–620. <https://doi.org/10.1016/j.ijbiomac.2020.04.086>
- 24 Kolosova, O.Yu., Karelina, P.A., Vasil'ev, V.G., Grinberg, V.Ya., Kurochkin, I.I., Kurochkin, I.N., & Lozinsky, V.I. (2021). Cryostructuring of polymeric systems. 58. Influence of the H₂N-(CH₂)_n-COOH-type amino acid additives on formation, properties, microstructure and drug release behaviour of poly(vinyl alcohol) cryogels. *Reactive and Functional Polymers*, 167(1), Article 105010. <https://doi.org/10.1016/j.reactfunctpolym.2021.105010>
- 25 Nambu, M. (1990). Rubber-like poly(vinyl alcohol) gel. *Kobunshi Ronbunshu*, 47(5), 695–703. <https://doi.org/10.1295/koron.47.695> (In Japanese)

- 26 Peppas, N.A., & Stauffer, S.R. (1991). Reinforced uncrosslinked poly (vinyl alcohol) gels produced by cyclic freezing-thawing processes: A short review. *Journal of Controlled Release*, 16(3), 305–310. [https://doi.org/10.1016/0168-3659\(91\)90007-Z](https://doi.org/10.1016/0168-3659(91)90007-Z)
- 27 Lozinsky, V.I. (1998). Cryotropic gelation of poly(vinyl alcohol) solutions. *Russian Chemical Reviews*, 67(7), 573–586. <https://doi.org/10.1070/RC1998V067N07ABEH000399>
- 28 Hassan, C.M., & Peppas, N.A. (2000). Structure and applications of poly(vinyl alcohol) hydrogels produced by conventional crosslinking or by freezing/thawing methods. *Advances in Polymer Science*, 153, 37–65. https://doi.org/10.1007/3-540-46414-X_2
- 29 Lozinsky, V.I., Damshkaln, L.G., Shaskol'skii, B.L., Babushkina, T.A., Kurochkin, I.N., & Kurochkin, I.I. (2007). Study of cryostructuring of polymer systems. 27. Physicochemical properties of poly(vinyl alcohol) cryogels and features of their macroporous morphology. *Colloid Journal*, 69(6), 747–764. <https://doi.org/10.1134/S1061933X07060117>
- 30 Lozinsky, V.I., Damshkaln, L.G., Kurochkin, I.N., & Kurochkin, I.I. (2008). Study of cryostructuring of polymer systems. 28. Physicochemical and morphological properties of poly(vinyl alcohol) cryogels formed via multiple freezing-thawing technique. *Colloid Journal*, 70(2), 189–198. <https://doi.org/10.1134/S1061933X08020117>
- 31 De Rosa, C., Auriemma, F., & Girolamo, R.D. (2014). Kinetic analysis of cryotropic gelation of poly(vinyl alcohol)/water solutions by small-angle neutron scattering. *Advances in Polymer Science*, 263, 159–197. https://doi.org/10.1007/978-3-319-05846-7_4
- 32 Suzuki, A., & Sasaki, S. (2015). Swelling and mechanical properties of physically crosslinked poly(vinyl alcohol) hydrogels. *Journal of Engineering in Medicine*, 229(12), 828–844. <https://doi.org/10.1177/0954411915615469>
- 33 Teodorescu, M., Bercea, M., & Morariu, S. (2018). Biomaterials of poly(vinyl alcohol) and natural polymers. *Polymer Reviews*, 58(2), 247–287. <https://doi.org/10.1080/15583724.2017.1403928>
- 34 Rogozhin, S.V., Lozinsky, V.I., Vainerman, E.S., Domotenko, L.V., Mamtsis, A.M., Ivanova, S.A., Shtil'man, M.I., & Korshak, V.V. (1984). Noncovalent cryostructuring in polymer systems. *Doklady Akademii Nauk SSSR*, 278(1), 129–133. (in Russian) ISSN 0869-5652.
- 35 Lozinsky, V.I., Domotenko, L.V., Vainerman, E.S., Mamtsis, A.M., & Rogozhin, S.V. (1986). On the possibility of mechanodestruction of poly(vinyl alcohol) molecules under moderate freezing of its concentrated water solutions. *Polymer Bulletin*, 15(4), 333–340. <https://doi.org/10.1007/BF00254852>
- 36 Lozinsky, V.I., Vainerman, E.S., Domotenko, L.V., Mamtsis, A.M., Titova, E.F., Belavtseva, E.M., & Rogozhin, S.V. (1986). Study of cryostructuring of polymer systems. VII. Structure formation under freezing of poly(vinyl alcohol) aqueous solutions. *Colloid Polymer Science*, 264(1), 19–24. <https://doi.org/10.1007/BF01410304>
- 37 Nishinari, K., Watase, M., & Tanaka, F. (1996). Structure of junction zones in poly(vinyl alcohol) gels by rheological and thermal studies. *Journal de Chimie Physique (Paris)*, 93(5), 880–886. <https://doi.org/10.1051/jcp/1996930880>
- 38 Ricciardi, R., Auriemma, F., De Rosa, C., & Lauprêtre, D. (2004). X-ray diffraction analysis of poly(vinyl alcohol) hydrogels, obtained by freezing and thawing techniques. *Macromolecules*, 37(5), 1921–1927. <https://doi.org/10.1021/ma035663q>
- 39 Lozinsky, V.I., & Okay, O. (2014). Basic principles of cryotropic gelation. *Advances in Polymer Science*, 263, 49–102. https://doi.org/10.1007/978-3-319-05846-7_2
- 40 De Rosa, C., Auriemma, F., & Girolamo, R.D. (2014). Kinetic analysis of cryotropic gelation of poly(vinyl alcohol)/water solutions by small-angle neutron scattering. *Advances in Polymer Science*, 263, 159–197. https://doi.org/10.1007/978-3-319-05846-7_4
- 41 Adelnia, H., Ensandoost, R., Moonshi, S.S., Gavvani, J.N., Vasafi, E.I., & Ta, H.T. (2022). Freeze/thawed polyvinyl alcohol hydrogels: present, past and future. *European Polymer Journal*, 164, Article 110974. <https://doi.org/10.1016/j.eurpolymj.2021.110974>
- 42 Chu, K.C., & Rutt, B.K. (1997). Poly(vinyl alcohol) cryogel: An ideal phantom material for MR studies of arterial flow and elasticity. *Magnetic Resonance in Medicine*, 37(3), 314–319. <https://doi.org/10.1002/mrm.1910370220>
- 43 Baker, M.I., Walsh, S.P., Schwatz, Z., & Boyan, B.D. (2012). A review of polyvinyl alcohol and its uses in cartilage and orthopedic applications. *Journal of Biomedical Materials Research, Part B*, 100(5), 1451–1457. <https://doi.org/10.1002/jmb.b32694>
- 44 Gajra, B., Pandya, S.S., Vidyasagar, G., Rabari, H., Dedania, R.R., & Rao, S. (2012). Poly(vinyl alcohol) hydrogel and its pharmaceutical and biomedical applications: A review. *International Journal of Pharmaceutical Research*, 4(2), 20–26. ISSN 0975-2366.
- 45 Iatridis, J.C., Nicoll, S.B., Michalek, A.J., Walter, B.A., & Gupta, M.S. (2013). Role of biomechanics in intervertebral disc degeneration and regenerative therapies: What needs repairing in the disc and what are promising biomaterials for its repair? *Spine Journal*, 13(2), 243–262. <https://doi.org/10.1016/j.spinee.2012.12.002>
- 46 Wan, W., Bannerman, A.D., Yang, L., & Mak, H. (2014). Poly(vinyl alcohol) cryogels for biomedical applications. *Advances in Polymer Science*, 263, 283–321. https://doi.org/10.1007/978-3-319-05846-7_8
- 47 Hyon, S.H., Cha, W.I., & Ikada, Y. (1989). Preparation of transparent poly(vinyl alcohol) hydrogel. *Polymer Bulletin*, 22(1), 119–122. <https://doi.org/10.1007/BF00255200>
- 48 Trieu, H.H., & Qutubuddin, S. (1995). Poly(vinyl alcohol) hydrogels. 2. Effects of processing parameters on structure and properties. *Polymer*, 36(13), 2531–2539. [https://doi.org/10.1016/0032-3861\(95\)91198-G](https://doi.org/10.1016/0032-3861(95)91198-G)
- 49 Mastri, C., Chagnon, G., & Favier, D. (2017). Influence of processing parameters on the macroscopic mechanical behavior of PVA hydrogels. *Materials Science and Engineering, Part C*, 75(6), 769–776. <https://doi.org/10.1016/j.msec.2017.02.045>

- 50 Lozinsky, V.I., Leonova, I.M., Ivanov, R.V., & Bakeeva, I.V. (2017). A study of cryostructuring of polymer systems. 46. Physicochemical properties and microstructure of poly(vinyl alcohol) cryogels formed from polymer solutions in mixtures of dimethyl sulfoxide with low-molecular-mass alcohols. *Colloid Journal*, 79(6), 788–796. <https://doi.org/10.1134/S1061933X17060114>
- 51 Lozinsky, V.I., Kolosova, O.Y., Michurov, D.A., Dubovik, A.S., Vasil'ev, V.G., & Grinberg, V.Y. (2018). Cryostructuring of polymeric systems. 49. Unexpected “kosmotropic-like” impact of organic chaotropes on the PVA freeze-thaw-induced gelation in DMSO. *Gels*, 4(4), Article 81. <https://doi.org/10.3390/gels4040081>
- 52 Kolosova, O.Y., Kurochkin, I.N., Kurochkin, I.I., & Lozinsky, V.I. (2018). Cryostructuring of polymeric systems. 48. Influence of organic non-ionic and ionic chaotropes or kosmotropes on the cryotropic gel-formation of aqueous poly(vinyl alcohol) solutions, as well as on the properties and microstructure of the resultant cryogels. *European Polymer Journal*, 102, 169–177. <https://doi.org/10.1016/j.eurpolymj.2018.03.010>
- 53 Kurochkin, I.I., Kurochkin, I.N., Kolosova, O.Yu., & Lozinsky, V.I. (2020). Cryostructuring of polymeric systems. 56. Application of deep neural networks for the classification of structural features peculiar to macroporous poly(vinyl alcohol) cryogels prepared without and with the additives of chaotropes or kosmotropes. *Molecules*, 25(19), Article 4480. <https://doi.org/10.3390/molecules25194480>
- 54 Lucas, O.N., & Albert, T.W. (1981). Epsilon aminocaproic acid in hemophiliacs undergoing dental extractions: a concise review. *Oral Surgery, Oral Medicine, and Oral Pathology*, 51(2), 115–120. [https://doi.org/10.1016/0030-4220\(81\)90025-6](https://doi.org/10.1016/0030-4220(81)90025-6)
- 55 Gordon, A., & Ford, R. (1973). *The Chemist's Companion. A Handbook of Practical Data, Techniques and References*. New York: John Wiley and Sons, 560 p. ISBN 978-0-471-31590-2.
- 56 Eldridge, J.E., & Ferry, J.D. (1954). Studies of the cross-linking process in gelatin gels. III. Dependence of melting point on concentration and molecular weight. *Journal of Physical Chemistry*, 58(11), 992–995. <https://doi.org/10.1021/j150521a013>
- 57 Gusev, D.G., Lozinsky, V.I., Vainerman, E.S., & Bakmutov, V.I. (1990). Study of the frozen water-poly(vinyl alcohol) system by ^2H and ^{13}C NMR spectroscopy. *Magnetic Resonance in Chemistry*, 28(7), 651–655. <https://doi.org/10.1002/mrc.1260280717>
- 58 Mikhalev, O.I., Serpinski, M., Lozinsky, V.I., Kapanin, P.V., Chkeidze, I.I., & Alfimov, M.V. (1991). Method for determination of liquid microphase volume: Application to the investigation of frozen H_2O -poly(vinyl alcohol) system. *Cryo-Letters*, 12(4), 197–206. ISSN 0143-2044.
- 59 Masuda, K., & Horii, F. (1998). CP/MAS ^{13}C NMR analyses of the chain conformation and hydrogen bonding for frozen poly(vinyl alcohol) solutions. *Macromolecules*, 31(17), 5810–5817. [https://doi.org/S0024-9297\(98\)00126-0](https://doi.org/S0024-9297(98)00126-0)
- 60 Pritchard, J.G. (1970). *Poly(vinyl alcohol): basic properties and uses*. Gordon & Breach Sci. Publ., London e.a. 139 p. ISBN 9780356033358
- 61 Papadopoulou, V., Kosmidis, K., Vlachou, M., & Macheras, P. (2006). On the use of the Weibull function for the discernment of drug release mechanisms. *International Journal of Pharmaceutics*, 309(1-2), 44–50. <https://doi.org/10.1016/j.ijpharm.2005.10.044>
- 62 Peppas, N.A., & Narasimhan, B. (2014). Mathematical models in drug delivery: How modeling has shaped the way we design new drug delivery systems. *Journal of Controlled Release*, 190(1), 75–81. <https://doi.org/10.1016/j.jconrel.2014.06.041>

Д.А. Мичуров, О.Ю. Колосова, В.И. Лозинский

Полимерлі жүйелерді криокұрылымдау.

61. ДМСО құрамында мочеви́на бар полимерлі ерітінділер негізінде дайындалған поливинил спирті криогельдерінің физикалық-химиялық қасиеттері және алынған гельдік материалдарды потенциалды дәрілік тасымалдаушылар ретінде бағалау

Поливинил спирті (ПВС) негізіндегі макрокеукті физикалық криогельдер құрамында мочеви́на қоспалары бар диметилсульфоксид полимер ерітінділерінен алынды. Криотропты гельдеу процесінің айнымалылары оның температурасы мен қосылған мочеви́на концентрациясы болды, бұл алынған криогельдердің қаттылығы мен жылуғатөзімділігінің жоғарылауын қамтамасыз етеді, сонымен қатар гель массасындағы макрокеуктердің кеңеюіне ықпал етеді. ДМСО-дан ісінген криогельдерді судың артық мөлшерімен жуғаннан кейін судан ісінген ПВС криогельдерінің пайда болуына, олардың қаттылығының бір мезгілде жоғарылауына әкелді. Бұл гельдік матрицалар дәрілік заттарды жеткізу жүйелерінде полимерлі тасымалдаушылар ретінде жұмыс істеу қабілетіне сыналған. Суда ісінген осындай криогельдерді модельдік препаратпен — ϵ -аминокапрон қышқылымен толтыру, содан кейін оның шығарылу кинетикасын зерттеу ДМСО-да ісінген криогельдерді мұздату-еріту арқылы туындаған бастапқы ПВС ерітінділеріндегі мочеви́на құрамы суда ісінген, құрамында дәрілік зат бар тасымалдаушы гельдің шығарылу сипаттамасында маңызды рөл атқарғанын көрсетті. Атап айтқанда, мочеви́на концентрациясы жоғары болған жағдайда дайындалған ПВС криогельдері үлкен тесіктерге ие болды, бұл препараттың біршама жылдамырақ шығарылуына әкелді.

Клт сөздер: поливинил спиртінң криогельдері, диметилсульфоксидті полимер ерітінділері, мочеви́на қоспалары, криогенді өңдеу температурасы, дәрілік заттарды жеткізуге арналған криогельді тасымалдаушылар.

Д.А. Мичуров, О.Ю. Колосова, В.И. Лозинский

Криоструктурирование полимерных систем.

61. Физико-химические свойства криогелей поливинилового спирта, приготовленных на основе мочевиносодержащих растворов полимера в ДМСО, и оценка полученных гелевых материалов как потенциальных носителей лекарственных средств

Макропористые физические криогели на основе поливинилового спирта (ПВС) получали из диметилсульфоксидных растворов полимера, содержащих добавки мочевины. Переменными криотропного процесса гелеобразования являлись его температура и концентрация добавляемой мочевины, что обуславливало повышение жесткости и теплостойкости полученных криогелей, а также способствовало расширению макропор в гелевой массе. Последующая промывка набухших от ДМСО криогелей избытком воды приводила к образованию набухших от воды криогелей ПВС с одновременным дальнейшим увеличением их жесткости. Эти гелевые матрицы были протестированы в отношении их способности работать в качестве полимерных носителей в системах доставки лекарственных средств. Наполнение таких набухших в воде криогелей модельным препаратом — ϵ -аминокапроновой кислотой, а затем изучение кинетики его высвобождения показало, что содержание мочевины в исходных растворах ПВС, использованных для индуцированного замораживанием-оттаиванием криогелей, набухших в ДМСО, играло ключевую роль в характеристиках высвобождения набухшего в воде геля-носителя, содержащего лекарственное средство. А именно, криогели ПВС, приготовленные в присутствии более высокой концентрации мочевины, имели более крупные поры, в результате чего высвобождение лекарственного вещества происходило несколько быстрее.

Ключевые слова: криогели поливинилового спирта, растворы полимеров диметилсульфоксида, добавки мочевины, температура криогенной обработки, криогелевые носители для доставки лекарственных средств.

Information about authors*

Michurov, Dmitrii Alekseevich — Junior Researcher, A.N. Nesmeyanov Institute of Organoelement Compounds of Russian Academy of Sciences, Vavilov street 28, 119334 Moscow, Russia; e-mail: dmitriial7.8@gmail.com

Kolosova, Olga Yurievna — Candidate of Chemical Sciences, Senior Researcher, A.N. Nesmeyanov Institute of Organoelement Compounds of Russian Academy of Sciences, Vavilov street 28, 119334 Moscow, Russia; e-mail: kolosova@ineos.ac.ru, <https://orcid.org/0000-0002-0378-3464>;

Lozinsky, Vladimir Iosifovich (corresponding author) — Doctor of Chemical Sciences, Professor, Head of the Laboratory for Cryochemistry of (Bio)Polymers, A.N. Nesmeyanov Institute of Organoelement Compounds of Russian Academy of Sciences, Vavilov street 28, 119334 Moscow, Russia; e-mail: loz@ineos.ac.ru; <https://orcid.org/0000-0002-8111-1161>

*The author's name is presented in the order: *Last Name, First and Middle Names*

O.B. Avazova^{*}, R.Yu. Milusheva, I.N. Nurgaliev, S.Sh. Rashidova

Institute of Polymer Chemistry and Physics, Academy of Sciences, Tashkent, Uzbekistan

(*Corresponding author's e-mail: avazova1972@mail.ru)

Polymolecular Complexes of Chitosan with the *Bombyx Mori* Protein

The interaction of chitosan (ChS) and the *Bombyx mori* protein on different pH ranges was studied, and the fundamental possibility of obtaining complexes of ChS with the *Bombyx mori* protein was revealed. The formation of a polymolecular complex of protein with ChS in aqueous solutions was confirmed by the results of physico-chemical methods. It is shown that the ChS structure is characterized by a certain rigidity and ionogenicity. The results indicate the complexation of the pupae protein with ChS in 2% acetic acid in the range of pH = 4.8–6.7. The detected changes and shifts of the absorption bands in the IR spectra confirm the occurrence of the complex formation reaction between the molecules of ChS and protein at pH = 4.8–6.7, which is characterized by absorption bands in the IR spectra at 1641 cm⁻¹, 1538 cm⁻¹ and 1068 cm⁻¹. Quantum-chemical DFT study of ChS complexes with amino acids (AAs) was carried out. The stability of complexes of ChS with AAs (ChS-AA) was shown except for the complex formed with histidine in the gas phase. The calculation results indicate the presence of a strong thermodynamic driving force in the complexation of ChS with AAs.

Keywords: silk production waste, silkworm pupae, alkaline hydrolysis, protein, chitin, chitosan, polymolecular complexes, conformational characteristics.

Introduction

The main waste products of silk production are silkworm pupae, which have a high nutritional and biological value. The mass of dry pupae consists of 60–65 % protein, 3–5 % chitin, 10–25 % lipids, and 2–6 % minerals [1]. Obtaining polymolecular complexes of protein and chitosan (ChS) from pupae of the silkworm *Bombyx mori* with valuable chemical and biological properties that will have antibacterial activity due to the natural ChS polysaccharide is an urgent task [2].

ChS is obtained from the natural biopolymer of chitin including the chitinous coatings of silkworm pupae in an aqueous solution of NaOH (30–50 %) in the temperature range of 90–150 °C [3]. This polysaccharide is considered as a promising biomaterial of the future; interest in it is associated with unique physiological and environmental properties, such as biocompatibility, biodegradation, physiological activity in the absence of toxicity and the availability of raw materials, as well as local sources for its production [4].

Since biopolymers including ChS are more capable of intermolecular interactions, one of the most effective ways to improve its characteristics is the formation of polymolecular complexes (PMCs) with other biopolymers and polar synthetic polymers [4]. Although amino acids (AAs) are the building blocks of proteins, elucidation of the nature of their interactions with ChS remains poorly understood. Understanding the strength of the interaction between ChS and AAs, as well as studying the reactivity of the complexes formed as a result of these interactions, is an urgent task. Despite the ubiquitous presence of such interactions in biological systems, there are few theoretical and experimental studies on the preparation of PMCs of *Bombyx mori* protein and ChS in solutions and in the solid state.

In this regard, physical and chemical phenomena and patterns of interaction of proteins with anionic and cationic polysaccharides are of great practical interest. A detailed study was made on the effect of both the ionogenic nature of the protein and the rigidity of ChS chains on its behavior in solutions with various concentrations subjected to various thermodynamic changes.

This paper presents the results of an experimental study of the production of PMCs preparations based on *Bombyx mori* protein and ChS, which have a different chemical structure of macromolecules due to the formation of complex compounds, and analyzes the role of ionogens in the structural and phase transformations of the biopolymer. Based on the density functional theory (DFT) method the formation of complexes between ChS and AAs (asparagine, threonine, serine, glutamine, alanine, tyrosine, histidine, and lysine), which are part of the protein isolated from the pupae of the silkworm *Bombyx mori*, was analyzed.

Experimental

Protein hydrolysis was carried out in 1 % NaOH aqueous solution at 90 °C for 3 hours. The modulus of the reaction mass “silkworm pupae: alkaline solution” was 1:10. The protein was separated from chitin by filtration. It was revealed that the mass of chitin was 5.6 %. After filtration, 1 % alkaline hydrolysate contained about 8.83 % pupal protein, hydrolysate density was 1028 kg/m³, and pH was 10.96. After separation of the hydrolysate, the resulting chitin was deacetylated with 50 % NaOH at 120 °C for 3 hours. ChS with a degree of deacetylation of 86 % was obtained. A sample of *Bombyx mori* chitosan is characterized by the elementary unit [(C₆H₅O(OH)CH₂OH(NH₂))_n], the presence of an amino group (–NH₂), aliphatic methylene (–CH)–group and hydroxyl (–OH)–groups at C-3 and C-6. The molecular weight of the elementary unit is M₀ = 161. The content of amine and carboxyl groups was determined by the method of conductometric titration (on a Seven Easy Conductivity Mettler-Toledo AG8603 instrument).

A simple and effective method of viscometry was used with the solvent outflow time t₀ = 94 s for acetic acid to determine the viscosity characteristics of ChS solutions depending on the concentration (C) of polymers. Sodium acetate (CH₃COONa) was added to the ChS solution to suppress the polyelectrolyte effect. At least 5 measurements were performed for each dilution of the solutions. The calculations were carried out using the Huggins equation:

$$\eta_{\text{spec}}/C \approx [\eta] + k[\eta]^2 C,$$

where $\eta_{\text{spec}} \approx \eta_{\text{rel}} - 1$ — specific viscosity, in which relative viscosity $\eta_{\text{rel}} \approx t_{\text{sol-n}}/t_{\text{sol-t}}$ (where $t_{\text{sol-n}}$ is the solution outflow time and $t_{\text{sol-t}}$ is the solvent); k — the Huggins coefficient; $[\eta]$ — the inherent viscosity of the solution, which is determined from the dependence of η_{spec}/C on C extrapolating $C \rightarrow 0$ and used to calculate the relative molecular weight (M_{η}) of the polymer using the Mark-Kuhn-Houwink equation, i.e.:

$$M_{\eta} \approx ([\eta]/K)^{1/\alpha},$$

where $K = 1.4 \times 10^{-4}$ and $\alpha = 0.83$ [5].

Quantitative determination of the AA composition in protein samples was carried out on an amino acid analyzer (Amino acid analyzer T-339). Preliminarily freeze-dried portions (50 mg each) of the samples were hydrolyzed with 5.7 N HCl for 24 hours at a temperature of 110 °C in a vacuum. The obtained hydrolysates were evaporated on a rotary evaporator (DLAB RE 100-Pro). IR spectroscopic studies were carried out on an Inventio-S IR-Fourier spectrophotometer (Bruker, Germany) with a spectral resolution of 2 cm⁻¹. The IR spectrometer is equipped with an attenuated total internal reflection attachment in the range from 4000 to 500 cm⁻¹ since absorption bands of almost all functional groups of organic molecules lie in this spectral range. The samples were prepared in the form of tablets with KBr under a pressure of 7 × 10⁸ Pa. Turbidimetric studies were carried out on a Turbidimeter TB300IR instrument (Germany). The TB300 IR is a portable turbidity meter that complies with ISO 7027.

The instrument has an auto-ranging feature ranging from 0.01 to 1100 NTU/FNU. The light source is an infrared LED (light emitting diode) with a wavelength of 860 nm. The emitted light is reflected by haze in the sample. Stray light will be detected at a 90° angle by the photodiode. This principle is a part of ISO 7027. Formazin solution is the international standard for turbidity. The results associated with this standard are designated as FNU (formazin nephelometric units).

Computational methods

Although a huge number of experimental works are focused on the interaction of different amino acids/proteins and chitosan, only a few computational studies have been reported. The interactions between chemicals and chitosan toward two specific emergent pollutants were studied by using the density functional theory (DFT) [6]. It is broadly used to understand and predict the interactions of a specific molecule over a polymeric structure, proving suitable correlations with the experimental results [7–13].

The calculations were performed using the GAUSSIAN 09 package and the Gaussview 5.0.9 molecular visualization program using DFT with the standard set basis 6-31++G (d,p) [6]. The first stage of the theoretical calculation was the determination of the optimized molecular structures of ChS and AA. The charges of atoms were calculated, diagrams of boundary molecular orbitals were constructed: the highest occupied (HOMO) and lowest unoccupied (LUMO) molecular orbitals and their energies were determined. Interactions of ChS with AAs were studied using reactivity descriptors. A monomeric link was taken as the structural unit of ChS; in calculations in the gas phase, AAs were considered as a nonionic form due to the greater intrinsic affinity for the proton of the carboxylate oxygen atom compared to the nitrogen atom of the amino group. The interaction energy (ΔE_{inter}) was calculated using the equation-based approach:

$$\Delta E_{\text{inter}} = E_{\text{ChS-AA}} - (E_{\text{ChS}} + E_{\text{AA}}) + E_{\text{BSSE}},$$

where $E_{\text{ChS-AA}}$, E_{ChS} and E_{AA} are the energy of the complex, ChS and AA, respectively. EBSSE is a basis set superposition error (BSSE) correction calculated using the direct difference method for calculating molecular interactions based on a bivariate transcorrelation approach together with special methods for estimating other errors [14]. Of several reactivity descriptors, the energy of the HOMO, total rigidity, chemical potential and electrophilicity were considered to analyze the reactivity of ChS and AAs complexes in the present study. The following reactivity descriptors [15] were calculated: chemical hardness (η) = $1/2(E_{\text{HOMO}} - E_{\text{LUMO}})$, where E_{HOMO} is the energy of the HOMO, and E_{LUMO} is the energy of the LUMO, softness $\zeta = 1/\eta$, chemical potential $\mu = 1/2(E_{\text{HOMO}} + E_{\text{LUMO}})$, electrophilicity (ω) is expressed as $\omega = \mu^2/2\eta$.

Results and Discussion

Since ChS molecules are more capable of intermolecular interactions, one of the most effective ways to improve its characteristics is the formation of PMCs with various compounds including proteins [4]. However, the preparation of PMCs of *Bombyx mori* protein and ChS, especially in electrolyte solutions, has not been sufficiently studied. In this regard, a detailed study of the influence of both the ionogenic nature of the protein and the rigidity of ChS chains on its behavior in solutions with different concentrations and pH was carried out.

Previously, we presented the results of an experimental study of protein structural changes in solutions and an analysis of the behavior of the R group of AA residues present in the *Bombyx mori* protein [16]. According to the amino acid composition, it is shown that the R-groups of AA residues present in the *Bombyx mori* protein consist of 16 AA residues, eight of which are non-polar, which is 1.98 %; five — uncharged, but polar, they make up 1.9 %, as well as three — charged, which make up 0.8 %. Conductometric titration showed that the content of $-\text{NH}_2$ groups in the *Bombyx mori* protein chain was 4.8 % and the obtained proteins in solutions exhibited polyampholytic properties characteristic of protein molecules. Based on the structural properties of the protein it is possible to obtain biologically active PMCs preparations with polysaccharides on its basis.

In polysaccharides, in particular, in ChS, amine and hydroxyl groups are functional, while in proteins, the chemical properties are determined by the nature of the amide bond and functional groups (carboxyl, hydroxyl, amine, disulfide) [17]. Through these functional groups and thermodynamic conditions, the interactions of the polysaccharide and protein are carried out through hydrogen bonds, electrostatic forces, van der Waals and hydrophobic interactions.

The process of obtaining complexes based on *Bombyx mori* protein and ChS is inevitably accompanied by the breakdown of the supramolecular and molecular structure due to the interaction of individual functional groups and elements of its macromolecules. In this case, the rate of the complex formation process depends on the pH of the medium and temperature. However, the efficiency of complex formation is also largely determined by the initial behavior of the biopolymer macromolecule in bulk.

Table 1

The physicochemical characteristics of the *Bombyx mori* ChS sample

Nitrogen content, %	Ash content, %	$[\eta]$, dl/g	M_{η} (kDa)	DP	L, nm	N	Solubility, %
8.20	2.6	2.7	14.6	910	465	23.3	94.0

Values: M_{η} is viscosity average molecular weight, DP is degree of polymerization, L is contour length and N is number of Kuhn segments for ChS samples.

As can be seen from Table 1, ChS molecules are characterized by a certain rigidity and ionogenicity. These results are in good agreement with the literature data [18]. The influence of both ionogenicity and kinetic rigidity of ChS and protein on their behavior in solutions with different concentrations and pH was determined to select the optimal conditions necessary to obtain complexes based on the *Bombyx mori* protein and chitosan. The preparation of complexes depends on the initial concentration of protein substances. Therefore, protein alkaline hydrolysate and a solution of *Bombyx mori* ChS in acetic acid were used to effectively carry out the process.

When obtaining complexes by direct titration of pH from alkaline to neutral media a monotonous increase in turbidity to pH = 7 occurs, the yield of the obtained complexes changes insignificantly. According to [19], the amino group of ChS at a pH value above 7 is deprotonated, exhibits nucleophilic properties, and

participates in the nucleophilic substitution reaction. However, in an alkaline environment, the protein molecule acquires a negative charge and exhibits ionogenic properties.

We have previously shown [16] that the *Bombyx mori* protein has five AAs that are uncharged but have polar side chains. They include asparagine, threonine, serine, glutamine, and tyrosine, as well as three AAs, namely lysine, arginine, and histidine with charged basic groups. These AAs are hydrophilic and can interact through electrostatic, hydrogen bonds, hydrophobic and steric interactions with water. They make up 1.9 % of one protein chain, at the N- and C-terminals of the polypeptide chains there are amino and carboxyl groups that contain functional groups capable of ionization. The degree of ionization of the functional groups of these radicals depends on the pH value.

In an alkaline environment at pH 10.96 with an excess of NaOH and the presence of a larger amount of Na⁺ ions, the charge and degree of ionization in the protein molecule decreases and the conformation of the protein macromolecule looks like a coil [17]: HONH₃-R-COONa.

Due to the presence of a large ionization group the interaction of the *Bombyx mori* protein with ChS does not result in a nucleophilic substitution reaction. Also in protein molecules, because of the large number of hydroxyl ions the positive charge decreases and the protein behaves like an acid (according to the reaction shown in the diagram).



At pH = 7 all ionogenic groups of the protein are in an ionized state.

It is known [20] that at low pH values (pK_a<6.5) the amino group is protonated, ChS is a cationic water-soluble polyelectrolyte and is capable of various types of interaction with the formation of 4 main types of bonds, namely ionic, hydrogen, hydrophobic, bonds by the type of complexation in which ChS acts as the core of the complex.

In this regard, the study is aimed at identifying the pH range from neutral to acidic during the formation of the complex of the protein and *Bombyx mori* ChS, as well as determining the special characteristics of the obtained samples. For titration of the protein solution 2 % solutions of ChS were prepared in a 2 % aqueous solution of CH₃COOH — pH=2.8. The resulting precipitate was filtered off, washed to pH=7 and freeze-dried for 2 hours.

Table 2 presents the results of obtaining complexes by direct titration from neutral to acidic value. The influence of the pH of the titrant at the stage of obtaining the complex from the protein hydrolysate was evaluated by elemental analysis and the weight of the complex referred to the maximum possible.

Table 2

Influence of medium pH on the physicochemical characteristics of the complex

No.	Protein hydrolysate, ml	2 % acetic acid, ml	2 % ChS pH 3.94	Solution 2 % ChS (pH 3.94), ml	pH	Yield, g	Nitrogen, %	Sulfur, %	Ash content, %
1	50	-	77	77	4.8	1.9	12.6	5.8	2.0
2	50	-	40	40	6.3	1.6	14.4	4.8	2.7
3	50	-	30	30	6.7	1.0	15.4	4.1	5.5
4	50 (control)	90	-	-	4.8	1.2	11.7	4.6	5.6

It can be seen from Table 2 that an increase in pH from 4.8 to 6.7 in the system (samples No. 1–3) leads to an increase in the degree of nitrogen content and ash content, as well as a decrease in sulfur and the complex yield. With an increase in pH from the isoionic point (IIP) to a neutral value the *Bombyx mori* protein macromolecule monotonously acquires a negative charge and entropy decreases while the coil of the macromolecule in this medium unfolds and the chain becomes flexible. At pH 6.3–6.7 (samples No. 2–3) the interaction of ChS with the *Bombyx mori* protein occurs efficiently, with a decrease in pH < 7 the protein and ChS have ionogenic properties: the protonated amino group of ChS is a cation and the protein is an anion. In this case, an increase in the nitrogen content occurs: an increase by 14–22 % (in relation to sample No. 1), respectively, due to the synergistic effect of the nitrogen content in the protein and ChS. With an increase in the acidity of the value pH = 6.7–4.8 the process of mineralization occurs and the ash content decreases in samples No. 1–3. This result is confirmed by the literature data [20]. As can be seen from Table 2 with IIP of the *Bombyx mori* protein which is at pH = 4.8 (sample 4), the yield of the control sample decreases by 60 % and the nitrogen content by 7.5 % because of the absence of *Bombyx mori* ChS (in relation to sample No. 1).

IR spectroscopy is a reliable method showing the interaction between ChS molecules and the *Bombyx mori* protein at different pHs. Figure 1 illustrates comparative studies by IR spectroscopy.

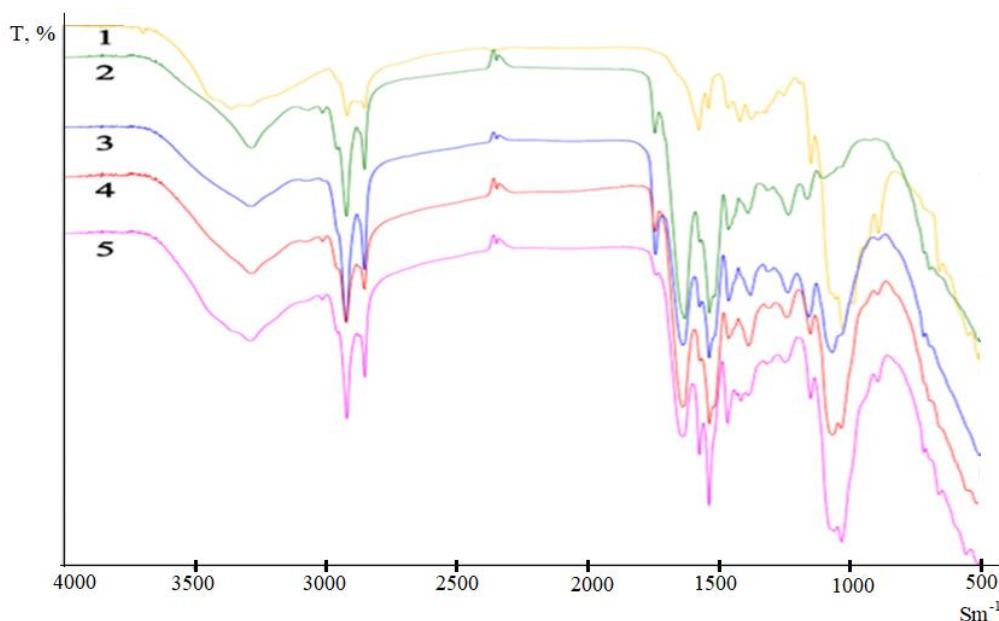


Figure 1. IR spectra of the initial ChS (1), protein (2) and their complexes at pH = 4.8 (3), pH = 6.3 (4) and pH = 6.7 (5) of the value

It can be seen that the IR spectrum of the initial ChS (1) and *Bombyx mori* protein (2) has characteristic absorption bands for these compounds. The IR spectrum of ChS (sample 1) has absorption bands at 3320 cm^{-1} , 3288 cm^{-1} and 2950 cm^{-1} , 2880 cm^{-1} corresponding to the stretching vibrations of -NH , -OH and -CH , CH_2 -groups, respectively. Pronounced absorption bands at $1590\text{--}1620\text{ cm}^{-1}$ (amide I) and at $1510\text{--}1550\text{ cm}^{-1}$ (amide II), as well as 1440 cm^{-1} , correspond to the bending vibrations of NH- , CN- , CO- and CH- , CH_2 -groups. Absorption bands characterizing CO- , C-O-C ether bonds are observed at $1000\text{--}1150\text{ cm}^{-1}$.

In the IR spectrum of the *Bombyx mori* protein (sample 2), several relatively strong absorption bands appear which refer to vibrations of the peptide group -CO-NH- , as a common structural component of protein molecules. There is a peak of -NH , -OH at wave numbers 3282 cm^{-1} , as well as peaks in the region of 2919 cm^{-1} , 2851 cm^{-1} and 1744 cm^{-1} , corresponding to the stretching vibrations of CH- , CH_2 -, -COOH groups, respectively. The presence of two main absorption bands due to stretching vibrations of the -NH bond, a peak at 1631 cm^{-1} , and in-plane bending vibrations of the -NH_2 bond — a peak at 1537 cm^{-1} , are characteristic of the protein structure.

The complex should be realized at a pH above the isoelectric point of the protein ($\text{pH} \approx 4.8$), at which the ion-dipole interaction occurs between the negatively charged protein and ChS with polar -NH_2 groups. As a result of the formation of complexes in samples at pH = 4.8 (3), 6.3 (4) and 6.7 (5), some changes occur in the absorption bands of the above groups and bonds. Namely, pronounced bands appear at wavenumbers of $3000\text{--}3500\text{ cm}^{-1}$ due to the shift of stretching vibrations of the band of -NH_2 groups of ChS and -NH groups of the protein. Particularly there are pronounced some changes and shifts in the absorption bands in the IR spectra of sample (5) obtained at pH 6.7. The absorption bands of bending vibrations at 3287 cm^{-1} are shifted by 13 cm^{-1} (3300 cm^{-1}) and become more pronounced and the absorption intensity of asymmetric angular deformation at 2918 cm^{-1} is more pronounced. The absence of absorption bands of stretching vibrations at 1517 cm^{-1} characteristic of -NH_2 groups (amide I), as well as stretching vibrations in the region of 1467 cm^{-1} become pronounced in samples No. 3 and No. 4.

Natural polysaccharides and proteins have a pronounced optical anisotropy, which makes it possible to conduct studies at the molecular and supramolecular levels using optical methods [21]. Determination of optical density is an informative and widely used parameter for monitoring changes in the behavior of proteins and polysaccharides during the formation of complexes [22]. The most effective method is the turbidimetric method based on measuring the intensity of the light flux scattered by solid particles suspended in solution (usually at an angle of 90°). The intensity of scattered light depends on the number of suspended particles and

their size. A sample of complexes based on ChS and protein from *Bombyx mori* is practically insoluble and is a suspension at neutral pH. Figure 2 shows the results of a comparative study of changes in the regularity of optical density according to the precipitation of the complex at pH from an alkaline to an acidic medium determined by the turbidimetric method on a Turbidimeter TB300IR instrument (Germany). Graphically the dependence of optical density (NTU) determined by the turbidimetric method on pH is shown in Figure 2.

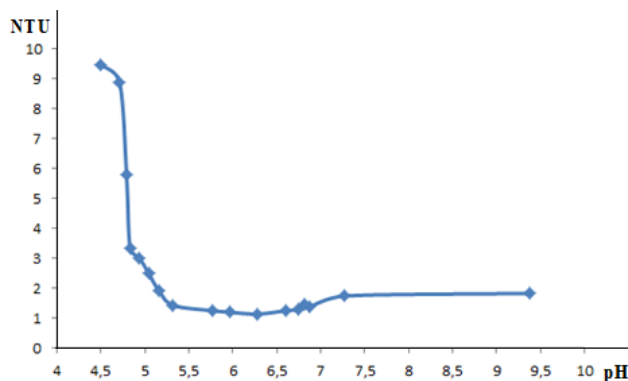


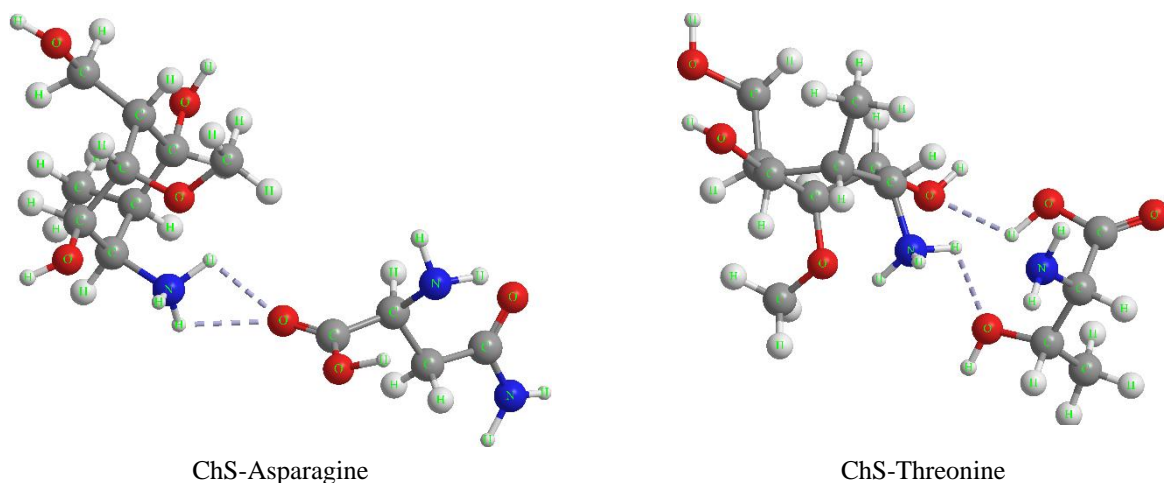
Figure 2. The dependence of the optical density of ChS-protein complexes on pH

From Figure 2 it can be seen that the lowest optical density is observed in the range of pH = 5.7–6.8, the values of the optical index of the complex sample decrease. In this interval, the maximum precipitation of the complex occurs and the volume of the solution becomes more transparent.

As studies have shown the interaction of ChS with protein is strongly influenced by the pH of the medium and the ratio of components. ChS and protein with opposite charges at pH 5.5 and 6.0 can interact with each other through electrostatic attraction. In addition, at these two pH values the interaction was further influenced by the concentration of ChS. It can be concluded that under these parameters the greatest interaction between the components of the system occurs and ultimately the formation of the ChS-protein complex.

At low pH values the protonated amino group gives ChS the ability to bind to negatively charged molecules via electrostatic interaction [23]. In addition, a number of earlier studies noted the decisive role of hydrogen bonds in the formation of complexes of protonated ChS with electrically neutral nitrogenous bases. It is known that amino acids form hydrogen bonds with various carrier molecules [24, 25].

The calculated group charge distribution for the tertiary hydrogen atom of the protonated amino group of ChS is 1.54 a.u [26]. These values indicate that these hydrogen atoms have a tendency to form hydrogen bonds with electronegative centers. Similarly, a group charge of 1.54 a.e. for two atoms of nitrogen and oxygen in histidine allowed us to evaluate the atypical ChS-histidine interaction between electronegative atoms with $-\text{OH}$ and $-\text{NH}_3^+$ ChS groups. Figure 3 demonstrates the optimized structure of the complexes under consideration.



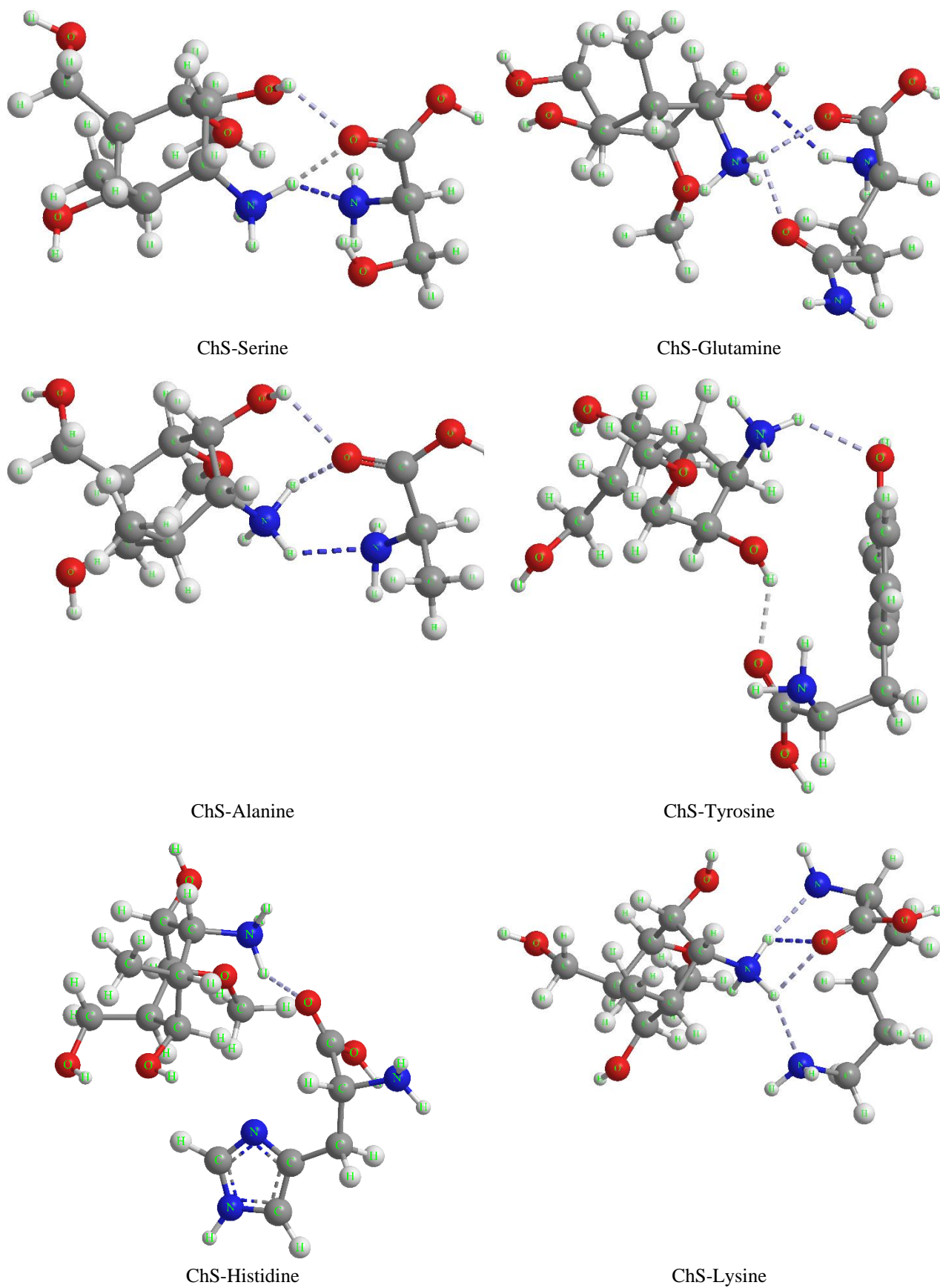


Figure 3. Optimized geometries of ChS complexes with AAs

The DFT calculations showed the presence of hydrogen bonds between the hydrogen atom of the amino group or $-OH$ of the ChS group and the O atom of the $-COO^-$ or $-OH$ groups of the studied amino acids (Table 3). According to Table 3, the distance between the H atom of the $-NH_3^+$ or $-OH$ -group of ChS and the O atom of the $-COO^-$ or $-OH$ groups of AAs is in the range of 0.96–1.34 Å, which is typical for hydrogen bonds [27]. This indicates that chitosan forms hydrogen bonds with amino acids during the formation of complexes. It is important to note the anomalously shorter $H_{ChS}-O_{Threonine}$ distance in the ChS-Threonine and $N_{Histidine}-O_{ChS}$ system (0.96 Å) for the ChS-Histidine interaction. Various protonation states of the complexes were tested as starting points for geometry optimization. The results confirmed the proton transfer only in the ChS-Histidine system while denying the same in the case of other complexes. Cationic or anionic AAs are well known for their ability to form hydrogen bonds with oppositely charged species [28, 29]. However, the formation of such a salt bridge in the gas phase of the complexes under consideration was not observed.

Studies have shown that ChS and its derivatives form stable complexes with proteins and peptides [30, 31]. The magnitude of the interaction energy (ΔE_{inter}) of complexes is of decisive importance from the point of view of the resistance of the complexing protein to degradation during the transition of the protein into the cell, as well as the transfer of the protein near or inside the cell nucleus. A high value of ΔE_{inter} promotes strong binding between ChS and AAs in the complex while a decrease in energy values promotes the complex dissociation. Moreover, on the basis of the ΔE_{inter} values the suitability of the carrier with respect to a particular AA can be assessed. The calculated values of ΔE_{inter} in the gas phase are presented in Table 3. As can be seen from the Table 3 with the exception of the complex with Histidine (-11.45 kcal/mol) the calculated values of ΔE_{inter} are negative in all cases, which contributes to the formation of complexes in the range from -17.56 to -129.46 kcal/mol. Other similar studies report that the binding energy of the most stable conformation of the ChS-Insulin complex is -38.0 kcal/mol [32], the release energy of doxorubicin by polyethylene glycol-chitosan biopolymer is 122.41 kcal/mol [33].

The formation of a complex of protonated ChS with a positively charged methionine is obviously not a spontaneous reaction, which indicates a repulsive interaction between them. The value of ΔE_{inter} ranges from 11.45 kcal/mol (ChS-Lysine) to -129.41 kcal/mol (ChS-Serine) in the gas phase and from -11.03 kcal/mol (ChS-Lysine) to -22.09 kcal/mol (ChS-asparagine). As for the anomalously high value of ΔE_{inter} , this may be due to the strong Coulomb force of attraction, which leads to hydrogen migration. The strength of the interaction is in the following order: ChS-Asparagine > ChS-Alanine > ChS-Glutamine > ChS-Serine > ChS-Tyrosine > ChS-Threonine > ChS-Lysine > ChS-Histidine.

As can be seen from Table 3, the influence of the aqueous phase largely affects the interaction energy of these systems. There is a progressive destabilization of ChS complexes with AAs with the exception of histidine. In addition, it is worth noting that the complex with asparagine (in which the two functional groups are charged oppositely) have a significant decrease in the values of ΔE_{inter} compared to other complexes. For example, the ΔE_{inter} value for the ChS-Serine complex in water is -16.83 kcal/mol in the aqueous phase, indicating a difference of about 112.58 kcal/mol with the value in the gas phase. In the case of ChS-Tyrosine this difference is about 2.31 kcal/mol, respectively, the values of the interaction energy are -18.38 (gas phase) and -16.07 (water phase). The results show that monomers with opposite charges are indeed more separated and more stable than complexes in water, which leads to a decrease in ΔE_{inter} .

This can also be explained by the fact that in polar environments the interaction with the environment (solvation) is probably more important than the electrostatic interaction between the two interacting molecules, which leads to their preferential stabilization. In addition, it is interesting to note the invariably negative value of ΔE_{inter} in the aqueous phase for the complex with histidine, which contrasts sharply with what is observed in the gas phase. Due to the solvation of positively charged fragments, the repulsive interaction between them decreases, which can increase the strength of their interaction with the formation of hydrogen bonds. The results obtained ΔE_{inter} in the gas and water phases are very important from the point of view of protein delivery. The results indicate a strong interaction between ChS and AAs in a non-polar environment and a gradual weakening of the interaction in the aqueous phase. These results are of interest in modeling the process of penetration of complexes through a cell membrane, which is non-polar in nature. Thus, it is assumed that in the cytoplasm (which is polar in nature) the interaction will be the weakest, which can promote the dissociation of the complex into the corresponding fragments. It is important to note that the ability of chitosan to release amino acids into the cytoplasmic environment is comparable to that of ChS derivatives [34, 35]. Significantly high value of ΔE_{inter} in the gas phase at a very low energy value in the aqueous phase for the complexes indicates its suitability for use in biomedicine. An increase in the efficiency of ChS as a carrier of nitrogenous bases RNA and DNA was also studied in [36–39].

Table 3

Hydrogen bond distance and BSSE corrected interaction energy of ChS with AAs complexes

Complex	Aqueous phase, Å	$\Delta E_{\text{inter.}}$, kkal/mol (Gas phase)	$\Delta E_{\text{inter.}}$, kkal/mol (Aqueous phase)
ChS-Asparagine	1.07	-110.81	-22.09
ChS-Threonine	0.96	-127.60	-15.54
ChS-Serine	1.07	-129.41	-16.83
ChS-Glutamin	1.09	-80.56	-16.95
ChS-Alanin	1.026	-42.62	-19.65
ChS-Tyrosin	1.047	-18.38	-16.07
ChS-Histidin	0.96	-11.45	-11.03
ChS-Lysin	1.046	-17.56	-21.14

The use of pure therapeutic peptides and proteins in medicine is relevant but the main problem is stability in the gastrointestinal environment. They are vulnerable to electrophilic attack by various ions present in the gastrointestinal tract resulting in protein degradation. Therefore, understanding the chemical activity of the studied complexes in various media is important from the point of view of their medical applications. Reactivity descriptors determined [40] on the basis of a theoretical physico-chemical study by the DFT and electronic structure have become an auxiliary tool for interpreting the chemical and biological activity of compounds.

The calculated values of these parameters among the selected systems in the gas and water phases are presented in Tables 4 and 5.

Table 4

Calculated electronic parameters in the gas phase of amino acids and complexes

Amino acid	E_{HOMO} , eV	E_{LUMO} , eV	ΔE	Complex	E_{HOMO} , eV	E_{LUMO} , eV	ΔE
Asparagine	-9.98	0.80	10.78	ChS-Asparagine	-9.62	0.56	10.19
Threonine	-9.91	1.02	10.93	ChS-Threonine	-9.15	0.51	9.66
Serine	-10.12	0.83	10.96	ChS-Serine	-9.49	0.35	9.84
Glutamine	-10.23	0.66	10.9	ChS-Glutamine	-9.68	0.5	10.19
Alanine	-9.97	0.77	10.74	ChS-Alanine	-8.78	1.6	10.38
Tyrosine	-9.14	0.14	9.28	ChS-Tyrosine	-8.97	0.35	9.32
Histidine	-8.31	-0.02	8.34	ChS-Histidine	-7.09	-1.13	8.23
Lysine	-9.29	0.92	10.21	ChS-Lysine	-9.53	0.75	10.29

Table 5

Calculated descriptors of reactivity in the gas phase of complexes

Complex	Chemical hardness (η), eV	Electrophilicity Index (ω), eV	Chemical potential (μ), eV	Softness (ζ), eV ⁻¹
ChS-Asparagine	4.52675	2.8691	-5.09665	0.220909
ChS-Threonine	4.32	2.7031	-4.8327	0.231481
ChS-Serine	4.56855	2.6514	-4.92205	0.218888
ChS-Glutamine	4.5875	2.8307	-5.0963	0.217984
ChS-Alanine	3.5879	3.7573	-5.1925	0.278715
ChS-Tyrosine	4.31255	2.5226	-4.66455	0.231881
ChS-Histidine	2.98245	5.9649	-5.9649	0.335295
ChS-Lysine	4.39235	3.0155	-5.14695	0.227669

The measurement of the E_{HOMO} of the complexes is an important factor since this characteristic indicates the electron donating capacity, i.e. reactivity of compounds. The narrow HOMO-LUMO band gap means that the molecule has low kinetic stability and high biological activity. According to the calculation results, there is a sharp drop in the HOMO energy in AAs during the formation of a complex with ChS, which speaks in favor of a more stable HOMO in complexes than in AAs. This result means that complexes of ChS with AAs are less prone to attack by any electrophile than the AAs themselves. Similarly, a high neg-

ative value of μ means a relatively large stability of the system. As can be seen from Tables 4 and 5, in accordance with E_{HOMO} and E_{LUMO} , data on the chemical potential also characterize the greater chemical stability of the complexes than AAs and also show differences in the nature of the interaction with respect to different AAs. The narrow energy gap characterizes the nucleophilic properties of the complexes. According to the calculation data given in Table 4, the smallest band gap ΔE (8.34 eV) is observed for the ChS-Histidine complex and 9.28 eV for ChS-Tyrosine. All complexes have a wide HOMO-LUMO band gap. This may be due to low chemical activity and high kinetic stability.

Chemical hardness quantitatively determines the chemical stability of a molecular system in various media [37]. The higher the electronegativity, the more electronegative the molecule is, and the higher the value of chemical hardness, the "harder" the molecule is [38–40]. According to Table 5, the value of chemical hardness (2.98) for ChS-Histidine indicates a greater stability of the complex than AAs but at the same time characterizes a large difference in the interaction energy compared to other AAs. The chemical mildness of ChS-Histidine increases and the activity increases. Moreover, in all cases, the maximum stiffness is not associated with a small value of electrophilicity. In addition, it is worth noting that the stability predicted by the change in the interaction energy of the gas phase coincides with the trend shown by the values of E_{HOMO} and η . The order of stability in the gas phase of the ChS-Histidine complex according to the values of E_{HOMO} , η , and ζ , which also correlates with the value of the interaction energy. However, this correlation of interaction energy values with reactivity descriptor values for the ChS-Histidine system is not consistent with those of other interactions of ChS with AAs. As in the case of complexes with lysine and tyrosine, the highest values of the interaction energy do not correlate with the values of η and ζ . This fact of discrepancy can be explained by the fact that the LUMO of AAs (acting as an H-donor/acceptor of electrons) in different complexes interact to a different extent. Although the nature of the change in η does not allow us to make any general conclusion about the chemical stability of the studied complexes, the values of HOMO and η do confirm the greater stability of the ChS-Histidine complex compared to histidine, as well as the orders of stability, the calculated values of η and ζ are in full agreement with calculated values ΔE_{inter} .

Conclusions

Thus, based on carried out studies, it was shown that the initial macromolecules of *Bombyx mori* protein and chitosan biopolymers have their own behavioral features. A protein alkaline hydrolysate was obtained from *Bombyx mori* pupae with a protein content that contains amino- and -carboxylic functional groups and amino acids radicals located in the protein chain, which are capable of ionization. It is shown that the structure of chitosan is characterized by a certain rigidity and ionogenicity. Based on the studies results, the fundamental possibility of obtaining complexes of chitosan with the *Bombyx mori* protein at various pH values was revealed.

The results of calculations based on the quantum-chemical theory of the density functional of the interaction of chitosan with amino acids that are part of the *Bombyx mori* protein confirm the presence of a hydrogen bond. Complexes are more chemically stable than pure amino acids. The calculated values of the reactivity descriptors and stability of the complexes are sensitive to the nature of the functional modification, as well as to the prevailing environment. It should be noted that the complex with histidine is unstable in the gas phase but acquires significant stability in the aqueous environment. Chitosan exhibits a stronger interaction in a nonpolar environment and a gradual weakening is observed with increasing polarity of the environment, although there is no linear correlation between the interaction energy and the permittivity of the environment.

References

- 1 Милушева Р.Ю. Белок из куколок тутового шелкопряда *Bombyx mori* L. Выделение, свойства, применение / Р.Ю. Милушева, О.Б. Авазова, С.Ш. Рашидова. — Ташкент: ФАН; Академия наук Республики Узбекистан, 2021. — 216 с.
- 2 Oliveira, J.M. Chitosan / J.M. Oliveira, H. Radhouani, R.L. Reis // Polysaccharides of Microbial Origin: Biomedical Applications. — Springer, 2022. — 1320 pp.
- 3 Авазова О.Б. Особенности получения и модификации хитозана *Bombyx mori* в сдвиговом потоке: дис. ... канд. хим. наук. — 02.00.06 — «Высокомолекулярные соединения»/ Авазова Ойнавад Баратовна. — Ташкент, 2012. — 130 с.
- 4 Каблов В.Ф. Использование хитозана как флокулянта в процессах выделения белка из молочной сыворотки / В.Ф. Каблов, Ю.П. Иощенко // Успехи современного естествознания. — 1985. — Т. 36, № 8, — С. 421–424.

- 5 Gamzazade, A.I. Investigation of the hydrodynamic properties of chitosan solutions / A.I. Gamzazade, B.M. Shlimak, A.M. Sklyar, E.V. Stykova, S.A. Pavlova, S.V. Rogozin // *Acta Polymerica*. — 1985. — Vol. 36, No. 8. — P. 421–424.
- 6 Becke, A.D. Density-functional thermochemistry. III. The role of exact exchange / A.D. Becke // *The Journal of Chemical Physic.* — 1993. — Vol. 98. — P. 5648–5652. <https://doi.org/10.1063/1.464913>
- 7 Ektirici, S. Computational investigation of the monomer ratio and solvent environment for the complex formed between sulfamethoxazole and functional monomer methacrylic acid / S. Ektirici, Ö. Kurç, M. Jalilzadeh, S. Aşır, D. Türkmen // *ACS Omega*. — 2022. — Vol. 7. — P. 17175–17184. <https://doi.org/10.1021/acsomega.2c00862>
- 8 Sarma, R. Short range interactions in molecular complexes of 1,4-benzenediboronic acid with aromatic N-oxides / R. Sarma, P.K. Bhattacharyya, J.B. Baruah // *Computational and Theoretical Chemistry*. — 2011. — Vol. 963. — P. 141–147. <https://doi.org/10.1016/j.comptc.2010.10.020>
- 9 Houshmand, F. Host-guest interaction in chitosan–MX (3-chloro-4-(dichloromethyl)-5-hydroxy-2(5H)-furanone) complexes in watersolution: Density Functional Study / F. Houshmand, H. Neckoudaria, M. Baghdadic // *Asian Journal of Nanoscience and Materials*. — 2018. — Vol. 2, No. 1. — P. 49–65.
- 10 Deka, B.C. Understanding chitosan as a gene carrier: A DFT study / B.C. Deka, P.Kr. Bhattacharyya // *Computational and Theoretical Chemistry*. — 2015. — Vol. 1051. — P. 35–41. <https://doi.org/10.1016/j.comptc.2014.10.023>
- 11 Deka, B.C. Response of chitosan–nucleobase interaction toward external perturbations: A computational study / B.C. Deka, P.Kr. Bhattacharyya // *Computational and Theoretical Chemistry*. — 2016. — Vol. 1078. — P. 72–80. <https://doi.org/10.1016/j.comptc.2015.12.016>
- 12 Jeremić, S. Insight into interaction properties between mercury and lead cations with chitosan and chitin: Density functional theory studies / S. Jeremić, H. Tran, Z. Marković, T.C. Ngo, D.Q. Dao // *Computational and Theoretical Chemistry*. — 2018. — Vol. 1138. — P. 99–106. <https://doi.org/10.1016/j.comptc.2018.06.010>
- 13 Anchique, L. Predicting the Adsorption of Amoxicillin and Ibuprofen on Chitosan and Graphene Oxide Materials: A Density Functional Theory Study / L. Anchique, J.J. Alcázar, A. Ramos-Hernandez, M. Méndez-López, J.R. Mora, N. Rangel, J. Luis Paz, E. Márquez // *Polymers*. — 2021. — Vol. 13. — P. 1620. <https://doi.org/10.3390/polym13101620>
- 14 Galano, A. A New approach to counterpoise correction to BSSE / A. Galano, J.R.A. Idaboy // *Journal of Computational Chemistry*. — 2006. — Vol. 27, No. 11. — P. 1203–1210. <https://doi.org/10.1002/jcc.20438>
- 15 Miehlich, B. Results obtained with the correlation energy density functionals of becke and Lee, Yang and Parr / B. Miehlich, A. Savin, H. Stoll, H. Preuss // *Chemical Physics Letters*. — 1989. — Vol. 157. — P. 200–206. [https://doi.org/10.1016/0009-2614\(89\)87234-3](https://doi.org/10.1016/0009-2614(89)87234-3)
- 16 Авазова О.Б. Поведение белка *Bombyx mori* в растворах и его структурные исследования / О.Б. Авазова, Р.Ю. Милушева, С.Ш. Рашидова // *Журн. Доклады Академии наук Республики Узбекистан*. — 2021. — № 4. — С. 39–42.
- 17 Ленинджер А. Биохимия / А. Ленинджер. — М.: Мир, 1974. — 960 с.
- 18 Цветков В.Н. Жесткоцепные полимерные молекулы / В.Н. Цветков. — Л.: Наука, 1986. — 380 с.
- 19 Буткевич Т.В. Использование хитозана в производстве молочных продуктов / Т.В. Буткевич, В.П. Варламов, И.А. Евдокимов, Л.Р. Алиева // *Тр. Белорус. гос. ун-та*. — 2014. — Т. 9, № 2. — С. 181–190.
- 20 Курченко В.П. Механизм взаимодействия хитозана с белками молочной сыворотки / Л.Р. Алиева, Т.В. Буткевич, Н.В. Гавриленко // *Тр. Белорус. гос. ун-та*. — 2013. — Т. 8, № 1. — С. 45–51.
- 21 Захарченко В.Н. Коллоидная химия / В.Н. Захарченко. — М.: Высш. шк., 1989. — 238 с.
- 22 Kurukji, D. Fabrication of sub-micron protein-chitosan electrostatic complexes for encapsulation and pH-Modulated delivery of model hydrophilic active compounds / D. Kurukji, I. Norton, F. Spyropoulos // *Food Hydrocolloids*. — 2016. — Vol. 53. — P. 249–260. <https://doi.org/10.1016/j.foodhyd.2015.02.021>
- 23 Patent US005747475A, 05.05.1998. Chitosan-derived biomaterials // United States Patent No 5,747,475 / Nordquist, R.E., Chen, W.R., Carubelli, R., Adams, R.
- 24 Jun, D. Properties and Applications of Amino-acid Complex / D. Jun, Z. Junhao, F. Bin // *Progress in Chemistry*. — 2003. — Vol. 53, No 4. — P. 288–294.
- 25 Xu, Q. Application of Amino Acids in the Structural Modification of Natural Products / Q. Xu, H. Deng, X. Li, Z.-S. Quan // *Frontiers in Chemistry*. — 2021. — Vol. 9. <https://doi.org/10.3389/fchem.2021.650569>
- 26 Emmanuel, M. Theoretical Study of the Interaction between Chitosan Constituents (Glucosamine and Acetylglucosamine Dimers) and Na⁺ Ions / M. Emmanuel, A. Pogrebnoi, T. Pogrebnya // *Open Access Library Journal*. — 2015. — Vol. 2, No. e1978. <https://doi.org/10.4236/oalib.1101978>
- 27 Deka, B.C. Understanding chitosan as a gene carrier: A DFT study / B.C. Deka, P.K. Bhattacharyya // *Computational and Theoretical Chemistry*. — 2015. — Vol. 1015. — P. 35–41. <https://doi.org/10.1016/j.comptc.2014.10.023>
- 28 Melo, A. Theoretical study of arginine–carboxylate interactions / A. Melo, M. Ramos, W. Floriano, J. Gomes, J. Leao, A. Magalhaes, B. Maigret, M. Nascimento, N. Reuter // *Journal of Molecular Structure: THEOCHEM*. — 1999. — Vol. 463, No. 1–2. — P. 82–90. [https://doi.org/10.1016/S0166-1280\(98\)00396-0](https://doi.org/10.1016/S0166-1280(98)00396-0)
- 29 Donald, J.E. Salt bridges: Geometrically specific, designable interactions. *Proteins: Structure, Functions* / J.E. Donald, D.W. Kulp, W.F. DeGrado // *Bioinformatics*. — 2010. — Vol. 79, No. 3. — P. 898–915. <https://doi.org/10.1002/prot.22927>
- 30 Calvo, P. Novel hydrophilic chitosan-polyethylene oxide nanoparticles as protein carriers / P. Calvo, C. Remunan-Lopez, J. Vila-Jato, M. Alonso // *Journal of Applied Polymer Science*. — 1997. — Vol. 63, No. 1. — P. 125–132. [https://doi.org/10.1002/\(SICI\)1097-4628\(19970103\)63:1<125::AID-APP13>3.0.CO;2-4](https://doi.org/10.1002/(SICI)1097-4628(19970103)63:1<125::AID-APP13>3.0.CO;2-4)

- 31 Lin, Y.-H. Preparation and Characterization of Nanoparticles Shelled with Chitosan for Oral Insulin Delivery / Y.-H. Lin, F.-L. Mi, C.-T. Chen, W.-C. Chang, S.-F. Peng, H.-F. Liang, H.-W. Sung // *Biomacromolecules*. — 2007. — Vol. 8, No. 1. — P. 146–152. <https://doi.org/10.1021/bm0607776>
- 32 Al-Sou'od K. Interaction Between Low Molecular Weight Chitosan and Some Types of Drugs and Insulin / K. Al-Sou'od // *Asian Journal of Chemistry*. — 2012. — Vol. 24, No. 9. — P. 3785–3790.
- 33 Srinophakun, T. Preliminary Study of Conformation and Drug Release Mechanism of Doxorubicin-Conjugated Glycol Chitosan, via cis-Aconityl Linkage, by Molecular Modeling / T. Srinophakun, J. Boonmee // *International Journal of Molecular Sciences*. — 2011. — Vol. 12, No. 3. — P. 1672–1683. <https://doi.org/10.3390/ijms12031672>
- 34 Thanou, M. Effect of degree of quaternization of N-trimethyl chitosan chloride for enhanced transport of hydrophilic compounds across intestinal Caco-2 cell monolayers / M. Thanou, A. Kotze, T. Scharringhausen, H. Luessen, A. De Boer, J. Verhoef, H. Junginger // *Journal of Controlled Release*. — 2000. — Vol. 64, No. 1–3. — P. 15–25. [https://doi.org/10.1016/S0168-3659\(99\)00131-5](https://doi.org/10.1016/S0168-3659(99)00131-5)
- 35 Liu, W.G. N-Alkylated Chitosan as a Potential Nonviral Vector for Gene Transfection / W.G. Liu, X. Zhang, S.J. Sun, G.J. Sun, K.D. Yao, D.C. Liang, G. Guo, J.Y. Zhang // *Bioconjugate Chemistry*. — 2003. — Vol. 14, No. 4. — P. 782–789. <https://doi.org/10.1021/bc020051g>
- 36 Deka, B.C. Reactivity of chitosan derivatives and their interaction with guanine: A computational study / B.C. Deka, P.K. Bhattacharyya // *Journal of Chemical Sciences*. — 2016. — Vol. 128, No. 4. — P. 589–598. <https://doi.org/10.1007/s12039-016-1064-6>
- 37 Parr, R.G. Principle of maximum hardness / R.G. Parr, P.K. Chattaraj // *Journal of the American Chemical Society*. — 1991. — Vol. 113, No. 5. — P. 1854–1855. <https://doi.org/10.1021/ja00005a072>
- 38 Bachrach, S.M. Population Analysis and Electron Densities from Quantum Mechanics / K.B. Lipkowitz, D.B. Boyd // *Reviews in Computational Chemistry*. — 2007. — P. 171–228. <https://doi.org/10.1002/9780470125823.ch3>
- 39 Chattaraj, P.K. Chemical reactivity theory: a density functional view, 1st edition / P.K. Chattaraj. — CRC Press, 2009. — 616 p.
- 40 Chattaraj, P.K. Update 1 of: Electrophilicity Index. / P.K. Chattaraj, D.R. Roy // *Chemical Reviews*. — 2007. — Vol. 113, No. 5. — P. PR46–PR74. <https://doi.org/10.1021/cr078014b>

О.Б. Авазова, Р.Ю. Милушева, И.Н. Нұрғалиев, С.Ш. Рашидова

Хитозан *Bombyx mori* бар ақуыздың полимолекулалық кешендері

Хитозан (ХЗ) мен *Bombyx mori* протеинінің әртүрлі реакция жағдайларындағы әрекеттесуі зерттеліп, хитозанның *Bombyx mori* ақуызымен кешендерін алудың негізгі мүмкіндігі анықталды. Ерітінділердегі хитозанмен ақуыздың полимолекулалық кешенінің түзілуі физикалық-химиялық әдістердің нәтижелерімен дәлелденді. Хитозанның құрылымы белгілі бір қаттылықпен және ионгенділікпен сипатталатыны көрсетілген. рН = 4,8–6,7 диапазонында 2 % сірке қышқылында хитозанмен дернәсілдер ақуызының кешені берілген. ИҚ-спектрлердегі жұтылу жолақтарының анықталған өзгерістері мен ығысулары рН = 4,88–6,7 кезінде хитозан мен ақуыз молекулалары арасында күрделі түзілу реакциясының болғанын растайды, ол 1641 см⁻¹, 1538 см⁻¹ және 1068 см⁻¹ ИҚ-спектрлердегі жұтылу жолақтарымен сипатталады. Тұт жібек құртының *Bombyx mori* дернәсілдерінен бөлініп алынған ақуыздың құрамына кіретін аминқышқылдарымен (АК) хитозан кешендерін кванттық-химиялық зерттеу DFT әдісімен жүргізілді. Кешеннің түзілуі кезінде сутектік байланыс арқылы газ фазасында гистидинмен түзілген кешенді қоспағанда, ХЗ-АК кешендерінің тұрақтылығы көрсетілген. Термодинамикалық қозғаушы күштің бар екені анықталған.

Кілт сөздер: жібек өндірісінің қалдықтары, тұт жібек құртының дернәсілдері, сілтілі гидролиз, ақуыз, хитин, хитозан, полимолекулалық кешендер, конформациялық сипаттамалар.

О.Б. Авазова, Р.Ю. Милушева, И.Н. Нурғалиев, С.Ш. Рашидова

Полимолекулярные комплексы белка с хитозаном *Bombyx mori*

Исследовано взаимодействие хитозана (ХЗ) и белка *Bombyx mori* при различных условиях реакции, выявлена принципиальная возможность получения комплексов ХЗ с белком *Bombyx mori*. Образование полимолекулярного комплекса белка с ХЗ в растворах подтверждено результатами физико-химических методов. Показано, что структура ХЗ характеризуется определенной жесткостью и ионогенностью. Показано комплексообразование куколичного белка с ХЗ в 2-процентной уксусной кислоте в диапазоне рН = 4,8–6,7. Обнаруженные изменения и смещения полос поглощений в ИК-спектрах подтверждают протекание реакции комплексообразования между молекулами ХЗ и белка при

pH = 4,88–6,7, которое характеризуется полосами поглощения на ИК-спектрах при 1641 см⁻¹, 1538 см⁻¹ и 1068 см⁻¹. Методом DFT проведено квантово-химическое исследование комплексов ХЗ с аминокислотами (АК), входящими в состав белка, выделенного из куколок тутового шелкопряда *Bombyx mori*. Показано, что стабильность комплексов ХЗ–АК, за исключением комплекса, образованного с гистидином в газовой фазе. Результаты расчетов свидетельствовали о наличии сильной термодинамической движущей силы при комплексообразовании ХЗ–АК.

Ключевые слова: отходы производства шелка, куколки тутового шелкопряда, щелочной гидролиз, белок, хитин, хитозан, полимолекулярные комплексы, конформационные характеристики.

References

- 1 Milusheva, R.Yu., Avazova, O.B., & Rashidova, S.Sh. (2020). *Belok iz kukolok tutovogo shelkopriada Bombyx mori L. Vydelenie, svoystva, primeneniye* [Protein from pupae of the silkworm *Bombyx mori* L. Isolation, properties, application]. FAN; Akademiya nauk Respubliki Uzbekistan — Academy of Sciences of the Republic of Uzbekistan, 216 [in Russian].
- 2 Oliveira, J.M., Radhouani, O.H., & Reis, R.L. (2022). *Polysaccharides of Microbial Origin: Biomedical Applications*, US: Springer.
- 3 Avazova, O.B. (2012). Osobennosti polucheniya i modifikatsii khitozana *Bombyx mori* v sdvigovom potoke [Features of obtaining and modification of *Bombyx mori* chitosan in shear flows]. *Candidate's thesis*. Tashkent [in Russian].
- 4 Kablov, V.F., & Ioshchenko, Yu.P. (1985). Ispolzovanie khitozana kak flokulianta v protsessakh vydeleniya belka iz molochnoi syvorotki [Using chitosan as a flocculant in the process of protein isolation from whey]. *Uspekhi sovremennogo estestvoznaniya — Advances in current natural sciences*, 36(8), 421–424 [in Russian].
- 5 Gamzazade, A.I., Shlimak, B.M., Sklyar, A.M., Stykova, E.V., Pavlova, S.A., & Rogozin, S.V. (1985). Investigation of the hydrodynamic properties of chitosan solutions. *Acta Polymerica*, 36(8), 421–424.
- 6 Becke, A.D. (1993). Density-functional thermochemistry. III. The role of exact exchange. *The Journal of Chemical Physics*, 98, 5648–5652. <https://doi.org/10.1063/1.464913>.
- 7 Ektirici, S., Kurç, Ö., Jalilzadeh, M., Aşır, S., & Türkmen, D. (2022). Computational investigation of the monomer ratio and solvent environment for the complex formed between sulfamethoxazole and functional monomer methacrylic acid. *ACS Omega* 7, 17175–17184. <https://doi.org/10.1021/acsomega.2c00862>.
- 8 Sarma, R., Bhattacharyya, P.K., & Baruah, J.B. (2011). Short range interactions in molecular complexes of 1,4-benzene-diboronic acid with aromatic N-oxides. *Computational and Theoretical Chemistry*, 963 141–147. <https://doi.org/10.1016/j.comptc.2010.10.020>.
- 9 Houshmand, F., Neckoudaria, H., & Baghdadic, M. (2018). Host-guest interaction in chitosan– MX (3-chloro-4-(dichloromethyl)-5-hydroxy-2(5H)-furanone) complexes in watersolution: Density Functional Study. *Asian Journal of Nanoscience and Materials*, 2(1), 49–65.
- 10 Deka, B.C., & Bhattacharyya, P.Kr. (2015). Understanding chitosan as a gene carrier: A DFT study. *Computational and Theoretical Chemistry*, 1051, 35–41. <http://dx.doi.org/10.1016/j.comptc.2014.10.023>.
- 11 Deka, B.C., & Bhattacharyya, P.Kr. (2016). Response of chitosan–nucleobase interaction toward external perturbations: A computational study. *Computational and Theoretical Chemistry*, 1078, 72–80. <http://dx.doi.org/10.1016/j.comptc.2015.12.016>.
- 12 Jeremić, S., Tran, H., Marković, Z., Ngo, T.C., & Dao, D.Q. (2018). Insight into interaction properties between mercury and lead cations with chitosan and chitin: Density functional theory studies. *Computational and Theoretical Chemistry*, 1138, 99–106. <https://doi.org/10.1016/j.comptc.2018.06.010>.
- 13 Anchique, L. Alcázar, J.J., Ramos-Hernandez, A., Méndez-López, M., Mora, J.R., Rangel, N., Luis Paz, J., & Márquez, E. (2021). Predicting the Adsorption of Amoxicillin and Ibuprofen on Chitosan and Graphene Oxide Materials: A Density Functional Theory Study. *Polymers*, 13, 1620. <https://doi.org/10.3390/polym13101620>.
- 14 Galano, A., & Idaboy, J.R.A. (2006). A new approach to counterpoise correction to BSSE. *Journal of Computational Chemistry*, 27(11), 1203–1210. <https://doi.org/10.1002/jcc.20438>.
- 15 Miehlich, B., Savin, A., Stoll, H., & Preuss, H. (1989). Results obtained with the correlation energy density functionals of Becke and Lee, Yang and Parr. *Chemical Physics Letters*, 157, 200–206. [https://doi.org/10.1016/0009-2614\(89\)87234-3](https://doi.org/10.1016/0009-2614(89)87234-3)
- 16 Avazova, O.B., Milusheva, R.Yu., & Rashidova, S.Sh. (2021). Povedeniye belka *Bombyx mori* v rastvorakh i ego strukturnyye issledovaniya [Protein behavior of *Bombyx mori* in solutions and its structural studies]. *Zhurnal Doklady Akademii nauk Respubliki Uzbekistan — Proceedings of Academy of Sciences of the Republic of Uzbekistan*, 4, 39–42 [in Russian].
- 17 Lenindzher, A. (1974). *Biokhimiya [Biochemistry]*. Moscow: Mir [in Russian].
- 18 Tsvetkov, V.N. (1986). *Zhestkotsepnyye polimernyye molekuly [Rigid-chain polymeric molecules]*. Leningrad: Nauka [in Russian].
- 19 Butkevich, T.V., Varlamov, V.P., Evdokimov, I.A., Alieva, L.R., & Kurchenko, V.P. (2014). Ispolzovanie khitozana v proizvodstve molochnykh produktov [Using Chitosan in the production of dairy products]. *Trudy Belorusskogo gosudarstvennogo universiteta — Proceedings of the Belarusian State University*, 9(2), 181–190 [in Russian].

- 20 Kurchenko, V.P., Alieva, L.R., Butkevich, T.V. & Gavrilenko, N.V. (2013). Mekhanizm vzaimodeistviia khitozana s belkami molochnoi syvorotki [Mechanism of interaction between chitosan and whey proteins]. *Trudy Belorusskogo gosudarstvennogo universiteta — Proceedings of the Belarusian State University*, 8(1), 45–51 [in Russian].
- 21 Zaharchenko, V.N. (1989). *Kolloidnaia khimiia* [Colloid chemistry]. Moscow: Vysshiaia shkola [in Russian].
- 22 Kurukji, D., Norton, I., & Spyropoulos, F. (2016). Fabrication of sub-micron protein-chitosan electrostatic complexes for encapsulation and pH-Modulated delivery of model hydrophilic active compounds. *Food Hydrocolloids*, 53, 249–260. <http://dx.doi.org/10.1016/j.foodhyd.2015.02.021>.
- 23 Nordquist, R.E., Chen, W.R., Carubelli, R., & Adams, R. (1998). *Patent No. 5,747,475*.
- 24 Jun, D., Junhao, Z., & Bin, F. (2003). Properties and Applications of Amino-acid Complex. *Progress in Chemistry*, 15(04), 288–294.
- 25 Xu, Q., Deng, H., Li, X., & Quan, Z.-S. (2021). Application of Amino Acids in the Structural Modification of Natural Products. *Frontiers in Chemistry*, 9. <https://doi.org/10.3389/fchem.2021.650569>.
- 26 Emmanuel, M., Pogrebnoi, A., & Pogrebnyaya, T. (2015). Theoretical Study of the Interaction between Chitosan Constituents (Glucosamine and Acetylglucosamine Dimers) and Na⁺ Ions. *Open Access Library Journal*, 2(e1978). <http://dx.doi.org/10.4236/oalib.1101978>.
- 27 Deka, B.C., & Bhattacharyya, P.K. (2015). Understanding chitosan as a gene carrier: A DFT study. *Computational and Theoretical Chemistry*, 1015, 35–41. <https://doi.org/10.1016/j.comptc.2014.10.023>.
- 28 Melo, A., Ramos, M., Floriano, W., Gomes, J., Leao, J., Magalhaes, A., Maigret, B., Nascimento, M., & Reuter, N. (1999). Theoretical study of arginine–carboxylate interactions. *Journal of Molecular Structure: THEOCHEM*, 463(1-2), 81–90. [https://doi.org/10.1016/S0166-1280\(98\)00396-0](https://doi.org/10.1016/S0166-1280(98)00396-0).
- 29 Donald, J.E., Kulp, D.W., & DeGrado, W. F. (2011). Salt bridges: Geometrically specific, designable interactions. *Proteins: Structure, Functions, Bioinformatics*, 79(3), 898–915. <https://doi.org/10.1002/prot.22927>.
- 30 Calvo, P., Remunan-Lopez, C., Vila-Jato, J., & Alonso, M. (1997). Novel hydrophilic chitosan-polyethylene oxide nanoparticles as protein carriers. *Journal of Applied Polymer Science*, 63(1), 125–132. [https://doi.org/10.1002/\(SICI\)1097-4628\(19970103\)63:1<125::AID-APP13>3.0.CO;2-4](https://doi.org/10.1002/(SICI)1097-4628(19970103)63:1<125::AID-APP13>3.0.CO;2-4)
- 31 Lin, Y.-H., Mi, F.-L., Chen, C.-T., Chang, W.-C., Peng, S.-F., Liang, H.-F., & Sung, H.-W. (2007). Preparation and Characterization of Nanoparticles Shelled with Chitosan for Oral Insulin Delivery. *Biomacromolecules*, 8(1), 146–152. <https://doi.org/10.1021/bm0607776>.
- 32 Al-Sou'od K. (2012). Interaction Between Low Molecular Weight Chitosan and Some Types of Drugs and Insulin. *Asian Journal of Chemistry*; 24(9), 3785–3790.
- 33 Srinophakun, T., & Boonmee, J. (2011). Preliminary Study of Conformation and Drug Release Mechanism of Doxorubicin-Conjugated Glycol Chitosan, via cis-Aconityl Linkage, by Molecular Modeling. *International Journal of Molecular Sciences*, 12(3), 1672–1683, <https://doi.org/10.3390/ijms12031672>.
- 34 Thanou, M., Kotze, A., Scharringhausen, T., Luessen, H., De Boer, A., Verhoef, J., & Junginger, H. (2000). Effect of degree of quaternization of N-trimethyl chitosan chloride for enhanced transport of hydrophilic compounds across intestinal Caco-2 cell monolayers. *Journal of Controlled Release*, 64(1–3), 15–25. [https://doi.org/10.1016/S0168-3659\(99\)00131-5](https://doi.org/10.1016/S0168-3659(99)00131-5).
- 35 Liu, W.G., Zhang, X., Sun, S.J., Sun, G.J., Yao, K.D., Liang, D.C., Guo, G., & Zhang, J.Y. (2003). N-Alkylated Chitosan as a Potential Nonviral Vector for Gene Transfection. *Bioconjugate Chemistry*, 14(4), 782–789, <https://doi.org/10.1021/bc020051g>
- 36 Deka, B.C., & Bhattacharyya, P.K. (2016). Reactivity of chitosan derivatives and their interaction with guanine: A computational study. *Journal of Chemical Sciences*, 128(4), 589–598. <https://doi.org/10.1007/s12039-016-1064-6>
- 37 Parr, R.G., & Chattaraj, P.K. (1991). Principle of maximum hardness. *Journal of the American Chemical Society*, 113(5), 1854–1855. <https://doi.org/10.1021/ja00005a072>.
- 38 Bachrach, S.M. (2007). Population Analysis and Electron Densities from Quantum Mechanics. *Reviews in Computational Chemistry*, 171–228. <https://doi.org/10.1002/9780470125823.ch3>.
- 39 Chattaraj, P.K. (2009). *Chemical reactivity theory: a density functional view, 1st edition*. CRC Press, 616.
- 40 Chattaraj, P.K., & Roy, D.R. (2007). Update 1 of: Electrophilicity Index. *Chemical Reviews*, 107(9), PR46–PR74. <https://doi.org/10.1021/cr078014b>

Information about authors*

Avazova, Oynavad Barotovna (*corresponding author*) — PhD, Department of Biologically Active Polymers, Institute of Chemistry and Physics of Polymers of the Academy of Sciences of the Republic of Uzbekistan. A. Kadyri street, 7 b, 100128, Tashkent, Uzbekistan; e-mail: avazova1972@mail.ru <https://orcid.org/000-0003-4552-6973>;

Milusheva, Rakiya Yunusovna — PhD, Department of Biologically Active Polymers, Institute of Chemistry and Physics of Polymers of the Academy of Sciences of the Republic of Uzbekistan. A. Kadyri street, 7 b, 100128, Tashkent, Uzbekistan; e-mail: rumulusheva@gmail.com <https://orcid.org/000-0003-2673-1013>;

Nurgaliev, Inar Nakipovich — Doctor of Sciences in Physics and Mathematics, Head of the Laboratory of Theoretical Foundations of Polymer Chemistry and Physics. Institute of Chemistry and Physics of Polymers of the Academy of Sciences of the Republic of Uzbekistan, A. Kadyri street, 7 b, 100128, Tashkent, Uzbekistan; e-mail: ilnarvodnik@gmail.com; <https://orcid.org/0000-0002-6983-4375>;

Rashidova, Sayyora Sharafovna — Doctor of Chemical Sciences, Professor, Academician, Director of the Institute of Chemistry and Physics of Polymers of the Academy of Sciences of the Republic of Uzbekistan. A. Kadyri street, 7 b, 100128, Tashkent, Uzbekistan; e-mail: polymer@academy.uz <https://orcid.org/00000003-3104-6004>

*The author's name is presented in the order: *Last Name, First and Middle Names*

B.Kh. Mussabayeva^{1*}, Zh.S. Kassymova², L.K. Orazzhanova²,
A.N. Klivenko², A.N. Sabitova², B.B. Bayakhmetova²

¹*Astana International University, Nur-Sultan, Kazakhstan;*

²*Shakarim University, Semey, Kazakhstan*

(*Corresponding author's e-mail: binur.mussabayeva@mail.ru)

Interpolyelectrolyte Complex Chitosan – Alginate for Soil Structuring

The interpolyelectrolyte complex of the composition [chitosan]:[alginate] = [1]:[4] was prepared by mixing a hydrochloric acid solution of cationic polyelectrolyte chitosan and an aqueous solution of anionic polyelectrolyte sodium alginate. The complex of chitosan and sodium alginate biopolymers was first used as a soil structurizer. Due to low humus and light mechanical composition, the dark chestnut soil of the dry-steppe zone of the East Kazakhstan region is subjected to erosion. Introducing a polymer complex into the specified soil contributed to the improvement of wind resistance, an increase in humidity, and a decrease in water permeability. The soil surface treated with a complex of biopolymers showed pronounced resistance to the action of planar and trickle water erosion due to aggregation of particles with a diameter of < 0.01 mm. The fraction of soil particles obtained by mechanical destruction of structured aggregates with a diameter of 3-1 mm has a well-expressed ability to self-aggregate during the humidification - drying process. The results of the vegetation and field experience in tillage with an interpolyelectrolyte complex showed a positive effect of the complex on the growth and development of radish of the Rubin variety and, as a result, an increase in radish yield by 2 times was achieved. The obtained results indicate the effectiveness of the structuring action of the chitosan-alginate complex for poorly structured soils.

Keywords: biopolymers, polysaccharides, interpolymer complex, vegetation experience, dark chestnut soil, radish.

Introduction

The physical and mechanical properties of soil, in particular its structure, are important conditions for the demonstration of soil fertility. The most complete provision of plants with moisture, air, and mineral nutrition occurs precisely on structural soils [1]. Such a valuable agroecological property of the soil as the degree of resistance to water and wind erosion is closely related to the structural state of the soil.

One of the modern and promising ways to improve the structural and aggregate state of the soil is the treatment of the surface soil layer with interpolyelectrolyte complexes (IPECs), which promote the gluing and aggregation of dusty particles into macro aggregates [2–4], thereby preventing wind and water transfer of poorly structured soils. The introduction of IPEC into the soil improves the water and air regimes of the soil, increasing its fertility and contributing to the improvement of plant growth and development [5].

Kabanov et al. [6] selected qualitative and quantitative compositions of polymer mixtures of variously charged synthetic and natural polymers suitable for the production of polymer binders. Moreover, special attention of the authors is paid to the search for ways of applying various polymer coatings to the surface layer of the soil.

There are two methods of introducing IPEC into the soil. In the sprinkling method [3], an IPEC solution is prepared by mixing aqueous solutions of anionic and cationic polyelectrolytes in the presence of a water-soluble alkali metal salt, ammonium, calcium, or magnesium. The resulting water-salt solution of IPEC is simultaneously applied to the soil surface, followed by washing out the salt with water. In the two-solution method, aqueous solutions of polyelectrolytes are prepared separately, while observing the total equimolar charge-charge ratio [4]. The soil is infused with a solution of the first polyelectrolyte until full saturation and then treated with the second. The insoluble complex is formed directly in the surface layer of the soil after applying a solution of the second polyelectrolyte.

To protect soils from erosion, separate synthetic polymers were used, for example, modified polyacrylamide [7], which attaches well to negatively charged soil particles. However, cationic polyelectrolytes

are easily washed off the soil surface by rain or irrigation water [3]. Nonetheless, the IPECs of synthetic polymers proved to be effective structure-forming agents of longer-acting soils [3, 5, 6].

IPECs of synthetic polymers with natural ones, such as a complex of sodium carboxymethylcellulose (Na-CMC) with urea–formaldehyde oligomers (UFOs) [8], poly(dimethyldiallylammonium chloride) with potassium humates [9], were also used to consolidate soils. We studied the structuring of the soil of IPEC chitosan with polyacrylic acid and obtained positive results [10].

However, the low biodegradability of synthetic polymers and their complexes makes them unsuitable for soil structuring. In this connection, to date, complexes of natural polymers and their derivatives are the most promising and environmentally safe for agroecological purposes among IPEC-soil structurizers [11, 12]. They are an affordable alternative to synthetic polymers and can be successfully used for soil structuring. In addition to high aggregating capacity, simple methods of operation, long-term action, biopolymer structure-forming agents have biocompatibility and biodegradability as a result of natural microbiological and biochemical processes, while the soil is not polluted by further polymer decomposition products. The widespread use of biopolymers is also facilitated by certain technological advantages, namely, the presence of a widespread and annually renewable raw material base, cheapness and the availability of production [12].

Polysaccharides and their derivatives — chitosan [4, 13], sodium carboxymethylcellulose [8, 11], gellan [14], alginates [15], etc. — are used in various practical applications from natural complexing polymers that are widely distributed and reproduced in nature.

The natural polymer chitosan (Ch) has proved to be an effective material for reducing water erosion [4, 16] and wind erosion of soils [17]. The introduction of chitosan into clay soil led to an increase in interparticle cohesion, and consequently, an improvement in the mechanical properties of the soil. However, its effect turned out to be short-term in conditions of moist soils [13].

The possibility of using sodium alginate (SA) for the restoration of abandoned lands has been studied [18]. It is shown that alginate easily forms a film on the surface of sandy soil, increases the compressive strength of sand. In addition, the studied polymer has a positive effect on the growth of cyanobacteria, thereby contributing to the restoration of abandoned lands.

Chitosan-alginate complexes are mainly used in medicine as drug delivery systems [19, 20] and for the preparation of wound dressings [21, 22]. In addition, chitosan-alginate complexes can be used in ecology as effective sorbents for water purification from pollutants [23].

Chitosan-alginate IPECs with unique biological properties of both biopolymers are of interest as promising environmentally safe binders of soil dispersions. In addition, experimental data on the restoration of optimal water-resistant and wind-resistant soil structures using the IPEC of these biopolymers are practically absent.

Earlier, we discovered complexation in the chitosan – sodium alginate system of molar composition [Ch]:[SA] = [1]:[4] using a set of physicochemical methods. It was revealed that alginate-chitosan polyionic complexes are formed due to ion-ion interaction between the carboxyl groups of alginate and amino groups of chitosan [24, 25].

In [26], we prepared an IPEC of the composition [Ch]:[SA] = [2]:[3]. To prepare it, chitosan was dissolved in citric acid. Laboratory experiments have shown that this IPEC increases soil resistance to water erosion and has a positive effect on the growth and development of cucumber [26].

This paper presents the results of studying the influence of IPEC Ch-SA on the water-physical and agrochemical properties of the dark chestnut soil of the dry-steppe zone of the East Kazakhstan region, as well as on the growth, development and yield of radishes in the conditions of a vegetation field experiment.

Experimental

The object of the study is the dark chestnut soil of the dry steppe zone of the East Kazakhstan region. The climate of the region is continental and arid. The average annual temperature is 2.5–3 °C, the duration of the warm period is 200 days, and 250–300 mm of precipitation falls per year. The soil sample was taken on a virgin plot located 18.3 km west of Semey (N 50°29', E 79°56'). The color of the soil is brownish-brownish. The power of the upper horizon is 20–22 cm. Soils are characterized by low humus, mainly light mechanical composition. However, on these soils, when carrying out measures for the accumulation and preservation of moisture, and when applying mineral and organic fertilizers, it is possible to successfully grow a wide range of agricultural crops: cereals (wheat, corn, barley), technical, vegetable, fruit.

Sigma Aldrich chitosan (USA), M = 500 kDa, 85 % deacetylation degree, was used without additional purification.

Sigma Aldrich (USA) sodium alginate, $M = 250,000$ kDa, was used without additional purification.

The selection of five-point soil samples with a total mass of at least 1 kg was carried out on a 100 m^2 site from the upper layer (0–20 cm) diagonally so that the combined sample was a typical sample for the arable horizon of this genetic soil type. The average sample of air-dry soil was taken by double quartering, the resulting sample was sifted through an appropriate sieve and placed in a jar with a ground stopper.

Radish of the Rubin variety (Ukraine, the Poisk company) is a widely cultivated precocious variety with a growing season of 26–28 days.

The agrochemical properties of the soil before and after the introduction of IPEC were determined according to the generally accepted methods [27].

Preparation of polymer solutions with a concentration of 10^{-3} mol/l

To prepare 1 liter of a solution 0.161 g of dry chitosan was transferred to a 1-liter volumetric flask, filled with a small amount of hydrochloric acid (10^{-1} mol/l) and stirred on a magnetic stirrer until the polymer was completely dissolved. After that, the volume of liquid in the flask was brought to the mark with a solution of hydrochloric acid (10^{-1} mol/l).

To prepare 1 liter of a solution 0.198 g of dry sodium alginate was transferred to a 1-liter volumetric flask, filled with a small amount of distilled water and after complete dissolution of the polymer, the volume of liquid in the flask was brought to the mark with distilled water. Then the solutions were kept at room temperature for 24 hours, after which solutions were used to structure the soil.

The treatment of the surface layer of the soil with biopolymers and IPEC based on them was carried out in a two-solution method by sequentially applying equimolar polymer solutions using a spray gun [6]. The synthesis of IPEC took place directly in the soil at the time of application of a sodium alginate solution to a surface previously saturated with a chitosan solution. At the same time, the volumes of equimolar polymer solutions used contain chitosan and sodium alginate in molar ratios $[\text{Ch}]:[\text{SA}] = [1]:[4]$ [24, 25].

Investigation of mechanical strength of soil structurates

To obtain the structure, a 0.5 m soil fraction was poured into a Petri dish with a 1.5 cm layer and treated with a two-solution method. The resulting structurates were dried at room temperature for 3 days, then mechanical strength tests were carried out using the TAXT texture analyzer (Stable Micro Systems, UK) in compression mode at a speed of 0.01 mm/sec using the P5/S nozzle.

Determination of resistance to water flushing of soil structurates formed as a result of tillage of IPEC Ch-SA was carried out according to the methodology described in the papers of Panova [9].

The Petri dish was filled with a 50 g soil sample passed through a sieve with holes $d = 0.25 \text{ mm}$, the thickness of the soil layer was 0.5 cm. Soil treatment with polymers and IPEC was carried out in the following variants:

1. Control (soil not treated with biopolymers and IPEC);
2. Soil treated with IPEC $[\text{Ch}]:[\text{SA}] = [1]:[4]$;
3. Soil treated with hydrochloric acid solution Ch (10^{-3} mol/l);
4. Soil treated with an aqueous solution of SA (10^{-3} mol/l).

The treated soil in Petri dishes was dried for 5 days, then cups with soil were installed at an angle of 15° and subjected to flushing by spraying with 100 ml water while collecting the flowing water from the cups. The remaining soil in the cups was dried at room temperature for 5 days, after which it was weighed.

Calculation of soil resistance to flushing was carried out according to the formula (1):

$$R, \% = \frac{m}{M} \cdot 100, \quad (1)$$

where R — the resistance of the soil to flushing, %; m — the mass of the remaining soil after the test, g; M — the mass of the soil sample, g.

The model experiment on trickle water erosion was carried out in the same sequence, while the flushing of soil structures with water was carried out by a drip method on a special installation (Fig. 1).

The ability of soil structurates to self-aggregation was studied after soil treatment with polymers and IPEC [27]. The soil sample was passed through a sieve with a hole diameter of 0.25 mm. 20 g of the obtained fraction of “free particles” (FP) were poured into 4 Petri dishes and 20 ml of water, sodium alginate, chitosan and IPEC were treated, respectively. The treated soil was dried at room temperature for 2 days.

Soil aggregates 3–1 mm were crushed in a mortar and passed through a 0.25 mm sieve. Thus, the so-called fraction of aggregates particles (AP) was obtained. Then the AP fraction was also processed, as well as the FP fraction.

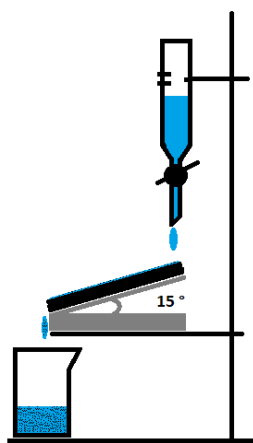


Figure 1. A model laboratory installation for studying trickle water erosion

To separate self-aggregating particles and loosely bonded soil particles, the attachments from Petri dishes were transferred to centrifuge tubes, then shaken on a LOIP LS-110 rotator (Russia) for 90 minutes at 25 rpm, after which the soil was transferred to a 0.25 mm sieve, the remaining soil on the sieve was sifted and weighed.

The resulting self-assembled aggregates were transferred to a pre-moistened 0.25 mm sieve and waited for the water held between the sieve cells to moisten the suspension of the aggregates, then the sieve with the aggregates was immersed in water for 10 minutes. Next, the aggregates were sifted in water, moving the sieve up and down and left and right 10 times. Water-tight aggregates capable of self-assembly after mechanical destruction remained on the sieve. The obtained water-tight aggregates, as well as the suspension with particles <0.25 mm passed through the sieve, were dried at a temperature of 105°C and weighed.

The number of self-assembling units was calculated according to the formula (2):

$$\eta_c = \frac{m_c}{M} \cdot 100\%, \quad (2)$$

where η_c — the number of aggregates capable of self-assembly, %; m_c — the mass of self-assembled soil aggregates, g; M — the mass of the soil sample, g.

The number of water-bearing aggregates capable of self-assembly was calculated by the formula (3):

$$\eta_e = \frac{m}{m_c} \cdot 100\%, \quad (3)$$

where η_e — the number of water-bearing aggregates capable of self-assembly, %; m — the mass of water-bearing self-assembled soil aggregates, g.

Investigation of the effect of IPEC on radish yield in vegetation and field conditions. Experiments with radish were carried out in the open ground on microplots measuring 20×20 cm² in 3-fold replication. A plot with a homogeneous plain relief is selected. Before laying the experimental plots, the site was dug up, weeds were removed. The marking of the experimental plots was carried out by the randomized square method according to the following scheme (Figure 2):

CONTROL	IPEC	CONTROL
IPEC	CONTROL	IPEC

Figure 2. Layout diagram of experimental plots in the vegetation experiment

The dividing boundaries between the individual plots were 10 cm.

The culture was sown in dry, windless weather. All variants of the experiment were laid down in one day along with planting seeds and making IPEC.

The duration of the experiment from sowing seeds to harvesting was 1 month. Care (watering, weeding from weeds) and recording of biometric and phenological observations were carried out daily for all variants of the experiment while considering the following indicators:

- the appearance of the first shoots of plants according to the experience options;
- the appearance of mass shoots of plants according to the variants of the experiment;
- dynamics of growth and onset of the main phenological phases according to the variants of the experiment;
- evaluation of the yield according to the variants of the experiment (30 days after sowing).

Before weighing, the plants were washed from the soil and dried with filter paper. The determination of the raw biomass of root crops and tops was carried out within 1–2 hours after digging to avoid weight loss during drying.

Statistical processing of the data. Statistical processing of the results was performed automatically using Origin Pro™ Data Analysis and Graphing Software. For mean value and standard deviation determination, the following parameters were used: confidence probability — 0.95; interpolation of quantiles – empirical distribution with averaging.

Results and Discussion

IPEC Ch – SA was successfully used for structuring dark chestnut soil of the dry steppe zone of the East Kazakhstan region.

The main agrochemical parameters of the soil before and after the introduction of IPEC were studied: mechanical composition, moisture capacity, humidity, acidity, water permeability, organic matter content, exchangeable ammonium, and mobile phosphorus.

Table 1 presents the analysis results of the mechanical composition of the dark chestnut soil of the dry steppe zone of the East Kazakhstan region before and after the introduction of IPEC.

Table 1

Content (%) of fractions of soil particles (mm) in untreated soil (control) and after application of IPEC

Variant	Physical Sand			Physical Clay		
	Coarse and medium sand, 0.25–1.0	Fine sand, 0.05–0.25	Coarse dust, 0.01–0.05	Medium dust, 0.005–0.01	Fine dust, 0.001–0.005	Mud, < 0.001
Control	27.95	41.75	19.65	5.04	3.95	1.66
	89.35 %			10.65 %		
IPEC	31.10	45.04	17.85	2.08	2.51	1.42
	93.99 %			6.01 %		

Depending on the content and ratio of various fractions of soil particles, in particular, on the ratio of physical sand (particle diameter >0.01 mm) and physical clay (particle diameter <0.01 mm), according to the agronomic classification of N.A. Kachinsky, a variety of soil is determined by mechanical composition. The studied soil by its mechanical composition belongs to sandy loam soils (in soils of the steppe type of soil formation) since the content of physical clay (10.65 %) is in the range from 10 to 20 %. Such soil is characterized by a low content of moisture and nutrients, is easily exposed to water and wind erosion [11].

The introduction of IPEC on the soil surface contributed to the aggregation of physical clay (<0.01 mm 6.01 %). The aggregating effect of IPEC when applied to the soil is associated with the formation of a soil-polymer crust due to the interaction of structural fragments (hydrophilic, hydrophobic, positively and negatively charged) of IPEC with particles of the dispersed phase of the soil [14].

Table 2 demonstrates the main agrochemical indicators of dark chestnut soil before and after the introduction of IPEC.

Table 2

Agrochemical indicators of untreated and treated IPEC soil

Variant	Soil moisture, %	Moisture capacity, %	pH _{H₂O}	pH _{KCl}	Content, mg/kg of soil		Organic matter, %	K _{f10} , mm·mm ⁻¹
					NH ₄ ⁺	exchange P ₂ O ₅		
Control	1.44	40.45	7.16	7.45	28.0	89.2	1.63	1.5
IPEC	1.62	52.60	7.24	7.21	33.9	91.7	1.65	0.4

According to the results of the study of agrochemical indicators of untreated soil, the following agrochemical characteristics were obtained: sandy loam mechanical composition, good water permeability, low organic matter content, slightly alkaline reaction of soil solution, low content of mobile nitrogen and exchangeable phosphorus. The obtained results also indicate a weak structural condition of the soil and a strong susceptibility to deflation and water erosion [11].

When applying chitosan – sodium alginate to the soil surface of IPEC, there is an increase in the content of mobile ammonium nitrogen by ~ 6 % and exchangeable phosphorus by 2.7 %, a relatively small increase in humidity (~ 0.2 %) and moisture capacity (1.3 %), as well as a pronounced decrease in water permeability (by 73%) of the soil after treatment with IPEC. The value of the filtration coefficient is reduced by almost 4 times (Table 2).

The increase in nitrogen and phosphorus content may be due to the presence of amino groups in the chitosan macromolecule, as well as saturation and retention of macronutrients in the surface layer of the soil as a result of gluing soil particles with a polymer complex.

The improvement of the water properties of the treated soil may be a consequence of the enlargement of soil pores and filling them with IPEC, hydrophilic fragments which have the ability to absorb and retain moisture.

Thus, when using IPEC as a structuring agent, the top layer of soil is saturated with water and the moisture necessary for vegetation is preserved, which contributes to the rationalization of the water regime of plants during their growing season.

Mechanical properties of soil-polymer structurators

An important characteristic of the aggregating properties of soil structurators is the mechanical strength of the formed soil structurates. For this purpose, the mechanical properties of soil samples treated with water, chitosan solutions, sodium alginate and IPEC [Ch]:[SA] = [1]:[4] were studied (Figure 3).

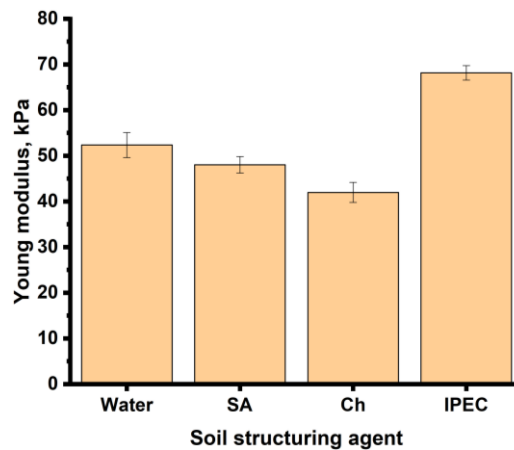


Figure 3. Mechanical properties of soil structurates

As can be seen from Figure 3, structures based on IPEC (68.74 kPa) exhibit the greatest mechanical strength, in comparison with structures treated with individual polymers, as well as water. It is important to note that for a short period of time, water is a good structuring agent [28].

Anti-erosion resistance of soil-polymer structurates

The resistance to planar and trickle erosion of soil structurates formed as a result of tillage with individual polymers and an interpolymer complex of chitosan – sodium alginate has been investigated. Figures 4 and 5 illustrate the results of the resistance of the soil treated with polymers and IPEC to water flushing.

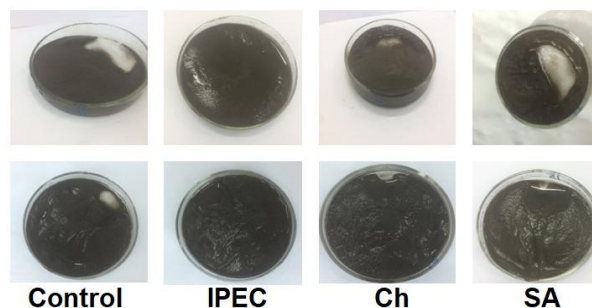


Figure 4. Resistance of soil aggregates to planar (upper row) and trickle erosion (lower row)

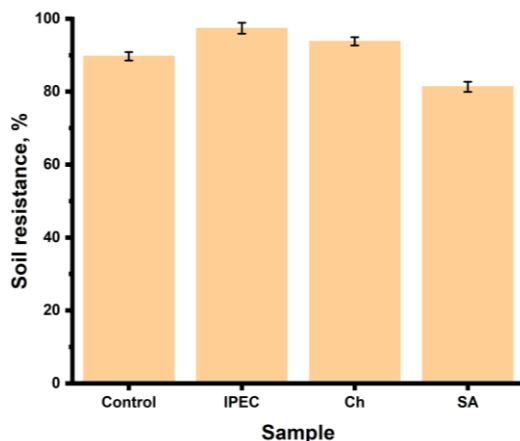


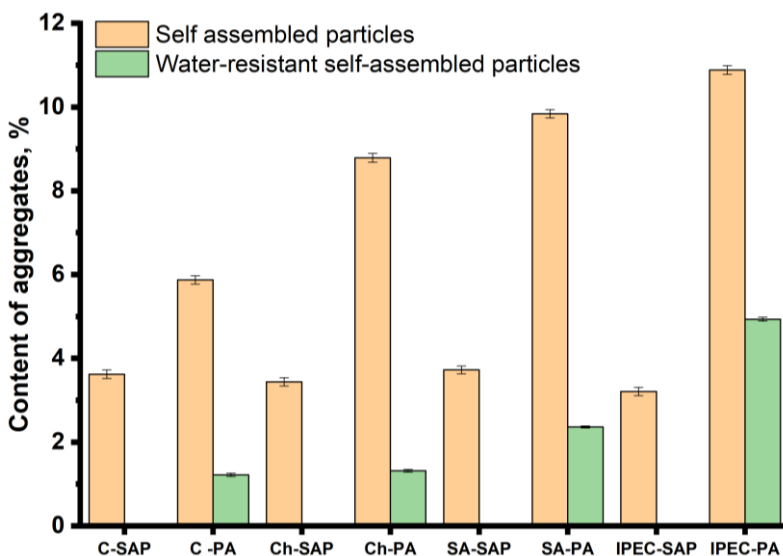
Figure 5. Diagram of soil resistance to trickle erosion

The maximum flushing of soil particles is observed in the variant with control and soil treated with SA. In the sample of soil treated with Ch, the soil washability is lower in comparison with the control and the soil treated with SA. The behavior of Ch in soil is related to its cationic characteristics, which provide electrical interaction between the biopolymer and the diffuse double layer of soil minerals (charged surface and distributed charge in the adjacent phase), which determines the interparticle behavior of the treated soil. It is assumed that upon contact of a negatively charged soil particle with a positively charged chitosan, the distribution of polymer cations concentrates on the surface of the soil particles, which leads to a balance in the overall electrical neutrality of the system. However, the distance from the charged particle leads to a gradual decrease in the concentration of counterions to the same conditions as in the Ch volume. This mechanism leads to an increase in mechanical properties due to the ionic bond between the biopolymer and soil particles.

The greatest soil washout with water in the case of using SA solution is caused by the same charge of SA macromolecules and the surface charge of soil particles [13].

Thus, the introduction of the Ch-SA complex on the soil surface helps to strengthen the upper layer of the soil by aggregating it and increases its resistance to water flushing.

The results of self-assembly of soil aggregates of natural composition <0.25 mm and from pre-destroyed structural lumps of 3-1 mm treated with polymers and IPEC, after moistening – drying, as well as the values of water-resistant self-assembled aggregates from the above-mentioned fractions are shown in Figure 6.



FP from structureless particles <0.25 mm in natural soil composition;
 FA obtained by mechanical destruction of soil fractions 3-1 mm

Figure 6. The ability to self-aggregate FP and AP and the water resistance of self-assembled aggregates

As can be seen from Figure 6, structureless FP, regardless of the polymer composition introduced for structuring, in almost all cases have a minimal aggregation ability and no water-resistant particles were found among them. On the contrary, according to experimental data, AP have a well-expressed ability to self-assemble after the humidification-drying process. When using IPEC, the water resistance index of self-assembled aggregates is the highest, which indicates the structuring of the IPEC soil. After IPEC treatment, self-organized AP of arable dark chestnut soil contain almost 4 times more water-resistant particles compared to AP structured with water.

Thus, when using biopolymers and IPEC, artificially destructured soil aggregates have a greater ability to self-aggregate than natural soil microaggregates. In this regard, polymer structure-forming agents can be recommended for effective use on soils with a destroyed structure.

Influence of the interpolyelectrolyte complex on radish development

From a practical point of view, the impact of IPEC Ch-SA introduced into the soil on the growth and development of plants that grow on it is important. In this work, radish (*Raphanus sativus*) of the “Ruby” variety was used as a model plant. Figures 7, 8 and Table 3 show data on the growth and development of radishes on dark chestnut soil treated with water and IPEC [Ch]:[SA] = [1]:[4] in a vegetative field experiment.

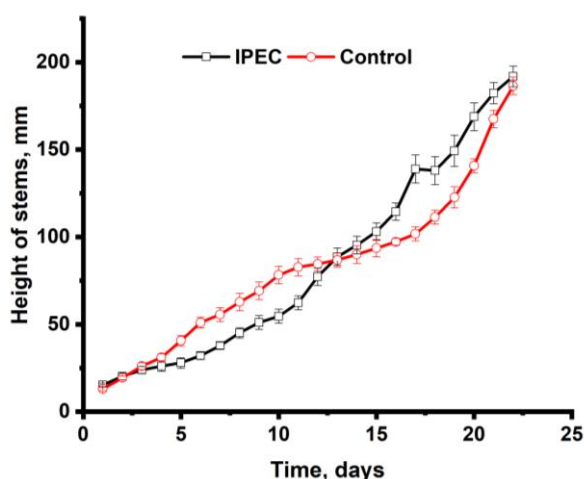


Figure 7. Dynamics of growth and development of radish of the “Rubin” variety

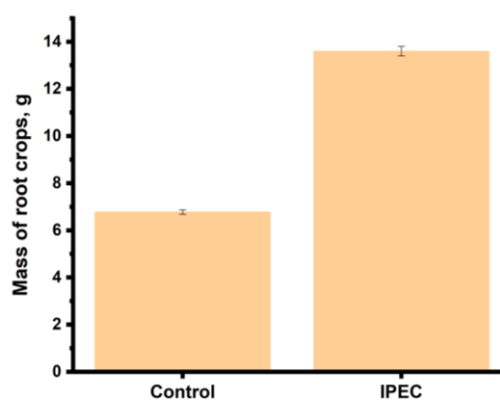


Figure 8. The average weight of the radish variety “Rubin” on the plots, g

Table 3

The influence of IPEC on the development of the radish variety “Rubin”

Parameter	Variant	
	Control	IPEC
Height, cm/vessel	18.50	19.10
Weight of the tops, g	35.13	51.8
Weight of root crops, g	6.43	20.78
Specific weight, g/unit	1.07	3.47
The period before the emergence of seedlings, a day	6	5
Germination, %	60	80

The results of daily monitoring of biometric indicators of radish development showed that the introduction of IPEC into the soil contributed to the best plant growth since radish seedlings were obtained earlier, and the height and weight of plants were more pronounced than in the control variant.

The yield of radish turned out to be 2 times higher than the control in the case of introduction of IPEC into the soil.

The positive effect on the growth and development of radish of the Rubin variety during tillage of IPEC may be due to its effect on the retention of moisture reserves in the soil by reducing evaporation and improving water absorption.

The results indicate that the use of environmentally friendly biodegradable IPEC Ch-SA had contributed to the growth of the plant, so seedlings were obtained 1 day earlier, and the height and weight of plants were greater than in the control variant, a 3-fold increase in fruit weight, a 2-fold increase in yield were achieved. Examples of the use of biodegradable polymer as floating row covers in field production of radish based on aliphatic-aromatic polyesters [29] and IPEC based on chitosan and sodium carboxymethylcellulose [30] are known. These systems lead to an increase in fruit weight by 2.9 and 1.45 times, respectively. Thus, the developed technology has significant advantages among known analogues.

Conclusions

To conclude, the analysis of the results of laboratory and vegetation-field studies confirms the possibility of using IPEC chitosan – sodium alginate for aggregation of poorly structured soils to create an erosion-resistant, agronomically valuable soil structure and ensure optimal water and air regimes for the cultivation of agricultural crops. The results of the application of soil treatment technology with biopolymers and IPEC show the need for further research on other agricultural soils and crops.

References

- 1 Karpachevskii L.O. Soil structure and modern methods for its examination. *Eurasian Soil Science*. — 2009. — Vol. 42. — P. 1423–1425. <https://dx.doi.org/10.1134/S1064229309120151>.
- 2 Kabanov V.A. Polyelectrolyte complexes in solution and in bulk. *Russian Chemical Reviews*. — 2005. — Vol. 74. — P. 3–20. <http://dx.doi.org/10.1070/RC2005v074n01ABEH001165>.
- 3 Zezin A.B. Polymeric stabilizers for protection of soil and ground against wind and water erosion / A.B. Zezin, S.V. Mikheikin, V.B. Rogacheva, M.F. Zansokhova, A.V. Sybachin, A.A. Yaroslavov // *Advances in Colloid and Interface Science*. — 2015. — Vol. 226. — P. 17–23. <https://doi.org/10.1016/j.cis.2015.06.006>
- 4 Izumrudov V.A. Interpolyelectrolyte complexes: advances and prospects of application / V.A. Izumrudov, B.Kh. Mussabayeva, Zh.S. Kassymova, A.N. Klivenko, L.K. Orazzhanova // *Russian Chemical Reviews*. — 2019. — Vol. 88. — P. 1046–1062. <https://doi.org/10.1070/RCR4877>.
- 5 Bimendina L.A. Application of Interpolymer Complexes of Novel Poly(ampholyte-electrolyte) as Soil Structuring Agents and for Extraction of Radioactive Strontium / L.A. Bimendina, M.G. Yashkarova, L.K. Orazzhanova, S.E. Kudaibergenov // *Eurasian Chemical Technological Journal*. — 2005. — Vol. 7(2). — P. 139–145. <https://doi.org/10.18321/ectj625>.
- 6 Kabanov V.A. Polyelectrolytes in the solution of ecological problems / V.A. Kabanov, A.B. Zezin, S.V. Mikheikin, V.A. Kasaikin, A.A. Yaroslavov, D.A. Topchiev // *Russian Chemical Reviews*. — 1991. — Vol. 60 (3). — P. 288–291. <http://dx.doi.org/10.1070/RC1991v060n03ABEH001063>.
- 7 Inbar A. Using polyacrylamide to mitigate post-fire soil erosion / A. Inbar, M. Ben-Hur, M. Sternberg, M. Lado // *Geoderma*. — 2015. — Vol. 239–240. — P. 107–114. <https://doi.org/10.1016/j.geoderma.2014.09.026>
- 8 Inagamov Ya. Structure and Physical-Mechanical Properties of Interpolymeric Complexes Based on Sodium Carboxymethylcellulose / Ya. Inagamov, G.I. Mukhamedov // *Journal of Applied Polymer Science*. — 2011. — Vol. 122 (3). — P. 1749–1757.
- 9 Panova I. Interpolyelectrolyte complexes as effective structure-forming agents for Chernozem soil / I. Panova, V. Demidov, P. Shulga, L. Ilyasov // *Land Degradation & Development*. — 2021. — Vol. 32 (2). — P. 1022–1033. <https://doi.org/10.1002/ldr.3743>
- 10 Orazzhanova L.K. Soil Structuring in the presence of the Chitosan — Polyacrylic Acid Interpolymer Complex / L.K. Orazzhanova, Zh.S. Kassymova, B.Kh. Mussabayeva, A.N. Klivenko // *Eurasian Soil Science*. — 2020. — Vol. 53(12). — P. 1773–1781. <https://doi.org/10.1134/S1064229320120091>
- 11 Kassymova Zh.S. Preparation and Properties of Interpolymer Complexes Capable of Soil Structuring Russ / Zh.S. Kassymova, L.K. Orazzhanova, A.N. Klivenko, B.Kh. Mussabayeva, D.K. Aserzhanov // *Russian Journal of Applied Chemistry*. — 2019. — Vol. 92(2). P. 208–217. <https://dx.doi.org/10.1134/S107042721902006X>.
- 12 Мусабаева Б.Х. Применение интерполимерных комплексов в экологических целях / Б.Х. Мусабаева, А.Н. Кливенко, Ж.С. Касымова, Л.К. Оразжанова // *Хим. журн. Казахстана*. — 2018. — № 4. — С. 187.
- 13 Klivenko A.N. Biocompatible cryogels: preparation and application / A.N. Klivenko, B.Kh. Mussabayeva, B.S. Gaisina, A.N. Sabitova // *Bulletin of the University of Karaganda — Chemistry*. — 2021. — Vol. 103 (3). — P. 4–20. <https://doi.org/10.31489/2021Ch3/4-20>
- 14 Nurakhmetova Zh.A. Immobilized anticancer agents and metal nanoparticles in a matrix of gellan: achievements and prospects / Zh.A. Nurakhmetova, G.S. Tatykhanova, S.E. Kudaibergenov // *Chemical Bulletin of Kazakh National University*. — 2020. — Vol. 99 (4). — P. 32–41. <https://doi.org/10.15328/cb1169>
- 15 Jadach B. Sodium Alginate as a Pharmaceutical Excipient: Novel Applications of a Well-known Polymer / B. Jadach, W. Świetlik, A. Froelich // *Journal of Pharmaceutical Sciences*. — 2022. — Vol. 111 (5). — P. 1250–1261. <https://doi.org/10.1016/j.xphs.2021.12.024>

- 16 Adamczuk A. Impact of Chitosan on Water Stability and Wettability of Soils / A. Adamczuk, M. Kercheva, M. Hristova, G. Jozefaciuk // *Materials*. — 2021. — Vol. 14. — P. 7724–7735. <https://doi.org/10.3390/ma14247724>
- 17 Adamczuk A. Impact of Chitosan on the Mechanical Stability of Soils / A. Adamczuk, G. Jozefaciuk // *Molecules*. — 2022. — Vol. 2. — P. 2273–2283. <https://doi.org/10.3390/molecules27072273>
- 18 Peng Ch. Application of sodium alginate in induced biological soil crusts: enhancing the sand stabilization in the early stage / Ch. Peng, J. Zheng, Sh. Huang, Sh. Li, D. Li, M. Cheng, Y. Liu // *Journal of Applied Phycology*. — 2017. — Vol. 29. — P. 1421–1426. <https://doi.org/10.1007/s10811-017-1061-2>
- 19 Aranaz I. Chitosan: An Overview of Its Properties and Applications / I. Aranaz, A.R. Alcántara, M.C. Civer, C. Arias, B. Elorza, A.H. Caballero, N. Acosta // *Polymers*. — 2021. — Vol. 13 (19): 3256. <https://doi.org/10.3390/polym13193256>
- 20 Longuinho M.M. Lapazine loaded Alginate/Chitosan microparticles: Enhancement of anti-mycobacterium activity / M.M. Longuinho, S.G. Leitaó, R.S.F. Silva, P.E.A. Silva, A.L. Rossi, P.V. Finotelli // *Journal of Drug Delivery Science and Technology*. — 2019. — Vol. 54: 101292. <https://doi.org/10.1016/j.jddst.2019.101292>
- 21 Sweeney I.R. Absorbent alginate fibres modified with hydrolysed chitosan for wound care dressings—II. Pilot scale development / I.R. Sweeney, M. Mirafab, G. Collyer // *Carbohydrate Polymers*. — 2014. — Vol. 102. — P. 920–927. <https://doi.org/10.1016/j.carbpol.2013.10.053>
- 22 Mndlovu H. Development of a fluid-absorptive alginate-chitosan bioplatform for potential application as a wound dressing / H. Mndlovu, L.C. du Toit, P. Kumar, Th. Marimuthu, V. Pillay // *Carbohydrate Polymers*. — 2019. — Vol. 222: 114988. <https://doi.org/10.1016/j.carbpol.2019.114988>
- 23 Bajpai A.K. Facile preparation of ionotropically crosslinked chitosan-alginate nanosorbents by water-in-oil (W/O) microemulsion technique: Optimization and study of arsenic (V) removal / A.K. Bajpai // *Journal of Water Process Engineering*. — 2019. — Vol. 32: 100920. <https://doi.org/10.1016/j.jwpe.2019.100920>
- 24 Kassymova Zh.S. Preparation of interpolymer complexes of chitosan and sodium alginate / Zh.S. Kassymova, L.K. Orazzhanova, B.B. Bayakhmetova, B.S. Gaisina, N.B. Kassenova, G.T. Yelemessova G.T. // *Bulletin of the University of Karaganda — Chemistry*. — 2019. — Vol. 93(1). — P. 17–24. <https://doi.org/10.31489/2019Ch1/17-24>
- 25 Klivenko A. Soil structuring using interpolyelectrolyte complexes of water-soluble polysaccharides / A. Klivenko, L. Orazzhanova, B. Mussabayeva, G. Yelemessova, Z. Kassymova // *Polymers for Advanced Technologies*. — 2020. — Vol. 31 (12). — P. 3392–3301. <https://doi.org/10.1002/pat.5053>
- 26 Mussabayeva B.Kh. Interpolymer complex of biopolymers as a soil structure-forming agent / B.Kh. Mussabayeva, Zh.S. Kassymova, M.A. Aldabergenova // *Bulletin of the University of Karaganda — Chemistry*. — 2020. — Vol. 97 (1). — P. 22–29. <https://doi.org/10.31489/2020Ch1/22-29>
- 27 Минеев В.Г. Практикум по агрохимии / В.Г. Минеев. — М.: Изд-во Моск. ун-та, 2001. — 689 с.
- 28 Kholodov V.A. The Capacity of Soil Particles for Spontaneous Formation of Macroaggregates after a Wetting–Drying Cycle / V.A. Kholodov // *Eurasian Soil Science*. — 2013. — Vol. 46 (6). — P. 660–667. <https://doi.org/10.1134/S1064229313040078>
- 29 Kalisz A. Biodegradable polymer as floating row covers in field production of radish / A. Kalisz, A. Grabowska, A. Sekara, E. Capecka, A. Libik, K. Sulak, R. Jurkow // *Chilean Journal of Agricultural Research*. — 2019. — Vol. 79(2). — P. 243–256. <http://dx.doi.org/10.4067/S0718-58392019000200243>
- 30 Касымова Ж.С. Улучшение водно-физических свойств почв с помощью биоразлагаемых полимеров / Ж.С. Касымова, А.Н. Кливенко, А.Д. Мукушева // *Вестн. Евраз. нац. ун-та им. Л.Н. Гумилева. Сер. Химия, география, экология*. — 2019. — № 4(129). — С. 13–24.

Б.Х. Мұсабаева, Ж.С. Қасымова, Л.К. Оразжанова,
А.Н. Кливенко, А.Н. Сабитова, Б.Б. Баяхметова

Хитозан – альгинат интерполиэлектродитті комплексі топырақты құрылымдау үшін

Құрамы [хитозан]:[альгинат] = [1]:[4] интерполиэлектродитті комплексі катиондық полиэлектродит хитозанның тұз қышқылды ерітіндісін және аниондық полиэлектродитті натрий альгинатының сулы ерітіндісін араластыру арқылы алынды. Хитозан және натрий альгинаты биополимерлерінің комплексі алғаш рет топырақ түзуші ретінде пайдаланылды. Шығыс Қазақстан облысының құрғақ далалы аймағының күңгірт-күрең топырағында қарашіріктің төмен болуынан және жеңіл механикалық құрамның салдарынан эрозияға ұшыраған. Аталған топыраққа полимерлі комплекстің енгізілуі желге төзімділікті жақсартуға, ылғалдылықты арттыруға және су өткізгіштігін төмендетуге ықпал етті. Биополимерлер комплексімен өңделген топырақ беті диаметрі < 0,01 мм бөлшектердің агрегациялануына байланысты жазықтық және ағынды су эрозиясының әсеріне айқын қарсылық көрсетті. Диаметрі 3–1 мм құрылымдалған агрегаттардың механикалық бұзылуымен алынған топырақ бөлшектерінің фракциясы ылғалдандыру–кептіру процесінде өзін-өзі реттеуге жақсы қабілетті. Топырақты интерполиэлектродитті комплекспен өңдеудегі вегетациялық-далалық тәжірибенің нәтижелері комплекстің Рубин сортты шалғамның өсуіне және дамуына оң әсерін көрсеткен,

нәтижесінде шалғамның өнімділігі 2 есе артты. Алынған нәтижелер нашар құрылымдалған топырақтарға арналған хитозан-альгинат комплексінің құрылымдық әсерінің тиімділігін көрсетеді.

Кілт сөздер: биополимер, полисахаридтер, интерполимерлі комплекс, вегетациялық тәжірибе, күңгірт-күрең топырақ, шалғам.

Б.Х. Мусабаева, Ж.С. Касымова, Л.К. Оразжанова,
А.Н. Кливенко, А.Н. Сабитова, Б.Б. Баяхметова

Интерполиэлектролитный комплекс хитозан–альгинат для структурирования почвы

Интерполиэлектролитный комплекс состава [хитозан]:[альгинат] = [1]:[4] получили методом смешения солянокислого раствора катионного полиэлектролита хитозана и водного раствора анионного полиэлектролита альгината натрия. Комплекс биополимеров хитозана и альгината натрия впервые использован в качестве структурообразователя почвы. Вследствие малогумусности и легкого механического состава темно-каштановая почва сухостепной зоны Восточно-Казахстанской области подвержена эрозии. Внесение в указанную почву полимерного комплекса способствовало улучшению ветроустойчивости, увеличению влажности и снижению водопроницаемости. Поверхность почвы, обработанная комплексом биополимеров, проявляла выраженную устойчивость к действию плоскостной и струйчатой водной эрозии за счет агрегирования частиц диаметром < 0,01 мм. Фракция почвенных частиц, полученная механическим разрушением структурированных агрегатов диаметром 3–1 мм, обладает хорошо выраженной способностью самоагрегироваться в процессе увлажнения–высушивания. Результаты вегетационно-полевого опыта по обработке почвы интерполиэлектролитным комплексом показали положительное влияние комплекса на рост и развитие редиса сорта «Рубин» и, как следствие, достигнуто повышение урожайности редиса в 2 раза. Полученные результаты свидетельствуют об эффективности структурирующего действия хитозан-альгинатного комплекса для слабоструктурированных почв.

Ключевые слова: биополимер, полисахариды, интерполимерный комплекс, вегетационный опыт, темно-каштановая почва, редис.

References

- 1 Karpachevskii, L.O. (2009). Soil structure and modern methods for its examination. *Eurasian Soil Science*, 42, 1423–1425. <https://dx.doi.org/10.1134/S1064229309120151>.
- 2 Kabanov, V.A. (2005). Polyelectrolyte complexes in solution and in bulk. *Russian Chemical Reviews*, 74, 3–20. <http://dx.doi.org/10.1070/RC2005v074n01ABEH001165>.
- 3 Zezin, A.B., Mikheikin, S.V., Rogacheva, V.B., Zansokhova, M.F., Sybachin, A.V., & Yaroslavov, A.A. (2015). Polymeric stabilizers for protection of soil and ground against wind and water erosion. *Advances in Colloid and Interface Science*, 226, 17–23. <https://doi.org/10.1016/j.cis.2015.06.006>.
- 4 Izumrudov, V.A., Mussabayeva, B.Kh., Kassymova, Zh.S., Klivenko, A.N., & Orazzhanova, L.K. (2019). Interpolyelectrolyte complexes: advances and prospects of application. *Russian Chemical Reviews*, 88, 1046–1062. <https://doi.org/10.1070/RCR4877>.
- 5 Bimendina, L.A., Yashkarova, M.G., Orazzhanova, L.K., & Kudaibergenov, S.E. (2005). Application of Interpolymer Complexes of Novel Poly(ampholyte-electrolyte) as Soil Structuring Agents and for Extraction of Radioactive Strontium. *Eurasian Chemical Technological Journal*, 7(2), 139–145. <https://doi.org/10.18321/ectj625>.
- 6 Kabanov, V.A., Zezin, A.B., Mikheikin, S.V., Kasaikin, V.A., Yaroslavov, A.A., & Topchiev, D.A. (1991). Polyelectrolytes in the solution of ecological problems. *Russian Chemical Reviews*, 60 (3), 288–291. <http://dx.doi.org/10.1070/RC1991v060n03ABEH001063>.
- 7 Inbar, A., Ben-Hur, M., Sternberg, M., & Lado, M. (2015). Using polyacrylamide to mitigate post-fire soil erosion. *Geoderma*, 239–240, 107–114. <https://doi.org/10.1016/j.geoderma.2014.09.026>
- 8 Inagamov, Ya., & Mukhamedov, G.I. (2011). Structure and Physical-Mechanical Properties of Interpolymeric Complexes Based on Sodium Carboxymethylcellulose. *Journal of Applied Polymer Science*. 122 (3), 1749–1757.
- 9 Panova, I., Demidov, V., Shulga, P., & Ilyasov, L. (2021). Interpolyelectrolyte complexes as effective structure-forming agents for Chernozem soil. *Land Degradation & Development*, 32 (2). 1022–1033. <https://doi.org/10.1002/ldr.3743>
- 10 Orazzhanova, L.K., Kassymova, Zh.S., Mussabayeva, B.Kh., & Klivenko, A.N. (2020). Soil Structuring in the presence of the Chitosan – Polyacrylic Acid Interpolymer Complex. *Eurasian Soil science*, 53 (12), 1773–1781. <https://doi.org/10.1134/S1064229320120091>

- 11 Kassymova, Zh.S., Orazzhanova, L.K., Klivenko, A.N., Mussabayeva, B.Kh., & Aserzhanov, D.K. (2019). Preparation and Properties of Interpolymer Complexes Capable of Soil Structuring. *Russian Journal of Applied Chemistry*, 92 (2), 208–217. <https://dx.doi.org/10.1134/S107042721902006X>.
- 12 Mussabayeva, B.Kh., Klivenko, A.N., Kassymova, Zh.S., & Orazzhanova, L.K. (2018). Primenenie interpolimernykh kompleksov v ekologicheskikh tseliakh [Application of interpolymer complexes in the ecological purposes]. *Khimicheskii zhurnal Kazakhstana – Chemical Journal of Kazakhstan*, 64 (4), 187–204 [in Russian].
- 13 Klivenko, A.N., Mussabayeva, B.Kh., Gaisina, B.S., & Sabitova, A.N. (2021). Biocompatible cryogels: preparation and application. *Bulletin of the University of Karaganda – Chemistry*, 103(3), 4–20. <https://doi.org/10.31489/2021Ch3/4-20>
- 14 Nurakhmetova, Zh.A., Tatykhanova, G.S., & Kudaibergenov, S.E. (2020). Immobilized anticancer agents and metal nanoparticles in a matrix of gellan: achievements and prospects. *Chemical Bulletin of Kazakh National University*, 99 (4), 32–41. <https://doi.org/10.15328/cb1169>
- 15 Jadach, B., Świetlik, W., & Froelich, A. (2022). Sodium Alginate as a Pharmaceutical Excipient: Novel Applications of a Well-known Polymer. *Journal of Pharmaceutical Sciences*, 111 (5), 1250–1261. <https://doi.org/10.1016/j.xphs.2021.12.024>
- 16 Adamczuk, A., Kercheva, M., Hristova, M., & Jozefaciuk, G. (2021). Impact of Chitosan on Water Stability and Wettability of Soils. *Materials*, 14, 7724–7735. <https://doi.org/10.3390/ma14247724>
- 17 Adamczuk, A., & Jozefaciuk, G. (2022). Impact of Chitosan on the Mechanical Stability of Soils. *Molecules*, 27, 2273–2283. <https://doi.org/10.3390/molecules27072273>
- 18 Peng, Ch., Zheng, J., Huang, Sh., Li, Sh., Li, D., Cheng, M., & Liu, Y. (2017). Application of sodium alginate in induced biological soil crusts: enhancing the sand stabilization in the early stage. *Journal of Applied Phycology*, 29, 1421–1426. <https://doi.org/10.1007/s10811-017-1061-2>
- 19 Aranaz, I., Alcántara, A.R., Civer, M.C., Arias, C., Elorza, B., Caballero, A.H., & Acosta, N. (2021). Chitosan: An Overview of Its Properties and Applications. *Polymers*, 13(19), 3256. <https://doi.org/10.3390/polym13193256>
- 20 Longuinho, M.M., Leitao, S.G., Silva, R.S.F., Silva, P.E.A., Rossi, A.L., & Finotelli, P.V. (2019). Lapazine loaded Alginate/Chitosan microparticles: Enhancement of anti-mycobacterium activity. *Journal of Drug Delivery Science and Technology*, 54, 101292. <https://doi.org/10.1016/j.jddst.2019.101292>.
- 21 Sweeney, I.R., Mirafteb, M., & Collyer, G. (2014). Absorbent alginate fibres modified with hydrolysed chitosan for wound care dressings--II. Pilot scale development. *Carbohydrate Polymers*, 102, 920–927. <https://doi.org/10.1016/j.carbpol.2013.10.053>
- 22 Mndlovu, H., du Toit, L.C., Kumar, P., Marimuthu, Th., & Pillay, V. (2019). Development of a fluid-absorptive alginate-chitosan bioplatfrom for potential application as a wound dressing. *Carbohydrate Polymers*, 222: 114988. <https://doi.org/10.1016/j.carbpol.2019.114988>
- 23 Bajpai, A.K. (2019). Facile preparation of ionotropically crosslinked chitosan-alginate nanosorbents by water-in-oil (W/O) microemulsion technique: Optimization and study of arsenic (V) removal. *Journal of Water Process Engineering*, 32: 100920. <https://doi.org/10.1016/j.jwpe.2019.100920>
- 24 Kassymova, Zh.S., Orazzhanova, L.K., Bayakhmetova, B.B., Gaisina, B.S., Kassenova, N.B., & Yelemessova, G.T. (2019). Preparation of interpolymer complexes of chitosan and sodium alginate. *Bulletin of the University of Karaganda – Chemistry*, 93 (1), 17–24. <https://doi.org/10.31489/2019Ch1/17-24>
- 25 Klivenko, A., Orazzhanova, L., Mussabayeva, B., Yelemessova, G., & Kassymova, Z. (2020). Soil structuring using interpolyelectrolyte complexes of water-soluble polysaccharides. *Polymers for Advanced Technologies*, 31 (12), 3392–3301. <https://doi.org/10.1002/pat.5053>
- 26 Mussabayeva, B.Kh., Kassymova, Zh.S., & Aldabergenova, M.A. (2020). Interpolymer complex of biopolymers as a soil structure-forming agent. *Bulletin of the University of Karaganda – Chemistry*, 97 (1), 22–29. <https://doi.org/10.31489/2020Ch1/22-29>
- 27 Mineev, V.G. (2001). *Praktikum po agrokhimii [Agrochemistry practicum]*. Moscow: Izdatelstvo Moskovskogo gosudarstvennogo universiteta [in Russian].
- 28 Kholodov, V.A. (2013). The Capacity of Soil Particles for Spontaneous Formation of Macroaggregates after a Wetting–Drying Cycle. *Eurasian Soil Science*, 46(6), 660–667. <https://doi.org/10.1134/S1064229313040078>
- 29 Kalisz, A., Grabowska, Sekara, A., Capecka, E., Libik, A., Sulak, K., & Jurkow, R. (2019). Biodegradable polymer as floating row covers in field production of radish. *Chilean Journal of Agricultural Research*, 79 (2), 243–256. <http://dx.doi.org/10.4067/S0718-58392019000200243>
- 30 Kasymova, Zh.S., Klivenko, A.N., & Mukusheva, A.D. (2019). Uluchshenie vodno-fizicheskikh svoystv pochv s pomoshchiu biorazlagaemykh polimerov [Improvement of water-physical properties of soils with the help of biodegradable polymers]. *Vestnik Evrazijskogo natsionalnogo universiteta imeni L.N. Gumilyova. Seriya Khimiia, geografii, ekologiya — Bulletin of the L.N. Gumilyov Eurasian National University. Chemistry, geography, ecology series*, 4(129), 13–24 [in Russian].

Information about authors*

Mussabayeva, Binur Khabasovna (corresponding author) — Candidate of Chemical Sciences, Professor of the Higher School of Natural Sciences, Astana International University, Kabanbai batyr Ave., 8,

010000, Nur-Sultan, Kazakhstan; e-mail: binur.mussabayeva@mail.ru; <https://orcid.org/0000-0003-2209-1209>;

Kassymova, Zhanar Saylaubekovna — Candidate of Biological Sciences, Associate Professor of Chemical Technologies and Ecology Department, Shakarim University, Glinka str., 20A, 071412, Semey, Kazakhstan; e-mail: kasymova-z@mail.ru; <https://orcid.org/0000-0002-4971-6638>

Orazzhanova, Lyazzat Kametayevna — Candidate of Chemical Sciences, Associate Professor of Chemical Technologies and Ecology Department, Shakarim University, Glinka str., 20A, 071412, Semey, Kazakhstan; e-mail: lyazzat.7070@mail.ru; <https://orcid.org/0000-0001-7881-0589>;

Klivenko, Alexey Nikolayevich — PhD of Chemistry, Acting Associate Professor of Chemical Technologies and Ecology Department, Shakarim University, Glinka str., 20A, 071412, Semey, Kazakhstan; e-mail: alexeyklivenko@mail.ru; <https://orcid.org/0000-0002-8971-686X>;

Sabitova, Alfira Nurzhanovna — PhD of Petrochemistry, Head of Chemical Technologies and Ecology Department, Shakarim University, Glinka str., 20A, 071412, Semey, Kazakhstan; e-mail: alfa-1983@mail.ru; <https://orcid.org/0000-0002-3360-7998>;

Bayakhmetova, Bulbul Bayakhmetovna — Candidate of Chemical Sciences, Associate Professor of Chemical Technologies and Ecology Department, Shakarim University, Glinka str., 20A, 071412, Semey, Kazakhstan; e-mail: bulbul.bayahmetova@mail.ru; <https://orcid.org/0000-0002-5663-5107>

*The author's name is presented in the order: *Last Name, First and Middle Names*

Juan Du^{1,2}, Shimei Xu^{3*}

¹Key Laboratory of Material Corrosion and Protection of Sichuan Province, College of Materials Science and Engineering, Sichuan University of Science and Engineering, Zigong, China;

²Key Laboratory of Oil and Gas Fine Chemicals, Ministry of Education Xinjiang Uyghur Autonomous Region, College of Chemistry and Chemical Engineering, Xinjiang University, Urumqi, China;

³College of Chemistry, Sichuan University, Chengdu, China
(*Corresponding author's e-mail: xushimei@scu.edu.cn)

Solvents Triggered Coil-to-Globule-to-Coil Transition of Dual Nanocomposite Hydrogels with Inorganic Hybrid Crosslinking

This paper presents the study on the reentrant solvation of dual nanocomposite hydrogel poly-N-isopropylacrylamide/Laponite/SiO₂ (PNIPAM/Laponite/SiO₂) upon shrinkage/reswelling process. Depending on the unique hierarchical microstructure of inorganic hybrid crosslinking of Laponite and SiO₂, as well as the preferential interaction of polar solvents with PNIPAM chains, the hydrogel exhibited rapid coil-to-globule-to-coil transition in water-polar solvent mixtures. The solvation behavior could be controlled through varying types of organic solvents. Shrinkage in water-polar solvent mixtures occurred as a consequence of strong interaction between polar solvents and PNIPAM chains, whereas reswelling resulted from the direct interaction of the solvent molecules with the intermolecular water in the hydrogel. The attractive competing effects on forming hydrogel-water and hydrogel-polar solvent hydrogen bonds were considered to be indispensable to the solvation. The rapid response rate was attributed to the synergistic effect of the unique heterogeneous microstructure with inorganic hybrid crosslinking and preferential interaction of polar solvents with polymer chains. The mechanism proposed in this paper provides a new reference on design of smart soft matter systems. Moreover, several solvation effects described in this paper can be incorporated in theory of cononsolvent-induced conformational transitions in the nanocomposite hydrogels with inorganic hybrid crosslinking.

Keywords: inorganic hybrid crosslinking, dual nanocomposite hydrogel, coil-to-globule-to-coil transition, poly-N-isopropylacrylamide, polar solvent.

Introduction

Smart hydrogels have attracted increasing attention since they can exhibit dramatic change of volume or other properties in responding to external stimuli, such as temperature [1–3], pH [4–8], humidity [9–12], special ions or molecules [13–16], ionic strength or electric field [17, 18]. They are often involved in liquid environments, i.e., salt solutions, organic solvents, or both of them when applied in the field of cell culture, drug delivery, plant cultivation, soft actuator, etc. Therefore, it is crucial to have a better understanding of the swelling behavior of gels in different medium. The swelling of chemically crosslinked hydrogels are mainly focused in different salt solutions [19–22], polymer aqueous solutions [21, 23], or aqueous solutions of organic solvents [24–29]. It was found that the composition of solution has a great impact on the swelling behavior of the hydrogel. Cononsolvency is one of the most intriguing phenomena in physical chemistry of polymers, where a polymer perfectly soluble in two different solvents becomes insoluble in mixtures of both. The typical example is poly-N-isopropylacrylamide (PNIPAM) in water-methanol mixtures [30–32]. At a fixed temperature, PNIPAM can be easily dissolved in both pure water and pure methanol to form an optically transparent solution. However, mixing the two solvents in certain proportions led to the precipitation of polymer phases. Many efforts have been made to control the cononsolvency of PNIPAM hydrogels by shifting the content of alcohols. So far, most of those trials focus on the cononsolvency of organically crosslinked PNIPAM hydrogels. However, such hydrogels usually have a limited application owing to poor mechanical properties [33].

Haraguchi et al. reported a physically crosslinked PNIPAM/Laponite nanocomposite hydrogel which has remarkable mechanical properties (i.e., elongation at break: about 1000 %, tensile strength: 1.00 MPa) [33–35]. The nanoscaled Laponite platelets are uniformly dispersed in the gel and a large number of polymer chains are attached to their surfaces forming physical crosslinking points [36]. As a result, the thermo-

sensitivities and swelling/deswelling of the nanocomposite hydrogel was subject to steric hindrance by clay platelets and the coil-to-globule transition was prohibited at high Laponite content (greater than 10×10^{-2} mol/L). This may be due to the restriction of the thermal molecular movement of PNIPAM chains attached to the hydrophilic clay nanosheets [34, 35]. In our previous work, a dual nanocomposite hydrogel (PNIPAM/Laponite/SiO₂) with inorganic hybrid crosslinking network was successfully fabricated through simultaneous sol-gel technique and free radical polymerization. The gel exhibited high stiffness and toughness (i.e., elongation at break: 1845%, fracture strength: 271.41 kPa; compression stress: 7.06 MPa; fracture energy: $1185.53 \text{ J} \cdot \text{m}^{-2}$) [37]. It is a promising candidate for various disciplines such as biomedicine, tissue engineering, soft actuators, etc.

We found that the hydrogel showed an interesting and rapid coil-to-globule-to-coil transition in polar solvents at ambient temperature. The hydrogel could become opaque (collapsed) quickly at first within short intervals when soaked in polar solvents (such as ethanol and dimethyl formamide), and then turned to transparent (reswelled) gradually in hundreds of minutes. The phenomenon inspired us to explore the solvation behaviors and possible mechanism. Herein, different polarity and contents of solvents were used to investigate the competitive interactions (hydrogen bond) between polymer-water and polymer-organic solvents. The dependence of the response rate of the hydrogel on the gel microstructure and interaction of polymer-solvents was discussed. The reentrant solvation mechanism was proposed.

Experimental

Materials

Tetraethyl orthosilicate (TEOS) was purchased from Sigma-Aldrich Co.; *N*-isopropylacrylamide (NIPAM) was bought from J&K Scientific; *N,N,N',N'*-tetramethylethylenediamine (TEMED) was provided by Aldrich Chemical Co.; potassium peroxydisulfate (KPS) was purchased from Beijing Beihua Fine Chemicals Co. and Laponite XLG [$\text{Mg}_{5.34}\text{Li}_{0.66}\text{Si}_8\text{O}_{20}(\text{OH})_4\text{Na}_{0.66}$] was provided by Rockwood Co.; *N,N'*-methylene-bis-acrylamide was obtained from China Medicine Group Shanghai Chemical Reagent Corporation; ethanol and acetone were supplied by Tianjin Yongsheng Fine Chemicals Co.; tetrasodium pyrophosphate ($\text{Na}_4\text{P}_2\text{O}_7$) was bought by Shanghai Kechang Fine Chemicals Company; dimethyl formamide (DMF) was purchased from Tianjin Yongda Chemical Reagents Co. Ltd.; dimethyl sulfoxide and cyclohexane were provided by Tianjin Zhiyuan Chemical Reagent Co. Ltd.; benzyl alcohol was bought from Tianjin Guangfu Institute of Fine Chemicals. All reagents were used as received without any further purification. Deionized water was used in all experiments.

Hydrogel synthesis

The PNIPAM/Laponite/SiO₂ dual nanocomposite hydrogel was prepared by simultaneous *in-situ* free radical polymerization and sol-gel technique. Typically, a transparent aqueous dispersion consisting of water (10.0 g), Laponite (0.5 g), $\text{Na}_4\text{P}_2\text{O}_7$ (0.0384 g), NIPAM (1.0 g) and TEOS (1.0 g) was prepared under stirring at room temperature for 48 h until a transparent and stable dispersion was obtained. Then, initiator KPS (2 wt%, 1.0 mL) and catalyst TEMED (50.0 μL) were added into the above dispersion with stirring, respectively. Afterwards, the pre-polymerization dispersion was transferred to a sealed glass tube and the polymerization was carried out at room temperature for 72 h to obtain the PNIPAM/Laponite/SiO₂ dual nanocomposite hydrogel.

As a control, PNIPAM/Laponite nanocomposite hydrogel was fabricated in a similar manner except for the free of TEOS, and the organically crosslinked PNIPAM hydrogel was synthesized by the same procedure described above except for using organic crosslinker *N,N'*-methylene-bis-acrylamide instead of Laponite and TEOS, respectively.

Characterization

Fourier transform infrared (FTIR) measurements were recorded on a Fourier transform infrared spectrometer (VERTEXFTIR, Bruker). All spectra in the range of $400\text{--}4000 \text{ cm}^{-1}$ with 2 cm^{-1} spectral resolution were obtained. Scanning electron microscope (SEM) images were obtained on a scanning electron microscope (TM3030, Hitachi) at an accelerating voltage of 20 kV. The SEM samples were prepared by immersing the gel into ethanol (or DMF), water and ethanol (or DMF) in turn to reach phase equilibrium. The samples obtained through the every procedure above were freeze drying (FD-1C-50, Beijing Boyikang) for 48 h. Afterwards, the dry hydrogels were coated with gold prior to SEM analysis. The heat effect associated to the coil-to-globule-to-coil transition of the dual nanocomposite hydrogels in water/organic solvent mixtures were

measured using a differential scanning micro-calorimeter (DSC, Q2000, TA) by modulation mode. The difference in the heat capacity of gels containing different volume fraction of water and organic solvents and the heat capacity of the gels were measured upon heating at a rate of 2°C/min.

Results and Discussion

Solvents triggered coil-to-globule-to-coil transition

The PNIPAM/Laponite/SiO₂ dual nanocomposite hydrogel exhibited an interesting solvation behavior when soaked in ethanol: it became opaque (collapsed) quickly at first within 0.25 min, and then turned to transparent (reswelled) gradually after 245 min. During this process, the gel underwent an uneven solvation, and the periphery became transparent more quickly than the center (Fig. 1a). We further immersed the gel into the mixtures with different volume fraction of ethanol and water, and found that the reentrant coil-to-globule-to-coil transition was dependent of volume fraction of ethanol. When the ethanol volume fraction was low (below 20%), the gel remained transparent and the collapse-reswelling transition did not occur. It was probably because that low content of ethanol was hardly disturbed the interaction between PNIPAM chains and water. The solvation occurred gradually with the increase of ethanol content. When the volume fraction of ethanol was 30%–60% ($n_{\text{ethanol}}:n_{\text{water}}$ from 0.13 to 0.47 accordingly), the gel turned to translucent within 0.25 min, and then became opaque (collapsed) gradually. There was no further change observed even after 3 days. These results were in good agreement with those reported by Hirotsu et al. and Wu et al. They found that the organically crosslinked PNIPAM gel and linear PNIPAM became opaque when $n_{\text{ethanol}}:n_{\text{water}}$ from 0.17 to 0.50 [38, 39]. This suggested that the coil-to-globule transition was independent of the type of crosslinking. However, further to increase the volume fraction of ethanol (above 80%), the gel could experience the reentrant coil-to-globule-to-coil transition (i.e., the transparent gel quickly became opaque after contacting with ethanol solution, and then became transparent again) in a relatively short period because of the dissolution of the aggregated PNIPAM chain segments (Fig. 1a). Those phenomena made it possible to realize controllable solvation of the dual nanocomposite hydrogels upon the composition of organic solvents and soak time. Besides, the unusual phase behavior was independent of the shape of the gel (Fig. 1b). These results provided the possibility of programmable control of solvation of the gel by changing the solvent composition.

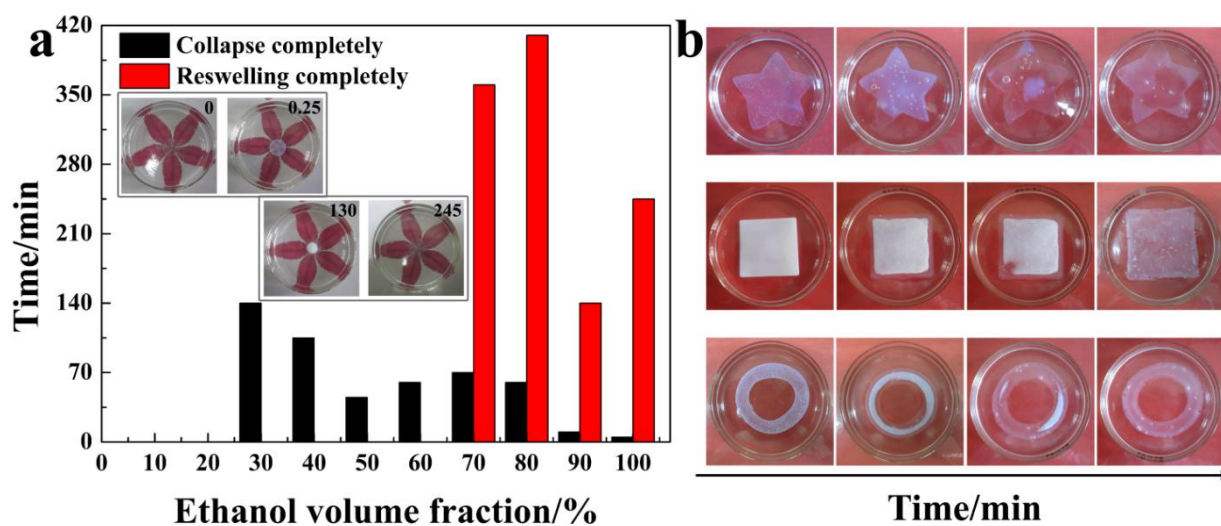


Figure 1. *a* — The influence of ethanol volume fraction on the reentrant coil-to-globule-to-coil transition of the dual nanocomposite gels (the inset: optical photographs of the reentrant solvation of the gels in 70% ethanol volume fraction observed at room temperature); *b* — The dual nanocomposite gels with various shapes (pentagram, square, and annulus) were immersed in ethanol

Both shrinkage and reswelling procedures of the dual nanocomposite hydrogel were reversible. When the gel reached phase equilibrium in ethanol first, and then immersed it in water, the transparent gel could become opaque quickly and eventually turned transparent. If the same gel block was re-submersed in ethanol again, it still showed a significant contraction-expansion transition in hundreds of minutes. As the gel fin-

ished solvation in ethanol, it exhibited a heterogeneous structure and the pores size of the gel network became more irregular (Fig. 2*b*) in contrast with the gel which reached swelling equilibrium in water (Fig. 2*a*). When the gel reached phase equilibrium in water again, the pore size of the gel network was recovered in some degree and became more uniform (Fig. 2*c*). Although the gel achieved phase separation in ethanol completely, the pores of the gel presented a serious irregular shrinkage due to further destruction of the gel network (Fig. 2*d*). The microstructure of the hydrogel is a critical factor in the response rate of the solvation process. The response rate of the hydrogel is inversely proportional to the size of the gel. However, in our work, the bulk dual nanocomposite gel could quickly collapse (opaque) in ethanol within 0.25 min and then reswell (transparent) again since the synergistic effect of the unique heterogeneous microstructure of dual nanocomposite and preferential interaction of ethanol with PNIPAM chains (Fig. 2*e*). The hydrophobic interaction led to rapid dehydration and solvation of the gel, while the dual nanocomposite configuration could provide an interconnected water release channel throughout the hydrogel and the free water could diffuse out quickly. Combined with the above results, it could be seen that the change of gel microstructure caused by solvent is closely related to its reentrant coil-to-globule-to-coil transition.

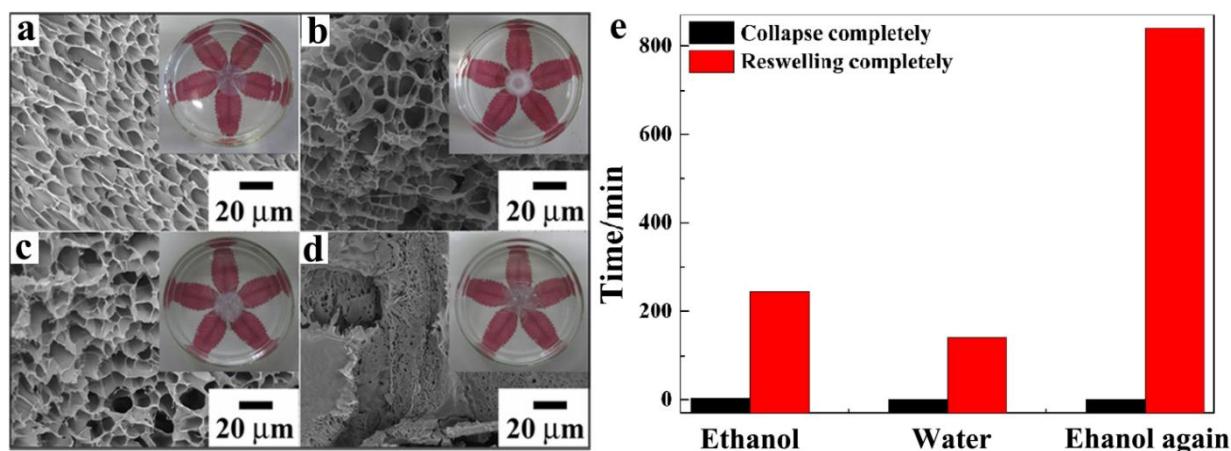


Figure 2. SEM micrographs of the dual nanocomposite hydrogels treated through following processing: *a* — the gel reached swollen equilibrium in water; *b* — the gel reached phase equilibrium in ethanol beforehand; *c* — and then in water; *d* — finally in ethanol again (the orange circles represent the gel collapsed completely, the pink circles represent the gel reswelled completely, respectively); *e* — The influence of alternate treated process on the reentrant coil-to-globule-to-coil transition of the dual nanocomposite hydrogels

Different solvents were used to account for the influence of polarity on the reentrant coil-to-globule-to-coil transition. It was found that these complex solvations were closely driven by the preferential binding of polar or non-polar solvents with PNIPAM chains in the hydrogel matrix (Fig. 3*a*). The gel experienced an obvious reentrant collapse-reswelling transition in polar solvents (such as dimethyl sulfoxide, DMF, ethanol, and acetone). However, the gel had no significant change when was immersed into non-polar solvent (such as cyclohexane). It is speculated that the favorable interaction with water and polar solvents lead to the different solvation behavior. Initially, the gel was surrounded by cages of water molecules due to the stable hydrogen bonds formed between polymer chains and water molecules. As a result, the gel was transparent. When non-polar solvents were added, the solvent could not destroy the structure of water due to the poor solute-solvent interactions. At this time, the gel could still remain transparent. However, when polar solvents were added with favorable interaction with the water surrounded the gel, the competition between PNIPAM molecular chain shrinkage and interchain aggregation decreased the stability of the hydrogen-bonded water structure, ultimately leading to phase separation (the coil-to-globule transition) of the dual nanocomposite hydrogel. As a result, the gel became opaque. This is consistent with the report of Grosberg and Yang [40, 41]. With the proceeding of process, all the water molecules around the gel were combined with the polar solvent, resulting in the interaction between the polar solvent and PNIPAM chains stronger than that between the polymer and water. Finally, the gel became transparent again (the transition of globule-to-coil).

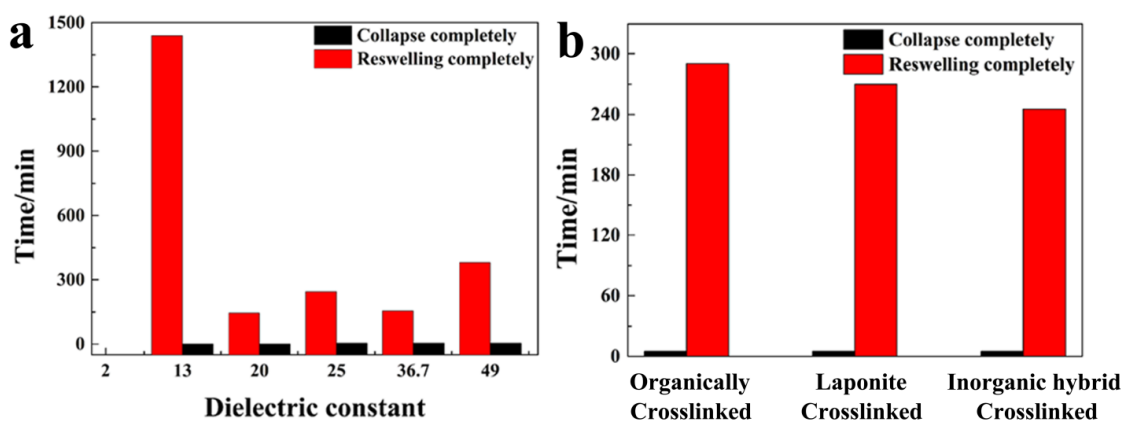


Figure 3. The influence of solvents polarity (a) and crosslinked network (b) on the reentrant coil-to-globule-to-coil transition of the dual nanocomposite hydrogels, respectively

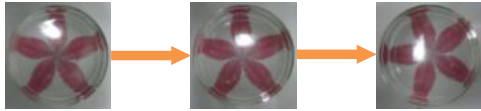
To figure out the impact of crosslinked network on the solvation, gels with different crosslinking networks (organically crosslinking, Laponite crosslinking, and hybrid inorganically crosslinking) were soaked in ethanol. The results showed that this uneven solvation behavior still existed despite the different types of crosslinking. In comparison, the gel with hybrid inorganically crosslinking network reached phase equilibrium in a relatively short time (Fig. 3b). Those were mainly attributed to the dual nanocomposite network structure in which clay platelets and SiO₂ particles, uniformly dispersed on nanoscale, act as multifunctional cross-linking units whereby a large number of polymer chains are attached to the surface of clay platelets and SiO₂ particles forming hybrid cross-linking points. The unique heterogeneous dual nanocomposite network structure could facilitate the diffusion of solvent in the gel network. It indicated that the solvation behavior was related to the strong interactions between the hydrogel backbone polymer and the polar solvents, while the response rate was mainly attributed to the unique nanocomposite network structure.

The pretreatment process would influence the solvation of the gel. When the gel reached swelling equilibrium in water at first, and then immersed into DMF solutions with different volume fractions, all gels experienced the same reentrant collapse-reswelling behavior: from transparent to opaque, and eventually become transparent again. However, if the gel reached phase equilibrium in DMF solutions with different volume fractions beforehand and then immersed into water, a different solvation phenomenon was observed instead. At low volume fractions of DMF (below 40%), the gel could maintain transparent all the time. As the DMF volume fraction increased (from 50% to 70%), the gel underwent an opaque-to-transparent transition. Further enhancing the volume fraction of DMF (from 80% to 100%), the transparent gel became opaque at first and then turned to transparent again in a few minutes (Table 1). When immersed into DMF first, the strong interaction between the water surrounded the gel and DMF molecules could disturb the hydrogen bonding between gel and water, which led to a decrease in the transparency of the gel after the phase equilibrium was reached. Afterwards, the competing interaction between DMF and water occurred, and finally the gel became transparent again in water in all circumstances due to formation of durable cages of water molecules surrounding the gel.

Table 1

The phenomena of the dual nanocomposite hydrogels reached phase equilibrium in the DMF-water mixture with different DMF volume fractions first, and then soaked it in water

DMF volume fraction	Phenomenon	
	Reached phase equilibrium in DMF-water beforehand → Then immersed in water → Reached phase equilibrium in water finally	
1	2	
0 %	Transparent	

1	2	
10 %	Transparent 	
20 %	Transparent 	
30 %	Transparent 	
40 %	Transparent 	
50 %	Opaque → Transparent 	
60 %	Opaque → Transparent 	
70 %	Opaque → Transparent 	
80 %	Transparent → Opaque → Transparent 	
90 %	Transparent → Opaque → Transparent 	
100 %	Transparent → Opaque → Transparent 	

Solvation mechanism

The effects of solvents on the solvation of the dual nanocomposite hydrogels were further investigated using DSC analysis. To avoid the evaporation of ethanol due to its low boiling point (78.0°C), DMF (152.8°C) was employed as the model solvent for exploration on solute-solvent interaction. The solvation temperature of the gel was 36.0°C in water, accompanying sharp change in polymer conformation from a

balance between hydrogen bonding of water on the chain (hydration) and hydrophobic aggregation of isopropyl groups, and presented an obvious endothermic peak in DSC curves [42]. The hydrogels demonstrated a significant shift in the transition temperature as the volume fraction of DMF varied (Fig. 4a). This observation was consistent with the initial experiments by Winnik et al., in which the effect of methanol as a cosolvent for linear PNIPAM in dilute aqueous solutions was investigated [31]. With the increasing of DMF volume fractions, the interaction between the gel and water was broken, and the interactions between the gel and polar solvents were dominated. As a consequence, the endothermic peak around 36.0 °C became unapparent and then disappeared gradually. Instead, some new endothermic peaks at higher solvation temperature were observed at low DMF volume fraction, suggesting a strong interaction formed between DMF and water. In the end, only a solvation temperature of 51.2 °C was found owing to the interaction between the gel and DMF. It is conjectured that there existed a competitive effect between the gel and water, as well as the gel and DMF. With the augment of DMF, the interaction between gel and water was substituted by DMF and gel. It was clearly observed that the solvation temperature was 51.2 °C when the gel was immersed in pure DMF, while it exhibited two distinct solvation temperatures (36.0 °C and 49.5 °C) when immersed in water afterwards. Finally, the solvation temperature changed to 50.5 °C when soaked in pure DMF again (Fig. 4b). SEM images showed that when the hydrogel was soaked in DMF first, the pores became irregular and collapsed to a certain extent (Fig. 4c) in contrast with the gel which reached swelling equilibrium in water (Fig. 2a). After the gel attained phase equilibrium in water again, the gel network was recovered in some degree (Fig. 4d). However, when the gel achieved phase separation in DMF completely once again, the pores of the gel were severely damaged again due to further destruction of the gel network (Fig. 4e). The SEM morphology of the gel in different solvents showed that the collapse and reswelling transformation was reversible, which also confirmed the strong interaction between the polar solvent DMF and the hydrogel.

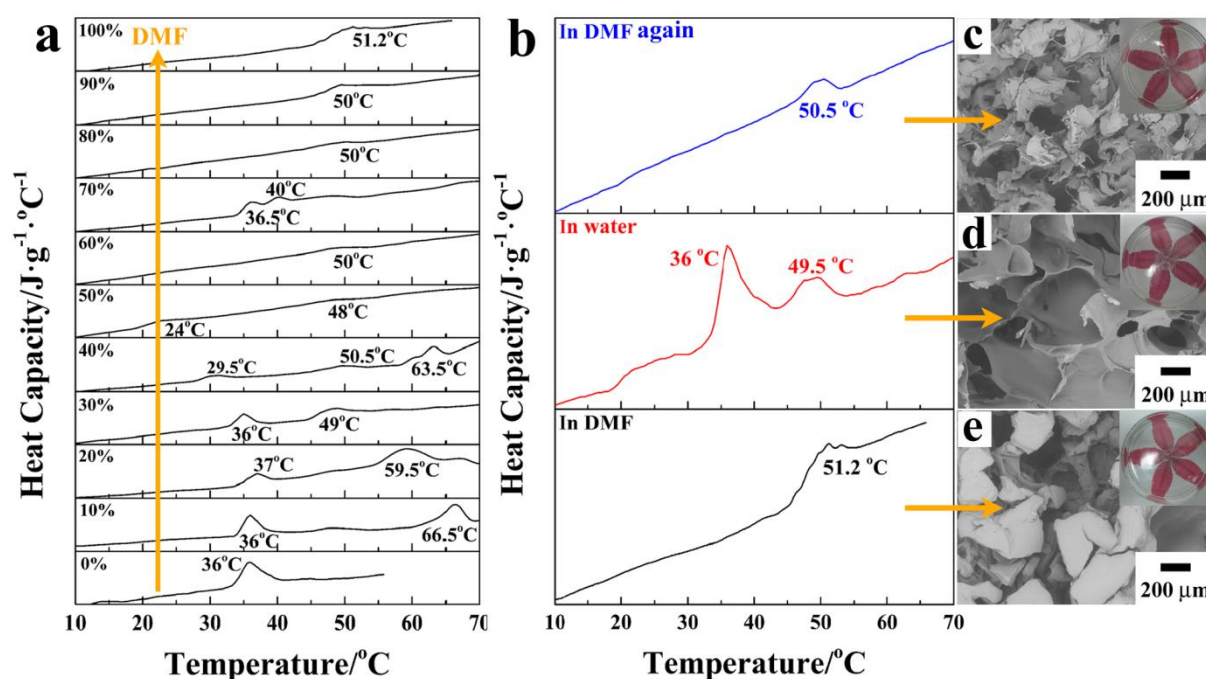


Figure 4. Temperature dependence of the heat capacity of PNIPAM/Laponite/SiO₂ dual nanocomposite hydrogels: *a* — in DMF-water mixtures with various volume fractions of DMF; *b* — treated through the following processing: the gel reached phase equilibrium in DMF beforehand, and then in water, finally in DMF again (left were the SEM images of the gels in above process)

To verify the conjecture above, the solvent dependence of the absorption bands of the dual nanocomposite hydrogel in varied volume fraction of DMF-water mixtures (0%–100%) was explored by FTIR. The absorption bands at about 1652 cm⁻¹ and 1500 cm⁻¹ could be attributed to the vibration of C=O hydrogen bonded with N–H from DMF (1600–1700 cm⁻¹) and C–N bond from DMF bonded with water and the gel (1500–1600 cm⁻¹), respectively [43–46]. The bands at 1652 cm⁻¹ shifted to higher wavenumbers while the intensity of the bands increased significantly with the increase of DMF volume fraction (Fig. 5a). Similarly, the bands at 1500 cm⁻¹ also shifted to higher wavenumber, while the intensity of the band rose but

in a lower degree compared with the one at 1652 cm^{-1} . This evidence confirmed that with the increase of DMF volume fraction, the C=O groups of the hydrogel dehydrated gradually and previous hydrogen bonds (C=O \cdots H-O) was replaced by new hydrogen bonds (C=O \cdots N-H). Thus, a blue shift and intensity increase were observed. Besides, it was further confirmed that intermolecular hydrogen bonds acted a key role in solvation behaviors owing to a blue shift of the adsorption peaks. A similar trend was found for the peaks at $1500\text{--}1600\text{ cm}^{-1}$ since it was contributed to breakage of C-N \cdots H-O-H and formation of C-N \cdots H-N. As Tanaka reported, the sharp reentrant coil-to-globule-to-coil transition of PNIPAM chain in a mixture of water and methanol was caused by competitive hydrogen bonds between water and methanol molecules onto the polymer chain [47]. In Figure 5b, after the same block of dual nanocomposite hydrogel was treated by DMF, water and DMF alternatively, there was a noticeable change concerning the bands of C=O hydrogen bonded with N-H ($1600\text{--}1700\text{ cm}^{-1}$) and C-N \cdots H-O-H, as well as C-N \cdots N-H ($1500\text{--}1600\text{ cm}^{-1}$) together with an intensity increase at about 1652 cm^{-1} and 1500 cm^{-1} when reached phase equilibrium in the presence of DMF. The destruction of C=O \cdots H-O-H hydrogen bonds between the gel and intermolecular water took place on a very short time scale, faster than the formation of C=O \cdots H-N, C-N \cdots H-O-H, and C-N \cdots H-N hydrogen bonds [48, 49]. Also, it is clearly observed that the gel has recovered in some degree, which was in consistent with SEM (Fig. 2a-d) and DSC analysis (Fig. 4b) of the gel. In conclusion, the competitive hydrogen bonding occurred between DMF and the gel was the main reason for the special solvation of the gel.

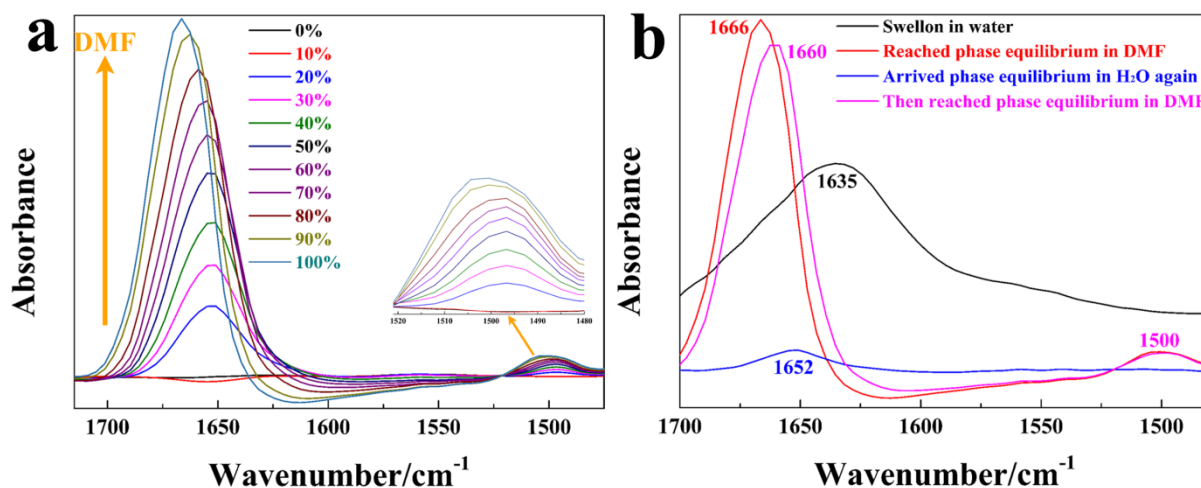


Figure 5. FTIR spectra of PNIPAM/Laponite/SiO₂ dual nanocomposite hydrogels recorded between $1750\text{--}1400\text{ cm}^{-1}$: *a* — as a function of DMF volume fraction; *b* — treated through the following processing: made the gel reach phase equilibrium in DMF beforehand, and then let the same block of gel reach phased equilibrium in water, finally made this gel reach phase equilibrium in DMF again

The solvation mechanism of the dual nanocomposite hydrogel in polar solvents was proposed as follows with DMF as an example: at a lower content of polar solvent, the interaction between PNIPAM chain and water is stronger than that between polar solvent and water. In this case, water clathrate cavities for DMF molecules may be formed (Figure 6a). Therefore, the gel maintains transparent and the collapse-swelling transition does not occur due to unbroken interaction between PNIPAM chains and water. With the increasing of polar solvent content, the interaction between gel and water is broken, and the interaction between gel and polar solvent is dominant. As a result, the gel undergoes a coil-to-globule transition (opaque) within a few minutes. It is because no sufficient water molecules to provide clathrate cavities for all the DMF molecules, and DMF breaks the partial hydrogen bonds of C=O \cdots H-O-H and C-N \cdots H-O-H while forms new hydrogen bonds of C=O \cdots N-H and C-N \cdots H-N (Scheme 1b). On this basis, by further increasing the contents of polar solvents, the gel can experience a coil-to-globule-to-coil transition in a relatively short period. In contrast, in non-polar solvents, they can coexist peacefully with the intermolecular water owing to the unfavorable interactions with non-polar solvents and the water surrounded the gel (Figure 6c).

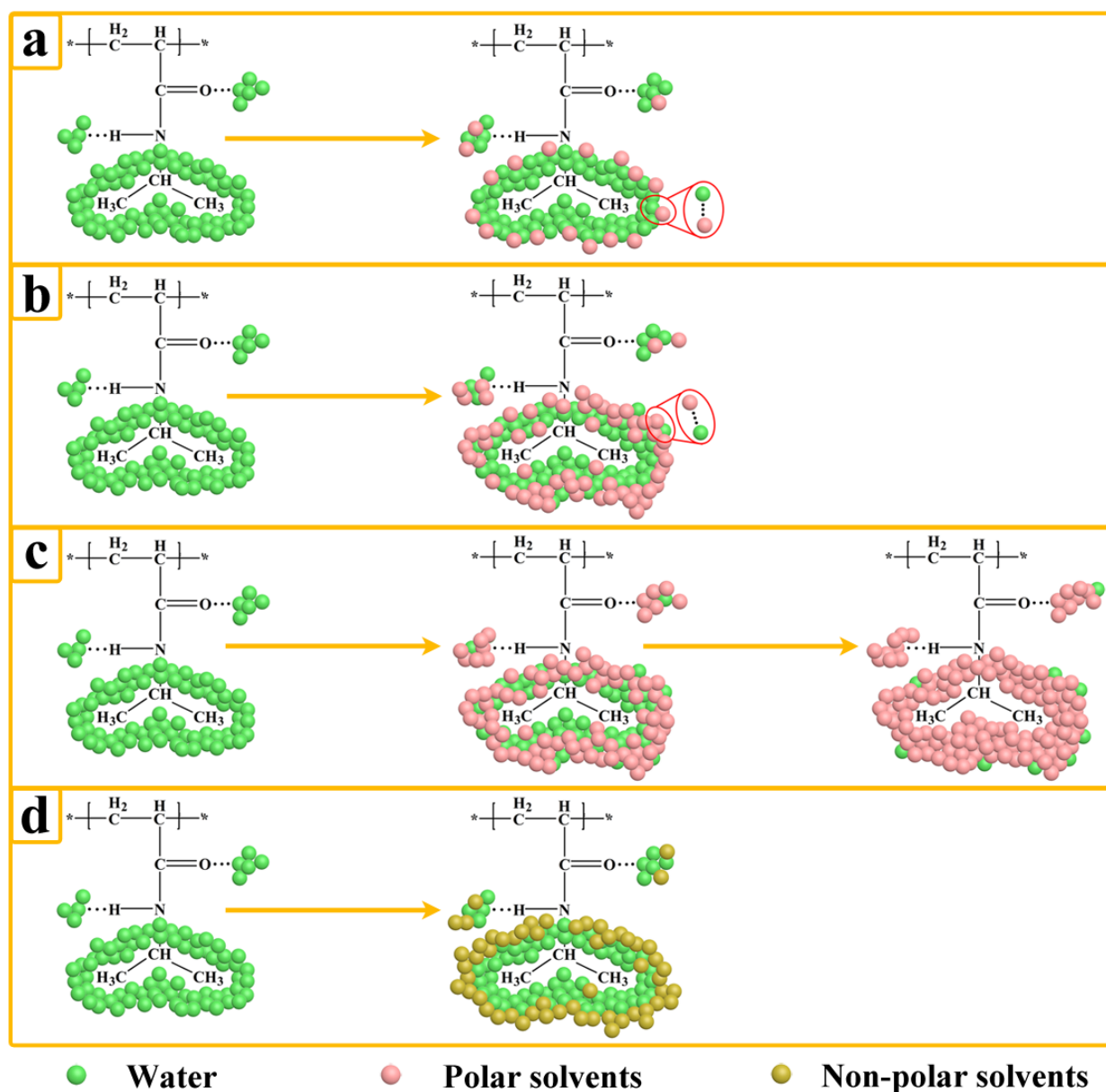


Figure 6. The reentrant solvation mechanism of PNIPAM/Laponite/SiO₂ dual nanocomposite hydrogel soaked in different solvents: *a*, *b* and *c* — in polar solvents (take DMF as an example: *a* — the volume fraction of DMF was below 50 %; *b* — the volume fraction of DMF was between 50 % and 70 %; *c* — the volume fraction of DMF was above 70 %); *d* — pure non-polar solvents

Conclusions

In conclusion, rapid collapse and reswelling behaviors were observed in dual nanocomposite hydrogels PNIPAM/Laponite/SiO₂. The solvation of the hydrogels could be easily controlled by adjusting the type and concentration of solvents and soaking time. The reentrant coil-to-globule-to-coil transition was attributed to competitive interactions between the hydrogel backbone polymer and the solvents: the breakdown or formation of hydrogen bonds between the polymer chains and water/polar solvents. With the increasing of polar solvents, the intramolecular hydrogen bonds between the C=O or C–N groups of PNIPAM and water molecules were damaged and new intra- and inter-chain bonds were formed between PNIPAM and polar solvents. Besides, the rapid response rate was attributed to the synergistic effect of the unique heterogeneous microstructure and preferential interaction of polar solvents with the polymer chains. The dual nanocomposite hydrogel exhibited fast and reversible solvent-responsive collapse-reswelling characteristics, as well as improved mechanical properties. It will be highly attractive and promising in many applications for on-off switches, artificial organs and actuators in liquid environments.

Acknowledgments

The work was supported by Sichuan Science and Technology Program (No. 2022JDRC0090).

References

- Juodkazis, S., Mukai, N., Wakaki, R., Yamaguchi, A., Matsuo, S., & Misawa, H. (2000). Reversible phase transitions in polymer gels induced by radiation forces. *Nature*, 408(6809): 178–181. <https://doi.org/10.1038/35041522>
- Yao, C., Liu, Z., Yang, C., Wang, W., Ju, X.J., Xie, R., & Chu, L.Y. (2015). Poly(N-isopropylacrylamide)-Clay Nanocomposite Hydrogels with Responsive Bending Property as Temperature-Controlled Manipulators. *Adv Funct Mater*, 25(20): 2980–2991. <https://doi.org/10.1002/adfm.201500420>.
- Fellin, C.R., & Nelson, A. (2022). Direct-Ink Write 3D Printing Multistimuli-Responsive Hydrogels and Post-Functionalization Via Disulfide Exchange. *ACS Appl Polym Mater*. <https://doi.org/10.1021/acsapm.1c01538>.
- Lee, B.P., & Konst, S. (2014). Novel Hydrogel Actuator Inspired by Reversible Mussel Adhesive Protein Chemistry. *Adv Mater*, 26(21): 3415–3419. <https://doi.org/10.1002/adma.201306137>.
- Ma, C., Li, T., Zhao, Q., Yang, X., Wu, J., Luo, Y., & Xie, T. (2014). Supramolecular Lego Assembly Towards Three-Dimensional Multi-Responsive Hydrogels. *Adv Mater*, 26(32): 5665–5669. <https://doi.org/10.1002/adma.201402026>.
- Soup, S.T., Shin-Hyun, K., Chul-Joon, H., Chul, J.H., & Yang, S.M. (2011). Controlled origami folding of hydrogel bilayers with sustained reversibility for robust microcarriers. *Angew Chem Int Edit*, 51(6): 1420–1423. <https://doi.org/10.1002/anie.201106723>.
- Shariatnia, Z., & Ziba, M., (2022). Smart pH-responsive drug release systems based on functionalized chitosan nanocomposite hydrogels. *Surf Interfaces*, 29: 101739. <https://doi.org/10.1016/j.surfin.2022.101739>.
- Wan, Q., Li, X., Ren, Y., Cao, Y., Ju, K., Yang, G., Sun, Y., & Zhang, X., (2022). Preparation and Characterization of Temperature/pH Dual-Responsive Gel Spheres for Immobilizing Nitro Bacteria. *ACS Omega*, 7(7): 5646–5656. <https://doi.org/10.1021/acsomega.1c04469>.
- Islam, M.R., Li, X., Smyth, K., & Serpe, M.J. (2013). Polymer-Based Muscle Expansion and Contraction. *Angew Chem Int Edit*, 52(39): 10330–10333. <https://doi.org/10.1002/anie.201303475>.
- Ma, Y., Zhang, Y., Wu, B., Sun, W., Li, Z., & Sun, J. (2011). Polyelectrolyte multilayer films for building energetic walking devices. *Angew Chem Int Edit*, 50(28): 6254–6257. <https://doi.org/10.1002/ange.201101054>.
- Ma, Y., & Sun, J. (2009). Humido- and Thermo-Responsive Free-Standing Films Mimicking the Petals of the Morning Glory Flower. *Chem Mater*, 21(5): 898–902. <https://doi.org/10.1021/cm8031708>.
- Deng, C., Fan, X., Tao, Y., Jiao, B., Liu, Y., Qu, L., Zhao, Y., Li, X., & Xiong, W. (2021). Femtosecond Laser Four-Dimensional Printing Based on Humidity Responsive Hydrogels. *Chin J Lasers*, 48(2): 202016–202011. <https://doi.org/10.3788/CJL202148.0202016>.
- Liu, Z., Liu, L., Ju, X.J., Xie, R., Zhang, B., & Chu, L.Y. (2011). K⁺-recognition capsules with squirting release mechanisms. *Chem Commun*, 47(45): 12283–12285. <https://doi.org/10.1039/C1CC15082K>.
- Mi, P., Ju, X.J., Xie, R., Wu, H.G., Ma, J., & Chu, L.Y. (2010). A novel stimuli-responsive hydrogel for K⁺-induced controlled-release. *Polymer*, 51(7): 1648–1653. <https://doi.org/10.1016/j.polymer.2010.02.018>.
- Tu, T., Fang, W., & Sun, Z. (2013). Visual-size molecular recognition based on gels. *Adv Mater*, 25(37): 5304–5313. <https://doi.org/10.1002/adma.201301914>.
- Xiong, Z., Zheng, M.L., Dong, X.Z., Chen, W.Q., Jin, F., Zhao, Z.S., & Duan, X.M. (2011). Asymmetric microstructure of hydrogel: two-photon microfabrication and stimuli-responsive behavior. *Soft Matter*, 7(21): 10353–10359. <https://doi.org/10.1039/C1SM06137B>.
- Peng, X., Li, Y., Zhang, Q., Shang, C., Bai, Q.-W., & Wang, H. (2016). Tough Hydrogels with Programmable and Complex Shape Deformations by Ion Dip-Dyeing and Transfer Printing. *Adv Funct Mater*, 26(25): 4491–4500. <https://doi.org/10.1002/adfm.201601389>.
- Shin, Y., Choi, M.Y., Choi, J., Na, J.-H., & Kim, S.Y. (2021). Design of an Electro-Stimulated Hydrogel Actuator System with Fast Flexible Folding Deformation under a Low Electric Field. *ACS Appl Mater Inter*, 13(13): 15633–15646. <https://doi.org/10.1021/acsaami.1c00883>.
- Nisato, G., Schosseler, F., & Candau, S. (1996). Swelling equilibrium properties of partially charged gels: the effect of salt on the shear modulus. *Polym Gels Netw*, 4(5): 481–498. [https://doi.org/10.1016/S0966-7822\(96\)00024-X](https://doi.org/10.1016/S0966-7822(96)00024-X).
- Orlov, Y., Xu, X., & Maurer, G. (2007). An experimental and theoretical investigation on the swelling of N-isopropyl acrylamide based ionic hydrogels in aqueous solutions of (sodium chloride or di-sodium hydrogen phosphate). *Fluid Phase Equilib*, 254(1): 1–10. <https://doi.org/10.1016/j.fluid.2007.02.010>.
- Sayil, Ç., & Okay, O. (2002). Swelling-shrinking hysteresis of poly(N-isopropylacrylamide) gels in sodium dodecylbenzenesulfonate solutions. *J Appl Polym Sci*, 83(6): 1228–1232. <https://doi.org/10.1002/app.2289>.
- Liu, X., Tong, Z., & Hu, O. (1995). Swelling equilibria of hydrogels with sulfonate groups in water and in aqueous salt solutions. *Macromolecules*, 28(11): 3813–3817. <https://doi.org/10.1021/ma00115a010>.
- Gündogan, N., & Okay, O. (2002). Reentrant phase transition of poly(N-isopropylacrylamide) gels in polymer solutions: Thermodynamic analysis. *J Appl Polym Sci*, 85(4): 801–813. <https://doi.org/10.1002/app.10669>.

- 24 Orlov, Y., Xu, X., & Maurer, G. (2006). Equilibrium swelling of N-isopropyl acrylamide based ionic hydrogels in aqueous solutions of organic solvents: Comparison of experiment with theory. *Fluid Phase Equilib*, 249(1): 6–16. <https://doi.org/10.1016/j.fluid.2006.08.015>.
- 25 Hüther, A., Xu, X., & Maurer, G. (2004). Swelling of N-isopropyl acrylamide hydrogels in water and aqueous solutions of ethanol and acetone. *Fluid Phase Equilib*, 219(2): 231–244. <https://doi.org/10.1016/j.fluid.2003.08.002>.
- 26 Orakdogan, N., & Okay, O. (2006). Reentrant conformation transition in poly(N,N-dimethylacrylamide) hydrogels in water-organic solvent mixtures. *Polymer*, 47(2): 561–568. <https://doi.org/10.1016/j.polymer.2005.11.066>.
- 27 Liu, X., Hu, O., & Tong, Z. (1997). Viscosity behavior of polyelectrolyte copolymers containing sulfonate groups in mixed organic solvents. *J Polym Sci Pol Phys*, 35(9): 1433–1438. [https://doi.org/10.1002/\(SICI\)1099-0488\(19970715\)35:9<1433::AID-POLB13>3.0.CO;2-7](https://doi.org/10.1002/(SICI)1099-0488(19970715)35:9<1433::AID-POLB13>3.0.CO;2-7).
- 28 Liu, X., Tong, Z., Cao, X., & Hu, O. (1996). Volume phase transition of polyelectrolyte gels in dimethyl sulfoxide/tetrahydrofuran mixtures. *Polymer*, 37(26): 5947–5949. [https://doi.org/10.1016/S0032-3861\(96\)00581-2](https://doi.org/10.1016/S0032-3861(96)00581-2).
- 29 Liu, X., Tong, Z., & Gao, F. (1998). Novel shrinking-swelling hysteresis in DMSO/THF mixtures of copolymer gels containing sulphonate groups. *Polym Int*, 47(2): 215–220. [https://doi.org/10.1002/\(SICI\)1097-0126\(1998100\)47:2<215::AID-PI58>3.0.CO;2-H](https://doi.org/10.1002/(SICI)1097-0126(1998100)47:2<215::AID-PI58>3.0.CO;2-H).
- 30 Hirotsu, S. (1987). Critical points of the volume phase transition in N-isopropylacrylamide gels. *J Chem Phys*, 88(1): 427–431. <https://doi.org/10.1063/1.454619>.
- 31 Winnik, F.M., Ringsdorf, H., & Venzmer, J. (1990). Methanol-water as a co-nonsolvent system for poly(N-isopropylacrylamide). *Macromolecules*, 23(8): 2415–2416. <https://doi.org/10.1021/ma00210a048>.
- 32 Schild, H.G., Muthukumar, M., & Tirrell, D.A. (2002). Cononsolvency in mixed aqueous solutions of poly(N-isopropylacrylamide). *Macromolecules*, 24(4): 948–952. <https://doi.org/10.1021/ma00004a022>.
- 33 Haraguchi, K., Taniguchi, S., & Takehisa, T. (2005). Reversible Force Generation in a Temperature-Responsive Nanocomposite Hydrogel Consisting of Poly(N-isopropylacrylamide) and Clay. *ChemPhysChem*, 6(2): 238–241. <https://doi.org/10.1002/cphc.200400398>.
- 34 Haraguchi, K., Li, H.J., Song, L., & Murata, K. (2007). Tunable Optical and Swelling/Deswelling Properties Associated with Control of the Coil-to-Globule Transition of Poly(N-isopropylacrylamide) in Polymer-Clay Nanocomposite Gels. *Macromolecules*, 40(40): 43–50. <https://doi.org/10.1021/ma071348i>.
- 35 Haraguchi, K., & Li, H.J. (2005). Control of the Coil-to-Globule Transition and Ultrahigh Mechanical Properties of PNIPA in Nanocomposite Hydrogels. *Angew Chem Int Edit*, 117(40): 6658–6662. <https://doi.org/10.1002/ange.200502004>.
- 36 Haraguchi, K., & Takehisa, T. (2002). Nanocomposite Hydrogels: A Unique Organic-Inorganic Network Structure with Extraordinary Mechanical, Optical, and Swelling/De-swelling Properties. *Adv Mater*, 14(16): 1120–1124. [https://doi.org/10.1002/1521-4095\(20020816\)14:16<1120::AID-ADMA1120>3.0.CO;2-9](https://doi.org/10.1002/1521-4095(20020816)14:16<1120::AID-ADMA1120>3.0.CO;2-9).
- 37 Du, J., Wang, D., Xu S., Wang, J., Liu Y., & Huang J. (2017). Stretchable dual nanocomposite hydrogels strengthened by physical interaction between inorganic hybrid crosslinker and polymers. *Appl Clay Sci*, 150: 71–80. <https://doi.org/10.1016/j.clay.2017.09.008>.
- 38 Hirotsu, S., Okajima, T., & Yamamoto, T. (1995). Anomalous Aggregation Pattern Observed on Gels in Mixed Solvent. *Macromolecules*, 28(3): 775–777. <https://doi.org/10.1021/ma00107a014>.
- 39 Zhang, G., & Wu, C. (2001). The water/methanol complexation induced reentrant coil-to-globule-to-coil transition of individual homopolymer chains in extremely dilute solution. *J Am Chem Soc*, 123(7): 1376–1380. <https://doi.org/10.1021/ja003889s>.
- 40 Grosberg, A.Y., & Kuznetsov, D.V. (1993). Single-chain collapse or precipitation? Kinetic diagram of the states of a polymer solution. *Macromolecules*, 26(16): 4249–4251. <https://doi.org/10.1021/ma00068a027>.
- 41 Yang, H. (2001). Coil-globule Transition of Aqueous Poly(N-isopropylacrylamide) Solution. Ph.D. Thesis. Nanjing: Nanjing University [in Chinese]. <https://d.wanfangdata.com.cn/thesis/Y371126>.
- 42 Schild, H.G. (1992). Poly(N-isopropylacrylamide)-experiment, theory and application. *Prog. Polym. Sci.* 17, 163–249. *Prog Polym Sci*, 17(2): 163–249. [https://doi.org/10.1016/0079-6700\(92\)90023-R](https://doi.org/10.1016/0079-6700(92)90023-R).
- 43 Dybal, J., Trchová, M., & Schmidt, P. (2009). The role of water in structural changes of poly(N-isopropylacrylamide) and poly(N-isopropylmethacrylamide) studied by FTIR, Raman spectroscopy and quantum chemical calculations. *Vib Spectrosc*, 51(1): 44–51. <https://doi.org/10.1016/j.vibspec.2008.10.003>.
- 44 Cheng, H., Shen, L., & Wu, C. (2006). LLS and FTIR Studies on the Hysteresis in Association and Dissociation of Poly(N-isopropylacrylamide) Chains in Water. *Macromolecules*, 39(6): 2325–2329. <https://doi.org/10.1021/ma052561m>.
- 45 Sun, B., Lin, Y., Wu, P., & Siesler, H.W. (2008). A FTIR and 2D-IR spectroscopic study on the microdynamics phase separation mechanism of the poly (N-isopropylacrylamide) aqueous solution. *Macromolecules*, 41(4): 1512–1520. <https://doi.org/10.1021/ma702062h>.
- 46 Fadeeva, Y.A., Demina, L.I., Gorbunova, Y.G., Shmukler, L.E., Safonova, L.P., & Tsvadze, A.Y. (2003). Orthophosphoric Acid-N,N-Dimethylformamide System: IR Study. *Russ J Coord Chem*, 29(7): 515–518. <https://doi.org/10.1023/A:1024791332656>.
- 47 Fumihiko, T., Tsuyoshi, K., & Winnik, F.O.M. (2008). Temperature-responsive polymers in mixed solvents: competitive hydrogen bonds cause cononsolvency. *Phys Rev Lett*, 101(2): 1676–1686. <https://doi.org/10.1103/PhysRevLett.101.028302>.
- 48 Tamai, Y., Tanaka, H., & Nakanishi, K. (1996). Molecular dynamics study of polymer-water interaction in hydrogels. 1. Hydrogen-bond structure. *Macromolecules*, 29(21): 6750–6760. <https://doi.org/10.1021/ma951635z>.
- 49 Tamai, Y., Tanaka, H., & Nakanishi, K. (1996). Molecular dynamics study of polymer-water interaction in hydrogels. 2. Hydrogen-bond dynamics. *Macromolecules*, 29(21): 6761–6769. <https://doi.org/10.1021/ma960961r>.

Хуан Ду, Шимей Сюй

Бейорганикалық гибридіт айқаспалы қос нанокөмпозитті гидрогельдердің еріткішпен индукцияланған «клубок–глобула–клубок» ауысуы

Жұмыста қос нанокөмпозитті поли-N-изопропилакриламид/лапонит/SiO₂ (PNIPAM/лапонит/ SiO₂) гидрогелінің шөгу/қайта ісіну кезіндегі кері сольватациясы зерттелген. Лапонит пен SiO₂ бейорганикалық гибридіт қиылысуының бірегей иерархиялық микроқұрылымына, сондай-ақ полярлы еріткіштердің PNIPAM тізбегімен преференциялық әрекеттесуіне байланысты гидрогель су-полярлы еріткіш қоспаларында жылдам «клубок–глобула–клубок» ауысуын көрсетті. Шешім әрекетін органикалық еріткіштердің әртүрлі түрлерімен басқаруға болады. Су-полярлы еріткіш қоспаларындағы шөгу полярлы еріткіштердің PNIPAM тізбегімен күшті әрекеттесуі нәтижесінде, ал қайта ісіну еріткіш молекулаларының гидрогельдегі молекулааралық сумен тікелей әрекеттесуі нәтижесінде пайда болды. Сольватация үшін алынған гидрогель-су және гидрогель-полярлы еріткіш сутегі байланыстарында бәсекелес тартылу эффектілері қажет деп саналды. Жоғары жауап беру жылдамдығы бейорганикалық гибридіт айқаспалы байланыстары бар бірегей гетерогенді микроқұрылымның синергиялық әсерімен және полярлы еріткіштердің полимерлі тізбектермен преференциялық әрекеттесуімен түсіндіріледі. Мақалада ұсынылған механизм интеллектуалды жұмсақ заттар жүйелерін жобалауға жаңа сілтеме береді. Сонымен қатар, мақалада сипатталған кейбір сольватционды әсерлерді бейорганикалық гибридіт айқаспалы байланысы бар нанокөмпозиттік гидрогельдердегі еріткішпен индукцияланған конформациялық ауысулар теориясына қосуға болады.

Кілт сөздер: бейорганикалық гибридіт кросс-байланыс, қос нанокөмпозитті гидрогель, «клубок–глобула–клубок» ауысуы, поли-N-изопропилакриламид, полярлы еріткіш.

Хуан Ду, Шимей Сюй

Индукцируемый расворителями переход «клубок–глобула–клубок» двойных нанокөмпозитных гидрогелей с неорганической гибридной сшивкой

В статье исследована возвратная сольватация двойного нанокөмпозитного гидрогеля поли-N-изопропилакриламид/лапонит/SiO₂ (PNIPAM/лапонит/SiO₂) в процессе усадки/повторного набухания. В зависимости от уникальной иерархической микроструктуры неорганического гибридного сшивания лапонита и SiO₂, а также предпочтительного взаимодействия полярных растворителей с цепями PNIPAM гидрогель демонстрировал быстрый переход «клубок–глобула–клубок» в смесях вода–полярный растворитель. Поведением сольватации можно управлять с помощью различных типов органических растворителей. Усадка в смесях вода–полярные растворители происходила в результате сильного взаимодействия полярных растворителей с цепями PNIPAM, тогда как повторное набухание возникло в результате прямого взаимодействия молекул растворителя с межмолекулярной водой в гидрогеле. Для сольватации считалось необходимым наличие конкурирующих эффектов притяжения в образующихся водородных связях гидрогель–вода и гидрогель–полярный растворитель. Высокая скорость отклика объясняется синергическим эффектом уникальной гетерогенной микроструктуры с неорганическими гибридными сшивками и преимущественным взаимодействием полярных растворителей с полимерными цепями. Предложенный авторами статьи механизм дает новую ссылку на проектирование интеллектуальных систем мягкой материи. Кроме того, описанные в статье некоторые эффекты сольватации могут быть включены в теорию индуцированных соразстворителем конформационных переходов в нанокөмпозитных гидрогелях с неорганической гибридной сшивкой.

Ключевые слова: неорганическая гибридная сшивка, двойной нанокөмпозитный гидрогель, переход «клубок–глобула–клубок», поли-N-изопропилакриламид, полярный растворитель.

Information about authors*

Xu, Shimei (*corresponding author*) — Professor, College of Chemistry, Sichuan University, Chengdu 610064, China; e-mail: xushimei@scu.edu.cn; <https://orcid.org/0000-0002-2217-2335>;

Du, Juan — Lecturer, College of Materials Science and Engineering, Sichuan University of Science and Engineering, Zigong 643000, China; College of Chemistry and Chemical Engineering, Xinjiang University, Urumqi 830046, China; e-mail: dujuan@suse.edu.cn; <https://orcid.org/0000-0003-4263-9550>.

*The author's name is presented in the order: *Last Name, First and Middle Names*

A.Ye. Ayazbayeva^{1,2*}, S.Z. Nauryzova², V.O. Aseyev³, A.V. Shakhvorostov¹

¹*Institute of Polymer Materials and Technology, Almaty, Kazakhstan;*

²*Satbayev University, Almaty, Kazakhstan;*

³*University of Helsinki, Helsinki, Finland*

(*Corresponding author's e-mail: ayazbayeva.aigerim@gmail.com)

Immobilization of Methyl Orange and Methylene Blue within the Matrix of Charge-Imbalanced Amphoteric Nanogels and Study of Dye Release Kinetics as a Function of Temperature and Ionic Strength

Cross-linked polyampholyte nanogels consisting of neutral N-isopropylacrylamide (NIPAM), negatively charged sodium salt of 2-acrylamido-2-methylpropanesulfonate (AMPS), and positively charged (3-acrylamidopropyltrimethylammonium chloride (APTAC) monomers were synthesized via conventional redox initiated free radical copolymerization using N,N-methylenebis(acrylamide) (MBAA) as a cross-linking agent. The resulting nanogels were characterized by means of FTIR and ¹H NMR spectroscopy, dynamic light scattering (DLS) and zeta-potential measurements. Surface morphology was analyzed using scanning electron microscopy. Due to the presence of thermally responsive NIPAM units and varying molar ratios of anionic (AMPS) and cationic (APTAC) units, the resulting nanogels were responsive to multiple stimuli in aqueous media and can be used for controlled delivery of dyes. Thus, the NIPAM₉₀-APTAC_{7.5}-AMPS_{2.5} nanogel with an excess of the cationic units was chosen for immobilization of the anionic dye, methyl orange (MO), whereas the NIPAM₉₀-APTAC_{2.5}-AMPS_{7.5} nanogel with an excess of the anionic units was chosen for immobilization of the cationic dye, methylene blue (MB). The release kinetics of the dyes from the nanogel was studied depending on the phase transition temperature and the salt content. Mechanism of the dye release from the nanogel matrix was determined using the Ritger-Peppas equation. Disappearance of the ionic contacts between the charged groups of the nanogels and the ionic dyes was suggested to be the main reason for the diffusion of the dyes through the dialysis membrane into the external solution.

Keywords: polyampholyte nanogels, methyl orange, methylene blue, polyampholyte-dye complex, phase transition temperature, dye release.

Introduction

Interaction between polyelectrolytes and low molar mass ionic dyes leads to the formation of polyelectrolyte-dye complexes with modified physical and chemical properties. The main driving force for this complexation is electrostatic binding. To develop novel materials with desired properties, which can be used in chemical separation, drug delivery, or waste treatment, it is necessary to deepen our understanding of the molecular interactions between dyes and polyelectrolytes.

Thus, the effect of the molecular architecture of synthetic polycations has been demonstrated using a complex formed between anionic dye, methyl orange (MO), and either linear strongly charged poly(diallyl dimethyl amine hydrochloride) (PDADMAC) or branched poly(ethyleneimine hydrochloride) (PEI). The complex formation is first determined by long-range electrostatic interactions accompanied by hydrophobic and π - π interactions on shorter distances [1].

Barcellona *et al.* [2] describe the release of three pseudo-drug molecules (caffeine, methylene blue or metanil yellow) from a nonfouling polyampholyte hydrogel based on [2-(acryloyloxy)ethyl]trimethylammonium chloride (TMA) and 2-carboxyethyl acrylate (CAA) depending on the density of the hydrogel, cross-linking agent, pH and the ionic strength (μ) of the solution. Release of the neutral caffeine molecule is influenced only by diffusion, while the release of the charged methylene blue (MB) or metanil yellow is controlled by their interaction with the charged groups of TMA and CAA. pH and μ influence the rate and degree of release of the charged pseudo drugs.

Cryogels based on sulfobetaine monomer 2-(N-3-sulfopropyl-N,N-dimethyl ammonium)ethyl methacrylate and dicationic cross-linking agent N,N,N',N'-tetramethyl-N,N'-bis(2-ethylmethacrylate)-propyl-1,3-diammonium dibromide are effective adsorbents for MO and MB [3]. The degree of MO adsorption is higher

than that of MB, and hence, anionic dyes may have a higher probability of being captured by the cryogel. Sulfobetaine groups have an advantage based on the stabilization of the hydrogel structure, which can be used in wastewater treatment [4].

Polyelectrolyte membranes, which remain solvated and functional in concentrated salt solutions or under strong acidic/basic conditions, are widely applied to separate dyes from wastewater by adjusting the polyelectrolyte-dye interaction [5–7]. For example, interactions between poly(2-acrylamide-2-methyl-1-propanesulfonic acid) (PAMPS) and poly(diallyldimethylammonium) chloride (PDDA) and cationic dyes MB and MO have been used to treat colored wastewater by polymer-enhanced ultrafiltration method (PEUF) [8].

Polyampholyte microgels based on the N-isopropylacrylamide backbone containing methacrylic acid and 2-(dimethylamino)ethyl methacrylate have been used to absorb and release cationic surfactants. Depending on the type of surfactant and pH of the medium, the absorption mechanism is determined by a combination of electrostatic and hydrophobic interactions, as well as H-bonding [9].

Despite some progress in the field of complex formation between polyelectrolytes and dyes, there is little information about complexes formed between amphoteric nanogels and dyes. In our previous study, the interaction of polyampholyte hydrogels consisting of (3-acrylamidopropyl) trimethylammonium chloride (APTAC) and sodium salt of 2-acrylamido-2-methyl-1-propanesulfonic acid (AMPS) with MB and MO was investigated. Hydrogels containing an excess of negative and positive charges effectively absorb up to 80–90 % of dyes owing to the electrostatic binding [10]. In this article, we describe synthesis and characterization of polyampholyte nanogels based on neutral N-isopropylacrylamide (NIPAM), anionic sodium salt of 2-acrylamido-2-methyl-1-propanesulfonic acid (AMPS) and cationic (3-acrylamidopropyl)trimethylammonium chloride (APTAC). Resulting nanogels have random distribution of repeating units, where 90 mol. % of NIPAM units bring in thermoresponsive behavior to the nanogels, while AMPS and APTAC provide electrostatic interaction. We investigate the immobilization of anionic and cationic dyes within the matrix of amphoteric nanogels and study the release kinetics of these dyes from the nanogel matrix as a function of temperature and salt concentration.

Experimental

Materials

Monomers — N-isopropylacrylamide (NIPAM, 97 % purity), 2-acrylamido-2-methylpropanesulfonic acid sodium salt (AMPS, 50 wt. %), and (3-acrylamidopropyl) trimethylammonium chloride (APTAC, 75 wt. %); the redox initiator — ammonium persulfate (APS, 98 % purity) and sodium metabisulfite (SMBS, 97 % purity); the surfactant — sodium dodecyl sulfate (SDS, 99 % purity); the crosslinker — N,N-methylenebis(acrylamide) (MBAA, 99 % purity); sodium chloride (NaCl); dialysis tubing cellulose membrane (12–14 kDa); anionic dye — methyl orange (MO, $\lambda_{\max} = 464$ nm); cationic dye — methylene blue (MB, $\lambda_{\max} = 662$ nm) were purchased from Sigma-Aldrich Chemical Co. and used as received.

Synthesis of nanogels based on NIPAM-APTAC-AMPS

Polyampholyte nanogels of various compositions NIPAM₉₀-APTAC_{7.5}-AMPS_{2.5} and NIPAM₉₀-APTAC_{2.5}-AMPS_{7.5} were synthesized via conventional redox-initiated free radical copolymerization (Figure 1).

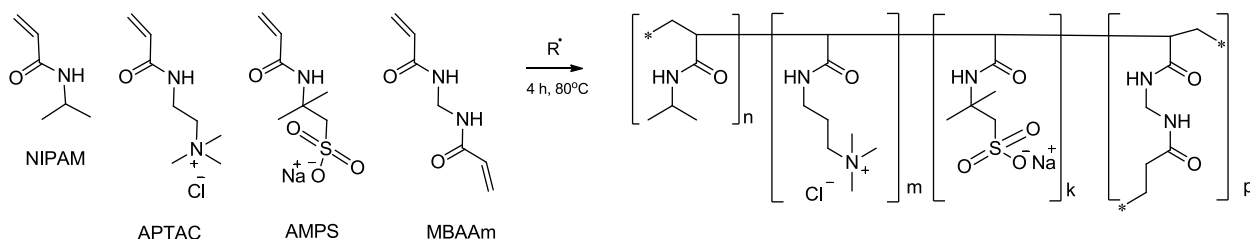


Figure 1. Free radical copolymerization of NIPAM, APTAC and AMPS monomers for synthesis of nanogels NIPAM₉₀-APTAC_{7.5}-AMPS_{2.5} and NIPAM₉₀-APTAC_{2.5}-AMPS_{7.5}

To obtain the nanogels, required amounts of monomers NIPAM, APTAC and AMPS, MBAA as a crosslinker, and SDS as a surfactant were dissolved in deionized water with constant stirring until complete

dissolution of the components (Table 1). Required amounts of APS and SMBS were added to this solution and stirred for 5 minutes. The solution was then transferred to a sealed round bottom flask. The conventional redox-initiated free radical copolymerization was carried out at 80 °C for 4 h under an argon atmosphere with constant stirring of the mixture. The obtained nanogel solutions were dialyzed in deionized water for 14 days to remove unreacted components.

Table 1

Polymerization protocol of NIPAM-APTAC-AMPS nanogels

Nanogel sample	NIPAM, g	APTAC, g	AMPS, g	APS, mg	MBAA, g	SMBS, mg	SDS, g	H ₂ O, mL	Yield, wt. %
NIPAM ₉₀ -APTAC _{7.5} -AMPS _{2.5}	0.735	0.149	0.082	20	0.11	10	0.35	98.5	88
NIPAM ₉₀ -APTAC _{2.5} -AMPS _{7.5}	0.735	0.049	0.248	30	0.11		0.23		72

Methods

The chemical structure of NIPAM-APTAC-AMPS nanogels were characterized using FTIR spectroscopy (Cary 660 FTIR, Agilent, USA). Measurements were carried out on freeze-dried nanogels at room temperature within the 500-4000 cm⁻¹ range of wavenumbers. ¹H NMR spectra were collected with a JNN-ECA Jeol 400 spectrometer (frequency 400 MHz) using D₂O as a solvent. Dynamic light scattering (DLS) and zeta-potential measurements were implemented by means of Zetasizer Nano ZS90 (Malvern, UK) with a 633 nm laser. Analysis of the surface morphology using MIRA3 LMU scanning electron microscopy (Tescan, Czech Republic) was performed for 0.1 wt. % solution of nanogels after drying at 25 °C. Absorption spectra of MO and MB were registered with a UV-Vis spectrophotometer Specord 210 plus (Germany) at 25 °C.

Immobilization of dyes within the matrix of charge-imbalanced amphoteric nanogels

Immobilization of anionic dye, methyl orange (MO) and a cationic dye, methylene blue (MB) into the matrix of nanogels was performed as follows. 2.5 mL of 1 mM MO solution and 2.5 mL of 0.4 wt. % NIPAM₉₀-APTAC_{7.5}-AMPS_{2.5} nanogel were poured into a 50 mL flask. Distilled water was then added up to the required volume. The final concentration of MO and NIPAM₉₀-APTAC_{7.5}-AMPS_{2.5} nanogel in the flask was 5 · 10⁻² mM and 0.1 wt. %, respectively.

The MB immobilization is identical to the procedure described above: 2.5 mL of 1 mM MB and 2.5 mL of 0.4 wt. % NIPAM₉₀-APTAC_{2.5}-AMPS_{7.5} nanogel were poured into a 50 mL flask; the required amount of water was added obtaining 5 · 10⁻² mM MB and 0.1 wt.% NIPAM₉₀-APTAC_{2.5}-AMPS_{7.5} nanogel.

The NIPAM₉₀-APTAC_{7.5}-AMPS_{2.5} nanogel with an excess of the positively charged APTAC monomer was chosen for the immobilization of the MO anionic dye. Whereas the NIPAM₉₀-APTAC_{2.5}-AMPS_{7.5} nanogel with an excess of the negatively charged AMPS monomer was chosen for immobilization of the cationic dye MB. Since the determination of the composition of the nanogel-dye complexes presents a certain experimental difficulty, we first carried out the conductometric titration of an aqueous solution of the linear terpolymer NIPAM₉₀-APTAC_{7.5}-AMPS_{2.5} with the anionic dye MO and the linear terpolymer NIPAM₉₀-APTAC_{2.5}-AMPS_{7.5} with the cationic dye MB at polymer concentrations 1 · 10⁻¹ mM and dye concentrations 1 mM (Figure 2).

In the case of the NIPAM₉₀-APTAC_{7.5}-AMPS_{2.5} linear terpolymer, the inflection point corresponds to the composition of the complex [NIPAM₉₀-APTAC_{7.5}-AMPS_{2.5}]/[MO] = 1:0.8 mol/mol, which is close to the equimolar ≈ 1:1. In case of the NIPAM₉₀-APTAC_{2.5}-AMPS_{7.5} system, the inflection point corresponds to the composition of the complex [NIPAM₉₀-APTAC_{2.5}-AMPS_{7.5}]/[MB] = 1:1 mol/mol. Thus, linear NIPAM-APTAC-AMPS polyampholytes with an excess of positive (APTAC) or negative (AMPS) monomers form a 1:1 equimolar complex with ionic dyes (MO and MB). For this reason, further study of the dyes release from the volume of the NIPAM-APTAC-AMPS nanogels was carried out for equimolar nanogel-dye compositions found for linear polyampholytes.

Figure 3 represents the electrostatic binding of anionic and cationic dyes by charged groups of amphoteric nanogels NIPAM-APTAC-AMPS with release of NaCl.

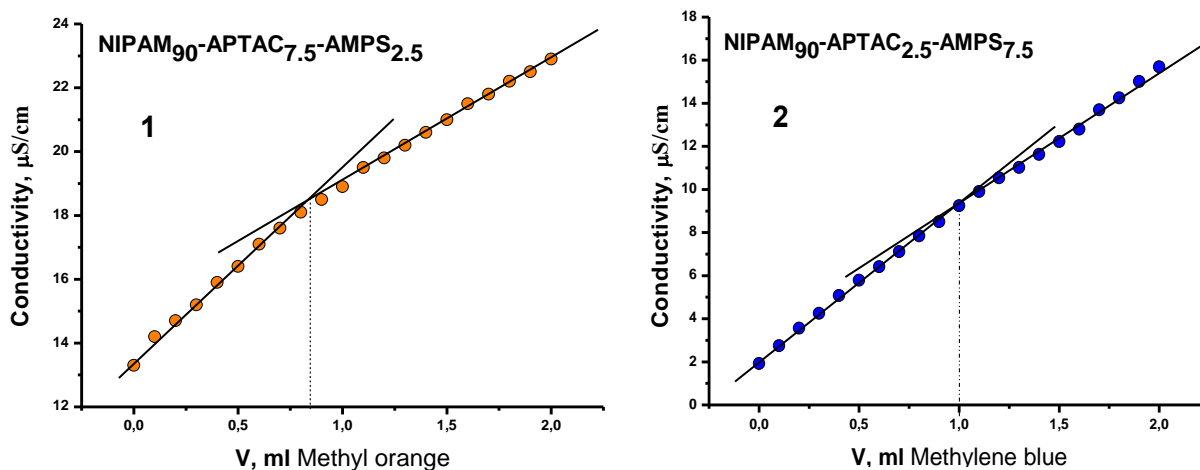


Figure 2. Conductometric titration of linear terpolymer NIPAM₉₀-APTAC_{7.5}-AMPS_{2.5} with anionic dye MO (1) and linear terpolymer NIPAM₉₀-APTAC_{2.5}-AMPS_{7.5} with cationic dye MB (2) at a polymer concentration of $1 \cdot 10^{-1}$ mM and concentration dyes 1 mM

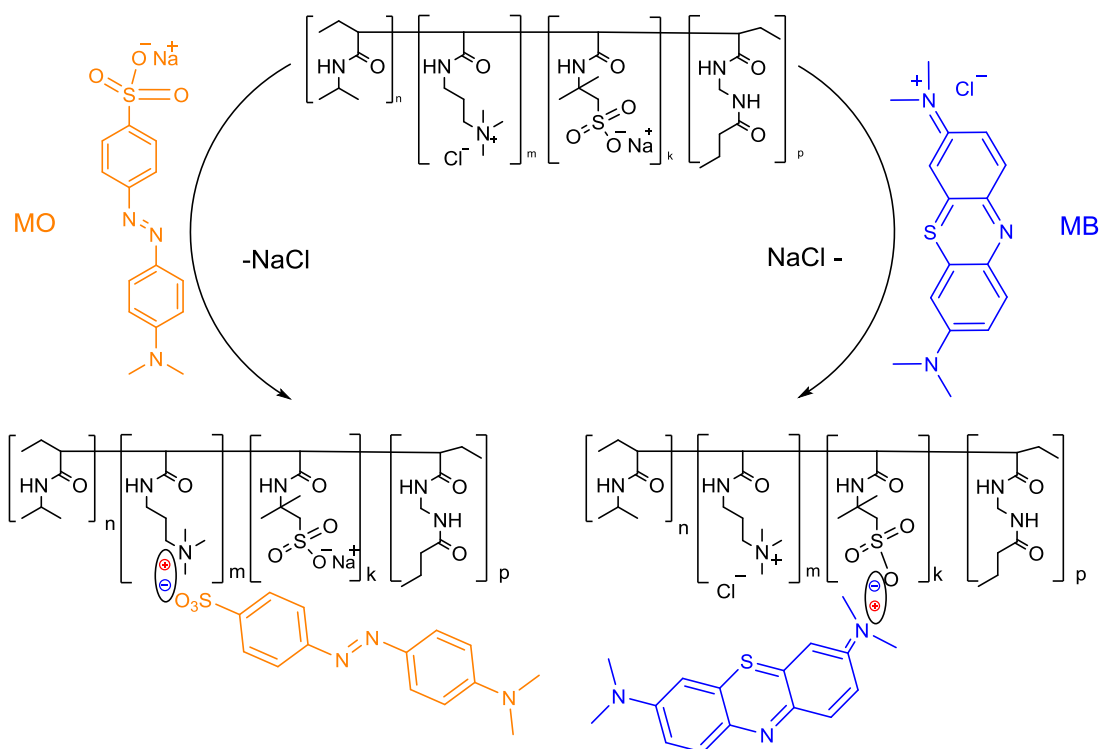


Figure 3. Formation of equimolar complexes between amphoteric nanogels and ionic dyes

Determination of phase transition temperatures for NIPAM-APTAC-AMPS nanogels

The phase transition temperatures ($T_{p.t.t.}$) of nanogels based on NIPAM-APTAC-AMPS in aqueous and aqueous-salt solutions were determined by observing the change in transmittance of the solution upon increasing temperature. Below the lower critical solution temperature (LCST), aqueous and aqueous-salt solutions of NIPAM-APTAC-AMPS nanogels are transparent. The solutions become milky white above the LCST when the polymer dehydrates and becomes more hydrophobic hence less soluble in water and transmittance decreases. Phase transition experiments were carried out at $\lambda = 700$ nm at a NIPAM-APTAC-AMPS nanogel concentration of 0.1 wt.%, a heating rate of $0.5 \text{ }^\circ\text{C min}^{-1}$, and a temperature range of 25–60 $^\circ\text{C}$, as described in [11]. $T_{p.t.t.}$ of NIPAM-APTAC-AMPS nanogels in aqueous NaCl solutions with the ionic strength $\mu = 1; 1 \cdot 10^1; 1 \cdot 10^2; 5 \cdot 10^2$ and $1 \cdot 10^3$ mM correspond to the minimum points on differential

curves. Figure 4 illustrates the examples for the NIPAM₉₀-APTAC_{7.5}-AMPS_{2.5} nanogel at different μ . It demonstrates that added salt screens the polymer charges. When $\mu = 1 \cdot 10^3$ mM, electrostatic interaction is totally screened and the nanogels behave similarly to pure PNIPAM. For the NIPAM₉₀-APTAC_{2.5}-AMPS_{7.5} nanogel, the experiments were carried out identically.

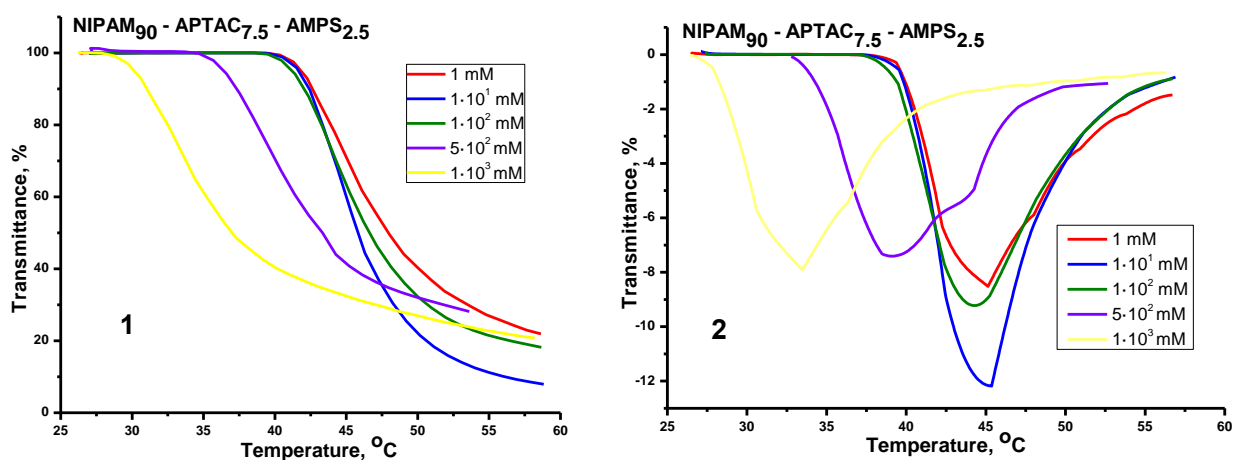


Figure 4. Integral (1) and differential (2) curves of temperature-dependent phase behavior of the nanogel NIPAM₉₀-APTAC_{7.5}-AMPS_{2.5} at different μ

Release of dyes from NIPAM-APTAC-AMPS nanogels

The release (or diffusion to the outer solution) of dyes was carried out using a simple “glass in a glass” device with constant stirring, as shown in Figure 5. For this, the inner glass, the bottom of which was covered with a dialysis membrane (molecular weight cut off is 12-14 kDa), was filled with a mixture of 10 mL of dye (MO or MB) with $5 \cdot 10^{-2}$ mM concentration and 0.1 wt. % of nanogel (NIPAM₉₀-APTAC_{2.5}-AMPS_{7.5} or NIPAM₉₀-APTAC_{7.5}-AMPS_{2.5}). It was dipped in the outer vessel containing 20 mL of distilled water or aqueous NaCl solution ($\mu = 1, 1 \cdot 10^1$ and $1 \cdot 10^2$ mM). All measurements were carried out under stirring at 25 °C and at $T_{p.t.t.}$ of nanogels determined as described above. Covering the bottom part of the inner glass with a dialysis membrane retains the nanogel in the inner vessel and keeps the concentration of nanogel constant. At the same time, pores of the dialysis membrane did not prevent diffusion of the released dye molecules (MB or MO) into the outer beaker. At certain time intervals, 2 mL of sample was taken from the outer beaker for the UV-Vis analysis. The experiments were performed under the sink conditions: to keep the volume of the solution constant, the 2 mL solution taken for analysis was compensated by adding 2 mL of distilled water or aqueous-salt solution.

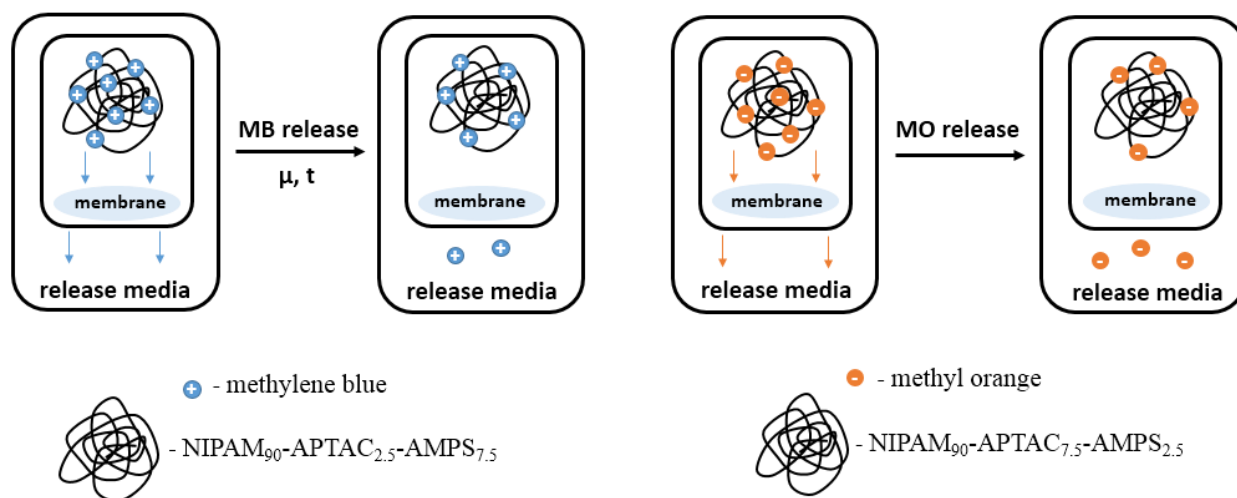


Figure 5. “Glass-in-glass” device for dye release from the nanogel matrix

The concentration of the dyes released into distilled water or aqueous-salt solutions was determined using a UV-Vis spectrophotometer at 464 nm for MO and 662 nm for MB and expressed by Equation 1:

$$\text{Dye release (\%)} = \frac{[\text{released dye}]}{[\text{total dye}]} \cdot 100. \quad (1)$$

Dye release kinetics

Kinetics and mechanism of the dye release from the nanogel matrix was determined using the Ritger-Peppas model for simple solute release, which is described by Equation 2 [12]:

$$M_t / M_\infty = kt^n, \quad (2)$$

where M_t — the concentration of dye released at time t ; M_∞ — the concentration of dye at infinite time t_∞ ; k — the kinetic constant; n — the exponent of diffusion indicating the mechanism of dye transport from the nanogel matrix.

The values of n can be the following: when $n = 0.5$, diffusion is the main driving force (Fickian diffusion); when $n = 1$, the dye release is largely controlled by degradation (Case II transport); when $0.5 < n < 1.0$, the dye release is followed by both diffusion and erosion controlled mechanisms (non-Fickian diffusion or anomalous mechanism of the drug release).

The cumulative release was calculated by Equation 3 [13]:

$$\text{Cumulative percentage release, \%} = \frac{\text{Volume of sample withdrawn, mL}}{\text{Bath volume, mL}} P_{(t-1)} + P_t, \quad (3)$$

where P_t — percentage release at time t ; $P_{(t-1)}$ — percentage release previous to t .

Results and Discussion

Synthesis and characterization of nanogels based on NIPAM-APTAC-AMPS

NIPAM₉₀-APTAC_{7.5}-AMPS_{2.5} and NIPAM₉₀-APTAC_{2.5}-AMPS_{7.5} nanogels were synthesized via conventional redox-initiated free radical copolymerization. Two molar ratios of the anionic (AMPS) and cationic (APTAC) monomers were used to obtain suitable stimuli-responsive systems with optimal properties for controlled dye release studies.

FTIR analysis of the nanogels

Figure 6 represents the FTIR spectra of NIPAM-APTAC-AMPS nanogels. The characteristic peaks of the functional groups found at $\nu = 3290\text{--}3500\text{ cm}^{-1}$ belong to the secondary and tertiary amine groups. Peaks at $\nu = 2800\text{--}3000\text{ cm}^{-1}$ and 1460 cm^{-1} are responsible for the CH groups. Peaks at $\nu = 1640$ and 1540 cm^{-1} are attributed to the N-substituted groups (amide I and amide II). S=O groups containing in AMPS fragments appear at $\nu = 1040\text{ cm}^{-1}$.

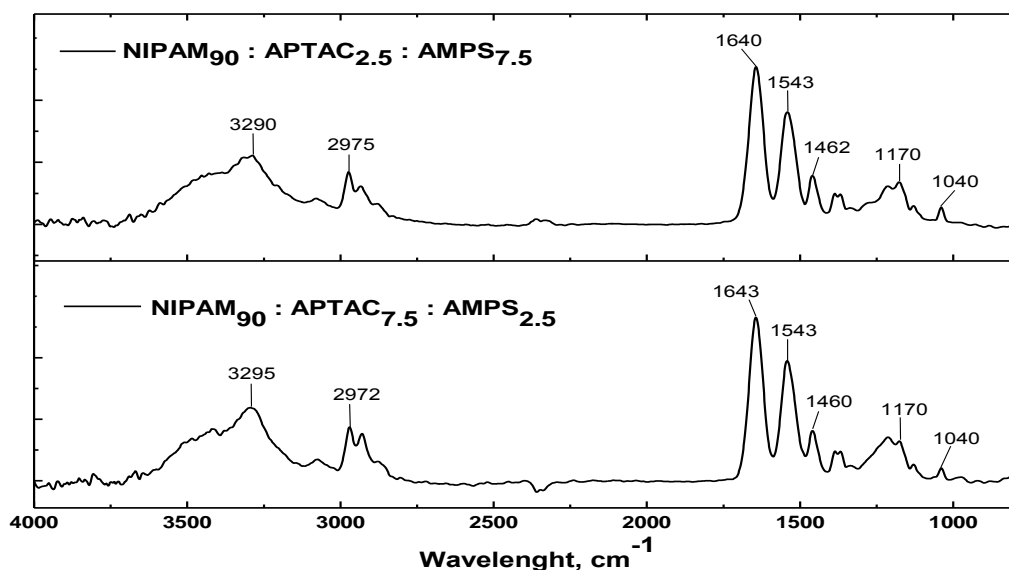


Figure 6. FTIR spectra of NIPAM-APTAC-AMPS nanogels

¹H NMR analysis of nanogels

The methylene and methine protons include resonance bands at 1.8 and 2.2 ppm, which also overlap with the peaks of the methyl and methylene protons of AMPS and APTAC. The suspended protons of the methyl and methylene groups in AMPS and APTAC include resonance bands at 3.2–3.4 ppm. Since these signals overlapped, the exact composition of the NIPAM₉₀-APTAC_{7.5}-AMPS_{2.5} and NIPAM₉₀-APTAC_{2.5}-AMPS_{7.5} nanogels could not be accurately determined from the ¹H NMR spectra (Figure 7). One should note that the reactivities of used monomers are the same and close to one. Therefore, it can be assumed that the ratio of the reacted repeating units in the nanogels is practically the same as that of the monomers in feed [14]. Considering all the reasons above, it can be argued that the NIPAM₉₀-APTAC_{7.5}-AMPS_{2.5} and NIPAM₉₀-APTAC_{2.5}-AMPS_{7.5} nanogels containing an excess of positively (APTAC) or negatively (AMPS) charged monomers are charge imbalanced.

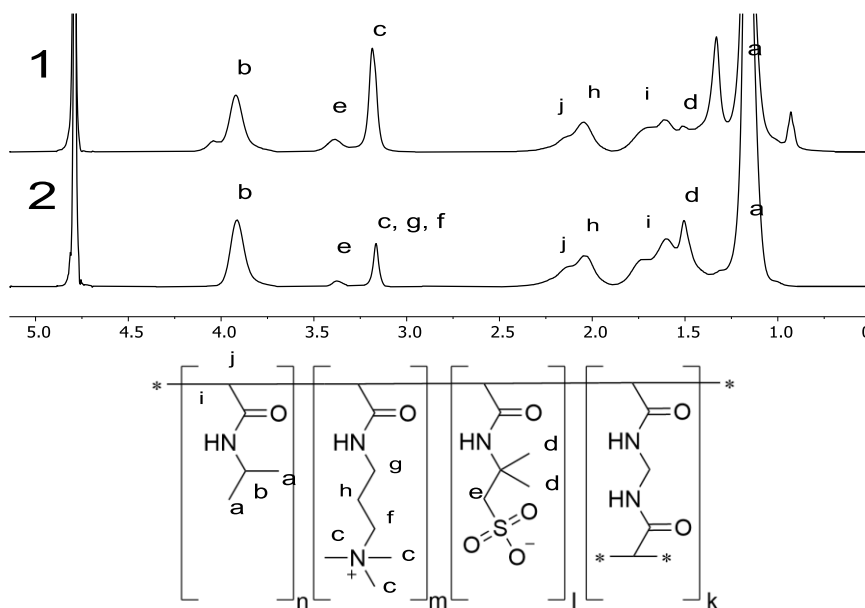


Figure 7. NMR spectra of NIPAM₉₀-APTAC_{7.5}-AMPS_{2.5} (1) and NIPAM₉₀-APTAC_{2.5}-AMPS_{7.5} (2) nanogels and identification of proton signals

The mean hydrodynamic radius (R_h) and zeta-potentials (ζ) of NIPAM-APTAC-AMPS nanogels in aqueous and aqueous-salt solutions

The mean hydrodynamic size was measured in a 0.1 wt.% solution of nanogels in the temperature range from 25 to 50 °C with an interval of 5 °C in DI water and in NaCl solutions with $\mu = 1, 1 \cdot 10^1$ and $1 \cdot 10^2$ mM (Table 2).

Table 2

The mean hydrodynamic size of NIPAM-APTAC-AMPS nanogels

T, °C	Hydrodynamic radius (R_h), nm							
	NIPAM ₉₀ -APTAC _{7.5} -AMPS _{2.5}				NIPAM ₉₀ -APTAC _{2.5} -AMPS _{7.5}			
	$\mu, \text{mol} \cdot \text{L}^{-1}$ (NaCl)							
	0	1	$1 \cdot 10^1$	$1 \cdot 10^2$	0	1	$1 \cdot 10^1$	$1 \cdot 10^2$
25	6.5 ± 1	8 ± 2	8 ± 1	90 ± 12	14 ± 1 $275 \pm 20^*$	14 ± 2 $480 \pm 8^*$	11 ± 1	11 ± 1 $160 \pm 20^*$
30	9 ± 1	9 ± 2	7 ± 0.5	138 ± 10	13 ± 1 $330 \pm 20^*$	12 ± 2 $735 \pm 10^*$	13 ± 0.5	120 ± 10
35	8 ± 3	7 ± 1	7 ± 1	197 ± 1	565 ± 15	740 ± 10	265 ± 20	170 ± 1
40	68 ± 4	90 ± 8	115 ± 9	220 ± 10	570 ± 10	744 ± 4	270 ± 20	172 ± 1
45	110 ± 0.5	148 ± 0.5	196 ± 1.5	201 ± 5	110 ± 1.5	265 ± 1	650 ± 15	172 ± 2
50	127 ± 0.5	171 ± 0.5	201 ± 7	200 ± 3	135 ± 5	307 ± 0.5	690 ± 10	410 ± 20

* nanogels in some solutions have a bimodal distribution.

Zeta-potentials of charge-imbalanced NIPAM-APTAC-AMPS nanogels were measured in 0.1 wt.% aqueous solution at 25 °C. An aqueous solution of NIPAM₉₀-APTAC_{7.5}-AMPS_{2.5} with an excess of positively charged APTAC monomer has $\zeta = +4 \pm 1$ mV. NIPAM₉₀-APTAC_{2.5}-AMPS_{7.5} with an excess of negatively charged AMPS monomer has $\zeta = -7 \pm 1$ mV.

SEM analysis of the nanogels

As is seen from SEM image, the nanogel particles contain glued or stuck aggregates (Figure 8). The narrow necks connecting the nanogel particles and few nanometer- and micron-sized voids are visible. Macroscopic gelation occurs due to multiple contacts between spherical or wormlike nanogels, which lead to the formation of a three-dimensional network of nanogels [15].

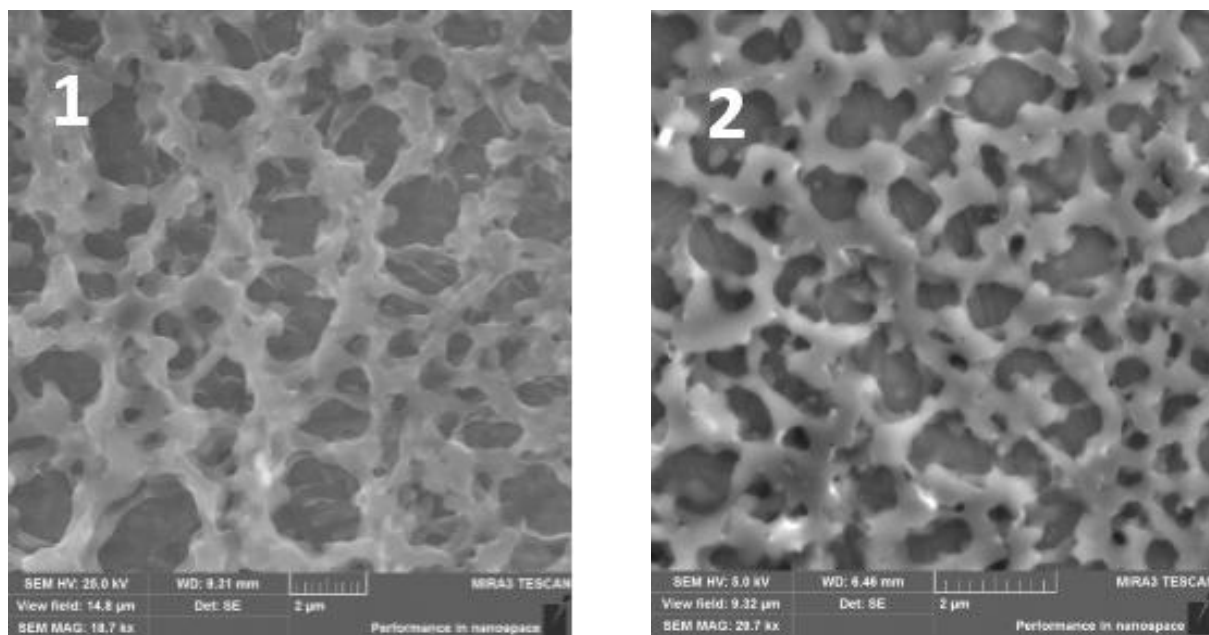
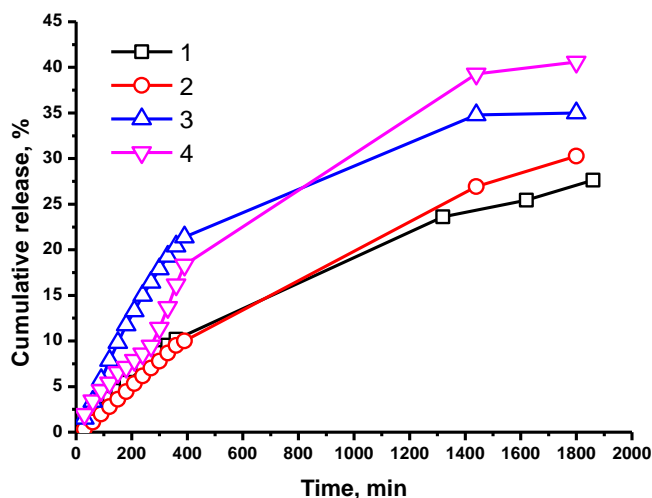


Figure 8. SEM images of NIPAM₉₀-APTAC_{7.5}-AMPS_{2.5} (1) and NIPAM₉₀-APTAC_{2.5}-AMPS_{7.5} (2) nanogels

Release kinetics of dyes from the matrix of charge-imbalanced amphoteric nanogels

Figure 9 shows the cumulative of release of MO from nanogel NIPAM₉₀-APTAC_{7.5}-AMPS_{2.5} into de-ionized water and aqueous-salt solution containing 1, 1·10¹ and 1·10² mM NaCl. The released amount of MO from the nanogel matrix is summarized in Table 3.



1 — DI water; 2 — 1 mM NaCl; 3 — 1·10¹ mM NaCl; 4 — 1·10² mM NaCl. [MO] = 5·10⁻² mM

Figure 9. Cumulative release of MO from NIPAM₉₀-APTAC_{7.5}-AMPS_{2.5} nanogel at 25 °C in different media

Table 3

The equilibrium release data of MO for nanogel NIPAM₉₀-APTAC_{7.5}-AMPS_{2.5} at 25 °C

μ , mol·L ⁻¹ (NaCl)	Released amount of MO during 30 h, (%)
0	27.0±0.5
1	30.0±0.5
1·10 ¹	35.0±0.5
1·10 ²	41.0±0.5

Gradually increasing MO release into the external solution is associated with destruction of the electrostatic interactions between the anionic groups of nanogel and the cationic dye upon increasing μ .

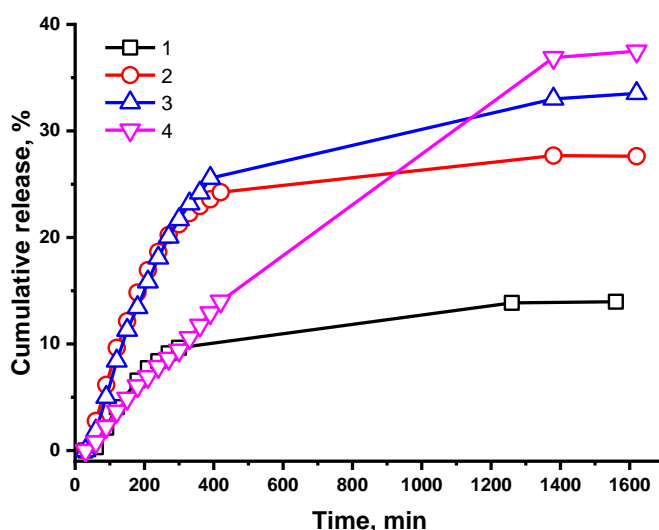
The release kinetics of MO from nanogel NIPAM₉₀-APTAC_{7.5}-AMPS_{2.5} were fit using the Ritger–Peppas equation. The values of n and k are presented in Table 4. The values of n in DI water, 1 and 1·10¹ mM NaCl are around 1 and indicate a case II transport release mechanism. When MO is released into 1·10² mM NaCl the n value equals 0.69, which indicates non-Fickian (anomalous) diffusion.

Table 4

The values of n and k of MO for nanogel NIPAM₉₀-APTAC_{7.5}-AMPS_{2.5} at 25 °C

Release medium	n	$k \cdot 10^2$	Release mechanism
MO+NIPAM ₉₀ -APTAC _{7.5} -AMPS _{2.5} into DI water	1.04±0.02	0.09	Case II transport
MO+NIPAM ₉₀ -APTAC _{7.5} -AMPS _{2.5} into 1 mM NaCl	1.12±0.02	0.05	Case II transport
MO+NIPAM ₉₀ -APTAC _{7.5} -AMPS _{2.5} into 1·10 ¹ mM NaCl	1.03±0.02	0.16	Case II transport
MO+NIPAM ₉₀ -APTAC _{7.5} -AMPS _{2.5} into 1·10 ² mM NaCl	0.69±0.02	0.50	non-Fickian diffusion

The release kinetics of MB from NIPAM₉₀-APTAC_{2.5}-AMPS_{7.5} nanogel was studied in aqueous-salt solutions at $\mu = 1, 1 \cdot 10^1$ and $1 \cdot 10^2$ mM NaCl (Figure 10). When $\mu = 1$ and $1 \cdot 10^1$ mM NaCl (up to 400 min), the intensive diffusion of MB from the nanogel matrix is observed. This owes to the step-by-step destruction of the nanogel-dye complex due to screening of the negative charges of the nanogel by NaCl ions. At a time interval from 400 to 1600 min, the MB diffusion rate reaches a plateau. This indicates the stationary nature of the release of the dye molecules from the bulk of the nanogel. At $\mu = 1 \cdot 10^2$ mM NaCl the rate of the dye diffusion from the nanogel matrix increases linearly, but after 1400 and 1600 min it reaches the limit value.



1 — DI water; 2 — 1 mM NaCl; 3 — 1·10¹ mM NaCl; 4 — 1·10² mM NaCl

Figure 10. Cumulative release of MB from NIPAM₉₀-APTAC_{2.5}-AMPS_{7.5} nanogel in different media at 25 °C

The released amount of MB from the nanogel matrix is summarized in Table 5.

Table 5

The equilibrium release data of MB for nanogel NIPAM₉₀-APTAC_{2.5}-AMPS_{7.5} at 25 °C

μ , mol·L ⁻¹ (NaCl)	Released amount of MB during 27 h, (%)
0	14.0±0.5
1	28.0±0.5
1·10 ¹	34.0±0.5
1·10 ²	37.0±0.5

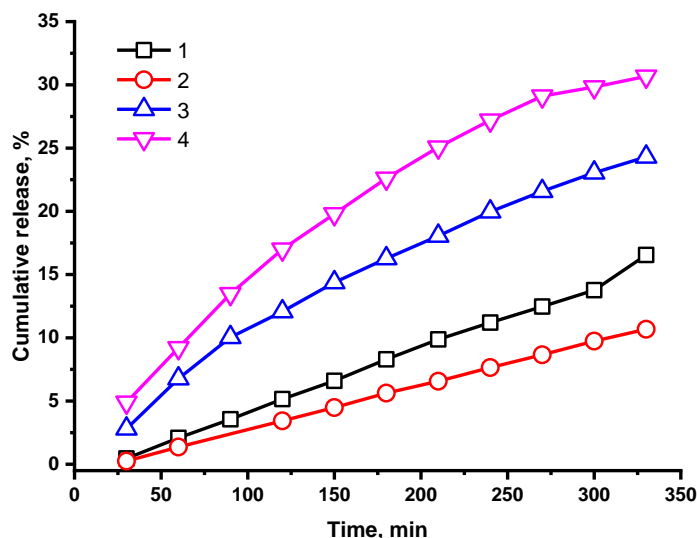
The values of n equal one upon release of MB from the NIPAM₉₀-APTAC_{2.5}-AMPS_{7.5} nanogel into deionized water and 1·10² mM NaCl solution indicating that the release mechanism is controlled by degradation, whereas the release into 1 and 1·10¹ mM NaCl corresponds to the diffusion and erosion-controlled mechanism (Table 6).

Table 6

The values of n and k for release of MB for nanogel NIPAM₉₀-APTAC_{2.5}-AMPS_{7.5} at 25 °C

Release medium	n	$k \cdot 10^2$	Release mechanism
MB+NIPAM ₉₀ -APTAC _{2.5} -AMPS _{7.5} into DI water	1.2±0.02	0.76	Case II transport
MB+NIPAM ₉₀ -APTAC _{2.5} -AMPS _{7.5} into 1 mM NaCl	0.7±0.02	1.25	non-Fickian diffusion
MB+NIPAM ₉₀ -APTAC _{2.5} -AMPS _{7.5} into 1·10 ¹ mM NaCl	0.9±0.02	0.32	non-Fickian diffusion
MB+NIPAM ₉₀ -APTAC _{2.5} -AMPS _{7.5} into 1·10 ² mM NaCl	1.3±0.02	0.016	Case II transport

Figure 11 shows the cumulative release of MO from the NIPAM₉₀-APTAC_{7.5}-AMPS_{2.5} nanogel into NaCl solutions at the phase transition temperatures measured during 5 hours.



1 — DI water; 2 — 1 mM NaCl; 3 — 1·10¹ mM NaCl; 4 — 1·10² mM NaCl

Figure 11. Cumulative release of MO from NIPAM₉₀-APTAC_{7.5}-AMPS_{2.5} nanogel in different media at T_{p.t.t.}

The effect of μ on the phase transition temperatures T_{p.t.t.} and released amount of MO from NIPAM₉₀-APTAC_{7.5}-AMPS_{2.5} nanogel is summarized in Table 7.

Table 7

Influence of the ionic strength (μ) on the phase transition temperatures ($T_{p.t.t.}$) and released amount of MO from NIPAM₉₀-APTAC_{7.5}-AMPS_{2.5} nanogel

μ , mol·L ⁻¹ (NaCl)	Phase transition temperature, $T_{p.t.t.}$ (°C)	Released amount of MO during 5 h, (%)
0	44.0±0.1	17.0±0.5
1	45.1±0.1	11.0±0.5
1·10 ¹	44.4±0.1	24.0±0.5
1·10 ²	44.3±0.1	31.0±0.5

The amount of released MO into deionized water at 44 °C equals 17 %. However, in a 1 mM solution at $T_{p.t.t.} = 45.1$ °C it decreases down to 11 %. The released amount of MO into 1·10¹ mM and 1·10² mM solutions at $T_{p.t.t.}$ equals 24 and 31 % respectively. Therefore, an increase in temperature increases the MO release from the nanogel into deionized water, 1·10¹ and 1·10² mM NaCl solutions (Table 6).

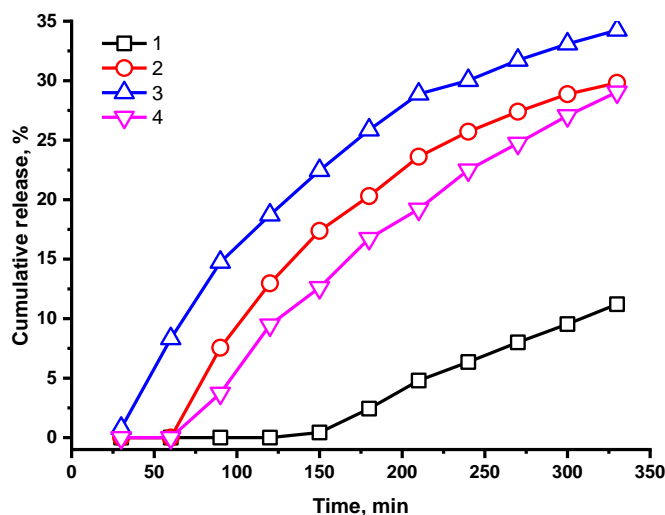
The release of MO from nanogel matrix into 1·10¹ mM salt solution at the phase transition temperature leads to a decrease in n down to 0.85 and the diffusion mechanism changes to non-Fickian (Table 8).

Table 8

The values of n and k for release of MO for nanogel NIPAM₉₀-APTAC_{7.5}-AMPS_{2.5} at $T_{p.t.t.}$

Release medium	n	$k \cdot 10^2$	Release mechanism
MO+NIPAM ₉₀ -APTAC _{7.5} -AMPS _{2.5} into DI water	1.4±0.02	0.04	Case II transport
MO+NIPAM ₉₀ -APTAC _{7.5} -AMPS _{2.5} into 1 mM NaCl	1.1±0.02	0.09	Case II transport
MO+NIPAM ₉₀ -APTAC _{7.5} -AMPS _{2.5} into 1·10 ¹ mM NaCl	0.85±0.02	0.08	non-Fickian diffusion
MO+NIPAM ₉₀ -APTAC _{7.5} -AMPS _{2.5} into 1·10 ² mM NaCl	0.77±0.02	1.3	non-Fickian diffusion

The effect of the phase transition temperature on the MB release from the NIPAM₉₀-APTAC_{2.5}-AMPS_{7.5} nanogel is shown in Figure 12. The dye release in deionized water did not change during 5 hours as the temperature increased from 25 to 41.6 °C. The diffusion of MB from the nanogel into NaCl solutions with different $\mu = 1, 1 \cdot 10^1$ and $1 \cdot 10^2$ mM at the phase transition temperature increases by 7–15 % (Table 9).



1 — DI water; 2 — 1 mM NaCl; 3 — 1·10¹ mM NaCl; 4 — 1·10² mM NaCl

Figure 12. Cumulative release of MB from NIPAM₉₀-APTAC_{2.5}-AMPS_{7.5} nanogel in different media at $T_{p.t.t.}$

Table 9

The equilibrium release data of MB for nanogel NIPAM₉₀-APTAC_{2.5}-AMPS_{7.5} at T_{p.t.t.}

μ , mol·L ⁻¹ (NaCl)	Phase transition temperature, T _{p.t.t.} (°C)	Release amount of MB during 5 hrs, (%)
0	41.6±0.1	11±0.5
1	40.8±0.1	30±0.5
1·10 ¹	41.8±0.1	34±0.5
1·10 ²	41.4±0.1	29±0.5

The influence of T_{p.t.t.} on the change in the diffusion mechanism occurred when the MB was released into a 1 M NaCl. The *n* value changed to 1 and the mechanism became - Case II transport (Table 10).

Table 10

The values of *n* and *k* for release of MB for nanogel NIPAM₉₀-APTAC_{2.5}-AMPS_{7.5} at T_{p.t.t.}

Release medium	<i>n</i>	<i>k</i> ·10 ²	Release mechanism
MB+NIPAM ₉₀ -APTAC _{2.5} -AMPS _{7.5} into 1 mM NaCl	1±0.04	0.33	Case II transport
MB+ NIPAM ₉₀ -APTAC _{2.5} -AMPS _{7.5} into 1·10 ¹ mM NaCl	0.76±0.02	1.3	non-Fickian diffusion
MB+NIPAM ₉₀ -APTAC _{2.5} -AMPS _{7.5} into 1·10 ² mM NaCl	1.2±0.02	0.063	Case II transport

Conclusions

Samples of polyampholyte nanogels NIPAM₉₀-APTAC_{7.5}-AMPS_{2.5} and NIPAM₉₀-APTAC_{2.5}-AMPS_{7.5} were obtained via conventional redox-initiated free radical copolymerization in presence of a cross-linking agent. The structure and composition of the nanogels were investigated through IR-Fourier and ¹H NMR spectroscopy.

The kinetics of release of dyes from the matrix of nanogels has been studied in aqueous solutions at various temperatures and ionic strengths. The MO release from the NIPAM₉₀-APTAC_{7.5}-AMPS_{2.5} nanogel matrix at 25 °C for 30 hours increases from 27 to 41 % with increasing μ . At the phase transition temperature, the release of MO with μ is preserved, except for 1 mM NaCl, for which the release is 11 % and less than in distilled water. The release of MB from the NIPAM₉₀-APTAC_{2.5}-AMPS_{7.5} nanogel within 27 hours rises from 14 to 37 % with μ . The upward trend in the MB release with μ persists at the phase transition temperature as well.

Gradual increase in the dye release from the nanogel matrix into the external solution is associated with the destruction/screening of electrostatic interactions of the nanogel-dye complex with μ . The release of the dye molecules is enhanced at the phase transition temperature of nanogels. Dye delivery systems developed in this study may be promising platforms for therapeutic applications.

Acknowledgments

This research was funded by the Science Committee of the Ministry of Education and Science of the Republic of Kazakhstan (Grant No. AP08855552). Aseyev V.O. thanks the Horizon 2020 research and innovation program of the European Union Marie Skłodowska-Curie Actions (grant agreement 823883-NanoPol-MSCA-RISE-2018) for financial support.

References

- Vleugels, L.F.W. (2018). Self-organization of polyelectrolytes : as mediated by surfactants, dyes and ions. Dissertation. Technische Universiteit Eindhoven.
- Barcellona, M.N., Johnson N., & Bernards, M.T. (2015). Characterizing Drug Release from Nonfouling Polyampholyte Hydrogels. *Langmuir*, 31(49), 13402–13409. <https://doi.org/10.1021/acs.langmuir.5b03597>
- Ihlenburg, R.B.J., Lehnen, A.-C., Koetz, J., & Taubert, A. (2021). Sulfobetaine Cryogels for Preferential Adsorption of Methyl Orange from Mixed Dye Solutions. *Polymers*, 13(2), 208. <https://doi.org/10.3390/polym13020208>
- Ihlenburg, R.B.J., Mai, T., Thünemann, A.F., Baerenwald, R., Saalwächter, K., Koetz, J., & Taubert, A. (2021). Sulfobetaine Hydrogels with a Complex Multilength-Scale Hierarchical Structure. *The Journal of Physical Chemistry B*, 125(13), 3398–3408. <https://doi.org/10.1021/acs.jpcc.0c10601>

- 5 Deen, G.R., Wei, T.T., & Fatt, L.K. (2016). New stimuli-responsive polyampholyte: Effect of chemical structure and composition on solution properties and swelling mechanism. *Polymer*, 104, 91–103. <https://doi.org/10.1016/j.polymer.2016.09.094>
- 6 Rabiee, A., Ershad-Langroudi, A., & Jamshidi, H. (2014). Polyacrylamide-based polyampholytes and their applications. *Reviews in Chemical Engineering*, 30(5). <https://doi.org/10.1515/revce-2014-0004>
- 7 Mi, L., & Jiang, S. (2012). Synchronizing nonfouling and antimicrobial properties in a zwitterionic hydrogel. *Biomaterials*, 33(35), 8928–8933. <https://doi.org/10.1016/j.biomaterials.2012.09.011>
- 8 Oyarce, E., Butter, B., Santander, P., & Sánchez, J. (2021). Polyelectrolytes applied to remove methylene blue and methyl orange dyes from water via polymer-enhanced ultrafiltration. *Journal of Environmental Chemical Engineering*, 106297. <https://doi.org/10.1016/j.jece.2021.106297>
- 9 Bradley, M., Vincent, B., & Burnett, G. (2008). Uptake and release of surfactants from polyampholyte microgel particles. *Colloid and Polymer Science*, 287(3), 345–350. <https://doi.org/10.1007/s00396-008-1978-8>
- 10 Toleutay, G., Dauletbekova, M., Shakhvorostov, A., & Kudaibergenov, S. (2019). Quenched Polyampholyte Hydrogels Based on (3-Acrylamidopropyl)trimethyl Ammonium Chloride and Sodium Salt of 2-Acrylamido-2-methyl-1-Propanesulfonic Acid. *Macromolecular Symposia*, 385(1), 1800160. <https://doi.org/10.1002/masy.201800160>
- 11 Ayazbayeva, A.Ye., Shakhvorostov, A.V., Seilkhanov, T.M., Aseyev, V.O., & Kudaibergenov, S.E. (2021). Synthesis and characterization of novel thermo- and salt-sensitive amphoteric terpolymers based on acrylamide derivatives. *Bulletin of the University of Karaganda – Chemistry*, 104(4), 9–20. <https://doi.org/10.31489/2021Ch4/9-20>
- 12 Ritger, P.L., & Peppas, N.A. (1987). A simple equation for description of solute release II. Fickian and anomalous release from swellable devices. *Journal of Controlled Release*, 5(1), 37–42. [https://doi.org/10.1016/0168-3659\(87\)90035-6](https://doi.org/10.1016/0168-3659(87)90035-6)
- 13 Chandrasekaran, A.R., Jia, C.Y., Theng, C.S., Muniandy, T., Muralidharan S., & Dhanaraj, S.A. (2011). In vitro studies and evaluation of metformin marketed tablets-Malaysia. *Journal of Applied Pharmaceutical Science*, 1(5), 214–217.
- 14 Braun, O., Selb, J., & Candau, F. (2001). Synthesis in microemulsion and characterization of stimuli-responsive polyelectrolytes and polyampholytes based on N-isopropylacrylamide. *Polymer*, 42(21), 8499–8510. [https://doi.org/10.1016/S0032-3861\(01\)00445-1](https://doi.org/10.1016/S0032-3861(01)00445-1)
- 15 Lovett, J.R., Derry, M.J., Yang, P., Hatton, F.L., Warren, N.J., Fowler, P.W., & Armes, S.P. (2018). Can percolation theory explain the gelation behavior of diblock copolymer worms? *Chemical Science*, 9(35), 7138–7144. <https://doi.org/10.1039/c8sc02406e>

А.Е. Аязбаева, С.З. Наурызова, В.О. Асеев, А.В. Шахворостов

Заряд бойынша теңгерімсіз амфотерлік наногельдердің матрицасына метил қызғылт сары мен метилен көк бояуларын иммобилизациялау және олардың температура мен иондық күшке байланысты босап шығу кинетикасын зерттеу

Гидрофобты (N-изопропилакриламид, НИПАМ), теріс зарядталған (2-акриламидо-2-метилпропан-сульфонат натрий тұзы, АМПС) және оң зарядталған (3-акриламидопропилтриметиламмоний хлориді, АПТАХ) мономерлерден тұратын өзара байланысқан полиамфолитті наногельдер N,N-метилен-бис(акриламид) айқастырғыш агент ретінде қолданылып, бос радикалды полимерлену жолымен синтезделді. Алынған наногельдер ИК-Фурье және ¹H ЯМР спектроскопиясы әдістерімен сипатталды, беттік морфология сканерлеу электронды микроскопия арқылы талданды. Термосезімтал НИПАМ және аниондық (АМПС) және катиондық (АПТАХ) мономерлердің әртүрлі молярлық коэффициенттерінің арқасында алынған наногельдер ынталандыруға сезімтал-жүйелерге ие және оларды бояғыштарды бақыланатын түрде жеткізу үшін пайдалануға болады. Артық катионды мономері бар NIPAM₉₀-APTAC_{7.5}-AMPS_{2.5} наногель анионды бояуды, метил қызғылт сарыны (МО), инкапсуляциялау үшін, ал артық анионды мономері бар NIPAM₉₀-APTAC_{2.5}-AMPS_{7.5} наногель катионды бояуды, метилен көкті (МВ) иммобилизациялау үшін таңдалды. Фазалық ауысу температурасына және тұз қоспасына байланысты наногельдің матрицасынан бояғыштардың шығарылу кинетикасы зерттелді, Ритгер-Пеппас теңдеуі негізінде наногель матрицасынан бояғыштың шығарылу механизмі анықталды. Зарядталған наногельдер топтары мен иондық бояғыштардың арасындағы иондық байланыстардың бұзылуы диализ мембранасы арқылы бояғыштардың сыртқы ерітіндіге таралуының негізгі себебі болып табылады.

Кілт сөздер: полиамфолит наногелі, метил қызғылт сары, метилен көк, полиамфолит-бояғыш кешені, фазалық ауысу температурасы, бояғышты босату.

А.Е. Аязбаева, С.З. Наурызова, В.О. Асеев, А.В. Шахворостов

Иммобилизация метилового оранжевого и метиленового синего в матрицу амфотерных наногелей с несбалансированным зарядом и изучение кинетики высвобождения красителей в зависимости от температуры и ионной силы

Сшитые полиамфолитные наногели, состоящие из гидрофобного (N-изопропилакриламид, НИПАМ), отрицательно заряженного (натриевая соль 2-акриламидо-2-метилпропансульфоната, АМПС) и положительно заряженного (3-акриламидопропилтриметиламмония хлорид, АПТАХ) мономеров, были синтезированы методом свободнорадикальной полимеризации с N,N-метиленбис(акриламидом) (МБАА) в качестве сшивающего агента. Полученные наногели охарактеризованы методами ИК-Фурье и ¹H ЯМР-спектроскопии, морфология поверхности проанализирована с помощью сканирующей электронной микроскопии. Из-за присутствия термочувствительного НИПАМ и различных молярных соотношений анионных (АМПС) и катионных (АПТАХ) мономеров, полученные наногели представляют собой стимул-чувствительные системы и могут использоваться для контролируемой доставки красителей. Нангель с избытком катионного мономера (NIPAM₉₀-APTAC_{7,5}-AMPS_{2,5}) был выбран для инкапсулирования анионного красителя метилового оранжевого (МО), а нангель с избытком анионного мономера (NIPAM₉₀-APTAC_{2,5}-AMPS_{7,5}) был выбран для иммобилизации катионного красителя метиленового синего (МС). Исследована кинетика высвобождения красителей из объема наногеля в зависимости от температуры фазового перехода и солевой добавки, определен механизм высвобождения красителей из матрицы наногеля на основе уравнения Ритгера-Пеппаса. Разрушение ионных контактов между заряженными группами наногелей и ионогенными красителями является основной причиной диффузии красителей через диализную мембрану во внешний раствор.

Ключевые слова: полиамфолитные наногели, метиловый оранжевый, метиленовый синий, комплекс «полиамфолит–краситель», температура фазового перехода, высвобождение красителя.

Information about authors*

Ayazbayeva, Aigerim Yerlanovna (*corresponding author*) — PhD student, Satbayev University, Satpayev str., 22, 050013, Almaty, Kazakhstan; e-mail: ayazbayeva.aigerim@gmail.com; <https://orcid.org/0000-0003-1313-895X>;

Nauryzova, Saule Zinagiyevna — PhD, Satbayev University, Satpayev str., 22, 050013, Almaty, Kazakhstan; e-mail: s.nauryzova@satbayev.university; <https://orcid.org/0000-0002-3012-7817>;

Aseyev, Vladimir Olegovich — PhD, Docent, University Lecturer, Department of Chemistry, University of Helsinki, P.O. Box 55 (A.I. Virtasen aukio 1), FIN-00014 HY, Helsinki, Finland; e-mail: Vladimir.Aseyev@helsinki.fi; <https://orcid.org/0000-0002-3739-8089>;

Shakhvorostov, Alexey Valerievich — PhD, Institute of Polymer Materials and Technology, Atyrau-1, 3/1, 050019, Almaty, Kazakhstan; e-mail: alex.hv91@gmail.com; <https://orcid.org/0000-0003-3502-6123>

*The author's name is presented in the order: *Last Name, First and Middle Names*

N. Mukhametgazy^{1,2*}, I.Sh. Gussenov^{1,2}, A.V. Shakhvorostov¹, Heikki Tenhu³

¹*Institute of Polymer Materials and Technology, Almaty, Kazakhstan;*

²*Satbayev University, Almaty, Kazakhstan;*

³*University of Helsinki, Helsinki, Finland*

(*Corresponding author's e-mail: Nurbatyr.kaz@gmail.com)

Oil Recovery at High Brine Salinity Conditions Using Amphoteric Terpolymer

The viscosity and the oil recovery ability of high molecular weight amphoteric terpolymer (ATP) were tested in different brines and compared with hydrolyzed poly(acrylamide) (HPAM) which is traditionally used in enhanced oil recovery (EOR). The results show that ATP provides higher viscosity at brine salinity ranging from 200 to 300 g·L⁻¹. This may give ATP an advantage over HPAM in high salinity reservoirs, which are abundant in Kazakhstan. Moreover, comparative polymer flooding experiments were carried out by injecting 0.25 wt.% ATP and HPAM dissolved in 200 g·L⁻¹ brine into sand packs. The HPAM flooding in high permeability (1.77 Darcy) sand pack leads to the increase of the oil recovery factor (ORF) by 18.5 % after 1 PV of brine injection. On the other hand, the injection of ATP into the low permeability (0.6 Darcy) sand pack results in the ORF increase by 28.5 %. The obtained results show that ATP has the potential to become an alternative to HPAM in 200 g·L⁻¹ and higher brine salinity reservoirs.

Keywords: amphoteric terpolymer, hydrolyzed poly(acrylamide), antipolyelectrolyte effect, sand pack model, water flooding, polymer flooding, oil recovery factor.

Introduction

Water is usually used to displace oil from matrix rocks. However, because of the unstable displacement front due to the differences in oil and water viscosities and the heterogeneous nature of matrix rocks the oil production rates often decline with the increase in water production [1].

If water viscosity is increased by dissolving high molecular weight polymers in it, the problem of viscous fingering and premature breakthrough can be minimized [2]. Such polymers are an important topic of modern research due to their practical application. For example, polyacrylamide is widely used in wastewater treatment, paper production, and oil industry because of its thickening, flocculation, and rheological properties [3, 4].

Even though different polymers were tested over the years, hydrolyzed polyacrylamide (HPAM) has found the widest application due to its low cost; commercial availability; remarkable capability to increase viscosity; acceptable and adjustable injectivity; and resistance to microbial degradation [5].

However, if cations are present in water the negative charges on the polymer chain are screened and as a result, the hydrodynamic volume of the polymer molecule is reduced [5, 6]. Thus, at higher salinities, higher concentrations of HPAM are required to achieve the target viscosity. Moreover, at extremely high salinity and temperature, the HPAM chains will coil up and precipitate [6].

Amphoteric copolymers and terpolymers can swell and enhance the viscosity in high salinity reservoirs, which is crucial for enhanced oil recovery (EOR) [7, 8]. The remarkable resistance of polyampholytes to high salinity makes them attractive for the application where thickeners are required in concentrated brine solutions [2, 9–13]. Special attention should be given to the hydrophobically associating polyampholytes which combine self-assembly and adjustable charge balance [14–17]. The application of acrylamide-based polyampholytes in EOR and drag reduction was reviewed in [18].

In this regard, amphoteric polyelectrolytes have great potential, because in high-salinity water anions and cations disperse macromolecular chains by reducing the electrostatic attraction between positively and negatively charged monomers. As a result, the viscosity of the solution increases [19]. The main problems of oil fields in Kazakhstan are the viscosity of oil and high salinity of reservoir water, which in some regions reaches 163–232 g·L⁻¹ and even higher. To solve these problems, it is recommended to use specially designed amphoteric terpolymers (with an “anti-electrolyte” effect) that can increase the viscosity of brine [20–25].

In this study, we compare the oil recovery efficiency of high molecular weight amphoteric terpolymer AAm-AMPS-APTAC = 80:10:10 mol.% with HPAM in sand pack models at high salinity conditions.

Experimental

Materials

Monomers — acrylamide (AAm, 97 % purity), 2-acrylamido-2-methylpropanesulfonic acid sodium salt (AMPS, 50 wt.%), (3-acrylamidopropyl) trimethylammonium chloride (APTAC, 75 wt.% in water), and ammonium persulfate (APS, 98% purity) were purchased from Sigma-Aldrich Chemical Co., and used without further purification. Commercially available hydrolyzed polyacrylamide (HPAM) (Flopaam 3630S, 98% purity SNF) with a hydrolysis degree of 30% and average molecular weight of 17.2 million Dalton was used as received.

Sand pack model

To simulate the oil displacement by water and polymers, 3-cm-diameter and 5-cm-length sand packs were used. The size of the sand grains varied between 0.25 and 0.5 mm. Initially, the sand packs were vacuumed and saturated with brine. The porosity of the models was determined by using the following formula:

$$\varphi = \frac{V_m - V_d}{V_t} \cdot 100 \%,$$

where φ — the porosity, %; V_m — the injected volume, cm³; V_d — the dead volume, cm³; V_t — total volume of the sand pack, cm³

Next, brine was injected through the sand packs at different flow rates and constant registration of pressure. Darcy equation was used to calculate permeability at 100 % water saturation. Table 1 presents the results of the porosity and permeability calculations.

Table 1

Properties of the sand packs

Sand pack	Pore volume, cm ³	Porosity, %	Permeability, Darcy
1	10.6	30	0.62
2	11.9	33.7	1.77

Brine

Table 2 demonstrates a list of brines with different salinities and chemical composition.

Table 2

Total salinity and chemical composition of synthetic brines

Total salinity, g·L ⁻¹	Concentration of salts, g·L ⁻¹		
	NaCl	CaCl ₂	MgCl ₂
200	180	10	10
232	208.8	11.6	11.6
250	225	12.5	12.5
275	247.5	13.75	13.75
300	270	15	15

Oil

Crude oil from Karazhanbas oil field well #1913 was used. Oil viscosity and density at 30°C are equal to 420 mPa·sec and 0.93 g·cm⁻³, respectively.

Methods

Elemental analysis of ATP and HPAM samples was performed using Vario EL-III elemental analyzer (Elementary Analyze System GmbH, Hanau, Germany). The dynamic viscosity of polymer solutions was measured by Ubbelohde viscometer at 24 and 60 °C. The sand pack experiments were done through core flooding apparatus “УИК-С (2)” (Russia).

Results and Discussion

Synthesis and characterization of AAm-APTAC-AMPS and HPAM

Synthesis and characterization of the AAm-AMPS-APTAC amphoteric terpolymer containing 80 mol.% AAm, 10 mol.% AMPS, and 10 mol.% APTAC with the weight-average molecular weight ($M_w = 2.9 \cdot 10^6$ Dalton) and the average number molecular weight ($M_n = 2.1 \cdot 10^6$ Dalton) are comprehensively described elsewhere [23, 24] (Fig. 1).

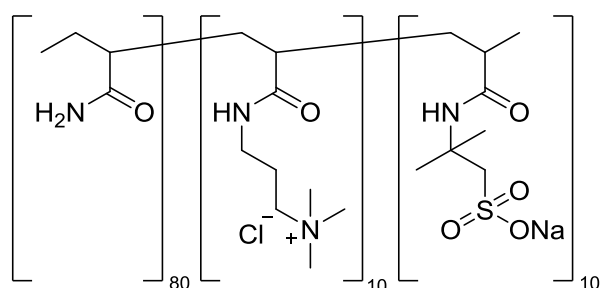


Figure 1. Repeating monomeric units and composition (mol.%) of AAm-AMPS-APTAC amphoteric terpolymer

Hydrolyzed polyacrylamide (HPAM) (Flopaam 3630S, 98% purity, SNF) with a hydrolysis degree of 30 % and an average molecular weight of $17.2 \cdot 10^6$ Dalton was used for the comparative experiments. The hydrolysis degree of HPAM 30 % means that the sample contains 70 mol. % of acrylamide (AAm) and 30 mol.% of sodium acrylate (SA) in the macromolecular chain (Figure 2).

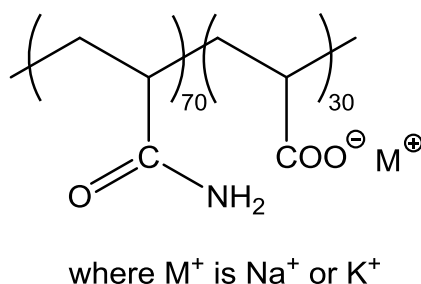


Figure 2. Repeating monomeric units and composition (mol.%) of HPAM

Table 3 presents the results of the elemental analysis of AAm-AMPS-APTAC and HPAM.

Table 3

Results of elemental analysis of AAm-AMPS-APTAC and HPAM

Samples	Monomer ratios in terpolymer and copolymer, mol. %			Percentages of elements, wt. %				
				Found/Calculated	N, %	C, %	H, %	S, %
ATP	AAm	APTAC	AMPS	Found	11.54	43.58	8.32	3.18
	80	10	10	Calculated	15.34	47.83	7.11	3.19
HPAM	AAm		SA	Found	8.49	38.29	6.46	0
	70		30	Calculated	11.84	43.52	5.36	0

Table 3 shows that the experimentally found and theoretically calculated amounts of elements C, N, H, and S are in good agreement. This confirms that the composition of the AAm-APTAC-AMPS (80:10:10 mol.%) terpolymer insignificantly deviates from the initial monomer composition in the feed. In the case of HPAM, the experimentally found and theoretically calculated amounts of elements C, N, and H are somewhat different. This is reasonable because the commercially available samples for oil recovery usually contain some impurities.

Viscosity of AAm-APTAC-AMPS and HPAM in synthetic brine

Figure 3 demonstrates the dynamic viscosities of amphoteric terpolymer AAm-AMPS-APTAC and HPAM versus the polymer concentrations at 24 and 60 °C in 250 g·L⁻¹ synthetic brine. The gradually decreasing dynamic viscosities of ATP and HPAM upon dilution testify to the absence of polyelectrolyte effect leading to the unfolding of macromolecular coils.

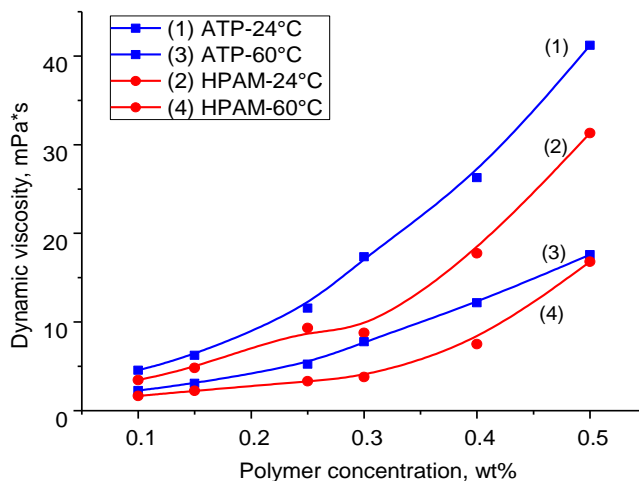


Figure 3. Dynamic viscosity of ATP and HPAM versus the polymer concentration in 250g·L⁻¹ synthetic brine at 24 and 60 °C

Figure 4 represents the dynamic viscosities of ATP and HPAM in brine solutions. The dynamic viscosity of 0.25 wt.% ATP solutions increases steadily from 7.45 to 14.25 mPa·s with the increase in the salinity from 200 to 300 g·L⁻¹. Whereas the dynamic viscosity of HPAM solution increases from 6.78 to 9.31 mPa·s upon the salinity increase from 200 to 250 g·L⁻¹, however, the further increase in the salinity up to 300 g·L⁻¹ causes a sharp falling of HPAM viscosity. This is explained by the precipitation of HPAM as a result of the “salting out” effect.

The increase of the dynamic viscosity of amphoteric terpolymer in high saline solution because of the screening of the positively and negatively charged monomers by anions and cations of salts leads to the unfolding of macromolecular chains. This phenomenon is called the *antipolyelectrolyte effect*. The dynamic viscosities of ATP solutions are higher than that of HPAM. It is explained by the unfolding of the AAm-AMPS-APTAC terpolymer molecule at high temperature and salinity.

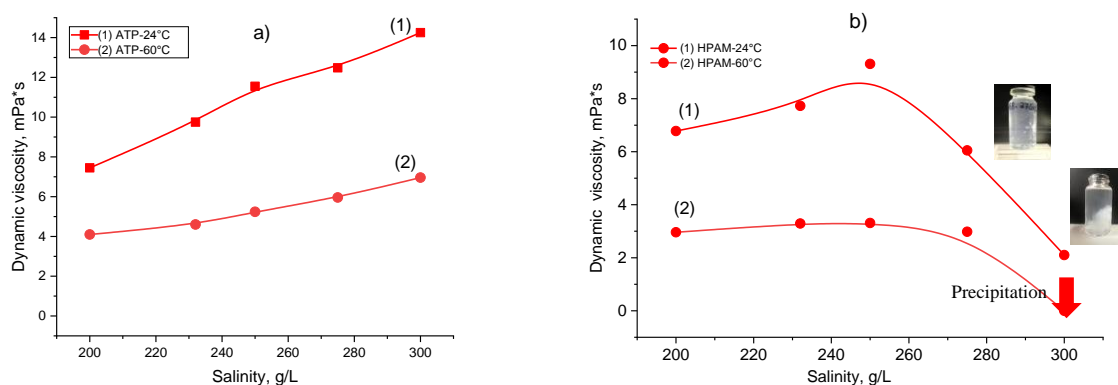
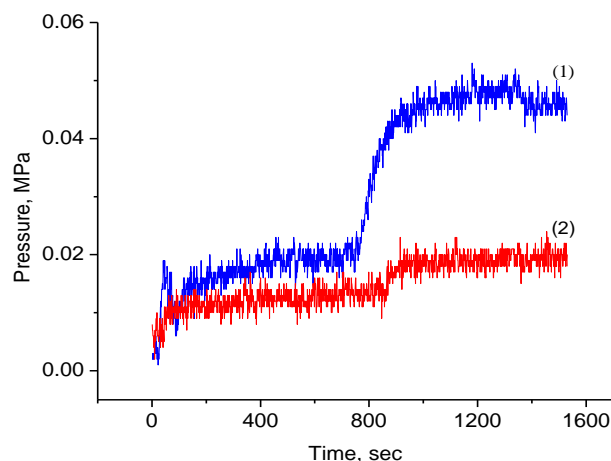


Figure 4. Salt-dependent dynamic viscosities of 0.25 wt.% amphoteric terpolymer (a) and HPAM (b) at 24°C (1) and 60°C (2) in the range of 200–300 g·L⁻¹ brine salinity

*Sand pack flooding**Water and oil saturation*

The saturation of the models with $200 \text{ g}\cdot\text{L}^{-1}$ brine was done after vacuuming to calculate the porosity (Table 1). Figure 5 shows the injection pressure change during the oil saturation process for the 0.62 D and 1.77 D sand packs. As can be seen, for the low-permeability sand pack model, the oil injection pressure reached 0.044–0.051 MPa and stabilized without further growth. For the high-permeability sand pack model, the oil injection pressure stabilized at 0.020–0.024 MPa. This is two times less than the oil saturation pressure for the low-permeability sand pack model. In addition, the mass of saturated oil in each model was calculated based on the material balance, and equal to 8.78 and 9.67 g for the 0.62D and 1.77D sand packs, respectively.

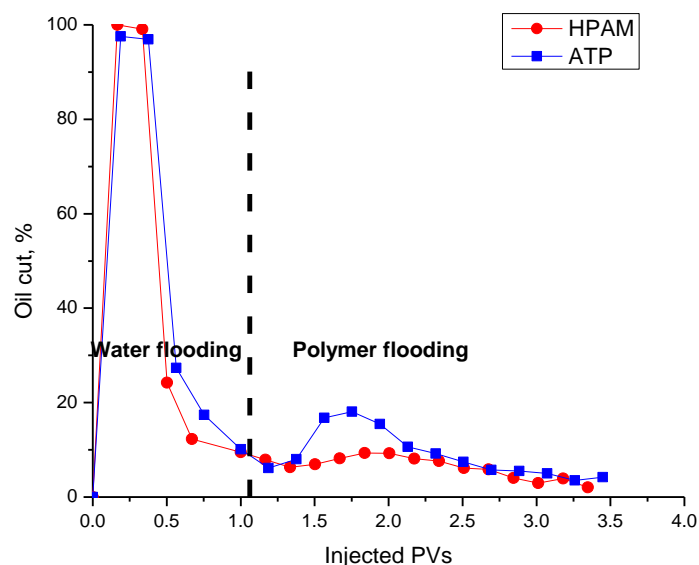


The permeability of sand pack model is 0.62D (1) and 1.77D (2). Flow rate — $0.15 \text{ cm}^3\cdot\text{min}^{-1}$. Temperature — $30 \text{ }^\circ\text{C}$

Figure 5. The oil injection pressure versus time during the oil saturation process

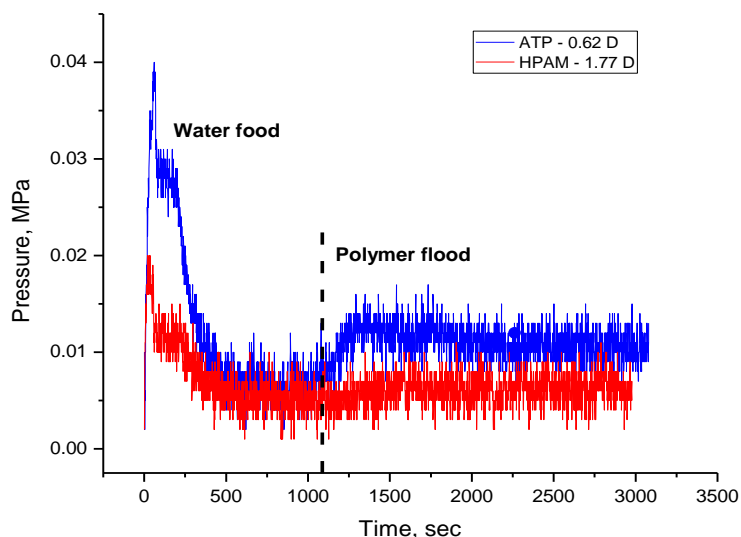
Water and polymer flooding

Figure 6 shows the oil cut versus the number of injected pore volumes. Water injection resulted in the production of almost the same portions of oil in both tests, even though in the case of low permeability (0.62D) sand pack, the injection pressure was significantly higher (Figure 7). The injection of the polymer solutions into this model shows that ATP provides a higher increase in oil production than HPAM does.



Flow rate — $0.15 \text{ cm}^3\cdot\text{min}^{-1}$. Temperature — $30 \text{ }^\circ\text{C}$

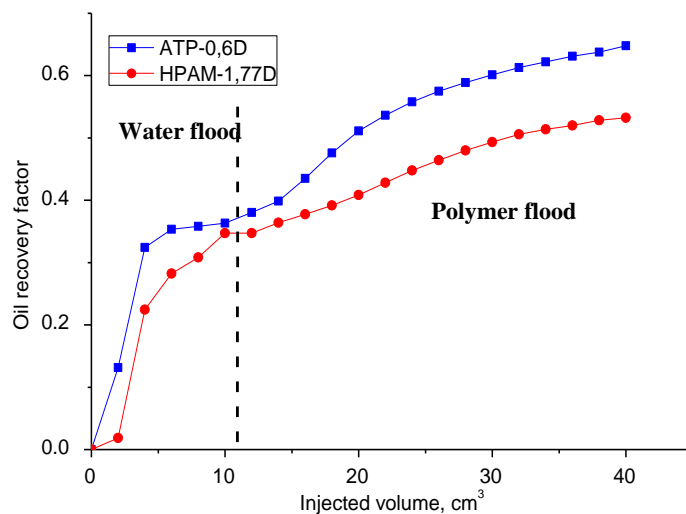
Figure 6. Oil cut versus injected pore volumes during water injection and polymer flooding by ATP (—■—) and HPAM (—●—)



The permeability of sand pack model is 0.62D (1) and 1.77D (2). Flow rate — $0.15 \text{ cm}^3 \cdot \text{min}^{-1}$. Temperature — $30 \text{ }^\circ\text{C}$

Figure 7. The injection pressure versus time during water and polymer flooding

Figure 8 illustrates the oil recovery factor (ORF) obtained during water and polymer flooding processes. Water injection allowed to produce 34.7–36 % of oil. Whereas the injection of 0.25 wt.% ATP and HPAM solutions in $200 \text{ g} \cdot \text{L}^{-1}$ brine into the 0.6D and 1.77D sand packs increased the oil recovery factor after water injection by 28.5 % and 18.5 %, respectively. Thus, 0.25 wt.% ATP produced 10 % more oil than HPAM.



Flow rate — $0.15 \text{ cm}^3 \cdot \text{min}^{-1}$. Temperature — $30 \text{ }^\circ\text{C}$

Figure 8. Oil recovery factor registered during ATP (- ■ -) and HPAM (- ● -) polymer flooding experiments

Conclusions

The results of the elemental analysis demonstrate that the composition of AAm-AMPS-APTAC terpolymer insignificantly deviates from the composition of initial monomer feed upon polymerization.

AAm-AMPS-APTAC terpolymers exhibit improved viscosifying behavior in high salinity media because of their polyampholytic nature and can find practical applications in EOR. For example, the increase of brine salinity from 200 to $300 \text{ g} \cdot \text{L}^{-1}$ at $24 \text{ }^\circ\text{C}$ leads to the increase of the dynamic viscosity of 0.25 % ATP solution from 7 to 14 mPa·s. Whereas the dynamic viscosity of HPAM solution increases from 6 to 9 mPa·s upon the salinity increase from 200 to $250 \text{ g} \cdot \text{L}^{-1}$ and then suddenly declines at $300 \text{ g} \cdot \text{L}^{-1}$ because of the severe polymer precipitation. This phenomenon is explained by hydrolyzed polyacrylamide poor solubility at 270–

300 g·L⁻¹. The obtained viscosity measurement results indicate that the amphoteric terpolymer is more stable at high brine salinity than HPAM.

The injection of 0.25% amphoteric terpolymer and HPAM solutions prepared in 200 g·L⁻¹ brine into the 0.62 and 1.77 Darcy sand packs resulted in the increase of the oil recovery factor by 28 and 18%, respectively. These results show that the amphoteric terpolymer has a higher oil displacement capacity than HPAM.

The introduction of the amphoteric terpolymer as an alternative to HPAM at extremely high salinity conditions adds to the relevance and novelty of this study.

However, some significant shortcomings of this study are

- 1) Limited number of sand pack flooding experiments;
- 2) The use of models with relatively low pore volume, which increases the probability of errors in oil recovery calculations;
- 3) No polymer retention measurements were done.

Thus, the future research will focus on the flooding tests with polymer retention measurements by using large pore volume sand packs and cores.

Acknowledgments

This research was funded by the Science Committee of the Ministry of Education and Science of the Republic of Kazakhstan (Grant No. AP09260574). Authors thank Prof. Nurxat Nuraje from Nazarbayev University for provision of assistance in providing of elemental analysis.

References

- 1 Tileuberdi, N., Zholtayev, G.Z.H., Abdeli, D.Zh., & Ozdov, S.M. (2021). Investigation of drainage mechanism of oil from pores of oil saturated rocks using nitrogen at the laboratory condition. *News of the National Academy of Sciences of the Republic of Kazakhstan, Series of Geology and Technical Sciences*, 5(449), 146–152. <https://doi.org/10.32014/2021.2518-170x.108>
- 2 Ezell, R.G., & McCormick, C.L. (2007). Electrolyte- and pH-responsive polyampholytes with potential as viscosity-control agents in enhanced petroleum recovery. *Journal of Applied Polymer Science*, 104(5), 2812–2821. <https://doi.org/10.1002/app.24999>
- 3 Siyam, T. (2001). Development of acrylamide polymers for the treatment of waste water. *Designed Monomers and Polymers*, 4(2), 107–168. <https://doi.org/10.1163/156855500300203377>
- 4 Tha, A., Agrawal, S., Mishra, A., & Rai, J.P. (2001). Synthesis, characterization and flocculation efficiency of poly(acrylamide-co-acrylic acid) in tannery waste-water. *Iranian Polymer Journal*, 10(2), 85–90.
- 5 Sydansk, R.D., & Romero-Zeron, L. (2011). *Reservoir conformance improvement. Society of Petroleum Engineers*. ISBN: 978-1-55563-302-8
- 6 Zhu, D., Zhang, J., Han, Y., Wang, H., & Feng, Y. (2013). Laboratory study on the potential EOR use of HPAM/ves hybrid in high-temperature and high-salinity oil reservoirs. *Journal of Chemistry*, 2013, 1–8. <https://doi.org/10.1155/2013/927519>
- 7 Kudaibergenov, S.E. (1999). Recent advances in the study of Synthetic Polyampholytes in solutions. *Polymer Latexes - Epoxide Resins - Polyampholytes*, 115–197. https://doi.org/10.1007/3-540-68384-4_3.
- 8 Kudaibergenov, S.E. (2002). *Polyampholytes: Synthesis, characterization and application*. Kluwer Academic/Plenum Publishers.
- 9 McCormick, C.L., & Johnson, C.B. (1998). Water-soluble copolymers 28. Ampholytic copolymers of sodium 2-acrylamido-2-methylpropanesulfonate with (2-acrylamido-2-methylpropyl) dimethylammonium chloride: Synthesis and characterization. *Macromolecules*, 21(3), 686–693. <https://doi.org/10.1021/ma00181a025>
- 10 McCormick, C.L., & Salazar, L.C. (1992a). Water soluble copolymers 43. Ampholytic copolymers of sodium 2-(acrylamido)-2-methylpropanesulfonate with 2-(acrylamido)-2-methylpropanetrimethylammonium chloride. *Macromolecules*, 25(7), 1896–1900. <https://doi.org/10.1021/ma00033a009>
- 11 McCormick, C.L., & Salazar, L.C. (1992b). Water soluble copolymers 44. Ampholytic terpolymers of acrylamide with sodium 2-acrylamido-2-methylpropanesulfonate and 2-acrylamido-2-ethylpropane-trimethyl-ammonium chloride. *Polymer*, 33(20), 4384–4387. [https://doi.org/10.1016/0032-3861\(92\)90284-4](https://doi.org/10.1016/0032-3861(92)90284-4)
- 12 McCormick, C.L., & Salazar, L.C. (1993). Water soluble copolymers 45. Ampholytic terpolymers of acrylamide with sodium 3-acrylamido-3-methylbutanoate and 2-acrylamido-2-methylpropane-trimethylammonium chloride. *J. Appl. Polym. Sci.*, 47(6), 1115–1120. <https://doi.org/10.1002/app.1993.070480617>
- 13 Fevola, M.J., Bridges, J.K., Kellum, M.G., Hester, R.D., & McCormick, C.L. (2004a). pH-responsive ampholytic terpolymers of acrylamide, sodium 3-acrylamido-3-methylbutanoate and (3-acrylamidopropyl)trimethylammonium chloride. I. Synthesis and characterization. *J. Appl. Polym. Sci.*, 42(13), 3236–3251. <https://doi.org/10.1002/pola.20173>
- 14 Fevola, M.J., Kellum, M.G., Hester, R.D., & McCormick, C.L. (2004b). pH-responsive ampholytic terpolymers of acrylamide, sodium 3-acrylamido-3-methylbutanoate and (3-acrylamidopropyl)trimethylammonium chloride. II. Solution properties. *J. Appl. Polym. Sci.*, 42(13), 3252–3270. <https://doi.org/10.1002/pola.20174>

- 15 Quan, H., Li, Z., & Huang, Z. (2016). Self-assembly properties of a temperature- and salt-tolerant amphoteric hydrophobically associating polyacrylamide. *RSC Adv.*, 6(54), 49281–49288. <https://doi.org/10.1039/C6RA05779A>
- 16 Kujawa, P., Rosiak, J.M., Selb, J., & Candau, F. (2000). Synthesis and properties of hydrophobically modified polyampholytes. *Mol. Cryst. and Liq. Cryst.*, 1(354), 401–407. <https://doi.org/10.1080/10587250008023632>
- 17 Kujawa, P., Rosiak, J.M., Selb, J., & Candau, F. (2001). Micellar synthesis and properties of hydrophobically associating polyampholytes. *Makromol. Chem. Phys.*, 8(202), 1384–1397. [https://doi.org/10.1002/1521-3935\(20010501\)202:8<1384::AID-MACP1384>3.0.CO;2-1](https://doi.org/10.1002/1521-3935(20010501)202:8<1384::AID-MACP1384>3.0.CO;2-1)
- 18 El-hoshoudy, A.N., Desouky, S.E.M., Elkady, M.Y., Alsabagh, A.M., Betiha, M.A., & Mahmoud, A.M. (2015). Investigation of optimum polymerization conditions for synthesis of cross-linked polyacrylamide-amphoteric surfer nanocomposites for polymer flooding in sandstone reservoirs. *Int. J. Polym. Sci.*, (4), 1–14. <https://doi.org/10.1155/2015/318708>
- 19 Ahmad, R., Amir, E., & Hajar, J. (2014). Polyacrylamide-based polyampholytes and their applications. *Rev Chem Eng.*, 30(5), 501–519. <https://doi.org/10.1515/revce-2014-0004>
- 20 Kudaibergenov, S. (2021). *Polyampholytes: Past, Present, Perspectives*. Almaty, Kazakhstan.
- 21 Kudaibergenov, S., & Okay, O. (2020). Synthetic and natural polyampholytes: Structural and behavioral similarity. *Polym. Adv. Technol.*, 32(7), 2639–2654. <https://doi.org/10.1002/pat.5145>
- 22 Mukhametgazy, N., Gussenov, I., Shakhvorostov, A., & Kudaibergenov, S. (2020). Salt tolerant acrylamide based quenched polyampholytes for polymer flooding. *Bulletin of the University of Karaganda – Chemistry*, 4(100), 119–127. <https://doi.org/10.31489/2020Ch4/119-127>
- 23 Gussenov, I., Mukhametgazy, N., Shakhvorostov, A., & Kudaibergenov, S. (2021). Synthesis and characterization of high molecular weight amphoteric terpolymer based on acrylamide, 2-acrylamido-2-methyl-1-propanesulfonic acid sodium salt and (3-acrylamidopropyl)trimethylammonium chloride for oil recovery. *Chemical Bulletin of Kazakh National University*, 103(4), 12–20. <https://doi.org/10.15328/cb1243>
- 24 Quan, Zh., Jincheng, M., Xiaojiang, Y., Chong, L., Heng, Zh., Tao, X., & Quanhong, W. (2022). Synthesis of a hydrophobic association polymer with an inner salt structure for fracture fluid with ultra-high-salinity water. *Colloids and Surfaces A: Physicochemical and Engineering Aspects*, 636, 128062. <https://doi.org/10.1016/j.colsurfa.2021.128062>
- 25 Gou, S., Yin, T., Ye, Z., Jiang, W., Yang, C., Ma, Y., Feng, M., & Xia, Q. (2014). High-temperature resistance water-soluble copolymer derived from acrylamide, DMDAAC, and functionalized sulfonamide for potential application in enhance oil recovery. *J. Appl. Polym. Sci.*, 131(17), 40727. <https://doi.org/10.1002/app.40727>

Н. Мухаметгазы, И.Ш. Гуссенов, А.В. Шахворостов, Хейкки Тенху

Амфотерлік терполимерді қолдану арқылы жоғары тұзды орта жағдайында мұнай өндіру

Жоғары молекулалық салмақты амфотерлі терполимердің (АТП) тұтқырлығы мен мұнайды ығыстырып шығару қабілеті әртүрлі тұзды ерітінділерде сыналған және мұнайдың өнімділігін арттыруда дәстүрлі түрде қолданыстағы гидролизденген полиакриламидмен (ГПА) салыстырылған. Нәтижелер АТП 200-ден 300 г/л-ге дейінгі тұзды ерітінділерде жоғары тұтқырлықты қамтамасыз ететінін көрсетеді. Бұл Қазақстанда көптеп кездесетін тұздылығы жоғары су қоймаларында ГПА-мен салыстырғанда АТП-ға елеулі артықшылық бере алады. Сонымен қатар, полимерлік айдау бойынша салыстырмалы тәжірибелер 0.25 % массалық үлестегі амфотерлі терполимер мен ГПА-ның 200–300 г/л тұзды судағы ерітінділерін құмды модельге айдау арқылы жүргізілді. ГПА ерітіндісімен жоғары өткізгішті (1.77 Дарси) құмды модель арқылы айдау 1PV тұзды сумен айдауға салыстырғанда мұнай өндіру коэффициентін (МӨК) 18.5%-ға арттырды. Екінші жағынан, өткізгіштігі төмен (0.6 Дарси) құмды модельге АТП айдауда МӨК-ті 28.5%-ға дейін жоғарылатты. Алынған нәтижелер АТП-ның 200 г/л және одан да жоғары тұзды су қоймаларында ГПА-ға балама бола алатынын көрсетеді.

Кілт сөздер: амфотерлік терполимер (АТП), гидролизденген полиакриламид, антиполиэлектролиттік эффект, тығыздық моделі, су арқылы айдау, полимер ерітіндісімен айдау, мұнайды ығыстыру коэффициенті.

Н. Мухаметгазы, И.Ш. Гуссенов, А.В. Шахворостов, Хейкки Тенху

Добыча нефти в условиях высокой минерализации с применением амфотерного терполимера

В статье протестированы реологические свойства и нефтевытесняющая способность высокомолекулярного амфотерного терполимера (АТП) в водах с различной минерализацией. Результаты сравнивались с частично гидролизованным полиакриламидом (ЧГПА), который традиционно

используется для увеличения добычи нефти. Результаты показали, что АТП обладает большей вязкостью в диапазоне минерализации от 200 до 300 г/л. Это даёт АТП преимущество над ЧГПА в пластах с высокой минерализацией воды, которых в Казахстане довольно много. Сравнительные эксперименты по полимерному заводнению проводились путём закачки 0,25 мас.% амфотерного терполимера и ЧГПА, растворённых в воде с минерализацией 200 г/л в насыпные песчаные модели. Закачка ЧГПА в высокопроницаемую модель (1,77 Дарси) привела к увеличению коэффициента вытеснения нефти (КВН) на 18,5% после закачки одного порового объёма воды. Соответственно, при закачке амфотерного терполимера в низкопроницаемую (0,6 Дарси) модель КВН был увеличен на 28,5%. Полученные результаты показали, что АТП может стать альтернативой ЧГПА в условиях, где минерализация воды превышает 200 г/л.

Ключевые слова: амфотерный терполимер, гидролизанный полиакриламид, антиполизлектролитный эффект, насыпная модель, заводнение, полимерное заводнение, коэффициент вытеснения нефти.

Information about authors*

Mukhametgazy, Nurbatyr (*corresponding author*) — 3rd year PhD student of Petrochemistry, Satbayev University, Satbayev street, 22a, 050013, Almaty, Kazakhstan; Junior Researcher of the Institute of Polymer Materials and Technology, Almaty, Kazakhstan; Atyrau-1, 3/1, 050019; e-mail: nurbatyr.kaz@gmail.com; <https://orcid.org/0000-0001-5957-0305>;

Gussenov, Iskander Shakhsavanovich — PhD of Petroleum Engineering Sciences, Satbayev University, Satbayev street, 22a, 050013, Almaty, Kazakhstan; Senior Researcher of the Institute of Polymer Materials and Technology, Almaty, Kazakhstan; Atyrau-1, 3/1, 050019; e-mail: iskander.gussenov@mail.ru; <https://orcid.org/0000-0002-9820-7952>;

Shakhvorostov, Alexey Valeryevich — PhD of Petrochemistry Sciences, Satbayev University, Satbayev street, 22a, 050013, Almaty, Kazakhstan; Senior Researcher of the Institute of Polymer Materials and Technology, Almaty, Kazakhstan; Atyrau-1, 3/1, 050019; e-mail: alex.hv91@gmail.com; <https://orcid.org/0000-0003-3502-6123>;

Tenhu, Heikki — PhD, Professor of Polymer Chemistry, Supervisor of Doctoral Programme in Chemistry and Molecular Sciences, Department of Chemistry, University of Helsinki, 55 (A. I. Virtasen aukio 1), 00014, Helsinki, Finland; heikki.tenhu@helsinki.fi; <https://orcid.org/0000-0001-5957-4541>

*The author's name is presented in the order: *Last Name, First and Middle Names*

A.A. Zhubanov^{1*}, V.G. Bondaletov², S.S. Kozhabekov¹, A.Z. Galymzhan¹

¹Kazakh-British Technical University, Almaty, Kazakhstan;

²Tomsk Polytechnic University, Tomsk, Russia

(*Corresponding author's e-mail: amin.zhuban@gmail.com)

Amidation of Polyethylene-Acrylic Acid Copolymer as Pour Point Depressants for Waxy Crude Oils

The present work aims to provide amine-modified polyethylene-acrylic acid (PEAA) copolymers as a pour point depressant (PPD) that will be evaluated for lower pour point of crude oil. For this, PEAA was amidated with butylamine and octadecylamine in the presence of xylene as a solvent at 150 °C for 10 hours to obtain copolymers PEAA/ODA and PEAA/BA. The copolymers were modified by amidation using the carboxyl groups of an ethylene-acrylic acid copolymer as reaction sites in reactions with RNH₂. The resulting copolymers were purified and analyzed by FTIR spectroscopy. The modified PEAA copolymers were evaluated for their effectiveness as depressants for crude oils by pour point measurements at 50 ppm, 100 ppm and 200 ppm and rheological measurements at 100 ppm. The pour point measurements of the crude oil showed that octadecylamine-modified PEAA copolymer performed better than butylamine-modified and unmodified PEAA copolymer. The effectiveness of the modified copolymers compared to unmodified PEAA can be explained by the polarity of the monoalkylamide groups in the peripheral substituents along the copolymer backbone, which plays a crucial role in preventing the agglomeration of wax crystals in crude oil.

Keywords: polyethylene-acrylic acid (PEAA), crude oil, pour point depressant (PPD), wax crude oil, copolymers, pour point, flow, modification, primary amines.

Introduction

The global petroleum industry is experiencing significant material costs, as well as technical and technological difficulties, due to the current trend of an increase in the share of heavy and highly waxy crude oil. According to forecasts this share is already 37–56 %, which is especially typical for crude oils from Kazakhstan fields (fields of the Mangyshlak Peninsula, South-Turgai trough, and other regions). In general, the anomalous properties of crude oils from Kazakhstan fields allow us to class them as solidifying at positive temperatures, highly waxy and high-viscosity ones. Even under standard conditions the viscosity of crude oils fluctuates within several hundred and sometimes thousands of centipoises. At low temperatures highly waxy crude oils show the pronounced non-Newtonian (viscous-plastic, viscoelastic, thixotropic) properties, without which it is impossible to organize rational well operation and crude oil transportation through pipelines. When the pumping process is stopped, crystalline structures are formed in crude oil, the strength of which depends on the content of wax fractions, the dormant time of the crude oils, and the conditions for their formation. From a scientific point of view, the most effective way to regulate the fluidity of crude oil is chemical action, that is, to achieve a significant change in the structural organization and phase state of crude oil dispersed systems. Thus, a chemical additive known as PPD is used to reduce the viscosity and pour point of crude oils [1–5]. These supplements are most recognized for their simplicity and cost effectiveness. When used in manufacturing processes, these PPDs minimize the problems associated with wax deposition on manufacturing equipment. Pour point depressants (PPDs) are polymeric compounds consisting of a hydrocarbon chain that interacts between the additive and wax, as well as a polar part that repels the wax crystals from each other, preventing the growth of wax crystals [6, 7]. Pour point depressants include poly (ethylene-vinyl acetate) (PEVA) copolymers, which have good PPD performance for crude oil, an alkyl ester, a copolymer of unsaturated carboxylic acid and olefin, olefin and maleic anhydride [8–11]. Thus, the development of new PPDs that can solve or minimize such problems is of great interest to the petroleum industry around the world.

Crude oil from the Akshabulak field (Kazakhstan) with high wax content is characterized by a high pour point, high viscosity, high gel strength, and a large amount of wax deposits. An increase in the wax con-

tent of crude oil leads to a deterioration in the solubility of the wax in the crude oil, in some cases with the formation of a separate solid phase.

Experimental

In the work, the PEAA modification was carried out. The characteristics of PEAA copolymers were investigated. The molecular weight and polydispersity index were determined. PEAA copolymers were characterized by FTIR spectroscopy. The effectiveness of the modified copolymers as a pour point depressant was shown. A rheological study of highly wax crude oil from the Akshabulak field was carried out.

Reagents

Poly(ethylene-co-acrylic acid) (acrylic acid 20 %, $t = 99\text{--}101\text{ }^\circ\text{C}$, density = 0.96), octadecylamine, butylamine, *o*-xylene, THF, toluenesulfonic acid from Sigma-Aldrich.

Amidation of poly(ethylene-co-acrylic acid)

Modification of the poly(ethylene-co-acrylic acid) copolymer with butylamine (mass ratio PEAA-BA was 1–0.4), octadecylamine (mass ratio PEAA-ODA was 1–1.5) was carried out according to the general procedure (Figure 1). A two-necked flask equipped with a Dean-Stark head with a reflux condenser, stirrer and thermometer was loaded with an poly(ethylene-co-acrylic acid) copolymer, a primary amine and *o*-xylene. The mixture was heated to a temperature of $150\text{ }^\circ\text{C}$ and toluenesulfonic acid dissolved in *o*-xylene (1 % wt based on total mass of reactants) was added. Then the reaction mixture was continuously stirred until the evolution of reaction water ceased, namely for 10 hours. The resulting mixture was cooled, washed with methanol and dried in a vacuum oven to remove residual solvent.

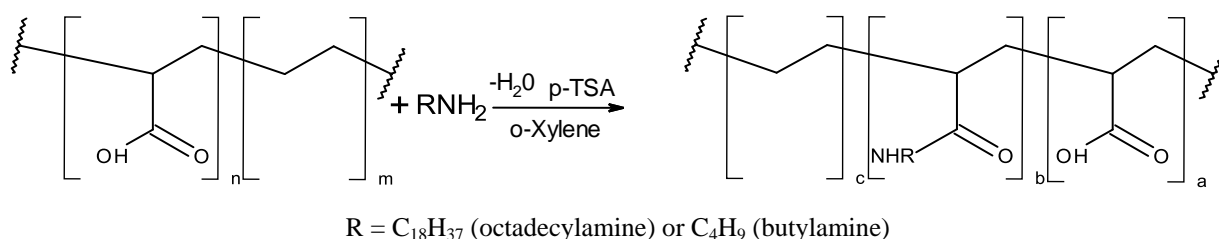


Figure 1. Structure of modified copolymers

Instrumental methods of analysis

The structure of the modified copolymers was analyzed using FTIR spectroscopy. The FTIR spectra of the copolymer samples were recorded on a Nicolet 5700 FTIR spectrometer in the range of $400\text{--}4000\text{ cm}^{-1}$.

The depression efficiency of the synthesized copolymers was evaluated for crude oil from the Akshabulak field. The pour point was determined following ASTM D 5853.

Rheological measurements were carried out using a RheoLab QC rheometer (Anton Paar, Austria) with Rheoplus 3.0 software equipped with a thermostated cooling system with a temperature control.

The chromatogram of crude oil from the Akshabulak field is presented in Figure 2. The analysis of the wax fraction was conducted in the form of a solution in carbon disulfide using a simulation program for the distillation of hydrocarbons on a PerkinElmer AutoSystemXL chromatograph (USA). The components of the waxy fraction were identified by chromatography using reference hydrocarbons.

The Gel Permeation Chromatography (GPC) method was used to determine the molecular weight and polydispersity index of the obtained copolymers. The measurements were carried out on an Agres 1100 instrument with Elitapex software. In measurements, tetrahydrofuran was used as a mobile phase at a flow rate of 0.7 ml/min , and polystyrene of various molecular weights was used as a standard.

Results and Discussion

Physical and Chemical Characteristics of Akshabulak Crude Oil

The rheological properties of crude oil depend on the physical and chemical characteristics of the crude oil (Table 1). Several factors affect the fluidity of a crude oil, including temperature, wax, asphaltene and tar content in the crude oil. Crude oil from the Akshabulak field is wax and low in resins and asphaltenes. The low tar content and the high wax content determine the high pour point values of this crude oil.

The main role in determining the pour point of crude oil is played by hard waxes C_{20} and above. For crude oil from the Akshabulak field, the molecular weight distribution of n-alkanes was determined using

gas chromatography (Fig. 2). The presented data show that the bulk of *n*-alkanes in crude oil are C₂₀–C₃₄ waxes. In turn, among this group, the largest percentage is accounted for by C₂₀–C₃₀ waxes, and the smallest one — by C₃₁–C₄₅. Waxes of the C₂₀–C₃₄ group melt in the temperature range of 36–70 °C.

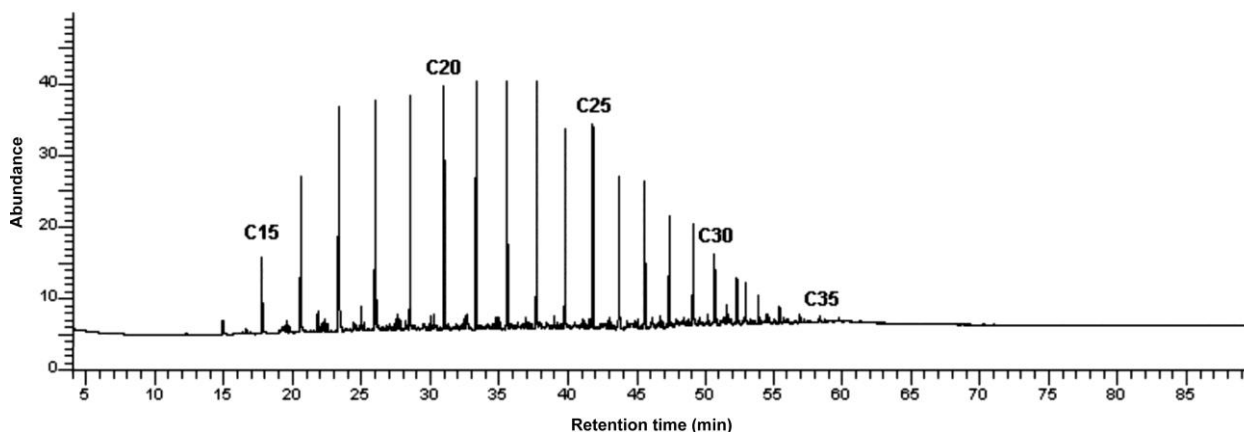


Figure 2. Chromatogram of the distribution of *n*-alkanes in Akshabulak crude oil

Table 1

Physical and chemical characteristics of Akshabulak crude oil

No.	Determined characteristics	Example	Test method
1	Density at 20°C, kg/m ³	813.3	ASTM D 1298
2	Water content, %	0.1	ASTM D 95
3	Concentration of chloride salts, mg/dm ³	20	ASTM D 3230
4	Pour point, °C	+15	ASTM D 97
		+9	ASTM D 5853
5	Mass fraction of wax, %	14.3	ASTM 3235-06
6	Mass fraction of silica gel resins, %	8.6	ASTM D 6560–00
7	Mass fraction of asphaltenes, %	0.6	ASTM D 6560–00
8	Kinematic viscosity at 40°C, mm ² /s	4.2	ASTM D 445–96

Characterization of the copolymers

The structure of the copolymers was analyzed using FTIR spectrometry in the range of 400–4000 cm⁻¹.

FTIR spectra of a copolymer of ethylene and acrylic acid are shown in Figure 3, where vibration bands are observed for ν_{as} methylene group in the region of 2918.5 cm⁻¹ and ν_s vibrations of methylene group in the region of 2849.9 cm⁻¹.

A wide band in the range of 3400–2800 cm⁻¹ is due to amino groups' ν vibrations in primary amides. The characteristic fluctuations in the 1703 cm⁻¹ range refer to the ν_s vibrations of acrylic acid carbonyl group. After modifications the peak at 1703 cm⁻¹ disappears, which indicates the conversion of carboxylic group of acrylic acid into amide. δ -vibrations of methyl and methylene group appear in the region of 1463.9 cm⁻¹ for aliphatic groups. The absorption at about 1409.7 cm⁻¹ is partly attributed to the hydroxy group of the COOH fragment [12]. The presented data indicate the presence of the main functional groups in the structure of the copolymers shown in the diagram (Fig. 1).

In Figure 3, all FTIR spectra of poly (ethylene-co-acrylic acid) copolymers modified with amines contain ν_{as} of methyl and methylene groups in the region of 2918–2920 cm⁻¹, as well as ν_s of methyl and methylene group in the region of 2850 cm⁻¹. Stretching vibrations of the carbonyl group in the amide and imide rings are in the range of 1640–1645 cm⁻¹. δ -vibrations of methyl and methylene group for aliphatic groups are presented in all spectra in the range of 1450–1460 cm⁻¹. δ vibrations of the hydroxy group of acrylic acid are presented in the region of 940 cm⁻¹ and practically completely disappears after modifications with amines [12].

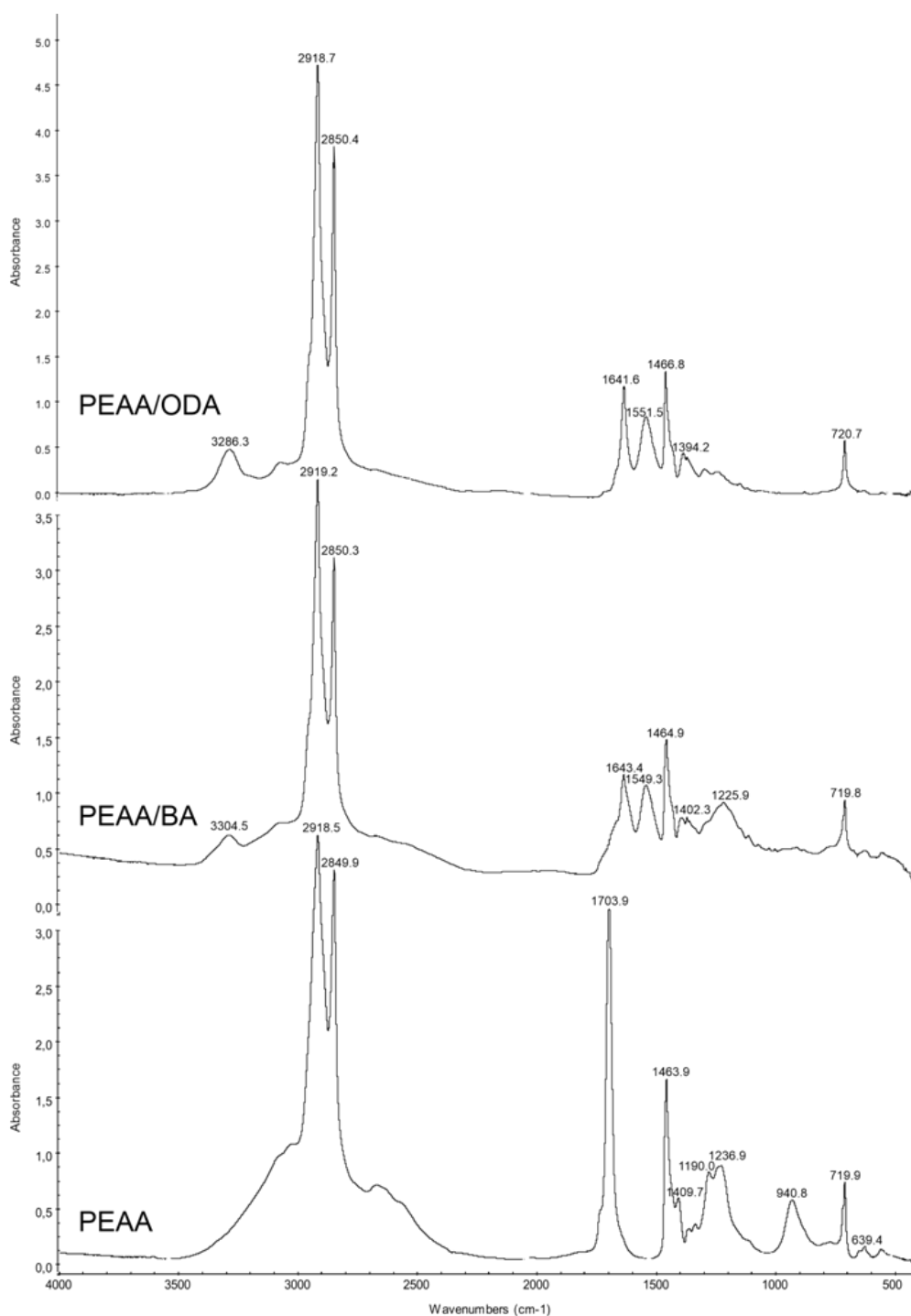


Figure 3. FTIR spectrum of the synthesized copolymers PEAA, PEAA/BA, PEAA/ODA

The Results of Measuring the Molecular Weight of the Copolymers

The measurement results showed that the molecular weight of PEAA (M_w is 2.21×10^5 g/mol) is lower than the molecular weight of PEAA modified with butylamine (M_w is 2.49×10^5 g/mol) and the molecular weight of PEAA modified with butylamine is lower than the molecular weight of PEAA modified with octadecylamine (M_w is 3.83×10^5 g/mol). The polydispersity index (M_w/M_n) ranges from 1.211 to 1.287 (Table 2). Comparing and analyzing the molecular weight and polydispersity index of the synthesized and modified copolymers improving the pour point of crude oil in various studies in similar directions, it was found that the molecular weight and polydispersity index of the modified copolymers were within the regulated norms. Therefore, it is possible to use modified copolymers as potential PPDs.

Molecular weight of PEAA copolymers

Sample	M_w , g/mol	M_n , g/mol	M_w/M_n
Poly(ethylene-co-acrylic acid)	221.315	182.754	1.211
Poly(ethylene-co-acrylic acid)/butylamine	249.412	199.051	1.253
Poly(ethylene-co-acrylic acid)/octadecylamine	383.124	297.687	1.287

Pour Point and Rheological Measurements

From the obtained data, we can observe that the PEAA copolymer modified with octadecylamine shows the best efficiency at lowering the pour point of crude oil to $-3\text{ }^\circ\text{C}$ at an additive concentration in crude oil of 100 ppm. Increasing or decreasing concentration of an additive, the pour point of the crude oil is $0\text{ }^\circ\text{C}$. The same trend is observed for PEAA copolymer, where the pour point of crude oil at 100 ppm is $0\text{ }^\circ\text{C}$, and with decreasing or increasing pour point concentration, it increases to $3\text{ }^\circ\text{C}$ and PEAA copolymer modified with butylamine, where the pour point of crude oil at 100 ppm is $3\text{ }^\circ\text{C}$, and with a decrease or increase in the concentration of pour point, it increases to $6\text{ }^\circ\text{C}$. Therefore, the most effective dosage for PEAA-based additives for Akshabulak crude oil is 100 ppm and when dosage changes, the achieved effectiveness deteriorates.

A $12\text{ }^\circ\text{C}$ decrease in pour point of crude oil (from $9\text{ }^\circ\text{C}$ to $-3\text{ }^\circ\text{C}$) of modified PEAA copolymer, compared to unmodified PEAA copolymer by $6\text{ }^\circ\text{C}$ (from $9\text{ }^\circ\text{C}$ to $3\text{ }^\circ\text{C}$) indicates that PEAA grafts have the ability to disperse wax crystals and reduce their nucleation (Table 3). According to the obtained data, the deposition and coagulation of wax crystals decrease with an increase in the length of the side group of the modified PEAA copolymers, which, in turn, shows the effect of the length of the pendant groups on the effectiveness of the depressant additive.

Table 3

Pour point of crude oil with the addition of PEAA copolymers and blank crude oil

Sample	Pour point temperature, $^\circ\text{C}$			ΔT , $^\circ\text{C}$
	50 ppm	100 ppm	200 ppm	
Crude oil blank $45\text{ }^\circ\text{C}$	+18			–
Crude oil blank $60\text{ }^\circ\text{C}$	+9			–
Crude oil with PEAA	6	3	6	6
Crude oil with PEAA/BA	3	0	3	9
Crude oil with PEAA/ODA	0	-3	0	12

The rheological properties of crude oil from the Akshabulak field were measured with and without the addition of PEAA copolymers at a concentration of 100 ppm. The PEAA copolymer and modified PEAA copolymers having octadecylamine and butylamine side chains show an improvement in the rheology curve (Fig. 4).

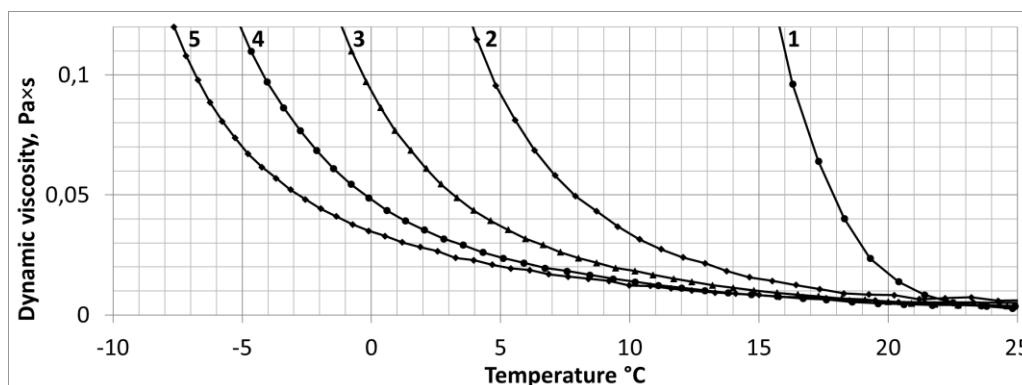


Figure 4. Curve of the dependence of the dynamic viscosity of Akshabulak crude oil on temperature with a heat treatment at $45\text{ }^\circ\text{C}$ ¹ and $60\text{ }^\circ\text{C}$ ² without PPD, and heat treatment at $60\text{ }^\circ\text{C}$ with dosage of 100 ppm depressants: PEAA³, PEAA-BA⁴, PEAA-ODA⁵

The addition of unmodified PEAA copolymer to crude oil is less effective than modified PEAA. The most effective additive for rheological measurements and for measuring the pour point of crude oil is PEAA copolymer modified with octadecylamine. The rheological data also show the dependence of the rheological curve on the heat treatment temperature. Crude oil heat treated at 60 °C performs better than crude oil heat treated at 45 °C.

The effectiveness of modified copolymers compared to unmodified PEAA can be explained by the polarity of nitrogen in the amide group along the copolymer chain, which plays a role in preventing the agglomeration of wax crystals in crude oil.

Conclusions

Modification of the PEAA copolymer was carried out using primary amines, namely long-chain octadecylamine and short-chain butylamine. The most effective concentration for copolymers based on PEAA as a pour point depressant for Akshabulak crude oil is 100 ppm. Octadecylamine-modified PEAA copolymer shows the best performance as Pour Point Depressant for Akshabulak crude oil. Rheological measurements demonstrate that the viscosity properties of the treated crude oil depend on the structure of the modified PEAA copolymers. The longer the pendant group is, the higher the effectiveness of the pour point depressants is.

The rheological properties and pour point of crude oil were found to decrease with the addition of modified PEAA even at low concentrations (50 ppm).

Acknowledgments

This study was supported by the Ministry of Education and Science of the Republic of Kazakhstan within the framework of Grant No. AP08855445 “Synthesis and modification of copolymers based on vinyl monomers as pour point depressants for wax crude oils” (2020–2022).

References

- 1 Atta, A.M., Al-Shafy, H.I., & Ismail, E.A. (2011). Influence of ethylene acrylic alkyl ester copolymer wax dispersants on the Rheological behavior of Egyptian crude oil. *Journal of Dispersion Science and Technology*, 32(9), 1296–1305. <https://doi.org/10.1080/01932691.2010.505806>
- 2 Shafey, A.H.I., Hameed, A.R.S., Ismail, E.A., & Azabawy, E.O.E. (2014). Studies of poly ethylene acrylic acid derivatives as pour point depressants of waxy crude oils. *Organic Chemistry: An Indian Journal*, 10, 308–14.
- 3 Xia, X., Li, C., Dai, S., Duan, Z., Lian, W., Yao, B., Sun, G., & Yang, F. (2022). Modification effect of macroporous comb-like polymeric pour point depressants on the flow behavior of model waxy oils. *Fuel*, 314, 123113. <https://doi.org/10.1016/j.fuel.2021.123113>
- 4 Elganidi, I., Elarbe, B., Ridzuan, N., & Abdullah, N. (2022). Synthesis, characterisation and pre-evaluation of a novel terpolymer as pour point depressants to improve the Malaysian crude oil flowability. *Journal of Petroleum Exploration and Production Technology*. <https://doi.org/10.1007/s13202-021-01445-2>
- 5 Atta, A.M., Elsockary, M.A., Kandil, O.F., & Mohamed, Z.M. (2008). Using of modified plastic waste based on poly(ethylene-co-acrylic acid) grafts to solve transportation problem of petroleum crude oil. *Journal of Dispersion Science and Technology*, 29(1), 7–19. <https://doi.org/10.1080/01932690701686767>
- 6 Bondaletov, V.G., Kopytov, M.A., Prozorova, I.V., & Antonov, I.G. (2004). Synthesis and research of dark oil-polymeric gums as regulators of rheological properties of average paraffinic oils. *Chemistry and chemical technology*, 47(8), 110–113.
- 7 Steckel, L., Nunes, R.C.P., Rocha, P.C.S., Ramos, A.C.S., Alvares, D.R.S., & Lucas, E.F. (2022). Pour point depressant: Identification of critical wax content and model system to estimate performance in crude oil. *Fuel*, 307, 121853. <https://doi.org/10.1016/j.fuel.2021.121853>
- 8 Kozhabekov, S.S., Zhubanov, A.A., & Toktarbay, Z. (2019). Study the rheological properties of waxy oil with modified pour point depressants for the South Turgai Oil Field in Kazakhstan. *Oil & Gas Science and Technology — Revue d'IFP Energies Nouvelles*, 74, 28. <https://doi.org/10.2516/ogst/2019004>
- 9 Xiu, Z., Dufils, P.-E., Zhou, J., Cadix, A., Hatchman, K., Decoster, T., & Ferlin, P. (2019). Amphiphilic wax inhibitor for tackling crude oil wax deposit challenges. Texas, USA. <https://doi.org/10.2118/193593-ms>
- 10 Li, N., Wu, W., & Mao, G. (2021). Effect of modified ethylene vinyl acetate copolymers pour point depressants on flow properties of crude oil and corresponding mechanism analysis. *Colloids and Surfaces A: Physicochemical and Engineering Aspects*, 630, 127602. <https://doi.org/10.1016/j.colsurfa.2021.127602>
- 11 Xu, J., Qian, H., Xing, S., Li, L., & Guo, X. (2010). Synthesis of poly(maleic acid alkylamide-co- α -olefin-co-styrene) copolymers and their effect on the yield stress and morphology of waxy gels with asphaltenes. *Energy & Fuels*, 25(2), 573–579. <https://doi.org/10.1021/ef1012215>
- 12 Kuptsov, A.H., & Zhizhin, G.N. (1998). *Handbook of Fourier transform Raman and infrared spectra of polymers*. Elsevier.

Ә.Ә. Жубанов, В.Г. Бондалетов, С.С. Кожобеков, А.З. Галымжан

Полиэтилен акрил қышқылының сополимерін парафинді шикі мұнайларға депрессант ретінде қолдану үшін амидациялау

Осы жұмыс депрессорлық қоспа ретінде пайдалану үшін модификацияланған аминдермен полиэтилен-акрил қышқылының (PEAA) сополимерлерін алуға және оларды шикі мұнайдың аққыштығының жоғалу температурасын жақсарту үшін бағалауға бағытталған. Ол үшін PEAA/ODA және PEAA/BA сополимерлерін алу үшін 150°C температурада 10 сағат бойы еріткіш ретінде ксилол қатысуымен PEAA бутиламинмен және октадециламинмен амидирленді. Сополимерлер RNH_2 реакцияларында реакция орталықтары ретінде этилен мен акрил қышқылы сополимерінің карбон қышқылының топтарын қолдана отырып, амидирлеу арқылы модификацияланды. Модификацияда негіз ретінде пайдаланылатын PEAA сополимері 20 моль акрил қышқылына ие. Алынған сополимерлер FTIR-спектроскопия әдісімен тазартылып, талданды. Модификацияланған PEAA сополимерлері 50 ppm, 100 ppm және 200 ppm концентрациялары кезінде аққыштықтың жоғалу температурасын өлшеу, сондай-ақ 100 ppm концентрациясы жағдайында реологиялық өлшеу арқылы шикі мұнайға арналған депрессорлық қоспалар ретінде олардың тиімділігі үшін бағаланды. Шикі мұнайдың аққыштығының жоғалу температурасын өлшеу нәтижелері октадециламинмен модификацияланған PEAA сополимерінің модификацияланған бутиламинге және модификацияланбаған PEAA сополимеріне қарағанда тиімділігі жоғары екенін көрсетті. Модификацияланбаған PEAA-мен салыстырғанда модификацияланған сополимерлердің тиімділігін шикі мұнайдағы парафин кристалдарының агрегациясын болдырмауда маңызды рөл атқаратын сополимер тізбегі бойындағы амидтер тобындағы азоттың полярлығымен түсіндіруге болады.

Кілт сөздер: полиэтилен-акрил қышқылы (PEAA), шикі мұнай, депрессорлық қоспалар (PPD), парафиндік мұнай, сополимерлер, кату температурасы, аққыштық, модификация, бастапқы аминдер.

А.А. Жубанов, В.Г. Бондалетов, С.С. Кожобеков, А.З. Галымжан

Амидирование сополимера полиэтилен-акриловой кислоты для использования в качестве депрессорных присадок для сырых парафинистых нефтей

Настоящая работа направлена на получение сополимеров полиэтилен-акриловой кислоты (PEAA), модифицированных аминами, для применения в качестве депрессорных присадок и оценку их на предмет улучшения температуры потери текучести сырой нефти. Для этого PEAA амидировали бутиламином и октадециламином в присутствии ксилола в качестве растворителя при 150 °C в течение 10 часов с получением сополимеров PEAA/ODA и PEAA/BA. Сополимеры были модифицированы путем амидирования с использованием групп карбоновой кислоты сополимера этилена и акриловой кислоты в качестве реакционных центров в реакциях с RNH_2 . Полученные сополимеры очищали и анализировали методом FTIR-спектроскопии. Модифицированные сополимеры PEAA были оценены на предмет их эффективности в качестве депрессорных присадок для сырой нефти посредством измерений температуры потери текучести при концентрациях 50 ppm, 100 ppm и 200 ppm, а также реологических измерений при концентрации 100 ppm. Результаты измерения температуры потери текучести сырой нефти показали, что большую эффективность показывает сополимер PEAA, модифицированный октадециламином, чем модифицированный бутиламином и не модифицированный сополимер PEAA. Эффективность модифицированных сополимеров по сравнению с немодифицированным PEAA можно объяснить полярностью азота в амидной группе вдоль цепи сополимера, которая играет роль в предотвращении агрегации кристаллов парафина в сырой нефти.

Ключевые слова: полиэтилен-акриловая кислота, сырая нефть, депрессорная присадка, парафиновая нефть, сополимеры, температура застывания, текучесть, модификация, первичные амины.

Information about authors*

Zhubanov, Amin Abdirasululy — PhD student, Researcher, Kazakh-British Technical University, Tole bi, 59, 050000, Almaty, Kazakhstan; e-mail: amin.zhuban@gmail.com; <https://orcid.org/0000-0003-1194-8094>;

Kozhabekov, Serik Samsalykovich — PhD, Professor, Kazakh-British Technical University, Tole bi, 59, 050000, Almaty, Kazakhstan; e-mail: skozhabekov.49@mail.ru; <https://orcid.org/0000-0002-7689-9089>;

Bondaletov, Vladimir Grigorievich — DScTech, Professor, National Research Tomsk Polytechnic University, Lenin Ave., 30, 634050, Tomsk, Russia; e-mail: bondaletovvg@mail.ru; <https://orcid.org/0000-0001-5076-6248>;

Galymzhan, Aknur Zeinkyzy — Master's student, Kazakh-British Technical University, Tole bi, 59, 050000, Almaty, Kazakhstan; e-mail: aknurzg@gmail.com; <https://orcid.org/0000-0002-3080-7206>.

*The author's name is presented in the order: *Last Name, First and Middle Names*

O. Toktarbaiuly^{1*}, A. Kurbanova¹, O. Ualibek¹, A. Seralin¹,
T. Zhunussova¹, G. Sugurbekova², N. Nuraje¹

¹National Laboratory Astana, Nazarbayev University, Nur-Sultan, Kazakhstan;

²LLP "EcoStandart.kz", Nur-Sultan, Kazakhstan

(*Corresponding author's e-mail: olzat.toktabaiuly@nu.edu.kz)

Fabrication of Superhydrophobic Self-Cleaning Coatings by Facile Method: Stable after Exposure to Low Temperatures and UV Light

Self-cleaning hydrophobic surfaces attracted public attention last few decades after discovering of lotus effect. Ability of lotus leaves to keep cleanness in relatively dirty places and to clean up itself during rains directed to the development of novel materials and surface structure modification. The surface with such smart properties may have the potential for cost-effectiveness in the case of application in skyscrapers, high buildings, etc. Two main criteria for the surface to express hydrophobic behavior are roughness and low surface energy of the coating material. In this study, superhydrophobic self-cleaning coatings were prepared by a simple, facile, and cheap method using easily available materials, such as polydimethylsiloxane (PDMS) and TiO₂ nanoparticles, and fully characterized for direct usage. PDMS is a bonding layer and TiO₂ nanoparticles are a reinforced composite to form roughness, which shows superhydrophobicity. Characterizations showed that the prepared superhydrophobic coating has a water contact angle of up to 165.5°, with sliding angle of less than 5°. Also self-cleaning and surface microfluidic properties have been studied. The superhydrophobic properties of these coatings do not change even after exposure to their surface to low temperatures and UV light. SEM images confirm the rough structure of obtained surface on glass and sand grains.

Keywords: superhydrophobic coating, superhydrophobic sand, polydimethylsiloxane, titanium oxide nanoparticles, contact angle, UV light, facile method, electrokinetic potential.

Introduction

Recently, the fabrication of superhydrophobic surfaces and coatings based on oxides and polymers with exceptional water repellency is a relevant topic. Superhydrophobic surfaces are essential for the energy-saving industry, because such surfaces are not limited to self-cleaning protection properties, but are also used for anti-icing applications [1]. The effect of roughness on the surface and energy of the fabricated substrate plays a key role in creating superhydrophobic properties and is used to prevent ice accumulation on the substrate [2, 3]. When a drop of water hits a solid surface, it tends to a lower energy state and is measured using the contact angle of water wetting (the radius of the three-phase contact line: solid-liquid-air) of each drop [1]. The hydrophobic surface is described as a surface in which the contact angle of water exceeds 110°, and a drop of water reluctantly slides off its surface [4].

At present, much attention is paid to the preparation of a hydrophobic surface, which is widely used as a self-cleaning coating [5], corrosion protection [6, 7], water-oil separation [8, 9], and anti-icing [10, 11]. Until now, many superhydrophobic coatings with proposed applications have been made with various methods, such as corrosion resistance [12–14], anti-fog surfaces [15–17], anti-icing surfaces [16–20], oil and water separation [21–24], self-cleaning surfaces [25–28], battery production technology [29], sensors [30, 31], water treatment [32], optical devices [33], etc.

Experimental

Chemicals

High purity titanium (IV) oxide nanoparticles (TiO₂, 99.5 %, size 21 nm), PDMS (Silicone Sealant), anhydrous hexane (95 %), borosilicate cover glasses were purchased from Sigma Aldrich. Mixed carbonate-silicate sand from the Akmola region of Kazakhstan with a grain size of 0.1 μm to 800 μm was used as raw material and quartz sand was purchased from LLP "Labopharma" with the GOST 9428-73.

Preparation of Superhydrophobic Solution

Firstly, 1 g PDMS was dissolved in 10 ml of hexane by magnetic stirring for 3 hours, then placed into an ultrasound bath for 1 h under a hermetically covered cap. Further, TiO₂ was added to the mixture and ultra-sonicated another 2 h.

Preparation of Superhydrophobic Coating on Glass by Coating with Sliding Scraper

The glass substrate was repeatedly cleaned several times with deionized water and ethanol, then dried in an oven at 60 °C. The as-prepared superhydrophobic solution was coated by a sliding scraper onto the surface of the glass substrate. Further, the glass substrate was placed in the driving oven at 70 °C for 30 min and annealed at 300 °C for 10 min. Figure 1 shows a complete schematic picture of the experimental synthesis of superhydrophobic coatings.

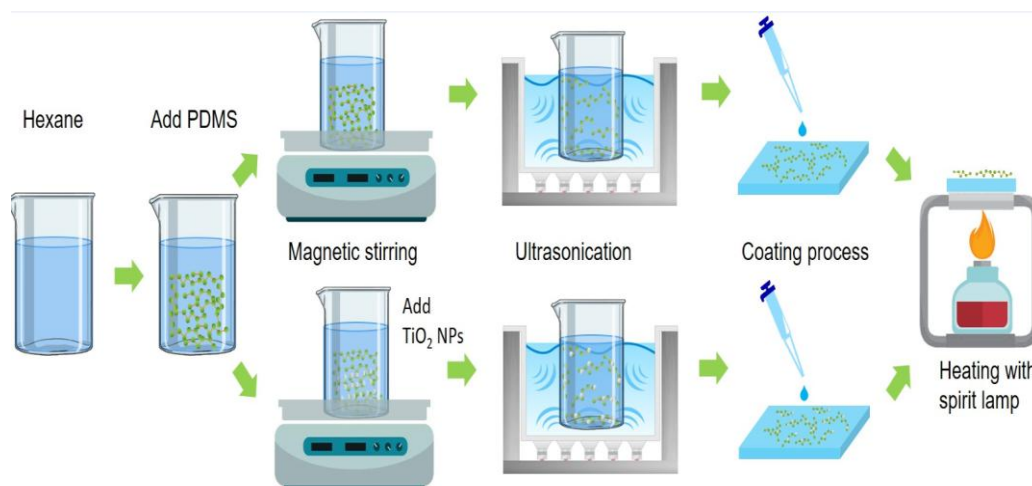


Figure 1. Schematic of a process for synthesis of a superhydrophobic solution and coating

Preparation of Superhydrophobic Sands

Carbonate-silicate sand from the Akmola region of Kazakhstan and quartz sand were used experimentally to make superhydrophobic sands. Akmola sand was cleaned with deionized water in an ultrasonic bath for 30 minutes. The cleaned sand was dried at 70 °C for 30 minutes. The synthesized superhydrophobic suspensions were applied to sand in the same manner as described above.

Characterization

The surface of the materials was studied by Scanning Electron Microscope (SEM) using a Zeiss Auriga Crossbeam 540. The zeta potential and size distribution of suspension were measured by a Zetasizer 3000 (Malvern Instruments). The static contact angle of the droplets was measured by a contact angle meter (OCA 15 EC, Neurtek Instruments). Zeta potential and size distribution were conducted three times. Also, all contact angle measurements were examined at least five times, the average value was taken. Standard deviation was calculated by following formulas:

$$STD = \sqrt{\frac{(x_1 - \bar{x})^2 + (x_2 - \bar{x})^2 + (x_3 - \bar{x})^2 + \dots}{n - 1}}; \quad (1)$$

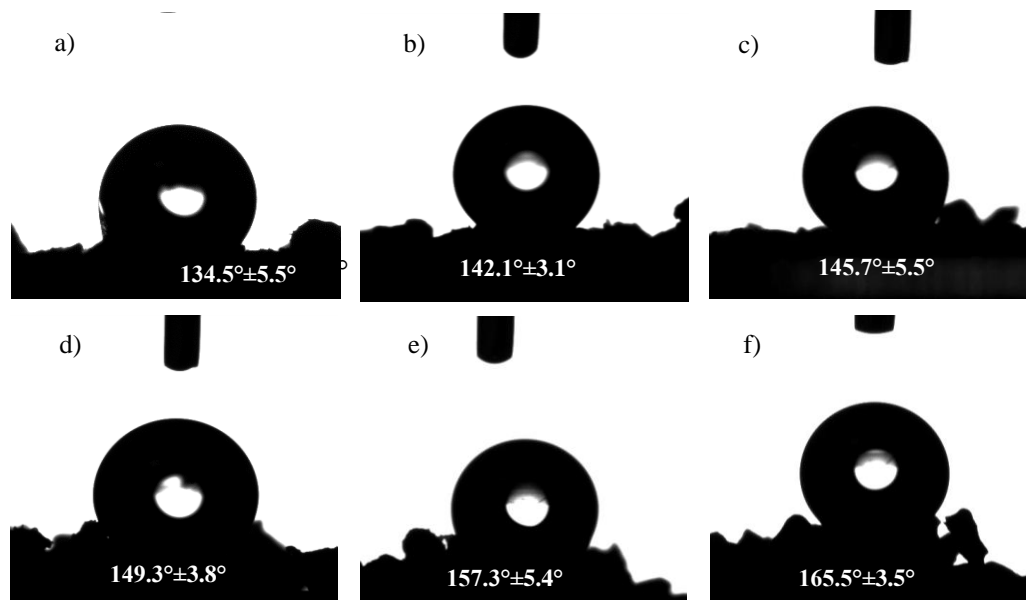
$$RSD = \frac{100}{\bar{x}}, \quad (2)$$

where \bar{x} — the average result; STD — the standard deviation; RSD — the relative standard deviation (%); n — the total number of observation.

Results and Discussion

Wettability of superhydrophobic sands was investigated with optical contact angle measuring and contour analysis system. To measure contact angle, sand particles were uniformly distributed on the surface of conductive double-sided carbon tape and thereafter placed in to sample stage. An amount of 10 μ l water droplet was applied to all samples. Figure 2 shows contact angle measurements of quartz sand, cleaned and not cleaned Akmola sand after processing with superhydrophobic coatings. Wettability of three different

sands (quartz sand, not cleaned, and cleaned Akmola sand) was analysed after coating PDMS and the results are shown in the top row of Figure 2. Water contact angles were $134.5^{\circ} \pm 5.5^{\circ}$, $142.1^{\circ} \pm 3.1^{\circ}$, and $145.7^{\circ} \pm 2.9^{\circ}$ for these sands, respectively. Furthermore, mixture of PDMS and TiO_2 nanoparticles (NPs) was coated on the surface of these sands. The bottom row of Figure 2 represents the contact angle analysis and superhydrophobic properties of these sands can be seen from the results. Water contact angles were $149.3^{\circ} \pm 3.8^{\circ}$, $157.3^{\circ} \pm 5.4^{\circ}$, and $165.5^{\circ} \pm 3.5^{\circ}$ for these sands.



Top row: *a* — PDMS coated quartz sand; *b* — uncleaned Akmola sand; *c* — cleaned Akmola sand. Bottom row: *d* — mixture of PDMS and TiO_2 NPs coated quartz sand; *e* — uncleaned Akmola sand; *f* — cleaned Akmola sand

Figure 2. Contact angle measurements of different sands before and after coating PDMS and PDMS/ TiO_2

Figure 3 demonstrates the comparison of TiO_2 NPs effects on hydrophobic properties of sand. An increase of contact angle can be seen after applying TiO_2 NPs with PDMS. This also indicates the useful impacts of TiO_2 on the process of superhydrophobic materials. The highest contact angle was achieved from cleaned Akmola sand after coating mixture of PDMS and TiO_2 NPs and it was $165.5^{\circ} \pm 3.5^{\circ}$. This result evidenced that cleaning procedure effectively improves superhydrophobic properties of sand.

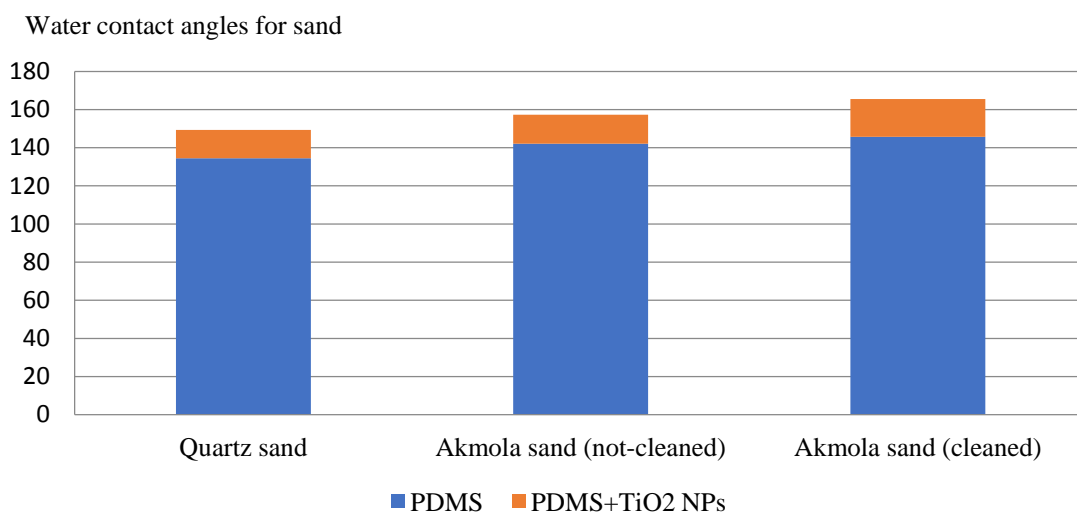
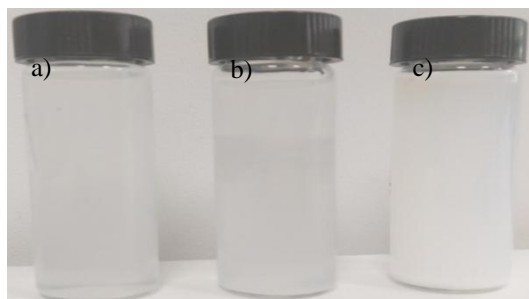


Figure 3. A diagram for water contact angle of obtained superhydrophobic sands

Inhomogeneous dispersion due to the pronounced tendency of nanoparticles to agglomerate is a common phenomenon in the synthesis of polymer nanocomposite. However, good dispersion is required to obtain nanocomposites with optimized properties. The dispersant has branched polysilicon chains that can bind to the -OH group on the TiO₂ surface. Figure 4 illustrates the dispersion of PDMS + TiO₂. A stable and homogenized dispersion indicates that the silicone polymer dissolved in hexane is bound to the surface of the TiO₂ particles.



a — TiO₂; b — PDMS; c — PDMS/TiO₂ in hexane

Figure 4. Visual comparison of solutions

The study results showed a rather large agglomeration with an average hydrodynamic diameter of 812.9 ± 3.6 nm and an average Pdi (polydispersity index) of 0.156 ± 0.003 , and the diameters of TiO₂, PDMS, PDMS/TiO₂ are equal at 501.5 ± 3.8 nm, 784.2 ± 4.2 nm, 1153.1 ± 2.7 nm, respectively (Table 1). Inhomogeneous dispersion due to the pronounced tendency of nanoparticles to agglomerate is a common phenomenon in the synthesis of polymer nanocomposite [34]. When titanium oxide was added to the silicone polymer, the particle size increased from ~ 500 nm to 1000 nm (Figure 5).

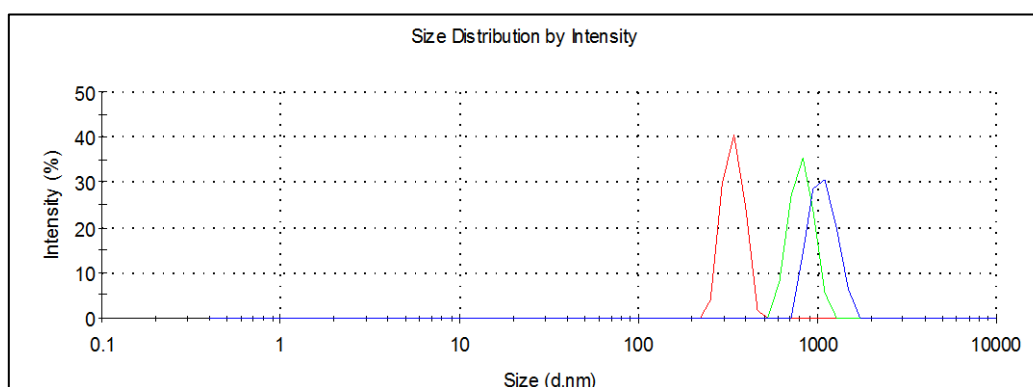


Figure 5. Zeta potential (ζ) of (red line) TiO₂, (green line) PDMS, (blue line) PDMS/TiO₂

The average electro kinetic (zeta " ζ ") dispersion potential was 0.0289 ± 0.02 mV and the average hydrodynamic diameter was 812.9 ± 3.6 nm (Table 1), indicating that some agglomerates and nanoparticles are present in the suspension.

Table 1

Stability of dispersion

Parameters	TiO ₂ in hexane	PDMS in hexane	PDMS/TiO ₂ in hexane	Average value
Size average (d, nm)	501.5 ± 3.8	784.2 ± 4.2	1153.1 ± 2.7	812.9 ± 3.6
PDI	0.163 ± 0.004	0.152 ± 0.002	0.155 ± 0.003	0.157 ± 0.003
ζ (mV)	0.0539 ± 0.02	0.0309 ± 0.04	0.00182 ± 0.002	0.0289 ± 0.02

The wettability of sand increased with the inflow due to an increase in the amount TiO₂, reaching a superhydrophobic effect with a contact angle of 165.5° at 6 mg of TiO₂, 157.3° at 5 mg of TiO₂. The increase in contact angle can be attributed to surface roughness due to the formation of a bonding of titanium parti-

cles. The contact angle of a sample was sharply decreased after 7 mg of TiO_2 , reaching 145.7° . Figure 6 demonstrates that all samples have a hydrophobic effect with a contact angle above 90° .

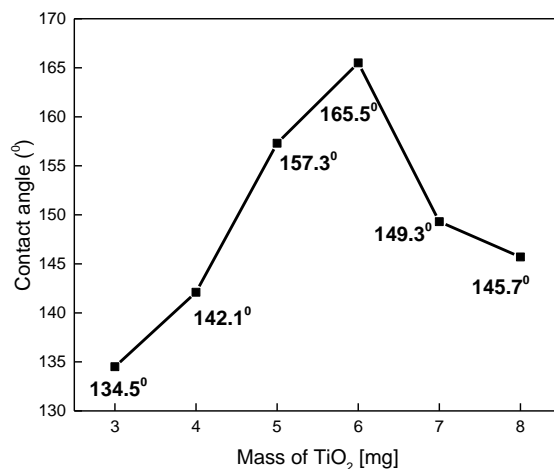


Figure 6. Dependence of contact angle on mass of TiO_2

The microstructure and surface morphology of various sands has been studied using SEM. Figure 7 shows SEM images of quartz sand before (a, b, c) and after coating PDMS (d, e, f) and PDMS/ TiO_2 (h, i, j) with different magnification. The images for micro area were confirmed effectively coating of superhydrophobic materials on the sand surface (see Figure 7 (c, f, g)). The microstructure of sand surface was changed and produced a rougher surface after applying PDMS and PDMS/ TiO_2 . The mixture of PDMS/ TiO_2 demonstrated a greater effect on superhydrophobicity. Moreover, cleaned and un-cleaned Akmol sands were imaged with SEM before and after processing with superhydrophobic materials. SEM images of cleaned (Figure 8) and uncleaned Akmol sand (Figure 9) before (a, b, c) and after coating PDMS (d, e, f), also PDMS/ TiO_2 (h, i, j) with different magnification. A smooth and uniform coating layer of superhydrophobic material can be seen in these images. Also, the effect of the cleaning process on the Akmol sand is clearly visible. Small dust and clay particles disappeared from the surface of sand after cleaning with water and difference can be seen in Figures 8 (b, c) and 9 (b, c). A clean surface provides better sticking of superhydrophobic material. For this reason, the highest contact angle was achieved from cleaned Akmol sand (the contact angle was increased from $157.3^\circ \pm 5.4^\circ$ to $165.5^\circ \pm 3.5^\circ$ after using cleaned Akmol sand).

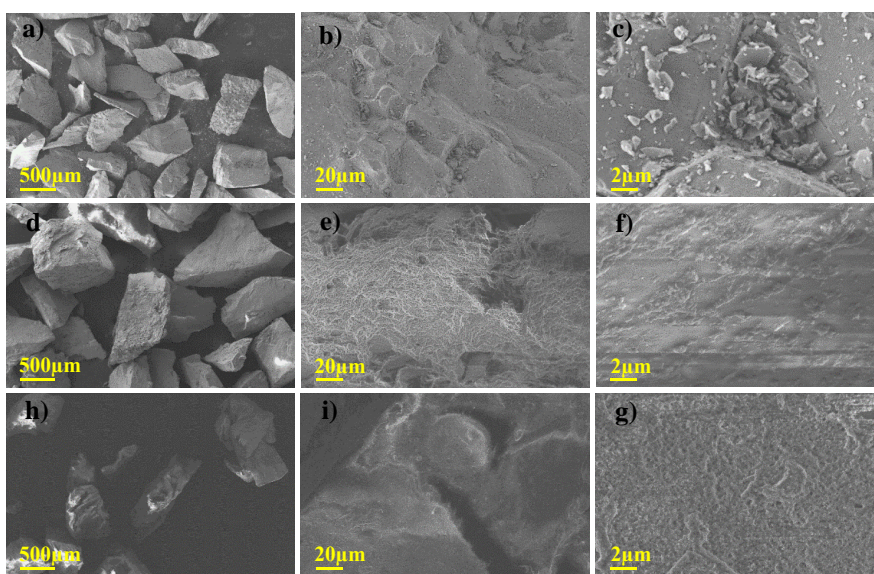


Figure 7. SEM images of quartz sand before (a, b, c) and after coating PDMS (d, e, f), also PDMS/ TiO_2 (h, i, j) with different magnification

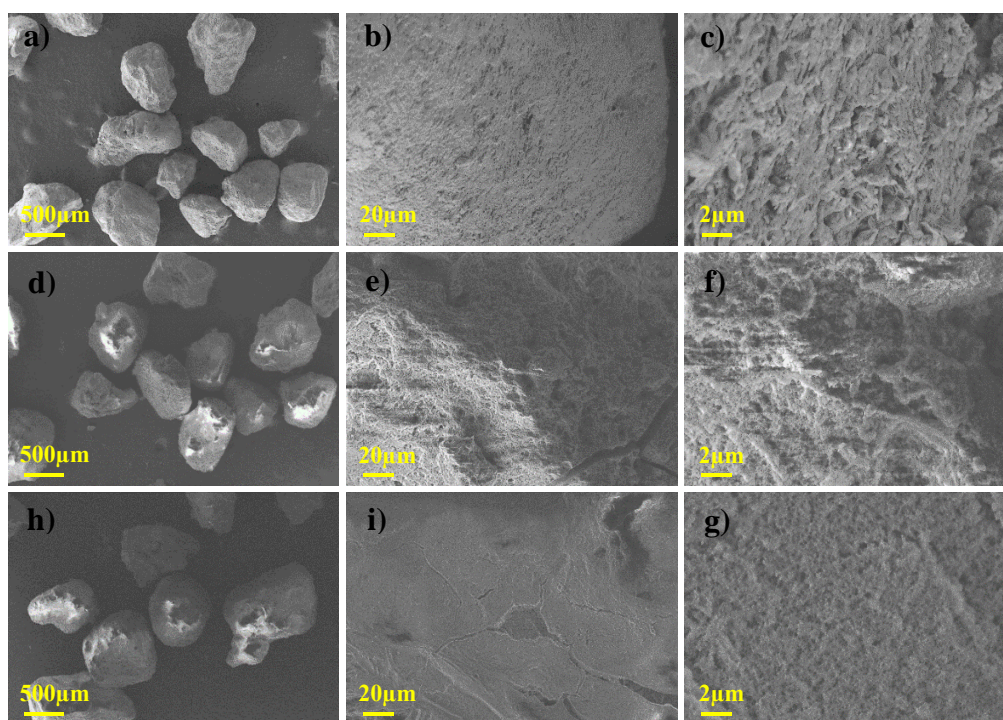


Figure 8. SEM images of uncleaned Akmol sand before (*a, b, c*) and after coating PDMS (*d, e, f*), also PDMS/TiO₂ (*h, i, j*) with different magnification

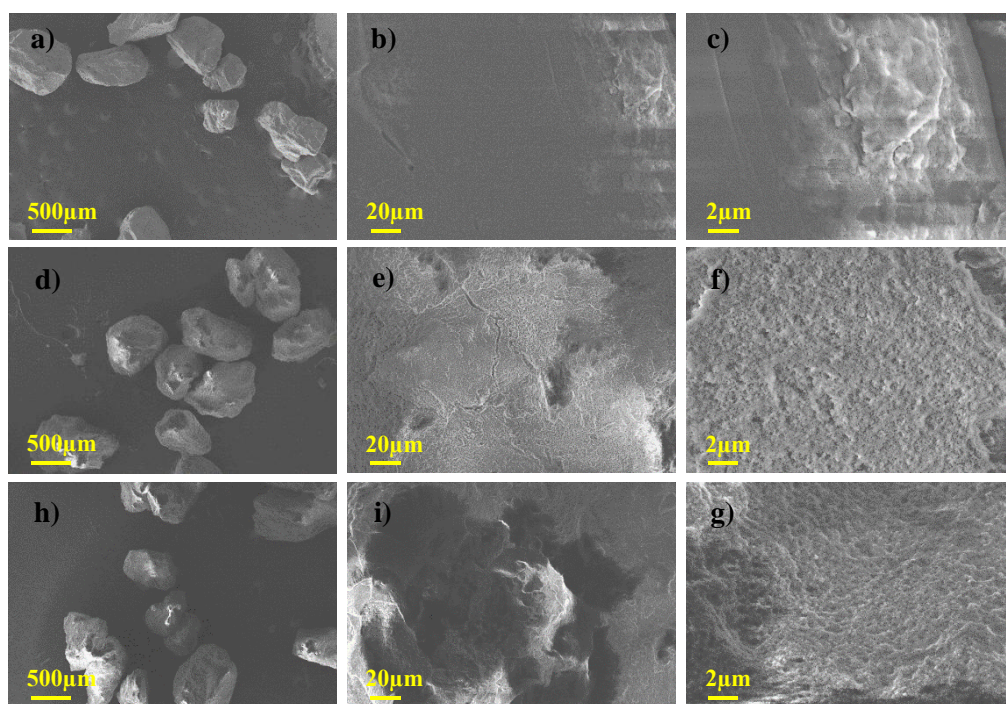


Figure 9. SEM images of cleaned Akmol sand before (*a, b, c*) and after coating PDMS (*d, e, f*), also PDMS/TiO₂ (*h, i, j*) with different magnification

Microfluidics was studied on the surfaces of superhydrophobic sand (Figure 10). The fluidity of water with blue dye on these surfaces is high with an inclination angle of 45°. These surfaces have a high self-cleaning ability because any dust or contamination can be easily removed with the water droplets at this inclination angle of 45° (Figure 11).



Figure 10. The microfluidity of water with blue dye on surfaces of superhydrophobic sands of quartz and Akmola region



Figure 11. Self-cleaning properties of superhydrophobic surfaces of quartz and Akmola region sand

The PDMS/TiO₂ coatings of quartz and uncleaned Akmola sand were placed in the lab refrigerator at low temperatures (−20 °C, −50 °C) for 72 hours. UV light (400 W) was exposed to these surfaces at room temperature for 24 hours to study the stability of their superhydrophobic properties. After exposure to low temperatures, these surfaces were warmed up to room temperatures to study contact angle properties. As seen in Figure 12, contact angle measurement demonstrates that both sands with coatings are still sable after low temperature and UV light exposure. This type of experiment was done three times to make sure that superhydrophobic properties do not change after a few cycles of temperature variety.

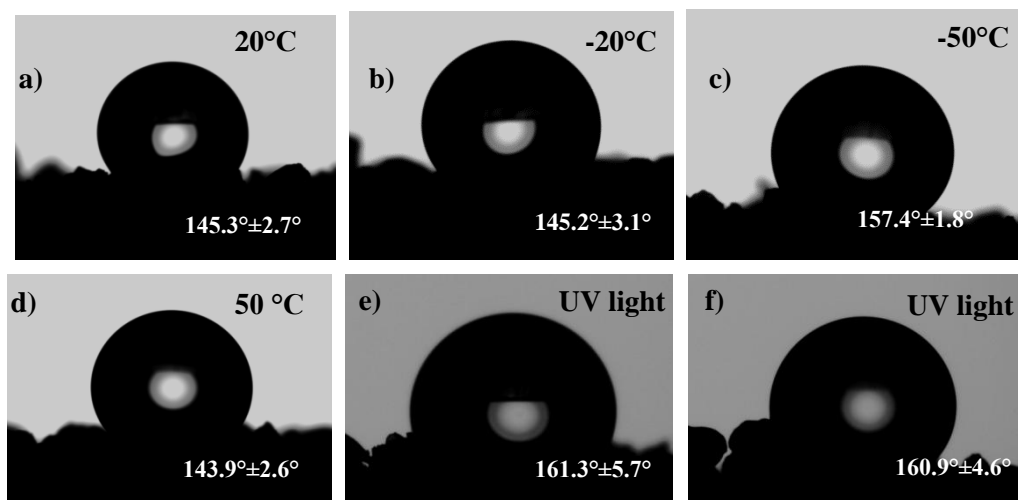


Figure 12. Contact angle measurements of quartz and uncleaned Akmola region sand with PDMS/TiO₂ coatings after exposure to low temperatures and UV light

Conclusions

Superhydrophobic self-cleaning coatings based on PDMS and PDMS/TiO₂ were synthesized using a facile chemical method. These superhydrophobic composites were applied to two different sands (quartz and sand from the Akmol region). The highest contact angle of water wetting of 165.5° was shown by the cleaned Akmol sand coated with PDMS/TiO₂, which has superhydrophobic properties.

The superhydrophobic properties of materials, such as wettability, particle size, and electrokinetic potential, were investigated. Also, these coatings demonstrated a microfluidity process on their surfaces, where the self-propelled flow is driven by the surface tension-induced pressure gradient. The superhydrophobic properties were retained after exposure to low temperatures and UV light.

These superhydrophobic self-cleaning materials by the facile method can be potentially used in construction to obtain concrete, anti-ice paving slabs, building facades, roofs, and waterproofing of buildings.

Acknowledgments

This research was funded by the Ministry of Education and Science of the Republic of Kazakhstan, grant AP08052848.

References

- 1 Si, Y., Dong, Z., & Jiang, L. (2018). Bioinspired Designs of Superhydrophobic and Superhydrophilic Materials. *ACS Central Science*, 4 (9), 1102–1112. <https://doi.org/10.1021/acscentsci.8b00504>
- 2 Ruan, M., Li, W., Wang, B., Deng, B., Ma, F., & Yu, Z. (2013). Preparation and Anti-icing Behavior of Superhydrophobic Surfaces on Aluminum Alloy Substrates. *Langmuir*, 29, 27, 8482–8491. <https://doi.org/10.1021/la400979d>
- 3 Wu, X., Silberschmidt, V.V., Hu, Z.-T., & Chen, Z. (2019). When superhydrophobic coatings are icephobic: Role of surface topology. *Surface & Coatings Technology*, 358: 207–214. <https://doi.org/10.1016/j.surfcoat.2018.11.039>
- 4 Tian, X., Verho, T., & Ras, R.H. (2016). SURFACE WEAR. Moving superhydrophobic surfaces toward real-world applications. *Science*. Apr 8; 352(6282):142–143. <https://doi.org/10.1126/science.aaf2073>.
- 5 Zhou, X., Yu, S., Jiao, S., Lv, Z., Liu, E., Zhao, Y., & Cao, N. (2019). Fabrication of superhydrophobic TiO₂ quadrangular nanorod film with self-cleaning, anti-icing properties. *Ceram. Int*, 45, 11508–11516. <https://doi.org/10.1016/j.ceramint.2019.03.020>
- 6 Xue, Y., Wang, S., Zhao, G., Taleb, A., & Jin, Y. (2019). Fabrication of Ni-Co coating by electrochemical deposition with high super-hydrophobic properties for corrosion protection. *Surface Coating Technology*, 363, 352–361. <https://doi.org/10.1016/j.surfcoat.2019.02.056>
- 7 Liang, J., Wu, X.-W., Ling, Y., Yu, S., & Zhang, Z. (2018). Trilaminar structure hydrophobic graphene oxide decorated organosilane composite coatings for corrosion protection. *Surface Coating Technology*, 339, 65–77. <https://doi.org/10.1016/j.surfcoat.2018.02.002>
- 8 Yu, L., Zhang, Z., Tang, H., & Zhou, J. (2019). Fabrication of hydrophobic cellulosic materials via gas-solid silylation reaction for oil/water separation. *Cellulose*, 26, 4021–4037. <https://doi.org/10.1007/s10570-019-02355-7>
- 9 Sun, S., Zhu, L., Liu, X., Wu, L., Dai, K., Liu, C., Shen, C., Guo, X., Zheng, G., & Guo, Z. (2018). Superhydrophobic shish-kebab membrane with self-cleaning and oil/water separation properties. *ACS Sustainable Chem. Eng*, 6, 9866–9875. <https://doi.org/10.1021/acssuschemeng.8b01047>
- 10 Nguyen, T.-B., Park, S., & Lim, H. (2018). Effects of morphology parameters on anti-icing performance in superhydrophobic surfaces. *Applied Surface Science*, 435, 585–591. <https://doi.org/10.1016/j.apsusc.2017.11.137>
- 11 Qi, Y., Chen, S., & Zhang, J. (2019). Fluorine modification on titanium dioxide particles: Improving the anti-icing performance through a very hydrophobic surface. *Appl. Surf. Sci*, 476, 161–173. <https://doi.org/10.1016/j.apsusc.2019.01.073>
- 12 Barkhudarov, P.M., Shan, P.B., Watkins, E.B., Doshi, D.A., Brinker, C.J., & Majewski, J. (2008). Corrosion inhibition using superhydrophobic films. *Corrosion Science*, 50, 897–902. <https://doi.org/10.1016/j.corsci.2007.10.005>
- 13 Ishizaki, T., & Saito, N. (2010). Rapid formation of a superhydrophobic surface on a magnesium alloy coated with a cerium oxide film by a simple immersion process at room temperature and its chemical stability. *Langmuir*, 26, 9749–9755. <https://doi.org/10.1021/la100474x>
- 14 Zhang, F., Chen, S., Dong, L., Lei, Y., Liu, T., & Yin, Y. (2011). Preparation of superhydrophobic films on titanium as effective corrosion barriers. *Appl. Surf. Sci*, 257, 2587–2591. <https://doi.org/10.1016/j.apsusc.2010.10.027>
- 15 Dong, H., Ye, P., Zhong, M., Pietrasik, J., Drumright, R.E., & Matyjaszewski, K. (2010). Superhydrophilic surfaces via polymer-SiO₂ nanocomposites. *Langmuir*, 26, 15567–15573. <https://doi.org/10.1021/la102145s>
- 16 Lu, X., Wang, Z., Yang, X., Xu, X., Zhang, L., Zhao, N., & Xu, J. (2011). Antifogging and antireflective silica film and its application on solar modules. *Surface Coating Technology*, 206, 1490–1494. <https://doi.org/10.1016/j.surfcoat.2011.09.031>
- 17 You, J.-H., Lee, B.-I., Lee, J., Kim, H., & Byeon, S.-H. (2011). Superhydrophilic and antireflective La(OH)₃/SiO₂-nanorod/nanosphere films. *J. Coll. Interf. Sci*, 354, 373–379. <https://doi.org/10.1016/j.jcis.2010.10.009>

- 18 Jung, S., Tiwari, M.K., Doan, N.V., & Poulikakos, D. (2012). Mechanism of supercooled droplet freezing on surfaces. *Nat. Comm.*, 3, 615. <https://doi.org/10.1038/ncomms1630>
- 19 Tourkine, P., Le Merrer, M., & Quèrè, D. (2009). Delayed freezing on water repellent materials. *Langmuir*, 25, 7214–7216. <https://doi.org/10.1021/la900929u>
- 20 Meuler, A.J., Smith, J.D., Varanasi, K.K., Mabry, J.M., McKinley, G.H., & Cohen, R.E. (2010). Relationships between water wettability and ice adhesion. *ACS Appl. Mater. Interf.*, 2, 3100–3110. <https://doi.org/10.1021/am1006035>
- 21 Gui, X., Li, H., Wang, K., Wei, J., Jia, Y., Li, Z., Fan, L., Cao, A., Zhu, H., & Wu, D. (2011). Recyclable carbon nanotube sponges for oil absorption. *Acta Mater.*, 59, 4798–4804. <https://doi.org/10.1016/j.actamat.2011.04.022>
- 22 Pan, Q., Wang, M., & Wang, H. (2008). Separating small amount of water and hydrophobic solvents by novel superhydrophobic copper meshes. *Appl. Surf. Sci.*, 254, 6002–6006. <https://doi.org/10.1016/j.apsusc.2008.03.034>
- 23 Wang, C., Yao, T., Wu, J., Ma, C., Fan, Z., Wang, Z., Cheng, Y., Lin, Q., & Yang, B. (2009). Facile approach in fabricating superhydrophobic and superoleophilic surface for water and oil mixture separation. *ACS Appl. Mater. Interf.*, 1, 2613–2617. <https://doi.org/10.1021/am900520z>
- 24 Wen, Q., Di, J., Jiang, L., Yu, J., & Xu, R. (2013). Zeolite-coated mesh film for efficient oil–water separation. *Chem. Sci.*, 4, 591–595. <https://doi.org/10.3866/PKU.WHXB201906044>
- 25 Blossey, R. (2003). Self-cleaning surfaces — virtual realities. *Nature Mater.*, 2, 301–306.
- 26 Liu, K., & Jiang, L. (2011). Multifunctional integration: from biological to bio-inspired materials. *ACS Nano*, 5, 6786–6790. <https://doi.org/10.1021/nn203250y>
- 27 Parkin, I.P., & Palgrave, R.G. (2005). Self-cleaning coatings. *J. Mater. Chem.*, 15, 1689–1695.
- 28 Sanchez, C., Arribart, H., & Guille, M.M.G. (2005). Biomimetism and bioinspiration as tools for the design of innovative materials and systems. *Nat. Mater.*, 4, 277–288. <https://doi.org/10.1038/nmat1339>
- 29 Lifton, V.A., Simon, S., & Frahm, R.E. (2005). Reserve battery architecture based on superhydrophobic nanostructured surfaces. *Bell Labs Tech. J.*, 10, 81–85. <https://doi.org/10.1002/bltj.20105>
- 30 Andreeva, N., Ishizaki, T., Baroch, P., & Saito, N. (2012). High sensitive detection of volatile organic compounds using superhydrophobic quartz crystal microbalance. *Sens. Actuators B*, 164, 15–21. <https://doi.org/10.1016/j.snb.2012.01.051>
- 31 Cho, D.J., Kim, S.E., Seo, E., Lee, M.C., Lee, J.M., & Ko, J.S. (2013). Underwater micro gas detector. *Sens. Actuators B*, 188, 347–353.
- 32 Zhu, H., Chen, D., Li, N., Xu, Q., Li, H., He, J., & Lu, J. (2017). Dual-layer copper mesh for integrated oil–Water separation and water purification. *Appl. Catal. B*, 200, 594–600. <https://doi.org/10.1016/j.apcatb.2016.07.028>
- 33 Lin, C.-Y., Andrew Lin, K.-Y., Yang, T.-W., Chen, Y.-C., & Yang, H. (2017). Self-assembled hemispherical nanowell arrays for superhydrophobic antireflection coatings. *J. Colloid Interface Sci.*, 490, 174–180. <https://doi.org/10.1016/j.jcis.2016.11.064>
- 34 Carpi, F., Gallone, G., Galantini, F., & De Rossi, D. (2008). Silicone-Poly(hexylthiophene) blends as elastomers with enhanced electromechanical transduction properties. *Adv. Funct Mater.*, 18, 235–242. <https://doi.org/10.1002/adfm.200700757>

О. Тоқтарбайұлы, А. Курбанова, О. Уалибек, А. Сералин,
Т. Жунусова, Г. Сугурбекова, Н. Нурадже

Жеңіл әдіспен төмен температура мен ультракүлгін сәулесінің әсерінен кейін тұрақты супергидрофобты өзін-өзі тазартатын жабындарды дайындау

Өзін-өзі тазартатын гидрофобты беттер лотос эффектісі ашылғаннан кейін соңғы бірнеше онжылдықта қоғамның назарын өзіне аударды. Лотос гүлінің жапырақтарының салыстырмалы түрде лайлы жерлерде таза болып қалуы және жаңбыр кезінде өзін-өзі тазарту қабілеті жаңа материалдар мен бет құрылымының модификациясын дамытуға әкелді. Мұндай ақылды жабыны бар беттер көк тіреген ғимараттарда, зәулім ғимараттарда және т.б. пайдаланған кезде экономикалық әлеуетке ие болуы мүмкін. Беттің гидрофобты болуының екі негізгі критерийі — бұл беттің кедір-бұдырлығы және жабын материалының төмен беттік энергиясы. Осы зерттеуде супергидрофобты өзін-өзі тазартатын жабындар полидиметилсилоксан (ПДМС) және TiO_2 нанобөлшектері сияқты оңай қол жетімді материалдарды пайдалана отырып, қарапайым, жеңіл және арзан әдіспен дайындалды және тікелей пайдалану үшін толығымен сипатталған. ПДМС байланыстырушы қабат болып табылады, ал TiO_2 нанобөлшектері супергидрофобтылықты тудыратын кедір-бұдыр түзуге арналған армиленген композитке ие. Сипаттама жаңадан дайындалған супергидрофобты жабынның сумен жанасу бұрышы $165,5^\circ$ дейін, сырғанау бұрышы 5° -ден аз екенін көрсетті. Сонымен қатар өзін-өзі тазарту және беттік микрофлюидтік қасиеттері зерттелді. Бұл жабындардың супергидрофобты қасиеттері оның бетіне төмен температура мен ультракүлгін сәулесінің әсерінен кейін де өзгермейді. СЭМ суреттері шыны және құм түйіршіктерінде алынған беттің өрескел құрылымын растайды.

Кілт сөздер: супергидрофобты жабын, супергидрофобты құм, полидиметилсилоксан, титан оксидінің нанобөлшектері, шеттік бұрышы, УК–сәулелену, жеңіл әдіс, электрокинетикалық потенциал.

О. Токтарбайулы, А. Курбанова, О. Уалибек, А. Сералин,
Т. Жунусова, Г. Сугурбекова, Н. Нурадже

Получение супергидрофобных самоочищающихся покрытий легким методом: устойчивых к воздействию низких температур и ультрафиолетового излучения

За последние несколько десятков лет самоочищающиеся гидрофобные поверхности привлекли обширное внимание после открытия эффекта лотоса. Способность листьев цветка лотоса сохранять чистоту в относительно грязных местностях и самоочищаться во время дождей направила к развитию новых материалов и модификации структуры поверхности. Поверхность с таким умным покрытием может иметь экономический потенциал в случае использования на небоскрёбах, высотных зданиях и т.д. Два главных критерия поверхности для обладания гидрофобности — это шероховатость поверхности и низкая поверхностная энергия покрываемого материала. В этом исследовании супергидрофобные самоочищающиеся покрытия были получены простым, легким и дешевым методом с использованием легкодоступных материалов, таких как полидиметилсилоксан (ПДМС) и наночастицы TiO_2 , и полностью охарактеризованы для прямого применения. ПДМС представляет собой связующий слой, а наночастицы TiO_2 — армированный композит для формирования шероховатости, проявляющей супергидрофобность. Характеристика показала, что свежеприготовленное супергидрофобное покрытие имеет угол смачивания водой до $165,5^\circ$ при угле скольжения менее 5° . Также были изучены самоочищающиеся и поверхностные микрожидкостные свойства. Супергидрофобные свойства этих покрытий не меняются даже после воздействия на их поверхность низких температур и УФ-излучения. Изображения СЭМ подтверждают шероховатую структуру полученной поверхности на стекле и песчинках.

Ключевые слова: супергидрофобное покрытие, супергидрофобный песок, полидиметилсилоксан, наночастицы оксида титана, краевой угол, УФ-излучение, фасильный метод, электрокинетический потенциал.

Information about authors*

Toktarbaiuly, Olzat (*corresponding author*) — PhD in Physical Sciences, Researcher, National Laboratory Astana, Nazarbayev University, Kabanbay batyr avenue, 53, 010000, Nur-Sultan, Kazakhstan; e-mail: olzat.toktarbaiuly@nu.edu.kz; <https://orcid.org/0000-0003-4594-3435>;

Kurbanova, Aliya — Master of Chemical Sciences, Junior Researcher, National Laboratory Astana, Nazarbayev University, Kabanbay batyr avenue, 53, 010000, Nur-Sultan, Kazakhstan; e-mail: aliya.kurbanova@nu.edu.kz; Scopus ID 57208865374; <https://orcid.org/0000-0002-1261-4582>;

Ualibek, Oral — PhD in Physical Sciences, Researcher, National Laboratory Astana, Nazarbayev University, Kabanbay batyr avenue, 53, 010000, Nur-Sultan, Kazakhstan; e-mail: oral.ualibek@nu.edu.kz; Scopus ID 57116439500; <https://orcid.org/0000-0002-8482-3623>;

Seralin, Aidar — PhD in Pharmaceutical Sciences, Junior Researcher, National Laboratory Astana, Nazarbayev University, Kabanbay batyr avenue, 53, 010000, Nur-Sultan, Kazakhstan; e-mail: aidar.seralin@nu.edu.kz; <https://orcid.org/0000-0001-6001-5755>;

Zhunossova, Tomiris — Master of Physical Sciences, Consultant, National Laboratory Astana, Nazarbayev University, Kabanbay batyr avenue, 53, 010000, Nur-Sultan, Kazakhstan; e-mail: zhunossovatomiris1@gmail.com; <https://orcid.org/0000-0002-4189-1618>;

Sugurbekova, Gulnar — Doctor of Chemical Sciences, Leading Researcher, LLP “EcoStandart.kz”, Technopark of Nazarbayev University, Kabanbay batyr avenue, 53, 010000, Nur-Sultan, Kazakhstan; e-mail: sugurbekova.g.55@gmail.com; <https://orcid.org/0000-0002-6894-7247>;

Nuraje, Nurxat — Doctor of Chemical Sciences, Associate Professor, National Laboratory Astana, Nazarbayev University, Kabanbay batyr avenue, 53, 010000, Nur-Sultan, Kazakhstan; e-mail: nurxat.nuraje@nu.edu.kz; <https://orcid.org/0000-0003-4751-2719>

*The author's name is presented in the order: *Last Name, First and Middle Names*

C.Y. Wu¹, W.Q. Ling², Y.C. Yao², M. Guo^{2*}, N. Nuraje³

¹College of Forestry, Tarim University, A'ler, Xinjinag, China;

²College of Chemistry and Materials Engineering, Zhejiang Agriculture & Forestry University, Hangzhou, Zhejiang, China;

³School of Engineering & Digital Science, Nazarbayev University, Nur-Sultan, Kazakhstan

(*Corresponding author's e-mail: guoming@zafu.edu.cn)

Three-Dimensional Fingerprint Spectroscopy Study on the Biopolymer System of Polyphenol Oxidase Binding with Cumalic Acid

The protection of Cumalic acid (CA), antioxidant, in the biochemical process in nature has aroused great interest. Polyphenol oxidase (PPO), an enzyme, plays a vital function in aging and browning of plants, such as vegetables, fruits, and mushrooms. The interaction of CA and PPO reveals the important information in metabolism and aging. Thus, the molecular mechanism of CA binding with polyphenol oxidase (PPO) was explored by combining spectroscopic methods with molecular modeling. A three-dimensional fingerprint of the CA-PPO complex was built for the first time to characterize the biopolymer interaction between CA and PPO. Application of the spectroscopic methods indicated that CA effectively quenched the intrinsic fluorescence of PPO. The enthalpy change (ΔH°) and entropy change (ΔS°) suggested that the CA-PPO complex was predominantly stabilized by hydrophobic interactions CA and PPO. Building the λ -UV-F fingerprint of CA-PPO made it possible to demonstrate the three-dimensional interactions between CA and PPO. Subsequently, molecular modeling demonstrated that CA was primarily bound to PPO by hydrophobic interactions and hydrogen bonds located at amino acid residues Ala202, His38, His54, and Ser206. The computational simulations were consistent with the spectral experiments demonstrating confidence in the three-dimensional model determined of the CA-PPO interaction.

Keywords: biopolymer, Cu-containing enzyme, coumaric acid, polyphenol oxidase, antioxidant, α -pyrone-5-carboxylic acid, spectroscopy, tyrosinase, molecular modeling.

Introduction

Polyphenol oxidase (PPO) is a multifunctional Cu-containing enzyme, which is also called tyrosinase and is found widely in living organisms, such as vegetables, fruits, and mushrooms [1, 2]. It is a paramount substance in the process of browning of fruits after contact with the oxygen in the air which occurs after damaged or long-term storage [3, 4]. The enzyme PPO is also involved in the production of melanin [5]. Specifically, PPO is involved in the formation of the melanin shield protecting plants from external stress.

The biochemical properties of phenolic resins have been extensively studied. They are reported to have antioxidants, anti-carcinogenic and other properties [6]. Due to the various pharmacological properties, antioxidants have been of great interest in recent years. The main mechanism proposed may play a protective role through the transfer of H atoms, single electron transfer, and metal chelation [7]. Cumalic acid (CA), also known as α -pyrone-5-carboxylic acid, is such an antioxidant (Figure 1). This antioxidant, CA, is the main active component of mature spores of tomato and lygodium japonicum plants [8]. It is also a potential candidate in the field of antioxidant, antibacterial and antiviral research [9]. According to the studies, both CA and PPO consist in the same plants and have effects on the metabolism of plants [10, 11]. Recently, several studies have been published related to molecular modeling studies of PPO [12–14]. However, research about interaction mechanism between CA and PPO has not yet been conducted.

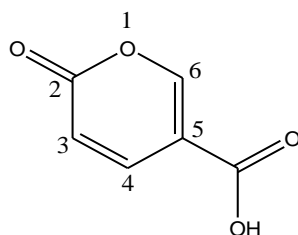


Figure 1. The structure of Cumalic acid

Rosario Goyeneche, Yue-Xiu Si, Mareike E. Dirks-Hofmeister, and many other professors have reported that PPO is associated with the active ingredient in plant tissues [15–17]. At present, some researchers mostly pay attention to the active molecule interactions with enzymes on the binding reaction between animal's protease and drug molecules [18–20], while others are focused on the reactive molecules inhibited enzyme activity [21, 22]. There are a plethora of investigations on the enzyme interactions and enzyme inhibitions in animals and humans because enzymes are one of the most important targets for drugs to exert effects on the body. However, there are a few studies on the interaction between plant enzymes and active plant components. Thus, it will be important to understand in more detail how plant processes such as aging or browning may affect enzyme activities.

Many research literature show that fluorescence and UV-*vis* absorption spectroscopy techniques are powerful tools for studying important data of complexes. The values of wavelength (λ), fluorescence intensity (F), and ultraviolet absorption (A) can be extracted from the spectral experiment, which helps to draw a three-dimensional fingerprint of $\lambda \sim F \sim A$ and analyze the fingerprint peaks to obtain the interaction characteristics of small molecules and enzymes. Therefore, the construction of traditional Chinese medicine fingerprint can primarily reflect the species and quantity of chemical composition in traditional Chinese medicine, and make an integral description and evaluation of the quality of medicine [23]. Based on the construction principle of traditional Chinese medicine fingerprint and spectrum experiment skills, we get and extract the absorption spectrum and emission spectrum data of CA binding with PPO.

In this work, fluorescence and UV-*vis* absorption spectroscopy are measured to detect the interaction mechanism between CA and PPO. The λ -UV-F fingerprint is built to analyze characteristic fingerprint peaks in the CA-PPO fingerprint chromatogram, which aims to explore and reveal the binding between CA and PPO. The molecular modeling is also constructed to explain and support data from the spectral experiment. We believe these findings will be useful for pharmaceutical research, especially for the synthesis and design of CA derivatives with enhanced activity.

Experimental

Reagents and Materials

$1.0 \times 10^{-6} \text{ mol} \cdot \text{L}^{-1}$ of PPO (3130 units/mg) (Sigma Chemical USA) in phosphate-buffered saline (PBS, pH 6.5) at CA ($\geq 97\%$) (Energy Chemical Shanghai), and $1.0 \times 10^{-4} \text{ mol} \cdot \text{L}^{-1}$ in ethanol were prepared separately. Ultrapure water was used to prepare for the above solutions. All chemicals are of analytical grade.

Spectroscopic techniques which were used to measure fluoresce and absorption include the F-7000 spectrofluorophotometer (Hitachi, Japan) and UV-2450 UV-*vis* spectrometer (Shimadzu, Japan). A BS224 Selectronic analytic weighing scale (Sartorius, China) was used to obtain the precise amount of the samples for experiment.

Experimental procedure for spectroscopic measurement

The absorption spectra of PPO in the presence of CA ranging from 0 to $5.6 \times 10^{-6} \text{ mol} \cdot \text{L}^{-1}$ were measured in the range of 200–800 nm at room temperature. The conditions for fluorescence measurement were set at 291 K, 300 K, and 308 K. The emission spectra were recorded in the wavelength range of 250–500 nm upon excitation at 282 nm with a scanning speed of 1200 nm/min. The widths of both the excitation slit and emission slit were set to 5 nm. The fluorescence emission spectra of PPO were recorded in the absence and presence of increasing concentrations of CA, corresponding to 0×10^{-6} , 0.4×10^{-6} , 0.8×10^{-6} , 1.0×10^{-6} , 1.8×10^{-6} , 2.4×10^{-6} , 3.2×10^{-6} , 4.0×10^{-6} , 4.8×10^{-6} , $5.6 \times 10^{-6} \text{ mol} \cdot \text{L}^{-1}$. Subtract the appropriate blank corresponding to the buffer to correct the fluorescent background.

λ -UV-F fingerprint

The three-dimensional fingerprint of the CA-PPO complex was built using emission wavelength, intensity of fluorescence, and UV absorption values from the CA-PPO spectral experiments. The interaction characteristics of the CA-PPO system were obtained by analyzing the peak distributions of fingerprint spectrum.

Molecular modeling: blind docking simulation

PPO (tyrosinase) belongs to the oxidase superfamily protein [24, 25]. To understand the basic mechanism of PPO and CA interaction, in the experiment, the docking mode of CA was checked at the catalytic site of PPO. The binding site was fixed near the three fluorophores (Trp, Tyr, and Phe) under the guidance of a fluorescence experiment. The three-dimensional structure of PPO was obtained from the Protein Data Bank (PDB ID: 1WX2). The CA structure was built using ChemDraw Ultra 8.0 software. For the docking of CA with PPO, the required files for ligand (CA) were created through Gaussian. The following steps taken for

the docking process were: (1) conversion of the 2D structure to a 3D structure; (2) addition of hydrogen atoms; (3) calculation of charges, and (4) location of pockets. The PyMOL software package was used for the visualization of the docked conformations. Finally, all experimental data calculations from our work were performed on a Silicon Graphics Ocatane2 workstation.

Calculation equations

Dynamic quenching is the mechanism of fluorescence quenching. The calculation is disclosed as follows [26]:

$$\frac{F_0}{F} = 1 + K_{sv}[Q] = 1 + K_q\tau_0[Q], \quad (1)$$

where K_q , K_{sv} , τ_0 and $[Q]$ — the quenching rate constant of the biomolecule, the dynamic quenching constant, the average lifetime of molecule without quencher and the concentration of quencher, respectively.

The K_{sv} and dynamic quenching parameters of CA and PPO can be obtained from the experimental data by using the calculated equation (1). For the fluorescence lifetime of the biopolymer is 10^{-8} s, the quenching constant K_q ($L \cdot mol^{-1} \cdot s^{-1}$) can be obtained from $K_q = K_{sv} / \tau_0$.

For static quenching interaction, experimental numerical calculation and determination can be performed according to formula (2) [27, 28]:

$$\lg[(F_0 - F)/F] = \lg K + n \lg [Q]. \quad (2)$$

Among them, F_0 , F , and $[Q]$ are the same as defined in formula (1), K is the binding constant in CA and PPO, and n is the number of binding sites in each PPO molecule, and it can be determined by the slope and intercept of double logarithm regression curve of $\lg [(F_0 - F)/F]$ vs. $\lg [Q]$ based on Equation (2) (Figure 4).

The thermodynamic parameters of CA-PPO are calculated by the van't Hoff equation:

$$\ln K = \frac{-\Delta H^\circ}{RT} + \frac{\Delta S^\circ}{R}, \quad (3)$$

$$\Delta G^\circ = \Delta H^\circ - T\Delta S^\circ, \quad (4)$$

where R — the universal gas constant, K at temperature T ; T — the Kelvin temperature (291 K, 300 K, and 308 K).

In this research work, we calculated the energy transfer efficiency E based on the Förster's non-radioactive energy transfer theory. For the distance r , we calculated the distance from the ligand to the protein tryptophan residue, and R_0 is the Förster critical distance, at which 50 % of the excitation energy is transferred to the receptor. It can be calculated by using formula (5):

$$E = 1 - \frac{F}{F_0} = \frac{R_0^6}{(R_0^6 + r^6)}, \quad (5)$$

$$R_0^6 = 8.8 \times 10^{-25} K^2 N^{-4} \phi J \quad (6)$$

where $K^2 = 2/3$, $N = 1.336$, $\phi = 0.118$, J — the overlap integral of the fluorescence emission spectrum of the donor and that of the absorption spectrum of the acceptor.

Therefore,

$$J = \int_0^\infty F(\lambda)\varepsilon(\lambda)\lambda^4 d\lambda / \int_0^\infty F(\lambda)d\lambda \quad (7)$$

where $F(\lambda)$ — the fluorescence intensity of the fluorescent donor at wavelength λ , $\varepsilon(\lambda)$ — the molar absorptivity of the acceptor at wavelength λ .

Results and Discussion

UV and fluorescence spectra of PPO in the presence of CA

In the UV-Vis absorption spectrum of PPO (Figure 2A), we observed a double absorption peak, but the peaks that appeared earlier in the study are generally ignored. Therefore, the maximum absorption peak of PPO is between 300 nm and 350 nm, and a red shift occurs, indicating that the existing CA ring molecular structure makes the system's hydrophobicity lower. The preliminary results indicated the formation of CA-PPO complex. In addition, because PPO molecules contain tryptophan, tyrosine, and phenylalanine, they have endogenous fluorescence (between 300 and 500 nm). When the excitation wavelength (λ_{ex}) is 282 nm, the maximum emission wavelength of PPO is about 351 nm. At this time, the fluorescence of PPO mainly comes from tryptophan residues.

At different concentrations of CA (1 to 10 in Figure 2B), the shape of the fluorescence spectrum of PPO did not change. As the concentration of CA increases, the maximum fluorescence emission peak of PPO red-shifts at 349 nm, indicating that the microenvironment of tryptophan (TRP) residues is reduced in hydrophobicity [29]. The increase in CA concentration leads to the contraction of the peptide chain near the binding site, and the hydrophobicity of the surrounding environment increases. The experimental results of different changes in the fluorescence spectrum and ultraviolet-visible spectrum show that there is an interaction between CA and PPO. Figure 2 shows that CA has no peak at the peak position of PPO and has no influence on the CA-PPO system.

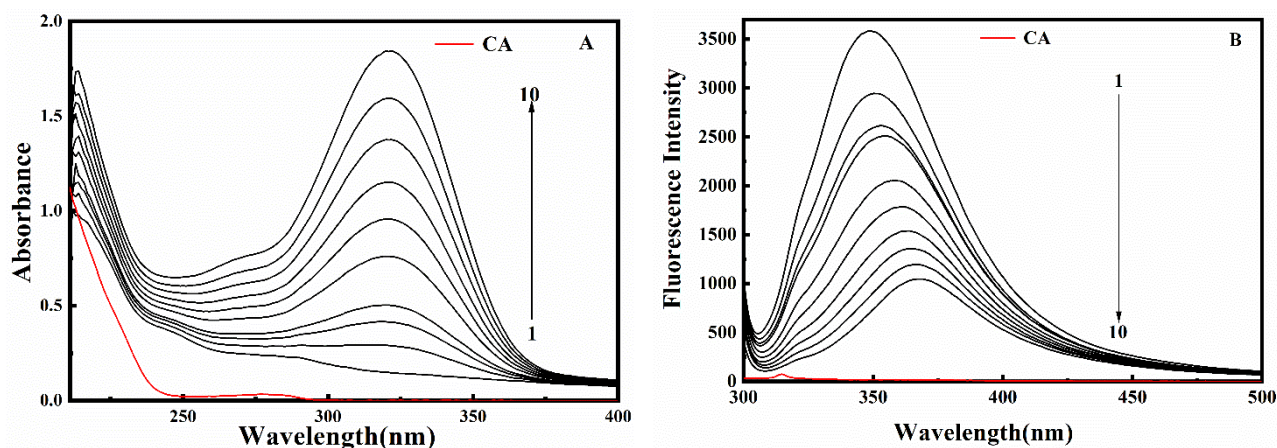
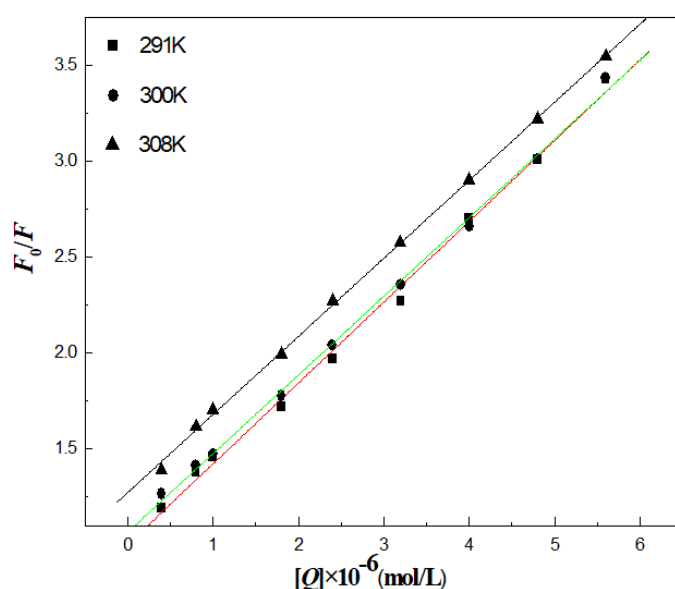


Figure 2. UV absorption spectra (A) and fluorescence spectra (B) of PPO in PBS solution in presence of various CA concentrations corresponding to 0×10^{-6} , 0.4×10^{-6} , 0.8×10^{-6} , 1.0×10^{-6} , 1.8×10^{-6} , 2.4×10^{-6} , 3.2×10^{-6} , 4.0×10^{-6} , 4.8×10^{-6} , 5.6×10^{-6} mol·L⁻¹ from 1 to 10; pH = 6.5; $c_{(ppo)} = 1.0 \times 10^{-6}$ mol·L⁻¹

Quenching mechanism of PPO with CA

It can be seen from Figure 2B that as the concentration of CA increases, the fluorescence of tryptophan residues decreases, which can be explained why the compound is formed from CA and PPO. If the process of fluorescence quenching is dynamic quenching, then it can be described by an equation (1).



(■ — 291K; ● — 300K; ▲ — 308K). $c_{(ppo)} = 1.0 \times 10^{-6}$ mol·L⁻¹; pH = 6.5; $\lambda_{ex} = 282$ nm

Figure 3. The Stern-Volmer plot of PPO quenched by CA

Table 1

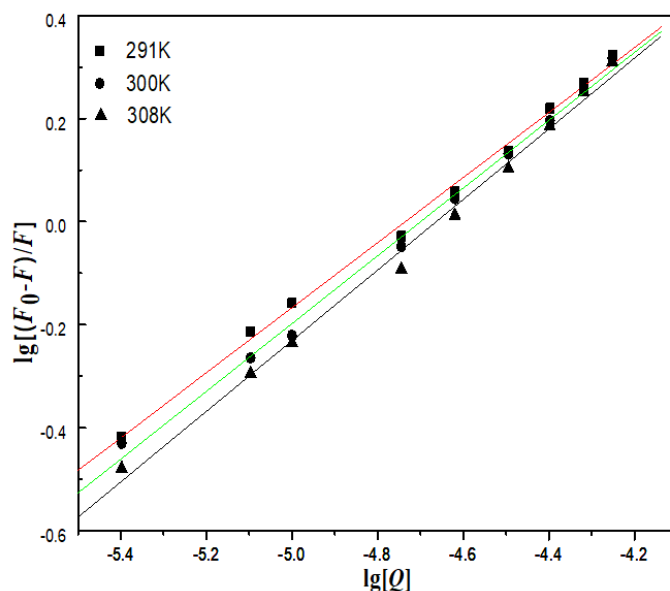
The parameters of the Stern-Volmer plots for the quenching of PPO by CA at 291 K, 300 K, and 308 K

System	$T(K)$	$K_{sv}(L \cdot mol^{-1})$	$K_q(L \cdot (mol \cdot s)^{-1})$	R	SD
CA-PPO	291	4.22×10^4	4.22×10^{12}	0.99812	0.05127
	300	4.18×10^4	4.18×10^{12}	0.99882	0.04029
	308	3.23×10^4	3.23×10^{12}	0.99958	0.01850

The experimental results in Figure 3 and Table 1 indicate that the quenching curves of CA and PPO are different at different experimental temperatures. The curve obtained at each experimental temperature shows a good linear relationship between F_0/F and Q ($R_{291}, R_{300}, R_{308} > 0.99$), which illustrates the uniformity of static quenching. In addition, because the rate constant of CA-induced PPO is much larger than the K_q value of the dispersion process $2.0 \times 10^{10} L \cdot (mol \cdot s)^{-1}$ [19], in this experiment, quenching was not initiated by dynamic quenching, but it was caused by static quenching. In this process, compounds are formed. All the above data and results confirm that quenching between substances was caused by static quenching.

Binding constant and binding sites of PPO with CA

The value of the static quenching interaction can be obtained from equation (2). The results are shown in Figure 4 and Table 2.



$C(\text{polyphenol oxidase}) = 1.0 \times 10^{-6} \text{ mol} \cdot \text{L}^{-1}$; $\text{pH} = 6.5$; $\lambda_{\text{ex}} = 282 \text{ nm}$

Figure 4. Plots of $\lg[(F_0-F)/F]$ vs. $\lg[Q]$ for CA-PPO

Table 2

The binding constants K , binding sites n and the thermodynamic parameters of CA-PPO system

System	$T(K)$	$K(L \cdot mol^{-1})$	n	R	$\Delta G^\circ(kJ \cdot mol^{-1})$	$\Delta H^\circ(kJ \cdot mol^{-1})$	$\Delta S^\circ(J \cdot (mol \cdot K)^{-1})$
CA-PPO	291	2.45×10^4	0.95	0.9983	-26.08	28.66	188.09
	300	1.86×10^4	0.92	0.9978	-27.21		
	308	1.58×10^3	0.69	0.9970	-29.27		

The n value of CA-PPO complex in Table 2 is approximately equal to 1, indicating that there is one binding site in PPO for CA during their interactions. In Table 2, the binding constants are shown as a straight line at the three test temperatures. The higher the substance concentration, the lower the K value, shows that the test temperature has an influence on it.

Thermodynamic parameters and binding Forces

The sign and size of the parameters related to the drug-protein interaction process (such as ΔH° and ΔS°) can be used as some potential tools for deciphering the activation binding force [30, 31]. The calculated thermodynamic parameters collected in Table 2 show that $\Delta H^\circ > 0$, $\Delta S^\circ > 0$ (According to the relative magnitudes of thermodynamic enthalpy change ΔH° and entropy change ΔS° before and after the reaction, the main force types between small molecules and proteins can be judged [32]: when $\Delta S^\circ > 0$, it may be hydrophobic and electrostatic forces. $\Delta S^\circ < 0$ may be hydrogen bonding and van der Waals force, $\Delta H^\circ > 0$, $\Delta S^\circ > 0$ is a typical hydrophobic force; $\Delta H^\circ < 0$, $\Delta S^\circ < 0$ is mainly hydrogen bonding and van der Waals force), which manifest that the predominance of hydrophobic forces as the responsible factor for CA-PPO binding. This inference is well supported from blind docking simulation result which shows a hydrophobic force between the two molecules.

Energy transfer from PPO to CA

From Equation (5), Equation (6) and Equation (7), the following data was obtained: $E = 0.708$, $J = 1.11 \times 10^{-14} \text{ (cm}^3 \cdot \text{L)} \cdot \text{mol}^{-1}$, $R_0 = 2.46 \text{ nm}$, and $r = 2.13 \text{ nm}$ for the CA-PPO system. The donor-acceptor distances (r) of above CA-PPO system was less than 7 nm [33, 34], suggesting that the energy transfer from PPO to CA occurred with high probability. The distance values here are a theoretical value [35].

Three-dimensional fingerprint study

The three-dimensional spectrum of fluorescence intensity-absorbance-wavelength of CA-PPO system is preliminary constructed based on fingerprint construction technology (Figure 5). λ -UV-F fingerprint showed 4 characteristic peaks (Table 3).

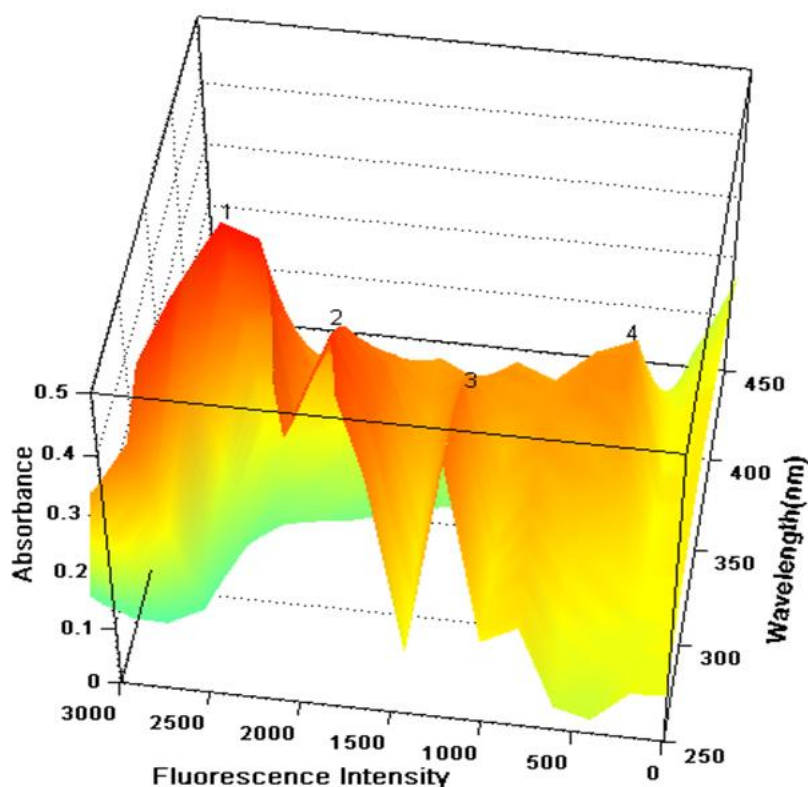


Figure 5. The three-dimensional spectra of wavelength-fluorescence intensity-absorbance ($C_{CA} : C_{PPO} = 1:1$)

Table 3

The data information of the CA-PPO three-dimensional fingerprint

Peak numbers	1	2	3	4
Absorbance(A)	0.164	0.298	0.372	0.1
Fluorescence intensity(F)	2511	2188	1288	2433
$F \times A$ (%)	4.12	6.52	4.79	2.43

effective fluorescence quenching of PPO emission in the presence of CA. Spectrum experiment results showed that the microdomain of the PPO tryptophan residues and CA have obvious interactions with each other. The distance between PPO tryptophan (the donor) and CA (the acceptor) obtained from the fluorescence quenching experiment is nearly 2 nm. This distance measurement was corresponding to the combined distance measured by docking, which fully provides evidence that CA can quench the fluorescence spectra of PPO.

As shown in Figure 6B, the hydrophobic cavity in PPO has the function of containing active ingredients and an important position in various processes of CA. It can be seen from Figure 6C that the hydrogen-bond interaction occurred between oxygen atom on 2-bit =O and Ala202, between the oxygen atom on 5-bit formic =O and His54, between the oxygen atom on 5-bit formic -OH and His38, and between hydrogen atom and Ser206. CA rings were embedded in the bonded zone, PPO amino acids showed the stability of the CA-PPO system. Hydrogen bonding has the effect of reducing hydrophilicity and increasing hydrophobicity and can keep the CA-PPO system stable. Therefore, it can be concluded that hydrophobic forces and hydrogen bonding play a role between CA and PPO. Although there is little difference in the result between spectroscopic experiment and molecular modeling, the result of molecular modeling correlated well with the binding mode observed by the fluorescence quenching mechanism of PPO in presence of CA, *i.e.*, the hydrophobic interactions as the predominant interaction.

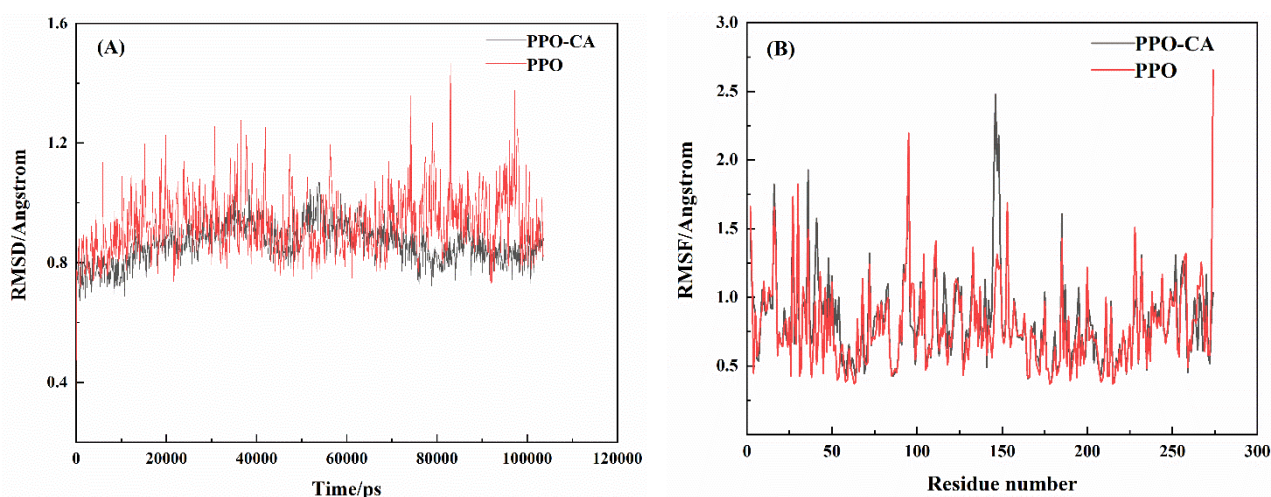


Figure 7. (A) Curves of RMSD values of PPO and PPO-CA over time; (B) RMSF values and time of $C\alpha$ carbon atoms in the skeletons of PPO and PPO-CA systems

The spatial conformation of the interaction between CA and PPO was studied by molecular dynamics simulation, and different parameters were calculated *in vitro*. RMSD (Figure 7A) demonstrates that within 90–110 ns, the fluctuation value of PPO-CA's RMSD is relatively low. The average RMSD value of PPO-CA is 0.863 Å, and that of PPO is 0.927 Å. It can be noticed that PPO-CA has a relatively rigid structure compared to PPO. CA has a significant effect on the conformation of PPO. The RMSF value reflects the fluctuation of amino acid residues in PPO relative to the average position and determines the flexibility of PPO in a given region of protein. The greater the RMSF value, the greater the fluctuation of amino acid residues. According to the RMSF (Figure 7B), the RMSF value fluctuates within the range of 0–3, indicating that the overall structure of PPO and PPO-CA is stable. The amino acid residue of PPO-CA is SER14, compared with that of CA-free PPO, ALA14 and ARG9 have large RMSF values, indicating that these parts are relatively flexible. Compared with the same parts of PPO residues, amino acid residues such as ALA40, LEU274, ALA41, ARG53 and ARG95 had lower RMSF values, and the amino acids in the active site were relatively stable and moved less, resulting in lower structural flexibility in this region. The results showed that PPO-CA was stable after equilibrium.

Conclusions

Based on the traditional drug-protein binding theory, this paper examined the interaction between CA and PPO from multiple perspectives. According to the fluorescence spectrum results, CA quenched the fluorescence of PPO by forming a PPO-CA complex, *i.e.*, the static quenching, which is consistent with the hy-

potheses. CA can strongly bind to PPO. The increase in the temperature caused a decrease in the binding strength. According to the results of thermodynamic analysis, the binding force between CA and PPO is mainly hydrophobic interaction. The donor-acceptor distance (r) of the CA-PPO system was less than 7 nm, which indicates that the energy transfer from PPO to CA occurred. Three-dimensional spectrums (fluorescence intensity-absorbance-wavelength) of CA-PPO were preliminary constructed based on spectrum dates and the characteristic peaks of the interaction to verify the results ultimately.

Experimental results confirmed the interaction and micro binding domain between CA and PPO. Here it can be pointed out that the interaction was dominated by hydrophobic interaction and hydrogen bonding, which is consistent with the spectroscopy experiments.

The saturation of the enzyme PPO binding sites can be measured by the equilibrium experiment method, and it can help to analyze the binding mechanism. Important insights into the interaction of PPO with CA provided a useful guideline for further pharmacology research.

Acknowledgments

The project was supported by the Open Fund of The National and Local Joint Engineering Laboratory of High Efficiency and Superior-Quality Cultivation and Fruit Deep Processing Technology of Characteristic Fruit Trees in South Xinjiang (FE201802).

References

- 1 Siddiq, M., & Dolan, K.D. (2017). Characterization of polyphenol oxidase from blueberry (*Vaccinium corymbosum* L.). *Food Chem.*, 218, 216–220. <https://doi.org/10.1016/j.foodchem.2016.09.061>
- 2 Anaya-Esparza, L.M., Velázquez-Estrada, R.M., Sayago-Ayerdi, S.G., Sánchez-Burgos, J.A., Ramírez-Mares, M.V., LourdesGarcía-Magaña, M., & Montalvo-González, E. (2017). Effect of thermosonication on polyphenol oxidase inactivation and quality parameters of soursop nectar. *LWT--Food Sci. Technol.*, 75, 545–551. <https://doi.org/10.1016/j.lwt.2016.10.002>
- 3 Li, J., Wang, H., Yang, L., Mao, T., Xiong, J., He, S.L., & Liu, H. (2019). Inhibitory effect of tartary buckwheat seedling extracts and associated flavonoid compounds on the polyphenol oxidase activity in potatoes (*Solanum tuberosum* L.). *J. Integr. Agric.*, 18(9), 2173–2182. [https://doi.org/10.1016/S2095-3119\(19\)62692-4](https://doi.org/10.1016/S2095-3119(19)62692-4)
- 4 Truong A., N., Thor, Y., Harris, G. K., Simunovic, J., & Truong, V.D. (2019). Acid Inhibition on Polyphenol Oxidase and Peroxidase in Processing of Anthocyanin-Rich Juice and Co-product Recovery from Purple-Fleshed Sweetpotatoes: Sweetpotato juice. *J. Food Sci.*, 84(7), 1730–1736. <https://doi.org/10.1111/1750-3841.14664>
- 5 Jiang, Y., Duan, X., Qu, H., & Zheng, S. (2016). Browning: Enzymatic Browning. *Encycl. Food Health*, 508–514. <https://doi.org/10.1016/B978-0-12-384947-2.00090-8>
- 6 Pollastro, F., Minassi, A., & Fresu, L.G. (2018). Cannabis Phenolics and their Bioactivities. *Curr. Med. Chem.*, 25(10), 1160–1185. <https://doi.org/10.2174/0929867324666170810164636>
- 7 Zhaoming, Y., Yinzhao, Z., Yehui, D., Qinghua, C., & Fengna, L. (2020). Antioxidant mechanism of tea polyphenols and its impact on health benefits. *Animal Nutrition.*, 6(2), 115–123. <https://doi.org/10.1016/j.aninu.2020.01.001>
- 8 Erdinc, C., Ekincialp, A., Gundogdu, M., Eser, F., & Sensoy, S. (2018). Bioactive components and antioxidant capacities of different miniature tomato cultivars grown by altered fertilizer applications. *J. Food Meas. Charact.*, 12, 1519–1529. <https://doi.org/10.1007/s11694-018-9767-7>
- 9 Wen, R., Lv, H., Jiang, Y., & Peng, F.T. (2018). Anti-inflammatory isoflavones and isoflavanones from the roots of *Pongamia pinnata* (L.) Pierre. *Bioorg. Med. Chem. Lett.*, 28(6), 1050–1055. <https://doi.org/10.1016/j.bmcl.2018.02.026>
- 10 Sukhonthara, S., Kaewka, K., & Theerakulkait, C. (2016). Inhibitory effect of rice bran extracts and its phenolic compounds on polyphenol oxidase activity and browning in potato and apple puree [J]. *Food Chem.*, 190, 922–927. <https://doi.org/10.1016/j.foodchem.2015.06.016>
- 11 Guo, M., Zhao, X.X., Brodelius, P. E., Fang, L., Sun, Z.H., & Wang, R. (2020). The difference of Serum Protein Transport between Echinoides and Verbascoside. *Journal of the Chemical Society of Pakistan*, 42(3), 369–381. <https://doi.org/10.52568/000651/jcsp/42.03.2020>
- 12 Liu, F., Zhao, J.H., Wen, X., & Ni, Y.Y. (2015). Purification and structural analysis of membrane-bound polyphenol oxidase from Fuji apple. *Food Chem.*, 183, 72–77. <https://doi.org/10.1016/j.foodchem.2015.03.027>
- 13 Zhou, Q.T., Guo, M., Ni, K.J., & Francesca, M.K. (2021). Construction of supramolecular laccase enzymes and understanding of catalytic dye degradation using multispectral and molecular docking approaches. *Reaction Chemistry & Engineering*, 6: 1940–1949. <https://doi.org/10.1039/D1RE00111F>
- 14 Brasil, E.M., Canavieira, L.M., Cardoso, É.T., Silva, E.O., Lameira, J., Nascimento, J., Eifler-Lima, V.L., Macchi, B.D., Sriram, D., Bernhardt, P.V., Silva, J.R., Williams, C.M., & Alves, C.N. (2017). Inhibition of tyrosinase by 4H chromene analogs: Synthesis, kinetic studies, and computational analysis. *Chemical Biology & Drug Design*, 90, 804–810. <https://doi.org/10.1111/cbdd.13001>

- 15 Guo, M., Lv, D., Shao, C Y, Kuang, Y., & Sun, Z.H. (2019). Analysis of the interaction mechanisms of polysaccharide homologs binding with serum albumin using capillary electrophoresis. *Journal of the Chemical Society of Pakistan*, 41(4), 640–649. <https://doi.org/10.52568/000780/jcsp/41.04.2019>
- 16 Guo, M., Wang, Y., Wang, X.M., Jiang, Y.K., & Zhang, Y. (2018). Molecular interaction mechanism of tyramine, phenethylamine binding with adrenergic receptor β_2 . *Journal of The Chemical Society of Pakistan*, 40(1), 145–157. https://inis.iaea.org/search/search.aspx?orig_q=RN:49051002
- 17 Yue, L., Lee, J., Lü, Z., Yang, J., Ye, Z., & Park, Y. (2017). Effect of Cd^{2+} on tyrosinase: Integration of inhibition kinetics with computational simulation. *International journal of biological macromolecules*, 94 Pt B, 836–844. <https://doi.org/10.1016/j.ijbiomac.2016.09.001>
- 18 Sukhonthara, S., Kaewka, K., & Theerakulkait, C. (2016). Inhibitory effect of rice bran extracts and its phenolic compounds on polyphenol oxidase activity and browning in potato and apple puree. *Food chemistry*, 190, 922–927. <https://doi.org/10.1016/j.foodchem.2015.06.016>
- 19 Agudelo, D., Bourassa, P., Bariyanga, J., & TajmirRiahi, H.A. (2018). Loading efficacy and binding analysis of retinoids with milk proteins: a short review. *Journal of Biomolecular Structure and Dynamics*, 36, 4246–4254. <https://doi.org/10.1080/07391102.2017.1411833>
- 20 Guo, M., Wang, X.M., Lu, X.W., Wang H.Z., & Brodelius, P.E. (2016). α -Mangostin extraction from the native mangosteen (*Garcinia mangostana* L.) and the binding mechanisms of α -mangostin to HSA or TRF. *PLOS one*, 11(9), 1–22. <https://doi.org/10.1371/journal.pone.0161566>
- 21 Nixha, A.R., Ergun, A., Gençer, N., Arslan, O., & Arslan, M. (2019). Development of carbazole-bearing pyridopyrimidine-substituted urea/thiourea as polyphenol oxidase inhibitors: synthesis, biochemistry, and theoretical studies. *Archives of Physiology and Biochemistry*, 125, 263–269. <https://doi.org/10.1080/13813455.2018.1453523>
- 22 Nguyen, K., Cuellar, C., Mavi, P.S., LeDuc, D., Bañuelos, G., & Sommerhalter, M. (2018). Two poplar hybrid clones differ in phenolic antioxidant levels and polyphenol oxidase activity in response to high salt and boron irrigation. *J. Agric. Food Chem.*, 66(28), 7256–7264. <https://doi.org/10.1080/13813455.2018.1453523>
- 23 Shao, M., Li, X., Zheng, K., Jiang, M., Yan, C., & Li, Y. (2016). Inorganic elemental determinations of marine traditional Chinese Medicine *Meretricis concha* from Jiaozhou Bay: The construction of inorganic elemental fingerprint based on chemometric analysis. *Journal of Ocean University of China*, 15, 357–362. <https://doi.org/10.1007/s11802-016-2749-7>
- 24 Hu, Y., Wang, Y., Deng, J., & Jiang, H. (2015). The structure of a prophenoloxidase (PPO) from *Anopheles gambiae* provides new insights into the mechanism of PPO activation. *BMC Biology*, 14(2), 1–13. <https://doi.org/10.1186/s12915-015-0225-2>
- 25 He, T.Z., Yuan, J.D., LI, W., He, B., & Duan, H.G. (2015). Enzymatic Properties of Polyphenol Oxidase from *Dysosma versipellis* (Hance.) M. Cheng. *Food Sci.*, 36(13), 137–142. <https://doi.org/10.7506/spkx1002-6630-201513026>
- 26 Li, D. (2017). Studies on the Interaction of Cefepime Hydrochloride with Bovine Serum Albumin by Fluorescence, Synchronous Fluorescence, Three-Dimensional Fluorescence and Circular Dichroism. *Journal of Bioanalysis & Biomedicine*, 1–7. <https://doi.org/10.4172/1948-593X.1000162>
- 27 Magdum, P.A. Gokavi, N.M., & Nandibewoor, S.T. (2017). Study on the interaction between anti-tuberculosis drug ethambutol and bovine serum albumin: multispectroscopic and cyclic voltammetric approaches. *Lumin.*, 32(2), 206–216. <https://doi.org/10.1002/bio.3169>
- 28 Gu, Y., Wang, Y., & Zhang, H. (2018). Study on the interactions between toxic nitroanilines and lysozyme by spectroscopic approaches and molecular modeling. *Spectrochim. Acta, Part A*, 202, 260–268. <https://doi.org/10.1016/j.saa.2018.05.008>
- 29 Li, J.H., Bian, L., Tian, S.Y., Kong, J.M., & Zhu, L.Z. (2017). Spectroscopic study on the interaction of human cytoglobin with copper (II) ion. *Spectrosc. Spectral Anal.*, 37, 321–326. [https://doi.org/10.3964/j.issn.1000-0593\(2017\)01-0321-06](https://doi.org/10.3964/j.issn.1000-0593(2017)01-0321-06)
- 30 Fernández-Sainz, J., Pacheco-Liñán, P.J., & Granadino-Roldán, J.M. (2017). Binding of the anticancer drug BI-2536 to human serum albumin. A spectroscopic and theoretical study. *J. Photochem. Photobiol. B, Biology*, 172, 77–87. <https://doi.org/10.1016/j.jphotobiol.2017.05.016>
- 31 Jiang, Y.Y., Wang, X.L., Wang, H.H., Zhang, L., Wang, H., Ji, L.N., & Liu, H.Y. (2016). The Interaction Between a New Water-Soluble Meso-Tetrakis (Carboxyl) Zinc (–) Porphyrin and Human Serum Albumin. *Spectrosc. Spectral Anal.*, 36(9), 2894–2900. PMID: 30084622
- 32 An, X., Zhao, J., Cui, F., & Qu, G. (2017). The investigation of interaction between Thioguanine and human serum albumin by fluorescence and modeling. *Arabian Journal of Chemistry*, 10, 2935–2947. <https://doi.org/10.1016/j.arabjc.2013.06.031>
- 33 García-Jiménez, A., Teruel-Puche, J.A., Berna, J.L., Rodríguez-López, J.N., Tudela, J., García-Ruiz, P.A., & García-Cánovas, F. (2016). Characterization of the action of tyrosinase on resorcinols. *Bioorganic & medicinal chemistry*, 24(18), 4434–4443. <https://doi.org/10.1016/j.bmc.2016.07.048>
- 34 Ploch-Jankowska, A., & Pentak, D. (2020). A Comprehensive Spectroscopic Analysis of the Ibuprofen Binding with Human Serum Albumin, Part I. *Pharmaceuticals*, 13, 205–230. <https://doi.org/10.3390/ph13090205>
- 35 Wani, T.A., Bakheit, A.H., Zargar, S., Rizwana, H., & Al-majed, A. (2019). Evaluation of competitive binding interaction of neratinib and tamoxifen to serum albumin in multidrug therapy. *Spectrochimica acta. Part A, Molecular and biomolecular spectroscopy*, 117691(19), 31081-9. <https://doi.org/10.1016/j.saa.2019.117691>

Цуйюнь Ву, Ваньцин Лин, Есен Яо, Мин Гуо, Нуршат Нурадже

Полифенол оксидазасын кумар қышқылымен байланыстырудың биополимерлік жүйесінің үш өлшемді саусақ іздері спектроскопия әдісімен зерттеу

Табиғаттағы биохимиялық процестерде антиоксидант болып келетін кумар қышқылын (КК) қорғау үлкен қызығушылық тудыруда. Полифенолоксидазасы (ПФО) көкөністер, жемістер мен саңырау-құлақтар сияқты өсімдіктердің ескіруі мен қараюында маңызды рөл атқаратын фермент болып табылады. КК және ПФО өзара әрекеттесуі метаболизм мен ескіру туралы маңызды ақпарат береді. Сондықтан, КК-ын полифенолоксидазасымен (ПФО) байланыстырудың молекулалық механизмі спектроскопиялық әдістерді молекулалық модельдеумен біріктіру арқылы зерттелді. Алғаш рет КК мен ПФО арасындағы биополимердің өзара әрекеттесуін сипаттау үшін КК-ПФО кешенінің үш өлшемді іздері жасалды. Спектроскопиялық әдістерді қолдану КК ПФО өзіндік флуоресценциясын тиімді түрде басатындығын көрсетті. Энтальпияның өзгеруі (ΔH°) және энтропияның өзгеруі (ΔS°) КК-ПФО кешені негізінен КК және ПФО гидрофобты әрекеттесуімен тұрақтандырылған деп болжайды. КК-ПФО кешенінің λ -UV-F ізінің құрылысы КК мен ПФО арасындағы үш өлшемді өзара әрекеттесуді көрсетуге мүмкіндік берді. Кейіннен молекулалық модельдеу КК мен ПФО негізінен гидрофобты өзара әрекеттесулер мен Ala202, His38, His54 және Ser206 аминқышқылдарының қалдықтарында орналасқан сутегі байланыстарымен байланысты екенін көрсетті. Компьютерлік модельдеу КК-ПФО өзара әрекеттесуі үшін анықталған үш өлшемді модельге деген сенімділікті көрсететін спектрлік эксперименттерге сәйкес келді.

Кілт сөздер: биополимер, құрамында Cu бар фермент, кумар қышқылы, полифенол оксидазы, антиоксидант, α -пирон-5-карбон қышқылы, спектроскопия, тирозиназа, молекулалық модельдеу.

Цуйюнь Ву, Ваньцин Лин, Есен Яо, Мин Гуо, Нуршат Нурадже

Исследование методом трехмерной спектроскопии отпечатков пальцев биополимерной системы связывания полифенолоксидазы с кумаровой кислотой

Защита кумаровой кислоты (КК), антиоксиданта, в биохимическом процессе в природе вызвала большой интерес. Полифенолоксидаза (ПФО) — это фермент, который играет жизненно важную роль в старении и потемнении растений, таких как овощи, фрукты и грибы. Взаимодействие КК и ПФО раскрывает важную информацию о метаболизме и старении. Поэтому молекулярный механизм связывания КК с полифенолоксидазой (ПФО) был исследован путем объединения спектроскопических методов с молекулярным моделированием. Впервые был создан трехмерный отпечаток комплекса КК–ПФО для характеристики взаимодействия биополимера между КК и ПФО. Применение спектроскопических методов показало, что КК эффективно подавляет собственную флуоресценцию ПФО. Изменение энтальпии (ΔH°) и энтропии (ΔS°) предполагает, что комплекс КК–ПФО был преимущественно стабилизирован гидрофобными взаимодействиями КК и ПФО. Построение λ -UV-F отпечатка КК–ПФО позволило продемонстрировать трехмерные взаимодействия между КК и ПФО. Впоследствии молекулярное моделирование показало, что КК, в основном, связана с ПФО гидрофобными взаимодействиями и водородными связями, расположенными в аминокислотных остатках Ala202, His38, His54 и Ser206. Компьютерное моделирование соответствовало спектральным экспериментам, демонстрирующим уверенность в трехмерной модели, определенной для взаимодействия КК–ПФО.

Ключевые слова: биополимер, Cu-содержащий фермент, кумаровая кислота, полифенолоксидаза, антиоксидант, α -пирон-5-карбоновая кислота, спектроскопия, тирозиназа, молекулярное моделирование.

Information about authors *

Wu, Cuiyun — Candidate of Chemical Sciences, Leading Researcher of Red jujube fruit team, Tarim University, A'ler, 843301, Xinjinag, China; e-mail: wcyby@163.com; <https://orcid.org/0000-0002-0178-3524>;

Ling, Wanqing — Master of chemical sciences, assistant researcher, Zhejiang Agriculture and Forestry University, 310007, Lin'an City, Hangzhou, Zhejiang, China; e-mail: lwq9901@163.com;

Yao, Yecen — Master of Chemical Sciences, Assistant Researcher, Zhejiang Agriculture and Forestry University, 310007, Lin'an City, Hangzhou, Zhejiang, China; e-mail: 2020104062016@zafu.edu.cn;

Guo, Ming — PhD in Chemistry, Professor at Zhejiang Agriculture and Forestry University, 310007, Lin'an City, Hangzhou, Zhejiang, China; e-mail: guoming@zafu.edu.cn; <https://orcid.org/0000-0002-5255-9952>;

Nuraje, Nurxat — PhD in Chemistry, Head of ASEMS, National Laboratory Astana, Nazarbayev University, Kabanbay batyr avenue, 53, 010000, Nur-Sultan, Kazakhstan; e-mail: nurxat.nuraje@nu.edu.kz; <https://orcid.org/0000-0003-4751-2719>

*The author's name is presented in the order: *Last Name, First and Middle Names*

T.R. Deberdeev, A.I. Akhmetshina*, L.K. Karimova, S.V. Grishin, D.V. Kochemasova

Kazan National Research Technological University, Kazan, Russia

(*Corresponding author's e-mail: aai-89@mail.ru)

Thermal Behavior of Novel Aromatic Oligoesters and Oligoesteramides

Liquid crystalline polymers, depending on their structure and macromolecular architecture, are found in a number of commercial applications, ranging from state-of-the-art engineering plastics to soft matter artificial muscles and microrobots. Rigid chain liquid crystalline polymers are known as indispensable materials for high technology industries. However, their relatively high costs provoke the search for novel cost-effective mesogenic monomers. In this regard, a series of aromatic oligoesters and oligoesteramides were synthesized via high-temperature polycondensation of aromatic dicarboxylic acids with 4-hydroxybenzoic acid (or 4-aminobenzoic acid) and 1,5-naphthalene diol. The structure of the synthesized compounds was identified using FTIR spectra analysis. According to polarizing microscopy observations, novel oligoester based on 4-hydroxybenzoic acid, 1,5-naphthalene diol and terephthalic acid demonstrated liquid crystallinity with nematic texture, whereas other samples occurred in amorphous state in case of oligoester or in crystalline state in case of oligoesteramides. A relatively wide range of mesophase existence from 120 to 290 °C was found for the thermotropic oligoester using differential scanning calorimetry. While aromatic oligoesters at the beginning of the degradation processes were highly stable towards heat with comparable values of T10, which were equal to 372–378 °C, aromatic oligoesteramides started to decompose at the temperatures lower by more than 50 °C than those for oligoesters.

Keywords: liquid crystalline polymers, phase transitions, polarizing microscopy, thermal stability, solubility, high-temperature polycondensation.

Introduction

Liquid crystals (LCs) are substances that exhibit some degree of order along with fluidity all at once. Depending on the conditions of liquid crystal formation, those substances can be subdivided into thermotropic and lyotropic [1–3]. The first ones undergo a transition from a crystal phase to a mesophase under heating, while the lyotropic LCs are formed in a solution in a certain concentration range. According to the arrangement of molecules in space, the following types of LCs may be differentiated, namely nematic phase, smectic phase, cholesteric phase, and discoid column phase [4].

High-molecular compounds can also demonstrate liquid crystallinity in case of rigid-rod macromolecules. Most examples reported in the literature vary in the position of the liquid crystalline unit and can be divided into the main chain type, side chain type, composite main side chain type, bowl type, star shape, net shape, and shell type. The main-chain thermotropic polymers are advanced materials, which have recently gained considerable attention for high-tech products, such as high-precision, thin-walled electronic components [5–10].

It is necessary to mention that despite their extraordinary properties, e.g., high thermal stability, low thermal expansion, outstanding mechanical properties, chemical resistance and so on, the first representatives of liquid crystalline polymers (poly-4-hydroxybenzoate, poly(1,4-phenylene terephthalamide)) faced challenges of intractability and poor processability [11].

Several approaches have been developed to improve the processability of LC polymers (LCP). One implied disruption of chains' regularity by inserting bulky groups of spacers into the macromolecules. Another method is to combine various mesogenic monomers with different length (p-phenyl, p-biphenyl, p-triphenyl, naphthalene moieties) along the chain direction thereof partially excluding intermolecular interactions between the polar linking groups [12]. As such, industrially produced thermotropic LCPs consist of para-linked aromatic monomers and one mesogenic monomer with enlarged length. Vectra A950, which is copolyester composed of HBA and 2,6-hydroxynaphthoic acid, is a striking example of the aforementioned approach. Addition of 6-hydroxy-2-naphthoic acid into the regular chain of poly-4-hydroxybenzoate makes the polymer tractable and processable [12]. Copolymerization of 4-hydroxybenzoic acid with p-phenylene-2,6-dicarboxylate reduces the melting point to 325 °C [12].

On the other hand, incorporation of the amide group into the polymer chain results in enhanced intermolecular interaction and, therefore, makes such polymers preferably lyotropic. In some cases, aromatic polyesteramides maintain their thermotropicity and are molded by traditional methods of plastic processing. Commercially available thermotropic polyesteramide Vectra B950 is made of 2,6-hydroxynaphthoic acid, *p*-hydroxyl acetanilide, and terephthalic acid [13].

Preceding commercialization, scientific research has established that among other isomers, it is 2,6-substituted naphthalene derivatives ensure the stability of the mesophase in a wide temperature range and an acceptable processing temperature [14]. However, it should be mentioned that the cost of this monomer is high and enlarges the cost of the final product.

1,5-substituted naphthalene based LC compounds are also capable to form a mesophase, but in a narrower temperature range than those based on the 2,6-substituted monomer [14]. According to [14], aromatic polyester composed of 4-hydroxybenzoic acid (HBA), terephthalic acid and 1,5-dihydroxynaphthalene residues at any molar ratio of the initial components melts at temperatures above 290 °C, and its mesomorphic properties are poorly researched.

It is worth noting that incorporation of this monomer into the LCPs reduces the cost of the final product by 30–50 % compared to the case of 6-hydroxy-2-naphthoic acid.

Herein, 1,5-naphthalene diol-based aromatic oligoesters and oligoesteramides were selected as possible objects, being able to form a mesophase; their thermal and optical properties were investigated to reveal the liquid crystallinity.

Experimental

4-Hydroxybenzoic acid (4-HBA, 99 %), 4-aminobenzoic acid (4-ABA, 99 %), terephthalic acid (TA, 98 %), isophthalic acid (IA, 99 %), 1,5-dihydroxynaphthalene (DHN, 97 %) were purchased from Sigma-Aldrich. Ditolylmethane (reagent grade) and titanium tetrabutoxide (97 %) were supplied from Angara-reaktiv. Isopropyl alcohol (98 %) was obtained from LLC Chimmed.

The phenyl esters (PE) of corresponding carboxylic acids were synthesized by the reaction of equimolar amount of phenol and carboxylic acid (TA, IA, 4-ABA, 4-HBA). The copolyester was obtained in one stage: a calculated amount of raw materials (the molar ratio of [4-HBA]:[PE of dicarboxylic acid]:[aromatic diol] = 1:1:1) and the catalyst (1 wt%) were added to the 500 mL three-necked round-bottom flask and mixed with 300 ml of ditolylmethane (Table 1, Figure 1). The reaction mixture was heated rapidly up to 200–250 °C with stirring under the nitrogen steam, following the evolution of the calculated amount of phenol+water mixture. The reaction was quenched after reaching the desired amount of side-products.

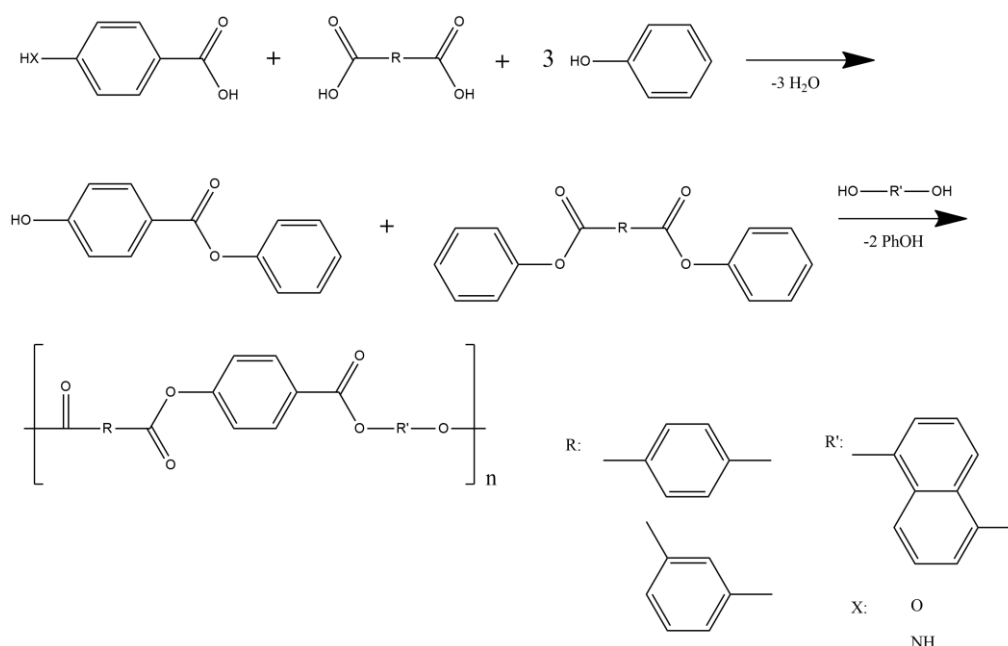


Figure 1. Synthetic route of the aromatic oligoesters and oligoesteramides

General properties of the aromatic oligoesters

LCP	The ratio of monomers	T _g [°C]	T _m [°C]	T _i [°C]	LC Phase
S-1	[4-HBA]:[IA]:[DHN] = 1:1:1	104	–	–	–
S-2	[4-HBA]:[TA]:[DHN] = 1:1:1	–	120	290	Nematic
S-3	[4-ABA]:[IA]:[DHN] = 1:1:1	–	–	–	–
S-4	[4-ABA]:[TA]:[DHN] = 1:1:1	–	307	–	–

The FTIR spectra of the products were recorded on an InfraLUM FT 08 Fourier transform spectrometer using the attenuated total reflection technique. The spectral resolution was 4 cm⁻¹, and the number of scans was 60.

Differential scanning calorimetry (DSC) measurements and thermogravimetric analysis were performed using thermal analyzer TGA/DSC 3+ (Mettler Toledo). The samples (0.1 g) were loaded in alumina pans and ramped to 773 K at a heating rate of 5 K/min in a nitrogen atmosphere.

Optical observation was carried out using the Polam P-312 polarizing microscope equipped with a heating stage in the temperature range of 25–300 °C.

Results and Discussion

Aromatic polyesters and polyesteramides were synthesized via a two-step condensation procedure as described previously. All polymers were obtained in high yields after the precipitation in non-solvent.

Since all used carboxylic acids exhibit approximately equal pK_a values, we expected their similar reactivity and, therefore, the incorporation of these monomers into macromolecules. Indeed, the results of FTIR spectroscopy revealed this assumption and the IR spectra demonstrated embedding of all raw materials into the polymeric chains.

Figure 2 depicts the FTIR graph of the polymeric samples and their characteristic bands. Ones ($\nu_{C=C}$) for the C=C stretching vibrations of aromatic (benzene and naphthalene) rings were found at 1450–1624 cm⁻¹. The peak located at 1740 cm⁻¹ is assigned to the C=O group stretching. Besides, the OH in-plane bending vibrations for end-groups may be found as low-intensity band at 1455 cm⁻¹. The IR band with a mild intensity at 1257 cm⁻¹ is originated by the C(Ar)-O bond presence. Moreover, the peaks that appeared at 1257 and 1057 cm⁻¹ are attributed to asymmetrical and symmetrical stretching of the C-O-C group. The C-H bending vibrations in oligoesters were observed at 750–900 cm⁻¹.

For the synthesized polyesteramides, the amide I band was resolved into two bands at about 1681 cm⁻¹ (a “free” carbonyl group) and 1651 cm⁻¹ (a hydrogen-bonded carbonyl group). The intensive shoulder at 1530–1550 cm⁻¹ is attributed to NH deformation vibrations, as well as the peak at 1507 is assigned to N-H bending vibrations. The C-C stretching vibrations in the aromatic ring remain unchanged compared to aromatic polyesters. The stretching vibrations of the C-O-C group in S-3 and S-4 is observed at 1250 cm⁻¹ and 1270 cm⁻¹, respectively.

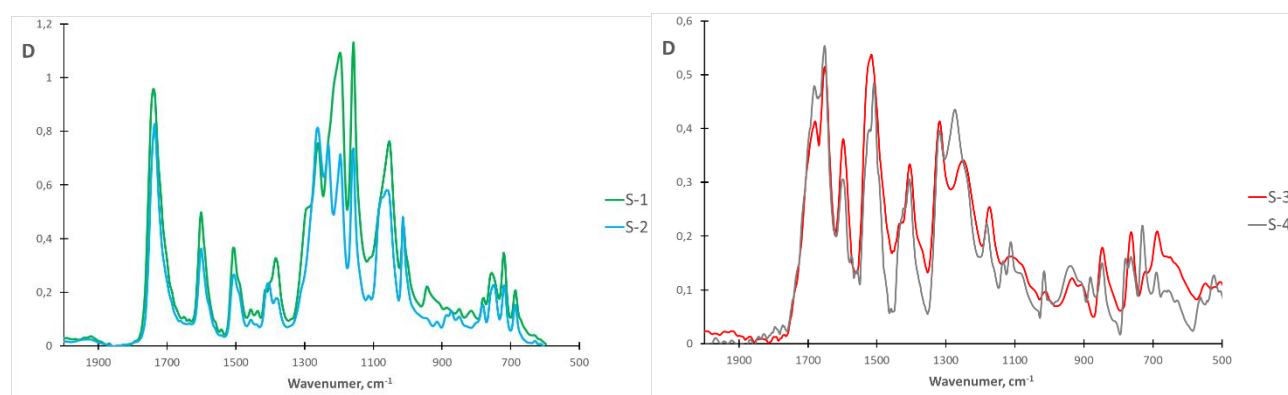


Figure 2. FTIR spectra of aromatic polyesters and polyesteramides

Hot-stage polarized optical microscopy (POM) was performed to observe the LC behavior of the polymeric samples. Among the synthesized compounds, the oligoester S-2 solely demonstrated the presence of a

nematic texture in a temperature range from 120 to 290 °C. Whereas the recent reports have claimed about instability of mesophase, which is formed by low-molecular LCs containing the residue of 1,5-naphthalene diol. The present work shows the opposite trend. Aromatic polyester S-2 tends to form a stable nematic phase with a wide processing window. When a linear configuration of TA is completely replaced by a bent-core geometry of IA, the polyester S-1 loses the ability to form a LC phase. Therefore, the images of POM show only the isotropic melt, appearing after the glass transition temperature. In case of polyestheramides, S-3 and S-4, those samples were intractable up to 290 °C, limited by an upper temperature bound of the microscope.

The phase transitions in the samples were confirmed using differential scanning calorimetry. From DSC data, it was evident that introduction of IA into the linear aromatic chain resulted in an absence of a mesophase. No endothermic peaks for this sample attributed to melting of the crystalline phase or isotropization were found on the thermograms (Figure 3).

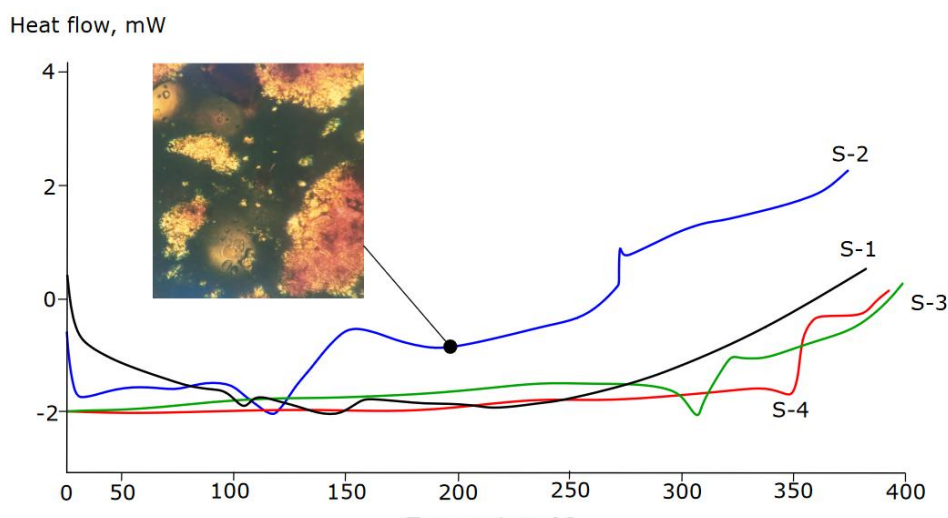


Figure 3. DSC scans of the samples

Figure 3 illustrates that the polymer S-2 clearly undergoes a phase transition and forms a mesophase at 120 °C with subsequent melting at 270 °C. Those data are consistent with results obtained from the optical microscopy. Upon introducing of 4-ABA instead of 4-HBA, polyestheramides have no accessible melting point and maintain intractability up to thermal decomposition temperatures. However, in case of S-4, one endotherm at 307 °C probably corresponding to the melting process was detected.

Some representatives of aromatic polyestheramides are recognized as thermotropic LCs; others are structured in an ordered state, only being dissolved in harsh conditions of aggressive solvents. To estimate the processability of the samples through solution casting, we have calculated the solubility parameter of the polymers using a group contribution method [15].

Solubility parameter δ is closely related to the cohesive energy according to the following equation:

$$\delta = \left(\frac{E_{coh}}{V} \right)^{1/2},$$

where E_{coh} is the cohesive energy (cal/mol), V is the molar volume (\AA^3).

Group contributions to E_{coh} and V are represented in the aforementioned reference. As can be concluded from the solubility parameter calculations, aromatic oligoesters and oligoesteramides dissolve presumably in amide solvents ($\delta_{\text{DMSO}} = 12.93$, $\delta_{\text{DMF}} = 12.14$) (Table 2).

Qualitative tests of the solubility in DMSO and DMF revealed that both oligoesters were completely soluble, whereas the close packing through hydrogen bonds between amide groups resulted in reduced solubility of S-3 and S-4. Oligoesteramides were soluble in concentrated H_2SO_4 and it made possible to form a lyotropic phase only under harsh conditions.

Cohesive energy and solubility parameters of the samples

Samples	E_{coh} , kcal/mol	V , Å ³	δ , (cal/cm ³) ^{0.5}
S-1	24.351	357.0	10.61
S-2	24.351	357.0	10.61
S-3	29.343	360.9	11.58
S-4	29.393	352.5	11.72
DMSO	–	–	12.93
DMF	–	–	12.14

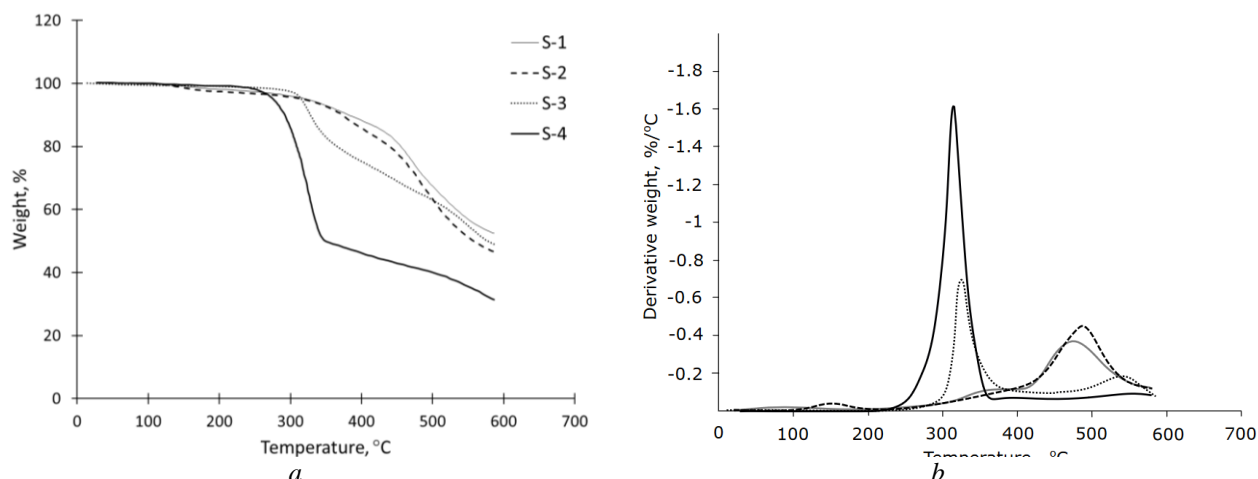


Figure 4. TGA and DTG curves of the samples

To study the thermal decomposition of the polymers, thermogravimetric analysis was performed between 25–600 °C in flowing N₂ at a heating rate of 10 °C/min. Figure 4a depicts the TGA curves for experiments with oligoesters and oligoesteramides. Figure 4b represents the curves plotting the first derivative of TGA thermograms. Noteworthy is that the thermal stability of oligoesters exceeded that for oligoesteramides. The weight loss percentages are close at different heating rates for S-1 and S-2. The temperature for 10 % gravimetric loss ($T_{10\%}$), which is the key indicator for thermal stability, was in the range of 372–378 °C for oligoesters and 291–326 °C for oligoesteramides, respectively. The temperatures at 10 % weight loss percentages and the temperature of maximal rate of the weight loss T_{dm} are listed in Table 3, from which it can be seen that the order of thermal stability is S-1 > S-2 > S-3 > S-4 in N₂. Most probably, the lowering of thermal stability in case of oligoesteramides is closely related to the fact that the average bond dissociation energy of C-N (about 73 kcal/mol) is smaller than that of C-O (approximately 85 kcal/mol). Therefore, the introduction of amide bonds into the structure makes S-3 and S-4 less thermally stable than S-1 and S-2.

It was established (Figure 4b) that the major decomposition of the oligoesters occurred in the temperature range from 250 to 350 °C. The highest rates of thermal decomposition for oligoesteramides were achieved in a range of 420–500 °C. Therefore, the kinetic parameters of thermal decomposition were evaluated only for the major decomposition range. The kinetic parameters were calculated using Coats-Redfern method [16]:

$$\ln \left[\frac{-\ln(1-\alpha)}{T^2} \right] = \ln \frac{AR}{\beta E_a} - \frac{E_a}{RT},$$

where α is fraction of decomposition, E_a is the activation energy, A is the pre-exponential factor, R is the universal gas constant, β is the heating rate.

Plotting $\ln \left[\frac{-\ln(1-\alpha)}{T^2} \right]$ against $1/T$ should give a straight line with a slope proportional to the activation energy ($-E_a/R$). Figure 5 demonstrates the Coats-Redfern plots of the decomposition step for the sam-

ples. The coefficient of correlation (R^2) is obtained by plotting $\ln \left[\frac{-\ln(1-\alpha)}{T^2} \right]$ versus $(1/T)$ using a linear approximation function. The relatively high values of R^2 offer an ability of the proposed model to fit the experimental TGA data.

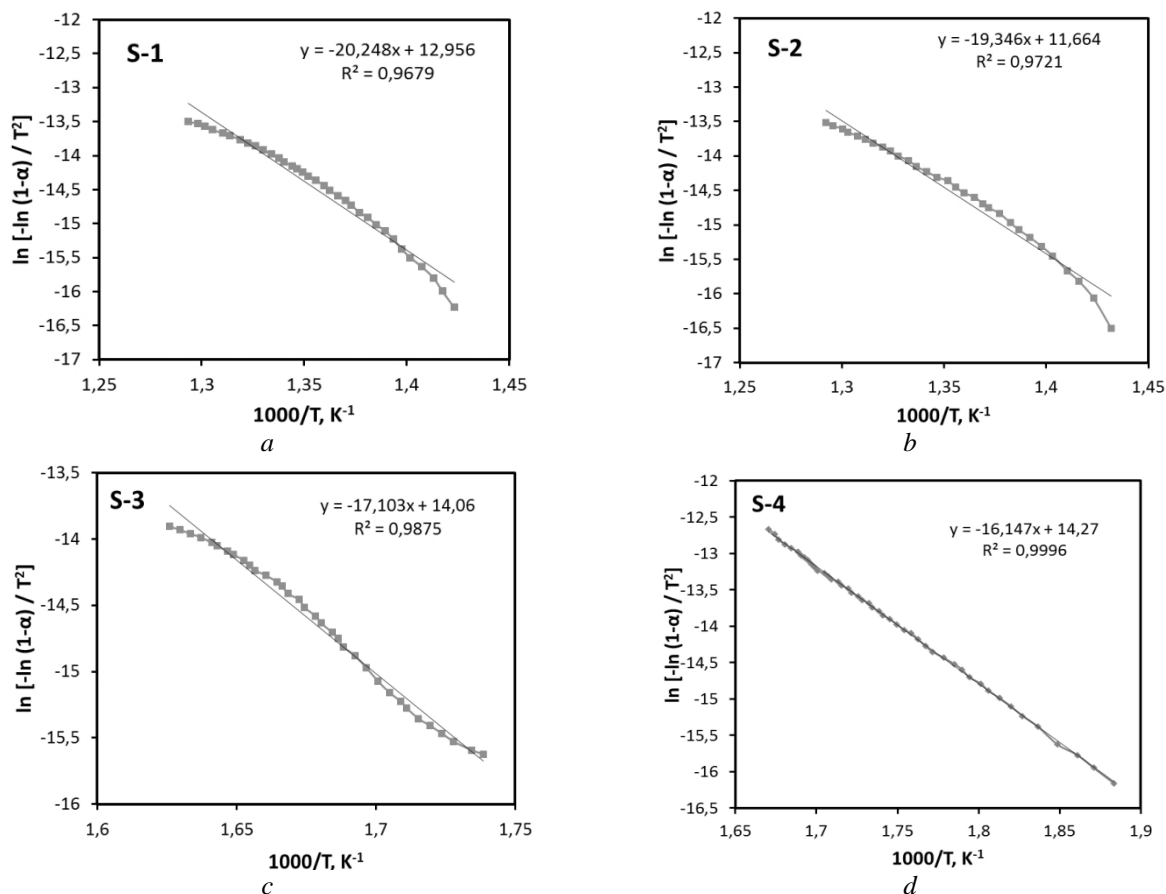


Figure 5. Coats-Redfern plots for the samples

Table 3 presents the results of the calculated activation energies for each sample. It is clear that the results highly correlated with the Coats-Redfern model since R^2 values exceeded 0.9. The activation energy of thermal decomposition of oligoester S-2 was $161.10 \text{ kJ mol}^{-1}$, slightly less than that ($168.35 \text{ kJ mol}^{-1}$) of oligoester S-1. The E_a was found to be $142.20 \text{ kJ mol}^{-1}$ and $134.25 \text{ kJ mol}^{-1}$ for oligoesteramides S-3 and S-4. In general, the findings of a kinetic study were in consistent with the thermal behavior of the samples given above. A relatively weak bond dissociation energy of oligoesteramides contributed to loosening of stability.

Table 3

Results of TGA analysis of the samples

Samples	$T_{10}, ^\circ\text{C}$	$T_{dm}, ^\circ\text{C}$	Residue, %	$E_a, \text{kJ/mol}$
S-1	378	464	52.5	168.35
S-2	372	494	46.6	161.10
S-3	326	325	48.8	142.20
S-4	291	323	31.3	134.25
Vectra A950 [19]	503	–	–	232.04
Vectra B950 [19]	502	–	–	196.71

The TGA results are different from the ones for the commercially available polyesters Vectra A650 and Vectra B950, as shown in Table 3. The explanation given for this large variance is related to a molecular

weight of the samples. The synthesized samples are noticeably inferior in terms of thermal stability, which can depend both on the chemical structure of oligoesters or oligoesteramides and on the content of end groups. Faster degradation of oligomers, most probably, is associated with the relatively low molecular weight of the samples [17] and the increased content of end groups, which are the first to be involved in the thermal degradation process [18]. However, due to the samples contain reactive end groups, the heat treatment of the samples, accompanied by post-polycondensation, is expected to improve their thermal stability.

Conclusions

In this work, we synthesized and characterized the mesomorphic and thermal behavior of aromatic oligoesters and oligoesteramides containing the 1,5-naphtalene moiety. DSC experiments revealed the existence of a phase transition in the temperature range of 120–290 °C in case of oligoester based on 4-hydroxybenzoic acid, 1,5-naphtalene diol, and terephthalic acid. Study of phase transitions using polarized light microscopy evidenced an optical activity of the sample and formation of a mesophase with a nematic texture. Replacement of linear terephthalic acid with kinked isophthalic acid resulted in an amorphous nature of the synthesized oligoester. Oligoesteramides showed no phase transitions associated with existing of a mesophase. Since those samples had been slightly soluble in amide solvents, but completely dissolved in sulfuric acid, they were presumptively capable of ordering in a lyotropic liquid crystalline phase. Aromatic oligoesters possessed higher thermal stability among polymeric samples and similar values of the 10 % weight loss temperature at 372–378 °C.

References

- 1 Shibaev, V.P. (2014). Liquid-crystalline polymer systems: From the past to the present. *Polymer Science Series A*, 56(6), 727–762. <https://www.doi.org/10.1134/S0965545X14060091>
- 2 Deberdeev, T.R., Akhmetshina, A.I., Karimova, L.K., Ignat'eva, E.K., Deberdeev, R.Ya., & Berlin, A.A. (2020). Heat-Resistant Polymer Materials Based on Liquid Crystal Compounds. *Polymer Science, Series C*, 62(2), 145–164. <https://doi.org/10.1134/s1811238220020034>
- 3 Ohm, C, Brehmer, M, & Zentel, R. (2010). Liquid Crystalline Elastomers as Actuators and Sensors. *Advanced Materials*, 22(31), 3366–3387. <https://doi.org/10.1002/adma.200904059>
- 4 Donnio, B. (2014). Liquid-crystalline metallodendrimers. *Inorganica Chimica Acta*, 409, 53–67. <https://doi.org/10.1016/j.ica.2013.07.045>
- 5 Ji, Y., Bai, Y., Liu, X., & Jia, K. (2020). Progress of liquid crystal polyester (LCP) for 5G application. *Advanced Industrial and Engineering Polymer Research*, 3(4), 160–174. <https://doi.org/10.1016/j.aiepr.2020.10.005>
- 6 Wang, L., & Li, Q. (2016). Stimuli-Directing Self-Organized 3D Liquid-Crystalline Nanostructures: From Materials Design to Photonic Applications. *Advanced Functional Materials*, 26(1), 10–28. <https://doi.org/10.1002/adfm.201502071>
- 7 Gantenbein, S., Masania, K., Woigk, W., Sesseg, J.P.W., Tervoort, T.A., & Studart, A.R. (2018). Three-dimensional printing of hierarchical liquid-crystal-polymer structures. *Nature*, 561(7722), 226–230. <https://doi.org/10.1038/s41586-018-0474-7>
- 8 Kato, T., Uchida, J., Ichikawa, T., & Soberats B. (2018). Functional liquid-crystalline polymers and supramolecular liquid crystals. *Polymer Journal*, 50(1), 149–166. <https://doi.org/10.1038/pj.2017.55>
- 9 Zhang, Y., Wang, Z., Yang, Y., Chen, Q., Qian, X., Wu, Y., Liang, H., Xu, Y., Wei, Y., & Ji, Y. (2020). Seamless multimaterial 3D liquid-crystalline elastomer actuators for next-generation entirely soft robots. *Science Advances*, 6(9). <https://doi.org/10.1126/sciadv.aay8606>
- 10 Chen, T., Han, J.Y., Okonski, D.A., Kazerooni, D., Ju, L., & Baird, D.G. (2021). Thermotropic liquid crystalline polymer reinforced polyamide composite for fused filament fabrication. *Additive Manufacturing*, 40, 101931. <https://doi.org/10.1016/j.addma.2021.101931>
- 11 Thakur, V.K., & Kessler, M.R. (2015). *Liquid Crystalline Polymers Volume 2-Processing and Applications*. Heidelberg: Springer Cham. <https://doi.org/10.1007/978-3-319-20270-9>
- 12 Jackson, W.J., & Kuhfuss, H.F. (1976) Liquid crystal polymers. I. Preparation and properties of p-hydroxybenzoic acid copolyesters. *Journal of Polymer Science: Polymer Chemistry Edition*, 14(8), 2043–2058. <https://doi.org/10.1002/pol.1976.170140820>
- 13 Han, J.Y., Chen, T., Mu, Q., & Baird, D.G. (2021). Thermotropic liquid crystalline polymer reinforced polypropylene composites enhanced with carbon nanotubes for use in fused filament fabrication. *Polymer Composites*, 42(8), 4115–4127. <https://doi.org/10.1002/pc.26134>
- 14 Jackson, W.J. (1983). Liquid crystalline polymers. 5. Liquid crystalline polyesters containing naphthalene rings. *Macromolecules*, 16(7), 1027–1033. <https://doi.org/10.1021/ma00241a001>
- 15 Askadskii, A.A. (2003). *Computational Materials Science of Polymers*. Cambridge: Cambridge international science publishing. [https://doi.org/10.1016/s1369-7021\(03\)00438-3](https://doi.org/10.1016/s1369-7021(03)00438-3)

16 Coats, A.W., & Redfern, J.P. (1964). Determination of kinetic parameters from thermogravimetric data. *Thermochimica Acta*, 24 (1), 182–185. [https://doi.org/10.1016/0040-6031\(78\)85150-8](https://doi.org/10.1016/0040-6031(78)85150-8)

17 Chrissafis, K., Paraskevopoulos, K.M., & Bikiaris, D.N. (2006). Effect of molecular weight on thermal degradation mechanism of the biodegradable polyester poly(ethylene succinate). *Thermochimica Acta*, 440(2), 166–175. <https://doi.org/10.1016/j.tca.2005.11.002>

18 Bosnyak, C.P., Knight, G.J., & Wright, W.W. (1981). Thermal stability of some aromatic polyesters and poly(ester carbonates). *Polymer Degradation and Stability*, 3(4), 273–283. [https://doi.org/10.1016/0141-3910\(81\)90023-9](https://doi.org/10.1016/0141-3910(81)90023-9)

19 Jin, X., & Chung, T.-S. (1999). Thermal decomposition behavior of main-chain thermotropic liquid crystalline polymers, Vectra A-950, B-950, and Xydar SRT-900. *Journal of Applied Polymer Science*, 73(11), 2195–2207. [https://doi.org/10.1002/\(sici\)1097-4628\(19990912\)73:11<2195::aid-app17>3.0.co;2-3](https://doi.org/10.1002/(sici)1097-4628(19990912)73:11<2195::aid-app17>3.0.co;2-3)

Т.Р. Дебердеев, А.И. Ахметшина, Л.К. Каримова, С.В. Гришин, Д.В. Кочемасова

Жаңа ароматты олигоэфирлер мен олиготерамидтердің жылулық қасиеттері

Химиялық құрылымы мен макромолекулярлық құрылысына байланысты сұйық кристалды полимерлер супер құрылымды инженерлік пластиктен бастап жасанды бұлшықеттер мен микророботтарға дейін әртүрлі жоғары технологиялық салаларда қолданылуы мүмкін. Қаттытiзбектi сұйық-кристалды полимерлер жоғары берiктiк қасиеттерi бар ыстыққа төзiмдi материалдар ретiнде кеңiнен тарады. Алайда, олардың айтарлықтай жоғары құны оларды синтездеу үшiн жаңа экономикалық тиiмдi мезогендi мономерлердi iздеуге әкелетiнiн атап өткен жөн. Осыған байланысты осы жұмыста жоғары температурада каталитикалық поликонденсациялау арқылы ароматты дикарбон қышқылдары, 4-гидроксibenзой қышқылы (немесе 4-аминбензой қышқылы) және 1,5-нафталендиол негiзiндегi бiрқатар ароматты олигоэфирлер мен олиготерамидтер синтезделдi. Синтезделген қосылыстардың құрылымы ИК-спектроскопия көмегiмен анықталды. Поляризацияланған оптикалық микроскопия арқылы алынған нәтижелерге сәйкес, 4-гидроксibenзой қышқылы, 1,5-нафталендиол және терефтал қышқылы негiзiндегi жаңа олигоэфир нематикалық құрылымды сұйық кристалды фазаның болуын көрсеттi, ал басқа үлгiлер аморфты күйде (олигоэфир) немесе кристалдық күйде (олиготерамидтер) болды. Термотропты олигоэфир үшiн дифференциалды сканерлеу калориметриясын қолдана отырып, температура интервалы 120-дан 290 °C-қа дейiнгi болып табылатын мезофазаның бар болу диапазоны сипатталды. Ароматты олигоэфирлер ыдырау процестерiнiң басында 372–378 °C-қа тең T10 салыстырмалы мәндерiнде температура әсерiне айтарлықтай жоғары тұрақтылық көрсеттi. Ароматты олиготерамидтер олигоэфирлерге қарағанда 50 °C төмен температурада ыдырай бастады.

Кiлт сөздер: сұйық кристалды полимерлер, фазалық ауысулар, поляризациялық микроскопия, термиялық тұрақтылық, ерiгiштiк, жоғары температурадағы поликонденсация.

Т.Р. Дебердеев, А.И. Ахметшина, Л.К. Каримова, С.В. Гришин, Д.В. Кочемасова

Термические свойства новых ароматических олигоэфиров и олигоэфирамидов

В зависимости от своего химического строения и макромолекулярной архитектуры жидкокристаллические полимеры могут быть применимы в различных высокотехнологичных отраслях, начиная с суперконструкционных инженерных пластиков и завершая искусственными мышцами и микророботами. Жесткоцепные жидкокристаллические полимеры получили распространение в качестве термостойких материалов с высокими прочностными свойствами. Однако стоит отметить, что их достаточно высокая стоимость обуславливает поиск новых экономически более рентабельных мезогенных мономеров для их синтеза. В связи с этим в данной статье синтезирован ряд ароматических олигоэфиров и олигоэфирамидов на основе ароматических дикарбоновых кислот: 4-гидроксibenзойной кислотой (или 4-аминобензойной кислотой) и 1,5-нафталиндиола методом высокотемпературной каталитической поликонденсации. Структуру синтезированных соединений идентифицировали с использованием ИК-спектроскопии. Согласно результатам, полученным методом поляризационной оптической микроскопии, новый олигоэфир на основе 4-гидроксibenзойной кислоты, 1,5-нафталиндиола и терефталевой кислоты проявлял наличие жидкокристаллической фазы с нематической текстурой, тогда как другие образцы находились в аморфном состоянии (олигоэфир) или в кристаллическом состоянии (олигоэфирамиды). С помощью дифференциальной сканирующей калориметрии для термотропного олигоэфира охарактеризован диапазон существования мезофазы, составляющий температурный интервал от 120 до 290 °C. Ароматические олигоэфир в начале процессов деструкции проявляли доста-

точно высокую стабильность к воздействию температуры при сопоставимых значениях T_{10} , равных 372–378 °С, ароматические олигоэфирамиды начинали разлагаться при температурах более чем на 50°С ниже, чем у олигоэфиров.

Ключевые слова: жидкокристаллические полимеры, фазовые переходы, поляризационная микроскопия, термическая стабильность, растворимость, высокотемпературная поликонденсация.

Information about authors*

Deberdeev, Timur Rustamovich — Doctor of Technical Sciences, Chair of Department, Kazan National Research Technological University, Karl Marx street, 68, 420015, Kazan, Russia; e-mail: deberdeev@mail.com; <https://orcid.org/0000-0003-2714-519X>;

Akhmetshina, Alsu Islamovna (*corresponding author*) — Candidate of Chemical Sciences, Associate Professor, Kazan National Research Technological University, Karl Marx street, 68, 420015, Kazan, Russia; e-mail: aai-89@mail.ru; <https://orcid.org/0000-0003-3960-8462>;

Karimova, Liana Katifyanovna — Candidate of Technical Sciences, Associate Professor, Kazan National Research Technological University, Karl Marx street, 68, 420015, Kazan, Russia; e-mail: li-karimova@yandex.ru; <https://orcid.org/0000-0002-3061-296X>;

Grishin, Sergey Vaycheslavovich — PhD student, Kazan National Research Technological University, Karl Marx street, 68, 420015, Kazan, Russia; e-mail: svg95@list.ru;

Kochemasova, Darya Vladimirovna — PhD student, Kazan National Research Technological University, Karl Marx street, 68, 420015, Kazan, Russia; e-mail: d_kochemasova@inbox.ru.

*The author's name is presented in the order: *Last Name, First and Middle Names*

A.T. Kazhmuratova¹, M.S. Zhunissova^{1*}, J. Plocek²,
V.N. Fomin¹, A.Zh. Sarsenbekova¹, T.O. Khamitova³

¹Karagandy University of the name of academician E.A. Buketov, Karaganda, Kazakhstan;

²Institute of Inorganic Chemistry of the Czech Academy of Sciences, Husinec-Rez, Czech Republic;

³S. Seifullin Kazakh Agro Technical University, Nur-Sultan, Kazakhstan

(*Corresponding author's e-mail: meruert_zhunusova@mail.ru)

Influence of the RAFT Agent on the Reaction Direction of the Copolymerization of Polypropylene Glycol Maleate with Acrylic Acid

This work demonstrates the capability of synthesizing new polymers based on unsaturated polyester and acrylic acid in the presence of a chain-transfer agent in a dioxane solution. The initial unsaturated polyester resin was derived from the polycondensation reaction of alcohol and maleic anhydride. The molecular weight of the polypropylene glycol maleate was determined by gel permeation chromatography. The dependence of the structure, network density and product yield on the concentration of the RAFT agent was proven. It was found that the greater the amount of chain-transfer agent in the monomer mixture, the lower the yield of the crosslinked polymer and the greater the yield of the branched copolymer. The composition of the studied copolymers was determined by FTIR spectroscopy in conjunction with the chemometric method of partial least squares in the R environment. The synthesized objects were characterized by infrared spectroscopy methods and were approximated by Gaussian contours. The study results show that the RAFT agent concentration, as well as the initial ratio of monomers in the copolymer affects the products yield. The surface topography of the studied copolymers was recorded by scanning electron microscopy. The molecular chain structure of the branched copolymers was confirmed by NMR spectroscopy.

Keywords: unsaturated polyester, polypropylene glycol maleate, acrylic acid, RAFT-polymerization.

Introduction

Currently the interest of researchers is directed to the search for new materials for the synthesis of polymers with desired properties and controlled characteristics [1, 2]. From this point of view, unsaturated polyester resins based on polypropylene glycol maleate and acrylic acid are interesting objects for theoretical and practical research, since they have been used in the production of smart systems with a wide range of applications [3, 4].

Due to the presence of a reactive double bond in the composition, unsaturated polyester resins easily enter into a copolymerization reaction with ionic monomers, forming cross-linked copolymers with a random network arrangement. As practice shows, this is because radical polymerization has limitations in terms of the degree of control over the molar mass distribution, copolymer composition, and macromolecular architecture [5].

In this regard, the attention of researchers is attracted by new effective polymers that provide unlimited possibilities for controlling their properties under conditions of reversible chain transfer by the addition-fragmentation mechanism (RAFT) [6]. The RAFT agent influence on the radical polymerization process is due to a change in the course of the reaction of bimolecular chain termination through its interaction with the growing macroradical and transition to a dormant state up to a certain point. There is a possibility of further chain growth under certain conditions, when a radical removal from the latter is possible and, thus, a step-wise growth of a macromolecule is formed, and an impression of a “pseudo-living” radical polymerization is created [7–9]. Such behavior of the polymerizing system is used to obtain polymers with a narrow molecular weight distribution, as well as block copolymers and graft copolymers [10, 11].

Previously, we established the possibility of synthesizing [12] and studying the properties [13] of new RAFT polymers based on polypropylene glycol maleate with acrylic acid. These results showed that the concentration of the chain-transfer agent affected the network density and also led to the formation of a soluble branched polymer. The obtained results demonstrate that work in this direction is promising in terms of obtaining new “smart” systems with desired properties.

However, for the purpose of a comprehensive in-depth study of the obtained materials it seemed interesting to continue research in this direction and follow the reaction course of radical copolymerization of polypropylene glycol maleate with acrylic acid in the RAFT agent presence. It was promising to establish the regularity and feature of RAFT-polymerization, calculate the composition and also study the density of the spatial network of the obtained copolymers.

Experimental

There were used the following reagents in this work: propylene glycol, maleic anhydride, acrylic acid (AA), benzoyl peroxide, zinc chloride, 1,4-dioxane, RAFT-agent (2-Cyano-2-propyl dodecyl trithio-carbonate CPDT) from Sigma-Aldrich.

Polypropylene glycol maleate (p-PGM) was derived from the polycondensation reaction of propylene glycol and maleic anhydride at a temperature of 433–443 K. The polycondensation was carried out according to the standard procedure [14] in the presence of a zinc chloride catalyst in a nitrogen flow to avoid gelatinization. Polycondensation was carried out for 16 hours. The molecular weight of the synthesized p-PGM was determined by gel permeation chromatography (GPC).

Radical copolymerization of p-PGM with AA (10:90 mol %) was carried out in a dioxane solution (1:1 by mass) in the presence of benzoyl peroxide (PB) as an initiating agent at 333 K. After purging with an inert gas for 30 minutes, the radical copolymerization was carried out for 52 hours. The resulting copolymers were repeatedly washed with dioxane and dried to a constant weight in a vacuum drying oven.

RAFT polymerization of p-PGM-AA was carried out in a dioxane solution with the addition of the RAFT agent. Monomer solutions were poured into ampoules, degassed in a vacuum unit, and then sealed; the ampoules were placed in a thermostat, in which the temperature was maintained with an accuracy of $\pm 0.10\text{C}$ for 52 hours. After a period of time, the ampoules were cooled and opened. The products obtained as a result of the reaction were divided quantitatively: the cross-linked polymers were filtered from the mother liquor and sent to dry in a vacuum oven until a constant weight was established. Branched polymers were precipitated from the mother liquor in alcohol.

The structural parameters of the molecular chain of branched p-PGM-AA-CPDT copolymers and the initial p-PGM oligomer were determined through $^1\text{H-NMR}$ spectroscopy in deuterated CDCl_3 using a JNM-ECA Jeol 400 NMR spectrometer.

The composition of the derived polymers was determined by HPLC on a Shimadzu (Japan) chromatograph by the amount of unreacted monomers, as well as by IR spectroscopy.

Fourier-transform infrared spectra of the copolymerization products were recorded on an FSM 1201. For complete reliability of the obtained data, the IR spectra of the reaction products were recorded in a KBr tablet, absorption spectra were recorded in the range of $450\text{--}4000\text{ cm}^{-1}$.

The surface topography of the samples was carried out on a MIRA3 scanning electron microscope (TESCAN, Czech Republic).

The swelling behavior of the copolymers was identified gravimetrically by the formula:

$$\alpha(\%) = \frac{m_1 - m_0}{m_0} \times 100,$$

where, m_1 and m_0 are the masses of swollen and dry copolymer, respectively.

Results and Discussion

In our previous studies [12], the use of controlled radical polymerization in the presence of RAFT agents made it possible to obtain polymer matrices with a less rigid structure, capable of sorbing a significantly larger volume of water, as well as to obtain branched copolymers. Thus, in continuation of these works, this article studied the effect of RAFT agent concentrations on the direction of the copolymerization reaction of polypropylene glycol maleate (p-PGM) with acrylic acid (AA) at a molar ratio of 10:90. Table 1 illustrates the calculated data for copolymerization with the addition of a RAFT agent.

According to Table 1, the copolymerization of p-PGM with AA yields two products, branched and cross-linked copolymers. It is established that the higher the concentration of the RAFT agent contained in the monomer mixture, the greater the yield of branched copolymers. It should be noted that the yield of network copolymers is higher than in the case in the ratio of 50:50 [13]. Also, with an increase in the amount of chain transfer agent, the degree of swelling of network copolymers increases, which is associated with a decrease in network density.

Table 1

Radical copolymerization of polypropylene glycol maleate with acrylic acid in a dioxane solution in the presence of a RAFT agent. [M1]:[M2] = 9.9: 90.1 mol %, T = 343 K, [PB] = $8 \cdot 10^{-3}$ mol/l

[RAFT], mM	Cross- linked Copolymer			Branched copolymer	
	Yield, %	[m ₁]:[m ₂] Mol, %	Swelling, α , %	Yield, %	[m ₁]:[m ₂] Mol, %
–	97.16	10.74:89.26	109.14	–	–
10.01	93.15	10.43:89.57	133.18	3.46	5.5:94.5
30.03	91.02	10.61:89.39	156.21	5.23	8.33:91.67
50.01	81.81	10.78:89.22	191.13	13.70	7.9:92.1
80.02	74.23	9.80:90.20	204.18	20.59	9.67:90.33

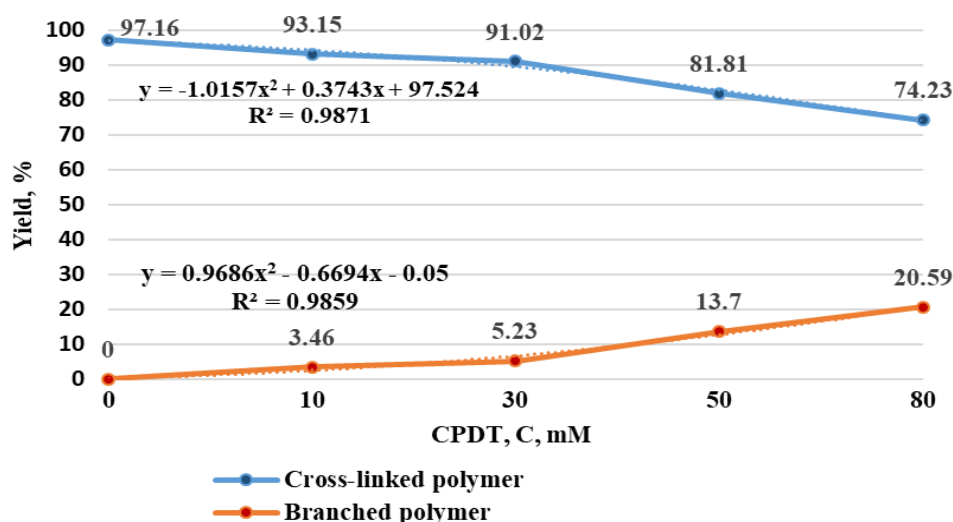


Figure 1. Dependence of the RAFT agent concentration on the polymer yield

From Figure 1 it can be seen that the dependence of the products yield is polynomial of the second order.

The mass ratio of polyacrylic acid units and polypropylene glycol maleate units in the synthesized objects was determined by FTIR spectroscopy in compatibility with the chemometric method of partial list squares [15] performed in the R environment [16, 17]. Mixtures of p-AA and p-PGM were prepared for the calibration spectrum. A homopolymer mixture with compositions of 1.0, 3.0, 5.0, 7.0, 9.0, and 10.0 % p-AA and p-PGM was ground to 100 % for a long time in a mechanical agate mortar together with potassium chloride. To achieve the ultimate accuracy of the IR spectra in three repeated samples, abrasion was carried out for 30 minutes.

The sample preparation of the synthesized copolymers was carried out in a similar way. Three tablets were prepared from a carefully homogenized mixture. The infrared spectra of tablets containing 4.0 mg of polymers in 300.0 mg of KBr were recorded in the range of 450...4000 cm^{-1} . The data from the spectra were entered into the R environment for the next mathematical processing. Model training with cross-validation was performed on averaged samples. To calculate the mass fraction of polyacrylic acid units in polymers (Table 1) for three parallel samples, the Student's coefficient was taken into account with a confidence level $p=0.95$. The obtained mass values were converted to molar ratios.

Figure 2 shows the IR spectra of p-PGM-AA and p-PGM-AA-CPDT copolymers.

The IR spectra of the copolymers show (Fig. 2 a) absorption bands in the region of 787 cm^{-1} attributed to CH_2 - bonds and bands in the region of 1133 cm^{-1} indicating the presence of $-\text{C}-\text{O}-\text{C}-$ ester bonds. The spectrum exhibits a pronounced peak in the region of 1282 cm^{-1} , which is responsible for the $-\text{C}=\text{C}-$ moiety of the polyester group. Further, the presence of signals at 1627 cm^{-1} and 3027 cm^{-1} indicates $\text{C}=\text{O}$ bonds of the $-\text{COOH}$ group and symmetrically located $-\text{CH}$ bonds in CH_2 , respectively. It is worth noting the signal in the region of 3711 cm^{-1} indicating the presence of $-\text{OH}$ groups.

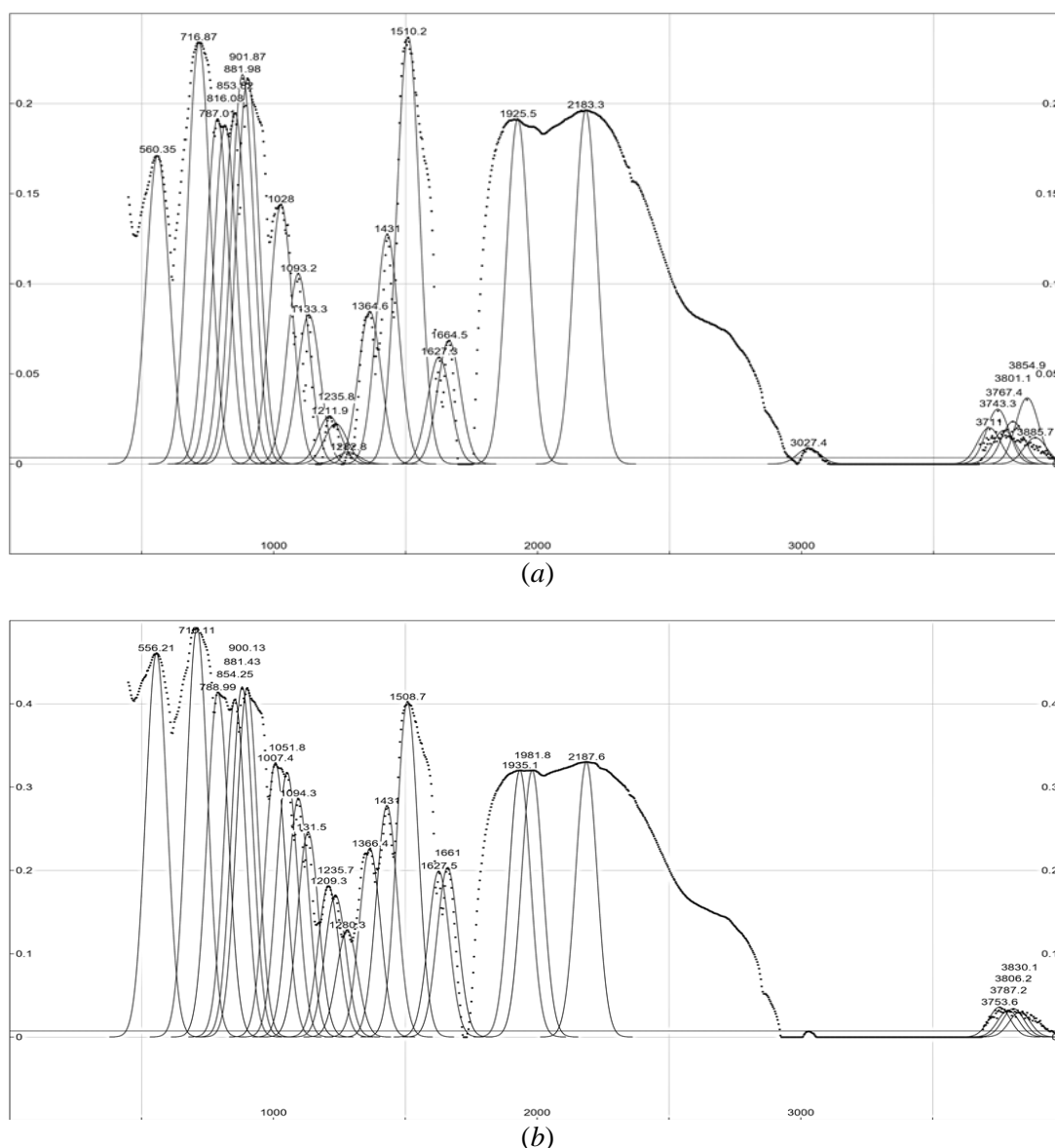


Figure 2. The IR spectra of p-PGM-AA (a) and p-PGM-AA-[CPDT] = 80mM (b)

Further, the IR spectra of RAFT polymers, namely p-PGM-AA-CPDT (Fig. 2b) were obtained. There was a signal in the region of 3753 cm^{-1} , which was characteristic of hydroxyl groups. An absorption band in the region of 3787 cm^{-1} was attributed to the $=\text{C}-\text{H}$ bonds of the aromatic compound and a weak band in the region of 2187 cm^{-1} was due to $\text{C}-\text{H}$ groups of the aliphatic compound.

An analysis of the IR spectra showed that the p-PGM-AA molecular chain contained $-\text{COOH}$ and $-\text{CH}_2$ groups, which served as transverse bridges in the formation of the cross-linked structure of copolymers. Thus, the mechanism of the copolymerization reaction of p-PGM with AA in the presence of benzoyl peroxide initiator can proceed according to the following scheme shown in Figure 3.

Figure 3(b) shows the formation of branched copolymers by reducing bimolecular chain terminations with the help of adding a RAFT agent.

In order to identify branched polymers, their NMR spectra were obtained. In the spectrum, signals of maleic groups and groups characteristic of p-PGM are observed, which are similar to the data of the initial oligomer (Fig. 4). The ^1H NMR spectrum of p-PGM-AA-CPDT shows a broad signal in the region of 1.13-1.28 ppm that corresponds to the $-\text{CH}_2$ protons of the Hb groups, which are closer to oxygen. Two multiplet signals in the region of 4.01-4.27 and 3.64 ppm point to the protons of simple and ester methine as well as methylene groups of the aliphatic hydrocarbon Hc and Hd. Multiplet signals at 5.02-5.22 and high-intensity multiplet at 6.78-6.82 ppm are assigned to the $-\text{CH}=\text{CH}-$ proton of the He group.

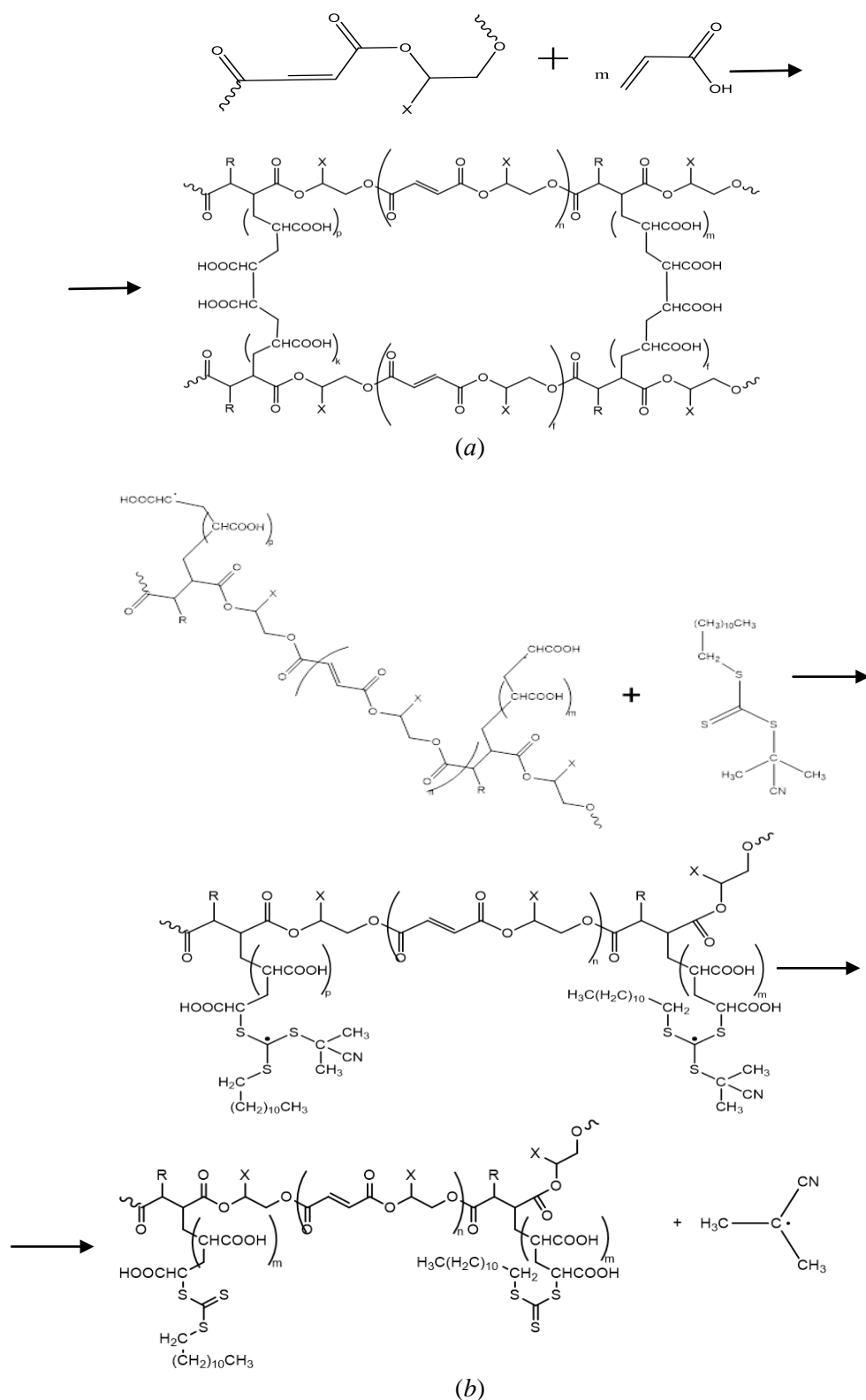


Figure 3. Schematic structure of p-PGM-AA (a), p-PGM-AA-CPDT (b)

In the ^{13}C NMR spectrum of the copolymer Ca and Cb signals at 16.35 ppm correspond to methyl and methylene carbon atoms. Signals of alkyl groups, Cc and Cd, located next to simple and complex ether groups are in the region of 66.67 and 69.22 ppm. Signals with a chemical shift of 133.83 ppm indicate ethylene carbon atoms, namely Ce. The carbon atoms of $-\text{COOH}$ groups and $\text{C}=\text{O}$ fragments appear at 134.09 ppm.

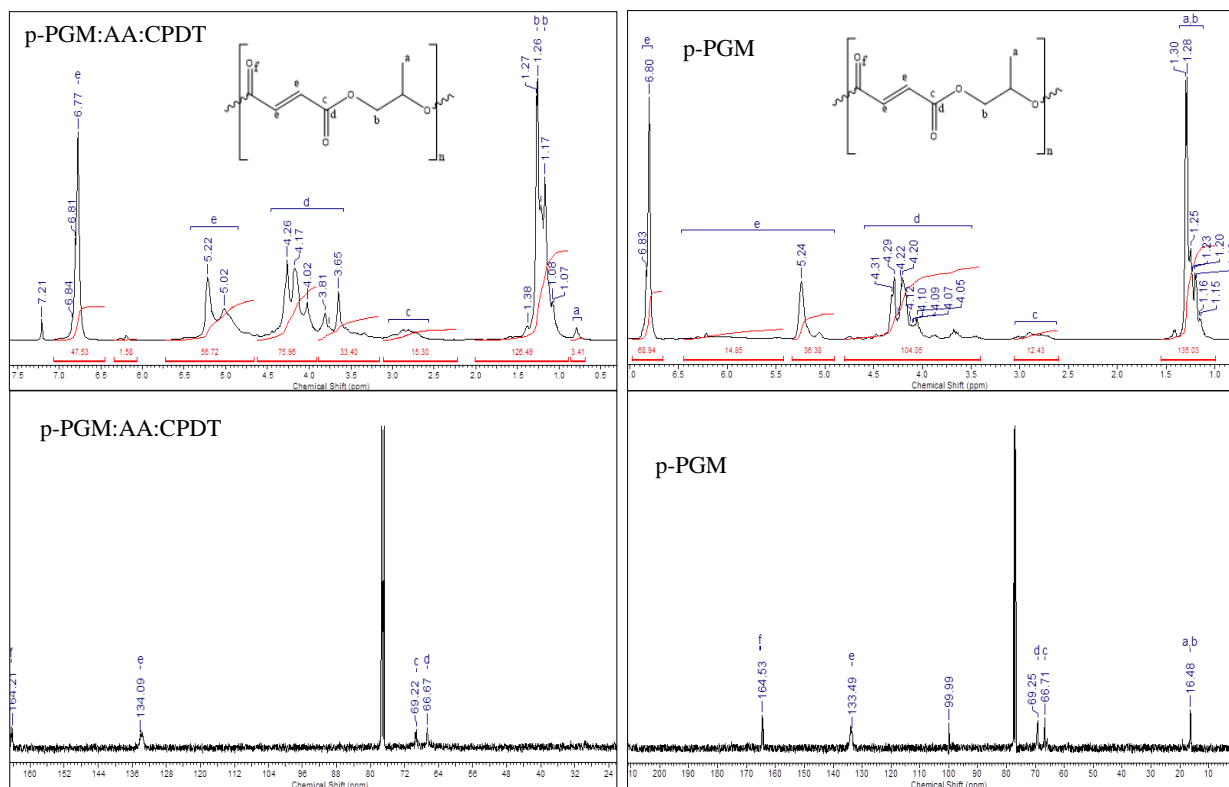


Figure 4. NMR spectra of p-PGM:AA:[CPDT] = 80 mM and p-PGM copolymers

In continuation of the study, the surface topography of the copolymers was determined by SEM.

From Fig. 5(a), under a magnification of 2 nm, it is observed that the surface of the p-PGM-AA cross-linked copolymer particles (a) has brittle cleavages corresponding to solid objects.

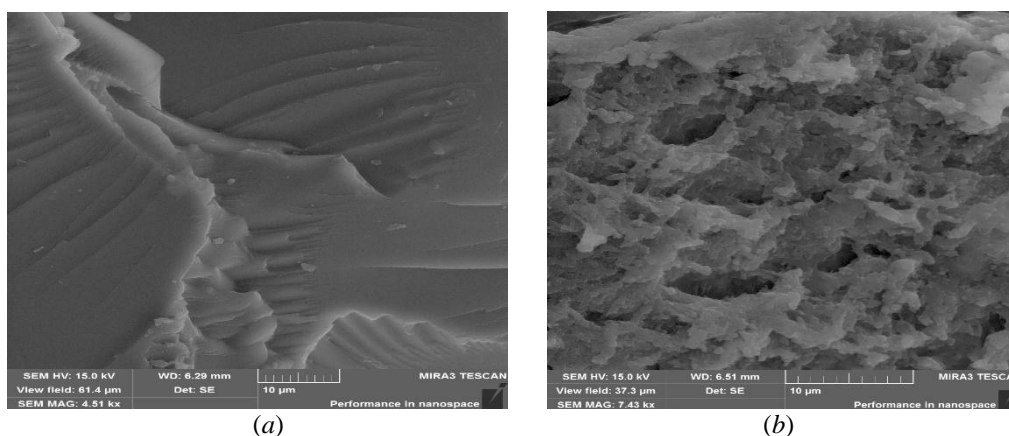


Figure 5. Surface morphology of p-PGM-AA polymer (a); polymer surface morphology p-PGM-AA-[CPDT] = 80 · 10⁻³ mM (b)

Micrographs of samples containing the RAFT agent p-PGM-AA-CPDT (b) show that the surface has a layered, loose structure with pores. The surface of RAFT polymers is softer and more airy compared to p-PGM-AA copolymers. The electron microscopy images confirm that an increase in the concentration of the chain transfer agent in the composition of the monomer mixture leads to an increase in pores in the network structure of the crosslinked copolymer.

Conclusions

As a result of the attempt to change the directions of the copolymerization reactions of polypropylene glycol maleate with acrylic acid, it was found that varying the amount of chain transfer agent allowed the

reaction to be carried out in two directions, forming cross-linked and branched copolymers. Scanning electron microscopy showed that polymers containing a RAFT agent had a looser, airy surface with the formation of pores. It was established by the gravimetric method that the swelling ability of the obtained hydrogels containing CPDT in the composition of the monomer mixture at a molar ratio of 10:90 PGM and AA made it possible to obtain products with satisfactory sorbing properties.

Summarizing the above, it should be noted that the behavior of the synthesized copolymers during swelling directly depends on the amount of the RAFT agent included in the polymers composition. In addition, it can be concluded that the network construction and the products yield depend on the concentration of the RAFT agent, as well as on the comonomers, which prevents randomness in the structure. Thus, this method makes it possible to purposefully obtain copolymers with polyfunctional properties, which makes them promising hydrogels.

References

- 1 Zhang L.Q. A photo-thermal dual-regulated latent monomer strategy for sequence control of polymers/ L.Q. Zhang., Y.Y. Song., Y.H. Cao., Z. Wang., Z.H. Huang., S.T. Xuan., Z.B. Zhang // *Polymer chemistry*. — 2021. — Vol. 12, № 35. — P. 4996–5002. <https://doi.org/10.1039/d1py00961c>
- 2 Aoyagi T. Optimization of the elastic properties of block copolymers using coarse-grained simulation and an artificial neural network / T. Aoyagi / *Computational Materials Science*. — 2022. — Vol.207, № 111286. <https://10.1016/j.commat.2022.111286>
- 3 Sarsenbekova A.Z. Comparative Analysis of the Thermal Decomposition Kinetics of Polyethylene Glycol Fumarate–Acrylic Acid Copolymers/ A.Z. Sarsenbekova, G.K. Kudaibergen, M.Z. Burkeev, G.K. Burkeeva // *Russian Journal of Physical Chemistry A*. — 2019. — Vol. 93, № 7. — P. 1252–1257. <https://doi.org/10.1134/s0036024419060281>
- 4 Hu, J. Smart polymers for textile applications/ J. Hu, J. Lu // *Smart Polymers and Their Applications*. — 2014. — P. 437–475. <https://doi.org/10.1533/9780857097026.2.437>
- 5 Burkeev M.Zh. Poly(propylene fumarate phthalate) and acrylic acid radical copolymerization constants and parameters / M.Zh. Burkeev, G.M. Zhumanazarova, E.M. Tazhbayev, G.K. Kudaibergen, S.B. Aukadiev, E.Z. Zhakupbekova // *Bulletin of the university of Karaganda – Chemistry*. — 2020. — № 97. — P. 68–74. <https://doi.org/10.31489/2020Ch1/68-74>
- 6 Wang X. New Insights into RAFT Dispersion Polymerization-Induced Self-Assembly: From Monomer Library, Morphological Control, and Stability to Driving Forces/ X.Wang, Z. An // *Macromolecular Rapid Communications*. — 2018. — Vol. 40, № 2. — P. 1–14. <https://doi.org/10.1002/marc.201800325>
- 7 Barner-Kowollik C. *Handbook of RAFT polymerization*. — Weinheim: Wiley-vch, 2008. — 541 p. <https://10.1002/9783527622757>
- 8 Chiefari, J. *Living Free-Radical Polymerization by Reversible Addition–Fragmentation Chain Transfer: The RAFT Process*/ J. Chiefari, Y.K. (Bill) Chong, F. Ercole, J. Krstina, J. Jeffery, T.P.T. Le, R.T.A. Mayadunne, G.F. Meijs, C.L. Moad, G., Moad, E. Rizzardo, S.H. Thang // *Macromolecules*. — 1998. — Vol. 31, № 16. — P. 5559–5562. <https://doi.org/10.1021/ma9804951>
- 9 Chong, Y.K. A More Versatile Route to Block Copolymers and Other Polymers of Complex Architecture by Living Radical Polymerization: The RAFT Process / Y.K. Chong, T. P.T. Le, G. Moad, E. Rizzardo, S.H. Thang // *Macromolecules*. — 1999. — Vol. 32, № 6. — P. 2071–2074. <https://doi.org/10.1021/ma981472p>
- 10 Han S. Utilization of Poor RAFT Control in Heterogeneous RAFT Polymerization/ S. Han, J. Wu, Y. Zhang, J. Lai, Y. Chen, L. Zhang, J. Tan // *Macromolecules*. — 2021. — Vol. 54, № 10. — P. 4669–4681. <https://doi.org/10.1021/acs.macromol.1c00381>
- 11 Easterling C.P. Block Copolymer Sequence Inversion through Photoiniferter Polymerization / C.P. Easterling, Y. Xia, J. Zhao, G.E. Fanucci, B.S. Sumerlin // *ACS Macro Letters*. — 2019. — P. 1461–1466. <https://doi.org/10.1021/acsmacrolett.9b00716>
- 12 Burkeev M.Zh. Influence of RAFT Agent on the Mechanism of Copolymerization of Polypropylene Glycol Maleinate with Acrylic Acid / M.Zh. Burkeev, M.S. Zhunisova, Y.M. Tazhbayev, V.N. Fomin, A.Zh. Sarsenbekova, G.K. Burkeyeva, A.T. Kazhuratova, T.S. Zhumagalieva, E.Zh. Zhakupbekova, T.O. Khamitova // *Polymers*. — 2022. — Vol.14, № 9. — P. 1884 <https://doi.org/10.3390/polym14091884>
- 13 Burkeyev M.Zh. Properties of cross-linked copolymers of polypropylene glycol maleate with acrylic acid obtained at various concentrations of the RAFT agent/ M.Zh. Burkeyev, M.S. Zhunisova, Jiri Plocek, A.T. Kazhuratova, T.S. Zhumagalieva // *Bulletin of the University of Karaganda – Chemistry*. — 2022. — Vol. 105, № 1. — P. 15–24. <https://doi.org/10.31489/2022Ch1/15-24>
- 14 Торопцева А.В. Лабораторный практикум по химии и технологии высокомолекулярных соединений / А.В. Торопцева, К.В. Белгородская, В.М. Бондаренко. — М.: Химия, 1972. — С. 231–233.
- 15 Wold S. PLS-regression: a basic tool of chemometrics / S. Wold, M. Sjörström, L. Eriksson // *Chemometrics and Intelligent Laboratory Systems*. — 2001. — Vol. 58, № 2. — P. 109–130. [https://doi.org/10.1016/S0169-7439\(01\)00155-1](https://doi.org/10.1016/S0169-7439(01)00155-1)
- 16 R Core Team (2021). R: A language and environment for statistical computing. R Foundation for Statistical Computing, Vienna, Austria. 04.04.22. <https://www.R-project.org/>
- 17 Mevik B.H. Principal component and partial least squares regression in R/ B.H. Mevik, R. Wehrens // *Journal of Statistical Software* — 2007. — Vol.18, № 2. — P. 1–24.

А.Т. Қажмұратова, М.С. Жүнісова, Ю. Плоцек,
В.Н. Фомин, А.Ж. Сарсенбекова, Т.Ө. Хамитова

RAFT-агентінің полипропиленгликольмалеинатының акрил қышқылымен сополимерлену реакциясының бағытына әсері

Мақалада қанықпаған полиэфир және акрил қышқылы негізінде диоксан ерітіндісіндегі тізбекті тасымалдаушы агенттің қатысуымен жаңа полимерлерді синтездеу мүмкіндігі көрсетілген. Бастапқы қанықпаған полиэфир шайыры спирт пен малеин ангидридіннің поликонденсациялану реакциясынан алынған. Полипропиленгликольмалеинатының молекулалық салмағы гелді-өткізу хроматографиясы арқылы анықталған. Құрылымның, полимердің тығыздығының және өнім шығымының RAFT-агентінің концентрациясына тәуелділігі дәлелденді. Мономер қоспасында тізбекті тасымалдағыштың мөлшері неғұрлым көп болса, соғұрлым тігілген полимердің шығымы төмен, ал тармақталған сополимердің шығымы соғұрлым жоғары болатыны табылған. Зерттелетін сополимерлердің құрамы R ортасында ішінара ең кіші квадраттардың (Жартылай тізім квадраттары немесе жасырын құрылымдарға проекциялау) химометриялық әдісімен бірге FTIR-спектроскопия арқылы анықталған. Синтезделген объектілер инфрақызыл спектроскопиялық әдістермен сипатталды және Гаусс контурларымен жақындатылды. Осы зерттеу нәтижелері сополимердегі мономер буындарының қатынасы өнімдердің шығымына әсер ететінін көрсетеді. Зерттелген сополимерлер бетінің топографиясы сканерлеуші электронды микроскоп арқылы жазылды. Тармақталған сополимерлердің молекулалық тізбек құрылымы ЯМР спектроскопиясымен расталды.

Кілт сөздер: қанықпаған полиэфир, полипропиленгликольмалеинаты, акрил қышқылы, RAFT-полимерлеу.

А.Т. Кажмуратова, М.С. Жунисова, Ю. Плоцек,
В.Н. Фомин, А.Ж. Сарсенбекова, Т.О. Хамитова

Влияние RAFT-агента на направление реакции сополимеризации полипропиленгликольмалеината с акриловой кислотой

В статье показана возможность синтеза новых полимеров на основе ненасыщенного полиэфира и акриловой кислоты в присутствии агента передачи цепи в растворе диоксана. Исходная ненасыщенная полиэфирная смола была получена реакцией поликонденсации спирта и малеинового ангидрида. Молекулярная масса полипропиленгликольмалеината определена с помощью гель-проникающей хроматографии. Доказана зависимость строения, плотности сетки и выхода продуктов от концентрации RAFT-агента. Установлено, что чем больше содержится агента передачи цепи в мономерной смеси, тем меньше выход шитого полимера и больше выход разветвленного сополимера. Состав исследуемых сополимеров определен посредством FTIR-спектроскопии совместно с хемометрическим методом частичных наименьших квадратов (Partial List Squares or Projection to Latent Structures) в среде R. Синтезированные объекты охарактеризованы методами инфракрасной спектроскопии и были аппроксимированы контурами Гаусса. Результаты данного исследования показывают, что соотношение мономерных звеньев в сополимере влияет на выход продуктов. Топография поверхности исследуемых сополимеров зафиксирована посредством сканирующей электронной микроскопии. Структура молекулярной цепи разветвленных сополимеров подтверждена ЯМР-спектроскопией.

Ключевые слова: ненасыщенный полиэфир, полипропиленгликольмалеинат, акриловая кислота, RAFT-полимеризация.

References

- 1 Zhang, L.Q., Song, Y.Y., Cao, Y.H., Wang, Z., Huang, Z.H., Xuan, S.T., & Zhang Z.B. (2021). A photo-thermal dual-regulated latent monomer strategy for sequence control of polymers. *Polymer chemistry*, 12(35), 4996–5002. <https://doi:10.1039/d1py00961c>
- 2 Aoyagi, T. (2022). Optimization of the elastic properties of block copolymers using coarse-grained simulation and an artificial neural network. *Computational Materials Science*, 207(111286). <https://10.1016/j.commatsci.2022.111286>
- 3 Sarsenbekova, A.Z., Kudaibergen, G.K., Burkeev, M.Z., & Burkeeva, G.K. (2019). Comparative Analysis of the Thermal Decomposition Kinetics of Polyethylene Glycol Fumarate–Acrylic Acid Copolymers. *Russian Journal of Physical Chemistry A*, 93(7), 1252–1257. <https://doi:10.1134/s0036024419060281>
- 4 Hu, J., & Lu, J. (2014). Smart polymers for textile applications. *Smart Polymers and Their Applications*, 437–475. <https://doi:10.1533/9780857097026.2.437>

- 5 Burkeev, M.Zh., Zhumanazarova, G.M., Tazhbayev, E.M., Kudaibergen, G.K., Aukadiyeva, S.B., & Zhakupbekova, E.Zh. (2020). Poly(propylene fumarate phthalate) and acrylic acid radical copolymerization constants and parameters. *Bulletin of the University of Karaganda — Chemistry*, 97(4), 68–74. <https://doi:10.31489/2020Ch1/68-74>
- 6 Wang, X., & An, Z. (2018). New Insights into RAFT Dispersion Polymerization-Induced Self-Assembly: From Monomer Library, Morphological Control, and Stability to Driving Forces. *Macromolecular Rapid Communications*, 40(2), 1–14. <https://doi:10.1002/marc.201800325>
- 7 Barner-Kowollik, C. (2008). Handbook of RAFT polymerization. Weinheim: Wiley-vch, 541 p. <https://10.1002/9783527622757>
- 8 Chiefari, J., Chong, Y.K. (Bill), Ercole, F., Krstina, J., Jeffery, J., Le, T.P.T., Mayadunne, R.T.A., Meijs, G.F., Moad, C.L., Moad, G., Rizzardo, E., & Thang, S.H. (1998). Living Free-Radical Polymerization by Reversible Addition–Fragmentation Chain Transfer: The RAFT Process. *Macromolecules*, 31(16), 5559–5562. <https://doi:10.1021/ma9804951>
- 9 Chong, Y.K., Le, T.P.T., Moad, G., Rizzardo, E., & Thang, S.H. (1999). A More Versatile Route to Block Copolymers and Other Polymers of Complex Architecture by Living Radical Polymerization: The RAFT Process. *Macromolecules*, 32(6), 2071–2074. <https://doi.org/10.1021/ma981472p>
- 10 Han, S., Wu, J., Zhang, Y., Lai, J., Chen, Y., Zhang, L., & Tan, J. (2021). Utilization of Poor RAFT Control in Heterogeneous RAFT Polymerization. *Macromolecules*, 54(10), 4669–4681. <https://doi:10.1021/acs.macromol.1c00381>
- 11 Easterling, C.P., Xia, Y., Zhao, J., Fanucci, G.E., & Sumerlin, B.S. (2019). Block Copolymer Sequence Inversion through Photoiniferter Polymerization. *ACS Macro Letters*, 1461–1466. <https://doi.org/10.1021/acsmacrolett.9b00716>
- 12 Burkeev, M.Zh., Zhunissova, M.S., Tazhbayev, Y.M., Fomin, V.N., Sarsenbekova, A.Zh., Burkeyeva, G.K., Kazhuratova, A.T., Zhumagalieva, T.S., Zhakupbekova, E.Zh., & Khamitova, T.O. (2022). Influence of RAFT Agent on the Mechanism of Copolymerization of Polypropylene Glycol Maleinate with Acrylic Acid. *Polymers*, 14(9). <https://doi.org/10.3390/polym14091884>
- 13 Burkeyev, M.Zh., Zhunissova, M.S., Plocek, Jiri, Kazhuratova, A.T., & Zhumagalieva, T.S. (2022). Properties of cross-linked copolymers of polypropylene glycol maleate with acrylic acid obtained at various concentrations of the RAFT agent. *Bulletin of the University of Karaganda — Chemistry*, 105(1), 15–24. <https://doi.org/10.31489/2022Ch1/15-24>
- 14 Toroptseva, A.V., Belogorodskaya, K.V., & Bondarenko, V.M. (1972). *Laboratornyi kurs po khimii i tekhnologii vysokomolekuliarnykh soyedinenii [Laboratory course on chemistry and technology of macromolecular compounds]*. Moscow: Khimiia [in Russian].
- 15 Wold S., Sjöström M., & Eriksson L. (2001). PLS-regression: a basic tool of chemometrics. *Chemometrics and Intelligent Laboratory Systems*, 58(2), 109–130. [https://doi.org/10.1016/S0169-7439\(01\)00155-1](https://doi.org/10.1016/S0169-7439(01)00155-1)
- 16 R Core Team (2021). R: A language and environment for statistical computing. R Foundation for Statistical Computing, Vienna, Austria. 04.04.22. <https://www.R-project.org/>
- 17 Mevik B.H., & Wehrens, R. (2007). The pls package: Principal component and partial least squares regression in R. *Journal of Statistical Software*, 18(2), 1–24.

Information about authors*

Kazhuratova, Akerke Temirgalievna — Candidate of Chemical Sciences, Karagandy University of the name of academician E.A. Buketov, Universitetskaya street, 28, 100024, Karaganda, Kazakhstan; e-mail: kazhuratova@mail.ru; <https://orcid.org/0000-0003-4044-8419>;

Zhunissova, Meruyert Serikhanovna (corresponding author) — 2st year PhD student, Karagandy University of the name of Academician E.A. Buketov, Universitetskaya street, 28, 100024, Karaganda, Kazakhstan; e-mail: meruert_zhunissova@mail.ru; <https://orcid.org/0000-0001-6376-8955>;

Plocek, Jiri — PhD, CSc. Institute of Inorganic Chemistry of the Czech Academy of Sciences, Czech Republic, Husinec-Rez 1001 25068 Rez; e-mail: plocek@iic.cas.cz; <https://orcid.org/0000-0001-6082-5766>;

Fomin, Vitaliy Nikolaevich — Candidate of Chemical Sciences, Karagandy University of the name of academician E.A. Buketov, Universitetskaya street, 28, 100024, Karaganda, Kazakhstan; e-mail: vitfomin@mail.ru; <https://orcid.org/0000-0002-2182-2885>

Sarsenbekova, Akmaral Zhakanovna — PhD, Associate Professor, Karagandy University of the name of academician E.A. Buketov, Universitetskaya street, 28, 100024, Karaganda, Kazakhstan; e-mail: chem_akmaral@mail.ru; <https://orcid.org/0000-0002-8951-3616>

Khamitova, Tolkyndy Ondirisovna — PhD, Department of Soil Science and Agrochemistry, Agronomic Faculty, S. Seifullin Kazakh Agro Technical University, 010000, Nur-Sultan, Kazakhstan; e-mail: khamitova.t@inbox.ru; <https://orcid.org/0000-0002-4691-3732>

*The author's name is presented in the order: *Last Name, First and Middle Names*

M.Zh. Burkeyev¹, S.R. Shibayeva^{1*}, T.O. Khamitova², Jiri Plocek³,
M.T. Nurmaganbetova¹, A.T. Kazhmuratova¹, T.S. Zhumagalieva¹

¹Karagandy University of the name of academician E.A. Buketov, Karaganda, Kazakhstan;

²S. Seifullin Kazakh Agro Technical University, Nur-Sultan, Kazakhstan;

³Institute of Inorganic Chemistry of the Czech Academy of Sciences, Husinec-Rez, Czech Republic

(*Corresponding author's e-mail: sali_r@mail.ru)

Synthesis and Investigation of the Properties of Polymer-immobilized Silver- and Gold Nanoparticles

Metal–polymer composites (MPC) based on copolymers of polypropylene glycol maleate phthalate with acrylic acid and metallic gold and silver were synthesized for the first time. The structure of nanocomposites is characterized with the help of microscopy and spectroscopy. Antimicrobial activity of novel metal-polymeric complexes based on silver and gold was studied. Metal-polymeric complexes were stabilized for the first time with polymeric matrix based on the copolymers of polypropyleneglycolmaleatephthalate with acrylic acid (p-PGMPH/AA:Ag, p-PGMPH/AA:Au). Obtained nanocomposites contain the nanoparticles of silver and gold of rhomboidal and cylindrical shapes with the sizes of 40–50 and 35–50 nm correspondingly. The size of more than 80 % of the nanoparticles are from 20 to 50 nm and has a spherical and rhombic shape. For determination of antimicrobial activity of the MPC the reference test-microorganisms such as facultative-anaerobe gram-positive *Staphylococcus aureus*, aerobic gram-positive spore-forming *Bacillus subtilis*, gram-negative facultative anaerobe of *Escherichia coli*, aerobic *Pseudomonas aeruginosa* and yeast fungi *Candida albicans* have been used. The resulting nanocomposites are stable and promising for the creation of new photochromic and nonlinear optical materials, as well as for using in medicine in the development of antiseptic and antimicrobial materials that are needed during a pandemic.

Keywords: nanocomposites, nanoparticles, silver, gold, copolymer, polypropylene glycol maleate phthalate with acrylic acid, metal–polymer complex, antimicrobial activity.

Introduction

Nanocomposite materials, containing nanoparticles of silver and gold, possess unique properties and are promising for medicine, optoelectronics, nanophotonics, and catalytic systems. The study of the processes of self-organization of hybrid nanocomposites, the regularities of constructing zero-valency metals' nanoparticles, the problems of their stabilization and accomplishment of narrow-disperse distribution are the fundamental tasks of the modern chemistry of nanomaterials [1–4].

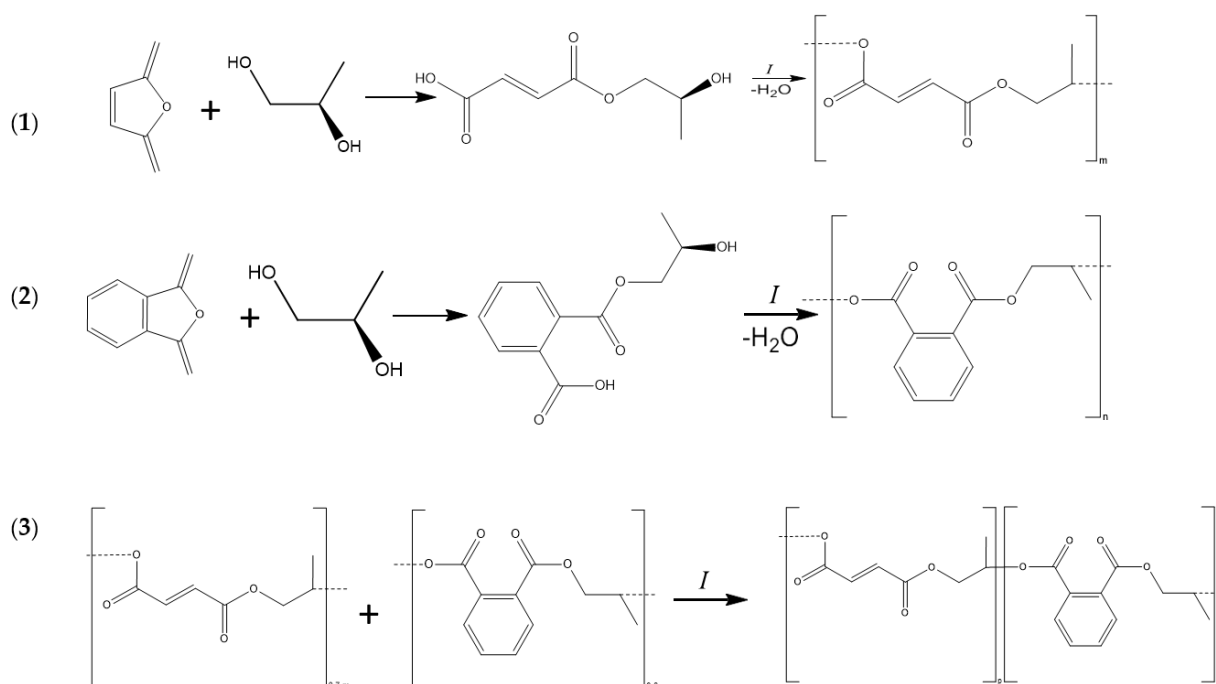
The nature of the nano-stabilizing matrix is substantially significant in designing metal-containing nanocomposites. The synthetic polymers shown previously in [5] are extensively studied as such matrices. The investigations on the development of methods of synthesizing “smart”-polymers based on UPS (unsaturated polyester resins) with unsaturated carboxylic acids have been done. Polymeric materials obtained on their basis possess unique properties which provide using them in a wide range of fields such as agricultural industry, medicine, oil chemistry, and chemical synthesis. The possibility of using the copolymers of p-PGMPH/AA as a matrix for obtaining effective catalysts for hydrogenization has been shown in [5]. Obtained metal-polymer complexes (MPC) contain isolated metal nanoparticles with diameters of 100–112 nm; they are mainly spherical and are evenly distributed within a polymer matrix. In terms of the abovesaid, it is evident, that the synthesis of smart-copolymers with the high water-absorbing volume based on available and rather cheap raw material (UPR cured with ionogenic vinyl monomers) and their study are of great importance [6–10]. The stability of nanoparticles in polymer matrices is maintained for a long time. Large-scale fundamental and applied research to develop innovative materials and technologies, especially nanocomposites, is an urgent task and of great scientific and practical interest. Using metal nanoparticles immobilized in polymers with bactericidal properties, it is possible to obtain medical materials for a wide range of applications: implants, drug delivery systems, antibacterial coatings for biomedical devices, and antimicrobial packaging.

The aim of this work is to synthesize new hybrid nanocomposites with a uniform stable distribution of silver and gold nanoparticles based on copolymers of polypropylene glycol maleate phthalate with acrylic acid (p-PGMP/AA) and evaluate their antibacterial properties.

Experimental

Synthesis of polypropylene glycol maleate phthalate. For obtaining the nanoparticles of metal silver and gold, a chemical way of dispersing these metals by reduction of Argentum nitrate and aurichlorohydric acid with sodium borohydride in an aqueous medium in the presence of polypropylene glycol maleate phthalate with the acrylic acid (p-PGMPh:AA) was used [5].

Polypropylene glycol maleate phthalate (p-PGMPh) was obtained by condensation polymerization of propyleneglycol with maleic, phthalic anhydride at a temperature of 423–433 K in a four-neck flask supplied with a reverse condenser, stirrer (from the top), thermometer, Dean-Stark trap in a nitrogen air. Polycondensation was carried out according to the standard procedure [11] at a constant stirring in the presence of catalyst zinc chloride in nitrogen air to avoid the processes of gelation (Fig. 1).



(1) the formation of an acidic ester of maleic anhydride; (2) the formation of acidic ester of phthalic anhydride; (3) obtaining polypropylene glycol maleate phthalate

Figure 1. Synthesis of polypropylene glycol maleate phthalate

Synthesis of nanocomposites of silver and gold. Immobilization of silver particles in p-PGMP:AA copolymer substrates (1 g) was added to 2 ml of an aqueous solution containing 0.034 g – 0.340 g of AgNO_3 and containing 0.510 g – 1.019 g of HAuCl_4 . The reduction was carried out for 5 h at room temperature. Then 0.012 g – 0.120 g of $\text{Na}(\text{PH}_2\text{O}_2)$ was added in small portions and 0.8 ml of NH_4OH was continued to be vigorously stirred for 12 h at room temperature. Dark gray powders (60–87 % yield) with 20–22 % silver content and dark purple powder (65–80 % yield) with 12–15 % gold content were obtained.

Figure 2 presents the schematic structure of p-PGMPh/AA: Au^0 .

Physicochemical methods of investigation of MPC. The samples for the IR-spectroscopy were prepared by long-termed triturating 2 ± 0.1 mg sample with 200 ± 0.1 mg anhydrous KBr (KBr was a background sample). The samples were pressed under the pressure of 200 atm. IR spectra of obtained materials were recorded on a device FSM1201 (RF, OOO “Infraspec”) in the range of $450\text{--}4000\text{ cm}^{-1}$ with the best possible resolution in a regimen of measuring a relative emission. The number of repeated scanning was increased to maximum – 100 (Fig. 3).

The content of metals in the nanocomposites was determined on an Agilent 4210 atomic emission spectrometer with microwave plasma, in which the flame was acetylene-air, a lamp with a full cathode, a wave-

length of 328 nm, and a slit width of 0.5 nm Agilent 4210 (MP-AES). The study of the structure of samples' surfaces was made on an SEM MIRA3 (TESCAN, Czech Republic). Before the study, the samples were covered with a carbon layer on a sputtering apparatus Quorum Q150R ES (Quorum Technology, Great Britain). The images (Fig. 4) were obtained by using the detector of secondary electrons (SE detector) at an accelerating tension of (HV) 20 kV. Thermal stability of the composites was studied thermogravimetrically on a synchronic TGA/DTA/DC analyzer LabSYSEvo (2014) within the temperature interval of 30–1000 °C in the aluminum oxide crucibles at a heating rate of 5 °C/min in air with the expense of 30 ml/min by putting the weighing of 20 mg (Fig. 5).

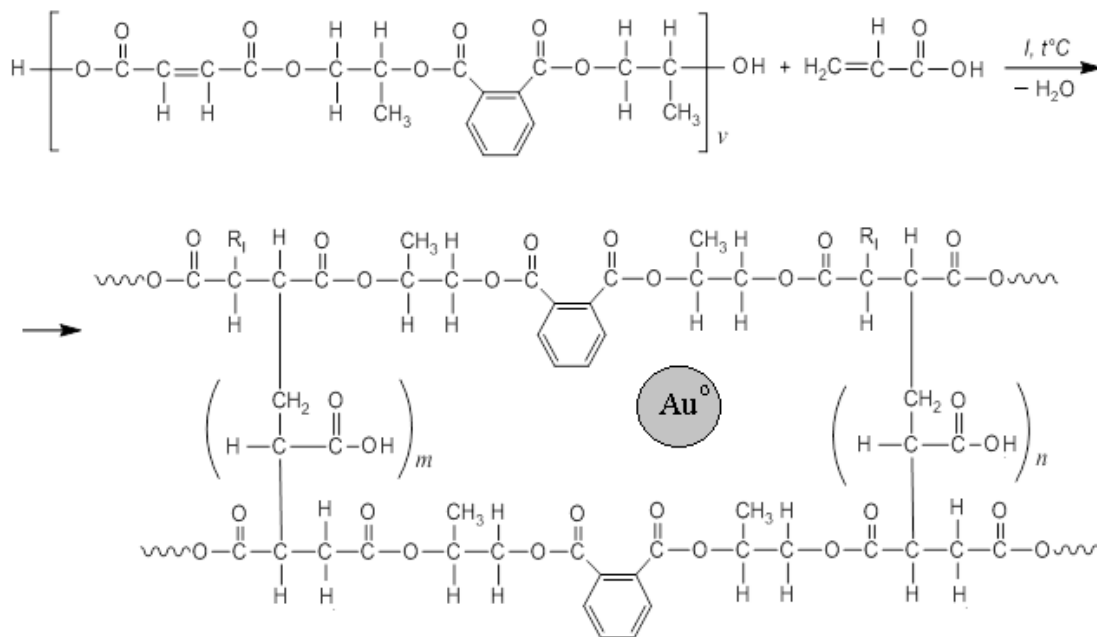


Figure 2. Schematic structure of p-PGMPh/AA:Au⁰

Antimicrobial activity. For determination of the antimicrobial activity of the metal-polymer complexes of p-PGMPh/AA:Au and p-PGMPh/AA:Ag, the reference test microorganisms, such as facultative-anaerobe gram-positive *Staphylococcus aureus* ATCC 6538, aerobic gram-positive spore-forming *Bacillus subtilis* ATCC 6633, gram-negative facultative anaerobe of *Escherichia coli* ATCC 25922, aerobic *Pseudomonas aeruginosa* ATCC 27853, and yeast fungi *Candida albicans* ATCC 10231, were used. Test bacteria of microorganisms used in this study were obtained from the American collection of type cultures. For the antimicrobial studies of complexes of the polymers, the suspensions of test bacteria at concentrations 10⁶ CFU/ml were used. Standard bacterial suspensions were prepared from daily cultures which were grown on an agar slant at a temperature of 37 °C within 24 hours by breeding the culture 1:1000 in a sterile isotonic 0.9 % solution of sodium chloride. 1 mkg of particles' complexes of the polymers p-PGMPh/AA:Au and p-PGMPh/AA:Ag were added to the testing tubes separately. The test tubes were incubated within 1 hour at room temperature [12]. Then the content of the test tubes was poured into the Petri dish with Muller-Khilton agar and they were incubated for 24 hours at a temperature of 37 °C. The results were estimated by defining the presence or absence of growth of microorganisms in the Petri dish which contains testing polymeric complexes in comparison with control.

Results and Discussion

Showing a plasma resonance (PR) is characteristic of gold and silver nanoparticles, which occurs when the frequency of the incident radiation coincides with the frequency of the collective vibration of excited electrons in metal nanoparticles. As a result, an absorption band appears in the visible region of the spectrum, its position significantly depends on the size, shape, and state of the surface of the nanoparticles, as well as on the presence of stabilizing substances and other compounds. The resistance of gold to oxidation and high sensitivity of plasma resonance peak to the state of the surface of nanoparticles allow using them in

the creation of sensors for selective determination of individual substances solving a wide range of analytical problems.

The structure of synthesized monometallic polymeric complexes was confirmed by IR-spectroscopy (Fig. 3) (cm^{-1}).

- Polypropylene glycole maleate phthalate /AA, white powder: 3449 (O–H); 2936 (C–H_{st}); 2361 (C–H_{st}, CH₂–N_{st}); 1724 [C=O bond with OH(COOH)]; 1269 (CH₂ δ); 1169 (CH₃ δ);
- Polypropylene glycole maleate phthalate /AA: Au⁰, dark purple powder: 3425 (O–H); 2939 (C–H_{st}); 2365 (C–H_{st}, CH₂–N_{st}); 1610 [C=O bond with OH(COOH)]; 1624 (CH₂ δ); 1277 (CH₃ δ); 659 (Au);
- Polypropylene glycole maleate phthalate /AA: Ag⁰, dark gray powder: 3429 (O–H); 2928 (C–H_{st}); 2372 (C–H_{st}, CH₂–N_{st}); 1604 [C=O bond with OH(COOH)]; 1454 (CH₂ δ); 1161 (CH₃ δ); 817 (Ag).

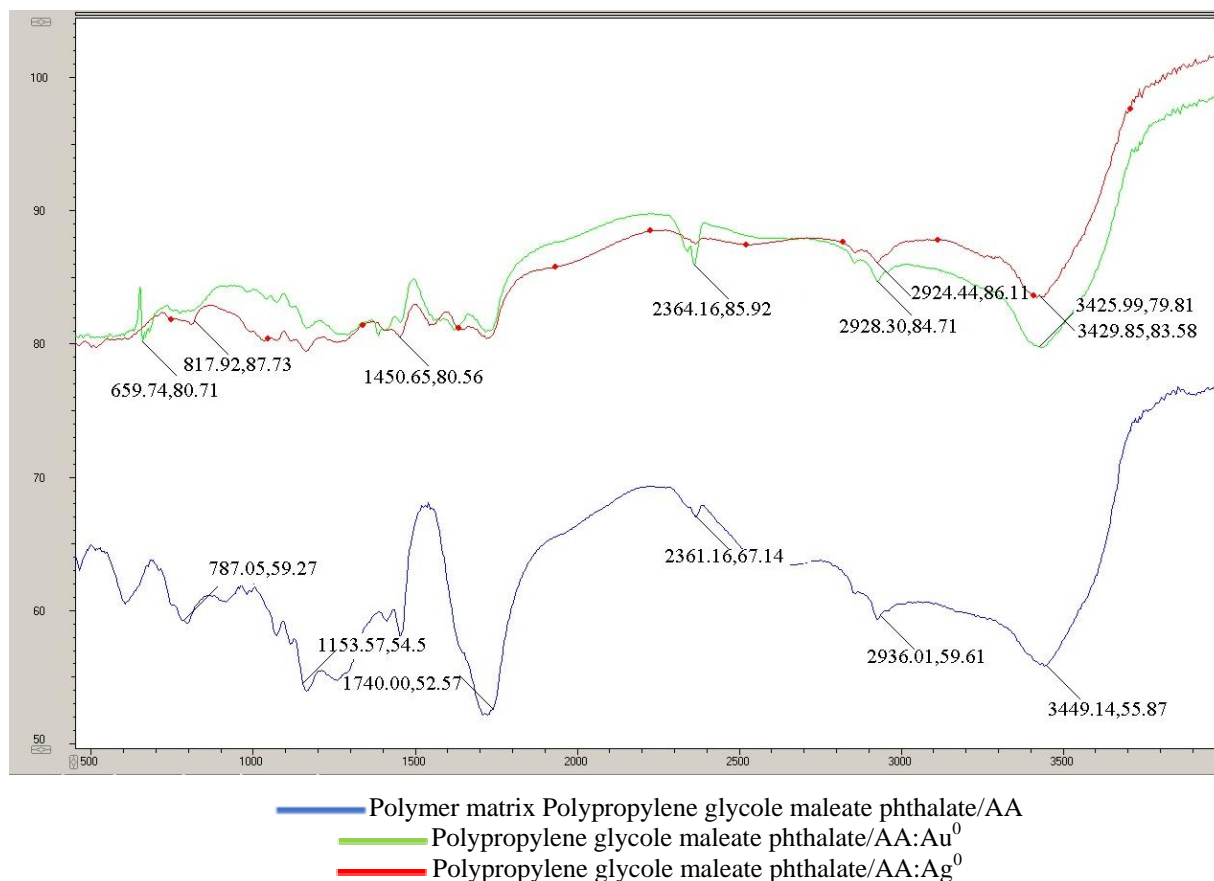


Figure 3. IR-spectra of the samples

In the IR-spectra of obtained composites, the corresponding PR bands appear with maxima in the region of 648–659 and 806–817 nm respectively which is characteristic for gold and silver of nano-sized zero-valency state; consequently, the original properties of polymer matrix are not changed.

IR-spectra of the samples of p-PGMPH:AA/Au and p-PGMPH:AA/Ag are rather close according to their place to maximums of absorption and they are characterized by low contrast which is due to non-selective absorption of emission of metal particles. In comparison with the spectra of the initial polymer, there are no significant shifts in absorption frequencies in the spectra.

Figure 4 presents the composition and the structure of synthesized samples, and the sizes of metal-NPs. The images are obtained using the SE detector at an accelerating voltage (HV) of 5 kV. From all sides of the pictures, there are observed the porous; the layer (porous) structure is mostly dominated. It is established that the pore sizes are 0.9–1.1 μm in these samples, which is characteristic of three-dimensional network polymers.

In electron microscopy images (Fig. 4), obtained metal-polymer composites consist of the nanoparticles of silver and gold of rhomboidal and cylindrical shapes with the sizes of 40–50 and 35–50 nm correspondingly.

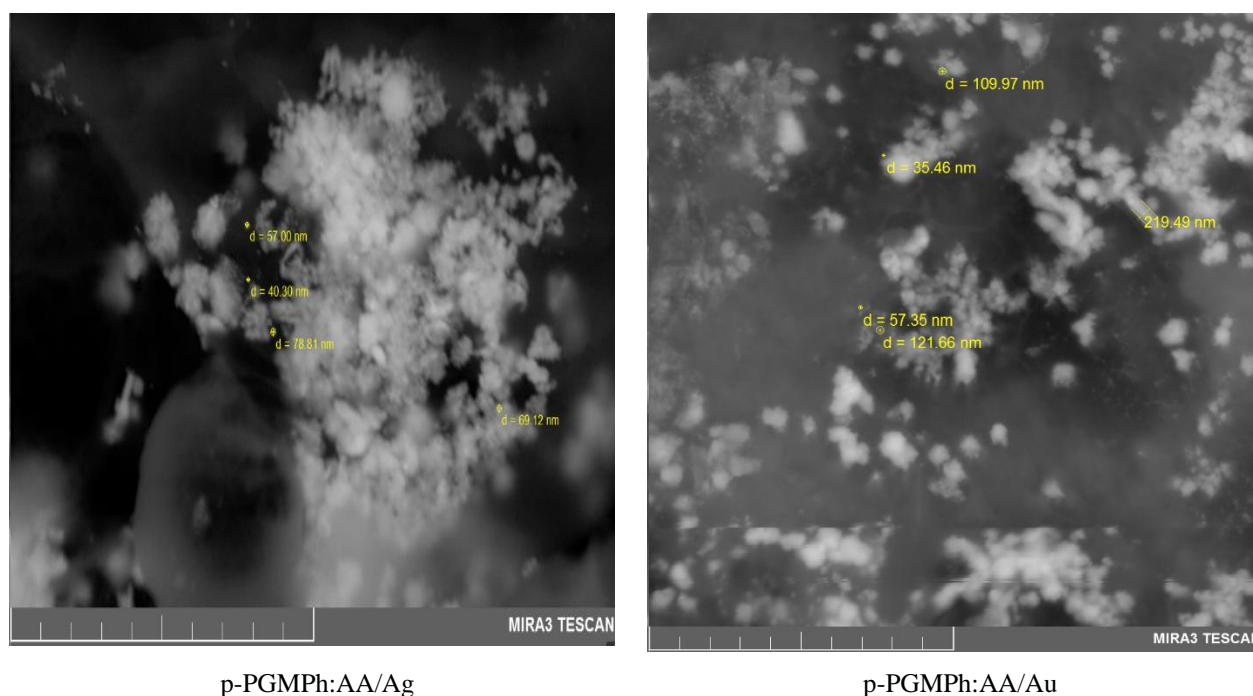


Figure 4. Electron microscopic images

According to data of atomic-adsorption spectroscopy, the content of the particles in nanocomposites is around 20–22 % for Ag and 12–15 % for Au. Dioxane was used as a solvent during sample preparation. Copolymers were dissolved in dioxane for 60–90 min. The solution is filtered with an autosampler and introduced into the column of the gas analyzer.

The nature of functional groups in the polymer structure, the molecular mass, and in the case of copolymers — their composition and distribution in a polymer matrix affect the size of forming particles (Table 1).

Compared to the results of a previous study [5], with metal nanoparticles of spherical (silver) and rhomboidal (nickel) forms distributed in the matrix of gel, the particle sizes are smaller. The main part of nanoparticles (about 80 % of total mass) are the particles with sizes within 20–60 nm and the less part is much bigger formations with sizes of 80–90 nm. The aggregates with sizes more than 200 nm ($\approx 10\%$) formed during the process of coalescence of nanoparticles which can be seen on the surface of the polymer. The content of Ag and Ni in nanocomplexes of p-PGMPh/AA:Ag⁰, p-PGMPh/AA:Ni⁰ is $\sim 23,21$ mass. % from the total mass of the complex correspondingly.

Table 1

Morphology of metal-containing copolymers

Sample	Content of metal, % (mass.)	Particle size, nm	Morphology of NPs, nm
Ag	20–22	40 \pm 10	sphere
Au	12–15	35 \pm 10	Rhomb

Figure 5 illustrates the thermograms of metal-polymer complexes of the composition of p-PGMPh/AA-Au and p-PGMPh/AA-Ag. The first thermogram (a) shows that the metal-polymer complex p-PGMPh/AA-Au is stable till 800.0 °C; 10 % mass loss at 200.0 °C with the maximum value of endothermal effect at 297.0 °C on DTG curve is observed. When thermal decomposition of the metal-polymer complex of p-PGMPh/AA-Au, the DTG curve (Fig. 5b) with three peaks at maximums $T_{\max} = 134.0, 292.5,$ and 410.0 °C is obtained. Low-temperature peak is due to the elimination of crystalline water, whereas the second and third peaks are explained by the destruction of the main chains which takes place as zipping. Metal-polymer complex p-PGMPh/AA-Ag (Fig. 5c) is stable till 800.0 °C; there is a 12 % mass loss at 190.0 °C and the residual mass is 58 %. As can be seen from Figure 5b, the process of thermal decomposition of the p-PGMPh/AA-Ag metal-polymer complex is a multiple-stage and, for many studied compounds, includes four stages of thermal decomposition, in which the bends on the curves correspond to the mass loss point.

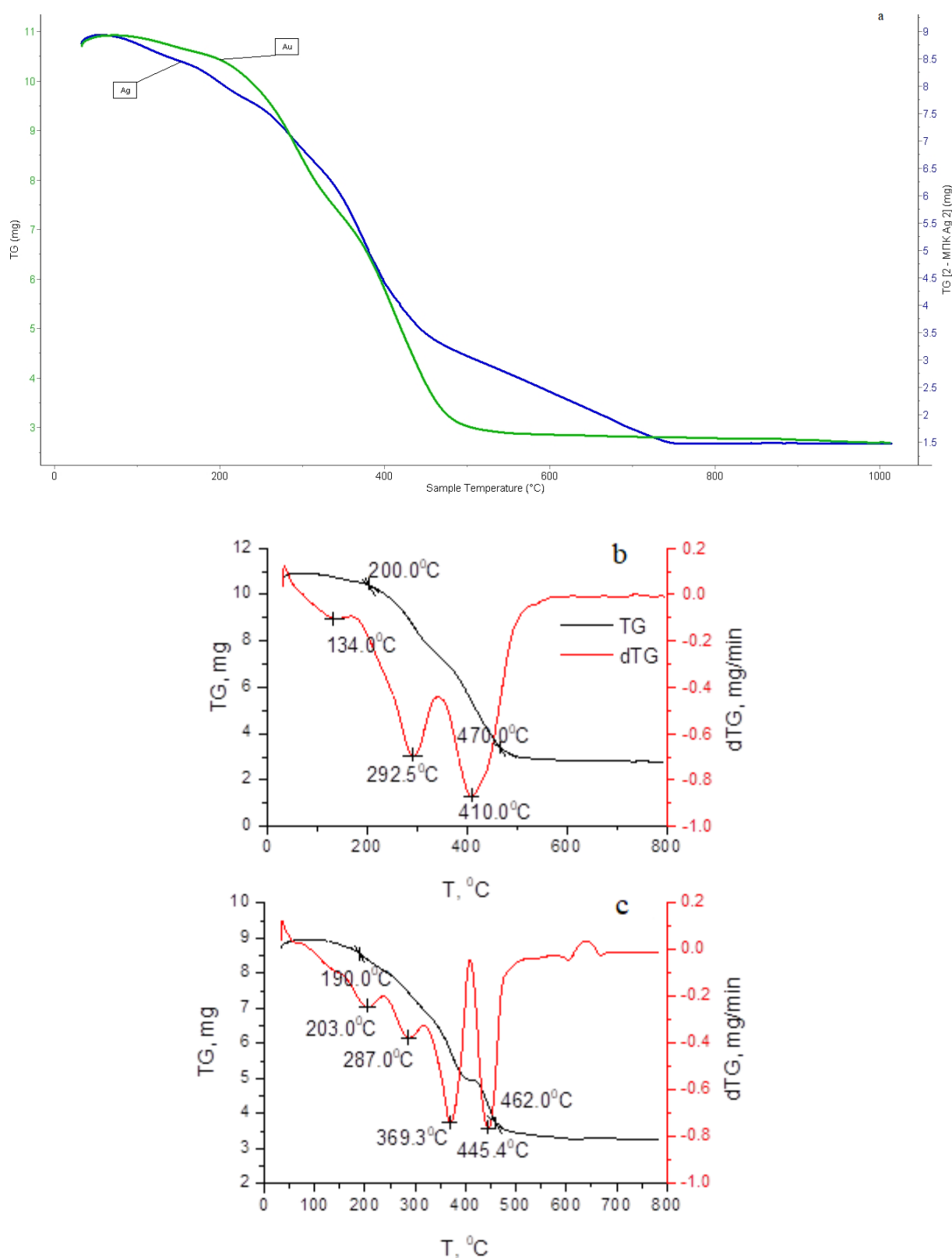


Figure 5. Temperature dependences of change of the mass (TG curve) (a) and the rate of change of the mass (DTG curve) for metal-polymer complexes: p-PGMPh/AA-Au (b) and p-PGMPh/AA-Ag (c)

As the thermal analysis of the studied p-PGMPh/AA-Ag and p-PGMPh/AA-Au, metal-polymer complexes containing the elements Ag and Au showed (Fig. 5b, c) that the complexes are stable up to 800.0 °C and gradually decompose in the range from 0.0 °C to 800.0 °C. In all cases, there is an exothermal effect $T_{\text{beginning}} = 350.0 \pm 0.1$ °C (at 410.0 °C) for p-PGMPh/AA-Au and $T_{\text{beginning}} = 400.0 \pm 0.1$ °C (at 445.0 °C) which

is absent in initial polymeric matrix which confirms the presence of the elements Ag and Au in the network of the polymer complex.

Antimicrobial activity. In the next step of the work, the antimicrobial activity of metal-polymer composites of the samples of p-PGMPh/AA:Au, p-PGMPh/AA:Ag to the strains of gram-positive bacteria of *Staphylococcus aureus*, *Bacillus subtilis*, gram-negative bacteria of *Escherichia coli*, *Pseudomonas aeruginosa* and yeast fungi of *Candida albicans* was studied. To determinate the antimicrobial effect of metal-polymer complexes of p-PGMPh/AA:Au and p-PGMPh/AA:Ag, a comparative experiment using several pharmacopeia testing bacteria was done. Table 2 presents the results of the study of antimicrobial activity metal-polymer complexes of PGMPh/AA:Au and p-PGMPh/AA:Ag.

Table 2

Antimicrobial activity of the samples

Bacteria/Sample	<i>Staphylococcus aureus</i>	<i>Bacillus subtilis</i>	<i>Escherichia coli</i>	<i>Pseudomonas aeruginosa</i>	<i>Candida albicans</i>
MPC Au	+	+	+	+	+
MPC Ag	–	–	–	+	–
Control	+	+	+	+	+

Conventional signs: “–” — no growth, “+” — significant growth.

As a result of antimicrobial analysis, it was found that in the sample of MPC-Ag there was no growth of presented testing bacteria except *Pseudomonas aeruginosa*. This points to the antimicrobial effect of the sample — MPC Ag; in this case the activity is higher than in the other testing samples. The sample of MPC-Au did not show an antimicrobial effect related to the presented test microorganisms.

Conclusions

Thus, the use of the polymer as a stabilizing matrix allowed obtaining hybrid nanocomposites with an equally stable distribution of nanoparticles of silver and gold. Synthesized nanoparticles were characterized (size and particle size distribution) with the help of electron microscopy and showed that the nanocomposites contain nanoparticles of silver and gold of rhomboidal and cylindrical shapes with the sizes 40–50 and 35–50 nm accordingly. Metal–polymer composites based on copolymers of polypropylene glycolmaleate-phthalate with acrylic acid and metallic gold and silver were synthesized for the first time. The results demonstrated an equal distribution of nano-sized particles in the volume of polymeric matrix; the sizes of more than 80% of metal nanoparticles are in the range of 20 to 50 nm and have the shape of a sphere and rhomboidal shape.

Obtained nanocomposites are stable and promising for the creation of novel photochromic and non-linear-optical materials, and the use in medicine in the creation of antiseptic and antimicrobial materials which are necessary during pandemic.

References

- 1 Kolzunova L. Polymethylolacrylamide/AuNPs Nanocomposites: Electrochemical Synthesis and Functional Characteristics / Switzerland, Cham: eBook Packages L. Kolzunova, E. Shchitovskaya, M. Karpenko // *Polymers*. — 2021. — Vol. 13, № 14. — P. 2382. <https://doi.org/10.3390/polym13142382>
- 2 Sadasivuni K.K. Silver Nanoparticles and Its Polymer Nanocomposites—Synthesis, Optimization, Biomedical Usage, and Its Various Applications / K.K. Sadasivuni, S. Rattan, S. Waseem, S.K. Brahme, S.B. Kondawar, S. Ghosh // *Methods in Molecular Biology*. — 2019. — Vol. 1, № 28. — P. 331–373. https://doi.org/10.1007/978-3-030-04741-2_11
- 3 Nicolais L. Metal-Polymer Nanocomposites / L. Nicolais, G. Carotenuto. — Weinheim, Germany: John Wiley & Sons, Inc., 2004. — 320 p. <https://doi.org/10.1002/0471695432>
- 4 Wu X. Preparation of noble metal/polymer nanocomposites via in situ polymerization and metal composite reduction / X. Wu, S. Takeshita, K. Tadumi, W. Dong, S. Horiuchi, H. Niino, T. Furuya, S. Yoda // *Materials Chemistry and Physics*. — 2019. — Vol. 222, — P. 300–308. <https://doi.org/10.1016/j.matchemphys.2018.10.031>
- 5 Burkeyev M.Z. Synthesis and Catalytic Properties of New Polymeric Monometallic Composites Based on Copolymers of Polypropylene Glycol Maleate Phthalate with Acrylic Acid / M.Z. Burkeyev, S.R. Shibayeva, T.O. Khamitova, J. Plocek, Y.M. Tazhbayev, S.Z. Davrenbekov, M.T. Nurmagambetova, A.T. Kazhmuratova, T.S. Zhumagalieva, A.T. Kezdikbayeva // *Polymers*. — 2021. — Vol. 13. — P. 4369. <https://doi.org/10.3390/polym13244369>

- 6 Peponi L. Smart polymers / L. Peponi, M.P. Arrieta, G.A. Mujica, D. López. — Norwich, UK: William Andrew, 2017. — P. 131–154. <https://doi.org/10.1016/B978-0-323-44353-1.00006-3>
- 7 Hitchcock J.P. Adsorption of Catalytic Nanoparticles onto Polymer Substrates for Controlled Deposition of Microcapsule Metal Shells / J.P. Hitchcock, A.L. Tasker, K. Stark, A. Leeson, E.A. Baxter, S. Biggs, O.J. Cayre. — Langmuir. — 2018. — Vol. 34. — P. 1473–1480. <https://doi.org/10.1021/acs.langmuir.7b02874>
- 8 Tamayo L. Polymer Composites With Metal Nanoparticles / L. Tamayo, H. Palza, J. Bejarano, P.A. Zapata // Amsterdam, The Netherlands: Elsevier, 2019. — P. 249–286. <https://doi.org/10.1016/b978-0-12-814064-2.00008-1>
- 9 Dzhardimalieva G.I. Polymer-Immobilized Clusters and Metal Nanoparticles in Catalysis / G.I. Dzhardimalieva, A.K. Zharmagambetova, S.E. Kudaibergenov, I.E. Uflyand // Kinetics and Catalysis. — 2020. — Vol. 61. — P. 198–223. <https://doi.org/10.1134/s0023158420020044>
- 10 Mansour A. Distribution of metal nanoparticles in a plasma polymer matrix according to the structure of the polymer and the nature of the metal / A. Mansour, F. Poncin-Epaillard, D. Debarnot // Thin Solid Films. — 2019. — Vol. 699. — P. 137–261. <https://doi.org/10.1016/j.tsf.2019.04.036>
- 11 Salmi T. Kinetics of melt polymerization of maleic acid phthalic acids with propylene glycol / T. Salmi, E. Paatero, P. Nyholm, M. Still, K. Narhi // Chemical Engineering Science. — 1994. — Vol. 49. — P. 5053–5070. [https://doi.org/10.1016/0009-2509\(94\)00358-0](https://doi.org/10.1016/0009-2509(94)00358-0)
- 12 Хабриев Р.У. Руководство по экспериментальному (доклиническому) изучению новых фармакологических веществ. — 2-е изд., перераб. и доп. / Р.У. Хабриев — М.: Медицина, 2005. — 832 с.

М.Ж. Буркеев, С.Р. Шибаетова, Т.О. Хамитова, Иржи Плоцек,
М.Т. Нурмаганбетова, А.Т. Кажмуратова, Т.С. Жумагалиева

Күміс пен алтын полимер-иммобилизацияланған нанобөлшектерінің синтезі және олардың қасиеттерін зерттеу

Полипропиленгликольмалеинатфталаттың акрил қышқылымен және алтын мен күміспен сополимерлері негізіндегі металл-полимерлі композиттері алғаш рет синтезделді. Нанокompозиттердің құрылымы микроскопия мен спектроскопияның көмегімен сипатталды. Күміс пен алтын негізіндегі жаңа металл-полимерлі кешендердің микробқақарсы белсенділігі зерттелді. Металл-полимерлі кешендер алғаш рет акрил қышқылымен полипропиленгликольмалеинатфталаттың сополимерлеріне негізделген полимерлі матрицамен тұрақтандырылды (п-ПГМФ/АК:Ag, п-ПГМФ/АК:Au). Алынған нанокompозиттердің құрамында сәйкесінше 40–50 және 35–50 нм өлшемдегі ромб тәрізді және цилиндрлік пішіндегі күміс пен алтынның нанобөлшектері бар. Нанобөлшектердің 80 %-дан астамының өлшемі 20-дан 50 нм-ге дейінгі аралықта жатыр және сфералық және ромб тәрізді пішінге ие. Металл-полимерлі композиттердің микробқақарсы белсенділігін анықтау үшін факультативті-анаэробты грамаң *Staphylococcus aureus*, аэробты грамаң спора түзетін *Bacillus subtilis*, *Escherichia coli-idaa*-ға қарсы грамтеріс факультативті анаэробтар қолданылған. Алынған нанокompозиттер тұрақты және жаңа фотохромды және сызықты емес оптикалық материалдарды жасау үшін, сондай-ақ пандемия кезінде қажет антисептикалық және микробқақарсы материалдарды әзірлеуде медицинада қолдану үшін перспективті болып табылады.

Кілт сөздер: нанокompозиттер, нанобөлшектер, күміс, алтын, сополимер, акрил қышқылымен полипропиленгликольмалеинатфталат, металл-полимер кешені, микробқақарсы белсенділік.

М.Ж. Буркеев, С.Р. Шибаетова, Т.О. Хамитова, Иржи Плоцек,
М.Т. Нурмаганбетова, А.Т. Кажмуратова, Т.С. Жумагалиева

Синтез и исследование свойств полимер-иммобилизованных наночастиц серебра и золота

Впервые синтезированы металл-полимерные композиты на основе сополимеров полипропиленгликольмалеинатафталата с акриловой кислотой и металлического золота и серебра. Структура нанокompозитов охарактеризована с помощью микроскопии и спектроскопии. Изучена антимикробная активность новых металл-полимерных комплексов на основе серебра и золота. Металл-полимерные комплексы впервые стабилизированы полимерной матрицей на основе сополимеров полипропиленгликольмалеинатафталата с акриловой кислотой (п-ПГМФ/АК:Ag, п-ПГМФ/АК:Au). Полученные нанокompозиты содержат наночастицы серебра и золота ромбовидной и цилиндрической форм размерами 40–50 и 35–50 нм соответственно. Размер более 80 % наночастиц лежит в пределах от 20 до 50 нм и имеет сферическую и ромбическую формы. Для определения антимикробной активности МПК референс-тест-микроорганизмы были использованы факультативно-анаэробные грамположительные

Staphylococcus aureus, аэробные грамположительные спорообразующие *Bacillus subtilis*, грамотрицательные факультативные анаэробы *Escherichia coli*, аэробные *Pseudomonas aeruginosa* и дрожжевые грибы *Candida albicans*. Полученные наноконпозиты стабильны и перспективны для создания новых фотохромных и нелинейно-оптических материалов, а также для применения в медицине при разработке антисептических и антимикробных материалов, необходимых в условиях пандемии.

Ключевые слова: наноконпозиты, наночастицы, серебро, золото, сополимер, полипропиленгликоль-малеинатфталат с акриловой кислотой, металл-полимерный комплекс, антимикробная активность.

References

- 1 Kolzunova, L., Shchitovskaya, E., & Karpenko, M. (2021). Polymethylolacrylamide/AuNPs Nanocomposites: Electrochemical Synthesis and Functional Characteristics. *Polymers*, 13(14), 2382. <https://doi.org/10.3390/polym13142382>
- 2 Sadasivuni, K.K., Rattan, S., Waseem, S., Bramhe, S.K., Kondawar, S.B., Ghosh, S., & Mazumdar, P. (2019). Silver Nanoparticles and Its Polymer Nanocomposites — Synthesis, Optimization, Biomedical Usage, and Its Various Applications. *Methods in Molecular Biology*, 331–373. https://doi.org/10.1007/978-3-030-04741-2_11
- 3 Nicolais, L., & Carotenuto, G. (2004). *Metal-Polymer Nanocomposites*; Wiley: VCH Verlag GmbH & Co: Weinheim, Germany. <https://doi.org/10.1002/0471695432>
- 4 Wu, X., Takeshita, S., Tadumi, K., Dong, W., Horiuchi, S., Niino, H., & Yoda, S. (2018). Preparation of noble metal/polymer nanocomposites via in situ polymerization and metal complex reduction. *Materials Chemistry and Physics*, 222, 300–308. <https://doi.org/10.1016/j.matchemphys.2018.10.031>
- 5 Burkeyev, M. Zh., Shibayeva, S. R., Khamitova, T. O., Plocek, J., Tazhbayev, Y. M., Davrenbekov, S. Zh., Nurmaganbetova, M. T., Kazhmuratova, A. T., Zhumagalieva, T. S., & Kezdikbayeva, A. T. (2021). Synthesis and Catalytic Properties of New Polymeric Monometallic Composites Based on Copolymers of Polypropylene Glycol Maleate Phthalate with Acrylic Acid. *Polymers*, 13(24), 4369. <https://doi.org/10.3390/polym13244369>
- 6 Peponi, L., Arrieta, M. P., Mujica-Garcia, A., & López, D. (2017). *Smart Polymers. Modification of Polymer Properties*, 131–154. <https://doi.org/10.1016/b978-0-323-44353-1.00006-3>
- 7 Hitchcock, J. P., Tasker, A. L., Stark, K., Leeson, A., Baxter, E. A., Biggs, S., & Cayre, O. J. (2018). Adsorption of Catalytic Nanoparticles onto Polymer Substrates for Controlled Deposition of Microcapsule Metal Shells. *Langmuir*, 34(4), 1473–1480. <https://doi.org/10.1021/acs.langmuir.7b02874>
- 8 Tamayo, L., Palza, H., Bejarano, J., & Zapata, P.A. (2019). Polymer Composites With Metal Nanoparticles. In *Polymer Composites with Functionalized Nanoparticles*; Elsevier: Amsterdam, Netherlands, 249–286. <https://doi.org/10.1016/b978-0-12-814064-2.00008-1>
- 9 Dzhardimalieva, G. I., Zharmagambetova, A. K., Kudaibergenov, S. E., & Uflyand, I. E. (2020). Polymer-Immobilized Clusters and Metal Nanoparticles in Catalysis. *Kinetics and Catalysis*, 61(2), 198–223. <https://doi.org/10.1134/s0023158420020044>
- 10 Mansour, A., Poncin-Epaillard, F., & Debarnot, D. (2019). Distribution of metal nanoparticles in a plasma polymer matrix according to the structure of the polymer and the nature of the metal. *Thin Solid Films*. <https://doi.org/10.1016/j.tsf.2019.04.036>
- 11 Salmi, T., Paatero, E., Nyholm, P., Still, M., & Na`rhi, K. (1994). Kinetics of melt polymerization of maleic acid phthalic acids with propylene glycol. *Chemical Engineering Science*, 49(24), 5053–5070. [https://doi.org/10.1016/0009-2509\(94\)00358-0](https://doi.org/10.1016/0009-2509(94)00358-0)
- 12 Khabriyev, R.U. (2005). *Rukovodstvo po eksperimentalnomu (doklinicheskomu) izucheniiu novykh farmakologicheskikh veshchestv [Guidelines for the experimental (preclinical) study of new pharmacological substances]*. 2nd ed., revised and additional. Moscow: Meditsina [in Russian].

Information about authors*

Burkeyev, Meyram Zhunusovich — Full Professor, Doctor of Chemical Sciences, Karagandy University of the name of academician E.A. Buketov, Universitetskaya street, 28, 100024, Karaganda, Kazakhstan; e-mail: m_burkeyev@mail.ru; <https://orcid.org/0000-0001-8084-4825>;

Shibayeva, Saliman Ramazanovna (*corresponding author*) — 2nd year PhD student, Karagandy University of the name of academician E.A. Buketov, Universitetskaya street, 28, 100024, Karaganda, Kazakhstan; e-mail: Sali_r@mail.ru; <https://orcid.org/0000-0002-3520-3962>

Khamitova, Tolkyn Ondirisovna — PhD, Department of Soil Science and Agrochemistry, Agronomic Faculty, S. Seifullin Kazakh Agro Technical University, Nur-Sultan 010000, Kazakhstan; e-mail: khamitova.t@inbox.ru <https://orcid.org/0000-0002-4691-3732>

Plocek, Jiri — PhD., CSc. Institute of Inorganic Chemistry of the Czech Academy of Sciences, Czech Republic, Husinec-Rez 1001 25068 Rez; e-mail: plocek@iic.cas.cz; <https://orcid.org/0000-0001-6082-5766>;

Nurmaganbetova, Margarita Taukenovna — Candidate of Chemical Sciences, Karagandy University of the name of academician E.A. Buketov, Universitetskaya street, 28, 100024, Karaganda, Kazakhstan; e-mail: ritunur@mail.ru <https://orcid.org/0000-0002-1785-1069>

Kazhmuratova, Akerke Temirgalievna — Candidate of Chemical Sciences, Karagandy University of the name of academician E.A. Buketov, Universitetskaya street, 28, 100024, Karaganda, Kazakhstan; e-mail: kazhmuratova@mail.ru; <https://orcid.org/0000-0003-4044-8419>;

Zhumagalieva, Tolkyng Sergazyevna — Candidate of Chemical Sciences, Professor, Karagandy University of the name of academician E.A. Buketov, Universitetskaya street, 28, 100024, Karaganda, Kazakhstan; e-mail: Zhumagalieva79@mail.ru; <https://orcid.org/0000-0003-1765-752X>

*The author's name is presented in the order: *Last Name, First and Middle Names*

-

A.R. Galiyeva^{*}, Ye.M. Tazhbayev, T.S. Zhumagaliyeva, A.T. Daribay

Karagandy University of the name of academician E.A. Buketov, Kazakhstan

(*Corresponding author's e-mail: aldana_karaganda@mail.ru)

Encapsulation of Isoniazid in Polylactide-Co-Glycolide Nanoparticles by Nanoprecipitation

The use of polymeric materials as drug carriers has several advantages, such as prolongation of drug action and reduction of drug side effects. In this study, we consider the methods for the preparation of polylactide-co-glycolide (PLGA) polymeric nanoparticles with the anti-tuberculosis drug (ATD), isoniazid, by nanoprecipitation. Polymeric nanocarriers were obtained by varying individual parameters such as the nature of solvent and non-solvent, drug/polymer ratio, and stabilizer concentration. It was determined that the average particle size depends on the type of non-solvent. When alcohols were used, the average size increased in the sequence: ethanol < isopropanol < isobutanol. The type of solvent is an important factor in the formation of nanoparticles and their final characteristics. With an increase in the drug/polymer ratio, the average size of nanoparticles also increased. The size of obtained nanoparticles varied from 93 to 869 nm. Thermogravimetric and differential scanning calorimetry analyses were carried out to confirm the incorporation of the drug into the polymer matrix. In addition, polymer degradation and the degree of release of isoniazid from the polymeric matrix at different pH were studied. It was identified that the nanoprecipitation method can be used not only for hydrophobic but also for hydrophilic drugs.

Keywords: nanoparticles, polylactide-co-glycolide, PLGA, isoniazid, nanoprecipitation, hydrophilic drugs, anti-tuberculosis drugs.

Introduction

There are currently many drugs available for the treatment of tuberculosis. Due to the need for intensive use, they have significant toxic effects on the body and lead to the development of resistance to many drugs [1–3]. When using new dosage forms in the form of polymer nanoparticles (NPs) for the delivery of anti-TB drugs (ATD), the following results can be achieved: providing prolonged drug release while maintaining effective drug concentration in blood for a given period of time; reducing the side effects of the drug, thereby increasing its therapeutic effect [4–7].

However, the choice of polymer materials and methods should be based on many factors such as particle size, solubility and stability in water, permeability and charge of drug molecules, degree of biodegradation, biocompatibility, and toxicity [8, 9]. Encapsulation of hydrophilic compounds is not easy and remains a problem for highly loaded drug delivery systems, mainly due to drugs leaking into the external aqueous phase during nanoparticle production [10]. Since water-soluble drugs can be immobilized into nanoparticles in various ways, the nanoprecipitation method was chosen.

Nanoprecipitation was patented by Fessi et al. in 1989 [11]. It has mainly been used to encapsulate hydrophobic drug molecules since its development. Several polymers have been developed for this purpose, in particular biodegradable polyesters such as polylactide (PLA), polylactide-co-glycolide copolymer (PLGA), and poly-ε-caprolactone (PCL) [3, 12–15]. As nanoprecipitation is a direct method, it has many advantages: easy to perform, no energy or time consumption.

At the same time, the nanoprecipitation method has a number of disadvantages. This method is mainly suitable for compounds of a hydrophobic nature, soluble in ethanol or acetone, but exhibiting limited solubility in water. Consequently, reduced or even zero leakage of the drug into the external medium results in an unsatisfactory degree of binding [11, 16, 17]. Some studies concerning the immobilization of hydrophilic drugs have also given promising results. Yoo et al. [18] proved that the correct choice of solvent and non-solvent can lead to the formation of nanoparticles, which means that the nanoprecipitation method can be carried out with other solvents and can be extended to hydrophilic preparations.

This study aims to optimize the nanoprecipitation method for obtaining PLGA-based nanoparticles immobilized with isoniazid, which exhibit a controlled particle diameter up to 300 nm, a narrow size distribu-

tion, with high encapsulation efficiency and loading capacity. For this purpose, we choose different alcohols as non-solvents, different solvents, and varied parameters, such as stabilizer concentration and drug/polymer ratio.

Experimental

Materials

Isoniazid (INH) ($\geq 99\%$), polyvinyl alcohol (PVA) (hydrolyzed, MW 9000–10000), poly(lactide-co-glycolide) copolymer (PLGA 50:50, MW 24 000 to 38 000), ethyl acetate ($\geq 99\%$) (all from Sigma Aldrich, Steinheim, Germany) were used without further purification. Ethanol was purchased from DosFarm (Almaty, Kazakhstan). The organic solvents (Dichloromethane (DCM), Dimethyl Sulfoxide (DMSO), and Chloroform) were obtained from Component Reagent (Russia). Sodium hydrophosphate and potassium dihydrophosphate were used to prepare the phosphate-buffered saline solution.

Preparation of poly(lactide-co-glycolide) nanoparticles immobilized with isoniazid by nanoprecipitation

To obtain nanoparticles by nanoprecipitation, the polymer was dissolved in a suitable organic solvent and isoniazid in alcohol (drug/polymer ratio from 1:1 to 1:5). The resulting polymer solution is then mixed with the isoniazid. The obtained solution is then added to the dispersed phase (0.1–1 % PVA) by stirring on a magnetic stirrer. The resulting suspension was stirred at room temperature for 6 h on a magnetic stirrer to remove the solvent completely. INH-loaded PLGA nanoparticles were extracted by centrifugation (MiniSpi, Eppendorf, Hamburg, Germany) (14,000 rpm, 20 min). The obtained nanoparticle suspension was washed with distilled water using three centrifugation steps at 14,000 rpm for 15 min each to remove dissolved solids and organic solvent from the mixture. The obtained nanoparticles were dried to a constant weight.

Particle size, polydispersity, and morphology of the obtained nanoparticles

Particle size and polydispersity index (PDI) were determined by dynamic light scattering (DLS) using the Malvern Zetasizer Nano S90 (Malvern Instruments Ltd., Malvern, UK). Each batch of nanoparticles was appropriately diluted with distilled water immediately after production. The shape and surface morphology of the PLGA-INH NPs were examined by scanning electron microscopy (MIRA 3LM TESCAN, Brno, Czech Republic, EU).

Encapsulation efficiency, loading capacity, and PLGA-INH NPs' yield

The amount of isoniazid encapsulated in the polymer nanoparticles was determined by measuring the amount of unencapsulated isoniazid in the aqueous solution recovered after ultracentrifugation and particle washing. The amount of drug in solution was determined by high-performance liquid chromatography (HPLC) (Shimadzu LC-20 Prominence). The encapsulation efficiency, loading capacity, and yield of nanoparticles were calculated as follows:

$$\text{Encapsulation Efficiency (EE\%)} = \frac{\text{Mass of the total drug} - \text{Mass of free drug}}{\text{Mass of total drug}} \times 100\%$$

$$\text{Loading Capacity (\%)} = \frac{\text{Mass of the total drug} - \text{Mass of free drug}}{\text{Mass of total nanoparticles}} \times 100\%$$

$$\text{Nanoparticles Yield (\%)} = \frac{\text{Mass of total nanoparticles}}{\text{Mass of the total drug} + \text{Mass of total PLGA}} \times 100\%$$

In vitro study of drug release from polymer NPs

Isoniazid release kinetics from the polymeric matrix was determined by dialysis, in phosphate-saline buffer (pH 7.4) at 37°C. The obtained nanoparticles were resuspended in phosphate-buffered saline using ultrasound and placed in a dialysis membrane. The membrane, sealed with clamps, was placed in a beaker with 250 ml of buffer solution, closed with a lid and stirred on a magnetic stirrer at 200 rpm. Dialysates were sampled periodically (3 mL at a time). To study the degree of release from the polymer nanoparticles, the amount of drug released was recorded by HPLC and calculated by the formula:

$$\text{Drug Release (\%)} = \frac{\text{Mass of released drug}}{\text{Mass of the total drug in nanoparticles}} \times 100\%$$

The amount of degraded polymer was determined on a UV spectrophotometer (HP LC-20 Prominence, Shimadzu, Japan) at wavelength $\lambda_{\text{max}} = 240$ nm for the polymer.

Thermogravimetric analysis and differential scanning calorimetry

Thermogravimetric and differential thermal analyses were performed on a LabSYS evo TGA/DTA/DSC analyzer (Setaram, France) in the 30–550 °C temperature range in an aluminum oxide crucible at a heating rate of 10 °C/min in nitrogen inert medium and flow rate was 30 mL/min by decomposition of a nanoparticle sample.

Statistical analysis

The data are expressed as mean \pm standard deviation and analysis was carried out statistically by Minitab 19 Statistical Software. The analysis of data was taken place via one-way analysis of variance (ANOVA).

Results and Discussion

Burkeev et al. [19] synthesized polylactide nanoparticles immobilized with isoniazid by the nanoprecipitation method. In this method, they used water as a non-solvent and acetone as a solvent and obtained NPs with a drug loading of 50 %. Since we used a more hydrophilic polymer, PLGA, and using distilled water as a non-solvent, NPs were not obtained. Therefore, to select a suitable non-solvent, the polymer was dissolved in organic solvent (DMSO) and the drug was dissolved in various non-solvents such as ethanol, isobutanol, isopropanol. The obtained drug solution was added to the polymer solution while stirring on a magnetic stirrer. The suspension was then added to the PVA solution, resulting in the formation of nanoparticles. Table 1 demonstrates the results of the average particle size and PDI of the obtained NPs.

Table 1

The effect of non-solvent on nanoparticle formation and characteristics

№	Type of non-solvent	Average particle size, nm	PDI	NPs' yield, %
1	Ethanol	182 \pm 6	0.104 \pm 0.031	68 \pm 9
2	Isopropanol	415 \pm 8	0.701 \pm 0.072	28 \pm 6
3	Isobutanol	870 \pm 9	1 \pm 0	32 \pm 4

As can be seen from Table 1, the average particle size depends on the nature of the dispersing solvent. Ethanol results in smaller nanoparticles, while the use of isobutanol or isopropanol gives even larger nanoparticles. The size values measured by DLS for ethanol are obtained with high reproducibility (less than 2% deviation between triplicate instances) and with a PDI that shows a homogeneous suspension of nanoparticles. When the drug/polymer ratio and PVA concentration remains constant, the particle size gradually increases in the series of homologous alcohols used as non-solvent.

The interest in using alcohols as insoluble substances lies in their relatively low dielectric constant (ϵ value) [17]. If the dielectric constant is lower, the insoluble substance will dissolve hydrophilic compounds and prevent drug leakage. Therefore, ethanol is the most suitable in this regard, as its dielectric constant is 24.6, which is far from the value of water (80.1) [17].

In the next step of the study, four different organic solvents were chosen to select a suitable solvent for the polymer: DMSO, DCM, acetone, chloroform, and the drug were dissolved in ethanol. Table 2 presents the obtained results.

Table 2

The effect of solvent type on average size and yield of nanoparticles

№	Solvent type	Average particle size, nm	PDI	NPs' yield, %
1	DMSO	182 \pm 6	0.104 \pm 0.031	68 \pm 9
2	Acetone	289 \pm 7	0.229 \pm 0.052	34 \pm 8
3	DCM	385 \pm 9	0.613 \pm 0.300	29 \pm 4
4	Chloroform	378 \pm 7	0.598 \pm 0.200	32 \pm 4

As can be seen from Table 2, nanoparticles with the smallest size and polydispersity are formed in DMSO. Other solvents (acetone, chloroform, DCM) are able to dissolve the PLGA copolymer, but they form large nanoparticles, while the solubility of polymers in DMSO is higher, and this solvent mixes well with the external phase, in our case with distilled water. This leads to the fastest diffusion of the two phases and more

nanoparticles. Accordingly, the lower the phase tension or the lower the interaction parameter of the organic solvent and the external phase, the higher the yield of nanoparticles [20, 21]. Accordingly, a lower phase tension or a weaker interaction parameter of the organic solvent and the external phase corresponds to a higher yield of nanoparticles. Consequently, the particle size obtained with the DMSO solvent is smaller and the NPs' yield is higher than with other solvents.

Drug and polymer ratios were varying parameters. Thus, the dependence of the polymer-drug ratio on particle size was investigated; for best results, nanoparticles should be in the range of 50–500 nm for alveolar macrophage phagocytosis [22]. Other characteristics, such as the encapsulation efficiency and loading capacity, were also investigated during the study. PLGA nanoparticles immobilized with isoniazid were obtained in five different ratios. The average size of the obtained NPs did not exceed 400 nm. Table 3 shows the physicochemical characteristics of the nanoparticles obtained by the DLS method.

Table 3

Average size and polydispersity of NPs at different INH/PLGA ratios

INH/PLGA ratio	Average particle size, nm	PDI	Encapsulation efficiency, %	Loading capacity, %	NPs' yield, %
1:1	221±8	0.124±0.023	42±6	39±6	41±9
1:2	275±4	0.335±0.044	48±8	42±9	44±9
1:3	288±5	0.372±0.040	52±6	46±6	57±9
1:4	322±7	0.444±0.041	60±5	58±8	63±5
1:5	317±9	0.448±0.012	56±8	53±9	59±7

With an increase in the drug/polymer ratio from 1:1 to 1:5, the particle sizes changed from 221±8 to 322±7 nm, and PDI from 0.124±0.023 to 0.448±0.012. An increase in the PLGA concentration led to an increase in particle size. This can be explained by the fact that an increase in the polymer concentration leads to an increase in the viscosity of the organic phase, which in turn increases the forces that counteract particle breakdown, leading to the formation of larger NPs [23, 24].

Besides the average size and polydispersity of the NPs, the nanoparticle production efficiency, such as the encapsulation efficiency and loading capacity, as well as the NPs' yield, are also important factors. The values of encapsulation efficiency for PLGA-INH NPs ranged from 42±6 % to 60±5 % and loading capacity from 39±6 % to 58±8 %. It can be seen from these results that increasing the PLGA concentration increases the encapsulation efficiency and drug loading into the polymer matrix. This can be explained by the fact that increasing the polymer concentration is likely to increase the viscosity of the organic phase, thus increasing the diffusion resistance between the organic and aqueous phases, thereby capturing more drugs in the NPs [25]. Based on the obtained data, it can be concluded that the optimal INH/PLGA ratio is 1:4, although it gives the largest size, but also the highest encapsulation efficiency and NPs' yield (60±5 and 63±5 %, respectively).

The study of the effect of various stabilizer concentrations on the formation of nanoparticles was a continuation of our work. PVA was used as a stabilizer. Figure 1 illustrates the results.

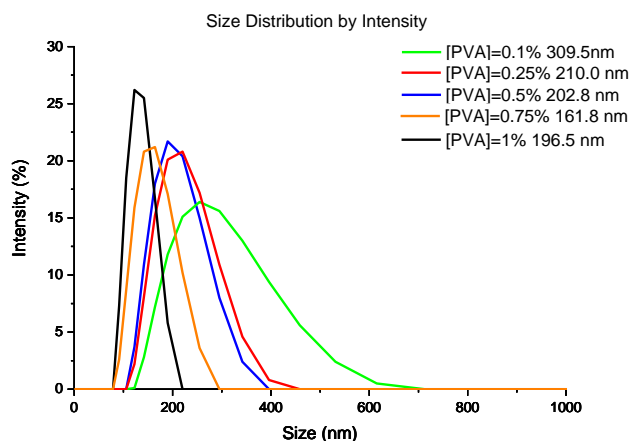


Figure 1. Distribution curves of NPs produced at different PVA concentrations

Figure 1 shows that with an increase in PVA concentration from 0.1 to 0.75 %, the average particle size of the NPs decreases (from 309.5 ± 8 nm to 161.8 ± 5 nm) due to stabilization of the medium. The small particle size of the obtained NPs is because of the high concentration of surfactant, which prevents coalescence of the globules, protects and stabilizes the droplets formed during emulsification, and leads to the formation of smaller emulsion droplets [26].

The morphological characteristics of the dried nanoparticles were determined by SEM, showing a regular spherical shape and smooth surface. Figure 2 shows a microphotograph of PLGA nanoparticles obtained by nanoprecipitation under the following conditions: non-solvent — ethanol, organic solvent — DMSO, INH/PLGA ratio 1:4, at different concentrations of PVA. The image shows both aggregates and individual parts of nanoparticles. The formation of aggregates can be explained by incomplete washing of the surfactant and the drying process.

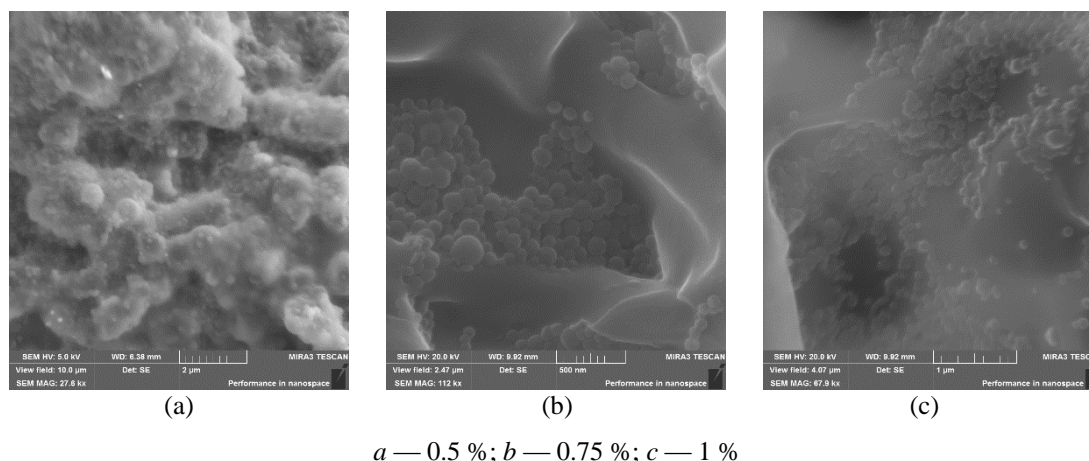


Figure 2. SEM image of PLGA – INH NPs at different PVA concentrations

Thermogravimetric analysis of the individual components of the system and the obtained NPs was performed to confirm the incorporation of isoniazid into the polylactide-co-glycolide NPs complex. Figure 3 illustrates TGA and DSC curves of isoniazid, empty PLGA nanoparticles, and PLGA nanoparticles immobilized with isoniazid.

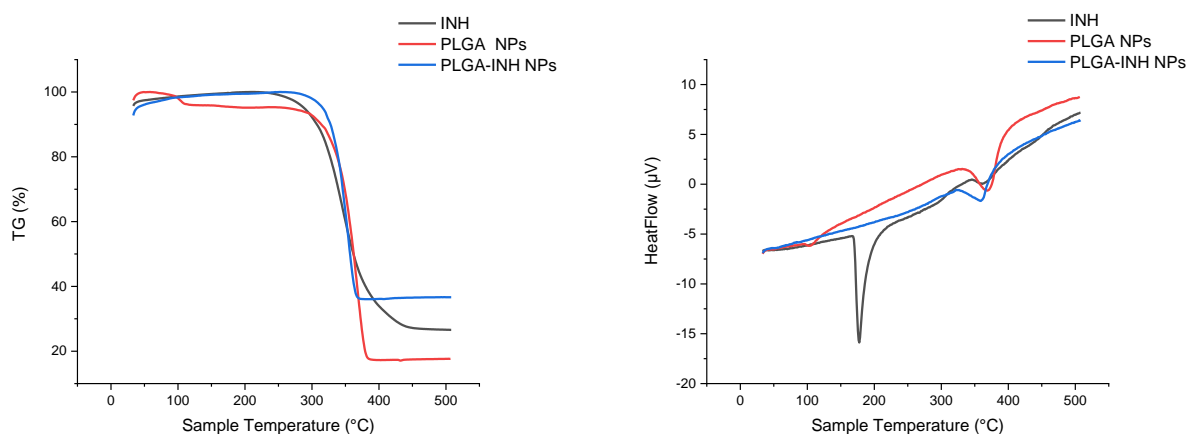


Figure 3. TGA and DSC of isoniazid, PLGA nanoparticles and PLGA particles immobilised with isoniazid

Thermal analysis (Figure 3) of pure INH showed an endothermic peak at 172 °C corresponding to its melting point and decomposition, which indicates that the drug could be in a crystalline form. Empty PLGA nanoparticles show an endothermic peak at 367 °C, which probably corresponds to their melting stage. The weight loss of the polymer NPs exceeds 76 % in the temperature range of 300 – 385 °C. For PLGA-INH NPs, the DSC curve shows an endothermic peak at 360 °C. On the TGA curve, the nanoparticles decompose at 300 – 370 °C and the weight loss exceeds 66 %. From the curves obtained, it can be concluded that the thermal degradation of polylactide-co-glycolide with the drug is slower than the degradation of free

poly(lactide-co-glycolide) nanoparticles. In addition, a shift of the melting peak indicates an interaction of the drug with the polymer.

In vitro release of isoniazid from poly(lactide-co-glycolide) NPs was studied by dialysis at different pH values, simulating the *in vitro* conditions of the gastrointestinal tract of people. Figure 4 shows a cumulative drug release from nanoparticles prepared by nanoprecipitation under the following conditions: non-solvent — ethanol, organic solvent — DMSO, INH/PLGA ratio 1:4, PVA concentration 0.75%. *In vitro* drug release from NPs typically consists of two phases: a first “burst release” phase followed by a second phase of prolonged release [27]. The first phase is caused by the release of the drug substance, which is adsorbed on the surface of the NPs or dispersed near the surface. The second phase is due to the release of the drug substance residing in the core [28–31]. As shown in Figure 4, “burst release” of the drug is observed at pH 6.86 after 2 hours; at pH 7.4 after 5 hours; and at pH 1.2 was 27 % within an hour. In the simulated stomach fluid (pH 1.2) there is a total (mean) release of the INH dose incorporated in the NPs after 2 h, which corresponds to the estimated transit time of the pharmaceutical form in the stomach environment [32]. After 6 hours, the release rate of isoniazid at pH 7.4 was 55 %, and at pH 6.86, a high release rate of 80 % was detected. This may be because the solubility of isoniazid increases with pH decreasing. We have previously studied the release of a drug from a dialysis membrane in a conventional dosage form (the conventional isoniazid tablet), which provides a single and short-term release of the drug [29]. At pH = 1.2, the drug is released normally and the next doses of the drug are required to achieve a therapeutic effect [33, 34].

From the experimental data, it can be concluded that the pH of the medium has a great influence on drug release. The solubility of the drug increased as the pH of the medium decreased [35, 36]. This partly explains the differences in drug release with changes in pH. However, this could not be the dominant factor in drug release. The release of small drug molecules from a biodegradable matrix may be due to polymer degradation [37].

Further, it was interesting to investigate the polymer degradation process. The polymer biodegradation was determined by dialysis at different pH values at 37°C [38]. Figure 5 shows data on degradation kinetics of PLGA NPs studied by UV-spectrophotometry.

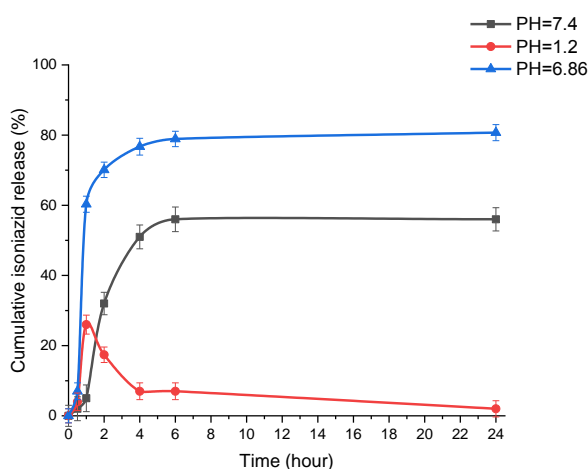


Figure 4. Degree of release of isoniazid from the polymeric matrix at different pH values

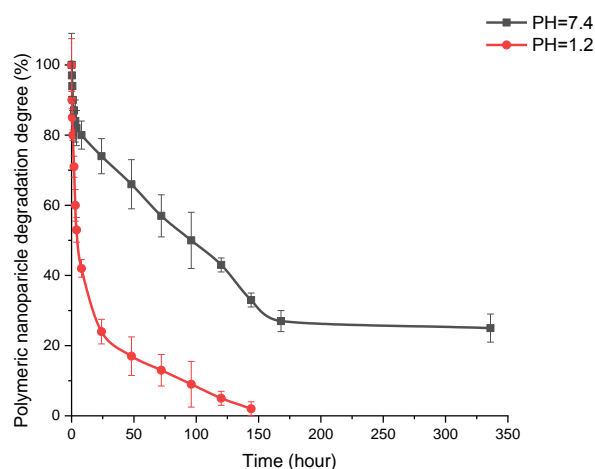


Figure 5. Degradation of PLGA NPs at different pH values

A decrease in the optical density of polymer solutions indicates a decrease in molecular weight as a direct result of degradation [36]. The degradation process over a period of 2 weeks shows that the polymer degrades faster in an acidic than in a neutral medium. At pH 1.2, the polymer is completely degraded in six days, but in the beginning it degrades rapidly (60 %) and the remaining 40% is stable and slow to degrade. At pH 7.4, the polymer slowly, evenly degrades to 70 % within two weeks.

Conclusions

This study successfully developed INH-loaded PLGA NPs using the nanoprecipitation method. A number of studies have been carried out to select optimal conditions (non-solvents, solvents, drug-to-polymer ratio, and concentration of surfactant) for the immobilization of the anti-TB drug isoniazid in PLGA NPs. Optimized PLGA nanoparticles were prepared by nanoprecipitation under the following conditions:

non-solvent – ethanol, organic solvent — DMSO, INH/PLGA ratio 1:4, PVA concentration 0.75 % with satisfactory physicochemical characteristics and a loading capacity of up to 50 %. An *in vitro* release analysis confirmed that isoniazid has a controlled release in a neutral medium. It was determined that the degradation of polymeric nanoparticles is faster in an acidic medium and correspondingly the kinetics of isoniazid release from the polymeric matrix is higher than in a neutral medium. This study provides future opportunities for the development of polylactide-co-glycolide-based inhalation dry powders for aerosol delivery of anti-TB drugs to the lungs. In addition, TGA and DSC analyses were performed to confirm the incorporation of isoniazid into the polylactide-co-glycolide matrix. The study results indicate that optimized polymeric nanoparticle formulation could be potentially used for hydrophilic drug delivery systems for tuberculosis treatment.

Acknowledgments

The work was fulfilled within the framework of program-targeted funding of the Ministry of Education and Science of the Republic of Kazakhstan No. AP14871344 “Development of colloidal drug delivery systems based on biopolymers for tuberculosis chemotherapy”.

References

- 1 Fatima, R., Ashraf, M., Ejaz, S., Rasheed, M. A., Altaf, I., Afzal, M., & Anwar, K. (2013). In vitro toxic action potential of anti tuberculosis drugs and their combinations. *Environmental Toxicology and Pharmacology*, 36(2), 501–513. <https://doi.org/10.1016/j.etap.2013.05.008>
- 2 Arbex, M.A., Varella, M.D., Siqueira, H.R., & Mello, F.A. (2010). Antituberculosis drugs: drug interactions, adverse effects, and use in special situations. Part 2: second line drugs. *Jornal brasileiro de pneumologia : publicacao oficial da Sociedade Brasileira de Pneumologia e Tisiologia*, 36, 5, 641–56. <https://doi.org/10.1590/S1806-37132010000500016>
- 3 Tazhbayev, Ye.M., Burkeyev, M.Zh., Zhaparova, L.Zh., Zhumagalieva, T.S., & Arystanova, Zh.T. (2018). Nanoparticles on the basis of polylactic acid and polylactic-co-glycolic acids loaded with drugs. *Bulletin of the University of Karaganda – Chemistry*, 90(2), 31–39. <https://doi.org/10.31489/2018ch2/31-39>
- 4 Hussain, A., Singh, S., Das, S. S., Anjireddy, K., Karpagam, S., & Shakeel, F. (2019). Nanomedicines as Drug Delivery Carriers of Anti-Tubercular Drugs: From Pathogenesis to Infection Control. *Current Drug Delivery*, 16(5), 400–429. <https://doi.org/10.2174/1567201816666190201144815>
- 5 Nasiruddin, M., Neyaz, M. K., & Das, S. (2017). Nanotechnology-Based Approach in Tuberculosis Treatment. *Tuberculosis research and treatment*, 2017, 4920209. <https://doi.org/10.1155/2017/4920209>
- 6 Baranyai, Z., Soria-Carrera, H., Alleva, M., Millán-Placer, A. C., Lucia, A., Martín-Rapún, R., la Fuente, J. M. (2020). Nanotechnology-Based Targeted Drug Delivery: An Emerging Tool to Overcome Tuberculosis. *Advanced Therapeutics*, 4(1), 2000113. <https://doi.org/10.1002/adtp.202000113>
- 7 Wang, W., Guo, H., Lin, S., Xiao, X., Liu, Y., Wang, Y., & Zhou, D. (2022). Biosafety materials for tuberculosis treatment. *Biosafety and Health*. <https://doi.org/10.1016/j.bsheal.2022.03.013>
- 8 Mitchell, M. J., Billingsley, M. M., Haley, R. M., Wechsler, M. E., Peppas, N. A., & Langer, R. (2020). Engineering precision nanoparticles for drug delivery. *Nature Reviews Drug Discovery*, 20(2), 101–124. <https://doi.org/10.1038/s41573-020-0090-8>
- 9 Elmowafy, E. M., Tiboni, M., & Soliman, M. E. (2019). Biocompatibility, biodegradation and biomedical applications of poly(lactic acid)/poly(lactic-co-glycolic acid) micro and nanoparticles. *Journal of Pharmaceutical Investigation*, 49(4), 347–380. <https://doi.org/10.1007/s40005-019-00439-x>
- 10 Becker Peres, L., Becker Peres, L., de Araújo, P. H. H., & Sayer, C. (2016). Solid lipid nanoparticles for encapsulation of hydrophilic drugs by an organic solvent free double emulsion technique. *Colloids and Surfaces B: Biointerfaces*, 140, 317–323. <https://doi.org/10.1016/j.colsurfb.2015.12.033>
- 11 Fessi, H., Puisieux, F., Devissaguet, J. P., Ammoury, N., & Benita, S. (1989). Nanocapsule formation by interfacial polymer deposition following solvent displacement. *International Journal of Pharmaceutics*, 55(1), R1–R4. [https://doi.org/10.1016/0378-5173\(89\)90281-0](https://doi.org/10.1016/0378-5173(89)90281-0)
- 12 Martínez Rivas, C. J., Tarhini, M., Badri, W., Miladi, K., Greige-Gerges, H., Nazari, Q. A., Elaissari, A. (2017). Nanoprecipitation process: From encapsulation to drug delivery. *International Journal of Pharmaceutics*, 532(1), 66–81. <https://doi.org/10.1016/j.ijpharm.2017.08.064>
- 13 Govender, T., Stolnik, S., Garnett, M. C., Illum, L., & Davis, S. S. (1999). PLGA nanoparticles prepared by nanoprecipitation: drug loading and release studies of a water soluble drug. *Journal of controlled release: official journal of the Controlled Release Society*, 57(2), 171–185. [https://doi.org/10.1016/s0168-3659\(98\)00116-3](https://doi.org/10.1016/s0168-3659(98)00116-3)
- 14 Da Costa, D., Exbrayat-Héritier, C., Rambaud, B., Megy, S., Terreux, R., Verrier, B., & Primard, C. (2021). Surface charge modulation of rifampicin-loaded PLA nanoparticles to improve antibiotic delivery in Staphylococcus aureus biofilms. *Journal of Nanobiotechnology*, 19(1). <https://doi.org/10.1186/s12951-020-00760-w>
- 15 Rani, S., Gothwal, A., Pandey, P. K., Chauhan, D. S., Pachouri, P. K., Gupta, U. D., & Gupta, U. (2018). HPMa-PLGA Based Nanoparticles for Effective In Vitro Delivery of Rifampicin. *Pharmaceutical Research*, 36(1). <https://doi.org/10.1007/s11095-018-2543-x>

- 16 Barichello, J. M., Morishita, M., Takayama, K., & Nagai, T. (1999). Encapsulation of Hydrophilic and Lipophilic Drugs in PLGA Nanoparticles by the Nanoprecipitation Method. *Drug Development and Industrial Pharmacy*, 25(4), 471–476. <https://doi.org/10.1081/ddc-100102197>
- 17 Bilati, U., Allémann, E., & Doelker, E. (2005). Development of a nanoprecipitation method intended for the entrapment of hydrophilic drugs into nanoparticles. *European Journal of Pharmaceutical Sciences*, 24(1), 67–75. <https://doi.org/10.1016/j.ejps.2004.09.011>
- 18 Yoo, H. S., Choi, H. K., & Park, T. G. (2001). Protein-fatty acid complex for enhanced loading and stability within biodegradable nanoparticles. *Journal of pharmaceutical sciences*, 90(2), 194–201. [https://doi.org/10.1002/1520-6017\(200102\)90:2<194::aid-jps10>3.0.co;2-q](https://doi.org/10.1002/1520-6017(200102)90:2<194::aid-jps10>3.0.co;2-q)
- 19 Burkeev, M. Z., Tazhbaev, E. M., Zhaparova, L. Z., Zhappar, N. K., & Zhumagalieva, T. S. (2016). Synthesis and Characterization of Poly(DL-Lactic Acid) Nanoparticles Loaded with the Antituberculosis Drug Isoniazid. *Pharmaceutical Chemistry Journal*, 50(9), 608–611. <https://doi.org/10.1007/s11094-016-1500-4>
- 20 Song, K. C., Lee, H. S., Choung, I. Y., Cho, K. I., Ahn, Y., & Choi, E. J. (2006). The effect of type of organic phase solvents on the particle size of poly(D,L-lactide-co-glycolide) nanoparticles. *Colloids and Surfaces A: Physicochemical and Engineering Aspects*, 276(1-3), 162–167. <https://doi.org/10.1016/j.colsurfa.2005.10.064>
- 21 Galindo-Rodríguez, S., Allémann, E., Fessi, H., & Doelker, E. (2004). Physicochemical Parameters Associated with Nanoparticle Formation in the Salting-Out, Emulsification-Diffusion, and Nanoprecipitation Methods. *Pharmaceutical Research*, 21(8), 1428–1439. <https://doi.org/10.1023/b:pham.0000036917.75634.be>
- 22 Costa, A., Pinheiro, M., Magalhães, J., Ribeiro, R., Seabra, V., Reis, S., & Sarmiento, B. (2016). The formulation of nanomedicines for treating tuberculosis. *Advanced Drug Delivery Reviews*, 102, 102–115. <https://doi.org/10.1016/j.addr.2016.04.012>
- 23 Tefas, L. R., Tomuța, I., Achim, M., & Vlase, L. (2015). Development and optimization of quercetin-loaded PLGA nanoparticles by experimental design. *Medicine and Pharmacy Reports*, 88(2), 214–223. <https://doi.org/10.15386/cjmed-418>
- 24 Elsewedy, H. S., Dhubiab, B. E. A., Mahdy, M. A., & Elnahas, H. M. (2020). Development, optimization, and evaluation of PEGylated brucine-loaded PLGA nanoparticles. *Drug Delivery*, 27(1), 1134–1146. <https://doi.org/10.1080/10717544.2020.1797237>
- 25 Chishti, N., Jagwani, S., Dhamecha, D., Jalalpure, S., & Dehghan, M. H. (2019). Preparation, Optimization, and In Vivo Evaluation of Nanoparticle-Based Formulation for Pulmonary Delivery of Anticancer Drug. *Medicina*, 55(6), 294. <https://doi.org/10.3390/medicina55060294>
- 26 Khan, R., Inam, M., Khan, S., Jiménez, A., Park, D., & Yeom, I. (2019). The Influence of Ionic and Nonionic Surfactants on the Colloidal Stability and Removal of CuO Nanoparticles from Water by Chemical Coagulation. *International Journal of Environmental Research and Public Health*, 16(7), 1260. <https://doi.org/10.3390/ijerph16071260>
- 27 Chorny, M., Fishbein, I., Danenberg, H. D., & Golomb, G. (2002). Lipophilic drug loaded nanospheres prepared by nanoprecipitation: effect of formulation variables on size, drug recovery and release kinetics. *Journal of Controlled Release*, 83(3), 389–400. [https://doi.org/10.1016/s0168-3659\(02\)00211-0](https://doi.org/10.1016/s0168-3659(02)00211-0)
- 28 Wang, Y., & Tan, Y. (2016). Enhanced drug loading capacity of 10-hydroxycamptothecin-loaded nanoparticles prepared by two-step nanoprecipitation method. *Journal of Drug Delivery Science and Technology*, 36, 183–191. <https://doi.org/10.1016/j.jddst.2016.09.012>
- 29 Tazhbayev, Ye.M., Galiyeva, A.R., Zhumagaliyeva, T.S., Burkeyev, M.Zh., Kazhmuratova, A.T., Zhakupbekova, E.Zh., Zhaparova, L.Zh., & Bakibayev, A.A. (2021). Synthesis and characterization of isoniazid immobilized poly(lactide-co-glycolide) nanoparticles. *Bulletin of the University of Karaganda – Chemistry*, 101(1), 61–70. <https://doi.org/10.31489/2021Ch1/61-70>
- 30 Galiyeva, A.R., Tazhbayev, Ye.M., Zhumagaliyeva, T.S., Sadyrbekov, D.T., Kaikenov, D.A., Karimova, B.N., & Shokenova, S.S. (2022). Poly(lactide-co-glycolide) nanoparticles immobilized with isoniazid: Optimization using the experimental Taguchi method. *Bulletin of the University of Karaganda – Chemistry*, 105(1), 69–77. <https://doi.org/10.31489/2022Ch1/69-77>
- 31 Burkeev, M.Zh., Kreuter, J., Tazhbayev, Ye.M., Zhaparova, L.Zh., Zhumagalieva, T.S., Arystanova, Zh.T., & Mukhanova, D.A. (2017). Preparation, characterization and investigation of in vitro release of anti-tuberculosis drug p-amino salicylic acid based on human serum albumin. *Bulletin of the University of Karaganda – Chemistry*, 87(3), 38–44. <https://doi.org/10.31489/2017ch3/38-44>
- 32 De Almeida, J. M. F., Júnior, E. D., Verríssimo, L. M., & Fernandes, N. S. (2019). pH-Dependent release system of isoniazid carried on nanoparticles of silica obtained from expanded perlite. *Applied Surface Science*, 489, 297–312. <https://doi.org/10.1016/j.apsusc.2019.05.317>
- 33 Pavani, J., Deepika, B., Nagaraju, K., Regupathi, T., Rao, K.N.V., & Rajeswar Dutt, K. (2017). Formulation development and in vitro evaluation of sustained release matrix tablets of tramadol hydrochloride. *Innovat International Journal Of Medical & Pharmaceutical Sciences*, 2(6), 28–38.
- 34 Angajala, Gangadhara, & Subashini, R. (2014). Transdermal Nanocarriers: New Challenges and Prospectives in the Treatment of Diabetes mellitus. *Journal of Chemistry and Applied Biochemistry*, 1(2): 107, 1–10.
- 35 Becker, C., Dressman, J. B., Amidon, G. L., Junginger, H. E., Kopp, S., Midha, K. K., Shah, V.P., Stavchansky, S., Barends, D. M. (2007). Biowaiver Monographs for Immediate Release Solid Oral Dosage Forms: Isoniazid**A project of the International Pharmaceutical Federation FIP, Groupe BCS, www.fip.org/bcs. *Journal of Pharmaceutical Sciences*, 96(3), 522–531. <https://doi.org/10.1002/jps.20765>
- 36 Nkanga, C. I., Walker, R. B., & Krause, R. W. (2018). pH-Dependent release of isoniazid from isonicotinic acid (4-hydroxybenzylidene)-hydrazide loaded liposomes. *Journal of Drug Delivery Science and Technology*, 45, 264–271. <https://doi.org/10.1016/j.jddst.2018.03.016>

37 Li, J., Jiang, G., & Ding, F. (2008). The effect of pH on the polymer degradation and drug release from PLGA-mPEG microparticles. *Journal of Applied Polymer Science*, 109(1), 475–482. <https://doi.org/10.1002/app.28122>

38 Burkeev, M. Z., Zhaparova, L. Z., Tazhbaev, E. M., Zhumagalieva, T. S., Ali, S. I., & van Herk, A. M. (2013). In Vitro Studies of Capreomycin Sulfate Release from Polyethylcyanoacrylate Nanoparticles. *Pharmaceutical Chemistry Journal*, 47(3), 154–156. <https://doi.org/10.1007/s11094-013-0916-3>

А.Р. Галиева, Е.М. Тажбаев, Т.С. Жұмағалиева, А.Т. Дәрібай

Полилактид-со-гликолид нанобөлшектеріне нанопретрация әдісімен изониазидті инкапсуляциялау

Дәрілік заттарды тасымалдаушы ретінде полимерлі материалдарды қолданудың бірқатар артықшылықтары бар, мысалы, препараттың әсерін ұзарту, дәрілік заттардың жанама әсерлерін азайту және т.б. Мақалада «Изониазид» туберкулезгеарсы препараттың (ТҚП) полилактид-ко-гликолид (ПЛГА) полимерлі нанобөлшектерін нанотұндыру әдісі арқылы алу қарастырылған. Еріткіш емес пен еріткіш табиғатының, дәрі пен полимердің қатынасы және тұрақтандырғыштың концентрациясы сияқты жеке параметрлерді өзгерту арқылы полимерлік нанотасымалдаушылар алынды. Бөлшектердің орташа мөлшері еріткіш емес түріне тығыз байланысты екені анықталды. Спирттерді пайдаланған кезде орташа өлшем мына реттілікпен өсті: этанол < изопропанол < изобутанол. Нанобөлшектердің пайда болуының және олардың соңғы сипаттамаларының маңызды факторы еріткіштің түрі болып табылады. Дәрілік зат/полимер қатынасы ұлғайған сайын нанобөлшектердің орташа мөлшері де өсті. Алынған нанобөлшектердің өлшемі 93–869 нм аралығында болды. Препараттың полимерлі матрицаға қосылғанын дәлелдеу үшін термогравиметриялық және дифференциалды сканерлеуші калориметриялық талдаулар жүргізілді. Сонымен қатар, әртүрлі рН мәндерінде полимердің ыдырауы және полимер матрицасынан изониазидтің босап шығу дәрежесі зерттелді. Алынған нәтижелер нанотұндыру әдісін тек гидрофобты препараттарға ғана емес, сонымен қатар гидрофильді препараттарға да қолдануға болатынын көрсетті.

Кілт сөздер: нанобөлшектер, полилактид-со-гликолид, PLGA, изониазид, нанотұндыру, гидрофильді препараттар, туберкулезгеарсы препараттар.

А.Р. Галиева, Е.М. Тажбаев, Т.С. Жұмағалиева, А.Т. Дәрібай

Инкапсуляция изониазида в наночастицы полилактида-со-гликолида методом наносоаждения

Применение полимерных материалов в качестве носителей лекарственных препаратов имеют ряд преимуществ, такие как пролонгирование действия препарата, уменьшение побочных эффектов лекарства и т.д. В данной статье рассмотрены способы получения полимерных наночастиц полилактида-со-гликолида (ПЛГА) с противотуберкулезным препаратом (ПТП) «Изониазид» методом наносоаждения. Варьируя отдельные параметры, такие как природа растворителя и нерастворителя, соотношение лекарства и полимера, концентрация стабилизатора, были получены полимерные наноносители. Было определено, что средний размер частиц тесно зависит от типа нерастворителя. При использовании спиртов средний размер увеличивался в последовательности: этанол < изопропанол < изобутанол. Немаловажным фактором для образования наночастиц и их конечных характеристик является тип растворителя. При увеличении соотношения лекарство/полимер средний размер наночастиц также увеличивался. Размер полученных наночастиц варьировался в пределах 93–869 нм. Для подтверждения включения лекарственного препарата в полимерную матрицу были проведены анализы термогравиметрии и дифференциальной сканирующей калориметрии. Кроме того, были исследованы деградация полимера и степень высвобождения изониазида из полимерной матрицы при различных рН среды. Полученные результаты показывают, что метод наносоаждения может быть применен не только для гидрофобных лекарств, но и для гидрофильных препаратов.

Ключевые слова: наночастицы, полилактид-со-гликолид, ПЛГА, изониазид, гидрофильные препараты, противотуберкулезные препараты, наносоаждение.

Information about authors*

Galiyeva, Aldana Rymzhanovna — 3rd year PhD student, Department of Organic Chemistry and Polymers, Karagandy University of the name of academician E.A. Buketov, Universitetskaya street, 28,

100024, Karaganda, Kazakhstan; e-mail: aldana_karaganda@mail.ru; <https://orcid.org/0000-0002-8551-6297>;

Tazhbayev, Yerkeblan Muratovich — Full Professor, Doctor of Chemical Sciences, Karagandy University of the name of academician E.A. Buketov, Universitetskaya street, 28, 100024, Karaganda, Kazakhstan; e-mail: tazhbayev@mail.ru; <https://orcid.org/0000-0003-4828-2521>;

Zhumagaliyeva, Tolkyn Sergazyevna — Candidate of Chemical Sciences, Associate Professor, Karagandy University of the name of academician E.A. Buketov, Universitetskaya street, 28, 100024, Karaganda, Kazakhstan; e-mail: zhumagaliyeva79@mail.ru; <https://orcid.org/0000-0003-1765-752X>;

Daribay, Arailym Turashkyzy — Department of Organic Chemistry and Polymers, Karagandy University of the name of academician E.A. Buketov, Universitetskaya street, 28, 100024, Karaganda, Kazakhstan; e-mail: arailymdaribay@gmail.com

*The author's name is presented in the order: *Last Name, First and Middle Names*

I.N. Nurgaliev

Institute of Polymer Chemistry and Physics, Tashkent, Uzbekistan
(*Corresponding author's e-mail: ilnarvodnik@gmail.com)

DFT Study of Chitosan Ascorbate Nanoparticles Structure

In recent years, use of chitosan (CS) nanoparticles as nanocarriers has received much attention due to their biodegradability, biocompatibility, and non-toxicity. CS nanoparticles containing drugs, flavors, enzymes, and antimicrobial agents can maintain their activity. Such nanoparticles can stimulate the stabilization of ascorbic acid (AA) and improve controlled release. This study investigates the interaction of CS monomer with AA and sodium triphosphate (TPP) using density functional theory (DFT) during the formation of chitosan ascorbate (CA) nanostructure (CAN). Based on existing results, the formation of the CS monomer from the complexes occurs due to the donor-acceptor interaction, which is energetically favorable in all considered interactions according to the calculations. At close range, proton transfer has been identified with interaction energies, namely CS-AA (-6.82 kcal/mol), CS-TPP (-4.56 kcal/mol) in the aqueous phase, which indicates that in the process of CAN formation, in most cases, the formation of a donor-acceptor bond occurs between the amino groups of CS with the enol group of AA and the relative coordination of CS with TPP. The introduction of the aqueous phase led to a drop in the interaction energy. Based on our results for the linking types (interaction energies), we propose a simple mechanism for their impact on the CAN formation process.

Keywords: chitosan, ascorbic acid, sodium triphosphate, chitosan ascorbate, nanoparticles, modeling.

Introduction

Chitosan (CS) is a polysaccharide consisting of N-acetyl-D-glucosamine and D-glucosamine linked by the β -(1 \rightarrow 4) bonds [1]. CS is recognized as a natural biopolymer that includes numerous functional groups, such as the amine (NH_2) and hydroxyl (OH), and it is made via the deacetylation of chitin. Ascorbic acid (AA) plays an important role in metabolism, acting as both an acceptor and a proton donor in enzymatic systems, due to the mobility of hydrogen atoms in enol hydroxyls at C-3 ($\text{pK}_a = 4.2$) and C-2 ($\text{pK}_a = 11.6$) [2]. CS is a biodegradable, non-toxic biopolymer; it has properties that stimulate plant growth and inhibit phytopathogenic fungi; it possesses immunological modulation and antiviral efficacy; it has a wide range of applications, particularly in anti-coronavirus applications [3, 4]. Water-soluble environmentally safe derivatives of CS, in particular, chitosan ascorbate (CA) are of great interest in the world. A wide possibility of CS modification allows one to obtain its water-soluble derivatives, among which CA is of special interest, that exhibit pronounced bioactivity in the growth and development of plants [5, 6].

CA is an organic salt formed by the reaction of CS with AA and it shows a more pH-independent solubility profile, thus providing more flexibility in biomaterial processing and fabrication. CA is synthesized by the direct reaction of CS and AA in water (Figure 1) [7–9].

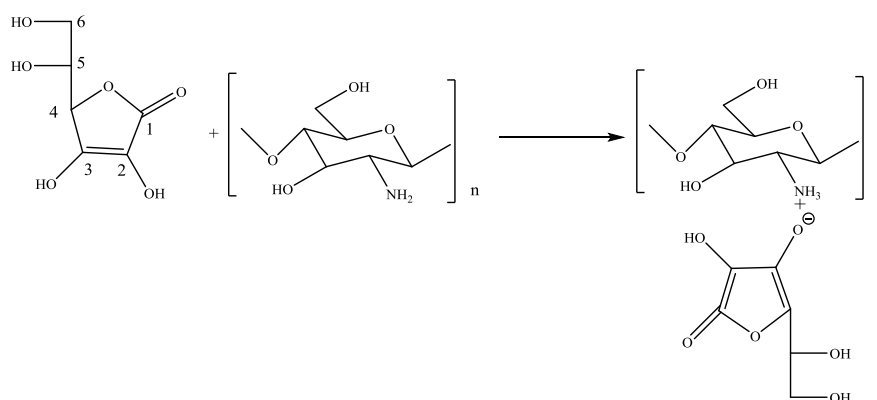


Figure 1. Mechanism of interaction between CS and AA

The product formed is the CS-AA complex, which is different from the CS-AA mixture in that no protonation of CS occurs in the latter [10]. AA presents several electrophilic groups. It contains four hydroxyl groups in positions 2, 3, 5, and 6 with different acidities allowing acid-base reactions. The -OH in position 3 is more acidic one ($pK_a = 4.2$), while the hydroxyl in position 2 has a pK_a of 11.6, and those in positions 5 and 6 behave as secondary and primary alcohol ($pK_a \approx 17$ and 16, respectively) [11]. The acidic hydroxyl in position 3 of AA was expected to react with the amino group of CS, converting it into ammonium ions. The FT-IR spectra demonstrate the formation of complex between CS and AA [11]. The peak at 1754.4 cm^{-1} , which was the stretching vibration of lactone C=O forming intramolecular H-bond in AA, was shifted to 1720.8 cm^{-1} at a reduced intensity. It could be seen that new absorption band characteristic of bending vibration of $-\text{NH}_3^+$ appeared at 1616.1 cm^{-1} . This result suggested that the $-\text{NH}_2$ groups on the CS chains were protonated by the H^+ supplied by AA [12]. The decrease of peak at 3428.2 cm^{-1} indicated the reduction of free $-\text{NH}_2$ groups after the formation of CS-AA complex [13].

Despite the ubiquitous presence of these interactions in chemical processes, few DFT studies on these systems exist in the literature [14–16]. There are few works on determining the activation energy of the formation reaction and modeling the structure of chitosan ascorbate nanostructure (CAN). Complexes of CS with organic acids are obtained mainly by the method of ionotropic gelation, coacervation precipitation, and ultrasonic dispersion [10, 13, 17–22]. However, there are advantages and disadvantages of the above methods for obtaining nanoparticles. If the method of ionotropic gelation is considered technologically acceptable and no additional purification is required for a long time of the final products, then by the method of coacervation precipitation, side compounds are formed due to ions of inorganic salts. When obtaining nanoparticles of CS derivatives by ultrasonic dispersion, it is impossible to control the process, which in turn makes it difficult to control their characteristics.

Thus, the formation of nanoparticles is a multifactorial process that depends on the ratio, concentration of components and solution pH [7–9]. The method of ionic gelation is the most well-known one among the methods for obtaining CAN. However, in studies when obtaining CAN, deprotonation of CS is not carried out; this stage plays a special role in the formation of a donor-acceptor bond between the amino group of CS and the enol group of AA [10, 17–20]. Since without deprotonation of the amino groups of CS, an excess amount of AA in the reaction system increases, this makes it impossible to analyze the properties of the final product [18, 21]. Therefore, in recent works, there was improvement in the method with the inclusion of the step of deprotonation of CS amino groups [7, 19, 22]. Based on the obtained deprotonated CS with varying pH and the ratio of the reaction components and the TPP stabilizer, it is possible to control the size of the resulting nanoparticles of CS derivatives with organic acids, including AA. Nano derivatives of CS with AA have growth-regulating, antimicrobial, and wound-healing properties; solutions of nano derivatives of CS are environmentally safe and low-toxic [10, 19, 20]. It is noted in the literature that the reaction of formation of CS nanoascorbate occurs due to the donor-acceptor bond. The ratio of components and solution pH play a special role in this process [24, 25]. Aqueous solutions of AA are used to obtain water-soluble nano derivatives of CS. The formation of CAN is carried out by varying the solution pH in the range from 4 to 5.5 [19, 26]. Physicochemical properties of biologically active nanostructured complexes of CS with AA are poorly studied, and theoretical works on the formation of CAN have not been found [3, 10, 21–26].

Computational research effectively helps to understand the nature of these interactions and it is less time-consuming and considerably less expensive than experimental analyses. Thus, the objective of the current work is to investigate the interaction of CS with AA and TPP using the DFT method to be a primer for understanding the CAN formation, as well as for theoretical validation of literature experimental results. The optimized geometry, frontier molecular orbitals (FMOs) and details of quantum molecular descriptors were calculated.

Experimental

Computational methods

In this work, we carry out quantum theoretical calculations and optimized the model of interaction of monomer form of CS with AA and TPP structure at the B3LYP/6-31++G(d,p) level (DFT) [28–30] by the GAUSSIAN09 program package [27] and calculate its properties. The charge state of atoms is calculated, diagrams of boundary molecular orbitals are constructed: the highest occupied (HOMO) and lowest free (LUMO) molecular orbitals, and their energies are determined. In DFT reactivity descriptors, such as global hardness (η) is determined using finite difference approximation and Koopmans' theorem [31] as:

$$\eta = \frac{1}{2} \left(\frac{\partial^2 E}{\partial N^2} \right)_{v(\bar{r})} = \frac{1}{2} \left(\frac{\partial \mu}{\partial N} \right)_{v(\bar{r})}, \quad (1)$$

where E — the energy and N is the number of electrons in the electronic system at constant external potential (v), μ — the chemical potential:

$$(\mu = 1/2(E_{\text{HOMO}} + E_{\text{LUMO}})). \quad (2)$$

η is calculated in terms of ionization potential ($-E_{\text{HOMO}}$) and electron affinity ($-E_{\text{LUMO}}$) using the following formulae:

$$\eta = (E_{\text{LUMO}} - E_{\text{HOMO}}) / 2. \quad (3)$$

Free energy of solvation is computed by equation:

$$\Delta G_{\text{sol}} = G_{\text{solvent}} - G_{\text{gas}}, \quad (4)$$

that numerical values obtained by using Solvation Model of Density (SMD) [32]. The interaction energy (ΔE_{int}) between CS and AA, TPP is calculated using super molecular approach

$$\Delta E_{\text{int}} = (E_{\text{CAN}}) - (E_{\text{CS}} + E_{\text{AA}} + E_{\text{TPP}}), \quad (5)$$

where E_{CAN} — the energy of the CAN adduct; E_{CS} — the energy of CS; E_{AA} — the energy of the AA and, E_{TPP} — the energy of the TPP.

The energy difference was taken before or after the proton transfer, for example, between CS^+ and AA^- , TPP^- ions. Global reactivity descriptor, namely the global hardness is calculated using global hardness values. To quantify the reactivity in aqueous phase, solvation energies are calculated using self-consistent reaction field theory through the Polarizable Continuum Model (PCM) [33, 34]. In calculating interaction energy, basis set superposition error (BSSE) is considered by using counterpoise = N [35, 36].

Results and Discussion

Model structures were built for simulating the possibility of CAN structure. Models were presented as one unit of CS representing the main model molecule. The interactions between CS molecules with AA and TPP can occur, as observed in the results addressed so far, by donor-acceptor interaction involving $-\text{OH}$ or $-\text{NH}_3^+$ groups from CS. To evaluate this interaction, as well as describe some quantum properties of the CAN model, which are scarce in the literature, a computational study was realized. FMOs were calculated to gain a deeper insight into the quantum properties of the CAN model. The FMOs results provide knowledge about the energy gap and electronic properties between the HOMO and LUMO of the CS-AA and CS-TPP interactions. The HOMO can be considered the outermost orbital containing electrons, which characterizes the ability of electron donor, while LUMO is considered the innermost orbital containing free places to accept electrons [37].

The optimized CS-AA and CS-TPP structures have been calculated by B3LYP/6-31++G(d,p), the level of theory is shown in Figure 2. The distance between the hydrogen atom of the CS amino group and the oxygen atoms of AA and TPP is in the range of 1.52–1.98 Å, which is typical for donor-acceptor interaction and thus establishes the fact that the product of the interaction of one monomer units of CS with AA and TPP are held together by a donor-acceptor mechanism. A bond is formed in the case of interaction of CS with AA ($r = 1.60$ Å, $\theta = 171.1^\circ$), as well as CS with TPP ($r = 1.53$ Å, $\theta = 178.7^\circ$).

According to calculations, the hydroxyl group of AA in position 3 (C3-O) will react with the amino group of CS, converting it into ammonium ions. The enol group of AA reacts with the $-\text{NH}_3^+$ group of CS with the formation of oxoammonium (Figure 1), due to the donor-acceptor interaction, a CS complex is formed. Amino groups in CS chains can be protonated by AA to form a positively charged water-soluble polysaccharide. CA in an acidic solution undergoes ionic gelation and forms CAN particles with a crosslinking agent added to the solution. Crosslinking occurs due to electrostatic interaction between positively charged amino groups of CS and negatively charged oxygen atoms of TPP. The size of the formed particle mainly depends on the concentration of the acid (acetic acid) and deacetylation degree (DD) of CS [24, 25]. CS with a higher DD is characterized by a large number of effective binding points, i.e., amino groups that are protonated in an acidic solution [7]. Moreover, in an acidic solution, the degree of protonation of amino groups in the chains of CS increases, which, as a result, increases the ability to form cross-links with TPP. The binding of TPP to the polymer occurs until the degree of binding that also depends on the concentration of TPP, decreases, which eventually leads to the formation of smaller nanoparticle sizes, and after saturation, excessive binding will lead to the formation of aggregates, resulting in large particle size [8–10, 25, 26].

The magnitude of interaction is of paramount importance for nanostructure stabilization. A strong or weak interaction, both are equally unfavorable for biological activity. The weak interaction is unfavorable for the stability of such nanoparticles. For exhibiting biological activity, a suitable interaction energy range is 10 kcal/mol [10, 21–23]. To examine the magnitude of the interaction between CS and AA, TPP, we estimated the interaction energy using a supermolecular approach. Initially, we calculated the interaction energies (ΔE_{int}) in the gas phase and then observed the impact of aqueous phase on the interaction energy (Table 1). In the gas phase, ΔE_{int} is observed to be high and the order is CS-AA (–68.76 kcal/mol) > CS-TPP (–64.58 kcal). The observed trend does not corroborate with that predicted from the bond angle (θ) values in donor-acceptor bonding. This indicates that the bond angle in donor-acceptor bonding is not the sole criterion that governs the interaction energies between two compounds.

During CAN delivery, transfection of nanoparticles takes place through a complex physiological medium, whose main constituent is water [13, 17]. Cationic charge of CS attracts a large scale of solvation and thereby enhances stability of CS. Therefore, incorporation of aqueous phase produces a spiky fall in interaction energies as compared to the gas phase. The aqueous phase ΔE_{int} (using PCM model) values of interactions are in the order: CS-AA (–13.67 kcal/mol) > CS-TPP (–11.2 kcal/mol). We have further calculated the free energy of solvation (ΔG_{sol}) (using SMD solvation model) of the chosen CS-AA and CS-TPP. The order is observed to be: CS-AA (–66.32 kcal/mol) > CS-TPP (–62.45 kcal/mol), higher values are due to positive charge inherent in the interactions.

Quantum chemical methods are important for obtaining information about the molecular structure and the interaction behavior. In the synergic effect of interactions of the type CS + nucleophile(AA,TPP) = CAN, intermolecular donor-acceptor interaction formation is favored when the HOMO of the CAN has lower energy than the HOMO of CS or LUMO of AA and TPP [33]. Hence, we have calculated the energy separation $\Delta E_{gas, aq} = (E_{HOMO(gas, aq)}^{CAN} - E_{HOMO(gas, aq)}^{nucleophile(AA, TPP)})$. It is evident from Table 1 that $E_{HOMO,CAN}$ is lower than $E_{HOMO, nucleophile(AA,TPP)}$ and $E_{LUMO,CS}$. This indicates that the formation of donor-acceptor interactions is beneficial in all considered interactions from the HOMO-LUMO energy data. Figure 2 illustrates the mapping of HOMO and LUMO orbitals.

Earlier, [38–40] reported a correlation between the energy separation $\Delta E_{gas, aq}$ values and interaction energy, ΔE_{int} which showed an increase in interaction energy with an increment in ΔE values (ΔE_{int} against $\Delta E_{gas, aq}$). Here we observe high ΔE_{gas} values (–51.49 kcal/mol to –72.42 kcal/mol) for interactions in the gas phase in compliance with high magnitude of the gas phase interaction energies (–64.58 kcal/mol to –68.76 kcal/mol). Incorporation of aqueous phase lowers ΔE_{aq} values (–4.56 kcal/mol to –6.82 kcal/mol) along with a fall in interaction energy (–11.2 kcal/mol to –13.67 kcal/mol). However, no linear relationship between ΔE and ΔE_{int} is observed. Apart from ΔE values, shape of the LUMO of the donor and HOMO of the acceptor is also important. Figure 2 reveals that HOMO and LUMO of CS-TPP are localized over the $-\text{NH}_3^+$ group, and this facilitates the $-\text{NH}_3^+$ group to participate in donor-acceptor interactions. Moreover, LUMO of CS-AA is spreading over the O atoms of AA and TPP, which makes them hydrogen acceptor during donor-acceptor bonding formation.

Gas phase BSSE corrected ΔE_{int} calculated values of the chosen adducts are presented in Table 1. We observe high ΔE_{gas} values for CS-AA and CS-TPP interactions (–72.42 kcal/mol and –51.49 kcal/mol) in the gas phase. Incorporation of aqueous phase lowers ΔE_{aq} values (–6.82 kcal/mol and –4.56 kcal/mol), respectively. However, no linear relationship between ΔE and ΔE_{int} is observed. Apart from ΔE values, shape of the LUMO of the donor and HOMO of the acceptor is also important. Figure 2 reveals that HOMO of CS-AA is localized over the $-\text{NH}_3^+$ group, whereas the LUMO orbital resides on the lactone-ring of AA molecule, which makes them hydrogen acceptor during donor-acceptor bonding formation. The LUMO of CS-TPP is localized over the TPP molecule, HOMO is slightly spreading over on $-\text{NH}_3^+$ group of CS molecule.

Table 1

Calculated parameters (in kcal/mol) of the studied systems

Structure	ΔE_{int} (BSSE correct)	ΔE_{int}	ΔE_{int} (using PCM model)	ΔG_{sol} (using SMD solvation model)	ΔE_{gas}	ΔE_{aq}	ΔG_{gas}	ΔG_{aq}	η , gas phase	η , aqueous phase
CS-AA	–68.76	–70.21	–13.67	–66.32	–72.42	–6.82	–40.34	–3.37	63.7	60.3
CS-TPP	–64.58	–66.32	–11.2	–62.45	–51.49	–4.56	–41.35	–3.08	49.7	59.3

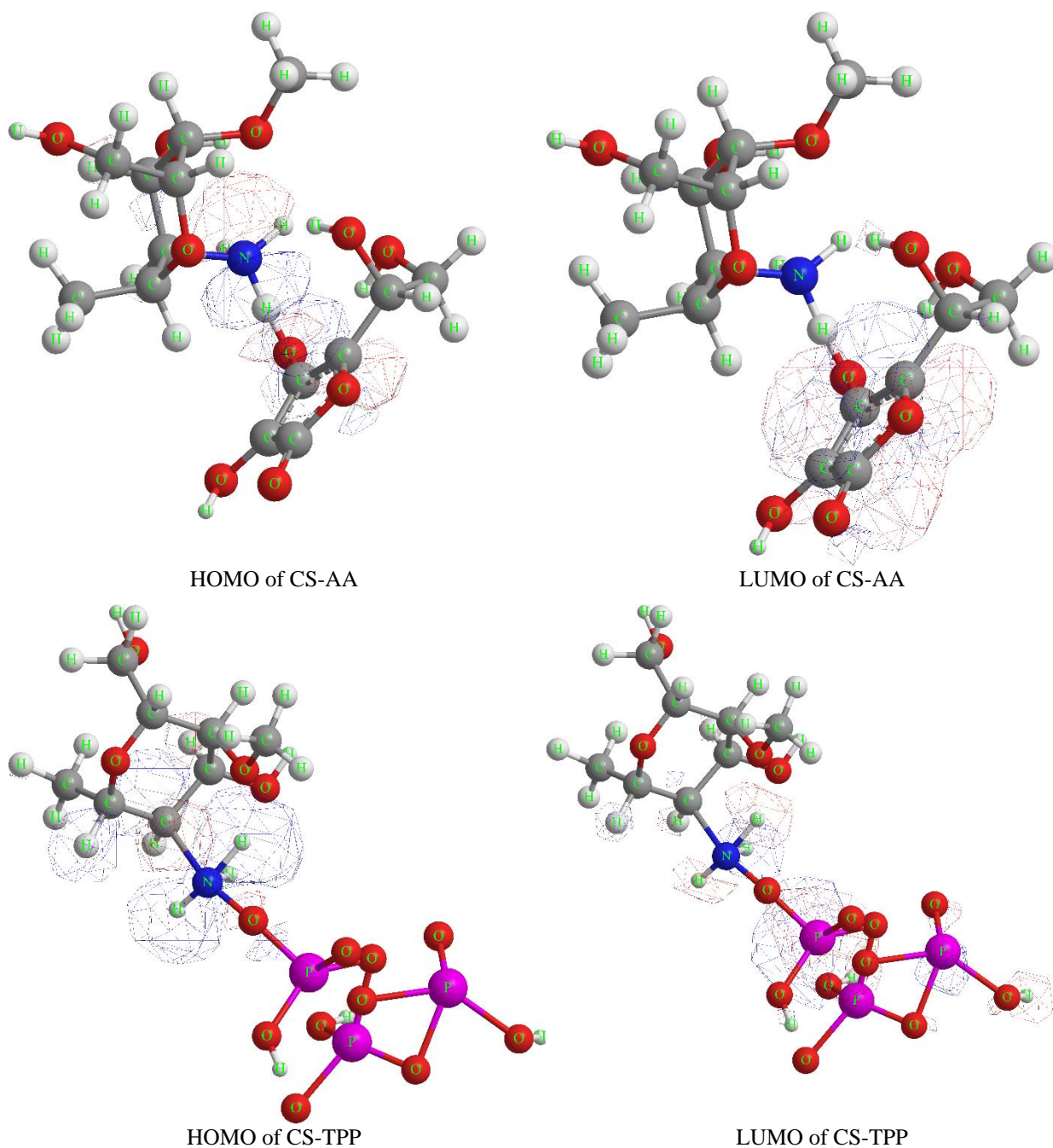


Figure 2. Molecular orbital surfaces for HOMO and LUMO of CS-AA and CS-TPP

We performed thermochemical analysis, to examine the thermodynamic driving force involved in the interactions. The ΔG_{gas} and ΔG_{aq} values are presented in Table 1. It is evident that in the gas phase, free energy favors interactions. In the gas phase, ΔG values follow the order CS-AA (-40.34 kcal/mol) < CS-TPP (-41.35 kcal/mol). However, a spiky fall in ΔG values is observed in the aqueous phase exhibiting negative ΔG_{aq} values. ΔG_{aq} values are in the order: CS-AA (-3.37 kcal/mol) < CS-TPP (-3.08 kcal/mol). This demonstrates the influence of solvent polarity on the parameter and the large role of thermodynamic driving forces in the aqueous phase, also for other systems [16, 38–44].

In accordance with the literature data [17–19] and the data of the calculation results, we proposed a model of CAN, which is represented in Figure 3.

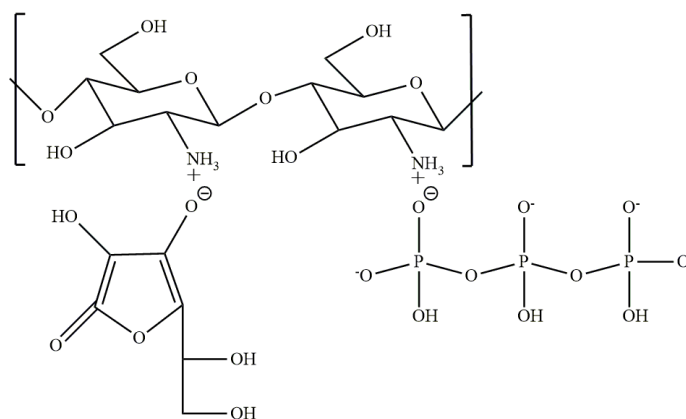


Figure 3. Interaction mechanism of CS-AA-TPP

Stability of the CAN can be monitored in terms of global hardness, in both gas and aqueous phases. The result in Table 1 elucidates the gas and aqueous phase global hardness of CS-AA and CS-TPP. Global hardness of the interaction values in both phases is comparable but slightly lower values in the aqueous phase imply that they are less stable in the aqueous phase.

Conclusions

In the present study, the electronic structure of interaction of CS to interact with AA and TPP has been analyzed using the DFT calculations B3LYP/6-31++G(d,p). The DFT results establish the existence of strong donor-acceptor interactions between CS and the AA and TPP in the gas phase. The introduction of the aqueous phase led to a drop in the interaction energy. The results show that the HOMO of CS-AA and CS-TPP is localized over the $-\text{NH}_3^+$ group, whereas the LUMO orbital resides on the lactone-ring of AA molecule, which makes them hydrogen acceptor during donor-acceptor bonding formation. The LUMO of CS-TPP is localized over the TPP molecule. According to the frontier orbital analysis, the AA had the greatest contributions to HOMO and LUMO. In addition, an increase in the acidity of the medium, the concentration of AA and TPP as well as the DD of CS can be considered as a tool for obtaining nanoparticles of various sizes. CS nanoparticles can protect AA from degradation and improve the stability of AA. CS-based drug delivery systems can be improved by adopting different theoretical and synthetic techniques and selecting appropriate process parameters and functional properties.

References

- Miguel, J., Radhouani, O.H., & Reis, R.L. (2021). Chitosan. *Chapter in book: Polysaccharides of Microbial Origin*, Springer, Cham, 1–18. https://doi.org/10.1007/978-3-030-35734-4_14-1
- Evdokimov, I.A., Alieva, L. R., Varlamov, V.P., Kharitonov, V.D., Butkevich, T.V., & Kurchenko, V.P. (2015). Usage of chitosan in dairy products production. *Foods and Raw Materials*, 3(2), 29–39. <https://doi.org/10.12737/13117>
- Safer, A.-M., & Leporatti, S. (2021). Chitosan nanoparticles for antiviral drug delivery: A Novel Route for COVID-19 Treatment. *International Journal of Nanomedicine*, 16, 8141–8158. <https://doi.org/10.2147/IJN.S332385>
- Mondal, A., Dhar, A.K., Banerjee, S., Hasnain, Md S., & Nayak, A.K. (2022). Antimicrobial uses of chitosan. *Chapter in book: Chitosan in Biomedical Application*, Academic Press, Elsevier, 13–36. <https://doi.org/10.1016/B978-0-12-821058-1.00009-5>
- Balusamy, S.R., Rahimi, S., Sukweenadhi, J., Sunderraj, S., Shanmugam, R., Thangavelu, L., Mijakovic, I., & Perumalsamy, H. (2022). Chitosan, chitosan nanoparticles and modified chitosan biomaterials, a potential tool to combat salinity stress in plants. *Carbohydrate Polymers*, 284(2), 19189. <https://doi.org/10.1016/j.carbpol.2022.119189>
- Gayen, K., Pabale, S., Shirolka Sarkar, S., & Roychowdhury, S. (2022). Chitosan biomaterials: Natural resources for dentistry. *International Journal of Oral Health Sciences*, 11(2), 75–79. https://doi.org/10.4103/ijohs.ijohs_18_21
- Sekar, V., Rajendran, K., Vallinayagam, S., Deepak, V., & Mahadevan, S. (2018). Synthesis and characterization of chitosan ascorbate nanoparticles for therapeutic inhibition for cervical cancer and their in silico modeling. *Journal of Industrial and Engineering Chemistry*, 62, 239–249. <https://doi.org/10.1016/j.jiec.2018.01.001>
- Rossi, S., Marciello, M., Sandri, G., Bonferoni, M.C., Ferrari, F., & Caramella, C. (2008). Chitosan ascorbate: a chitosan salt with improved penetration enhancement properties. *Pharmaceutical Development and Technology*, 13, 513–521. <https://doi.org/10.1080/10837450802288865>

- 9 Elbarbary, A.M., Shafik, H.M., Ebeid, N.H., Ayoub, S.M., & Othman S.H. (2015). Iodine-125 chitosan-vitamin C complex: preparation, characterization and application. *Radiochimica Acta*, 103, 663–671. <https://doi.org/10.1515/ract-2014-2303>
- 10 Tian, X.L., Tian, D.F., Wang, Z.Y., & Mo, F.K. (2009). Synthesis and evaluation of chitosan-vitamin C complex. *Indian Journal of Pharmaceutical Sciences*, 71(4), 371–376. <https://doi.org/10.4103/0250-474X.57284>
- 11 Capuzzi, G., Nostro, P.L., Kulkarni, K., & Fernandez, J.E. (1996). Mixtures of stearyl- 6-O-ascorbic acid and α -tocopherol: A monolayer study at the gas/water interface. *Langmuir*, 12, 3957–3963. <https://doi.org/10.1021/la960001y>
- 12 Zheng, C., Yan, X., Si, J.G., Meng, Y., Qi, Z., & Tao, Z. (2008). Ionic interactions between sulfuric acid and chitosan membranes. *Carbohydrate polymers*, 73, 111–116. <https://doi.org/10.1016/j.carbpol.2007.11.009>
- 13 Mao, S.R., Shuai, X.T., Unger, F., Simona, M., Bi, D.Z., & Kissel, T. (2004). The depolymerization of chitosan: Effects on physicochemical and biological properties. *International Journal of Pharmaceutics*, 281(1-2), 45–54. <https://doi.org/10.1016/j.ijpharm.2004.05.019>
- 14 Pacheco-García, P.F., Perez-Gonzalez, A., Ramos-Flores, A., Flores-Gonzalez, L.A., Lopez-Oglesby, J.M., & Gonzalez-Perez, M. (2017). Experimental study and calculation of the electron transfer coefficients on the dissolution behavior of chitosan in organic acids. *International Journal of Advanced Engineering, Management and Science*, 3(6), 703–709. <https://dx.doi.org/10.24001/ijaems.3.6.14>
- 15 An, X., Kang, Y., & Li, G. (2019). The interaction between chitosan and tannic acid calculated based on the density functional theory. *Chemical Physics*, 520, 100–107. <https://doi.org/10.1016/j.chemphys.2018.12.009>
- 16 Siahaan, P., Sasongko, N.A., Lusiana, R.A., Prasasty, V.D., & Martoprawiro, M.A. (2021). The validation of molecular interaction among dimer chitosan with urea and creatinine using density functional theory: In application for hemodialysis membrane. *International Journal of Biological Macromolecules*, 168, 339–349. <https://doi.org/10.1016/j.ijbiomac.2020.12.052>
- 17 Deshmukh, A.R., & Kim, B.S. (2019). Chitosan-vitamin C nanoparticles. *Korean Society for Biotechnology and Bioengineering Journal*, 34(4), 221–232. <https://doi.org/10.7841/ksbbj.2019.34.4.221>
- 18 Augustine, R., Dan, P., Schlachet, I., Rouxel, D., Menu, P., & Sosnik, A. (2019). Chitosan ascorbate hydrogel improves water uptake capacity and cell adhesion of electrospun poly(epsilon-caprolactone) membranes. *International Journal of Pharmaceutics*, 559(25), 420–426. <https://doi.org/10.1016/j.ijpharm.2019.01.063>
- 19 Othman, N., Masarudin, M.J., Kuen, C.Y., Dasuan, N.A., Abdullah, L.Ch., & Jamil, Md. S.N.A. (2018). Synthesis and optimization of chitosan nanoparticles loaded with L-ascorbic acid and thymoquinone. *Nanomaterials*, 8(11), 920. <https://doi.org/10.3390/nano8110920>
- 20 Liu, J., Pu, H., Zhang, X., Xiao, L., Kan, J., & Jin, Ch. (2018). Effects of ascorbate and hydroxyl radical degradations on the structural, physicochemical, antioxidant and film forming properties of chitosan. *International Journal of Biological Macromolecules*, 114, 1086–1093. <https://doi.org/10.1016/j.ijbiomac.2018.04.021>
- 21 Baek, J., Ramasamy, M., Carly Willis, N., Kim, D.S., Anderson, W.A., & Tam, K.C. (2021). Encapsulation and controlled release of vitamin C in modified cellulose nanocrystal/chitosan nanocapsules. *Current Research in Food Science*, 4, 215–223. <https://doi.org/10.1016/j.crfs.2021.03.010>
- 22 Alishahi, A., Mirvaghefi, A., Tehrani, M.R., Farahmand, H., Shojaosadati, S.A., Dorkoosh, F.A., & Elsabee, M.Z. (2011). Shelf life and delivery enhancement of vitamin C using chitosan nanoparticles. *Food Chemistry*, 126, 935–940. <https://doi.org/10.1016/j.foodchem.2010.11.086>
- 23 Esraa Abu El, Q.M., Mohamed, A.S., Fahmy, S.R., Soliman, A.M., & Gaafar, Kh. (2021). Silver/chitosan/ascorbic acid nanocomposites ameliorate diabetic nephropathy in the model of type 1 diabetes. *GSC Biological and Pharmaceutical Sciences*, 16(03), 091–102. <https://doi.org/10.30574/gscbps.2021.16.3.0263>
- 24 Pirmiyazov, K.K., & Rashidova, S.Sh. (2020a). Synthesis of ascorbate and nanoascorbate of chitosan and their biologically active properties. *Science and innovative development*, 5, 47–62.
- 25 Pirmiyazov, K.K., & Rashidova, S.Sh. (2020b). Study of the kinetics of Bombyx mori chitosan ascorbate formation. *Bulletin of the University of Karaganda – Chemistry*, 99(3), 38–43. <https://doi.org/10.31489/2020Ch3/38-43>.
- 26 Rossi, S., Vigani, B., Puccio, A., Bonferoni, M.C., Sandri, G., & Ferrari, F. (2017). Chitosan ascorbate nanoparticles for the vaginal delivery of antibiotic drugs in atrophic vaginitis. *Marine Drugs*, 15(10), 319. <https://doi.org/10.3390/md15100319>.
- 27 Frisch, M.J., Trucks, G.W., Schlegel, H.B., Scuseria, G.E., Robb, M.A., Cheeseman, J.R., Scalmani, G., Barone, V., Mennucci, B., Petersson, G.A., et al. (2010). Gaussian, Inc., Wallingford CT.
- 28 Becke, A.D. (1993). Density-functional thermochemistry. III. The role of exact exchange. *The Journal of Chemical Physics*, 98, 5648–5652. <https://doi.org/10.1063/1.464913>.
- 29 Lee, C., Yang, W., & Parr, R.G. (1988). Development of the Colle-Salvetti correlation-energy formula into a functional of the electron density. *Physical Review B*, 37, 785–789. <https://doi.org/10.1103/physrevb.37.785>.
- 30 Miehlich, B., Savin, A., Stoll, H., & Preuss, H. (1989). Results obtained with the correlation energy density functionals of Becke and Lee, Yang and Parr. *Chemical Physics Letters*, 157, 200–206. [https://doi.org/10.1016/0009-2614\(89\)87234-3](https://doi.org/10.1016/0009-2614(89)87234-3).
- 31 Koopmans, T. (1934). über Die Zuordnung Von Wellenfunktionen Und Eigenwerten Zu Den Einzelnen Elektronen Eines Atoms. *Physica*, 1, 104–113. [https://doi.org/10.1016/S0031-8914\(34\)90011-2](https://doi.org/10.1016/S0031-8914(34)90011-2)
- 32 Marenich, V., Cramer, C.J., & Truhlar, D.G. (2009). Universal solvation model based on solute electron density and a continuum model of the solvent defined by the bulk dielectric constant and atomic surface tensions. *The Journal of Physical Chemistry B*, 113(18), 6378–6396. <https://doi.org/10.1021/jp810292n>.

- 33 Miertus, S., Scrocco, E., & Tomasi, J. (1981). Electrostatic interaction of a solute with a continuum. A direct utilization of AB initio molecular potentials for the prevision of solvent effects. *Chemical Physics*, 55(1), 117–129. [https://doi.org/10.1016/0301-0104\(81\)85090-2](https://doi.org/10.1016/0301-0104(81)85090-2).
- 34 Mennucci, B. (2012). Polarizable continuum model. *Wiley interdisciplinary reviews: Computational Molecular Science*, 2(3), 386–404. <https://doi.org/10.1002/wcms.1086>.
- 35 Chalasiński, G., & Szczesniak, M.M. (1994). Origins of structure and energetics of van der Waals clusters from ab initio calculations. *Chemical Reviews*, 94, 1723–1765. <https://doi.org/10.1021/cr00031a001>.
- 36 Galano A., & Idaboy J.R.A. (2006). A new approach to counterpoise correction to BSSE. *Journal of Computational Chemistry*, 27(11), 1203–1210. <https://doi.org/10.1002/jcc.20438>.
- 37 Ozdemir, M.C., Ozgün, B., & Aktan, E. (2019). 1-Aryl-3,5-dimethylpyrazolium based tunable protic ionic liquids (TPILs). *Journal of Molecular Structure*, 1180, 564–572. <https://doi.org/10.1016/j.molstruc.2018.12.027>.
- 38 Ektirici, S., Kurç, Ö., Jalilzadeh, M., Aşır, S., & Türkmen, D. (2022). Computational investigation of the monomer ratio and solvent environment for the complex formed between sulfamethoxazole and functional monomer methacrylic acid. *ACS Omega* 7, 17175–17184. <https://doi.org/10.1021/acsomega.2c00862>.
- 39 Sarma, R., Bhattacharyya, P.K., & Baruah, J.B. (2011). Short range interactions in molecular complexes of 1,4-benzenediboronic acid with aromatic N-oxides. *Computational and Theoretical Chemistry*, 963 141–147 <https://doi.org/10.1016/j.comptc.2010.10.020>.
- 40 Houshmand, F., Neckoudaria, H., & Baghdadic, M. (2018). Host-guest interaction in chitosan–MX (3-chloro-4-(dichloromethyl)-5-hydroxy-2(5H)-furanone) complexes in watersolution: Density Functional Study. *Asian Journal of Nanoscience and Materials*, 2(1), 49–65.
- 41 Deka, B.C., & Bhattacharyya, P.Kr. (2015). Understanding chitosan as a gene carrier: A DFT study. *Computational and Theoretical Chemistry*, 1051, 35–41 <http://dx.doi.org/10.1016/j.comptc.2014.10.023>.
- 42 Deka, B.C., & Bhattacharyya, P.Kr. (2016). Response of chitosan–nucleobase interaction toward external perturbations: A computational study. *Computational and Theoretical Chemistry*, 1078, 72–80. <http://dx.doi.org/10.1016/j.comptc.2015.12.016>.
- 43 Jeremić, S., Tran, H., Marković, Z., Ngo, T.C., & Dao, D.Q. (2018). Insight into interaction properties between mercury and lead cations with chitosan and chitin: Density functional theory studies. *Computational and Theoretical Chemistry*, 1138, 99–106. <https://doi.org/10.1016/j.comptc.2018.06.010>.
- 44 Anchique, L., Alcázar, J.J., Ramos-Hernandez, A., Méndez-Lopez, M., Mora, J.R., Rangel, N., Paz, J.L., & Márquez, E. (2021). Predicting the Adsorption of Amoxicillin and Ibuprofen on Chitosan and Graphene Oxide Materials: A Density Functional Theory Study. *Polymers*, 13(10), 1620. <https://doi.org/10.3390/polym13101620>.

И.Н. Нұрғалиев

Хитозан аскорбат нанобөлшектерінің құрылымын DFT зерттеу

Соңғы жылдары хитозан (ХЗ) нанобөлшектерін нанотасымалдаушылар ретінде пайдалану олардың биоыдырағыштығына, биоүйлесімділігіне және уытты еместігіне байланысты көп көңіл бөлінуде. Құрамында препараттар, дәмдер, ферменттер және микробқақарсы агенттері бар ХЗ нанобөлшектері өз белсенділігін сақтай алады. Мұндай нанобөлшектер аскорбин қышқылының (АҚ) тұрақтануын ынталандырып, бақыланатын босатуды жақсарта алады. Бұл зерттеу хитозан аскорбатының нанокұрылымының (ХАН) түзілуі кезінде тығыздық функционалдық теориясы (DFT) арқылы ХЗ мономерінің АҚ және натрий-триполифосфатымен (ТПФ) өзара әрекеттесуін зерттейді. Қолданыстағы нәтижелер негізінде кешендерден түзілген ХЗ мономері донорлық-акцепторлық әрекеттесу есебінен пайда болады, ол есептеулер бойынша барлық қарастырылатын әрекеттесулерде энергетикалық жағынан қолайлы. Жақын қашықтықта өзара әрекеттесу энергиялары бар протонның тасымалдануы анықталды: сулы фазадағы ХЗ-АҚ (–6,82 ккал/моль), ХЗ-ТПФ (–4,56 ккал/моль). Бұл ХАН түзілу процесінде көп жағдайда донорлық-акцепторлық байланыстың түзілуі АҚ энол тобымен ХЗ амин топтары және ТПФ-мен ХЗ салыстырмалы координациясы арасында жүретінін көрсетеді. Сулы фазаның енгізілуі өзара әрекеттесу энергиясының төмендеуіне әкелді. Байланыс түрлеріне (өзара әрекеттесу энергиясы) нәтижелер негізінде олардың ХАН түзілу процесіне әсер етуінің қарапайым механизмі ұсынылған.

Кілт сөздер: хитозан, аскорбин қышқылы, натрий триполифосфаты, хитозан аскорбаты, нанобөлшектер, модельдеу.

И.Н. Нурғалиев

DFT исследование структуры наночастиц аскорбата хитозана

В последние годы большое внимание уделяется использованию наночастиц хитозана (ХЗ) в качестве наноносителей в связи с их биоразлагаемостью, биосовместимостью и нетоксичностью. Наночастицы ХЗ, содержащие лекарства, ароматизаторы, ферменты и противомикробные агенты, могут сохранять свою активность. Такие наночастицы могут стимулировать стабилизацию аскорбиновой кислоты (АК) и улучшать контролируемое высвобождение. В этой статье исследовано взаимодействие мономера ХЗ с АК и триполифосфатом натрия (ТПФ) с помощью теории функционала плотности (DFT) при формировании наноструктуры аскорбата хитозана (НАХ). На основании имеющихся результатов образования мономера ХС из комплексов происходит за счет донорно-акцепторного взаимодействия, которое, согласно расчетам, является энергетически выгодным во всех рассмотренных взаимодействиях. На близком расстоянии идентифицирован перенос протона с энергиями взаимодействия: ХЗ-АК (-6,82 ккал/моль), ХЗ-ТПФ (-4,56 ккал/моль) в водной фазе, что свидетельствует о том, что в процессе образования НАХ в большинстве случаев происходит образование донорно-акцепторной связи между аминогруппами ХЗ с енольной группой АК и относительная координация ХЗ с ТПФ. Введение водной фазы привело к падению энергии взаимодействия. На основании полученных результатов для типов связей (энергий взаимодействия) авторами предложен простой механизм их влияния на процесс формирования НАХ.

Ключевые слова: хитозан, аскорбиновая кислота, триполифосфат натрия, аскорбат хитозан, наночастицы, моделирование.

Information about the author*

Nurgaliev, Inar Nakipovich (*corresponding author*) — Doctor of Sciences in Physics and Mathematics, Head of the Laboratory of Theoretical Foundations of Polymer Chemistry and Physics, Institute of Chemistry and Physics of Polymers of the Academy of Sciences of the Republic of Uzbekistan, A. Kadyri street, 7 b, 100128, Tashkent, Uzbekistan; e-mail: ilnarvodnik@gmail.com; <https://orcid.org/0000-0002-6983-4375>

*The author's name is presented in the order: *Last Name, First and Middle Names*

A.A. Mashentseva^{1*}, N.A. Aimanova^{1,2}, N. Parmanbek^{1,2},
L.Sh. Altynbaeva^{1,2}, D.T. Nurpeisova²

¹*Institute of Nuclear Physics of the Republic of Kazakhstan, Almaty, Kazakhstan;*

²*L.N. Gumilyov Eurasian National University, Nur-Sultan, Kazakhstan*

(*Corresponding author's e-mail: a.mashentseva@inp.kz)

Application of the Cu@PET Composite Track-Etched Membranes for Catalytic Removal of Cr(VI) Ions

This research examines the features of obtaining composite track-etched membranes based on copper microtubes using various compositions of a deposition solution and various types of reducing agents, such as formaldehyde (Cu_CHO@PET), dimethylamine borane (Cu_DMAB@PET), glyoxylic acid (Cu_Gly@PET). The structure and composition of the membrane composites were studied by scanning electron microscopy and X-ray phase analysis. It was shown that in the case of using dimethylamine borane as a reducing agent, the obtained composites consisted of copper(I) oxide (37.4 %) and copper(0) (62.6 %), in other cases single-component copper microtubes were obtained. The reduction reaction of chromium(VI) ions was used to evaluate the catalytic ability of prepared composites. It was found that the removal efficiency of chromium ions reached up to 95–97 % in the case of single-component composites; the presence of a copper(I) oxide phase in the structure of the Cu_DMAB@PET composites significantly reduced the activity of catalysts and under similar conditions, only 41% of the contaminant was removed from the reaction system. The degradation reaction of Cr(VI) was found to follow the Langmuir-Hinshelwood mechanism and a pseudo-first-order kinetic model. The calculated value of the reaction rate constant k_a for composites of the Cu_DMAB@PET composition (0.017 min^{-1}) was more than 9 times less than that of composites obtained using glyoxylic acid (0.156 min^{-1}) and more than 15 times less than the k_a value of Cu_CHO@PET samples (0.249 min^{-1}). Effect of temperatures on the catalytic ability of composites was studied in the temperature range of 10–38 °C. Some thermodynamic characteristics such as activation energy, enthalpy, and entropy of activation were calculated. It was found that the minimum value of the activation energy was obtained for the Cu_CHO@PET samples.

Keywords: composite track-etched membranes, catalysts, copper microtubes, chromium removal, template synthesis, electroless plating.

Introduction

In recent decades, technological waste based on heavy metals has been considered one of the most significant environmental problems in the world, and emissions containing heavy metals are still a big problem for the aquatic ecosystem of our planet [1].

Chromium is the seventh most common element on Earth, which is distributed in underground and surface waters due to its extensive industrial applications, such as chromite mining, leather, textile and electroplating industries, steel and rubber production, pigment synthesis, etc. Cr(VI) is considered its most harmful form and is usually represented as chromate (CrO_4^{2-}) or dichromate ($\text{Cr}_2\text{O}_7^{2-}$) ions [2, 3]. Compounds based on Cr(VI) are among the 14 most significant chemicals that pose a threat to humans even at ppb concentrations. The Environmental Protection Agency (EPA) identified it as a group of pollutants and proposed a maximum permissible limit of Cr(VI) concentration in drinking water of 0.05 mg/L [4].

According to the World Health Organization (WHO), the maximum permissible limits of Cr(VI) content in drinking water and its discharge into inland waters are also 0.05 mg/L and 0.1 mg/L, respectively. All types of Cr(VI) are toxic to bacteria, animals, plants, and humans because of their permeability and biotransformation properties. They are not only potentially carcinogenic and mutagenic [5], but they can also cause many harmful health consequences such as allergic reactions, weakened immune system, kidney and liver damage, stomach ulcers, skin rash, genetic changes, irritation of the epidermis and even death [6].

Due to the above-mentioned serious impact of Cr(VI) on human health and the environment, the issue of wastewater treatment containing Cr(VI) compounds before being released into the environment or converted into less toxic forms is relevant and much in demand. In several previously published papers, various

approaches were used to remove Cr(VI) from aqueous solutions: adsorption, photocatalysis, membrane technologies, ion exchange, coagulation, etc. [1, 7–9]. Photocatalysis is one of the most popular techniques because of the simplicity of the hardware design, high efficiency, and low cost of the process [10, 11]. Various types of nanoscale materials have previously been studied as effective catalysts for the removal of chromium(VI) ions [8, 12–15].

Composite track-etched membranes (TeMs) are flexible nanoporous membranes with deposited nano- and microtubes of various metals or their oxides. A characteristic feature of this class of composites is the high precision of the density and distribution of pores and their diameters. The composite TeMs are due to the high chemical resistance of these polymers and their exceptional performance characteristics. Moreover, the directed modification of the polymer template is one of the effective ways to increase the catalytic efficiency of the final composites [16, 17]. The variation of the deposition conditions and the composition of the deposition solution make it possible to synthesize nano- and microtubes of composition and morphology with improved characteristics [18–20].

Chemical template synthesis comprises several successive stages, namely sensitization and activation of the template and the final stage of deposition [21]. A group of authors led by F. Muench previously conducted several experimental studies on the influence of various factors on the process of chemical deposition of metals into polycarbonate TEMs. It was shown that the structure of synthesized nanomaterials was largely determined by both the conditions of processing the template at the preparatory stages and the composition of the deposition solution, in particular the nature of the introduced complexing agents [22, 23].

Cu@PET composite TeMs are both effective catalysts for various types of chemical reactions [24–27] and promising sorbents for the removal of heavy metal ions from aqueous media [28, 29]. Moreover, a formaldehyde-based deposition solution is most often used to deposit copper into TEM channels. However, in the light of the increasingly strict requirements for the safety of the obtained nanomaterials, an increasing number of studies are focused on compliance with the basic principles of green chemistry, i.e., minimizing the use of toxic reagents. Alternative options for formaldehyde can be considered deposition solutions based on dimethylamine borane (DMAB), glyoxylic acid.

We studied the features of the synthesis process of composite TEMs of Cu@PET composition using glyoxylic acid as a reducing agent in a deposition solution and investigated the catalytic properties of synthesized composite TeMs in the reaction of removal of chromium(VI) ions in aqueous solutions as well as to conduct a comparative analysis of the effectiveness of this type of TeMs with samples obtained using formaldehyde and DMAB as a reducing agent.

Experimental

Chemical reagents. Copper sulfate pentahydrate ($\text{CuSO}_4 \cdot 5\text{H}_2\text{O}$), tin(II) chloride (SnCl_2), potassium sodium tartrate ($\text{KNaC}_4\text{H}_4\text{O}_6 \cdot 4\text{H}_2\text{O}$), palladium chloride (PdCl_2), glyoxylic acid, sodium lauryl sulfate, ethylenediaminetetraacetic acid (EDTA), potassium dichromate, dimethylamine borane (DMAB), and carbendazim (Czm) were purchased from Sigma Aldrich (Schnelldorf, Germany) and used without further purification. Deionized water (18.2 Mohm/cm, “Aquilon-D301” Aquilon, Podolsk, Russia) was used in all experiments.

Electroless copper deposition. The polymer template was made of PET TEM (film thickness was 12.0 microns; pore density was 4×10^7 ion/cm²). After the standard etching procedure in 2.2 M NaOH solution, the pore diameter of the track-etched membranes did not exceed 395.2 ± 4.73 nm. The sensitization and activation procedure were carried out under the procedure described in [30].

Cu_Gly@PET plating solution: $\text{CuSO}_4 \cdot 5\text{H}_2\text{O}$ — 7.63 g/L; EDTA — 10.26 g/L; sodium lauryl sulfate — 4.0 mg/L; glyoxylic acid — 8.14 g/L, deposition was performed at a temperature of 65 °C, the deposition time was 60 sec, the pH of the solution was 12.65 [31].

Cu_CHO@PET plating solution: $\text{KNaC}_4\text{H}_4\text{O}_6 \cdot 4\text{H}_2\text{O}$ — 18 g/L; $\text{CuSO}_4 \cdot 5\text{H}_2\text{O}$ — 5 g/L; NaOH — 7 g/L, CH_2O — 0.13 M; pH = 12.45 (H_2SO_4), deposition was carried out at a temperature of 10 °C, the deposition time was 40 minutes [32].

Cu_DMAB@PET: $\text{CuSO}_4 \cdot 5\text{H}_2\text{O}$ — 10 g/L; EDTA — 14 g/L; DMAB — 6 g/L, pH = 1.85, deposition was carried out at a temperature of 70 °C, the deposition time was 20 min [27].

The structure and properties of the synthesized composites were studied using a JEOL JFC-7500F scanning electron microscope (SEM). X-ray diffraction analysis of copper nanotubes in a polymer matrix was performed on a D8 Advance diffractometer (Bruker, Germany) in the angular range $2(\theta)$ 20–90° with a

step of $2(\theta) = 0.02^\circ$, measuring time was 1 s (voltage on the X-ray tube was 40 kV, current was 40 mA). The average size of the crystallites was determined by the Scherrer equation [25].

Study of catalytic activity

The catalytic reduction of Cr(VI) to Cr(III) in the presence of methanoic acid was performed in accordance with the paper [33]: 1 mL of HCOOH (88 %) was added to 25 ml of $K_2Cr_2O_7$ (2.0×10^{-4} M) and thermostated, stirring intensively at a temperature of 30 °C for 20 minutes. After that, a 2×2 cm composite catalyst was immersed in the reaction mixture. An aliquot of the reaction mixture with a volume of 1.0 ml was taken every 1–2 minutes and measured on a Specord-250 spectrophotometer (Jena Analytical, Germany) in the wavelength range of 200–500 nm. The degree of decomposition of Cr(VI) (D%) was determined by the formula (1):

$$D = \frac{C_0 - C_t}{C_0} \times 100\% = \frac{A_0 - A_t}{A_0} \times 100\%, \quad (1)$$

where C_0 and C_t — the concentration values of the $K_2Cr_2O_7$ solution at the initial time and time t ; A_0 and A_t — the values of the optical density of the $K_2Cr_2O_7$ solution at the initial time and time t at 285 nm.

The effect of pH on the decomposition efficiency of Cr(VI) ions was evaluated in the range of values 1.5–7.0 (0.1 M NaOH or 0.1 M HCl) at 30 °C, other conditions were similar to those described above. The effect of temperature on the efficiency of Cr(VI) decomposition was studied in the temperature range of 20–38 °C (pH=2, Cr(VI) concentration was 2.0×10^{-4} M).

Results and Discussion

Classical chemical processes of copper plating [34, 35] are widely used in the production of various types of nanoscale materials [36]. In previous studies, various types of reducing agents, such as formaldehyde [35], ascorbic [37, 38] or glyoxylic [31, 39, 40] acid, hydrazine hydrate [41], hypophosphite [42], dimethylamine borane [43, 44], etc., were used in copper deposition solutions. At room temperature, the reduction reaction of copper(II) ions is possible only when using formaldehyde as a reducing agent, but its high toxicity limits the use of this composition for coatings used in pharmaceuticals and biomedicine [45]. The use of hypophosphite or hydrazine is possible only at elevated temperatures, which limits their widespread use in practice.

Figure 1 shows electron micrographs of the synthesized composite TeMs. In these SEM images, besides the nanochannels that are still visible in places, the accumulation of nanoparticles (NPs) is visible as an abundant phase covering the entire surface of PET TeMs and the interior of the nanochannels.

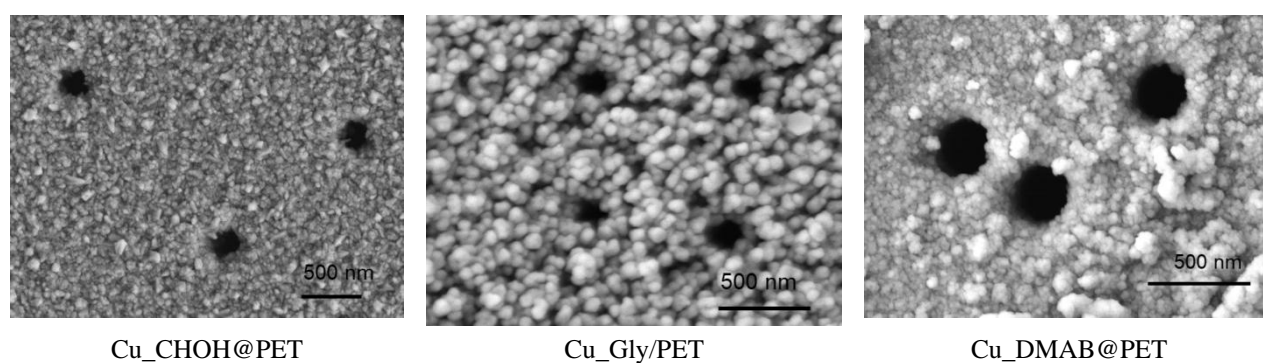


Figure 1. SEM images of the surfaces of synthesized composites

As can be seen from the XRD patterns of synthesized composite membranes in Figure 2, characteristic peaks consistent with the metallic copper, and PET template are apparent in the diffractograms of the Cu_CHO@PET as well as Cu_Gly/PET samples; Cu_DMAB@PET composite has an additional peak revealed to the Cu_2O phase.

Table 1 presents the data of X-ray phase analysis of composites obtained using various reducing agents. The quantitative phase composition was determined using the Rietveld method, which is based on estimating the areas of diffraction peaks by approximating them and determining convergence with reference values for each phase [29]. As can be seen from the data presented, when using DMAB-based deposition solutions, the formation of two phases is observed — pristine copper (0) and copper (I) oxide. In other cases, monophasic copper microtubes with a degree of crystallinity of 72.8 and 61.7 %, respectively, are formed for deposition

solutions based on formaldehyde and glyoxylic acid. The sizes of copper crystallites of the order of 19.4 ± 4 nm were calculated according to the Scherrer equation for Cu_CHOH@PET samples, for Cu_Gly@PET KTM was of the order of 25 nm.

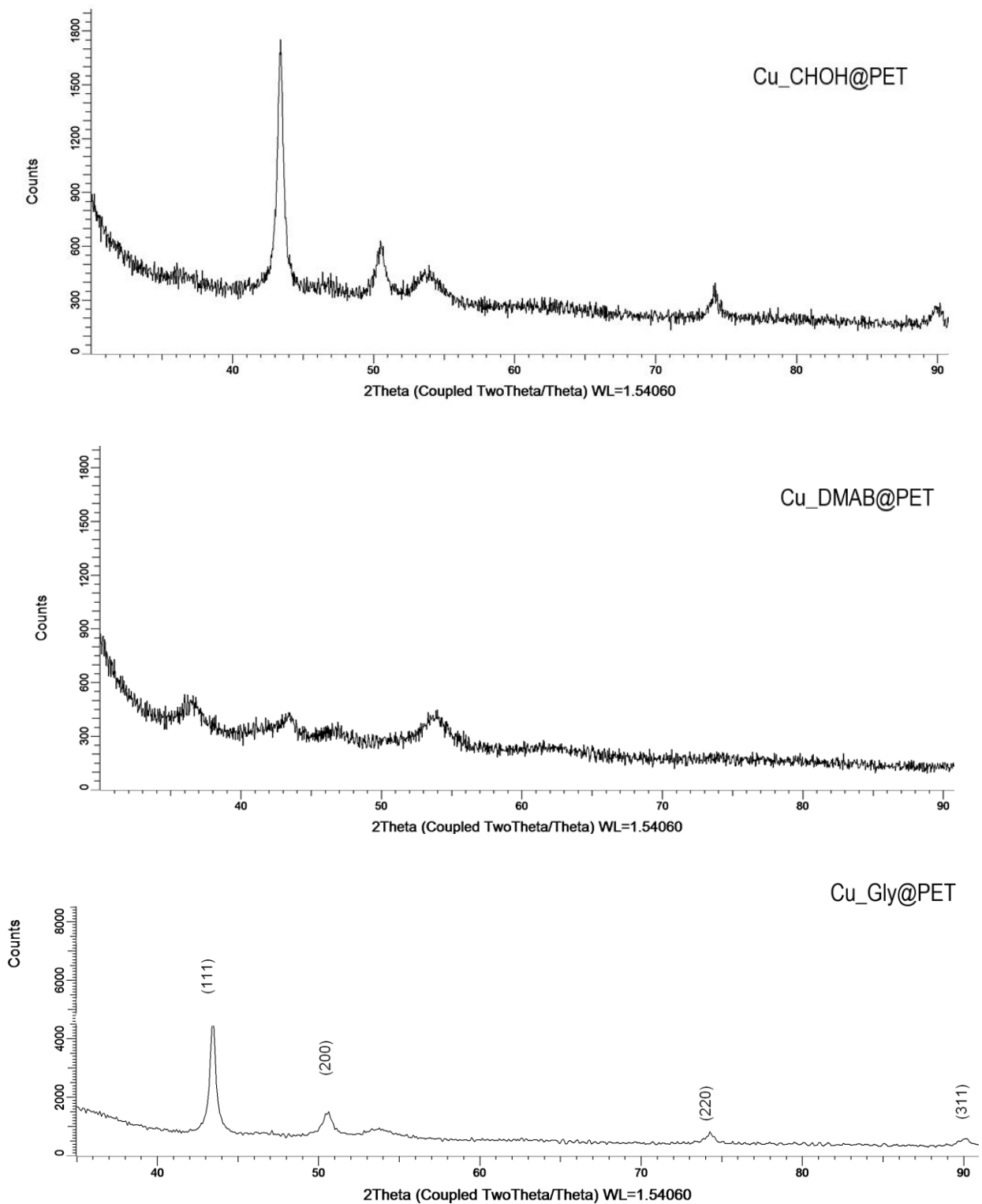


Figure 2. X-ray diffraction (XRD) patterns of composite membranes

Changes in the crystal structures of the composites according to XRD data

Composite	Phase/ phase content %	Symmetry group	(hkl)	2 θ	d, Å	Average L, nm	FWHM	Cell parameter, Å	Crystallinity degree, %
Cu_DMAB@PET	Cu ₂ O/ 37.4	Pn-3m(224)	211	53.64	1.707	65.6±16	1.775	4.205	67.0
			220	62.37	1.488		0.122		
			221	66.61	1.403		0.187		
	Cu/ 62.6	Fm-3m(225)	111	43.49	2.079	58.2±30	0.438	3.598	
			200	50.70	1.799		0.113		
			200	50.79	1.796		0.277		
			220	74.63	1.271		0.189		
			311	90.27	1.087		0.066		
Cu_Gly@PET	Cu/ 100	Fm-3m(225)	111	43.60	2.075	24.7±7	0.349	3.603	61.7
			200	50.71	1.808		0.571		
			220	74.09	1.279		0.366		
Cu_CHOH@PET	Cu/ 100	Fm-3m(225)	111	43.48	2.08	19.4±4	0.404	3.604	72.8
			200	50.41	1.81		0.655		
			220	74.24	1.28		0.513		
			311	89.94	1.09		0.715		

The catalytic activity of composite TeMs was investigated by converting toxic Cr(VI) to Cr(III) in the presence of formic acid as a reducing agent at 38 °C. K₂Cr₂O₇ was selected as a chromium source. The Cr(VI) reduction process was monitored using UV-visible spectroscopy. Figure 3(a-c) illustrates the optical density spectra of solutions containing Cr(VI) after the addition of catalysts. First of all, it should be noted that the reduction of Cr(VI) in the presence of formic acid and without the addition of a composite catalyst does not lead to an effective spectral change in the absorption of Cr(VI) (Fig. 3d). The intensity of the characteristic absorption peak at 352 nm for Cr₂O₇²⁻, which is caused by the charge transfer transition of ligand (oxygen) to the metal (Cr(VI)), decreases over time confirming the rapid reduction of Cr(VI). Thus, the reduction efficiency of Cr(VI) after 10 minutes of reaction was about 98 % for composites of the Cu_Gly@PET and Cu_CHOH@PET compositions. This indicator was only about 37 % after 10 minutes for Cu_DMAB@PET composite TeM samples. Visually, there is a change in the solution's color from yellow to colorless within 10 minutes, which indicates an effective conversion of Cr(VI) (yellow) to Cr(III) (colorless). The presence of Cr(III) ions as a reaction product is confirmed by the addition of an excess of sodium hydroxide solution, and the appearance of a green color characteristic of hexahydroxochromate (III) (Figure 3e) [46].

It is believed that the adsorption of both chromate and hydrogen donor (formic acid) on the surface of nanoscale catalysts leads to the redox decomposition of formic acid into carbon dioxide and hydrogen, which leads to the reduction of Cr(VI) to Cr(III) by proton transfer (Figure 3f).

Initially, the effect of the pH of the initial solution on the effectiveness of the studied catalysts in the decomposition reaction of Cr(VI) chromium ions (Figure 4) was studied. The studies were carried out for a series of Cu_Gly@PET samples. From the presented graphical data, it is obvious that the efficiency of the reduction of chromium ions Cr(VI) significantly decreases with an increase in pH from 2.0 to 7.0. The results showed that the low pH was favorable for the adsorption and decomposition of formate and dichromate reagents. For one part, the addition of dilute hydrochloric acid provides the required level of acidity of the reaction mixture and promotes the transfer of hydrogen atoms. For the other part, a low pH is most favorable for formate and dichromate reagents, which both have a negative charge and are adsorbed on a composite catalyst. In addition, it should be noted that at all studied pH levels, Cu_Gly@PET porous composite catalysts retain good catalytic reduction activity and physical and chemical stability. It was previously shown that due to the prolonging effect of catalytic agents and the strong binding force existing between ions, the surface acidity of catalysts increased at low pH values and, as a result, an increase in catalytic properties was observed [7]. Considering the obtained results, all further studies and tests were carried out in solutions with a pH value of 2.0.

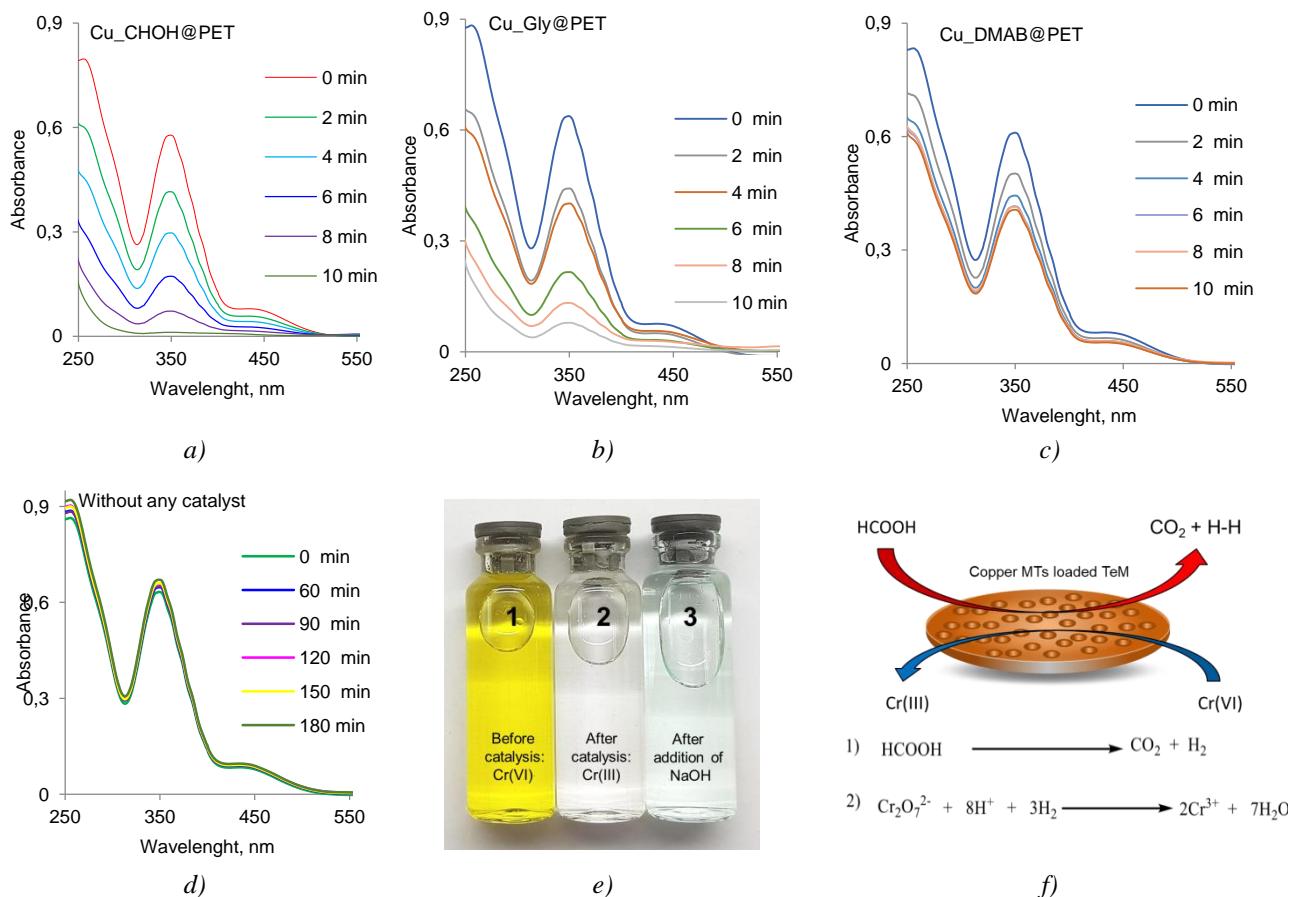


Figure 3. UV-vis absorption spectra of Cr(VI) ion reduction reaction in the presence of various types of composites as a function of time (a–c) without any catalyst and (d) and the image of the initial feed solution of Cr(VI) ions before and after catalysis and after the addition of excess NaOH (e) and the proposed mechanism of Cr(VI) reduction up to Cr(III) in the presence of Cu@PET composite catalyst (f)

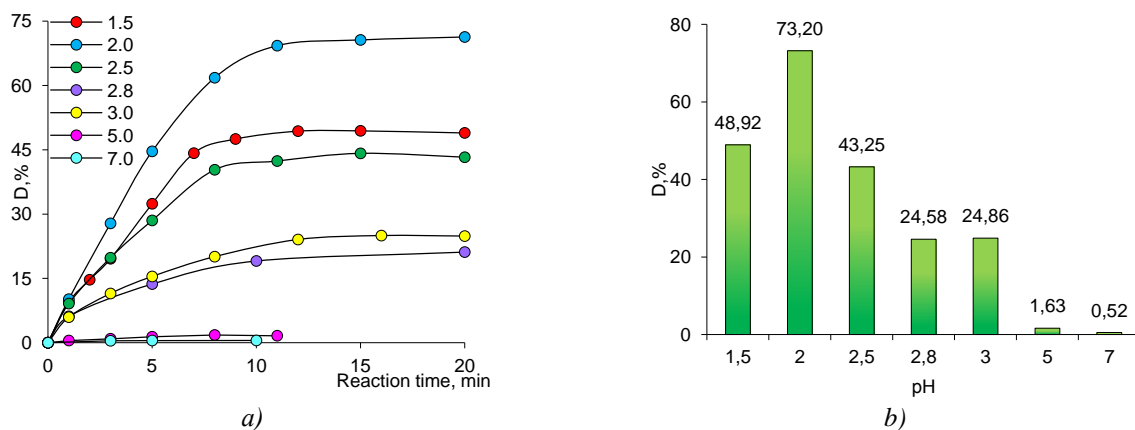


Figure 4. Variations in Cr(VI) ions degradation degree (D , %) as a function of pH for Cu_Gly@PET ZnO@PET composite membrane (a) and corresponding values of D parameter (b)

Figure 5a indicates the graphical dependences of the change in the D value as a function of the reaction time for all three types of catalysts under study. It can be seen that composites obtained using DMAB as a reducing agent have the least activity in the decomposition reaction of Cr(VI) ions, which is most likely due to the presence of the copper(I) oxide phase in the composite [27]. The Cr(VI) chromium ion decomposition reaction proceeds according to the Langmuir-Hinshelwood mechanism and has a pseudo-first order [35], which makes it possible to calculate the rate constant by changing the concentration of the key component (Fig. 5b). The calculated value of the reaction rate constant k_a for composites of the Cu_DMAB@PET com-

position (0.017 min^{-1}) is more than 9 times less than that of composites obtained using glyoxylic acid (0.156 min^{-1}) and more than 15 times less than the k_a value of Cu_CHO@PET samples (0.249 min^{-1}).

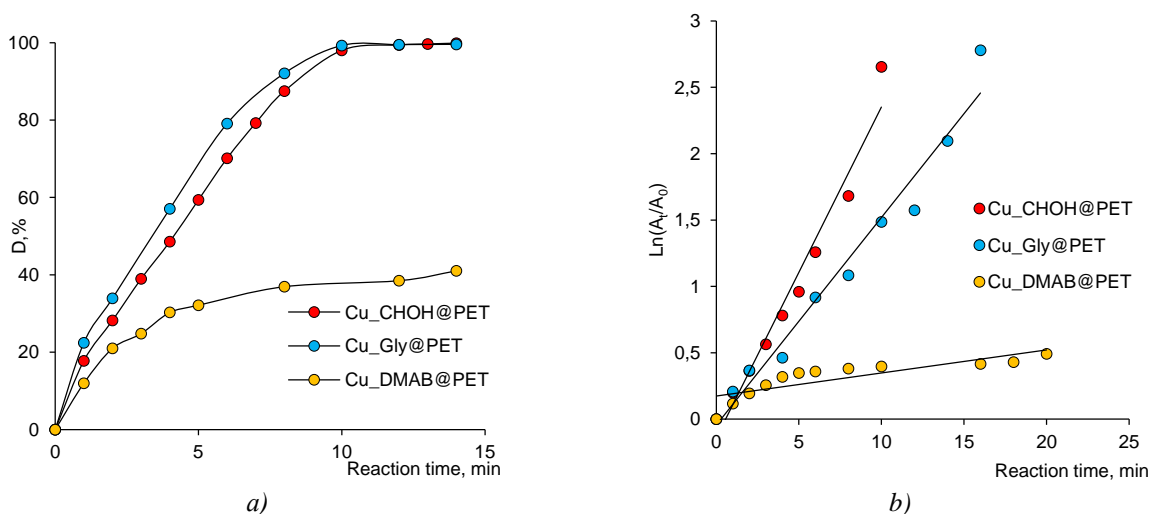


Figure 5. The variation in the degree of Cr(VI) degradation ($D, \%$) as a function of irradiation time in the presence of different composite catalysts (a), and Langmuir-Hinshelwood plots for photodegradation of Cr(VI) catalyzed by different composites (b)

The effect of temperature on the efficiency of composites in the Cr(VI) ion removal reaction was studied in the temperature range of 20–38 °C, which also allowed us to evaluate a number of such thermodynamic characteristics of catalysts as activation energy, enthalpy and entropy of activation according to the methods described in paper [27]. Figure 6 demonstrates the change in the efficiency of Cr(VI) decomposition at different temperatures. It can be noticed that catalysts based on Cu_CHO@PET effectively remove chromium ions Cr(VI) even at low temperatures, which is paramount for the further use of catalysts in technological processes.

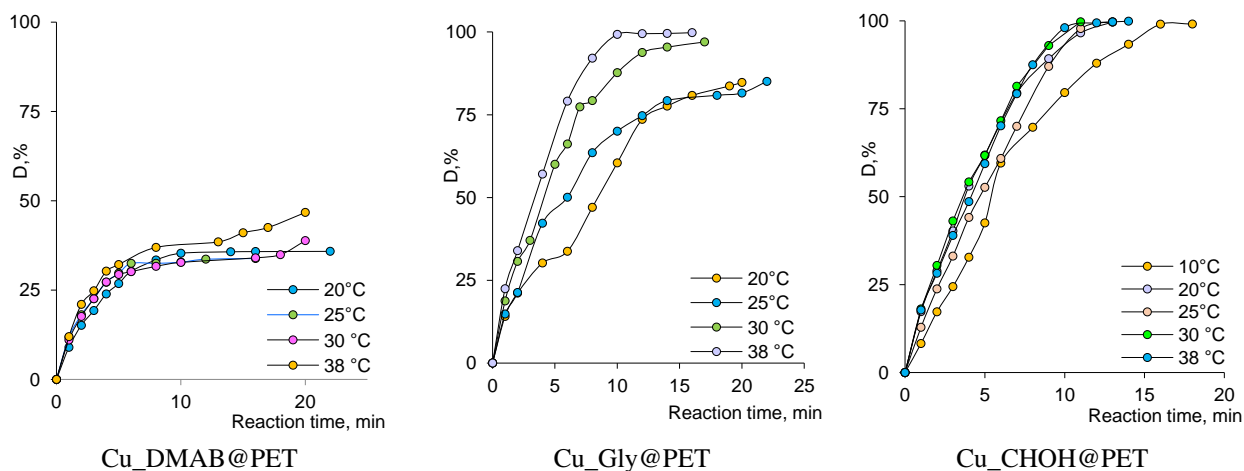


Figure 6. Variation of Cr(VI) degradation degree with irradiation time at different temperatures in the presence of composite membranes

Also, it is indicated that for all catalyst systems, there is a general tendency to increase the amount of degradation with an increase in temperature, and after a certain period, the degradation reaches almost equilibrium at all temperatures. The highest activity in the degradation of Cr(VI) over the entire temperature range was demonstrated by the Cu_CHO@PET catalysts, which catalyzed the degradation of almost all the contaminants in the medium after 15 minutes at 10 °C. Since Cu_CHO@PET catalysts demonstrate undeniable catalytic activity even at low temperatures (e.g. 10 °C); the developed membrane catalysts seem suitable to be used for wastewater treatment without preheating, especially considering their ease of use.

Table 2

**Thermodynamic parameters of the Cr(VI) decomposition reaction
in the presence of the copper loaded composite catalysts**

Composite catalyst	E_A , kJ/mol	ΔH , kJ/mol	ΔS , J/(mol×K)
Cu_CHOH@PET	10.8	13.21	-163.1
Cu_Gly@PET	35.96	38.47	-83.65
Cu_DMAB@PET	37.00	97.19	-58.05

Given the positive ΔH^\ddagger and negative ΔS^\ddagger values in Table 2, it appears that endothermic interactions and a decrease in entropy occur at the solid-liquid interface during the degradation process of Cr(VI) ions on the surface of the studied composite TeMs.

Table 3 presents the data on the efficiency of Cr(VI) ions degradation in the presence of different types of nanocatalysts. Note that the direct comparison of the D values, as well as corresponding k_a , is hardly possible, because such parameters as irradiation conditions (lamp capacity and type), amount of the loaded catalyst, and pollutant concentration in tests exert a considerable effect on degradation efficiency value. Nevertheless, it can be noted that our results compete closely with the existing alternatives and that the obtained composite membranes prepared with formaldehyde and glyoxylic acid are promising objects, considering particularly their practicality and high surface areas.

Table 3

Catalytic activity of nanocatalysts in the reaction of the Cr(VI) ions reduction

Catalyst	Testing conditions				D , %	k_a , min ⁻¹	E_A , kJ/mol	Ref.
	Cr(VI) concentration, ppm	Amount of catalysts, mg	Pollutant volume, ml	Lamp type				
Biogenic Pd NPs	250	0.043	0.1	Visible	95.5	0.0971	–	[47]
TiO ₂ nanotubes	100	–	100.0	Sunlight	37.0	0.0249	–	[8]
Pd NPs/Fe ₃ O ₄ @nanocellulose	354	10.0	25.0	Sunlight	98.6	–	–	[33]
Cu _{1-x} Fe _x S ($x = 9\%$) NPs	100	2.4	40.0	UV-light	100	0.093	43.0	[48]
Cu_CHOH@PET	58.8	2.68	25.0	Sunlight	99.88	0.249	10.8	This work
Cu_Gly@PET		0.7			99.56	0.156	35.96	
Cu_DMAB@PET		2.0			41.04	0.017	37.00	

Conclusions

This paper demonstrates the possibility of obtaining composite catalysts based on track-etched membranes and tubular microstructures of copper using various reducing agents of copper deposition solutions (formaldehyde, glyoxylic acid, dimethylamine borane). Through X-ray diffraction, we revealed that the copper(I) oxide phase was formed in the composition of synthesized copper microtubules when using DMAB as a reducing agent, while in other cases single component copper microstructures were formed. All synthesized samples effectively removed chromium ions Cr(VI) in a wide range of pH values and at various temperatures including low ones. When studying the kinetic parameters of the reaction, it was found that the reaction rate constant k_a of Cu_DMAB@PET composites (0.017 min⁻¹) was more than 9 times less than that of composites obtained using glyoxylic acid (0.156 min⁻¹) and more than 15 times less than the k_a value of Cu_CHOH@PET samples (0.249 min⁻¹).

Analysis of the calculated activation energy values showed that the most effective catalyst could be considered composite TeMs samples obtained using formaldehyde as a reducing agent.

Acknowledgments

This research was funded by the Ministry of Education and Science of the Republic of Kazakhstan under the project “Development of Functionalized Composite Track-Etched Membranes for Environmental Applications” (grant No. AP08855527).

The authors thank Dr. A. Kozlovskiy for his kind support and assistance in XRD analysis.

References

- 1 Karimi-Maleh, H., Ayati, A., Ghanbari, S., Orooji, Y., Tanhaei, B., Karimi, F., Alizadeh, M., Rouhi, J., Fu, L., & Sillanpää, M. (2021). Recent Advances in Removal Techniques of Cr(VI) Toxic Ion from Aqueous Solution: A Comprehensive Review. *Journal of Molecular Liquids*, 329, 115062. <https://doi.org/10.1016/j.molliq.2020.115062>
- 2 Saha, B., & Orvig, C. (2010). Biosorbents for Hexavalent Chromium Elimination from Industrial and Municipal Effluents. *Coordination Chemistry Reviews*, 254, 2959–2972. <https://doi.org/10.1016/j.ccr.2010.06.005>
- 3 Tumolo, M., Ancona, V., De Paola, D., Losacco, D., Campanale, C., Massarelli, C., & Uricchio, V.F. (2020). Chromium Pollution in European Water, Sources, Health Risk, and Remediation Strategies: An Overview. *International Journal of Environmental Research and Public Health*, 17, 5438. <https://doi.org/10.3390/ijerph17155438>
- 4 Islam, M.A., Angove, M.J., & Morton, D.W. (2019). Recent Innovative Research on Chromium (VI) Adsorption Mechanism. *Environmental Nanotechnology, Monitoring & Management*, 12, 100267. <https://doi.org/10.1016/j.enmm.2019.100267>
- 5 Kimbrough, D.E., Cohen, Y., Winer, A.M., Creelman, L., & Mabuni, C. (1999). A Critical Assessment of Chromium in the Environment. *Critical Reviews in Environmental Science and Technology*, 29, 1–46. <https://doi.org/10.1080/10643389991259164>
- 6 Zhitkovich, A. (2011). Chromium in Drinking Water: Sources, Metabolism, & Cancer Risks. *Chemical Research in Toxicology*, 24, 1617–1629. <https://doi.org/10.1021/tx200251t>
- 7 Li, S., Tang, L., Zeng, G., Wang, J., Deng, Y., Wang, J., Xie, Z., & Zhou, Y. (2016). Catalytic Reduction of Hexavalent Chromium by a Novel Nitrogen-Functionalized Magnetic Ordered Mesoporous Carbon Doped with Pd Nanoparticles. *Environmental Science and Pollution Research, Environmental Science and Pollution Research*, 23, 22027–22036. <https://doi.org/10.1007/s11356-016-7439-x>
- 8 Rosli, S.A., Alias, N., Bashrom, N., Ismail, S., Tan, W.K., Kawamura, G., Matsuda, A., & Lockman, Z. (2021). Hexavalent Chromium Removal via Photoreduction by Sunlight on Titanium–Dioxide Nanotubes Formed by Anodization with a Fluorinated Glycerol–Water Electrolyte. *Catalysts*, 11, 1–19. <https://doi.org/10.3390/catal11030376>
- 9 Peng, H., Leng, Y., Cheng, Q., Shang, Q., Shu, J., & Guo, J. (2019). Efficient Removal of Hexavalent Chromium from Wastewater with Electro-Reduction. *Processes*, 7, 1–12. <https://doi.org/10.3390/pr7010041>
- 10 Byrne, C., Subramanian, G., & Pillai, S.C. (2018). Recent Advances in Photocatalysis for Environmental Applications. *Journal of Environmental Chemical Engineering*, 6, 3531–3555. <https://doi.org/10.1016/j.jece.2017.07.080>
- 11 Sarkar, S., Ponce, N.T., Banerjee, A., Bandopadhyay, R., Rajendran, S., & Lichtfouse, E. (2020). Green Polymeric Nanomaterials for the Photocatalytic Degradation of Dyes: A Review. *Environmental Chemistry Letters*, 18, 1569–1580. <https://doi.org/10.1007/s10311-020-01021-w>
- 12 Bashir, M.S., Ramzan, N., Najam, T., Abbas, G., Gu, X., Arif, M., Qasim, M., Bashir, H., Shah, S.S.A., & Sillanpää, M. (2022). Metallic Nanoparticles for Catalytic Reduction of Toxic Hexavalent Chromium from Aqueous Medium: A State-of-the-Art Review. *Science of The Total Environment*, 829, 154475. <https://doi.org/10.1016/j.scitotenv.2022.154475>
- 13 Hussain, M.B., Khan, M.S., Loussala, H.M., & Bashir, M.S. (2020). The Synthesis of a BiOCl_x Br_{1-x} Nanostructure Photocatalyst with High Surface Area for the Enhanced Visible-Light Photocatalytic Reduction of Cr(VI). *RSC Advances*, 10, 4763–4771. <https://doi.org/10.1039/C9RA10256F>
- 14 Bashir, M.S., Jiang, X., Yang, X., & Kong, X.Z. (2021). Porous Polyurea Supported Pd Catalyst: Easy Preparation, Full Characterization, and High Activity and Reusability in Reduction of Hexavalent Chromium in Aqueous System. *Industrial & Engineering Chemistry Research*, 60, 8108–8119. <https://doi.org/10.1021/acs.iecr.1c01376>
- 15 Bashir, M.S. (2021). Benign Fabrication Process of Hierarchical Porous Polyurea Microspheres with Tunable Pores and Porosity: Their Pd Immobilization and Use for Hexavalent Chromium Reduction. *Chemical Engineering Research and Design*, 175, 102–114. <https://doi.org/10.1016/j.cherd.2021.08.037>
- 16 Korolkov, I. V., Borgekov, D.B., Mashentseva, A.A., Güven, O., Atlcl, A.B., Kozlovskiy, A.L., & Zdorovets, M.V. (2017). The Effect of Oxidation Pretreatment of Polymer Template on the Formation and Catalytic Activity of Au/PET Membrane Composites. *Chemical Papers*, 71, 2353–2358. <https://doi.org/10.1007/s11696-017-0229-1>
- 17 Mashentseva, A.A. (2019). Effect of the Oxidative Modification and Activation of Templates Based on Poly(Ethylene Terephthalate) Track-Etched Membranes on the Electroless Deposition of Copper and the Catalytic Properties of Composite Membranes. *Petroleum Chemistry*, 59, 1337–1344. <https://doi.org/10.1134/S0965544119120089>
- 18 Muench, F. (2021). Electroless Plating of Metal Nanomaterials. *ChemElectroChem*, 8, 2993–3012. <https://doi.org/10.1002/celec.202100285>
- 19 Mashentseva, A.A., Kozlovskiy, A.L., & Zdorovets, M.V. (2018). Influence of Deposition Temperature on the Structure and Catalytic Properties of the Copper Nanotubes Composite Membranes. *Materials Research Express*, 5, 065041. <https://doi.org/10.1088/2053-1591/aacb5f>
- 20 Muench, F., Kunz, U., Neetzel, C., Lauterbach, S., Kleebe, H.-J., & Ensinger, W. (2011). 4-(Dimethylamino)Pyridine as a Powerful Auxiliary Reagent in the Electroless Synthesis of Gold Nanotubes. *Langmuir*, 27, 430–5. <https://doi.org/10.1021/la104015a>
- 21 Hossain, U.H., Jantsen, G., Muench, F., Kunz, U., & Ensinger, W. (2022). Increasing the Structural and Compositional Diversity of Ion-Track Templated 1D Nanostructures through Multistep Etching, Plastic Deformation, and Deposition. *Nanotechnology*, 33, 245603. <https://doi.org/10.1088/1361-6528/ac59e5>
- 22 Muench, F., Fuchs, A., Mankel, E., Rauber, M., Lauterbach, S., Kleebe, H.-J., & Ensinger, W. (2013). Synthesis of Nanoparticle/Ligand Composite Thin Films by Sequential Ligand Self Assembly and Surface Complex Reduction. *Journal of colloid and interface science*, 389, 23–30. <https://doi.org/10.1016/j.jcis.2012.09.003>

- 23 Muench, F., Rauber, M., Stegmann, C., Lauterbach, S., Kunz, U., Kleebe, H.-J., & Ensinger, W. (2011). Ligand-Optimized Electroless Synthesis of Silver Nanotubes and Their Activity in the Reduction of 4-Nitrophenol. *Nanotechnology*, 22, 415602. <https://doi.org/10.1088/0957-4484/22/41/415602>
- 24 Yeszhanov, A.B., Mashentseva, A.A., Korolkov, I. V., Gorin, Y.G., Kozlovskiy, A.L., & Zdorovets, M.V. (2018). Copper Nanotube Composite Membrane as a Catalyst in Mannich Reaction. *Chemical Papers*, 72, 3189–3194. <https://doi.org/10.1007/s11696-018-0539-y>
- 25 Mashentseva, A.A., Shlimas, D.I., Kozlovskiy, A.L., Zdorovets, M. V, Russakova, A.V, Kassymzhanov, M., & Borisenko, A.N. (2019). Electron Beam Induced Enhancement of the Catalytic Properties of Ion-Track Membranes Supported Copper Nanotubes in the Reaction of the P-Nitrophenol Reduction. *Catalysts*, 9, 737. <https://doi.org/10.3390/catal9090737>
- 26 Altynbaeva, L.S., Mendibaeva, A.Z., Aimanova, N.A., Nurmakhan, A.E., Dzhakupova, Z.E., Tuleuov, B.I., & Mashentseva, A.A. (2021). Kinetic and Thermodynamic Characteristics of the Potassium Hexationoferrate (III) Decomposition Catalytic Reaction in the Presence of Composite Track-Etched Membranes. *NNC RK Bulletin*, 1, 15–24. <https://doi.org/10.52676/1729-7885-2021-1-15-24>
- 27 Altynbaeva, L.S., Barsbay, M., Aimanova, N.A., Jakupova, Z.Y., Nurpeisova, D.T., Zdorovets, M.V., & Mashentseva, A.A. (2022). A Novel Cu₂O/ZnO@PET Composite Membrane for the Photocatalytic Degradation of Carbendazim. *Nanomaterials*, 12, 1724. <https://doi.org/10.3390/nano12101724>
- 28 Russakova, A.V., Altynbaeva, L.S., Barsbay, M., Zheltov, D.A., Zdorovets, M.V., & Mashentseva, A.A. (2021). Kinetic and Isotherm Study of As(III) Removal from Aqueous Solution by PET Track-Etched Membranes Loaded with Copper Microtubes. *Membranes*, 11, 116. <https://doi.org/10.3390/membranes11020116>
- 29 Mashentseva, A.A., Barsbay, M., Zdorovets, M.V., Zheltov, D.A., & Güven, O. (2020). Cu/CuO Composite Track-Etched Membranes for Catalytic Decomposition of Nitrophenols and Removal of As(III). *Nanomaterials*, 10, 1552. <https://doi.org/10.3390/nano10081552>
- 30 Mashentseva, A.A., Kozlovskiy, A.L., Turapbay, K.O., Temir, A.M., Seytbaev, A.S., & Zdorovets, M.V. (2018). Determination of Optimal Conditions for Electroless Synthesis of Copper Nanotubes in the Polymer Matrix. *Russian Journal of General Chemistry*, 88, 1213–1218. <https://doi.org/10.1134/S1070363218060270>
- 31 Honma, H. (1994). Electroless Copper Deposition Process Using Glyoxylic Acid as a Reducing Agent. *Journal of The Electrochemical Society*, 141, 730. <https://doi.org/10.1149/1.2054800>
- 32 Mashentseva, A.A., & Zdorovets, M.V. (2019). Catalytic Activity of Composite Track-Etched Membranes Based on Copper Nanotubes in Flow and Static Modes. *Petroleum Chemistry*, 59, 552–557. <https://doi.org/10.1134/S0965544119050074>
- 33 Kalantari, E., Khalilzadeh, M.A., & Zareyee, D. (2021). Effective Reduction of Cr(VI) and Organic Dyes Using Pd NPs/Fe₃O₄@nanocellulose as a Recoverable Catalyst in Aqueous Media. *Journal of Inorganic and Organometallic Polymers and Materials*, 31, 319–330. <https://doi.org/10.1007/s10904-020-01784-3>
- 34 Ghosh, S. (2019). Electroless Copper Deposition: A Critical Review. *Thin Solid Films*, 669, 641–658. <https://doi.org/10.1016/j.tsf.2018.11.016>
- 35 Sharma, A., Cheon, C.-S., & Jung, J.P. (2016). Recent Progress in Electroless Plating of Copper. *Journal of the Microelectronics and Packaging Society*, 23, 1–6. <https://doi.org/10.6117/kmepps.2016.23.4.001>
- 36 Bercu, B., Enculescu, I., & Spohr, R. (2004). Copper Tubes Prepared by Electroless Deposition in Ion Track Templates. *Nuclear Instruments and Methods in Physics Research, Section B: Beam Interactions with Materials and Atoms*, 225, 497–502. <https://doi.org/10.1016/j.nimb.2004.06.011>
- 37 Liu, Q., Yasunami, T., Kuruda, K., & Okido, M. (2012). Preparation of Cu Nanoparticles with Ascorbic Acid by Aqueous Solution Reduction Method. *Transactions of Nonferrous Metals Society of China*, 22, 2198–2203. [https://doi.org/10.1016/S1003-6326\(11\)61449-0](https://doi.org/10.1016/S1003-6326(11)61449-0)
- 38 Valenzuela, K., Raghavan, S., Deymier, P.A., & Hoying, J. (2008). Formation of Copper Nanowires by Electroless Deposition Using Microtubules as Templates. *Journal of Nanoscience and Nanotechnology*, 8, 3416–3421. <https://doi.org/10.1166/jnn.2008.122>
- 39 Qin, W., & Guo, R. (2015). Metallization of Polyester Fabric by Autocatalytic Copper Plating Process Using Glyoxylic Acid as a Reducing Agent. *Fibers and Polymers*, 16, 1671–1675. <https://doi.org/10.1007/s12221-015-4943-4>
- 40 Shacham-Diamand, Y.Y. (1999). Electroless Copper Deposition Using Glyoxylic Acid as Reducing Agent for Ultralarge Scale Integration Metallization. *Electrochemical and Solid-State Letters*, 3, 279. <https://doi.org/10.1149/1.1391124>
- 41 Feng, H., Li, Y., Lin, S., Van der Eycken, E.V., & Song, G. (2014). Nano Cu-Catalyzed Efficient and Selective Reduction of Nitroarenes under Combined Microwave and Ultrasound Irradiation. *Sustainable Chemical Processes*, 2, 14/1-14/6, 6 pp. <https://doi.org/10.1186/2043-7129-2-14>
- 42 Li, J., & Kohl, P.A. (2003). The Deposition Characteristics of Accelerated Nonformaldehyde Electroless Copper Plating. *Journal of The Electrochemical Society*, 150, C558. <https://doi.org/10.1149/1.1591760>
- 43 Zhang, W., & Ding, D. (2016). Electroless Copper Plating on Liquid Crystal Polymer Films Using Dimethylamine Borane as Reducing Agent. *Journal of the Chinese Chemical Society*, 63, 222–228. <https://doi.org/10.1002/jccs.201500412>
- 44 Liao, Y., Zhang, S., & Dryfe, R. (2012). Electroless Copper Plating Using Dimethylamine Borane as Reductant. *Particuology*. *Chinese Society of Particuology*, 10, 487–491. <https://doi.org/10.1016/j.partic.2011.09.009>
- 45 Darken, J. (1991). Electroless Copper-an Alternative to Formaldehyde. *Transactions of the IMF*, 69, 66–69. <https://doi.org/10.1080/00202967.1991.11870895>

46 Huang, Y., Ma, H., Wang, S., Shen, M., Guo, R., Cao, X., Zhu, M., & Shi, X. (2012). Efficient Catalytic Reduction of Hexavalent Chromium Using Palladium Nanoparticle-Immobilized Electrospun Polymer Nanofibers. *ACS Applied Materials and Interfaces*, 4, 3054–3061. <https://doi.org/10.1021/am300417s>

47 Tripathi, R.M., & Chung, S.J. (2020). Reclamation of Hexavalent Chromium Using Catalytic Activity of Highly Recyclable Biogenic Pd(0) Nanoparticles. *Scientific Reports*, 10, 1–14. <https://doi.org/10.1038/s41598-020-57548-z>

48 Ain, N. ul, Rehman, Z. ur, Nayab, U., Nasir, J.A., & Aamir, A. (2020). Facile Photocatalytic Reduction of Carcinogenic Cr(VI) on Fe-Doped Copper Sulfide Nanostructures. *RSC Advances*, 10, 27377–27386. <https://doi.org/10.1039/D0RA04852F>

А.А. Машенцева, Н.А. Айманова, Н. Парманбек, Л.Ш. Алтынбаева, Д.Т. Нурпейсова

Хром(VI) иондарын каталитикалық жою үшін Cu@PET құрамды композитті тректі мембраналарын қолдану

Мақалада формальдегид (Cu_CHON@PET), диметиламинборан (Cu_DMAB@PET) және глиоксил қышқылы (Cu_Gly@PET) сияқты әртүрлі құрамды тұндыру ерітінділерін және әртүрлі түрдегі тотықсыздандырғыштарды пайдалана отырып, мыс микротүтікшелері негізінде композитті тректі мембраналарды алу ерекшеліктері қарастырылған. Композиттердің құрылымы мен құрамы порометрия, сканерлеуші электронды микроскопия және рентгендік фазалық талдау арқылы зерттелді. Тотықсыздандырғыш ретінде диметиламинборанды пайдаланған жағдайда алынған композиттер мыстан (0) (62,6 %) және мыс (I) оксидінен (37,4 %) тұратындығы, басқа жағдайларда монокомпонентті мыс микротүтікшелері алынғаны көрсетілген. Каталитикалық белсенділік хром (VI) иондарының тотықсыздану реакциясының мысалында зерттелді. Монокомпонентті композиттерді қолданған жағдайда хром иондарын жою тиімділігі 95–99 %-ға дейін жетеді, ал Cu_DMAB@PET композиттерінің құрамында оксидтік фазаның болуы катализаторлардың белсенділігін айтарлықтай төмендетеді және ұқсас жағдайларда реакция жүйесінен ластаушы заттардың 41%-ы ғана жойылады. Cr(VI) тотықсыздану реакциясының псевдо-бірінші ретті болатыны және Ленгмюр-Хиншельвуд механизмі бойынша жүретіні көрсетілген. Cu_DMAB@PET үлгілері үшін реакция жылдамдығы константасының есептелген мәні (0,017 мин⁻¹) Cu_Gly@PET үлгілерінен (0,156 мин⁻¹) 9 есе аз және Cu_CHON@PET композиттерінің k_a мәнінен (0,249 мин⁻¹) 15 есе аз. Зерттелетін композиттердің каталитикалық қасиеттеріне температураның әсері 10–38 °C температура аралығында зерттелді; активтену энергиясы, активтену энтальпиясы және энтропиясы сияқты термодинамикалық сипаттамалар есептелді. Ең төменгі активтену энергиясы Cu_CHON@PET үлгілері үшін алынғаны анықталды.

Кілт сөздер: композитті тректі мембраналар, катализаторлар, мыс микротүтікшелері, хромды жою, темплаттық синтез, химиялық тұндыру.

А.А. Машенцева, Н.А. Айманова, Н. Парманбек, Л.Ш. Алтынбаева, Д.Т. Нурпейсова

Применение композитных трековых мембран состава Cu@PET для каталитического удаления ионов хрома (VI)

В статье изучены особенности получения композитных трековых мембран на основе микротрубок меди с использованием различных составов раствора осаждения и различных типов восстановителей, таких как формальдегид (Cu_CHON@PET), диметиламинборан (Cu_DMAB@PET), глиоксиловая кислота (Cu_Gly@PET). Структура и состав композитов исследованы методами порометрии, растровой электронной микроскопии и рентгенофазового анализа. Показано, что в случае использования диметиламинборана в качестве восстановителя полученные композиты состоят из оксида меди (I) (37,4 %) и меди (0) (62,6 %), в остальных случаях были получены монокомпонентные медные микротрубки. Каталитическую активность исследовали на примере реакции восстановления ионов хрома (VI). Показано, что в случае применения монокомпонентных композитов эффективность удаления ионов хрома достигает 95–99 %, в то время как наличие оксидной фазы в составе Cu_DMAB@PET композитов значительно снижает активность катализаторов и при аналогичных условиях из реакционной системы удаляется лишь 41 % загрязнителя. Показано, что реакция восстановления Cr (VI) имеет псевдопервый порядок и протекает по механизму Ленгмюра-Хиншельвуда. Рассчитанное значение константы скорости реакции для образцов Cu_DMAB@PET (0,017 мин⁻¹) более чем в 9 раз меньше аналогичного показателя для образцов Cu_Gly@PET (0,156 мин⁻¹) и более чем в 15 раз меньше, чем величина k_a композитов состава Cu_CHON@PET (0,249 мин⁻¹). Влияние температуры на каталитические свойства исследуемых композитов изучали в интервале температур 10–38 °C; были рассчитаны такие термодинамические характеристики, как энергия активации, энтальпия и энтропия активации. Установлено, что минимальное значение энергии активации было получено для образцов Cu_CHON@PET.

Ключевые слова: композитные трековые мембраны, катализаторы, микротрубки меди, удаление хрома, темплатный синтез, химическое осаждение.

Information about authors*

Mashentseva, Anastassiya Alexandrovna (*corresponding author*) — Associate Professor, PhD, Head of the Technological Track-Etched Membranes Laboratory, Institute of Nuclear Physics of the Republic of Kazakhstan, Ibragimov street, 1, 050032 Almaty, Kazakhstan; e-mail: a.mashentseva@inp.kz; <http://orcid.org/0000-0003-4393-5845>;

Aimanova, Nurgulim Almasyzy — Ms. of Sci., Engineer of the Technological Track-Etched Membranes Laboratory, Institute of Nuclear Physics of the Republic of Kazakhstan, Ibragimov street, 1, 050032 Almaty, Kazakhstan; e-mail: nurgulim.a.a@gmail.com; <https://orcid.org/0000-0002-9150-5877>;

Parmanbek, Nursanat — Ms. of Sci., Engineer of the Technological Track-Etched Membranes Laboratory, Institute of Nuclear Physics of the Republic of Kazakhstan, Ibragimov street, 1, 050032 Almaty, Kazakhstan; e-mail: nursanat0509@mail.ru; <https://orcid.org/0000-0002-9860-1087>;

Altynbayeva, Lilya Sharifullova — 3-rd year PhD-student of the L.N. Gumilyov Eurasian National University, specialty “Chemistry”, Satpayev street, 2, 010008 Nur-Sultan, Kazakhstan; e-mail: lilija310378@gmail.com; <https://orcid.org/0000-0002-0474-3878>;

Nurpeisova, Dinara Temirbayevna — PhD, Senior Lecturer of the “Chemistry department”, the L.N. Gumilyov Eurasian National University, specialty “Chemistry”, Satpayev street, 2, 010008 Nur-Sultan, Kazakhstan; e-mail: nurpeisova_dt_1@enu.kz; <https://orcid.org/0000-0001-8789-1798>

*The author’s name is presented in the order: *Last Name, First and Middle Names*

V.A. Zhinzhilo¹, A.Yu. Litvinova¹, V.M. Lyamina¹, G.I. Dzhardimalieva^{2,3*}, I.E. Uflyand¹

¹*Southern Federal University, Rostov-on-Don, Russian Federation;*

²*Institute of Problems of Chemical Physics RAS, Chernogolovka, Russian Federation;*

³*Moscow Aviation Institute (National Research University), Moscow, Russian Federation*

(*Corresponding author's e-mail: dzhardim@icp.ac.ru)

Coordinating Polymers Based on Nickel(II) and Cobalt(II) Trimesinates as Promising Adsorbents of Organic Dyes

Metal-organic frameworks (MOFs) are crystalline compounds consisting of metal ions coordinated by bridging organic ligands. Depending on the coordination geometry of the metal and the direction of the bond of donor atoms, as well as on the geometry of the bridging ligand, 1D, 2D, or 3D polymer structures are formed. The characteristic features of metal-organic frameworks are low density, high porosity and crystallinity, and large specific surface. Wide attention is paid to the technological aspects of creating such materials and their integration into various devices. To obtain MOFs, various synthetic approaches have been developed based on precipitation reactions at room temperature and under convective heating, including hydrothermal and solvothermal syntheses. In this work, metal organic framework structures based on nickel and cobalt trimesinates were synthesized by a modified procedure by reacting nickel acetate and cobalt nitrate with trimesic acid in the presence of alkali. The obtained compounds were used to study the adsorption of Congo Red and Methylene blue organic dyes from their aqueous solutions. The degree of adsorption depends on temperature and reaches a value of 97% for Congo Red, while for Methylene blue it is 83%. The mechanisms and characteristic parameters of the adsorption process were analyzed using empirical models of Langmuir, Temkin, and Freundlich isotherms, of which the adsorption process was optimally described by the Freundlich model. The calculated thermodynamic parameters indicate the spontaneity of the process and its insignificant endothermic character.

Keywords: metal organic framework structures, coordination polymers, trimesic acid, pollutants, adsorption, Congo Red, methylene blue, thermodynamic parameters, adsorption isotherms, adsorption capacity.

Introduction

Metal-organic framework structures (MOFs) play an important role in science and technology since they are widely used in catalysis [1], separation and selective purification of substances [2], are necessary for the creation of nonlinear optical materials [3], and the synthesis of new compounds capable of a magnetic phase transition at high temperatures [4]. Due to the wide variety of organic and inorganic building blocks that make up MOFs, there are a huge number of opportunities for designing such materials with defined structures and desired properties [5]. In recent years, there has been a noticeable interest in MOFs based on benzenepolycarboxylic acids. Such MOFs are characterized by a regular structure and constant porosity after thermal/vacuum activation, which allows them to encapsulate various guest molecules in a bulk structure and makes them promising solid materials for a number of applications such as gas storage and separation of substances in solutions. In addition, they attract the attention of researchers because of their different modes of coordination with respect to metal ions, in particular, exhibiting monodentate, bridging, chelating modes, etc. For example, C_{3v}-symmetrical trimesic (1,3,5-benzenetricarboxylic) acid has been used to create MOF systems with interesting application possibilities. The first representative of this series of MOFs was synthesized in 1999 [6] and designated as HKUST-1 (HKUST – Hong Kong University of Science and Technology). A distinctive feature of Cu(II)-containing MOFs is the presence of binuclear fragments of the “Chinese lantern” type. This structure serves as a benchmark both in terms of stability and the ability to absorb various sorbates. Importantly, HKUST-1 stands out as a representative example, forming an isostructural series with other transition metal ions, including Zn [7], Mo [8], Cr [9, 10], Fe [11], Ni [12], Ru [13, 14], Co [15]. These MOFs have two important features: (1) the metal Lewis acid sites available for coordination by donor substrates are located within the pore walls; (2) materials can be activated (including removal of axially coordinated molecules) without destroying the underlying scaffold. An important role in their properties is played by a variety of supramolecular structures and such structural details as pores, channels, and voids of nanome-

ter dimensions. The latter circumstance makes it possible to use such polybenzene carboxylates as selective adsorbents, catalysts, electrodes for supercapacitors, etc. [16–21]. MOFs are of considerable interest for the extraction of technogenic pollutants, in particular, organic dyes from wastewater and the return of the latter to nature without damaging it [22]. It is important that many coordination polymers, in turn, are biologically and environmentally safe compounds. All metals and linkers can be used even for biomedical applications, but at different doses depending on several parameters, such as degradation kinetics, biodistribution, accumulation in tissues and organs, etc.

The synthesis of MOFs is usually carried out by the solvo- or hydrothermal method [23]. At present, the strategies for the synthesis of MOFs are well-developed, and, particularly, they are described in the literature for nickel and cobalt trimesinates [24, 25]. However, such methods are often laborious and require special equipment and a long time; at the same time, as shown in [26], they can be successfully replaced by more accessible synthetic methods carried out by the “RT” method.

The aim of this work is to develop procedures for the synthesis of nickel(II) and cobalt(II) complexes based on trimesic acid in aqueous solutions without the use of modulating agents. In addition, the investigation task is to study the ability of the resulting nickel and cobalt trimesinates to adsorb organic dyes from their aqueous solutions.

Experimental

Materials

Commercially available reagents were used in the work, namely trimesic acid (98 %, Acros Organics, cat. no. 105350500), NaOH (technical, AO Kaustik), $\text{Ni}(\text{CH}_3\text{COO})_2 \cdot 4\text{H}_2\text{O}$ (99 %+, Acros Organics, cat. no. 223141000), $\text{Co}(\text{NO}_3)_2 \cdot 6\text{H}_2\text{O}$ (99 %, Acros Organics, cat. no. 213091000). Ethanol, methanol, ethyl acetate, chloroform, and diethyl ether were used as solvents (all of the above reagents were produced by JSC Reakhim, chemically pure). All reagents were not subjected to additional preparation and purification. The solvents were dried by standard procedures. The sorbates were cationic Methylene blue and anionic Congo Red (Sigma-Aldrich, cat. nos. 556416 and B24310.14).

The synthesis of nickel and cobalt trimesinates consisted of two stages. In the first stage, a soluble form of trimesic acid was obtained in the form of a sodium salt. To an aqueous solution containing 0.09 mol of sodium hydroxide (in 50 mL of water), 0.03 mol of acid was added while heating to 80 °C, the process was controlled by the pH value of the solution, carrying it out in the range of 5.5–6.0. In the second stage, an aqueous solution containing 0.09 mol of $\text{Ni}(\text{CH}_3\text{COO})_2 \cdot 4\text{H}_2\text{O}$ or $\text{Co}(\text{NO}_3)_2 \cdot 6\text{H}_2\text{O}$ (calculated as anhydrous salt) in 30 mL of hot water was introduced into the resulting sodium (I) trimesinate solution. The resulting mixture was stirred for 6 h, maintaining the temperature at 80 °C, and left for crystallization for 12 h at room temperature. Cobalt(II) trimesinate precipitates almost immediately as a pink fine crystalline precipitate (hydrated form), while nickel(II) trimesinate precipitates within a few hours as a light green crystalline precipitate (hydrated form). The precipitated crystals were separated by filtration on a glass filter, washed with hot water and then with alcohol, and dried in air to an air-dry state. The dried product was treated sequentially in absolute ethanol, dry ethyl acetate, and chloroform, keeping in each solvent with constant stirring on a magnetic stirrer for 12 h. In the final stage, the compound was dried in air and kept for 36 h in a dynamic vacuum at a temperature of 150 °C (nickel(II) trimesinate) and 180 °C (cobalt(II) trimesinate). As a result, anhydrous salts were obtained with a yield of 73% (nickel(II) trimesinate), which is a yellow-green loose powder, and 88 % (cobalt(II) trimesinate) in the form of loose violet crystals. The weight loss on drying was 25.92 % for nickel(II) trimesinate (theoretical calculation for a loss of 12 water molecules, 26.6 %), for cobalt(II) trimesinate, 26.1 % (theoretical calculation for the loss of 12 water molecules is 26.57 %), which is in good agreement with the literature data. The resulting compounds were characterized by elemental analysis, the results are presented in Table 1.

Elemental analysis was performed on a Vario Micro cube analyzer (Elementar GmbH, Langenselbold). Ni and Co were determined on an AAS-3 atomic absorption spectrometer (Zeiss, Jena). X-ray phase analysis was performed on a Phywe XR 4.0 instrument ($\text{CuK}\alpha$, $\lambda = 0.15418$ nm, scanning speed 2 deg/min, step size 0.02°). Fourier transform infrared spectra were obtained on a Perkin-Elmer Spectrum 100 FTIR spectrometer using KBr pellets and Softspectra data analysis software (Shelton, CT). Scanning electron microscopy was performed on a ZEISS Crossbeam 340 instrument with an accelerating voltage of 3 kV. Secondary electrons were detected using an Everhart-Thornley detector (SE2) with a change in magnification from 1.92 to

50000 times. The dye concentration was determined using a UV-visible spectrophotometer (Varian, Cary 50) at $\lambda_{\max} = 492$ nm (Congo Red) and 664 nm (Methylene blue), respectively [28].

Table 1

Elemental Analysis of Synthesized nickel(II) and cobalt(II) trimesinates

Hydrated form				
Element	Found, %	Calculated for $C_{18}H_6O_{12}Ni_3 \cdot 12H_2O$, %	Found, %	Calculated for $C_{18}H_6O_{12}Co_3 \cdot 12H_2O$, %
C	25.93	26.58	26.93	26.56
H	3.44	3.70	3.58	3.69
Ni	22.12	21.67	–	–
Co	–	–	22.4	21.74
Anhydrous form				
Element	Found, %	Calculated for $C_{18}H_6O_{12}Ni_3$, %	Found, %	Calculated for $C_{18}H_6O_{12}Co_3$, %
C	35.3	36.2	36.8	36.17
H	1.1	1.00	0.99	1.00
Ni	30.0	29.5	–	–
Co	–	–	30.2	29.6

For adsorption studies, the dye solution with a volume of 200 mL and an initial concentration of $C_0 = 20$ mg/L was placed in a beaker with a capacity of 300 mL, thermostated at 283, 293, and 308 K on a magnetic stirrer, adjusting the rotation speed so that mixing was effective, but air in the liquid phase was not drawn in. When the desired temperature was reached, an adsorbent was introduced, which was the synthesized MOF. To determine the maximum adsorption capacity, a series of experiments was carried out, in which adsorbents were introduced into the dye solution under the same conditions, equal to 6.25, 12.5, 25, 50, 100 mg, and stirring was continued for 3 h, considering that this time was sufficient until equilibrium was reached in system. After the specified time, the mixture was centrifuged, and the residual concentration of the dye was determined in the supernatant.

The adsorption capacity of the MOF in aqueous solutions of Methylene blue and Congo Red at 283, 293, and 308 K was determined by suspending 0.1 g of MOF in 200 mL of the initial dye solution ($C_0 = 20$ mg/L) and the mixture was stirred. At predetermined time intervals, 10 mL of the mixture was taken, quickly centrifuged, and the residual concentration of the dye in the solution was determined. The obtained results were compared with the calibration curve and the equivalent concentration of the dye in a given time period was determined.

To obtain adsorption isotherms, 20 mL of a dye solution of various concentrations (10–200 mg/L) was added to a sample of the adsorbent (10 mg) and stirred for 3 hours. This time was considered sufficient to achieve equilibrium. Then a portion of the solution was taken and the concentration of the dye was determined.

The adsorption value was calculated using the following equations:

$$q_t = \frac{(C_0 - C_t)V}{m}; \quad (1)$$

$$q_e = \frac{(C_0 - C_e)V}{m}, \quad (2)$$

where q_t and q_e — the amounts (mg/g) of the dye adsorbed on the adsorbent at time t and in the equilibrium state, respectively; C_0 , C_t , and C_e — the concentrations of the dye in the solution (mg/L) at the initial stage, at time t , and in the state of equilibrium, respectively; m (g) and V (L) — the amount of adsorbent and the volume of dye solution, respectively.

The degree of adsorption R (%) (extraction ratio of the sorbate) was calculated by the formula:

$$R(\%) = \frac{(C_0 - C_e)}{C_0} \times 100. \quad (3)$$

Results and Discussion

Nickel(II) and cobalt(II) trimesinates were synthesized by direct interaction of metal salts and trimesic acid in water in the presence of alkali. The morphology of the synthesized nickel and cobalt(II) trimesinates was studied by scanning electron microscopy. Nickel(II) trimesinate consists of prismatic crystals ranging in size from $3 \times 1.2 \times 0.6$ (65 %) to $7.3 \times 2.3 \times 1$ μm (20 %), some of which are visualized as broken. A characteristic feature of the crystals is their layered character (Fig. 1A). Cobalt(II) trimesinate is also formed by elongated prismatic crystals, more uniform and monolithic (with a smooth surface) compared to nickel(II) trimesinate. The size of the crystals varies from $3.1 \times 0.6 \times 0.6$ (15 %) to $3.6 \times 0.5 \times 0.5$ (80 %) μm , and less than 2 % is represented by wide but short crystals (in the form of tablets) with dimensions of $2.6 \times 1.86 \times 0.33$ μm (Fig. 1B).

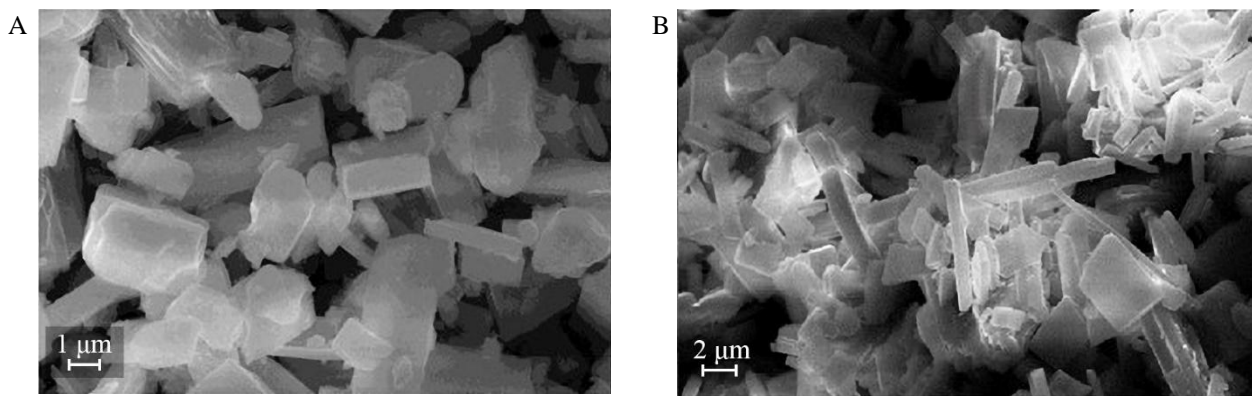


Figure 1. Images of nickel(II) (A) and cobalt(II) (B) trimesinate crystals obtained by scanning electron microscopy

X-ray phase analysis was carried out to identify the obtained compounds. The observed sharp and distinct diffraction peaks indicate that the prepared samples of nickel and cobalt trimesinates have good crystallinity and high phase purity. All positions of the diffraction peaks are in good agreement with the results of modeling performed in the program for processing X-ray phase analysis data “Match-3” (Fig. 2) and previously published works [24, 25]. In addition, X-ray diffraction data show that the peaks intensity does not completely match the theoretical calculation and may indicate the presence of crystals with a preferred growth orientation that are in the state of formation. The diffraction patterns of both compounds have much in common, which characterizes the compounds as isostructural [29].

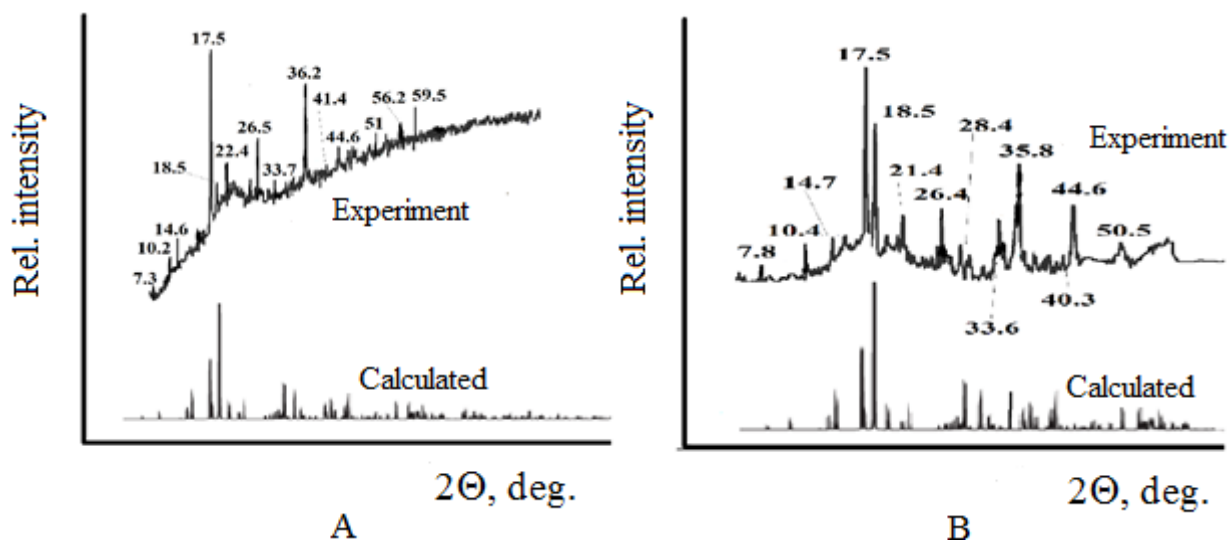
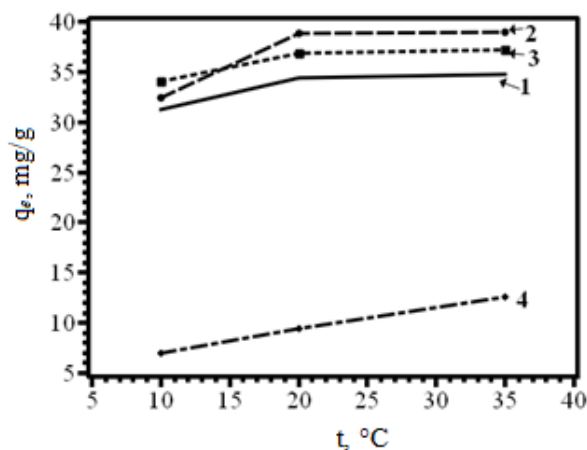


Figure 2. Calculated and experimental diffraction patterns of nickel(II) (A) and cobalt(II) (B) trimesinates

The IR spectra of trimesic acid and synthesized compounds were studied to determine the coordination mode of the organic ligand. The IR spectrum of trimesic acid shows bands with an absorption maximum in

the region of 1720, 1430 and 1276 cm^{-1} . The first band is characteristic of stretching vibrations of the carboxyl group; the other two are due to a combination of planar bending vibrations of the hydroxyl group and stretching vibrations of the C–O bond in carboxylic acid dimers. The IR spectra of nickel and cobalt trimesinates are almost identical and are in satisfactory agreement with the results previously published in the literature [25]. The IR spectrum of the resulting nickel(II) and cobalt(II) trimesinates lacks a band at 1720 cm^{-1} , which indicates complete deprotonation of carboxyl groups and their binding to metal ions. The latter is confirmed by the formation of the M–O bond and is proved by the formation of a new strong absorption band in the region of 765 cm^{-1} (Ni) and 768 cm^{-1} (Co). At the same time, absorption bands appear, which are not recorded in the spectrum of trimesic acid, located in the region of 1562 cm^{-1} (Ni) and 1565 cm^{-1} (Co), characteristic of asymmetric stretching vibrations of carboxylate ions. Stretching symmetric vibrations of this anion are fixed in the region of 1375 cm^{-1} (Ni) and 1376 cm^{-1} (Co). The difference between the wave numbers of asymmetric and symmetric stretching vibrations of carboxylate anions is 187 cm^{-1} (Ni) and 189 cm^{-1} (Co), which allows us to conclude that in this case, a bidentate-bridging mode of coordination of the carboxylate ion is possible.

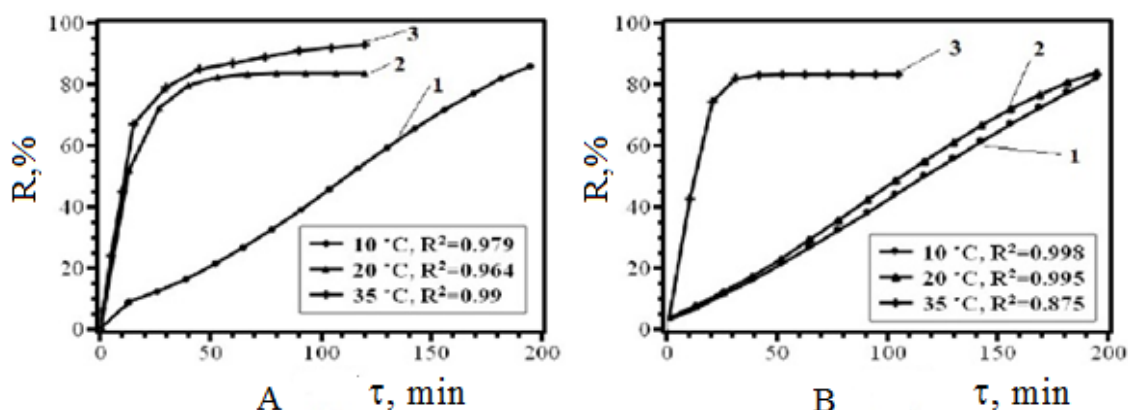
The ability of nickel(II) and cobalt(II) trimesinates to adsorb organic dyes from aqueous solutions at different temperatures was studied (Fig. 3). The dependences found indicate that the adsorption value tends to slightly increase with increasing temperature in the studied temperature range.



1 — Nickel(II) trimesinate – Congo Red; 2 — nickel(II) trimesinate – Methylene blue;
3 — cobalt (II) trimesinate – Congo Red; 4 — cobalt(II) trimesinate – Methylene blue

Figure 3. Effect of temperature on the adsorption of dyes in systems

The extraction efficiency versus the contact time of the sorbate with the sorbent is shown in Fig. 4. It can be seen from the presented figure that the degree of adsorption is higher in the case of Congo Red, reaching a value of 97 %, while for Methylene blue it is about 83 %.



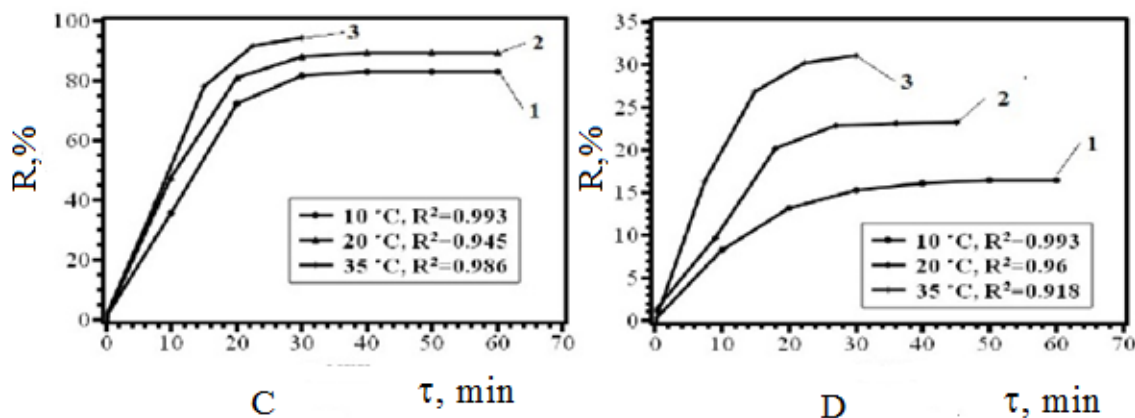


Figure 4. Time dependence of the adsorption degree of Congo Red (A, C) and Methylene blue (B, D) by nickel (A, B) and cobalt (C, D) trimesinates at different temperatures

The data obtained in the study of the adsorption of organic dyes by the studied MOFs were analyzed using various adsorption models. Preference was given to the models of Langmuir, Freundlich, and Temkin.

Langmuir adsorption model. This model gives a quite specific quantitative characteristic of the adsorption process at low and high sorbate concentrations. The Langmuir adsorption isotherm assumes that adsorption occurs at certain homogeneous sites within the adsorbent and has been successfully applied in many monolayer adsorption sorption processes [30]. The Langmuir isotherm can be written as [31]:

$$q_e = \frac{q_{max} K_L C_e}{1 + K_L C_e}, \quad (4)$$

where K_L — the Langmuir constant (L/mg) related to the set of binding sites and the free energy of adsorption; q_{max} — the limiting adsorption, which expresses the concentration of the dye during the formation of a monolayer on the adsorbent (mg/g).

Equation (4) is usually represented in a linear form:

$$\frac{C_e}{q_e} = \frac{1}{K_L q_{max}} + \frac{C_e}{q_{max}}. \quad (5)$$

For the Langmuir equation, the favorable nature of adsorption can be expressed in terms of the dimensionless equilibrium parameter R_L , which is determined as follows:

$$R_L = \frac{1}{1 + K_L C_0}. \quad (6)$$

R_L values indicate that the process type is irreversible ($R_L = 0$), favorable ($0 < R_L < 1$), linear ($R_L = 1$) or unfavorable ($R_L > 1$) [32].

Freundlich adsorption model. The empirical equation of the Freundlich isotherm is used to describe heterogeneous systems with medium coverages of the adsorbent surface [30]. It looks like this:

$$q_e = k_F C_e^{1/n_F}, \quad (7)$$

where K_F — a constant showing the adsorption capacity of the adsorbent ($\text{mg}^{1-1/n} \text{L}^{1/n} \text{g}^{-1}$); $1/n$ — an empirical constant related to the adsorption driving force.

The value of $1/n$ quantitatively determines the conditions favoring adsorption and characterizes the degree of inhomogeneity of the MOF surface [33]:

$$K_F = \frac{q_{max}}{C_0^{1/n}}. \quad (8)$$

It is necessary to work with a constant initial concentration C_0 and a variable mass of the adsorbent to determine the maximum adsorption (q_{max}).

Temkin's adsorption model. The Temkin model takes into account sorbent-sorbate interactions and assumes that the heat of adsorption as a function of the temperature of all molecules in the layer will decrease linearly as the layer is filled [34]. However, this model has specific limitations associated with the impossibility of using it at low or high sorbate concentrations in the solution. This model contains a parameter that takes into account interactions between adsorption sites and sorbate.

The experimental results on the determination of adsorption isotherms were processed according to the Temkin equations:

$$q_e = \frac{RT}{b} \ln K_T C_e; \quad (9)$$

$$B_T = \frac{RT}{b}. \quad (10)$$

Equation (9) can be expressed linearly:

$$q_e = B_T \ln K_T + B_T \ln C_e, \quad (11)$$

where T — the absolute temperature, K; R — the universal gas constant, $R = 8.314$ J/(mol K); K_T — the equilibrium constant; b — the constant associated with the heat of adsorption, J/mol; B_T — the Temkin isotherm constant.

The calculated values of the maximum adsorption and adsorption equilibrium constants at different temperatures are given in Table 2. The R_L values for dye adsorption on MOFs at different temperatures are less than 1 and greater than zero, which indicates the conditions favoring adsorption. In addition, experimental data show that the adsorption process is optimally described by the Freundlich model. The values of the coefficient $1/n$ range from 0 to 1, which also indicates favorable conditions for adsorption, while the lowest values are observed for the cobalt trimesinate – Methylene blue system, which is in good agreement with other experimental data and generally characterizes cobalt trimesinate as a relatively inefficient adsorbent with respect to cationic dyes (Methylene blue), while its adsorption capacity for anionic dyes (Congo Red) is satisfactory.

Table 2

Parameter values of adsorption isotherms

Model	Adsorbent	Sorbate	Parameter	T, K		
				283	293	308
1	2	3	4	5	6	7
Langmuir	Nickel(II) trimesinate	Congo Red	q_{\max}	123.4	128.2	161.3
			K_L	0.81	0.6	0.62
			R_L	0.058	0.076	0.074
			R^2	0.896	0.994	0.956
		Methylene blue	q_{\max}	107.5	119	153.8
			K_L	4.65	8.4	6.5
	R_L		0.01	0.006	0.007	
	Cobalt(II) trimesinate	Congo Red	q_{\max}	120.5	143	161
			K_L	8.3	7.0	6.2
			R_L	0.006	0.007	0.008
		Methylene blue	R^2	0.862	0.981	0.902
			q_{\max}	133	149	156
K_L			3.75	2.23	0.45	
Freundlich	Nickel(II) trimesinate	Congo Red	$1/n$	0.81	0.6	0.57
			K_F	0.51	0.690	0.75
			R^2	0.965	0.932	0.937
		Methylene blue	$1/n$	0.72	0.7	0.63
			K_F	0.7	2.3	4.1
			R^2	0.895	0.905	0.9
	Cobalt(II) trimesinate	Congo Red	$1/n$	0.72	0.7	0.65
			K_F	0.33	0.69	0.78
			R^2	0.911	0.932	0.92
		Methylene blue	$1/n$	0.71	0.67	0.75
			K_F	0.35	0.1	0.33
			R^2	0.83	0.815	0.865

Continuation of Table 2

1	2	3	4	5	6	7
Temkin	Nickel(II) trimesinate	Congo Red	b	36.18	40.58	46.53
			K_T	2.3	5.41	6.47
			R^2	0.929	0.944	0.958
		Methylene blue	b	33.6	38.64	44.9
			K_T	2.66	2.0	0.57
			R^2	0.926	0.949	0.968
	Cobalt(II) trimesinate	Congo Red	b	31.37	27.98	32.8
			K_T	12.5	43.5	78
			R^2	0.943	0.975	0.982
		Methylene blue	b	37.93	40.58	45.1
			K_T	2.48	0.9	0.45
			R^2	0.946	0.991	0.998

In addition, an analysis of dye adsorption isotherms shows that they refer to monomolecular adsorption isotherms and the curves monotonically approach a certain limiting value corresponding to monolayer filling.

The data obtained during the study of the adsorption process were analyzed using kinetic models of pseudo-first and pseudo-second order reactions. An equation that satisfactorily describes adsorption from a liquid medium by solid adsorbents was proposed by Lagergren and can be represented in the differential form as [35]:

$$\frac{dq_t}{dt} = k_1 (q_e - q_t), \quad (12)$$

where k_1 (min^{-1}) — the adsorption rate constant of the pseudo-first order model.

After a certain integration from $t = 0$ to $t = t$ and from $q = 0$ to $q = q_e$, equation (12) takes the form:

$$\ln (q_e - q_t) = \ln q_e - k_1 t. \quad (13)$$

The differential form of the classical pseudo second order velocity equation is:

$$\frac{dq_t}{dt} = k_2 (q_e - q_t)^2 \quad (14)$$

or

$$\frac{1}{q_t} = \frac{1}{k_2 q_e^2} + \frac{1}{q_e} t \quad (15)$$

transforming which you obtain:

$$q_t = \frac{t}{\frac{1}{k_2 q_e^2} + \frac{t}{q_e}}, \quad (16)$$

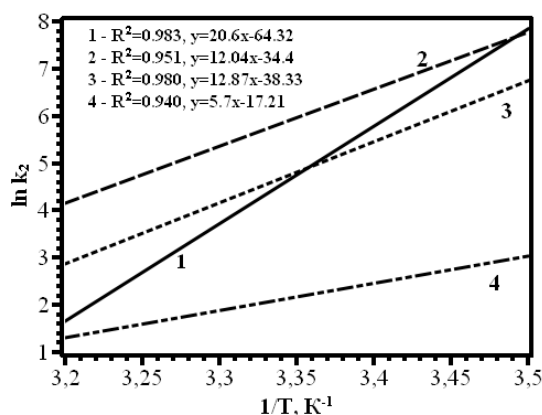
where k_2 — the adsorption rate constant of the pseudo second order model ($\text{g}/\text{mmol} \cdot \text{min}$).

Linear plots of $\ln(q_e - q_t)$ versus t for a pseudo-first-order reaction and t/q_t versus t for a pseudo second order reaction for dye adsorption were tested to obtain rate parameters. Kinetic parameters under various conditions were calculated from these graphs. They are given in Table 3. The applied pseudo-first-order equation satisfactorily describes the regularities of adsorption at the initial stages (up to 60 min in the experiment) of the adsorption process, when the phenomenon of film diffusion has a significant effect on the process. An increase in the concentration of sorbate molecules at the adsorbent surface at the initial moments at low degrees of filling of the adsorption space stimulates the movement of sorbate molecules into the adsorbent pores under the influence of the concentration gradient, but subsequently this process slows down, which in turn potentiates other mechanisms. The calculated values of the determination coefficient make it possible to judge that the pseudo-first-order kinetic model of adsorption describes the process less accurately, and, therefore, the pseudo-second-order kinetic model is preferable.

Kinetic parameters of the adsorption process

Adsorbent	t , °C	C_e , mg/g	Time to reach equilibrium, min	R^2		k_1 , min ⁻¹	k_2 , g/mg min
				Pseudo first order	Pseudo second order		
Congo Red							
Nickel(II) trimesinate	10	31.2	165	0.898	0.946	$8 \cdot 10^{-3}$	$3.44 \cdot 10^{-3}$
	20	34.4	120	0.949	0.925	$6 \cdot 10^{-2}$	$0.2 \cdot 10^{-3}$
	35	35.2	105	0.943	0.984	$8.6 \cdot 10^{-2}$	$0.06 \cdot 10^{-3}$
Cobalt(II) trimesinate	10	34.3	60	0.989	0.948	$1.6 \cdot 10^{-2}$	$0.69 \cdot 10^{-3}$
	20	36.8	60	0.981	0.909	$1.1 \cdot 10^{-2}$	$0.32 \cdot 10^{-3}$
	35	37.2	45	0.979	0.954	$1 \cdot 10^{-2}$	$0.016 \cdot 10^{-3}$
Methylene blue							
Nickel(II) trimesinate	10	32.4	195	0.978	0.985	$6.8 \cdot 10^{-3}$	$3.2 \cdot 10^{-3}$
	20	32.8	180	0.999	0.996	$7.3 \cdot 10^{-3}$	$0.44 \cdot 10^{-3}$
	35	35	120	0.961	0.992	$9.2 \cdot 10^{-2}$	$0.073 \cdot 10^{-3}$
Cobalt(II) trimesinate	10	7	90	0.949	0.999	$6.9 \cdot 10^{-2}$	$0.25 \cdot 10^{-2}$
	20	9.4	75	0.991	0.988	0.137	$0.09 \cdot 10^{-2}$
	35	12.6	60	0.998	0.986	0.152	$0.04 \cdot 10^{-2}$

The activation energies of the adsorption process of dyes on nickel(II) and cobalt(II) trimesinates were calculated from the dependence of $\ln k_2$ on the reciprocal temperature (Fig. 5), which amounted to 5.15 (nickel(II) trimesinate – Congo Red), 2.99 (nickel(II) trimesinate – Methylene blue), 3.32 (cobalt(II) trimesinate – Congo Red), 1.44 kJ/mol (cobalt trimesinate – Methylene blue). The activation energies are small values, which indicates the feasibility of the adsorption process under these conditions, in addition, since all values are below 40 kJ/mol, it can be assumed with a reasonable degree of confidence that the limiting process is physical adsorption.



1 — Nickel(II) trimesinate – Congo Red; 2 — nickel(II) trimesinate – Methylene blue, 3 — cobalt(II) trimesinate – Congo Red; 4 — cobalt(II) trimesinate – Methylene blue

Figure 5. Dependence of the pseudo-second order adsorption rate constant on the reciprocal temperature for the systems

To determine the spontaneity of the adsorption process and verify the obtained experimental data, three main thermodynamic parameters were used, namely the change in enthalpy (ΔH_0), entropy (ΔS_0), and Gibbs free energy (ΔG_0). The Gibbs equation was used to study the effect of temperature on the equilibrium adsorption:

$$\Delta G^0 = -RT \ln K_c, \quad (17)$$

where K_c — the thermodynamic equilibrium constant, which can be determined from the equation

$$K_c = \frac{C}{C_e}. \quad (18)$$

Considering the change in concentrations in the real time interval and depending on the dose of the adsorbent, equation (19) can be written as:

$$K_c = \frac{(C_0 - C_e)V}{mC_e} \quad (19)$$

The Gibbs equation can also be expressed as follows:

$$\Delta G^0 = \Delta H^0 - T\Delta S^0 \quad (20)$$

Combining the above equations, we obtain

$$\ln K_c = \frac{\Delta S^0}{R} - \frac{\Delta H^0}{RT} \quad (21)$$

The thermodynamic parameters of the process calculated graphically from the dependence of the thermodynamic equilibrium constant on the reciprocal temperature are given in Table 4.

Table 4

Thermodynamic parameters of the dye adsorption in the temperature range of 283–308 K

Adsorbent	Sorbate	T, K	K_c	ΔG^0 , kJ/mol	ΔH^0 , kJ/mol	ΔS^0 , J/mol K
Nickel(II) trimesinate	Congo Red	283	7.1	-4.6	3.2	27.5
		293	12.3	-6.1		
		308	13.4	-6.6		
Nickel(II) trimesinate	Methylene blue	283	8.5	-5.03	3	28.3
		293	9.1	-5.35		
		308	14.6	-9.91		
Cobalt(II) trimesinate	Congo Red	283	11.3	-5.7	1.3	24.7
		293	23	-7.6		
		308	26.6	-8.44		
Cobalt(II) trimesinate	Methylene blue	283	0.42	-2.04	0.4	6.1
		293	0.61	-1.21		
		308	0.92	-0.23		

It can be seen from Table 4 that for the compounds under study, the adsorption process is characterized by negative values of the Gibbs free energy, and the enthalpy of the process takes positive values, which describes the process as a whole as endothermic. However, the adsorption of Methylene blue with cobalt(II) trimesinate has much lower Gibbs free energy and minimal enthalpy values compared to other systems, which can be explained by the competition of sorbate and water molecules on the sorbent surface. The decrease in the value of the Gibbs free energy with increasing temperature indicates a greater efficiency of adsorption at moderately elevated temperatures. The endothermic nature of adsorption under these conditions is explained by the need for the particles of the organic dye to reach the active centers of the adsorbent, and for this, they should be free from the hydration shell, or at least part of it, for which energy must be expended. As a result, the calculated value of enthalpy is the resultant of two processes, namely dehydration of organic dye ions (endothermic process) and adsorption of the latter on the active centers of the adsorbent, which proceeds with the release of energy (heat of adsorption). A positive entropy value indicates an increase in the number of degrees of freedom at the solid-liquid interface during the dye adsorption process and reflects the sorbate affinity for adsorbent molecules. An exception is the system cobalt trimesinate – Methylene blue, which is characterized by the low heat of adsorption and the loss of some degrees of freedom of the adsorbent in relation to Methylene blue in the adsorption process, which is confirmed by the low system entropy.

Conclusions

In this work, we developed an easily accessible procedure for the synthesis of nickel and cobalt trimesates in water in the presence of alkali. The possibility of using nickel and cobalt trimesinates for the adsorption of organic dyes from aqueous solutions was studied. Equilibrium adsorption data were analyzed using three typical adsorption models, namely Langmuir, Freundlich, and Temkin in the temperature range of 283–308 K. It was found that the adsorption of organic dyes on nickel and cobalt trimesinates was best described by the Freundlich isotherm equation. The values of thermodynamic parameters (ΔG^0 , ΔH^0 , ΔS^0) indicate the competitive advantage of sorbate molecules over solvent molecules in the case of adsorption of Congo Red by cobalt(II) and nickel(II) trimesinates, and in the case of methylene blue adsorption, water

molecules have a competitive advantage over sorbate molecules. Cobalt(II) trimesinate has a good ability to adsorb anionic dyes, while it shows an average adsorption activity for cationic dyes and can be used as a selective adsorbent.

Acknowledgments

This research was carried out in accordance with the state task, state registration number AAAA-A19-119041090087-4.

References

- 1 Dybtsev D.N. Homochiral metal–organic material with permanent porosity, enantioselective sorption properties, and catalytic activity / D.N. Dybtsev, A.L. Nuzhdin, H. Chun, K.P. Bryliakov, E.P. Talsi, V.P. Fedin, K.A. Kim // *Angew. Chem. Int. Ed.* — 2006. — Vol. 45, No. 6. — P. 916–920. <https://doi.org/10.1002/anie.200503023>
- 2 Dybtsev D.N. Microporous manganese formate: a simple metal–organic porous material with high framework stability and highly selective gas sorption properties / D.N. Dybtsev, H. Chun, S.H. Yoon, D. Kim, K. Kim // *J. Am. Chem. Soc.* — 2004. — Vol. 126, No. 1. — P. 32–33. <https://doi.org/10.1021/ja038678c>
- 3 Lin W. Supramolecular engineering of chiral and acentric 2D networks. synthesis, structures, and second-order nonlinear optical properties of bis(nicotinato)zinc and bis{3-[2-(4-pyridyl)ethenyl]benzoato}cadmium / W. Lin, O.R. Evans, R.-G. Xiong, Z. Wang // *J. Am. Chem. Soc.* — 1998. — Vol. 120, No. 50. — P. 13272–13273. <https://doi.org/10.1021/ja983415h>
- 4 Toma L.M. $[\text{Mn}_2(\text{bipym})(\text{H}_2\text{O})_8]^{4+}$ and $[\text{Fe}(\text{bipy})(\text{CN})_4]^-$ as building blocks in designing novel bipym- and cyanide-bridged heterobimetallic complexes (bipym = 2,2'-bipyrimidine and bipy = 2,2'-bipyridine) / L.M. Toma, R. Lescouzec, L.D. Toma, F. Lloret, M. Julve, J. Vaissermann, M. Andruh // *J. Chem. Soc. Dalton Trans.* — 2002. — No. 50. — P. 3171–3176. <https://doi.org/10.1039/B202422P>
- 5 Kitagawa S. Functional porous coordination polymers / S. Kitagawa, R. Kitaura, S.-i. Noro // *Angew. Chem. Int. Ed.* — 2004. — Vol. 43, No. 18. — P. 2334–2375. <https://doi.org/10.1002/anie.200300610>
- 6 Chui S.S.-Y. A Chemically functionalizable nanoporous material $[\text{Cu}_3(\text{TMA})_2(\text{H}_2\text{O})_3]_n$ / S.S.-Y. Chui, S.M.-F. Lo, J.P. Charmant, A.G. Orpen, I.D. Williams // *Science*. — 1999. — Vol. 283, No. 5405. — P. 1148–1150. <https://doi.org/10.1126/science.283.5405.1148>
- 7 Feldblyum J. I., Liu M., Gidley D. W., Matzger A. J. Reconciling the discrepancies between crystallographic porosity and guest access as exemplified by Zn-HKUST-1 // *J. Am. Chem. Soc.* — 2011. — Vol. 133, No. 45. — P. 18257–18263. <https://doi.org/10.1021/ja2055935>
- 8 Kramer M. Synthesis and properties of the metal-organic framework $\text{Mo}_3(\text{BTC})_2(\text{TUDMOF-1})$ / M. Kramer, U. Schwarz, S. Kaskel // *J. Mater. Chem.* — 2006. — Vol. 16, No. 23. — P. 2245–2248. <https://doi.org/10.1039/B601811D>
- 9 Murray L.J. Highly-selective and reversible O_2 binding in $\text{Cr}_3(1,3,5\text{-benzenetricarboxylate})_2$ / L.J. Murray, M. Dinca, J. Yano, S. Chavan, S. Bordiga, C.M. Brown, J.R. Long // *J. Am. Chem. Soc.* — 2010. — Vol. 132, No. 23. — P. 7856–7857. <https://doi.org/10.1021/ja1027925>
- 10 Sumida K., Her J.-H., J.-H., Dinca M., Murray L. J., Schloss J. M., Pierce C. J., Thompson B. A., FitzGerald S. A., Brown C. M., Long J. R. Neutron scattering and spectroscopic studies of hydrogen adsorption in $\text{Cr}_3(\text{BTC})_2$ — A metal–organic framework with exposed Cr^{2+} sites // *J. Phys. Chem. C*. — 2011. — Vol. 115, No. 16. — P. 8414–8421. <https://doi.org/10.1021/jp200638n>
- 11 Xie L. Mixed-valence iron(II, III) trimesates with open frameworks modulated by solvents / L. Xie, S. Liu, C. Gao, R. Cao, J. Cao, C. Sun, Z. Su // *Inorg. Chem.* — 2007. — Vol. 46, No. 19. — P. 7782–7788. <https://doi.org/10.1021/ic062273m>
- 12 Maniam P. Investigation of porous Ni-based metal-organic frameworks containing paddle-wheel type inorganic building units via high-throughput methods / P. Maniam, N. Stock // *Inorg. Chem.* — 2011. — Vol. 50, No. 11. — P. 5085–5097. <https://doi.org/10.1021/ic200381f>
- 13 Noei H. CO adsorption on a mixed-valence ruthenium metal-organic framework studied by UHV-FTIR spectroscopy and DFT calculations / H. Noei, O. Kozachuk, S. Amirjalayer, S. Bureekaew, M. Kauer, R. Schmid, B. Marler, M. Muhler, R.A. Fischer, Y. Wang // *J. Phys. Chem. C*. — 2013. — Vol. 117, No. 11. — P. 5658–5666. <https://doi.org/10.1021/jp3056366>
- 14 Wade C.R. Investigation of the synthesis, activation, and isosteric heats of CO_2 adsorption of the isostructural series of metal-organic frameworks $\text{M}_3(\text{BTC})_2$ ($\text{M} = \text{Cr, Fe, Ni, Cu, Mo, Ru}$) / C.R. Wade, M. Dinca // *Dalton Trans.* — 2012. — Vol. 41, No. 26. — P. 7931–7938. <https://doi.org/10.1039/C2DT30372H>
- 15 Marri S.R. Two novel 3D-MOFs (Ca-TATB and Co-HKUST): synthesis, structure and characterization / S.R. Marri, N. Chauhan, R.K. Tiwari, J. Kumar, J.N. Behera // *Inorg. Chim. Acta.* — 2018. — No. 478. — P. 8–14. <https://doi.org/10.1016/j.ica.2018.03.014>
- 16 Suh M.P. Syntheses and functions of porous metallosupramolecular networks / M.P. Suh // *Coord. Chem. Rev.* — 2008. — Vol. 252. — P. 1007–1026. <https://doi.org/10.1016/j.ccr.2008.01.032>
- 17 Dzhardimalieva G.I. Design and synthesis of coordination polymers with chelated units and their application in nanomaterials science / G.I. Dzhardimalieva, I.E. Uflyand // *RSC Adv.* — 2017. — Vol. 7, No. 67. — P. 42242–42288. <https://doi.org/10.1039/C7RA05302A>

- 18 Dzhardimalieva G. I., Uflyand I.E. Chemistry of polymeric metal chelates / G.I. Dzhardimalieva, I.E. Uflyand. — Cham: Springer. — 2018. — P. 633–759.
- 19 Zhang H. Wire spherical-shaped Co-MOF electrode materials for high-performance all-solid-state flexible asymmetric supercapacitor device / H. Zhang, J. Wang, Y. Sun, X. Zhang, H. Yang, B. Lin // *J. Alloys Compd.* — 2021. — No. 879. — ID 160423. <https://doi.org/10.1016/j.jallcom.2021.160423>
- 20 Ramachandran R. Morphology-dependent electrochemical properties of cobalt-based metal organic frameworks for supercapacitor electrode materials / R. Ramachandran, C. Zhao, D. Luo, K. Wang, F. Wang // *Electrochim. Acta.* — 2018. — Vol. 267. — P. 170–180. <https://doi.org/10.1016/j.electacta.2018.02.074>
- 21 Horcajada P. Metal-Organic Frameworks in Biomedicine / P. Horcajada, R. Gref, T. Baati, P.K. Allan, G. Maurin, P. Couvreur, G. Ferey, R.E. Morris, C. Serre // *Chem. Rev.* — 2012. — Vol. 112. — P. 1232–1268. <https://dx.doi.org/10.1021/cr200256v>
- 22 Uflyand I.E. Recent strategies to improve MOF performance in solid phase extraction of organic dyes / I.E. Uflyand, V.A. Zhinzhilo, V.O. Nikolaevskaya, B.I. Kharisov, C.M. Oliva González, O.V. Kharissova // *Microchem. J.* — 2021. — No. 168. — ID 106387. <https://doi.org/10.1016/j.microc.2021.106387>
- 23 Yu G. Cobalt-based metal organic framework as precursor to achieve superior catalytic activity for aerobic epoxidation of styrene / G. Yu, J. Sun, F. Muhammad, P. Wang, G. Zhu // *RSC Adv.* — 2014. — Vol. 4, No. 73. — P. 38804–38811. <https://doi.org/10.1039/C4RA03746D>
- 24 Zhu H.-F. Hydrothermal synthesis and structural characterization of one-dimensional coordination polymers of cobalt(II) and nickel(II) with 1,3,5-benzenetricarboxylic acid / H.-F. Zhu, W.-Y. Sun, T. Okamura, N. Ueyama // *Inorg. Chem. Commun.* — 2003. — Vol. 6, No. 2. — P. 168–173. [https://doi.org/10.1016/S1387-7003\(02\)00714-1](https://doi.org/10.1016/S1387-7003(02)00714-1)
- 25 Дыбцев Д.Н. Синтез, структура и магнитные свойства слоистого координационного полимера 1,3,5-бензолтрикарбоксилата кобальта (II) / Д.Н. Дыбцев, М.П. Юткин, Е.В. Пересыпкина, А.В. Вировец, Й. Хасегава, Х. Нишихара, В.П. Федин // *Изв. РАН. Сер. хим.* — 2007. — № 9. — С. 1719–1723. <https://doi.org/10.1007/s11172-007-0277-8>
- 26 Lu H.-S. Surfactant media to grow new crystalline cobalt 1,3,5-benzenetricarboxylate metal-organic frameworks / H.-S. Lu, L. Bai, W.-W. Xiong, P. Li, J. Ding, G. Zhang, T. Wu, Y. Zhao, J.-M. Lee, Y. Yang, B. Geng, Q. Zhang // *Inorg. Chem.* — 2014. — Vol. 53, No. 16. — P. 8529–8537. <https://doi.org/10.1021/ic501113z>
- 27 Neff H. Periodic protein adsorption at the gold/biotin aqueous solution interface: evidence of kinetics with time delay / H. Neff, H.M. Laborde, A.M.N. Lima // *Sci. Rep.* — 2016. — Vol. 6. — ID 36232. <https://doi.org/10.1038/srep36232>
- 28 Dzhardimalieva G. Synthesis of copper(II) trimesinate coordination polymer and its use as a sorbent for organic dyes and a precursor for nanostructured material / G. Dzhardimalieva, R. Baimuratova, E. Knerelman, G. Davydova, S. Kudaibergenov, O. Kharissova, V. Zhinzhilo, I. Uflyand // *Polymers.* — 2020. — Vol. 12, No. 5. — ID 1024. <https://doi.org/10.3390/polym12051024>
- 29 Yaghi O. M. Construction of porous solids from hydrogen-bonded metal complexes of 1,3,5-benzenetricarboxylic acid / O.M. Yaghi, H. Li, T.L. Groy // *J. Am. Chem. Soc.* — 1996. — Vol. 118, No. 38. — P. 9096–9101. <https://doi.org/10.1021/ja960746q>
- 30 Wang S. A comparative study of dye removal using fly ash treated by different methods / S. Wang, Y. Boyjoo, A. Choueib // *Chemosphere.* — 2005. — Vol. 60, No. 10. — P. 1401–1407. <https://doi.org/10.1016/j.chemosphere.2005.01.091>
- 31 Hameed B.H. A novel agricultural waste adsorbent for the removal of cationic dye from aqueous solutions / B.H. Hameed, R.R. Krishni, S.A. Sata // *J. Hazard. Mater.* — 2009. — Vol. 162, No. 1. — P. 305–311. <https://doi.org/10.1016/j.jhazmat.2008.05.036>
- 32 Hamdaoui O. Batch study of liquid-phase adsorption of methylene blue using cedar sawdust and crushed brick / O. Hamdaoui // *J. Hazard. Mater.* — 2006. — No. 135. — P. 264–273. <https://doi.org/10.1016/j.jhazmat.2005.11.062>
- 33 Halsey G.D. The role of surface heterogeneity in adsorption / G.D. Halsey // *Adv. Catal.* — 1952. — Vol. 4. — P. 259–269. [https://doi.org/10.1016/S0360-0564\(08\)60616-1](https://doi.org/10.1016/S0360-0564(08)60616-1)
- 34 Dada A.O. Langmuir, Freundlich, Temkin and Dubinin-Radushkevich isotherms studies of equilibrium sorption of Zn²⁺ onto phosphoric acid modified rice husk / A.O. Dada, A.P. Olalekan, A.M. Olatunya, O. Dada // *IOSR J. Appl. Chem.* — 2012. — Vol. 3, No. 1. — P. 38–45. <https://doi.org/10.9790/5736-0313845>
- 35 Simonin J.-P. On the comparison of pseudo-first order and pseudo-second order rate laws in the modeling of adsorption kinetics / J.-P. Simonin // *Chem. Eng. J.* — 2016. — No. 300. — P. 254–263. <https://doi.org/10.1016/j.cej.2016.04.079>

В.А. Жинжило, А.Ю. Литвинова, В.М. Лямина, Г.И. Джардималиева, И.Е. Уфлянд

Органикалық бояғыштардың перспективті адсорбенттері ретінде никель және кобальт тримезинаттар негізіндегі координациялық полимерлер

Металлорганикалық каркастары (МОК) көпіршікті органикалық лигандтарды байланыстыратын металл иондарынан тұратын кристалдық қосылыстар. Металдың координациялық геометриясынан және донор атомдарының байланыс бағытына, сондай-ақ көпіршікті лигандтың геометриясына байланысты 1D, 2D, немесе 3D полимер құрылымдары түзіледі. Металлорганикалық каркастардың сипатты белгілері төмен тығыздық, жоғары кеуектілік пен кристалдылық және үлкен меншікті бетінің

ауданы болып табылады. Мұндай материалдарды жасаудың технологиялық аспектілеріне және оларды әртүрлі құрылғыларға біріктіруге көп көңіл бөлінеді. МОК алу үшін гидротермиялық және солвотермиялық синтезді қоса алғанда, бөлме температурасында және конвективтік қыздыру кезінде тұндыру реакцияларына негізделген әртүрлі синтетикалық тәсілдер әзірленген. Бұл жұмыста никель ацетаты мен кобальт нитратына сілтінің қатысуымен тримезин қышқылымен әрекеттесуі арқылы модификацияланған әдіспен никель және кобальт тримезинаттары негізіндегі металлорганикалық каркастық құрылымдар синтезделді. Алынған қосылыстар конго қызылы және метилен көгі органикалық бояғыштарының сулы ерітінділерінен адсорбциялануын зерттеу үшін пайдаланылды. Адсорбция дәрежесі температураға байланысты және шамасы конго қызылы үшін 97 % дейін жетеді, сол уақытта шама метилен көгі үшін 83 % құрайды. Адсорбция процесінің механизмдері мен сипаттамалық параметрлері Лангмюр, Темкин және Фрейндлих изотермаларының эмпирикалық үлгілері арқылы талданған, олардың ішінде адсорбция процесі Фрейндлих моделімен оптималды түрде сипатталған. Есептелген термодинамикалық параметрлер процесінің өздігінен жүретіндігін және оның елеусіз эндотермиялық сипатын көрсетеді.

Кілт сөздер: металлорганикалық каркас құрылымдары, координациялық полимерлер, тримез қышқылы, ластаушы заттар, адсорбция, конго қызылы, метилен көгі, термодинамикалық параметрлер, адсорбция изотермалары, адсорбциялық сыйымдылық.

В.А. Жинжило, А.Ю. Литвинова, В.М. Лямина, Г.И. Джардималиева, И.Е. Уфлянд

Координационные полимеры на основе тримезинатов никеля и кобальта как перспективные адсорбенты органических красителей

Металлоорганические каркасы (МОК) представляют собой кристаллические соединения, состоящие из ионов металлов, координированных мостиковыми органическими лигандами. В зависимости от координационной геометрии металла и направления связи донорных атомов, а также от геометрии мостикового лиганда формируются 1D-, 2D- или 3D-структуры полимера. Характерными особенностями металлоорганических каркасов являются низкая плотность, высокая пористость и кристалличность, большая удельная поверхность. Особое внимание уделено технологическим аспектам создания таких материалов и их интеграции в различные устройства. Для получения МОК разработаны различные синтетические подходы, основанные на реакциях осаждения при комнатной температуре и при конвективном нагреве, включая гидротермальный и сольвотермальный синтез. В настоящей статье металлоорганические каркасные структуры на основе тримезинатов никеля и кобальта были синтезированы по модифицированной методике взаимодействием ацетата никеля и нитрата кобальта с тримезиновой кислотой в присутствии щелочи. Полученные соединения использованы для изучения адсорбции органических красителей конго красного и метиленового синего из их водных растворов. Степень адсорбции зависит от температуры и достигает величины 97 % для конго красного, в то время как для метиленового синего она составляет порядка 83 %. Механизмы и характерные параметры процесса адсорбции проанализированы с применением эмпирических моделей изотерм Ленгмюра, Темкина и Фрейндлиха, из которых оптимально процесс адсорбции описывается моделью Фрейндлиха. Рассчитанные термодинамические параметры указывают на самопроизвольность процесса и незначительный его эндотермический характер.

Ключевые слова: металлоорганические каркасные структуры, координационные полимеры, тримезиновая кислота, поллютанты, адсорбция, конго красный, метиленовый синий, термодинамические параметры, изотермы адсорбции, адсорбционная емкость.

References

- 1 Dybtssev, D.N., Nuzhdin, A.L., Chun, H., Bryliakov, K.P., Talsi, E.P., Fedin, V.P., & Kim, K.A. (2006). Homochiral metal-organic material with permanent porosity, enantioselective sorption properties, and catalytic activity. *Angew. Chem. Int. Ed.*, 45 (6), 916–920. <https://doi.org/10.1002/anie.200503023>
- 2 Dybtssev, D.N., Chun, H., Yoon, S.H., Kim, D., & Kim, K. (2004). Microporous manganese formate: a simple metal-organic porous material with high framework stability and highly selective gas sorption properties. *J. Am. Chem. Soc.*, 126 (1), 32–33. <https://doi.org/10.1021/ja038678c>.
- 3 Lin, W., Evans, O.R., Xiong, R.-G., & Wang, Z. (1998). Supramolecular engineering of chiral and acentric 2D networks. synthesis, structures, and second-order nonlinear optical properties of bis(nicotinato)zinc and bis{3-[2-(4-pyridyl)ethenyl]benzoato}cadmium. *J. Am. Chem. Soc.* 120 (50), 13272–13273. <https://doi.org/10.1021/ja983415h>.
- 4 Toma, L.M., Lescouzec, R., Toma, L.D., Lloret, F., Julve, M., Vaissermann, J., & Andruh, M. (2002). [Mn₂(bipym)(H₂O)₈]⁴⁺ and [Fe(bipy)(CN)₄]⁻ as building blocks in designing novel bipym- and cyanide-bridged heterobimetallic complexes (bipym = 2,2'-bipyrimidine and bipy = 2,2'-bipyridine). *J. Chem. Soc. Dalton Trans.*, (50), 3171–3176. <https://doi.org/10.1039/B202422P>.

- 5 Kitagawa, S., Kitaura, R., & Noro, S.-I. (2004). Functional porous coordination polymers. *Angew. Chem. Int. Ed.*, 43 (18), 2334–2375. <https://doi.org/10.1002/anie.200300610>
- 6 Chui, S.S.-Y., Lo, S.M.-F., Charmant, J.P., Orpen, A.G., & Williams, I.D. (1999). A Chemically functionalizable nanoporous material [Cu₃(TMA)₂(H₂O)₃]_n. *Science*, 283 (5405), 1148–1150. <https://doi.org/10.1126/science.283.5405.1148>
- 7 Feldblyum, J.L., Liu, M., Gidley, D.W., & Matzger A.J. (2011). Reconciling the discrepancies between crystallographic porosity and guest access as exemplified by Zn-HKUST-1. *J. Am. Chem. Soc.*, 133 (45), 18257–18263. <https://doi.org/10.1021/ja2055935>.
- 8 Kramer, M., Schwarz, U., & Kaskel, S. (2006). Synthesis and properties of the metal-organic framework Mo₃(BTC)₂(TUDMOF-1). *J. Mater. Chem.*, 16 (23), 2245–2248. <https://doi.org/10.1039/B601811D>.
- 9 Murray, L.J., Dinca, M., Yano, J., Chavan, S., Bordiga, S., Brown, C.M., & Long, J.R. (2010). Highly-selective and reversible O₂ binding in Cr₃(1,3,5-benzenetricarboxylate)₂. *J. Am. Chem. Soc.*, 132 (23), 7856–7857. <https://doi.org/10.1021/ja1027925>.
- 10 Sumida, K., Her, J.-H., Dincă, M., Murray, L.J., Schloss, J.M., Pierce, C.J., Thompson, B.A., FitzGerald, S.A., Brown, C.M., & Long, J.R. (2011). Neutron scattering and spectroscopic studies of hydrogen adsorption in Cr₃(BTC)₂ — A metal-organic framework with exposed Cr²⁺ sites. *J. Phys. Chem. C.*, 115 (16), 8414–8421. <https://doi.org/10.1021/jp200638n>.
- 11 Xie, L., Liu, S., Gao, C., Cao, R., Cao, J., Sun, C., & Su, Z. (2007). Mixed-valence iron(II, III) trimesates with open frameworks modulated by solvents. *Inorg. Chem.*, 46 (19), 7782–7788. <https://doi.org/10.1021/ic062273m>.
- 12 Maniam, P., & Stock, N. (2011). Investigation of porous Ni-based metal-organic frameworks containing paddle-wheel type inorganic building units via high-throughput methods. *Inorg. Chem.*, 50 (11), 5085–5097. <https://doi.org/10.1021/ic200381f>.
- 13 Noei, H., Kozachuk, O., Amirjalayer, S., Bureekaew, S., Kauer, M., Schmid, R., Marler, B., Muhler, M., Fischer, R.A., & Wang, Y. (2013). CO adsorption on a mixed-valence ruthenium metal-organic framework studied by UHV-FTIR spectroscopy and DFT calculations. *J. Phys. Chem. C.*, 117 (11), 5658–5666. <https://doi.org/10.1021/jp3056366>.
- 14 Wade, C.R., & Dinca, M. (2012). Investigation of the synthesis, activation, and isosteric heats of CO₂ adsorption of the isostructural series of metal-organic frameworks M₃(BTC)₂ (M = Cr, Fe, Ni, Cu, Mo, Ru). *Dalton Trans.*, 41 (26), 7931–7938. <https://doi.org/10.1039/C2DT30372H>.
- 15 Marri, S.R., Chauhan, N., Tiwari, R.K., Kumar, J., & Behera, J.N. (2018). Two novel 3D-MOFs (Ca-TATB and Co-HKUST): synthesis, structure and characterization. *Inorg. Chim. Acta*, 478, 8–14. <https://doi.org/10.1016/j.ica.2018.03.014>.
- 16 Suh, M.P. (2008). Syntheses and functions of porous metallosupramolecular networks. *Coord. Chem. Rev.*, 252, 1007–1026. <https://doi.org/10.1016/j.ccr.2008.01.032>.
- 17 Dzhardimalieva, G.I., & Uflyand, I.E. (2017). Design and synthesis of coordination polymers with chelated units and their application in nanomaterials science. *RSC Adv.*, 7 (67), 42242–42288. <https://doi.org/10.1039/C7RA05302A>.
- 18 Dzhardimalieva, G.I., & Uflyand, I.E. (2018). Chemistry of polymeric metal chelates. Cham: Springer, 633–759.
- 19 Zhang, H., Wang, J., Sun, Y., Zhang, X., Yang, H., & Lin, B. (2021). Wire spherical-shaped Co-MOF electrode materials for high-performance all-solid-state flexible asymmetric supercapacitor device. *J. Alloys Compd.*, (879), 160423. <https://doi.org/10.1016/j.jallcom.2021.160423>.
- 20 Ramachandran, R., Zhao, C., Luo, D., Wang, K., & Wang, F. (2018). Morphology-dependent electrochemical properties of cobalt-based metal organic frameworks for supercapacitor electrode materials. *Electrochim. Acta*, 267, 170–180. <https://doi.org/10.1016/j.electacta.2018.02.074>
- 21 Horcajada, P., Gref, R., Baati, T., Allan, P.K., Maurin, G., Couvreur, P., Ferey, G., Morris, R.E., & Serre C. (2012). Metal-Organic Frameworks in Biomedicine. *Chem. Rev.*, 112, 1232–1268. <https://dx.doi.org/10.1021/cr200256v>
- 22 Uflyand, I.E., Zhinzhiro, V.A., Nikolaevskaya, V.O., Kharisov, B.I., Oliva, González, C.M., & Kharissova, O.V. (2021). Recent strategies to improve MOF performance in solid phase extraction of organic dyes. *Microchem. J.*, (168), 106387. <https://doi.org/10.1016/j.microc.2021.106387>.
- 23 Yu, G., Sun, J., Muhammad, F., Wang, P., & Zhu, G. (2014). Cobalt-based metal organic framework as precursor to achieve superior catalytic activity for aerobic epoxidation of styrene. *RSC Adv.*, 4 (73), 38804–38811. <https://doi.org/10.1039/C4RA03746D>
- 24 Zhu, H.-F., Sun, W.-Y., Okamura, T., & Ueyama, N. (2003). Hydrothermal synthesis and structural characterization of one-dimensional coordination polymers of cobalt(II) and nickel(II) with 1,3,5-benzenetricarboxylic acid. *Inorg. Chem. Commun.* 6 (2), 168–173. [https://doi.org/10.1016/S1387-7003\(02\)00714-1](https://doi.org/10.1016/S1387-7003(02)00714-1)
- 25 Dybtsev, D.N., Yutkin, M.P., Peresykina, E.V., Virovets, A.V., Hasegawa, Y., Nishihara, H., & Fedin, V.P. (2007). Sintez, struktura i magnitnye svoystva sloistogo koordinatsionnogo polimera 1,3,5-benzotrikarboxilata kobalta (II) [Synthesis, structure, and magnetic properties of the cobalt(II) 1,3,5-benzenetricarboxylate layered coordination polymer]. *Izvestiia Rossiiskoi akademii nauk. Seriya khimicheskaya — Bulletin of the Russian Academy of Sciences. Chemical series*, 56 (9), 1782–1786. <https://doi.org/10.1007/s11172-007-0277-8> [in Russian].
- 26 Lu, H.-S., Bai, L., Xiong, W.-W., Li, P., Ding, J., Zhang, G., Wu, T., Zhao, Y., Lee, J.-M., Yang, Y., Geng, B., & Zhang, Q. (2014). Surfactant media to grow new crystalline cobalt 1,3,5-benzenetricarboxylate metal-organic frameworks. *Inorg. Chem.*, 53 (16), 8529–8537. <https://doi.org/10.1021/ic5011133>
- 27 Neff, H., Laborde, H.M., & Lima, A.M.N. (2016). Periodic protein adsorption at the gold/biotin aqueous solution interface: evidence of kinetics with time delay. *Sci. Rep.*, 6, 36232. <https://doi.org/10.1038/srep36232>
- 28 Dzhardimalieva, G., Baimuratova, R., Knerelman, E., Davydova, G., Kudaibergenov, S., Kharissova, O., Zhinzhiro, V., & Uflyand, I. (2020). Synthesis of copper(II) trimesinate coordination polymer and its use as a sorbent for organic dyes and a precursor for nanostructured material. *Polymers*, 12 (5), 1024. <https://doi.org/10.3390/polym12051024>.

- 29 Yaghi, O.M., Li, H., & Groy, T.L. (1996). Construction of porous solids from hydrogen-bonded metal complexes of 1,3,5-benzenetricarboxylic acid. *J. Am. Chem. Soc.*, 118 (38), 9096–9101. <https://doi.org/10.1021/ja960746q>.
- 30 Wang, S., Boyjoo, Y., & Choueib, A. (2005). A comparative study of dye removal using fly ash treated by different methods. *Chemosphere*, 60 (10), 1401–1407. <https://doi.org/10.1016/j.chemosphere.2005.01.091>.
- 31 Hameed, B.H., Krishni, R.R., & Sata, S.A. (2009). A novel agricultural waste adsorbent for the removal of cationic dye from aqueous solutions. *J. Hazard. Mater.*, 162 (1), 305–311. <https://doi.org/10.1016/j.jhazmat.2008.05.036>
- 32 Hamdaoui, O. (2006). Batch study of liquid-phase adsorption of methylene blue using cedar sawdust and crushed brick. *J. Hazard. Mater.*, (135), 264–273. <https://doi.org/10.1016/j.jhazmat.2005.11.062>
- 33 Halsey, G.D. (1952). The role of surface heterogeneity in adsorption. *Adv. Catal.*, 4, 259–269. [https://doi.org/10.1016/S0360-0564\(08\)60616-1](https://doi.org/10.1016/S0360-0564(08)60616-1).
- 34 Dada, A. O., Olalekan, A. P., Olatunya, A. M., & Dada, O. (2012). Langmuir, Freundlich, Temkin and Dubinin-Radushkevich isotherms studies of equilibrium sorption of Zn²⁺ unto phosphoric acid modified rice husk. *IOSR J. Appl. Chem.*, 3 (1), 38–45. <https://doi.org/10.9790/5736-0313845>
- 35 Simonin, J.-P. (2016). On the comparison of pseudo-first order and pseudo-second order rate laws in the modeling of adsorption kinetics. *Chem. Eng. J.*, (300), 254–263. <https://doi.org/10.1016/j.cej.2016.04.079>.

Information about authors *

Zhinzhilo, Vladimir Anatolievich — Candidate of Chemical Sciences, Senior Lecturer, Chemistry Department, Southern Federal University, Zorge Str. 7, Rostov-on-Don 344090, Russian Federation; e-mail i06993@yandex.ru; <http://orcid.org/0000-0001-8423-7205>;

Litvinova, Alena Yurievna — 5th year student, Chemistry Department, Southern Federal University, Zorge Str. 7, Rostov-on-Don 344090, Russian Federation; e-mail: chemist01@mail.ru; <https://orcid.org/0000-0003-1416-4754>;

Lyamina, Veronika Mikhailovna — 5th year student, Chemistry Department, Southern Federal University, Zorge Str. 7, Rostov-on-Don 344090, Russian Federation; e-mail: veronichka.lyamina@yandex.ru; <https://orcid.org/0000-0001-5834-6600>

Dzhardimalieva, Gulzhian Iskakovna (*corresponding author*) – Doctor of Chemical Sciences, Head of Laboratory of Metallopolymers, Institute of Problems of Chemical Physics Russian Academy of Sciences, Chernogolovka, Moscow Region, and Professor of Moscow Aviation Institute (National Research University), Moscow, Russia; e-mail: dzhardim@icp.ac.ru; <https://orcid.org/0000-0002-4727-8910>;

Uflyand, Igor Efimovich — Doctor of Chemical Sciences, Professor, Chemistry Department, Southern Federal University, Zorge Str. 7, Rostov-on-Don 344090, Russian Federation; e-mail: ieuflyand@sfedu.ru; <http://orcid.org/0000-0002-7164-8168>

*The author's name is presented in the order: *Last Name, First and Middle Names*

A. Houbi^{1, 2*}, A.A. Zharmenov^{1, 2}, Y. Atassi³,
Z.T. Bagasharova^{1, 2}, S. Mirzalieva^{1, 2}, B.A. Karibayev⁴

¹National Center on Complex Processing of Mineral Raw Materials of the Republic of Kazakhstan, Almaty, Kazakhstan;

²Department of Chemical Technology of Inorganic Substances, Al-Farabi Kazakh National University, Almaty, Kazakhstan;

³Department of Applied Physics, Higher Institute for Applied Sciences and Technology, Damascus, Syria;

⁴Department of Physics and Technology, Al-Farabi Kazakh National University, Almaty, Kazakhstan

(*Corresponding author's e-mail: Anashoubi@gmail.com)

Synthesis and Microwave Absorption Properties of Ni_{0.5}Zn_{0.5}Fe₂O₄/CI Composite Coated with Polyaniline within Paraffin Wax Matrix

Ternary composites of polyaniline/Ni_{0.5}Zn_{0.5}Fe₂O₄/carbonyl iron (PANI/F/CI) are prepared via two stages. Firstly, Ni_{0.5}Zn_{0.5}Fe₂O₄ is prepared using a sol-gel method. After that, PANI/F/CI composites are prepared using an in-situ polymerization technique of PANI in the existence of the Ni_{0.5}Zn_{0.5}Fe₂O₄ and CI. X-ray diffractometry (XRD), Fourier transform infrared (FTIR) spectroscopy, Ultraviolet-visible (UV-vis) spectroscopy, and Thermogravimetric analysis (TGA) are utilized to characterize samples. The morphology of the powders is investigated by Scanning electron microscope (SEM). The electromagnetic interference (EMI) shielding and microwave absorption (MA) properties are measured in the frequency band of 8.8–12 GHz to investigate the microwave characterization. The results refer those microwave absorption properties are related to the absorber thickness and the loading ratio of the absorber within a paraffin matrix. Minimal reflection loss of –30.8 dB at the matching frequency (f_m) of 10.3 GHz and the absorption bandwidth under –10 dB (BW_{-10dB}) of 2.8 GHz for 3.4 mm thickness with a surface density (SD) of 3.38 kg/m² are noticed for the PANI/F/CI composite sample. The maximum shielding efficiency (SE) of 30.12 dB at 11.0 GHz for 3.2 mm thickness is observed for the PANI/F/CI composite sample.

Keywords: polyaniline, carbonyl iron, composites, lightweight microwave absorber, reflection loss, absorption bandwidth, shielding efficiency, matching frequency.

Introduction

Recent environmental pollution issues are appearing because of the quick evolution of electronic devices, involving smartphones, laptops, and intelligent devices. Electronic apparatuses emit undesirable EM waves, generating electromagnetic interference between various electronic apparatuses with a negative effect on their performance. Consequently, the disposal of EM waves resulting from EMI effectively is so important both for public protection security and electronic safety. Generally, there are two kinds of materials to absorb EM waves: firstly, magnetic loss materials such as hexagonal ferrites, spinel ferrites, and carbonyl iron, secondly, dielectric loss materials such as conductive polymers (e.g., polyaniline, polypyrrole) and carbonaceous materials (e.g., carbon black, activated carbon, carbon fibers, graphene) which have played a significant role for high-frequency EM wave absorption. Nevertheless, the drawbacks involving elevated density, low reflection absorption, and narrow wideband have hugely limited conventional loss materials' workable benefits for EM wave absorption [1, 2]. In recent years, microwave absorption composites based on polyaniline, ferrite, and carbonyl iron have obtained significant attention due to their excellent electrical and ferrimagnetic characteristics. Polyaniline-based composites have pulled in major attention for microwave absorption lately. Polyaniline is usually used to fit the requirements of high-effective microwave attenuation materials because of its superior characteristics, for example, low density, high permittivity, unique electronic conductivity, etc. Polyaniline has a unique place in the band of elevated-frequency microwave absorption materials (MAMs). Furthermore, spinel ferrites and carbonyl iron have excellent MA characteristics due to their unique magnetic characteristics. NiZn ferrites and carbonyl iron are considered suitable materials for high-frequency implementations [3, 4]. When NiZn ferrite and carbonyl iron are mixed with Polyaniline, the MA characteristics of the resultant composite are anticipated to enhance. According to this, PANI/NiZn ferrite microwave absorbers in the frequency range of 2–40 GHz were successfully prepared by Ting et al. [3].

The absorbers are prepared by dispersing PANI/NiZn ferrite nanocomposites with a weight ratio of 67% w/w within an epoxy resin matrix. The results indicated that by increasing polyaniline content in NiZn ferrite, a wide absorption frequency range could be obtained. Didehban et al. have designed microwave absorbers in the frequency band of 8–12 GHz based on NiZn ferrite-PANI (35:65) nanocomposites. The absorbers are formed by dispersing PANI/NiZn ferrite within an epoxy resin matrix of 20 w/w. The results have shown that the absorber had a RL_{\min} of -20 dB at 9.1 GHz and the absorption $BW_{-10\text{dB}}$ was 0.5 GHz for 2 mm thickness [5]. Wang et al. have designed absorbers in the frequency band of 2–8 GHz based on NiZn Ferrite/PANI (1:3) nanocomposites. The absorbers are formed by dispersing PANI/NiZn ferrite within a paraffin matrix of 75 w/w. The absorbers were prepared by the in-situ polymerization method. The results displayed that RL_{\min} was -32 dB at 9.5 GHz and the absorption $B.W_{-10\text{dB}}$ was 3.8 GHz [6]. Wang et al. have reported the MA properties of a one-dimensional uniform PANI/NiZn ferrite hybrid nanorods within a paraffin matrix of 70 % w/w in the frequency range of 2–18 GHz. They have found that the absorbers had broadband, and minimal reflection loss, where the results have indicated that the absorber had a RL_{\min} of -27.5 dB at 6.2 GHz and the absorption $BW_{-10\text{dB}}$ was 3 GHz for 2 mm thickness [7]. Wang et al. have designed absorbers in the frequency band of 2–18 GHz based on NiZn Ferrite/PANI nanocomposites. The absorbers were prepared by hydrothermal method. The results displayed that RL_{\min} was -17 dB at 11.1 GHz and the absorption $B.W_{-10\text{dB}}$ was 5 GHz [8]. Ma et al. have reported the MA properties of PANI/ $\text{Co}_{0.5}\text{Zn}_{0.5}\text{Fe}_2\text{O}_4$ nanocomposite. The MA properties were studied in the 8.2-26.5 GHz range. The absorbers were synthesized by the in-situ polymerization technique. They have found that the absorbers had broadband, and minimal reflection loss, where the results have indicated that the absorber had a RL_{\min} of -39.9 dB at 22.4 GHz and the absorption $BW_{-10\text{dB}}$ was 5 GHz for 2 mm thickness [9].

The aim of the study is to design lightweight and wide band absorbers with loading ratios not exceeding 35% with enhanced RL based on PANI/F/CI nanocomposites. The ferrite is prepared by the sol-gel method. Then, the aniline monomer is polymerized by the in-situ polymerization technique in the presence of NiZn ferrite and carbonyl iron. The prepared samples are characterized by XRD, FTIR spectroscopy, UV-vis spectroscopy and TGA. The morphologies of the ferrite and its nanocomposites are identified using SEM. The EMI shielding and MA properties are studied by measuring the minimal reflection loss, absorption bandwidth under -10 dB, and shielding efficiency of the absorbers in the frequency band of 8.8–12 GHz to achieve functional characterization. To the best of the authors' knowledge, the optimization of the performance of the current PANI/F/CI nanocomposites in terms of lightweight and wide bandwidth has not been reported before.

Experimental

Chemicals: Sodium dodecyl sulfate (SDS, 92.2 % purity), ammonium persulfate (APS, 95.3 % purity), nickel (II) nitrate hexahydrate ($\text{Ni}(\text{NO}_3)_2 \cdot 6\text{H}_2\text{O}$, 98.3 % purity), zinc nitrate hexahydrate ($\text{Zn}(\text{NO}_3)_2 \cdot 6\text{H}_2\text{O}$, 98.7% purity), and iron (III) nitrate nonahydrate ($\text{Fe}(\text{NO}_3)_3 \cdot 9\text{H}_2\text{O}$, 98.2 % purity) were purchased from TRADING COMPANY ANT, Russia. As well, Aniline monomer ($\text{C}_6\text{H}_5\text{NH}_2$, 99.5 % purity), Ammonium hydroxide (NH_4OH , 99.8 % purity), Citric acid ($\text{C}_6\text{H}_8\text{O}_7$, 99.0% purity) were purchased from Sigma Aldrich Company, Germany. On the other hand, carbonyl iron (CI, 99.6% purity) was purchased from Cabot Norit Company, Netherland.

Instruments used: A powder X-ray diffractometer (XRD, Rigaku Miniflex 600, Cu-Ka) is utilized for defining the crystal structures of the powders. Fourier Transform IR (FTIR) spectra are recorded on a Perkin Elmer spectrum 65 FTIR spectrometer in the range of 400–4000 cm^{-1} . The UV-vis absorption spectra of the samples (dispersed in dimethylformamide (DMF)) are recorded using the LAMBDA 365 UV-vis spectrophotometer in the range of 250–900 nm. Thermogravimetric analysis (TGA) is done utilizing a thermal analyzer (NETZSCH 449F3A-0372-M) under a nitrogen atmosphere, from room temperature to 1000 °C under constant heating rate of 10 °C/min. A scanning electron microscope (FEI Quanta 200 3D) is utilized for defining the morphology of the powders. Finally, energy-dispersive X-ray spectroscopy (EDX, Quanta 200 3D) is utilized to know the chemical composition of prepared samples.

The microwave absorption properties of the prepared samples are calculated by using the horn antenna connected to an oscilloscope (AKTAKOM ADS-2221M).

Methodology

1. Preparation of PANI/F/CI

Ferrite ($\text{Ni}_{0.5}\text{Zn}_{0.5}\text{Fe}_2\text{O}_4$) nanoparticles were prepared by a sol-gel method as illustrated in the following literature [10–14]. On the other hand, carbonyl iron powder was milled for 12 h at 300 rpm via the grinding

balls to obtain fine powders. NiZn ferrite and carbonyl iron were coated with polyaniline via the in-situ polymerization technique. Firstly, 6 g (90 % F and 10 % CI) was added to 100 ml distilled water under mechanical stirring at a speed of 250 rpm for 30 minutes. 3 g sodium dodecyl sulfate (SDS) and aniline were added to the solution while keeping mechanical stirring for 1 h. After that, 1 M HCl solution 80 mL was added to the solution under stirring for 1 h. Finally, 8.5 g APS was dissolved in 100 ml of an aqueous solution which was utilized as an oxidizing agent and added slowly dropwise into the solution to start the polymerization. The polymerization was allowed to proceed for 6 h with stirring in an ice bath. The resulting composite was filtered and washed many times with distilled water and ethanol, and then dried for 8 h in the furnace at 70 °C. The weight ratio of aniline/(F-CI) (1/1) was synthesized. Pure polyaniline was synthesized in a similar way but without NiZn ferrite and carbonyl iron solution for comparison purposes.

2. Preparation of samples for measuring the MA and EMI shielding properties

Microwave absorption and electromagnetic interference shielding properties of the samples were estimated with the free-space technique. According to this, 30–35 % w/w of the coated composites were dispersed in a paraffin wax matrix by heating and stirring for 15 min. Thereafter, the single-layer samples were molded to the dimensions of 100×100 mm to measure RL and SE in the frequency band of 8.8–12 GHz.

Results and Discussion

XRD patterns

Figure 1 demonstrates the XRD patterns of $\text{Ni}_{0.5}\text{Zn}_{0.5}\text{Fe}_2\text{O}_4$, CI, PANI/F/CI composite and PANI. For the $\text{Ni}_{0.5}\text{Zn}_{0.5}\text{Fe}_2\text{O}_4$ pattern, six diffraction peaks are noticed at 2θ values of 30.04° , 35.44° , 43.12° , 53.68° , 57.18° , and 62.14° , which conforms to (hkl) planes of (220), (311), (400), (422), (511) and (440), respectively. The ideal spinel structure is noticed by the peaks of NiZn ferrite [15]. The XRD pattern of $\text{Ni}_{0.5}\text{Zn}_{0.5}\text{Fe}_2\text{O}_4$ is matched with the reference XRD patterns (JCPDS, PDF no. 08–0234). The size of the NiZn ferrite grain ($2\theta = 35.44^\circ$) has been evaluated with Scherrer's equation, $D = 0.9 \lambda / \beta \cos\theta$, where D is the crystallite size (nm), λ is the X-ray wavelength, β is the bandwidth at half-height, and θ is the diffraction angle in degree. The calculated crystallite size of the NiZn ferrite is 27.6 nm. On the other hand, for the carbonyl iron pattern, three characteristic peaks are noticed at 2θ values of 44.61° , 64.92° and 82.33° , which conform to (hkl) planes of (100), (200), and (211), respectively. The XRD pattern of carbonyl iron resembles crystallites in which the sample mainly contains α -Fe phase [16]. All the observed peaks of CI are matched with the standard XRD pattern (JCPDS, PDF no. 06-0696). The characteristic peaks of the PANI/F/CI composite show matching the characteristic peaks of $\text{Ni}_{0.5}\text{Zn}_{0.5}\text{Fe}_2\text{O}_4$ as mentioned above. The XRD pattern of the pure PANI (Figure 1) displays an amorphous structure with two characteristic peaks at 20.22° and 25.36° which are attributed to the periodicity parallel to the polymer chains of PANI [17,18]. The XRD patterns of the PANI/F/CI composite (Figure 1) display crystalline peaks because of the existence of NiZn ferrite in this composite. The two characteristic peaks of the PANI disappeared due to the $\text{Ni}_{0.5}\text{Zn}_{0.5}\text{Fe}_2\text{O}_4$ nanoparticles [19, 20].

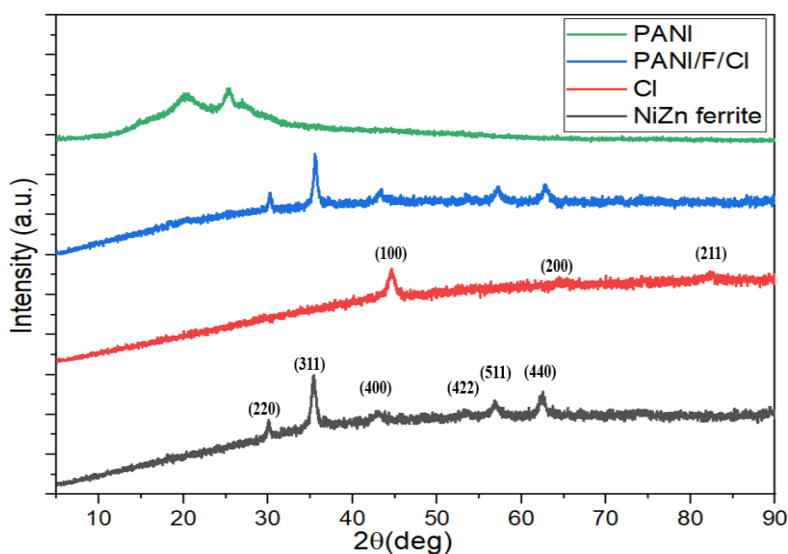


Figure 1. XRD patterns of $\text{Ni}_{0.5}\text{Zn}_{0.5}\text{Fe}_2\text{O}_4$, CI, PANI/F/CI composite and pure PANI

FTIR spectra

Figure 2 shows the FTIR spectra of the $\text{Ni}_{0.5}\text{Zn}_{0.5}\text{Fe}_2\text{O}_4$, CI, PANI/F/CI composite and PANI. For the $\text{Ni}_{0.5}\text{Zn}_{0.5}\text{Fe}_2\text{O}_4$ nanoparticles, two peaks at 563.1 cm^{-1} and 430.2 cm^{-1} are referring to the stretching vibration of (Fe–O), which emphasizes the formation of the metal-oxygen in ferrite-based [21]. In addition to that, the peak at 1630.4 cm^{-1} in $\text{Ni}_{0.5}\text{Zn}_{0.5}\text{Fe}_2\text{O}_4$, and CI is referring to C=O stretching vibration, and the peaks at 2348 cm^{-1} and 3452 cm^{-1} are referring to O–H stretching vibration [22, 23]. On the other hand, the characteristic peaks of PANI and PANI/F/CI composite are similar and they exhibited peaks at 1568 cm^{-1} , 1489 cm^{-1} , 1298 cm^{-1} , 1238 cm^{-1} , 1113 cm^{-1} , and 800 cm^{-1} [24, 25]. The characteristic peaks at 1568 and 1489 cm^{-1} are attributed to the C=N and C=C stretching modes of vibration for the quinonoid and benzenoid units of the polymer. The characteristic peaks at 1298 and 1238 cm^{-1} are related to N–H bending and asymmetric C–H stretching of the benzenoid ring, respectively. Finally, the characteristic peaks at 1113 cm^{-1} and 800 cm^{-1} are ascribed to the vibration mode of N=Q=N and the out-of-plane stretching vibration of C–H, respectively [19, 20]. In addition to that, the characteristic peak at 563.1 cm^{-1} of PANI/F/CI composite shows matching the characteristic peak of $\text{Ni}_{0.5}\text{Zn}_{0.5}\text{Fe}_2\text{O}_4$ as mentioned above. This indicates the stretching vibration of (Fe–O), which confirms the formation of the metal-oxygen in PANI/F/CI.

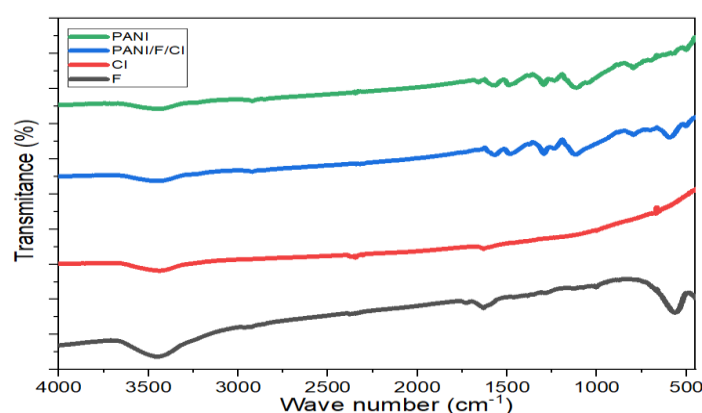


Figure 2. FTIR spectra of $\text{Ni}_{0.5}\text{Zn}_{0.5}\text{Fe}_2\text{O}_4$, CI, PANI/F/CI composite and pure PANI

UV-visible spectra

Figure 3 illustrates the UV–visible spectrum of the PANI and PANI/F/CI composite. For PANI, two characteristic peaks at around 302 nm and 629 nm are observed. The characteristic peak around 302 nm is ascribed to $\pi\text{--}\pi^*$ transition of the benzenoid ring and the characteristic peak around 629 nm is attributed to the benzenoid-to-quinoid excitonic transition [17, 26]. It can be seen that the characteristic peaks of PANI/F/CI composite show a clear red shift of 7 nm , as compared with that of polyaniline. The two characteristic peaks show the presence of PANI on the surface of $\text{Ni}_{0.5}\text{Zn}_{0.5}\text{Fe}_2\text{O}_4$ and carbonyl iron. These results may refer to the $\sigma\text{--}\pi$ interaction among $\text{Ni}_{0.5}\text{Zn}_{0.5}\text{Fe}_2\text{O}_4$, carbonyl iron and polyaniline backbone, which leads to the energy of the antibonding orbital decrease, the energy of the $\pi\text{--}\pi^*$ transition of the benzenoid and quinoid ring decreases, so the characteristic peaks of the composite show a red shift [26].

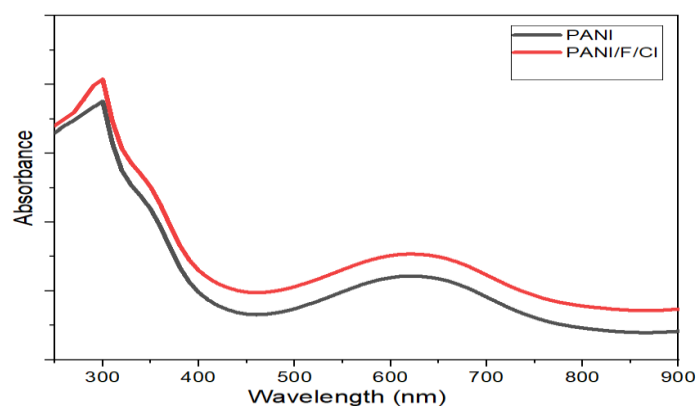


Figure 3. UV spectra of PANI and PANI/F/CI composite.

TGA analysis

Figure 4 shows the TGA curves of the $\text{Ni}_{0.5}\text{Zn}_{0.5}\text{Fe}_2\text{O}_4$, PANI/F/CI composite and PANI. For the $\text{Ni}_{0.5}\text{Zn}_{0.5}\text{Fe}_2\text{O}_4$ nanoparticles, no mass loss was noticed over the whole temperature range. PANI loses 4.87 % of its weight in the range of 110–130 °C because of the evaporation of moisture in the PANI. The thermal decomposition of the PANI is shown in the range of 230–1000 °C and has a big weight loss of 65.12 %. On the other hand, PANI/F/CI composite loses about 2.21 % of its weight in the range of 110–130 °C which is due to the evaporation of moisture in the composite. The thermal decomposition of the PANI/F/CI composite is shown in the range of 240–870 °C and has a big weight loss of 46.28 %.

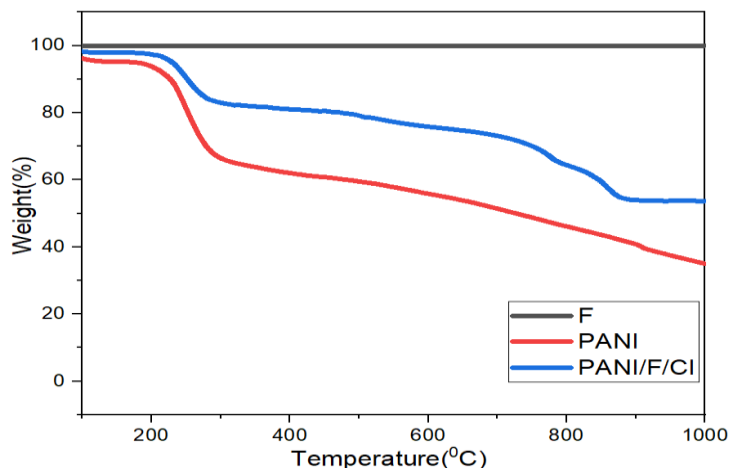


Figure 4. TGA thermograms of $\text{Ni}_{0.5}\text{Zn}_{0.5}\text{Fe}_2\text{O}_4$, PANI/F/CI composite and pure PANI

Morphology investigations

Figure 5 designates the morphology of the $\text{Ni}_{0.5}\text{Zn}_{0.5}\text{Fe}_2\text{O}_4$, CI, PANI and PANI/F/CI composite. The agglomerated spherical particles of NiZn ferrite and the spherical particles of carbonyl iron (Figure 5a, b) are observed with average diameters to be ranging between 27–63 nm and 0.2–2.4 μm , respectively. While a combination of rough surface sheets and short rods connected to each other of PANI is noticed (Figure 5c), distributed in the range between 60–220 nm. On the other hand, after coating with polyaniline, a continued overlayer of PANI is created on the CI and $\text{Ni}_{0.5}\text{Zn}_{0.5}\text{Fe}_2\text{O}_4$ nanoparticles' surface (Figure 5d).

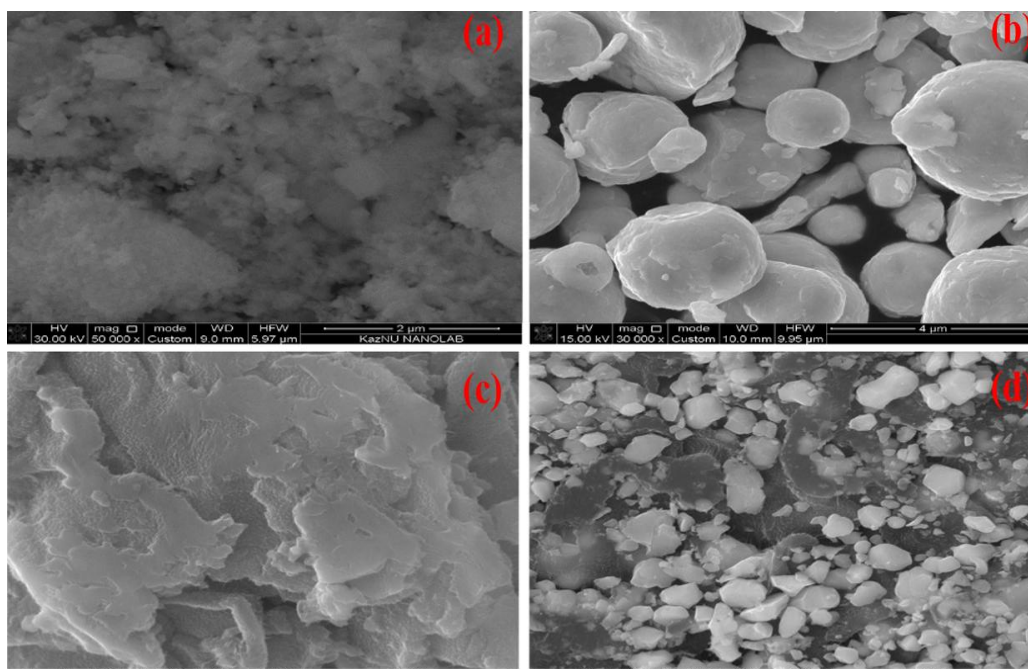


Figure 5. SEM images of (a) $\text{Ni}_{0.5}\text{Zn}_{0.5}\text{Fe}_2\text{O}_4$, (b) CI, (c) PANI and (d) PANI/F/CI composite

Energy-dispersive X-ray spectroscopy (EDX) analysis

Figure 6 and Table 1 present the energy-dispersive X-ray spectroscopy (EDX) analysis of $\text{Ni}_{10.5}\text{Zn}_{0.5}\text{Fe}_2\text{O}_4$, PANI and PANI/F/CI composite. The presence of C, O, Cl, S, Fe, Ni, Al, and Zn elements in the NiZn ferrite EDX spectrum is noticed. On the other hand, the presence of C, O, S and Cl elements in the PANI EDX spectrum is found. The presence of elemental Cl and S can be attributed to doping agents' hydrochloric acid and sodium dodecyl sulfate. Finally, the presence of C, O, Cl, S, Fe, Zn, Al, and Ni elements in the PANI/F/CI composite EDX spectrum is observed.

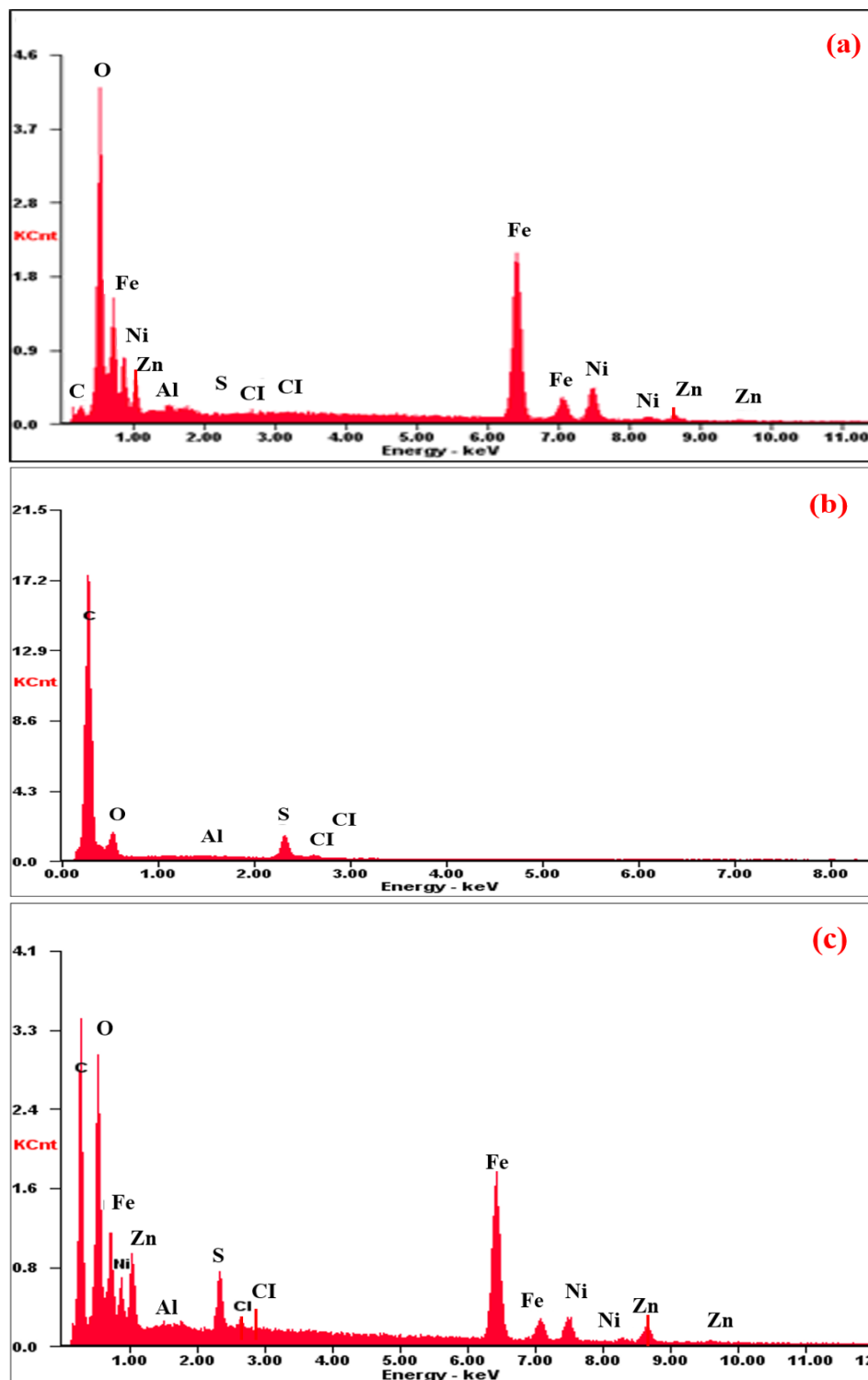


Figure 6. EDX of (a) $\text{Ni}_{10.5}\text{Zn}_{0.5}\text{Fe}_2\text{O}_4$, (b) PANI and (c) PANI/F/CI composite

EDX element composition of $\text{Ni}_{0.5}\text{Zn}_{0.5}\text{Fe}_2\text{O}_4$, PANI and PANI/F/CI composite

Element	C	Cl	O	S	Al	Fe	Ni	Zn
Ferrite (wt %)	3.30	0.13	19.26	0.02	0.41	53.02	13.04	10.82
PANI (wt %)	84.52	0.45	11.81	3.17	0.05	0	0	0
PANI/F/CI (wt %)	51.72	0.51	19.23	2.02	0.08	17.15	5.32	3.97

MA and EMI shielding properties

MA and EMI shielding properties of the prepared samples are estimated with the free-space technique as illustrated in the following literature [27–31]. SE is calculated for the EMI shielding by applying the equation (1) [32]:

$$SE (dB) = SE_R + SE_A + SE_M = 10 \log \frac{P_{in}}{P_T}, \quad (1)$$

where P_{in} and P_T — the incident power and transmitted power of the EM waves, respectively.

It is significant to note that the multiple reflection loss (SE_M) can be ignored if the absorption shielding (SE_A) of EMI shielding material is higher than 10 dB and equation (1) then can be rewritten as [32]:

$$SE (dB) = SE_R + SE_A = 10 \log \frac{P_{in}}{P_T}. \quad (2)$$

The shielding by reflection (SE_R) is calculated for the EMI shielding by applying the equation (3):

$$SE_R (dB) = -10 \log(1 - R) = -10 \log \left(1 - \frac{P_{ref}}{P_{in}} \right). \quad (3)$$

The shielding by absorption (SE_A) is calculated by equation (4) [33, 34]:

$$SE_A (dB) = -10 \log \left(\frac{T}{1 - R} \right) = -10 \log \left(\frac{P_T}{P_{in} - P_{ref}} \right), \quad (4)$$

where P_{ref} — the reflected power of the EM waves.

On the other hand, RL is calculated for the MA by applying the equation (5) [33, 34]:

$$RL (dB) = 10 \log \frac{P_{in}}{P_{ref}}. \quad (5)$$

Influence of the incorporation of $\text{Ni}_{0.5}\text{Zn}_{0.5}\text{Fe}_2\text{O}_4$, CI and PANI on the RL and the SE

EMI shielding and MA properties of the $\text{Ni}_{0.5}\text{Zn}_{0.5}\text{Fe}_2\text{O}_4$, CI, PANI and PANI/F/CI composite are studied. The results of this investigation are exhibited in Figures 7, 8 and Table 2. Figures 7, 8 illustrate the changing of the RL and SE as a function of the EM wave frequency for $\text{Ni}_{0.5}\text{Zn}_{0.5}\text{Fe}_2\text{O}_4$, CI, PANI and PANI/F/CI composite. The absorption of samples with specified thickness at 3.2 mm is molded to measure RL and SE in the frequency band of 8.8–12.0 GHz. As illustrated in Figures 7, 8, a weak reflection loss and low shielding efficiency for the $\text{Ni}_{0.5}\text{Zn}_{0.5}\text{Fe}_2\text{O}_4$ and CI are noticed. On the other hand, for the pure PANI, the reflection loss is in the range between 6.6–8.5 dB and the shielding efficiency is in the range between 9.8–12.9 dB. Furthermore, when PANI is incorporated with ferrite which is mixed with carbonyl iron, the reflection loss increases to –25.8 dB at 11.3 GHz for PANI/F/CI composite and the shielding efficiency increases to 30.12 dB at 11.0 GHz. Table 2 shows the reasonable surface density (SD) of all the prepared absorbers. As a result, one can notice the impact of incorporating $\text{Ni}_{0.5}\text{Zn}_{0.5}\text{Fe}_2\text{O}_4$ and CI (magnetic loss materials) and PANI (dielectric loss material) on the EMI and MA properties of the prepared absorber. This incorporation leads to an effective and low thickness absorber with a wide $\text{BW}_{-10\text{dB}}$ [35]. Figure 9 shows the SE_R and SE_A of the $\text{Ni}_{0.5}\text{Zn}_{0.5}\text{Fe}_2\text{O}_4$, CI, PANI and PANI/F/CI composite with a thickness of 3.2 mm at the frequency of 11.0 GHz.

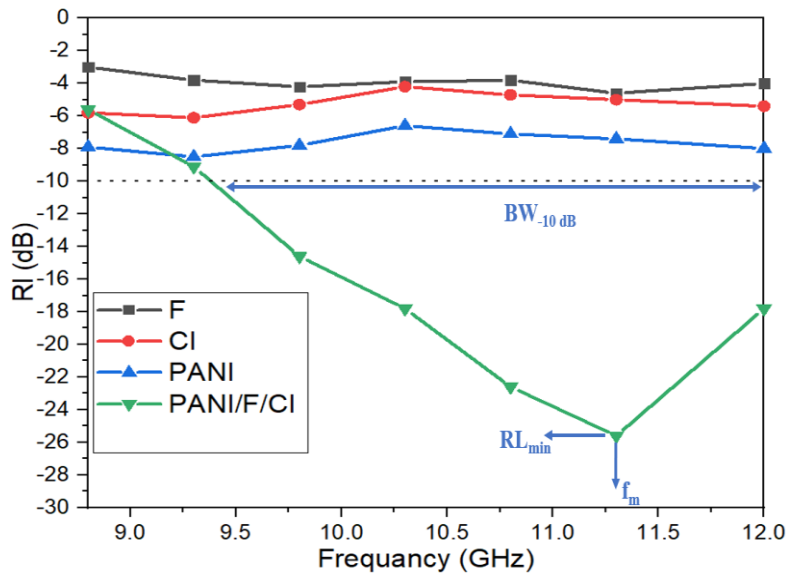


Figure 7. RL curves of $\text{Ni}_{0.5}\text{Zn}_{0.5}\text{Fe}_2\text{O}_4$, CI, PANI and PANI/F/CI composite at 3.2 mm thickness

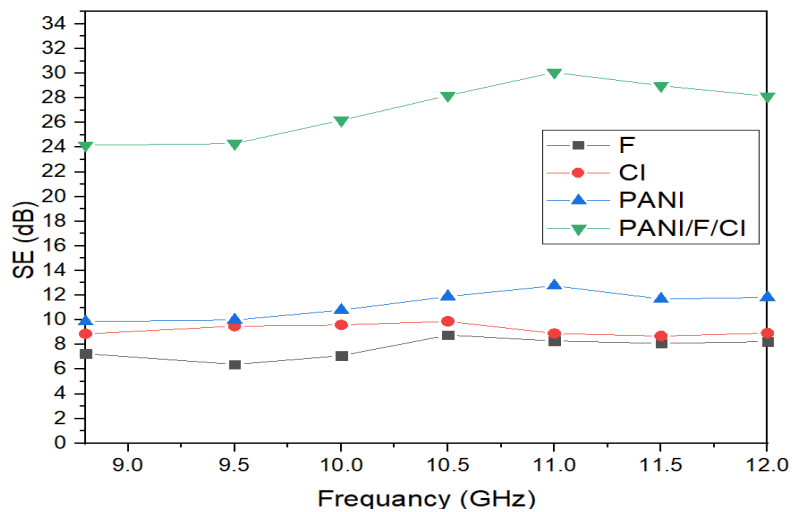


Figure 8. SE curves of $\text{Ni}_{0.5}\text{Zn}_{0.5}\text{Fe}_2\text{O}_4$, CI, PANI and PANI/F/CI composite at 3.2 mm thickness.

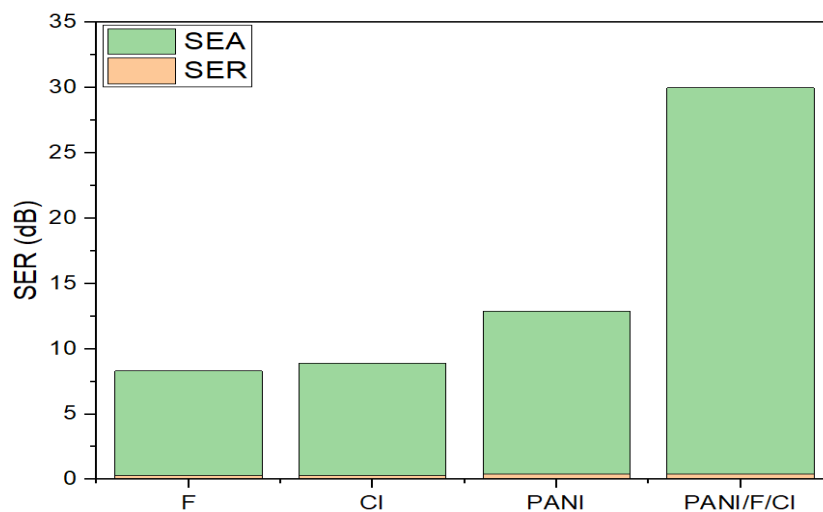


Figure 9. Bar plot for individual components of SE_R and SE_A of $\text{Ni}_{0.5}\text{Zn}_{0.5}\text{Fe}_2\text{O}_4$, CI, PANI and PANI/F/CI composite with a thickness of 3.2 mm at the frequency of 11.0 GHz

Table 2

MA behavior of Ni_{0.5}Zn_{0.5}Fe₂O₄, CI, PANI and PANI/F/CI composite at 3.2 mm thickness

Samples	RL _{min} (dB)	f _m (GHz)	BW _{-10dB} (GHz)	SD (kg/m ²)
Ni _{0.5} Zn _{0.5} Fe ₂ O ₄	-4.6	-	-	4.56
CI	-6.5	-	-	5.21
PANI	-8.5	-	-	2.25
PANI/F/CI	-25.7	11.3	2.6	3.31

Influence of the PANI/F/CI composite thickness and loading ratio on the RL

Figure 10 illustrates the RL of PANI/F/CI composite with various thicknesses (3.2, 3.4, 3.6 mm) at the various weight ratios of the absorber within a paraffin matrix (30, 35 % w/w). It can be seen that the RL attenuation peaks of samples moved to lower frequencies with increasing sample thickness. This phenomenon may be defined by the quarter-wavelength ($\lambda/4$) cancellation model, as shown in equation (6) [36–38]:

$$t_m = \frac{c}{4f_m \sqrt{|\mu_r||\epsilon_r|}}, \tag{6}$$

where $|\epsilon_r|$ and $|\mu_r|$ are the modulus of the measured complex relative permittivity (ϵ_r) and permeability (μ_r) at matching frequency (f_m), respectively; c is the velocity of light.

It can be noticed from equation (6) that the f_m is inversely proportionate to the thickness of an absorber. On the other hand, one can notice the minimum reflection loss moves gradually to a lower frequency with the increase in weight ratios of the absorber within a paraffin matrix (Figure 10). Furthermore, Table 3 shows the PANI/F/CI composites have reasonable surface density, ranging from 3.31 to 3.40 kg/m², and wide bandwidth extending from 2.5 to 3.0 GHz. One can conclude that optimal absorption can be accomplished by modifying the absorber thickness and the loading ratio of the absorber within a paraffin matrix.

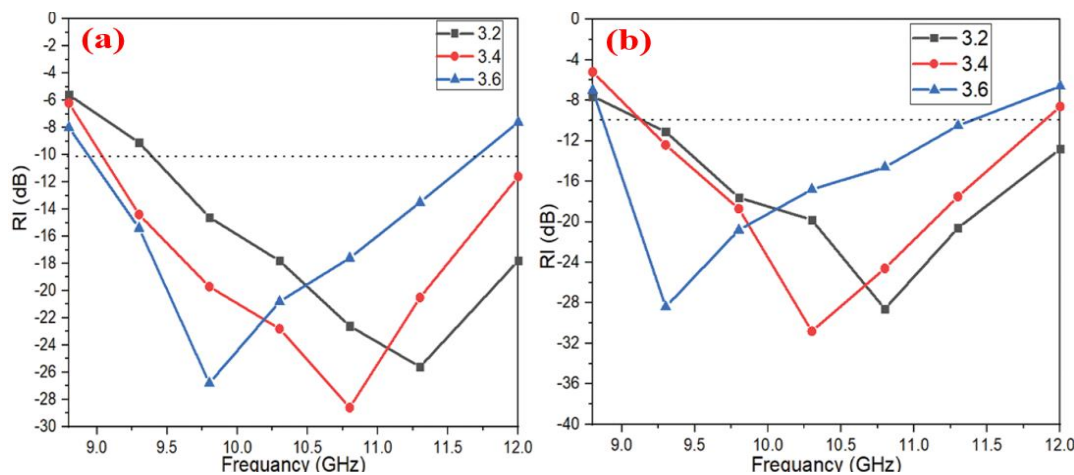


Figure 10. RL curves of PANI/F/CI composite with various thicknesses (3.2, 3.4, 3.6 mm) at the various weight ratios of the absorber within a paraffin matrix (a) 30 % and (b) 35 %

Table 3

MA behavior of PANI/F/CI composite at various thicknesses and various loading ratios within a paraffin matrix

Loading ratio %	t (mm)	RL _{min} (dB)	f _m (GHz)	BW _{-10dB} (GHz)	SD (kg/m ²)
30 %	3.2	-25.7	11.3	2.6	3.31
	3.4	-28.5	10.8	3.0	3.35
	3.6	-26.8	9.8	2.9	3.37
35 %	3.2	-28.6	10.8	2.5	3.33
	3.4	-30.8	10.3	2.8	3.38
	3.6	-28.4	9.3	2.6	3.40

To evaluate the beneficial impact of adding CI to the PANI/F on the microwave properties of the microwave absorber, Table 4 shows a comparison of MA properties of some lately reported PANI/NiZn ferrite absorbers with various loading ratios of the composites in the host matrix. Compared to PANI/NiZn ferrite absorbers reported by Ting et al. [3], Wang et al. and Wang et al. [7, 8], the current nanocomposite absorbers as-presented in this study display better MA in the frequency range of 8–12 GHz, lower loading ratio of the absorbers in the host matrix and relatively wider absorption bandwidth. However, the microwave absorber lately designed by Wang et al. [6] has comparable results with the current absorbers in terms of bandwidths and reflection losses, the lower loading ratios of the current absorbers are still an advantage. On the other hand, Didehban et al. designed absorbers with a low loading ratio similar to the ratio used in this study [5]. Although, the microwave properties of the current composites possess better reflection losses and larger bandwidths comparable with the result presented by Didehban et al. [5].

Table 4

Comparison of MA behavior of the current composites with similar absorbers in the literature

Specimen (relative weight ratio)/ host matrix	Loading percentage in the host matrix (%)	t (mm)	RL _{min} (dB)	f _m (GHz)	BW _{-10dB} (GHz)
PANI/F/CI/ Paraffin (current work)	30	3.4	-28.5	10.8	3.0
	35	3.4	-30.8	10.3	2.8
NiZn ferrite-PANI(50:50)/Epoxy [3]	67	2.00	-14	11.0	2.6
NiZn ferrite-PANI(35:65)/Epoxy [5]	20	2.00	-20	9.1	0.5
NiZn ferrite-PANI(1:3)/Paraffin [6]	75	3.50	-32	9.5	3.8
NiZn ferrite-PANI(2:1)/Paraffin [7]	70	2.00	-27.5	6.0	3.0
NiZn ferrite-PANI/Epoxy [8]	67	3.00	-17	11.1	2.8

These results prove that adding CI to the PANI/F has a beneficial role in enhancing the microwave properties of the absorber: It becomes lighter with wide bandwidth.

Conclusions

In the current research, we succeeded in the preparation of wideband and lightweight PANI/F/CI ferrite microwave absorbers with low loading ratios in paraffin wax 30–35 % w/w. The composites were structurally characterized using X-ray diffractometry, FTIR spectroscopy, UV-vis spectroscopy, and TGA. The morphology of the composites was investigated by scanning electron microscopy. The functional characterization was accomplished by measuring the EMI shielding and MA properties. The results show that by adequate control of the loading ratio and thickness of the absorber, one can tailor the design of a wideband and lightweight absorber based on PANI/F/CI in the frequency band of 8.8–12 GHz. Minimal reflection loss of -30.8 dB at the matching frequency of 10.3 GHz and the absorption bandwidth under -10 dB of 2.8 GHz for 3.4 mm thickness with a surface density of 3.38 kg/m² were noticed for the PANI/F/CI microwave absorber. The maximum shielding efficiency of 30.12 dB at 11.0 GHz for 3.2 mm thickness was observed for the PANI/F/CI microwave absorber.

References

- Xie, X. B., Wang, B., Wang, Y., Ni, C., Sun, X., & Du, W. (2022). Spinel structured MFe₂O₄ (M = fe, co, ni, Mn, Zn) and their composites for microwave absorption: A Review. *Chemical Engineering Journal*, 428, 131160. <https://doi.org/10.1016/j.cej.2021.131160>
- Bera, P., Lakshmi, R. V., Prakash, B. H., Tiwari, K., Shukla, A., Kundu, A. K., Biswas, K., & Barshilia, H. C. (2020). Solution combustion synthesis, characterization, magnetic, and dielectric properties of CoFe₂O₄ and Co_{0.5}Mn_{0.5}Fe₂O₄ (M = Mn, Ni, and Zn). *Physical Chemistry Chemical Physics*, 22(35), 20087–20106. <https://doi.org/10.1039/d0cp03161e>
- Ting, T. H., Yu, R. P., & Jau, Y. N. (2011). Synthesis and microwave absorption characteristics of polyaniline/NiZn ferrite composites in 2–40 GHz. *Materials Chemistry and Physics*, 126(1-2), 364–368. <https://doi.org/10.1016/j.matchemphys.2010.11.011>
- Houbi, A., Aldashevich, Z. A., Atassi, Y., Bagasharova Telmanovna, Z., Saule, M., & Kubanych, K. (2021). Microwave absorbing properties of ferrites and their composites: A Review. *Journal of Magnetism and Magnetic Materials*, 529, 167839. <https://doi.org/10.1016/j.jmmm.2021.167839>

- 5 Didehban, K., Yarahmadi, E., Nouri-Ahangarani, F., Mirmohammadi, S. A., & Bahri-Laleh, N. (2015). Radar absorption properties of $\text{Ni}_{0.5}\text{Zn}_{0.5}\text{Fe}_2\text{O}_4/\text{pani}/\text{epoxy}$ nanocomposites. *Journal of the Chinese Chemical Society*, 62(9), 826–831. <https://doi.org/10.1002/jccs.201500136>
- 6 Wang, M., Ji, G., Zhang, B., Tang, D., Yang, Y., & Du, Y. (2015). Controlled synthesis and microwave absorption properties of $\text{Ni}_{0.6}\text{Zn}_{0.4}\text{Fe}_2\text{O}_4/\text{Pani}$ composite via an in-situ polymerization process. *Journal of Magnetism and Magnetic Materials*, 377, 52–58. <https://doi.org/10.1016/j.jmmm.2014.10.066>
- 7 Wang, C.-P., Li, C.-H., Bi, H., Li, J.-C., Zhang, H., Xie, A.-J., & Shen, Y.-H. (2014). Novel One-dimensional polyaniline/ $\text{Ni}_{0.5}\text{Zn}_{0.5}\text{Fe}_2\text{O}_4$ hybrid nanostructure: Synthesis, magnetic, and electromagnetic wave absorption properties. *Journal of Nanoparticle Research*, 16(3). <https://doi.org/10.1007/s11051-014-2289-2>
- 8 Wang, C., Shen, Y., Wang, X., Zhang, H., & Xie, A. (2013). Synthesis of novel NiZn-Ferrite/polyaniline nanocomposites and their microwave absorption properties. *Materials Science in Semiconductor Processing*, 16(1), 77–82. <https://doi.org/10.1016/j.mssp.2012.06.015>
- 9 Ma, R.T., Zhao, H.T., & Zhang, G. (2010). Preparation, characterization and microwave absorption properties of polyaniline/ $\text{Co}_{0.5}\text{Zn}_{0.5}\text{Fe}_2\text{O}_4$ nanocomposite. *Materials Research Bulletin*, 45(9), 1064–1068. <https://doi.org/10.1016/j.materresbull.2010.06.021>
- 10 Chen, N., & Gu, M. (2012). Microstructure and microwave absorption properties of γ -substituted Ni-Zn Ferrites. *Open Journal of Metal*, 02(02), 37–41. <https://doi.org/10.4236/ojmetal.2012.22006>
- 11 Almessiere, M. A., Slimani, Y., Trukhanov, A. V., Demir Korkmaz, A., Guner, S., Akhtar, S., Shirsath, S. E., Baykal, A., & Ercan, I. (2020). Effect of ND- γ co-substitution on structural, magnetic, optical and microwave properties of NICUZN nanospinel ferrites. *Journal of Materials Research and Technology*, 9(5), 11278–11290. <https://doi.org/10.1016/j.jmrt.2020.08.027>
- 12 Almessiere, M.A., Slimani, Y., Güngüneş, H., Kostishyn, V.G., Trukhanov, S.V., Trukhanov, A.V., & Baykal, A. (2020). Impact of Eu^{3+} ion substitution on structural, magnetic and microwave traits of Ni-Cu-Zn spinel ferrites. *Ceramics International*, 46(8), 11124–11131. <https://doi.org/10.1016/j.ceramint.2020.01.132>
- 13 He, J., Deng, L., Luo, H., He, L., Shan, D., Yan, S., & Huang, S. (2019). Electromagnetic matching and microwave absorption abilities of Ti_3SiC_2 encapsulated with $\text{Ni}_{0.5}\text{Zn}_{0.5}\text{Fe}_2\text{O}_4$ Shell. *Journal of Magnetism and Magnetic Materials*, 473, 184–189. <https://doi.org/10.1016/j.jmmm.2018.10.061>
- 14 Niu, B., Zhang, F., Ping, H., Li, N., Zhou, J., Lei, L., Xie, J., Zhang, J., Wang, W., & Fu, Z. (2017). Sol-gel autocombustion synthesis of nanocrystalline high-entropy alloys. *Scientific Reports*, 7(1). <https://doi.org/10.1038/s41598-017-03644-6>
- 15 El Nahrawy, A. M., Salah El-Deen, H., Soliman, A. A., & Mosa, W. M. M. (2018). Crystallographic and magnetic properties of Al^{3+} Co-doped $\text{NiZnFe}_2\text{O}_4$ nano-particles prepared by sol-gel process. *Egyptian Journal of Chemistry*. <https://doi.org/10.21608/ejchem.2018.4504.1397>
- 16 Bahri-Laleh, N., Didehban, K., Yarahmadi, E., Mirmohammadi, S. A., & Wang, G. (2017). Microwave absorption properties of polyaniline/carbonyl iron composites. *Silicon*, 10(4), 1337–1343. <https://doi.org/10.1007/s12633-017-9609-y>
- 17 Ezzati, S. N., Rabbani, M., Leblanc, R. M., Asadi, E., Ezzati, S. M., Rahimi, R., & Azodi-Deilami, S. (2015). Conducting, magnetic polyaniline/ $\text{Ba}_{0.25}\text{Sr}_{0.75}\text{Fe}_{11}(\text{Ni}_{0.5}\text{Mn}_{0.5})\text{O}_{19}$ nanocomposite: Fabrication, characterization and application. *Journal of Alloys and Compounds*, 646, 1157–1164. <https://doi.org/10.1016/j.jallcom.2015.05.146>
- 18 Meng, X., Zhu, Y., Xu, S., & Liu, T. (2016). Facile synthesis of shell-core polyaniline/SRFE12O19 composites and magnetic properties. *RSC Advances*, 6(6), 4946–4949. <https://doi.org/10.1039/c5ra22200a>
- 19 Ali, N. N., Atassi, Y., Salloum, A., Charba, A., Malki, A., & Jafarian, M. (2018). Comparative study of microwave absorption characteristics of (polyaniline/NiZn ferrite) nanocomposites with different ferrite percentages. *Materials Chemistry and Physics*, 211, 79–87. <https://doi.org/10.1016/j.matchemphys.2018.02.017>
- 20 Prasanna, G. D., Jayanna, H. S., Lamani, A. R., & Dash, S. (2011). Polyaniline/ CoFe_2O_4 nanocomposites: A novel synthesis, characterization and magnetic properties. *Synthetic Metals*, 161(21-22), 2306–2311. <https://doi.org/10.1016/j.synthmet.2011.08.039>
- 21 Kondawar, S. B., & Nandapure, A. I. (2014). Magnetic and electrical properties of zinc-substituted nickel ferrite reinforced conducting polyaniline nanocomposites. *Journal of the Chinese Advanced Materials Society*, 2(3), 186–198. <https://doi.org/10.1080/22243682.2014.934919>
- 22 Abdel Rahim, M. (2017). Carbon supported mono- and bi-metallic dispersed thin film catalysts for oxygen electro-reduction reaction in acid medium. *International Journal of Electrochemical Science*, 7890–7910. <https://doi.org/10.20964/2017.08.23>
- 23 Kim, S. Y., Kwon, S. H., Liu, Y. D., Lee, J.-S., You, C.-Y., & Choi, H. J. (2013). Core-shell-structured cross-linked poly(glycidyl methacrylate)-coated carbonyl iron microspheres and their magnetorheology. *Journal of Materials Science*, 49(3), 1345–1352. <https://doi.org/10.1007/s10853-013-7818-3>
- 24 Gairola, S. P., Verma, V., Kumar, L., Dar, M. A., Annapoorni, S., & Kotnala, R. K. (2010). Enhanced microwave absorption properties in polyaniline and nano-ferrite composite in X-band. *Synthetic Metals*, 160(21-22), 2315–2318. <https://doi.org/10.1016/j.synthmet.2010.08.025>
- 25 Li, G., Yan, S., Zhou, E., & Chen, Y. (2006). Preparation of magnetic and conductive NiZn ferrite-polyaniline nanocomposites with core-shell structure. *Colloids and Surfaces A: Physicochemical and Engineering Aspects*, 276(1-3), 40–44. <https://doi.org/10.1016/j.colsurfa.2005.10.010>
- 26 Li, L., Jiang, J., & Xu, F. (2007). Synthesis and ferrimagnetic properties of novel SM-substituted LiNi Ferrite-polyaniline nanocomposite. *Materials Letters*, 61(4-5), 1091–1096. <https://doi.org/10.1016/j.matlet.2006.06.061>
- 27 You, K. Y. (2017). Materials characterization using microwave waveguide system. *Microwave Systems and Applications*. <https://doi.org/10.5772/66230>

- 28 Skocik, P., & Neumann, P. (2015). Measurement of complex permittivity in Free Space. *Procedia Engineering*, 100, 100–104. <https://doi.org/10.1016/j.proeng.2015.01.347>
- 29 Tamyis, N., Ramli, A., & Ghodgaonkar, D. K. (n.d.). Free space measurement of complex permittivity and complex permeability of magnetic materials using open circuit and short circuit method at microwave frequencies. *Student Conference on Research and Development*. <https://doi.org/10.1109/scored.2002.1033141>
- 30 Fwen, W., Ping, S., Abd Malek, M. F., & Hassas, N. (2012). Alternatives for PCB laminates: Dielectric Properties' measurements at microwave frequencies. *Dielectric Material*. <https://doi.org/10.5772/50718>
- 31 Gonçalves, F., Pinto, A., Mesquita, R., Silva, E., & Braccaccio, A. (2018). Free-space materials characterization by reflection and transmission measurements using frequency-by-frequency and multi-frequency algorithms. *Electronics*, 7(10), 260. <https://doi.org/10.3390/electronics7100260>
- 32 Verma, P., Bansala, T., Chauhan, S. S., Kumar, D., Deveci, S., & Kumar, S. (2021). Electromagnetic interference shielding performance of carbon nanostructure reinforced, 3D printed polymer composites. *Journal of Materials Science*, 56(20), 11769–11788. <https://doi.org/10.1007/s10853-021-05985-0>
- 33 Bayat, M., Yang, H., Ko, F. K., Michelson, D., & Mei, A. (2014). Electromagnetic interference shielding effectiveness of hybrid multifunctional Fe₃O₄/carbon nanofiber composite. *Polymer*, 55(3), 936–943. <https://doi.org/10.1016/j.polymer.2013.12.042>
- 34 Hong, Y. K., Lee, C. Y., Jeong, C. K., Lee, D. E., Kim, K., & Joo, J. (2003). Method and apparatus to measure electromagnetic interference shielding efficiency and its shielding characteristics in broadband frequency ranges. *Review of Scientific Instruments*, 74(2), 1098–1102. <https://doi.org/10.1063/1.1532540>
- 35 Ali, N. N., Atassi, Y., Salloum, A., Malki, A., Jafarian, M., & Almarjeh, R. K. (2019). Lightweight broadband microwave absorbers of core-shell (polypyrrole/nizn ferrite) nanocomposites in the X-band: Insights on Interfacial Polarization. *Journal of Materials Science: Materials in Electronics*, 30(7), 6876–6887. <https://doi.org/10.1007/s10854-019-01002-y>
- 36 Wang, S., Jiao, Q., Shi, Q., Zhu, H., Feng, T., Lu, Q., Feng, C., Li, H., Shi, D., & Zhao, Y. (2020). Synthesis of porous nitrogen-doped graphene decorated by γ -Fe₂O₃ nanorings for enhancing microwave absorbing performance. *Ceramics International*, 46(1), 1002–1010. <https://doi.org/10.1016/j.ceramint.2019.09.064>
- 37 Shu, R., Zhang, J., Guo, C., Wu, Y., Wan, Z., Shi, J., Liu, Y., & Zheng, M. (2020). Facile synthesis of nitrogen-doped reduced graphene oxide/nickel-zinc ferrite composites as high-performance microwave absorbers in the X-band. *Chemical Engineering Journal*, 384, 123266. <https://doi.org/10.1016/j.cej.2019.123266>
- 38 Jaiswal, R., Agarwal, K., Kumar, R., Kumar, R., Mukhopadhyay, K., & Prasad, N. E. (2020). EMI and microwave absorbing efficiency of polyaniline-functionalized reduced graphene oxide/ γ -Fe₂O₃/epoxy nanocomposite. *Soft Matter*, 16(28), 6643–6653. <https://doi.org/10.1039/d0sm00266f>

А. Хуби, А.А. Жарменов, И. Атасси, Ж.Т. Бағашарова, С. Мырзалиева, Б.А. Кәрібаев

Парафинді балауыз матрицасында полианилинмен қапталған Ni_{0,5}Zn_{0,5}Fe₂O₄/CI композитінің синтезі және микротолқынды сіңіру қасиеттері

Полианилин/Ni_{0,5}Zn_{0,5}Fe₂O₄/карбонил темірінің үштік композиттері (PANI/F/CI) екі кезең арқылы дайындалды: алдымен, Ni_{0,5}Zn_{0,5}Fe₂O₄ золь-гель әдісімен; содан соң PANI/F/CI композиттері Ni_{0,5}Zn_{0,5}Fe₂O₄ және CI болған кезде PANI-ның in-situ полимерлеу әдісі қолданылған. Үлгілерді сипаттау үшін рентгендік дифрактометрия (XRD — X-ray diffractometry), Фурье түрлендіру инфрақызыл спектроскопиясы (FTIR — Fourier transform infrared), ультракүлгін-көрінетін спектроскопиясы және термогравиметриялық талдау (TGA — Thermogravimetric analysis) пайдаланылды. Ұнтақтардың морфологиясы сканерлеуші электронды микроскоппен (SEM — Scanning electron microscope) зерттелген. Электромагниттік кедергілерді (EMI — electromagnetic interference) қорғау және микротолқынды жұту (MA — microwave absorption) қасиеттері 8,8–12 ГГц жиілік диапазонында өлшенді. Нәтижелер микротолқынды сіңіру қасиеттері абсорбердің қалыңдығына және парафиндік матрицадағы абсорбердің жүктеме қатынасына байланысты екенін көрсетті. Қалыңдығы 3,4 мм, бетінің тығыздығы 3,38 кг/м² болатын PANI/F/CI композиттік үлгісі үшін 10,3 ГГц сәйкес жиілікте (f_m) ең аз кері жоғалуы –30,8 дБ және жұту жолағы үшін 2,8 ГГц кезінде –10 дБ-ден (BW_{-10dB}) төмен болатыны анықталды. 3,2 мм қалыңдықтағы PANI/F/CI композиттік үлгісі үшін 11,0 ГГц жиілікте 30,12 дБ максималды экрандау тиімділігі байқалды.

Кілт сөздер: полианилин, карбонилді темір, композиттер, шағылысу жоғалуы, абсорбциялық жолақ ені.

А. Хуби, А.А. Жарменов, И. Атасси, Ж.Т. Багашарова, С. Мырзалиева, Б.А. Карибаев
**Синтез и микроволновые поглощающие свойства композита $\text{Ni}_{0,5}\text{Zn}_{0,5}\text{Fe}_2\text{O}_4/\text{CI}$,
покрытого полианилином в парафиновой матрице**

Тройные композиты полианилин/ $\text{Ni}_{0,5}\text{Zn}_{0,5}\text{Fe}_2\text{O}_4$ /карбонильное железо (PANI/F/CI) получены двумя стадиями: сначала методом золь–гель был получен $\text{Ni}_{0,5}\text{Zn}_{0,5}\text{Fe}_2\text{O}_4$, после этого был получен композит PANI/F/CI с использованием технологии полимеризации PANI в присутствии $\text{Ni}_{0,5}\text{Zn}_{0,5}\text{Fe}_2\text{O}_4$ и CI. Для характеристики образцов использовались рентгеновская дифрактометрия (XRD), инфракрасная спектроскопия с преобразованием Фурье (FTIR), спектроскопия в ультрафиолетовом и видимом (UV-vis) спектрах и термогравиметрический анализ (TGA). Морфологии порошков были исследованы с помощью сканирующего электронного микроскопа (СЭМ). Свойства экранирования электромагнитных помех и поглощения микроволн измерялись в полосе частот 8,8–12 ГГц для исследования микроволновых характеристик. Результаты относятся к тем свойствам поглощения микроволн, которые связаны с толщиной поглотителя и коэффициентом загрузки поглотителя в парафиновой матрице. Для композитного образца PANI/F/CI были определены, что на частоте согласования 10,3 ГГц (f_m) минимальные потери на отражение составляют –30,8 дБ и полоса поглощения ниже –10 дБ (BW_{10дБ}) на частоте 2,8 ГГц для толщины 3,4 мм с поверхностной плотностью 3,38 кг/м². Для образца композита PANI/F/CI с толщиной 3,2 мм наблюдалась максимальная эффективность экранирования 30,12 дБ на частоте 11,0 ГГц.

Ключевые слова: полианилин, карбонильное железо, композиты, потери на отражение, ширина полосы поглощения.

Information about authors *

Houbi, Anas (*corresponding author*) — 3rd year PhD student, Department of Chemical Technology of Inorganic Substances, Al-Farabi Kazakh National University, Al-Farabi street, 71, 050040, Almaty, Kazakhstan; e-mail: anashoubi@gmail.com; <https://orcid.org/0000-0001-9282-774X>

Zharmenov, Abdurassul Aldashevich — General Director of the RSE “National Center on Complex Processing of Mineral Raw Materials of the Republic of Kazakhstan”, Dr. Sci. (Eng.), Prof., academician of the NAS of RK, State Premium Double Laureate, Jandossov street, 67, 050036, Almaty, Kazakhstan; e-mail: nc@cmrp.kz; <https://orcid.org/0000-0001-5651-5343>

Atassi, Yomen — Professor of Chemistry of Materials, Director of Materials Science Laboratory, Higher Institute for Applied Science and Technology (HIASST), Barzeh street, Damascus, Syria; e-mail: yomen.atassi@gmail.com; <https://orcid.org/0000-0002-1338-4993>

Bagasharova, Zhenisgul Telmanovna — Candidate of Technical Sciences, RSE “National center for complex processing of mineral raw materials of the Republic of Kazakhstan”, Senior Lecturer at Al-Farabi Kazakh National University, Al-Farabi street, 71, 050040, Almaty, Kazakhstan; e-mail: zh.t_bagasharova@mail.ru; <https://orcid.org/0000-0001-8996-8656>

Mirzalieva, Saule — Doctor of Chemical Sciences, Professor, Head of Department for Training of Scientific Personnel National Center for Complex Processing of Mineral Raw Materials of the Republic of Kazakhstan, Professor at Al-Farabi Kazakh National University, Al-Farabi street, 71, 050040, Almaty, Kazakhstan; e-mail: saulekerchaiz@mail.ru; <https://orcid.org/0000-0003-2997-0716>

Karibayev, Beibit Abdirbekovich — Acting Assistant Professor of Physics and Technology, Al-Farabi Kazakh National University, Al-Farabi street, 71, 050040, Almaty, Kazakhstan; e-mail: beibitkaribaev7@gmail.com; <https://orcid.org/0000-0003-1057-0296>

*The author's name is presented in the order: *Last Name, First and Middle Names*

G.K. Mamytbekov, Zh.I. Beksultanov, V.I. Bannykh, I.V. Dan'ko

Institute of Nuclear Physics, Almaty, Kazakhstan
(*Corresponding author's e-mail: g.mamytbekov@inp.kz)

Synthesis, Structure and Properties of Hybrid Composite Bentonite-Based Materials

A systematic study of the synthesis of hybrid composite materials based on synthetic (poly-N-vinylpyrrolidone) and natural (agar-agar) macromolecules in the presence of plasticizers (PEG-400, glycerin) and mineral filler bentonite has been performed by the method of electron irradiation. The methods of X-ray diffraction analysis and SEM show that the structure of the resulted hybrid compositions is defined as an interpenetrating network with the distributed intercalated particles of mineral component inside its volume. It has been established that mechanical properties of the hybrid composition are determined mainly by the structural organization of the interpenetrating polymer network, formed during electron irradiation of the initial polymer mixture in the presence of plasticizers, as well as by the conditions for intercalation of polymer segments into the interpacket layers of the mineral matrix. During the process of crazing the sample under tension the shear stress is concentrated in the central part of the sample from the periphery of the fastening. It is shown that the degree of swelling for hybrid composition strongly depends on the concentration of a low molecular plasticizer in the polymeric interpenetrating network, which can easily impregnate into the interplanar layers of bentonite.

Keywords: hybrid composition material (HCM), polymer-inorganic compositions (PIC), electron irradiation, synthetic and natural polymers, bentonite, deformation, compression, tension, intercalation, interpenetrating networks (IPN).

Introduction

Hybrid nanocomposites represent a promising class of complex polymer-inorganic materials in which mineral particles are distributed in a polymer matrix of synthetic or natural origin [1–3]. The interphase boundary between the filler and the polymer matrix in nanocomposites occupies a larger area than in conventional microcomposites; therefore, it affects the properties of nanocomposites to a much greater extent even with a minimum amount of filler [4].

Among the variety of hybrid nanocomposites, a special place is occupied by systems where bentonite clays are used as an inorganic filler. The study of the structure and properties of minerals of the layered aluminosilicates class, produced from available and widespread natural raw materials, is an important scientific and practical task aimed to create new multifunctional materials [5, 6]. This is mainly defined by uniqueness of the physical-chemical properties of layered aluminosilicates, which appear in a developed specific surface, the presence of active reaction centers, high adsorption, and ion exchange abilities [7–9]. This suggests the possibility of using bentonite clays in medicine as drug carriers in the form of gel, film and injectable drug forms [10]. The main conditions for the use of polymer-clay composite materials for medical purposes are uniformity of the clay mineral composition, harmlessness of the components and relative indifference of their behavior in the polymer matrix.

There are a lot of publications devoted to the synthesis of polymer-clay systems based on natural and synthetic polymers [11–13], where the possibilities of designing new classes of hybrid polymer-inorganic compositions for solving various applied and technological problems are considered in detail.

Depending on the nature of used components (for example, chain, layered or zeolite silicate, polymer matrix) and the method of preparation, three main types of hybrid compositions can be produced in which layered silicates are bonded to the polymer matrix in various ways [13–15]: the first case when the polymer cannot intercalate between silicate layers resulting in formation of a microcomposite with separated phases. The second type of polymer compositions occurs when intercalation or exfoliation of the clay takes place, in which a single extended polymer chain is inserted between the silicate layers, which leads to formation of alternating layers of polymer and silicate particles. In the third case, the silicate layer is evenly and completely dispersed in a continuous polymer medium, resulting in a completely layered exfoliated structure.

The purpose of this paper is to review the mechanism of formation and structure of intercalated hybrid composite materials based on natural (agar-agar, bentonite) and synthetic medical-purpose polymers (poly-N-vinylpyrrolidone, PVP) in the presence of low and high molecular plasticizers (glycerol, polyethylene glycol PEG-400) produced by the method of electron irradiation.

The method of electron irradiation was used to obtain three-dimensional polymer structures due to the radiation cross-linking of polyvinylpyrrolidone macromolecules. Other options for cross-linking of a linear PVP are possible only by means of thermal degradation at the temperature of decomposition of the material at a temperature above 120 °C in a dry state, which is not acceptable for our purposes. Moreover, electron irradiation is a pure reagent-free method for obtaining three-dimensional polymer systems, that solves the issue of sterilization of polymer compositions, which is the main condition for their application in medical practice for use as an anti-burn and an anti-bedsore hydrogel coated on damaged tissue.

Experimental

Bentonite (BT) from the JSC “Ilsky plant Utyazhelitel” (Russia) TU-2164-003-00136716-2015 was used after washing with distilled water and drying to constant weight at a temperature of 70 °C.

Agar-agar (AA) “Grasar” 900 (Company “Bargus Trade”, Russia) is a white fine powder, manufactured in accordance with STO 010-96140533-2016, which was used with no additional purification.

Poly-N-vinylpyrrolidone (PVP) (Kollidon 90 F) and PEG400 (BASF Pharma, Germany) were used with no additional purification.

Preparation of a composite hydrogel solution included two stages: 1) dissolution of the required weight of PVP at a temperature of 15 °C with stirring on a magnetic stirrer until complete dissolution, after which plasticizer PEG-400 (P1) was added to this solution. Separately, a solution of agar-agar (P2) was prepared in distilled water at a temperature of 80–90 °C for 2 hours. Next, solutions P1 and P2 were mixed with addition of 0.5 g (0.5 %) of dry bentonite powder with vigorous stirring until a homogeneous system with a uniform distribution of the mineral component (for 1–2 hours) was obtained until a suitable temperature (40–45 °C) is reached for pouring the polymer-mineral mixture into the specially shaped containers.

Irradiation of a mixture of prepared solutions of polymer-inorganic compositions (PIC) of a given composition was performed in an accelerator ILU-10 with electron beam in the dose range from 5 to 25 kGy in special plastic molds with a rectangular cross-section of 10×12 cm-or in cylindrical ampoules with an inner diameter of 10 mm and a height 30 mm with the following processing mode: E — 5 MeV, I_{imp} — 350 mA; f — 26 Hz, V — 2.7 cm/s; I_{av} — 4.55 mA. The samples, obtained at the irradiation dose of 25 kGy, were used in the work.

X-ray diffraction analysis (XRD) was performed on a Bruker X-ray diffractometer with CuK_{α} radiation. A thin dried film of a hybrid composition and powdered bentonite up to 10 μ m in size were scanned in the 2 θ angle range from 20° to 70° with a step of 0.02°, a scanning speed of 2 s/point, with radiation parameters of 40 kV and 40 mA.

Scanning electron microscopy (SEM) was performed using a Hitachi model TM 4000 Plus microscope (Japan) equipped with an X-ray fluorescence energy dispersive analysis (EDS) attachment with a crystal detector. Samples were studied under low vacuum in back-scattered electron (BSE) mode.

IR-Fourier spectra were taken on a spectrometer Carry 660 (Agilent, USA) in the absorption mode in the frequency range 700–4000 cm^{-1} with a resolution of 4 cm^{-1} .

The mechanical properties of PIC samples were analyzed on a texture analyzer TA.XTplus-StableMicroSystems (England) with software. The principle of the texture analyzer is that the sample is subjected to the action of controlled forces using a probe while stretching a rectangular sample or compressing a cylindrical sample. The resistance of a material to tensile or compressive forces is measured using a torque sensor.

Results and Discussion

In our previous study [16], we considered the mechanism for formation of rare cross-linked composite hydrogels based on the natural polysaccharide agar-agar, a synthetic polymer for medical application, poly-N-vinylpyrrolidone (PVP), synthesized by electron irradiation. It was established that synthesis conditions and component composition of the initial mixture determine the structure and morphology of the formed hydrogel compositions and their mechanical properties. A new interpretation of the formation of the structure of composite hydrogels in the presence of various plasticizers was provided. It was shown that formation of a three-dimensional structure of PVP occurs as a result of electron irradiation of the reaction mixture in an

aqueous medium in the presence of low- and high-molecular plasticizers, the content of which can be controlled to obtain networks of various strengths and elasticity. The composite hydrogels P[AA-PVP-plasticizer] are a model of interpenetrating networks consisting of physical and covalent crosslinking points that provides them with a good combination of elastic and viscoelastic properties.

Considering the above, this article reviews the mechanism for the formation of intercalated structures of a natural mineral in the volume of a polymer matrix, synthesized by the method of electron irradiation of solutions of natural (AA) and synthetic (PVP) polymers mixtures in the presence of plasticizers. Content of the mineral filler was chosen equal to 0.5 wt.% to achieve a uniform distribution of natural silicate suspension in the volume of the polymer mixture solution while maintaining their aggregative stability.

The main rock-forming components of bentonite clays are minerals of the smectite group, mainly montmorillonites (more than 70 %). Their composition contains also quartz, feldspars, calcite, and rarely pyrite, as well as other clay minerals such as illite, kaolinite, and mixed-layered minerals [8, 11, 15, 17, 18].

Figure 1 shows the X-ray diffraction patterns of bentonite powder (1) and its intercalated complex (ICC) in the form of a film, scanned in the range of slip angles 2θ from 18° to 90° with a step of 0.02° . The X-ray diffraction data of bentonite (curve 1) shows characteristic diffraction reflections at 20.96° , 26.75° , 29.51° , 31.8° , 42.46° , and 61.54° , which correspond to the characteristic signals of quartz at 20.96° , 26.75° with interplanar distances (d) of 4.23 \AA and 3.32 \AA , respectively, and oxides of calcium, magnesium, and aluminum with frequent line overlap, which makes their identification difficult.

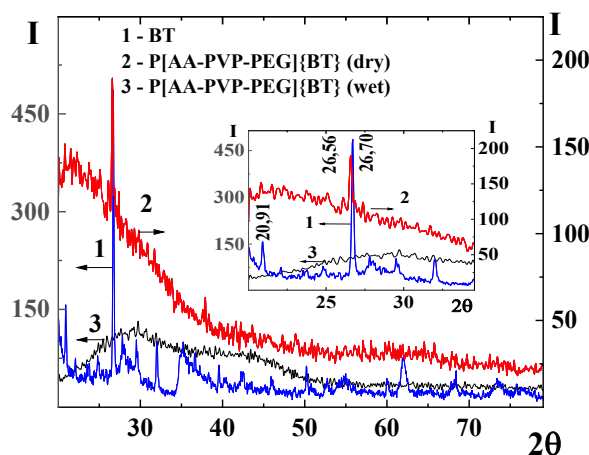


Figure 1. X-ray diffraction patterns of BT (1), (2) dry and (3) wet hybrid composition P[AA-PVP-PEG]{BT}

During the intercalation of bentonite particles into the volume of the polymer matrix P[AA-PVP-PEG], the characteristic maximum of the diffraction signal of quartz in the composition of clay shifts from 26.75° to 26.58° with an increase in the interplanar distance from 3.380 \AA to 3.342 \AA , respectively. However, in this case, there is a significant expansion of the range of diffraction signals in the range of $2020\text{--}40 \text{ \AA}$ and the growth of their intensity observed for the hybrid composite material P[AA-PVP-PEG]{BT}, which may indicate in favor of splitting of the layered packing of the polyoxide forms of aluminum and silicon included in the composition of bentonite clay. In the case of wet compositions, expansion of the range of diffraction signals is observed in a wider range from 30° to 50° . Disappearance of a number of characteristic diffraction bands of pure bentonite in the case of its intercalation into the volume of polymer matrix is explained by a decrease in the content or disappearance of some basic and impurity compounds, for example, quartz ($2\theta = 50.14^\circ$, 59.94°) and montmorillonite itself ($2\theta = 68.12^\circ$ and 68.31°), which may be caused by a complete filling of the interlayer space of the layered silicate with macromolecules of the interpenetrating network. A detailed explanation of this assumption will be considered in the analysis of the SEM data.

It was previously noted [19, 20] that clay minerals are divided into two types depending on alternation of tetrahedral [SiO_2] and octahedral [AlO_6] sheets and their mutual arrangement in the crystal lattice: (i) 2:1 composition clay (smectite and montmorillonite) and (ii) 1:1 clay (kaolinite). The high size ratio of smectite clay minerals is defined by their unique intercalation-separation properties, making them especially important and effective as reinforcing fillers for polymers [4–6].

Bentonite clay is mainly composed of thin layers of 1 nm thick composition 2:1 aluminum phyllosilicates with a central octahedral alumina sheet fused between two outer tetrahedral silica sheets by shared oxygen atoms, forming galleries between the alternating layers (Figure 2) [18].

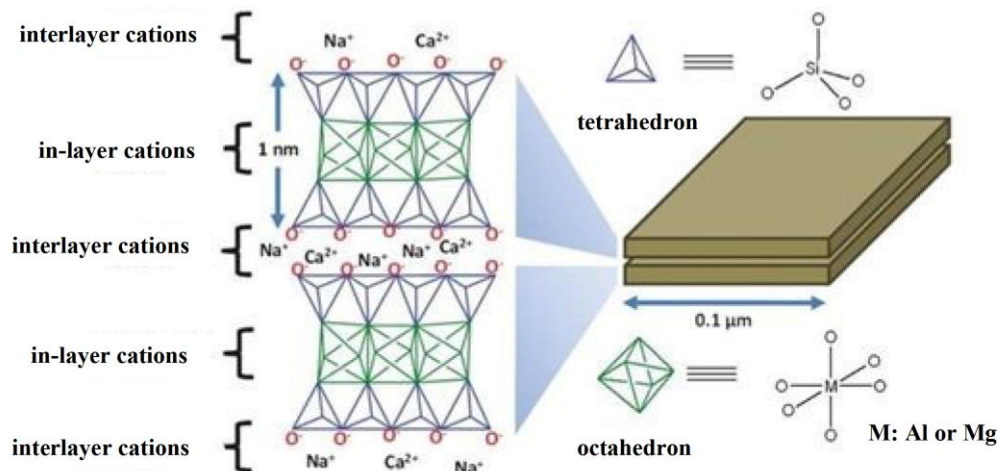


Figure 2. Structure of bentonite clay composition 2:1 [18]

The structured silicon and alumina layers are interconnected by covalent bonds, in which both the isomorphic substitution of silicon for aluminum in the tetrahedral chain and the substitution of aluminum in the octahedral layer for iron, magnesium, or alkaline earth metals take place. In addition, in stabilization of the covalently bonded layers of bentonite, an essential role is played by the electrostatic forces of interaction that arise between the ions of alkali and alkaline earth metals or impurity transition metals located in the gallery between the tetrahedral layers, thus tightly holding the stacks of clay layers together from disintegration either in dry or in wet state. Under such conditions the covalent bonds between the interlayers of aluminosilicate sheets of the clay create difficulties to penetrate into their bulk for most hydrophobic macromolecules [17, 18] due to the high hydrophilicity of the mineral matrix.

Introduction of massive cations or anions into the interlayer space also contributes to loosening of the crystallite structure, which makes it possible for surfactants and water-soluble polymers to penetrate. This leads to complete splitting of crystallites into primary nanosized silicate plates, i.e. exfoliation [18, 19, 21].

Figure 3a shows that bentonite particles represent a structure characterized by the presence of a complex non-oriented clay mass - a matrix, which contains randomly arranged dust-like sand grains that do not contact each other. When zoomed in from 120 (1) to 1000 (2) and 4000 (3) times, a clear picture of the surface structure of the layered and chain structure of natural polymer can be obtained.

This issue has been widely discussed in scientific publications and review articles [3, 4, 11, 17, 20, 21, 23]. Most researchers believe that the stage of modification of clay minerals with hydrophobizing or lyophilizing surfactants is necessary to obtain polymer-silicate (nano) compositions with acceptable mechanical characteristics and operational parameters, since surfactants are able to intercalate into the interlayer space of inorganic ionite with the formation of weak van der Waals (dispersion) or strong covalent chemical bonds.

The morphology of the polymer film is represented by macroporous segments with a developed surface and topological inhomogeneity typical of amorphous sparsely crosslinked polymer systems (Fig. 3b). It is characterized by a layered structure or cleavage of layers caused by formation of a matrix of an interpenetrating network with alternating layers of natural (agar-agar) and synthetic polymers (PVP) with lateral grafting of plasticizer molecules (PEG or glycerol), which we previously described in details in [15].

When forming a hybrid composition of bentonite-IPN, the picture changes significantly (Fig. 3c). It can be seen that the bentonite particles are unevenly distributed over the interlayer surfaces of the interpenetrating network. Particularly noteworthy is the shape of bentonite particles, which resemble the structure of γ -alumina. Traditionally, its crystal structure is described as feldspar, in which aluminum atoms are localized simultaneously in tetrahedral and octahedral positions, as a result of which its surface is much more hydroxylated compared to silica gel. It has been noted that the presence of water accelerates the rate of aluminum hydrolysis with formation of a lamellar large-pore structure of aluminum hydroxide [22–26], which also has an octahedral structure.

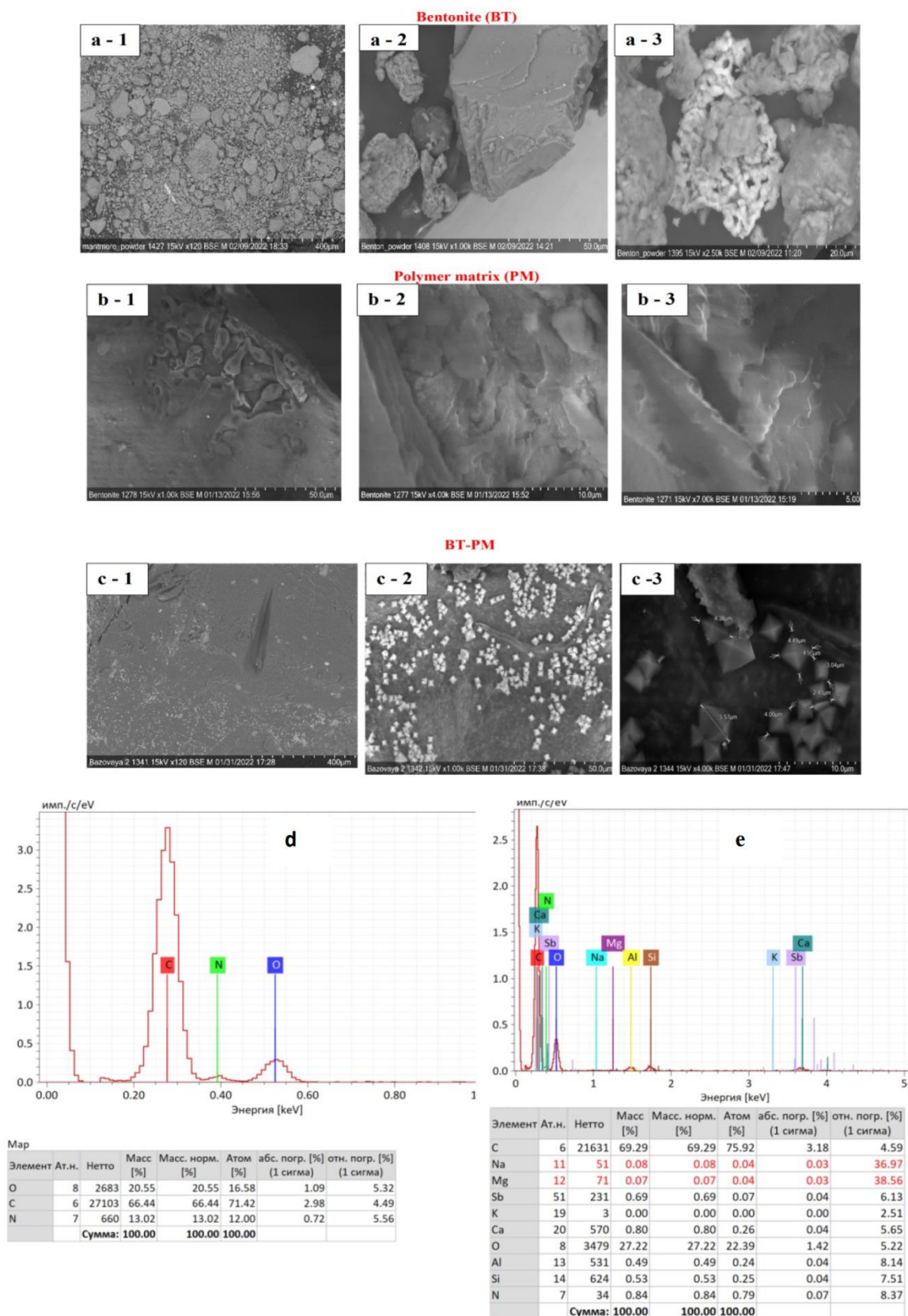


Figure 3. SEM micrographs of bentonite (a), P[AA-PVP-PEG] (b) and P[AA-PVP-PEG]{BT}(c) at various magnifications: 1 — 120; 2 — 1000 and 3 — 4000 times and X-ray fluorescence energy dispersive analysis for P[AA-PVP-PEG] (d) and P[AA-PVP-PEG]{BT} (e).

This conclusion about the chemical structure of the hybrid compositions is in good agreement with the X-ray fluorescence energy dispersive analysis data for P[AA-PVP-PEG] (Fig. 3d) and P[AA-PVP-PEG]{BT} (Fig. 3e).

It should be assumed that we are dealing with the process of partial or complete delamination of sheets with a composition of 2:1 until the complete separation of the silica and alumina layers from each other due to the excess negative charge arising in the process of hydration. Sequential analysis of the stages of montmorillonite hydration confirms the fact that 1 to 4 layers of water molecules can be located in the spaces between silicate layers [27–29].

However, in the studied system the particle sizes determined according to SEM data go far beyond nanoscale, in particular, the average size along the diagonal of octahedrons varies from 3.04 to 5.57 μm , that is, it exceeds the interplanar distances between layers by three orders of magnitude (Fig. 1). Therefore, the alternative explanation can be provided, according to which, in addition to delamination or exfoliation of bentonite particles in the intertwined polymer matrix of the interpenetrating PVP-AA network, microcrystallites of bentonite particles grow into more or less large aggregates in the form of a single monolithic structure of the same geometry as for individual molecules of hydrated alumina in the form of well-formed octahedra.

In the presence of polymers with bulky side pyrrolidone rings (PVP) linked to plasticizer molecules (PEG or glycerol) through a system of hydrogen bonds, as well as polysaccharides which macromolecules consist of cyclic units of D-galactose and 3,6-anhydro-L-galactose, deep splitting of aluminosilicate sheets from each other should be expected (Fig. 4).

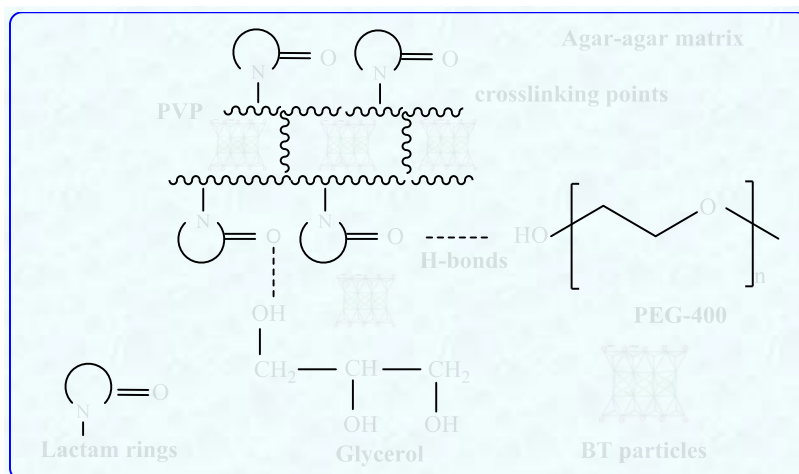


Figure 4. Schematic diagram of formation of composite hydrogels based on agar-agar and PVP in the presence of plasticizers by electron irradiation [15]

Thus, exfoliation begins with the splitting of sheets along the boundary of the gallery $\equiv\text{Si-O-Al-O-Si}\equiv$ $|\text{mMe}^{\text{n}+}\cdot\text{kH}_2\text{O}|$ $\equiv\text{Si-O-Al-O-Si}\equiv$ with subsequent destruction of the three-layer structure along the heterobond line $\equiv\text{Si-O-Al}$ along the oxygen atom. When bentonite particles are in a polymer matrix consisting of two complementary and intertwined macromolecules associated with the terminal hydroxyl groups of plasticizers, the exfoliation process can proceed until the complete rejection of not only sheets of aluminum phyllosilicates from each other, but also by splitting the structures of polyoxosilicon and polyoxoaluminum chains into separate fragments in the form of disparate $\gamma\text{-Al}_2\text{O}_3$ octahedron, as shown in Figure 5.

An increase in the interlayer space during exfoliation of silicates by the IPN matrix contributes to the further process of delamination of the layered filler due to growth of disjoining pressure between the packages and, subsequently, between the sheets of the packages (Fig. 5). The irradiation of the system with an electron beam exacerbates this process since the action of various types of radiation leads to the formation of radiation defects [30]. In this case, an uncontrolled redistribution of crosslinking sites and dimensions of the pore structures of the polymer matrix occur, where more or less hydrated bentonite particles are initially located according to the law of average distribution with nonlinear effects during structural transitions.

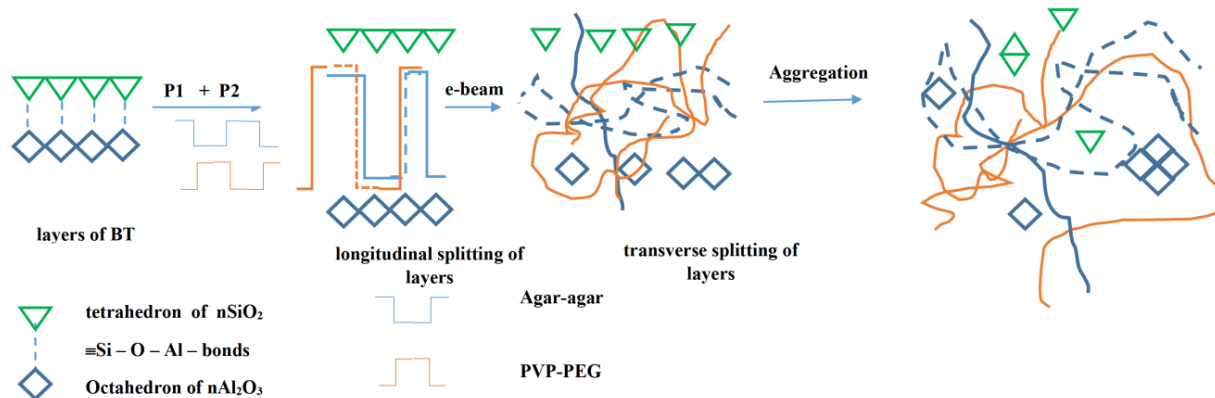


Figure 5. Scheme of exfoliation of bentonite sheets in the IPN matrix with subsequent ordering of BT crystallites into large aggregates

It can be assumed that during electron irradiation of the $\text{P}[\text{AA-PVP-PEG}]\{\text{BT}\}$ hybrid composition after partial exfoliation of sheets of mineral filler from each other by the polymer chains begins the stage of aggregation of disordered aluminosilicate sheets with each other along the side faces and edges of aluminum octahedron oxide, forming associates with more or less individual molecules of alumina or silicon oxide or from their linear sequences.

Consequently, recrystallization of bentonite nanoparticles into larger perfect crystals, consisting mainly of aluminum oxide, takes place. The absence of silica tetrahedral structures can be associated with a higher rate of its hydrolysis and dissolution in a water-alcohol medium with formation of polysilicic acid or their associated forms with a polymer matrix through hydrogen bonds according to the scheme compared to aluminum oxide (Fig. 5).

Complete destruction of clay packets in the form of separate sheets leads to formation of a layered structure, which is well distributed in the polymer matrix. This structure provides the most favorable improvement in the characteristics of the resulting polymer nanocomposites in comparison with the intercalated structure due to the high aspect ratio and intense surface reaction of clay particles with polymer chains [31–34].

In addition to the structures of $\gamma\text{-Al}_2\text{O}_3$, SEM micrographs revealed a small number of other geometric configurations (triangular, prismatic, and a number of distorted shapes) belonging to impurity compounds, a detailed study of which is beyond the scope of this article and requires additional in-depth studies.

Previously, the authors [35–37] studied the conditions for production of aluminosilicates by the sol-gel synthesis. It was found that introduction of templates into the aluminosilicate matrix, such as PEG, PEO, cationic surfactants, leads to rapid precipitation of aluminum hydroxide, while two phases of aluminum and silicon oxides condense with no formation of $\text{Si}-\text{O}-\text{Al}$ heterobonds. The resulting octahedra, with an aluminum atom in the center and hydroxyl groups at six corners, has the formula $[\text{Al}(\text{OH})_6]^{3-}$.

The molecular composition and structure of the hydrogel compositions produced by the mixing method followed by irradiation with electron beams were identified by IR-Fourier spectroscopy (Fig. 6). Spectra of the three-dimensional polymer matrix $\text{P}[\text{AA-PVP-PEG}]$ (curve 1) show a clear maximum at 1650 cm^{-1} , corresponding to the stretching vibration band of the carbonyl groups of the pyrrolidone ring, which shifts to the long-wavelength region of 1655 cm^{-1} during three-dimensional radiation polymerization. This indicates the formation of a strong hydrogen bond between the $\text{C}=\text{O}$ and $-\text{OH}$ groups of agar-agar or the terminal hydroxyl groups of PEG, confirming the previously accepted mechanism for the formation of three-dimensional structures in this system [15]. Thus, the synthetic and natural polymers of the hybrid composition are physically intertwined with each other within the three-dimensional framework of PVP and agar-agar, forming an interpenetrating network.

The intensity of the characteristic absorption length of PVP at 2942 cm^{-1} , corresponding to the stretching vibrations of the $\text{C}-\text{H}$ bond of the methylene groups, increases, indicating a possible superposition of different sections of crosslinked and non-crosslinked sections of polymer chains in the network. Bands of bending vibrations in the region of $1494, 1457, 14221$ and 1277 cm^{-1} ($\text{C}-\text{N}$ -groups) also appear in the spectra of the synthesized polymer hydrogels, which indicates the presence of linear PVP macromolecules, which are associated with both agar-agar and PEG chains.

Figure 6 below shows the Fourier IR spectra of the initial BT (2) and the final hybrid P[AA-PVP-PEG]{BT} (3) composition. It should be noted that the spectra have large overlaps with each other, but it makes it possible to qualitatively identify the structure of the hybrid composition. This is especially evident in the region of $3600\text{--}3200\text{ cm}^{-1}$, which characterizes the stretching vibrations of the hydroxyl groups of both BT and the polymer matrix, including adsorption or capillary water in the composition of the initial matrices. It is also possible to detect the spectra of stretching vibrations of Si–O–Si in the region of $1100\text{--}900\text{ cm}^{-1}$ and deformation vibrations of the Al–O–Al bond in the region of 918 cm^{-1} .

Vibrations in the region of $1018\text{--}1046\text{ cm}^{-1}$ can be attributed exclusively to stretching vibrations of the Si–O bond [18, 26]. These results show that chemical interaction occurs between the silicate groups of the inorganic matrix and the functional groups of the polymer matrix, leading to formation of a stable intercalated spatial IPN already from heterogeneous network structures of polymer macromolecules and inorganic ionite P[AA-PVP-PEG]{BT}.

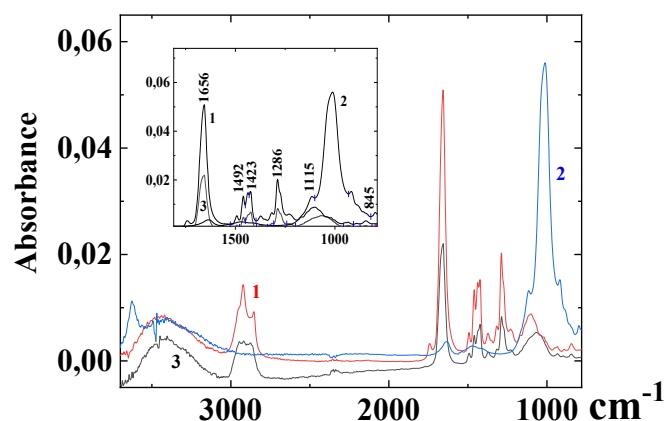


Figure 6. Fourier IR spectra BT (1), P[AA-PVP-PEG] (2) and their hybrid composition P[AA-PVP-PEG]{BT} (3)

Figure 7 shows the swelling kinetics of the compositions P[AA-PVP-PEG]{BT} synthesized in water (1) and in the presence of glycerol with a content of 0.1 wt.% (2) and 0.3 wt.% (3) in the initial reaction mixture. It can be seen that the presence of a low molecular plasticizer of glycerin along with PEG leads to swelling growth of the hybrid composition at the initial time, which can be judged by the tangent of slope angle in this time interval ($\text{tg}\alpha = \Delta K_{\text{sw}}/\Delta t$). So for the composition synthesized in water ($\text{tg}\alpha = 15.87^\circ$), in 0.1 and 0.3 wt.% glycerol is 9.963 and 7.53, respectively. Swelling profile in water and 0.1 wt. % glycerol has bends in the range from 0.5 to 1.5 hours, which may be defined by gradual hydration of the composition components when water molecules penetrate into its volume through the pores of the polymer matrix. It should be assumed that, first of all, fragments of the polymer matrix will be subjected to hydration, in particular, macromolecules of natural polysaccharide and PVP associated with PEG-400 chains through a system of hydrogen bonds, as noted above. The presence of a bend corresponds to the site when hydration of the mineral filler bentonite begins, the particles of which are distributed in the areas between the crosslinking nodes of the polymer matrix components. With a glycerol content of 0.3 mass. % such bend is not observed, which may be caused by a change in the structure of bentonite with an excess content of glycerol in the composition of the initial mixture.

We believe that at a low content of glycerol ($\omega_{\text{ГГ}} < 0.1\text{ wt.}\%$), there is a maximum flaking of aluminosilicate sheets from each other with the growth of interplanar distance between them in bentonite particles. This gives maximum rigidity to the polymer matrix they are located in. With the growth of glycerol content to 0.3 wt.%, its function from the expansion factor of the interplanar distance between the sheets changes to the function of a plasticizer, when its excess amount begins to bind to the hydrophilic ridges of the matrix macromolecules and the oxygen atoms of the aluminosilicate groups of bentonite due to hydrogen bonds. In this case, the interplanar spacing between the aluminosilicate layers can approach in value the initial parameters of the matrix with no glycerol additives due to enhancement of hydrophobic interactions stabilized by a system of hydrogen bonds. This can explain the twofold increase in the swelling coefficient of hybrid composition material in the presence of 0.1 wt. % glycerol.

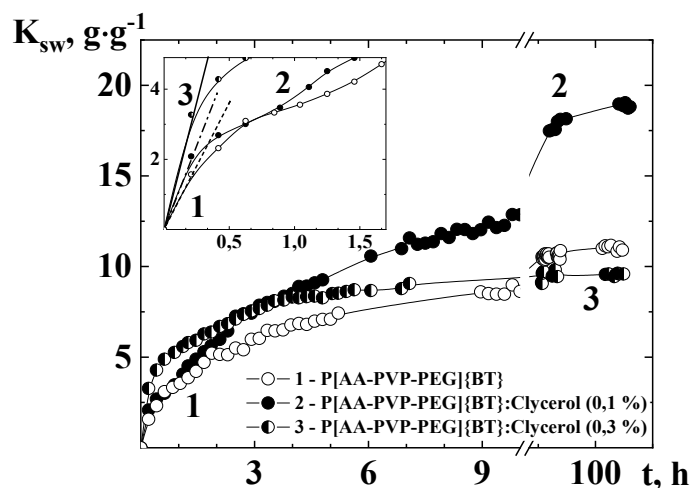


Figure 7. Change in the swelling coefficient of hydrogels P[AA-PVP-PEG]{BT} at different glycerol content

This conclusion is in good agreement with the results of strength measurements for hybrid composite materials. The strength properties and deformation behavior of hydrogel compositions are clearly illustrated by the stress–strain dependence ($P = f(\varepsilon)$), obtained by the method for determining the “puncture” strength of a material by pressing a ball through a layer of a flat composite hydrogel. Three main sections can be distinguished on the deformation curves (Fig. 8). The initial, gently sloping rectilinear section corresponds to the area of plastic, the second — to elastic, the third — to viscous-flowing deformation. In the interval of sections II–III, phase transitions and orientation of macromolecular chains take place between crosslinking sites in the direction of the applied tension and compression force, at which the segment mobility of macromolecules increases and the structure of the material is rearranged. In section III, the relaxation rate of the material becomes comparable with the strain rate of the sample. Outside the zone III, with further deformation, macrocracks appear in the sample of hydrogel composition, as a result, the thinning section of the composite hydrogel, which bears the load from the indented ball, is punctured from region I to region III [15].

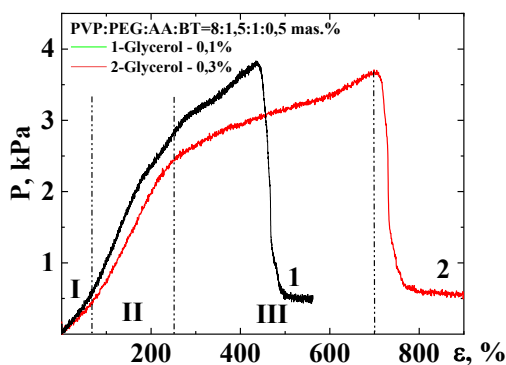


Figure 8. Deformation curves of hybrid composite materials P[AA-PVP-PEG]{BT} at different glycerol content

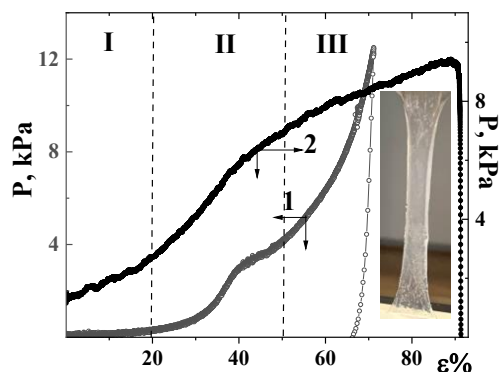


Figure 9. Stress-strain dependence of the composition P[AA-PVP-PEG]{BT}

It can be seen that when the content of glycerol in the hybrid composition is 0.1 wt. %, it shows a noticeable increase in the strength of material from 3680 Pa to 3834 Pa with a decrease in the strain value from 693% to 400% compared to the sample, where its content is 0.3 wt. %. This indicates an increase in interplanar distances between aluminosilicate sheets and the space between them is filled predominantly by the vertically oriented glycerol molecules. This leads to an increase in the disjoining pressure and stress, which affects the ultimate strength of the material and reduces its deformation during punching.

With the growth of glycerol content between sheets of aluminosilicates in bentonite particles, hydrophobic interactions increase and the material acquires viscous-flowing properties against the background of a slight decrease in puncture strength.

Figure 9 shows the stress-strain dependence for uniaxial compression (curve 1) and tension (curve 2) of a cylindrical and rectangular sample, respectively. Under uniaxial compression, the dependence $P = f(\varepsilon)$ shows a break in the deformation range of $\sim 30\%$ followed by a smooth increase in stress up to 12 kPa at $\varepsilon = 70\%$.

It is important to have a qualitative representation of the process leading to strengthening or weakening of the strength of the composite material under external loads to establish quantitative relationships between the structure and the property of a material to resist destruction. The absorption of the energy transferred to the polymer matrix occurs almost entirely. The function of fillers-plasticizers is to promote and control deformations in the matrix, providing significant stress concentrations in those places where local deformations can be initiated. Shear fluidity plays a role in the process, but crazing is the predominant hardening mechanism. Many researchers have shown that stress whitening is associated with formation of more crazes than microcracks [35].

With regard to the system we are considering, it can be assumed that mineral fillers play the role of stress absorbers caused by compression or tension of the sample.

The stress-strain dependence does not show a region of elastic deformation corresponding to the Hooke model. The dependence $P-f(\varepsilon)$ already at the initial stages resembles a plastic deformation profile, that is, not a sharp, but a gentle change in shear or compression stress up to $\varepsilon \approx 20\%$, which is not typical for most previously studied systems [38]. When a sample is compressed in the region of $\varepsilon \in 30-50\%$ there is a “consistent” orientation of mineral particles and layers of polymeric planes of a three-dimensional matrix, along the axis of tension or compression. It is natural in this case to expect some change in the morphological structure of the hybrid composition, which corresponds to the bend section on the stress-strain curve during compression, which is not observed in the absence of a mineral filler [15]. Such bends correspond to the region of the conformational transition of macromolecules “coil-globule” [38, 39].

Any parameter that affects the degree of intercalation and delamination, like the modulus, has a significant effect on the tensile strength of nanocomposites. Another effect of the nanoclay filler on the mechanical characteristics of nanocomposites is the value of elongation at break, which is affected by the interfacial reaction between the polymer and layered silicates [40].

In addition, introduction of a mineral filler into the volume of the polymer matrix resulted in a decrease in the degree of elongation by almost a factor of two [15]. In shear zones [38], molecules are oriented approximately parallel to the applied tensile stress and, therefore, normal to the planes where crazes form. Since both the initiation and growth of crazes are inhibited due to orientation in this direction, shear bands have an effect on inhibition of the crazes growth. As the number of shear bands increases, the length of newly formed crazes decreases, which is shown in the image (Figure 9).

Provision of the exfoliation conditions is of particular importance as it maximizes the interaction between the polymer and the clay particles, allowing the polymer to access the entire surface of the silicate layers, thus leading to the greatest changes in various physical properties. Nevertheless, there are still disputes about whether the system of polymer-clay nanocomposites contains entirely layered silicates, which is confirmed by the fact that a significant part of polymer nanocomposites in the literature has intercalated or mixed intercalated-layered nanostructures [41]. This is due to the fact that silicate layers are highly anisotropic, their side sizes vary from 100 to 1000 nm, and they cannot be arranged randomly in the polymer matrix even when separated at a large distance from each other [42].

In the course of crazing processes during sample stretching in tension, according to formation of microcracks in the area of material fastening and whitening in the central part from the fastening periphery, the shear stress is concentrated at break. Moreover, in the studied polymer compositions the formation of a “neck” is not observed, and the system rather passes into a viscous-fluid state than into a highly elastic state before destruction of the sample.

Most studies show that elastic modulus of polymer nanocomposites, fabricated using modified organoclay growth significantly, especially at increasing of load on the organoclay [43]. However, in some cases, the Young's modulus decreased, since completely exfoliated structures are replaced by partially exfoliated intercalated structures when the volume fraction of organoclay exceeds the threshold limit value [44, 45].

We propose to consider such hybrid composite materials as a new class of interpenetrating networks with promising applied properties (materials for tissue engineering and anti-burn hydrogel dressings with a wound healing effect and high bactericidal activity, etc.).

Conclusions

A systematic study of the synthesis of hybrid composite materials based on synthetic (PVP) and natural (AA) macromolecules in the presence of plasticizers (PEG-400, glycerol) and the mineral filler bentonite was carried out.

X-ray diffraction analysis and SEM showed that the structure of the resulting hybrid compositions is defined as an interpenetrating network, in the volume of which intercalated particles of the mineral component are distributed.

It was established that the mechanical properties of the hybrid composition are determined mainly by structural organization of the interpenetrating polymer network formed during electron irradiation of the initial polymer mixture in the presence of plasticizers, as well as by the conditions for intercalation of polymer segments into the interpacket layers of the mineral matrix. During the process of crazing of the sample under tension the shear stress is concentrated in the central part of the sample from the periphery of the fastening.

It was shown that the degree of swelling of the hybrid composition strongly depends on concentration of a low molecular plasticizer in the polymeric interpenetrating network, which can easily impregnate into the interplanar layers of bentonite.

Acknowledgements

The work was carried out within the framework of the Program “Development of nuclear physics methods and technologies for innovative modernization of the economy of Kazakhstan” (2021–2023) of the Ministry of Energy of the Republic of Kazakhstan (state registration number 0121RK00656, IRN number BR09158958).

The authors express their gratitude to LPP “Institute of Polymer Materials and Technologies” for providing the opportunity to measure mechanical characteristics of hybrid compositional materials.

References

- 1 Albdiry M.T. A critical review on the manufacturing processes in relation to the properties of nanoclay/polymer composites / M.T. Albdiry, B.F. Yousif, H. Ku, K.T. Lau // *J. Compos. Mater.* — 2013. — Vol. 47. — P. 1093–1115. <https://doi.org/10.1177/0021998312445592>
- 2 Du J.H. The fabrication, properties, and uses of graphene/polymer composites / J.H. Du, H.M. Cheng // *Macromol. Chem. Phys.* — 2012. — Vol. 213. — P. 1060–1077. <https://doi.org/10.1177/0021998312445592>
- 3 Müller K. Review on the processing and properties of polymer nanocomposites and nanocoatings and their applications in the packaging, automotive and solar energy fields / K. Müller, E. Bugnicourt, M. Latorre, M. Jorda, Y. Echegoyen Sanz, J.M. Lagaron, O. Miesbauer, A. Bianchin, S. Hankin, U. Bölz, G. Pérez, M. Jesdinszki, M. Linder, Z. Schuerer, S. Castello, M. Schmid // *Nanomaterials.* — 2017. — Vol. 7. — P. 74. <https://doi.org/10.3390/nano7040074>
- 4 Valapa R.B. An Overview of Polymer-Clay Nanocomposites / R.B. Valapa, S. Loganathan, G. Pugazhenthii, S. Thomas, T.O. Varghese // In *Clay-Polymer Nanocomposites*, Amsterdam, The Netherlands: Elsevier. — 2017. — P. 29–81, ISBN: 978-0-323-46153-5. <https://doi.org/10.1016/B978-0-323-46153-5.00002-1>
- 5 Kotal Moumita. Polymer nanocomposites from modified clays: Recent advances and challenges / Moumita Kotal, A. Bhowmick // *Progress in Polymer Science.* — 2015. — Vol. 51. — P. 127–187. <https://doi.org/10.1016/j.progpolymsci.2015.10.001>
- 6 Lee K.-Y. On the use of nanocellulose as reinforcement in polymer matrix composites / K.-Y. Lee, Y. Aitomäki, L.A. Berglund, K. Oksman, A. Bismarck // *Compos. Sci. Technol.* — 2014. — Vol. 105. — P. 15–27. <https://doi.org/10.1016/j.compscitech.2014.08.032>
- 7 Zhang J. Polymerically modified layered silicates: An effective route to nanocomposites / J. Zhang, E. Manias, C.A. Wilkie // *J. Nanosci. Nanotechnol.* — 2008. — Vol. 8. — P. 1597–1615.
- 8 Nosonovsky M. Green tribology: Principles, research areas and challenges / M. Nosonovsky, B. Bhushan // *Philos. Trans. R. Soc. A math. Phys. Eng. Sci.* — 2010. — Vol. 368. — P. 4677–4694. <https://doi.org/10.1098/rsta.2010.0200>
- 9 Каспржицкий А.С. Комплексное исследование состава и структурных особенностей порообразующих минералов бентонитовых глин Миллеровского месторождения / А.С. Каспржицкий, А.В. Морозов, Г.И. Лазоренко, Б.В. Талпа, В.А. Явна // *ИВД.* — 2013. — № 3. — С. 26. Режим доступа: <https://cyberleninka.ru/article>
- 10 Mamidi N. Development of ultra-high molecular weight polyethylene functionalized carbon nano-onions composites for biomedical applications / N. Mamidi, M.R.M. Gamero, J. Vilella-Castrejón, A. Elías-Zúñiga // *Diam. Relat. Mater.* — 2019. — Vol. 97. — P. 107435. <https://doi.org/10.1016/j.diamond.2019.05.020>
- 11 Гылымхан Н.Т. Возможности использования бентонитовых глин в медицине / Н.Т. Гылымхан, С.Н. Жумагалиева, Ж.А. Абилов // *Докл. НАН РК.* — 2016. — Т. 4. — № 308. — 24–33.

- 12 Tiwari J.N. Zero-dimensional, one-dimensional, two-dimensional and three-dimensional nanostructured materials for advanced electrochemical energy devices / J.N. Tiwari, R.N. Tiwari, K.S. Kim // *Prog. Mater. Sci.* — 2012. — Vol. 57. — P. 724–803. <https://doi.org/10.1016/j.pmatsci.2011.08.003>
- 13 Chan J.X. Effect of Nanofillers on Tribological Properties of Polymer Nanocomposites: A Review on Recent Development / J.X. Chan, J.F. Wong, M. Petru, A. Hassan, U. Nirmal, N. Othman, R.A. Ilyas // *Polymers.* — 2021. — Vol. 13. — P. 2867. <https://doi.org/10.3390/polym13172867>
- 14 Pavlidou S. A review on polymer-layered silicate nanocomposites / S. Pavlidou, C.D. Papaspyrides // *Prog. Polym. Sci.* — 2008. — Vol. 33. — P. 1119–1198. <https://doi.org/10.1016/j.progpolymsci.2008.07.008>
- 15 Alexandre M. Polymer-layered silicate nanocomposites: preparation, properties and uses of a new class of materials / M. Alexandre, P. Dubois // *Material Science and Engineering.* — 2008. — Vol. 28. — P. 1–63. [https://doi.org/10.1016/S0927-796X\(00\)00012-7](https://doi.org/10.1016/S0927-796X(00)00012-7)
- 16 Mamytbekov G. Synthesis, structure and mechanical properties of composite hydrogels for medical applications / G. Mamytbekov, Z. Beksultanov, V. Bannykh // *Chemical Bulletin of the Kazakh National University.* — 2022. — No. 104 (1). — P. 30–42. <https://doi.org/https://doi.org/10.15328/cb1264>
- 17 Dalia E. Abulyazied. Investigative Study on the Progress of Nanoclay-Reinforced Polymers: Preparation, Properties, and Applications / E. Abulyazied Dalia, E. Antoaneta // *Review Polymers.* — 2021. — No. 13. — P. 4401. <https://doi.org/10.3390/polym13244401>
- 18 Zhu W. Supramolecular ionic strength-modulating microstructures and properties of nacre-like biomimetic nanocomposites containing high loading clay / W. Zhu, L. Chu-Hua, F.-C. Chang, S.-W. Kuo // *RSC Adv.* — 2012. — No. 2. — P. 6295–6305. <https://doi.org/10.1039/c2ra20523h>
- 19 Gordeeva N.V. Influence of nanoparticles of layered silicates on the properties of aqueous dispersions of acrylate copolymers and films based on them / N.V. Gordeeva, I.A. Tolmachev, L.N. Mashlyakovsky, V.K. Vasiliev // *Proceedings of the St. Petersburg State Technological Institute (Technical University).* — 2012. — No. 14. — P. 41–44.
- 20 Botana A. Effect of modified montmorillonite on biodegradable PHB nanocomposites / A. Botana, M. Mollo, P. Eisenberg, R.M.T. Sanchez // *Applied Clay Science.* — 2010. — No. 47 (3–4). — 263–270. <https://doi.org/10.1016/j.clay.2009.11.001>
- 21 Srinivasan R. Advances in Application of Natural Clay and Its Composites in Removal of Biological, Organic, and Inorganic Contaminants from Drinking Water / R. Srinivasan // *Advances in Materials Science and Engineering.* — 2011. Article ID 872531, 17. <https://doi.org/10.1155/2011/872531>
- 22 Maršálek R. Comparative study of CTAB adsorption on bituminous coal and clay mineral / R. Maršálek, Z. Navrátilová // *Chemical Papers.* — 2011. — Vol. 65 (1). — P. 77–84. <https://doi.org/10.2478/s11696-010-0076-9>
- 23 Fischer H. Polymer nanocomposites: from fundamental research to specific applications / H. Fisher // *Materials Science and Engineering: C.* — 2003. — No. 23 (6–8). — P. 763–772. <https://doi.org/10.1016/j.msec.2003.09.148>
- 24 Nagornov R.S. Complex extraction of biologically active ingredients from oil-containing media using mineral sorbents / R.S. Nagornov, P.B. Razgovorov, E.A. Smirnova, M.P. Razgovorova // *Chemistry and Medicine: Abstract of report of X All-Russian conference with international participation.* In-t org. Chemistry USC RAS. Ufa-Abzakovo: Gilem, 2015.
- 25 Galan E. *Developments in Palygorskite-Sepiolite Research* / E. Galan, A. Singer // *A New Outlook of these Nanomaterials,* Oxford-Amsterdam: Elsevier. — 2011. ISSN 1572-4352. <https://doi.org/10.1016/1B978-0-444-53607-5.00001-3>
- 26 Тарасевич Ю.И. Строение и химия поверхности слоистых силикатов / Ю.И. Тарасевич. — Киев: Наук. думка, 1988.
- 27 Грег С. Адсорбция, удельная поверхность, пористость / С. Грег, К. Синг // пер. с англ. — 2-е изд. — М.: Мир, 1984.
- 28 Bonilla-Petriciolet A. *Adsorption Processes for Water Treatment and Purification* / A. Bonilla-Petriciolet, D.-I. Mendoza-Castillo, H.-E. ReynelÁvila // Cham.: Springer, 2017. <https://doi.org/10.1007/978-3-319-58136-1>
- 29 Gerasin V.A. New approaches to creation of hybrid polymer nanocomposites: structural materials to high-tech applications / V.A. Gerasin, E.M. Antipov, V.V. Karbushev, V.G. Kulichikhin, G.P. Karpacheva, R.V. Talroze, Ya.V. Kudryavtsev // *Advances in Chemistry.* — 2013. — No. 82 (4). — 303–332. <https://doi.org/10.1070/RC2013v082n04ABEH004322>
- 30 Купчишин А.И. Различные модели разрушения полимерных материалов и композитов электронными пучками / А.И. Купчишин, Б.Г. Таипова // *Вестн. НЯЦ РК.* — 2018. — № 4. — С. 107–110.
- 31 Kausar A. A review of fundamental principles and applications of polymer nanocomposites filled with both nanoclay and nano-sized carbon allotropes-graphene and carbon nanotubes / A. Kausar // *J. Plast. Film Sheeting.* — 2020. — No. 36. — P. 209–228. <https://doi.org/10.3390/polym13244401>
- 32 Jose A.J. 3 - Preparation and characterization of polysulfone-based nanocomposites / A.J. Jose, M. Alagar // *Manufacturing of Nanocomposites with Engineering Plastics.* — 2015. — P. 31–59. <https://doi.org/10.1016/B978-1-78242-308-9.00003-3>
- 33 Ke Y.C. *Polymer-Layered Silicate and Silica Nanocomposites* / Y.C. Ke, P. Stroeve // Elsevier: Amsterdam, The Netherlands, 2005. ISBN 0080457584.
- 34 Kumar A. Exfoliation of hematite: Morphological, structural and magnetic investigations / A. Kumar, R. Zhang, M. Venkatesan, P. Stamenov, J.M.D. Coey // *J. Magn. Magn. Mater.* — 2022. — Vol. 542. — P. 168507. <https://doi.org/10.1016/j.jmmm.2021.168507>
- 35 Hernandez C. Evolution of the texture and structure of SiO₂-Al₂O₃ xerogels and aerogels as a function of the Si to Al molar ratio / C. Hernandez, A.C. Pierre // *J. of sol-gel science and technology.* — 2001. — No. 20. — P. 227–243. <https://doi.org/10.1023/A:1008714617174>

- 36 Gordeeva N.V. Influence of nanoparticles of layered silicates on the properties of aqueous dispersions of acrylate copolymers and films based on them / N.V. Gordeeva, I.A. Tolmachev, L.N. Mashlyakovskiy, V.K. Vasiliev // Proceedings of the St. Petersburg State Technological Institute (Technical University). — 2012. — No. 14. — P. 41–44.
- 37 Sun Q. Water-based polymer/clay nanocomposite suspension for improving water and moisture barrier in coating / Q. Sun, F. Joseph Schork, Y. Deng // Composites Science and Technology. — 2007. — No. 67(9). — P. 1823–1829. <https://doi.org/10.1016/j.compscitech.2006.10.022>
- 38 Paul D. *Polymer blends* / D. Paul, S. Newman. — NY, USA: Academic Press, 1978. <https://doi.org/10.1016/B978-0-12-546802-2.X5001-5>
- 39 Morawetz H. *Macromolecules in solution* / H. Morawetz. — New York: Wiley, 1975. <https://doi.org/10.1002/pol.1976.130140914>
- 40 Burmistr M.V. Synthesis, structure, thermal and mechanical properties of nanocomposites based on linear polymers and layered silicates modified by polymeric quaternary ammonium salts (ionenes) / M.V. Burmistr, K.M. Skhyy, V.V. Shilov, P. Pissis, A. Spanoudaki, I.V. Sukha, V.I. Tomilo, Y.P. Gomza // Polymer. — 2005. — No. 46. — P. 12226–12232. <https://doi.org/10.1016/j.polymer.2005.10.094>
- 41 Jamshidian M. Structural, mechanical and barrier properties of active PLA-antioxidant films / M. Jamshidian, E.A. Tehrany, M. Imran, M.J. Akhtar, F. Cleymand, S. Desobry // J. FoodEng. — 2012. — No. 110. — P. 380–389. <https://doi.org/10.1016/j.jfoodeng.2011.12.034>
- 42 Ali F. Polymer-clay Nanocomposites, Preparations and Current Applications: A Review / F. Ali, H. Ullah, Z. Ali, F. Rahim, F. Khan, Z.U. Rehman // Curr. Nanomater. — 2016. — No. 1. — P. 83–95. <https://doi.org/10.2174/2405461501666160625080118>
- 43 Motawie A.M. Electrophysical characteristics of polyurethane/organo-bentonite nanocomposites / A.M. Motawie, M. Madani, E.A. Esmail, A.Z. Dacrorry, H.M. Othman, M.M. Badr, D.E. Abulyazied // Egypt. J. Pet. — 2014. — No. 23. — P. 379–387. <https://doi.org/10.1016/j.ejpe.2014.09.005>
- 44 Chen B. Polymer-clay nanocomposites: An overview with emphasis on interaction mechanisms / B. Chen // Br. Ceram. Trans. — 2004. — No. 103. — P. 241–249. <https://doi.org/10.1179/096797804X4592>
- 45 Shokrieh M.M. Fabrication and mechanical properties of clay/epoxy nanocomposite and its polymer concrete / M.M. Shokrieh, A.R. Kefayati, M. Chitsazzadeh // Mater. Des. — 2012. — No. 40. — P. 443–452. <http://dx.doi.org/10.1016/j.matdes.2012.03.008>

Г.К. Мамытбеков, Ж.И. Бексултанов, В.И. Банных, И.В. Данько

Бентонит негізіндегі гибриді композициялық материалдардың синтезі, құрылымы және қасиеттері

Пластификаторлар (ПЭГ-400, глицерин) мен бентонит минералды толтырғыштарының қатысуымен синтетикалық (поли-N-винилпирролидон) және табиғи (агар-агар) макромолекулалардың негізінде гибриді композициялық материалдарды электрондық сәулелену әдісімен синтездеу процесі жүйелі зерттелді. РСА және СЭМ әдістері көмегімен алынған гибриді композициялардың құрылымы минералды компоненттердің интеркаллиренген бөлшектерінің өзара өтімді тор ретінде қарастыруға болатындығы анықталды. Бентонит — өзара өтімді тор гибриді құрамы қалыптасу кезінде минералды толтырғыштың бөлшектері өзара өтімді тордың қабаттарының арасы бойынша біркелкі бөлінбейді. Гибриді композицияның механикалық қасиеттері пластификаторлардың қатысуымен бастапқы полимер қоспасының электронды сәулеленуі кезінде пайда болатын өзара өтімді полимер торының негізгі құрылымдылығымен, сондай-ақ полимер сегменттерінің минералды төсеніштің тораралық қабаттарына интеркаляция жағдайымен анықталады. Үлгіні созу кезінде крейзинг процесінде созылу кезінде ығысу кернеуі үлгінің бекіту перифериясынан орталық бөлігіне шоғырланады. Гибриді композицияның ісіну дәрежесі бентониттің аралық қабаттарына оңай ене алатын полимерлі өзара өтімді тордың құрамындағы төмен молекулалы пластификатордың концентрациясына байланысты екендігі көрсетілген.

Кілт сөздер: гибриді композициялық материалдар (ГКМ), полимерлік-бейорганикалық композициялар (ПБК), электрондық сәулелену, синтетикалық және табиғи полимерлер, бентонит, деформация, қысу, созылу, интеркаляция, өзара өтімді торлар (ӨӨТ).

Г.К. Мамытбеков, Ж.И. Бексултанов, В.И. Банных, И.В. Данько

Синтез, структура и свойства гибридных композиционных материалов на основе бентонита

Проведено систематическое исследование процесса синтеза гибридных композиционных материалов на основе синтетического (поливинил-N-пирролидон) и природного (агар-агар) макромолекул в при-

сутствии пластификаторов (ПЭГ–400, глицерин) и минерального наполнителя бентонита методом электронного облучения. Методами РСА и СЭМ показано, что структура полученных гибридных композиций определяется как взаимопроникающая сетка (ВПС), в объеме которой распределены интеркалированные частицы минеральной компоненты. При формировании гибридной композиции бентонит–ВПС частицы минерального наполнителя неравномерно распределяются по межслоевым поверхностям взаимопроникающей сетки. Установлено, что механические свойства гибридной композиции определяются преимущественно структурной организацией взаимопроникающей полимерной сетки, формирующейся в ходе электронного облучения исходной полимерной смеси в присутствии пластификаторов, а также условиями интеркаляции полимерных сегментов в межпакетные слои минеральной матрицы. В ходе процессов крейзования при растяжении образца происходит концентрирование напряжения сдвига в центральную часть образца от периферии крепления при разрыве. Показано, что степень набухания гибридной композиции сильно зависит от концентрации низкомолекулярного пластификатора в составе полимерной взаимопроникающей сетки, которая может легко импрегнировать в межплоскостные слои бентонита.

Ключевые слова: гибридные композиционные материалы, полимерно-неорганические композиции, электронное облучение, синтетические и природные полимеры, бентонит, деформация, сжатие, растяжение, интеркаляция, взаимопроникающие сети.

References

- 1 Albdiry, M.T., Yousif, B.F., Ku, H., & Lau, K.T. (2013). A critical review on the manufacturing processes in relation to the properties of nanoclay/polymer composites. *J. Compos. Mater.*, 47, 1093–1115. <https://doi.org/10.1177/0021998312445592>
- 2 Du, J.H., & Cheng, H.M. (2012). The fabrication, properties, and uses of graphene/polymer composites. *Macromol. Chem. Phys.* 213, 1060–1077. <https://doi.org/10.1177/0021998312445592>.
- 3 Müller, K., Bugnicourt, E., Latorre, M., Jorda, M., Echegoyen Sanz, Y., Lagaron, J.M., Miesbauer, O., Bianchin, A., Hankin, S., Bözl, U., Pérez, G., Jesdinszki, M., Linder, M., Schuerer, Z., Castello, S., & Schmid, M. (2017). Review on the processing and properties of polymer nanocomposites and nanocoatings and their applications in the packaging, automotive and solar energy fields. *Nanomaterials*, 7, 74. <https://doi.org/10.3390/nano7040074>
- 4 Valapa, R.B., Loganathan, S., Pugazhenthii, G., Thomas, S., & Varghese, T.O. (2017). An Overview of Polymer-Clay Nanocomposites. In *Clay-Polymer Nanocomposites*, Amsterdam, The Netherlands: Elsevier.; pp. 29–81, ISBN: 978-0-323-46153-5. <https://doi.org/10.1016/B978-0-323-46153-5.00002-1>
- 5 Kotal, Moumita., & Bhowmick, A. (2015). Polymer nanocomposites from modified clays: Recent advances and challenges. *Progress in Polymer Science*, 51, 127–187. <https://doi.org/10.1016/j.progpolymsci.2015.10.001>
- 6 Lee, K.-Y., Aitomäki, Y., Berglund, L.A., Oksman, K., & Bismarck, A. (2014). On the use of nanocellulose as reinforcement in polymer matrix composites. *Compos. Sci. Technol.*, 105, 15–27. <https://doi.org/10.1016/j.compscitech.2014.08.032>
- 7 Zhang, J., Manias, E., & Wilkie, C.A. (2008). Polymerically modified layered silicates: An effective route to nanocomposites. *J. Nanosci. Nanotechnol.*, 8, 1597–1615.
- 8 Nosonovsky, M., & Bhushan, B. (2010). Green tribology: Principles, research areas and challenges. *Philos. Trans. R. Soc. A math. Phys. Eng. Sci.*, 368, 4677–4694. <https://doi.org/10.1098/rsta.2010.0200>
- 9 Kasprzhitsky, A.S., Morozov, A.V. Lazorenko, G.I., Talpa, B.V., & Yavna, V.A. (2013). Kompleksnoe issledovanie sostava i strukturnykh osobennostei porodooobrazuyushchikh mineralov bentonitovykh glin Millerovskogo mestorozhdeniia [Complex research of the composition and structural characteristics of the rock-forming minerals in Millerovsky bentonite clay]. *Inzhenernyi vestnik Dona — Engineering bulletin of Don*, 3, 26. <https://cyberleninka.ru/article> [in Russian].
- 10 Mamidi, N., Gamero, M.R.M., Villela-Castrejón, J., & Elías-Zúñiga, A. (2019). Development of ultra-high molecular weight polyethylene functionalized carbon nano-onions composites for biomedical applications. *Diam. Relat. Mater.* 97, 107435. <https://doi.org/10.1016/j.diamond.2019.05.020>
- 11 Gylymkhan, N.T., Zhumagalieva, Sh.N., & Abilov, Zh.A. (2016). Vosmozhnosti ispolzovaniia bentonitovykh glin v meditsine [Possibilities of using bentonite clays in medicine]. *Doklady Natsionalnoi akademii nauk Respubliki Kazakhstan — Reports of the National Academy of Sciences of the Republic of Kazakhstan*, 4, 24–33 [in Russian].
- 12 Tiwari, J.N., Tiwari, R.N., & Kim, K.S. (2012). Zero-dimensional, one-dimensional, two-dimensional and three-dimensional nanostructured materials for advanced electrochemical energy devices. *Prog. Mater. Sci.*, 57, 724–803. <https://doi.org/10.1016/j.pmatsci.2011.08.003>
- 13 Chan, J.X., Wong, J.F., Petru, M., Hassan, A., Nirmal, U., Othman, N., & Ilyas, R.A. (2021). Effect of Nanofillers on Tribological Properties of Polymer Nanocomposites: A Review on Recent Development. *Polymers.*, 13, 2867. <https://doi.org/10.3390/polym13172867>
- 14 Pavlidou, S., & Papaspyrides, C.D. (2008). A review on polymer-layered silicate nanocomposites. *Prog. Polym. Sci.*, 33, 1119–1198. <https://doi.org/10.1016/j.progpolymsci.2008.07.008>
- 15 Alexandre, M., & Dubois, P. (2008). Polymer-layered silicate nanocomposites: preparation, properties and uses of a new class of materials. *Material Science and Engineering*, 28, 1–63. [https://doi.org/10.1016/S0927-796X\(00\)00012-7](https://doi.org/10.1016/S0927-796X(00)00012-7)

- 16 Mamytkbekov, G., Beksultanov, Z., & Bannykh, V. (2022). Synthesis, structure and mechanical properties of composite hydrogels for medical applications. *Chemical Bulletin of the Kazakh National University*, 104 (1), 30–42. <https://doi.org/https://doi.org/10.15328/cb1264>
- 17 Dalia, E. Abulyazied, & Antoaneta E. (2021). Investigative Study on the Progress of Nanoclay-Reinforced Polymers: *Preparation, Properties, and Applications*. *Review Polymers*, 13, 4401. <https://doi.org/10.3390/polym13244401>
- 18 Zhu, W., Chu-Hua, L., Chang, F.-C., & Kuo, S.-W. (2012). Supramolecular ionic strength-modulating microstructures and properties of nacre-like biomimetic nanocomposites containing high loading clay. *RSC Adv.*, 2, 6295–6305. <https://doi.org/10.1039/c2ra20523h>
- 19 Gordeeva, N.V., Tolmachev, I.A., Mashlyakovskiy, L.N., & Vasiliev, V.K. (2012). Influence of nanoparticles of layered silicates on the properties of aqueous dispersions of acrylate copolymers and films based on them. *Proceedings of the St. Petersburg State Technological Institute (Technical University)*, 14, 41–44.
- 20 Botana, A., Mollo, M., Eisenberg, P., & Sanchez, R. M. T. (2010). Effect of modified montmorillonite on biodegradable PHB nanocomposites. *Applied Clay Science*, 47 (3–4), 263–270. <https://doi.org/10.1016/j.clay.2009.11.001>
- 21 Srinivasan, R. (2011). Advances in Application of Natural Clay and Its Composites in Removal of Biological, Organic, and Inorganic Contaminants from Drinking Water. *Advances in Materials Science and Engineering*. Article ID 872531, 17. <https://doi.org/10.1155/2011/872531>
- 22 Maršálek, R., & Navrátilová, Z. (2011). Comparative study of CTAB adsorption on bituminous coal and clay mineral. *Chemical Papers.*, 65 (1), 77–84. <https://doi.org/10.2478/s11696-010-0076-9>
- 23 Fischer, H. (2003). Polymer nanocomposites: from fundamental research to specific applications. *Materials Science and Engineering: C*, 23 (6-8), 763–772. <https://doi.org/10.1016/j.msec.2003.09.148>
- 24 Nagornov, R. S., Razgovorov, P. B., Smirnova, E. A., & Razgovorova, M. P. (2015). Complex extraction of biologically active ingredients from oil-containing media using mineral sorbents. *Chemistry and Medicine: Abstract of report of X All-Russian conference with international participation*. In-t org. Chemistry USC RAS. Ufa-Abzakovo: Gilem.
- 25 Galan, E., & Singer A. (2011). *Developments in Palygorskite-Sepiolite Research. A New Outlook of these Nanomaterials*, Oxford-Amsterdam: Elsevier. ISSN 1572-4352. <https://doi.org/10.1016/1B978-0-444-53607-5.00001-3>
- 26 Tarasevich, Yu.I. (1988). Stroenie i khimiia poverkhnosti sloistykh silikatov [*Structure and chemistry of the surface of layered silicates*]. Kyiv: Naukova dumka [in Russian].
- 27 Greg, S., & Sing, K. (1984). Adsorbtsiia, udelnaia poverkhnost, poristost [*Adsorption, specific surface area, porosity*]. Translation from English. Moscow: Mir [in Russian].
- 28 Bonilla-Petriciolet, A., Mendoza-Castillo, D.-I., & ReynelÁvila, H.-E. (2017). *Adsorption Processes for Water Treatment and Purification*. Cham.: Springer. <https://doi.org/10.1007/978-3-319-58136-1>
- 29 Gerasin, V.A., Antipov, E.M., Karbushev, V.V., Kulichikhin, V.G., Karpacheva, G.P., Talroze, R.V., & Kudryavtsev, Ya.V. (2013). New approaches to creation of hybrid polymer nanocomposites: structural materials to high-tech applications. *Advances in Chemistry*, 82 (4), 303–332. <https://doi.org/10.1070/RC2013v082n04ABEH004322>
- 30 Kupchishin, A.I., & Taipova, B.G. (2018). Razlichnye modeli razrusheniia polimernykh materialov i kompozitov elektronnymi puchkami [Various models of destruction of polymeric materials and composites by electron beams]. *Vestnik Natsionalnogo yadernogo tsentra Respubliki Kazakhstan — Bulletin of National Nuclear Center of the Republic of Kazakhstan*, 4, 107–110 [in Russian].
- 31 Kausar, A. (2020). A review of fundamental principles and applications of polymer nanocomposites filled with both nanoclay and nano-sized carbon allotropes-graphene and carbon nanotubes. *J. Plast. Film Sheeting*, 36, 209–228. <https://doi.org/10.3390/polym13244401>
- 32 Jose, A.J., & Alagar, M. (2015). 3 - Preparation and characterization of polysulfone-based nanocomposites. *Manufacturing of Nanocomposites with Engineering Plastics*, 31–59. <https://doi.org/10.1016/B978-1-78242-308-9.00003-3>
- 33 Ke, Y.C., & Stroeve, P. (2005). *Polymer-Layered Silicate and Silica Nanocomposites*; Elsevier: Amsterdam, The Netherlands, ISBN 0080457584.
- 34 Kumar, A., Zhang, R., Venkatesan, M., Stamenov, P., & Coey, J.M.D. (2022). Exfoliation of hematite: Morphological, structural and magnetic investigations. *J. Magn. Magn. Mater.*, 542, 168507. <https://doi.org/10.1016/j.jmmm.2021.168507>
- 35 Hernandez, C., & Pierre, A.C. (2001). Evolution of the texture and structure of SiO₂-Al₂O₃ xerogels and aerogels as a function of the Si to Al molar ratio. *J. of sol-gel science and technology*, 20, 227–243. <https://doi.org/10.1023/A:1008714617174>
- 36 Gordeeva, N.V., Tolmachev, I.A., Mashlyakovskiy, L.N., & Vasiliev, V.K. (2012). Influence of nanoparticles of layered silicates on the properties of aqueous dispersions of acrylate copolymers and films based on them. *Proceedings of the St. Petersburg State Technological Institute (Technical University)*, 14, 41–44.
- 37 Sun, Q., Joseph Schork F., & Deng, Y. (2007). Water-based polymer/clay nanocomposite suspension for improving water and moisture barrier in coating. *Composites Science and Technology*, 67(9), 1823–1829. <https://doi.org/10.1016/j.compscitech.2006.10.022>
- 38 Paul, D., & Newman, S. (Eds.) (1978). *Polymer blends*, NY, USA: Academic Press. <https://doi.org/10.1016/B978-0-12-546802-2.X5001-5>
- 39 Morawetz, H. (1975). *Macromolecules in solution*. New York: Wiley. <https://doi.org/10.1002/pol.1976.130140914>

- 40 Burmistr, M.V., Skhyy, K.M., Shilov, V.V., Pissis, P., Spanoudaki, A., Sukha, I.V., Tomilo, V.I., & Gomza, Y.P. (2005). Synthesis, structure, thermal and mechanical properties of nanocomposites based on linear polymers and layered silicates modified by polymeric quaternary ammonium salts (ionenes). *Polymer*, 46, 12226–12232. <https://doi.org/10.1016/j.polymer.2005.10.094>
- 41 Jamshidian, M., Tehrani, E.A., Imran, M., Akhtar, M.J., Cleymand, F., & Desobry, S. (2012). Structural, mechanical and barrier properties of active PLA-antioxidant films. *J. FoodEng.*, 110, 380–389. <https://doi.org/10.1016/j.jfoodeng.2011.12.034>
- 42 Ali, F., Ullah, H., Ali, Z., Rahim, F., Khan, F., & Rehman, Z.U. (2016). Polymer-clay Nanocomposites, Preparations and Current Applications: A Review. *Curr. Nanomater.*, 1, 83–95. <https://doi.org/10.2174/2405461501666160625080118>
- 43 Motawie, A.M., Madani, M., Esmail, E.A., Dacrorry, A.Z., Othman, H.M., Badr, M.M., & Abulyazied, D.E. (2014). Electrophysical characteristics of polyurethane/organo-bentonite nanocomposites. *Egypt. J. Pet.*, 23, 379–387. <https://doi.org/10.1016/j.ejpe.2014.09.005>
- 44 Chen, B. (2004). Polymer-clay nanocomposites: An overview with emphasis on interaction mechanisms. *Br. Ceram. Trans.* 103, 241–249. <https://doi.org/10.1179/096797804X4592>
- 45 Shokrieh, M.M., Kefayati, A.R., & Chitsazzadeh, M. (2012). Fabrication and mechanical properties of clay/epoxy nanocomposite and its polymer concrete. *Mater. Des.* 40, 443–452. <http://dx.doi.org/10.1016/j.matdes.2012.03.008>

Information about the authors*

Mamytbekov, Galymzhan Kulamkadyrovich (*corresponding author*) — Doctor of Chemical Sciences, Full Professor, Chief Researcher, Center for Complex Environmental Research, Institute of Nuclear Physics, Ibragimov St., 1, 050032, Almaty, Kazakhstan, e-mail: g.mamytbekov@inp.kz; <https://orcid.org/0000-0003-3848-3709>;

Beksultanov, Zhomart Imuchanbetovich — Head of Research and Production Center for Radiation Technologies, Institute of Nuclear Physics, Ibragimov St., 1, 050032, Almaty, Kazakhstan, e-mail: bek@inp.kz; <https://orcid.org/0000-0002-4778-5023>;

Bannykh, Valentina Ivanovna — Head of the Quality Control Group, Institute of Nuclear Physics, Ibragimov St., 1, 050032, Almaty, Kazakhstan, e-mail: v.bannykh@inp.kz; <https://orcid.org/0000-0002-2779-6390>;

Dan'ko, Igor Vitalievich — Deputy Head of the Scientific and Technical Department of Accelerator Technologies, Institute of Nuclear Physics, Ibragimov St., 1, 050032, Almaty, Kazakhstan, e-mail: i.danko@inp.kz; <https://orcid.org/0000-0001-7377-5913>

*The author's name is presented in the order: *Last Name, First and Middle Names*

Q.N. Berdinazarov*, E.O. Khakberdiev, N.F. Normurodov, N.R. Ashurov

Uzbekistan Academy of Sciences, Institute of Polymer Chemistry and Physics, Tashkent, Uzbekistan

(*Corresponding author's e-mail: qodirberdinazarov@mail.ru)

Mechanical and Thermal Degradation Properties of Isotactic Polypropylene Composites with Cloisite15A and Cloisite20A

In this work, the influence of maleic anhydride grafted polypropylene (PP-g-MA) content on thermal and mechanical properties of polypropylene (PP) composites with two types of clays, differing modifier density in the interlayer space, Cloisite15A and Cloisite20A, was studied. PP/clay composites were melt blended in presence of different content of PP-g-MA from 3, 6, 9, and 12 wt.%. It was found that Cloisite15A with a high density of the modifier promotes the formation of intercalated structures, while Cloisite20A with a low density of the modifier, predominantly exfoliated nanocomposites are formed. In the first case, the structure tends to become intercalated whilst composites with Cloisite20A favor the formation of predominantly exfoliated structures. The formation of the nanocomposite is accompanied by a significant increase in thermal stability (50 % weight loss is observed at temperatures of 360 °C and 430 °C for polypropylene and nanocomposites based on it, respectively). An analysis of the mechanical properties of nanocomposites generally indicates an increase in the elastic modulus by 15–20 %, and this effect is more pronounced for exfoliated structures, the yield strength practically does not change and the elongation at break decreases noticeably.

Keywords: polypropylene, clay, composite, polypropylene grafted maleic anhydride, intercalation, exfoliation, oxidation, montmorillonite.

Introduction

Recent research in polymer science has shown finer dispersed inorganic layered silicates or smectite clays through the organic polymer, increasing its mechanical, thermal, barrier, and fire retardant properties [1–7]. Layered silicates are made up of several hundred thin platelets stacked in orderly particles or tactoids with dimensions of 8–10 µm. Each disk-shaped platelet has a large aspect ratio of approximately 100–1000 and is easily agglomerated due to the interlayer van der Waals forces. Each leaf contains an octahedral layer of alumina or magnesium flanked by two outer tetrahedral layers of silica, so the octahedral layer shares the tetrahedral layer with its oxygen atoms. Accordingly, clay particles should be homogeneously finer dispersed and exfoliated as individual platelets within the polymer matrices to accomplish the ultimate properties. Moreover, the lower clay content is also essential to achieve the large contact surface area between the polymer matrix and the fillers and to obtain good dispersion by alleviating the clay aggregation [8–9, 20].

Due to its hydrophilic properties, clay minerals are incompatible with organic polymers like polyolefins. Researchers employed surfactants aim to make compatible clay with PP. Alkyl amines are widely used surfactants in obtaining PP clay nanocomposites. In particular, exceeding amine modifiers number 12 provides exfoliation and self-assembly of individual silicate layers within the PP matrix [20]. Cloisite 15A and Cloisite 20A are organophilic clay minerals modified with dimethyl, dehydrogenated tallow, quaternary ammonium. Hydrogenated tallow includes 65 % C18, 30 % C16, and 5 % C14. The only difference between these two clays is the surfactant concentration between layers which accounts for 1,25 and 0.95 meq/g in Cloisite 15A and Cloisite 20A, respectively. Accordingly, the interlayer distance of Cloisite15A (3,06 nm) is bigger than Cloisite 20A (2,4 nm) [10].

Tessier et al. [11] used two types of clays: Cloisite 20A and Cloisite 30B (modified with a polar surfactant) to obtain starch-grafted polypropylene organoclay nanocomposites. They used Cloisite 20A due to its affinity to the polypropylene phase of the polymer matrix while Cloisite 30B has an affinity to the starch phase. They interpret that the initial inter-platelet distance of this non-polar modified montmorillonite (Cloisite 20A) is higher than that of its polar modified counterpart (Cloisite 30B). For this reason, on the occasion of Cloisite 20A, the exfoliation mechanism is more mechanically driven (by polypropylene chain insertion) rather than chemically in PP/clay nanocomposites.

Thermal stability of PP/clay composites was considerably increased as soon as obtained exfoliated structure [12–16]. The authors concluded that the improvement in the thermal properties was correlated with lower oxygen permeability resulting from an increased diffusion path for oxygen as well as volatile decomposition products. PP-g-MA was found the most effective compatibilizer for PP/clay composites in many articles [17–20]. There are a lot of publications that investigate the effect of different clay modification techniques [21, 22].

Phase diagram of polymer – clay mixture, proposed by Ginzburg et al., revealed that increased length and density of grafted chains led to improved miscibility of the clay and the polymer, in its turn, proper miscibility contributes to exfoliated structure in the wide range of clay volume ratio. In the case of short surfactant macromolecules, the polymer is not likely to insert space between the clay layers. This causes immiscibility for major values of the Flory – Huggins parameter and the clay volume ratio. There is also a limitation to the strong interaction between grafted chains and polymer macromolecules [23].

For different surfactant lengths, surfactant coverage and surfactant – matrix enthalpic, Balazs et al. studied morphological behavior of polymer clay composites by employing their model named self-consistent field calculation. According to their model, it turned out that a longer organic modifier provides better intercalation of polymer macromolecules to penetrate the space between clay platelets. However, the density of surfactant should be reasonable because dense coverage makes intercalation and/or exfoliation impossible [24].

Accordingly, in this paper isotactic PP, PP-g-MA, and two types of clays were chosen in obtaining composites and the aim of this study is to explore the properties of PP/clay nanocomposites obtained with different modifier densities between interlayer space in the variation of compatibilizer content.

Experimental

Materials

Isotactic PP (J-170T) with MFI = (2.16 kg, 230 °C) 21 g/10 min was kindly provided by JV Uz-Kor Gas Chemical LLC. PP-g-MA with 2.5 wt.% maleic anhydride content and MFI = (2.16 kg, 230 °C) >200 g/min was provided by JV UzAuto CEPLA LLC as a gift. Cloisite15A, (spacing $d_{001} = 3.06$ nm, dimethyl dehydrogenated tallow ammonium conc. 1.25 meq/g), Cloisite20A, (spacing $d_{001} = 2.4$ nm, dimethyl dehydrogenated tallow ammonium conc. 0.95 meq/g) Southern Clay Products, Inc., Gonzales, TX.

Preparation

Components melt blended in Brabender Plastograph (Germany). First PP and PP-g-MA were introduced into plastograph after getting molten mass clay was introduced and kept during 8 min 150 rpm in order to provide better mixing components one another. Next, tensile test samples were prepared by injection-molding machine Mercator 1971 (Poland). Name of samples and their content ratios are given in Table 1.

Table 1

Name of obtained samples and their contents

Name of samples	PP, %	PP-g-MA, %	Cloisite15A, %	Cloisite20A,%
PP	100	–	–	–
PP-g-MA	–	100	–	–
PP/MA10	90	10	–	–
PP/MA20	80	20	–	–
15A3	94	3	3	–
15A6	91	6	3	–
15A9	88	9	3	–
15A12	85	12	3	–
20A3	94	3	–	3
20A6	91	6	–	3
20A9	88	9	–	3
20A12	85	12	–	3

XRD measurements

XRD measurements were conducted with Rigaku Miniflex 600 (Japan) in the condition of 40 kV voltage, 15 mA current and 0.02° step.

DSC and TGA measurements

Thermal properties of the samples studied by DSC and TGA analysis were conducted simultaneously, in the range from room temperature to 600 °C by Linseis thermal analysis PT1610.

Mechanical analysis

Tensile tests were conducted according to ASTM D 638 in Shimadzu AG-X PLUS (Japan). For measuring tensile module (E), 1 mm/min crosshead speed was chosen until 0,3% deformation, after that crosshead speed increased immediately to 20 mm/min for further exploring yield stress (σ) and deformation (ϵ).

MFI measurement

MFI was measured according to ASTM D 1238 using Zwick extrusion plastometer (Germany) at 230 °C/2.16 kg.

Results and Discussion

Small angle X-ray diffraction

Small angle X-ray (SAXS) diffraction is identical for characterizing clay dispersion in polymer matrix [25–27]. The basal spacing of the silicate layer (d_{001}) was calculated with Bragg's law: $n\lambda = 2d\sin\theta$. Figures 1 and 2 show SAXS pattern of obtained samples. The difference between these two organically modified clays is modifier volume and interlayer distance d (which Cloisite15A has greater than Cloisite20A) [28]. Cloisites have two main peaks, the second peak at $2\theta = 7.2^\circ$ ($d_{001} = 1.2$ nm) corresponding to interlayer distance of pure unmodified montmorillonite (MMT), the first peak occurs at $2\theta = 2.88^\circ$ in Cloisite15A corresponding to intercalation of MMT as a result of modifier penetration during modification while in Cloisite20A, this peak accounts for in $2\theta = 3.68^\circ$. SAXS curves in Figures 1 and 2, compare the effect of PP-g-MA content on the intercalation degree of Cloisite15A and Cloisite20A. There was a considerable difference between the dispersion of clay through the PP matrix. While composites with Cloisite15A show an intercalated structure, Cloisite20A achieves exfoliation except for 20A3. In the case of Cloisite15A first peak in $2\theta = 2.8^\circ$ shifts towards small angles about $2\theta = 2.3^\circ$ corresponding to $d = 38.25$ Å, however, 15A9 has slightly smaller angles than others, indicating all samples' intercalation. The second peak also decreased from $2\theta = 7.2^\circ$ to $2\theta = 4.7^\circ$. With respect to the intensity of the peaks, the smallest intensity was seen in both main peaks in 15A9. This reduction in the peak intensity can be interpreted as the formation particular amount of exfoliated structure as well as intercalated. When it comes to Cloisite20A, except for composite with 20A3 all had a considerable shift in peaks to lower than $2\theta = 2^\circ$ angle, as a result of exfoliation. The reason for exception 20A3 is the lack of compatibilizer to achieve finer dispersion of clay in polymer matrix. Occurrence of exfoliation in the composites with Cloisite20A can be proved shifting of the first peak smaller angle relation to pure Cloisite20A.

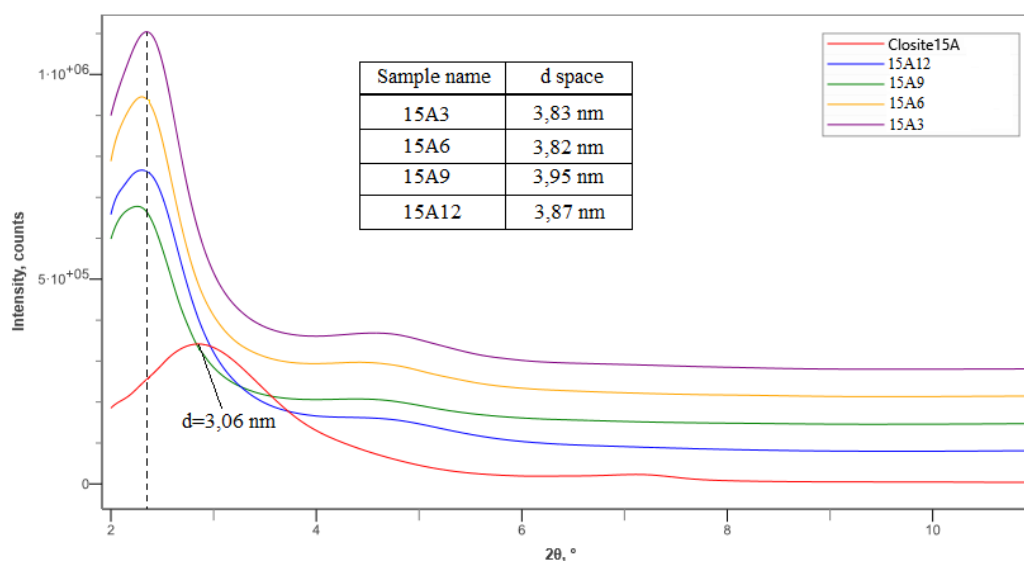


Figure 1. PP and Cloisite15A composites small angle X-ray curves

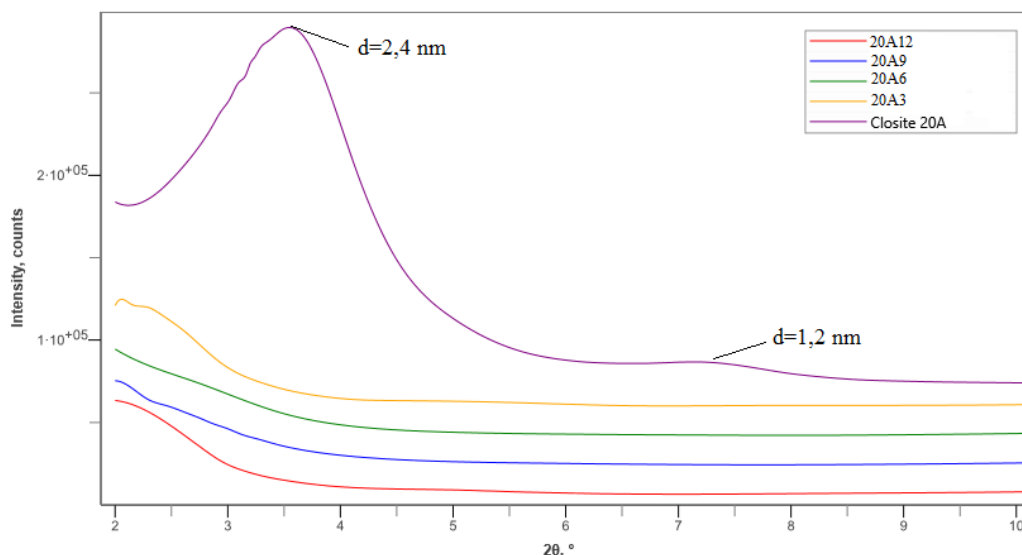


Figure 2. PP and Cloisite20A composites small angle X-ray curves.

MFI

Figure 3 compares MFIs of PP and PP-g-MA blends. PP-g-MA shows more than 200 g/10 min MFI while PP has 21 g/10 min. Presence of 10 wt.% PP-g-MA in PP/PP-g-MA blends MFI accounts for 56 g/10 min and further addition of PP-g-MA increases MFI to 94 g/10 min. This is due to the low molecular weight of PP-g-MA and, as shown in a number of works [14, 15, 23, 24], it is oligomeric functionalized PP that provides favorable conditions for intercalation in the interlayer space and subsequent exfoliation of MMT particles. For PP and clay systems, MFI decreases as soon as the formation of exfoliated and intercalated structures. Our compounds also exhibited these properties (Figure 4). For composites with Cloisite15A, when the ratio of compatibilizer/filler was 1, MFI is 58.6 g/10 min and as compatibilizer content increases MFI decreases to 17.5 g/10 min in the 15A9, however, subsequent addition of PP-g-MA causes slight growth in the 15A12. The initial reduction in MFI is related to the extension of clay particles dimensions as a result of intercalation. When PP-g-MA content reaches saturation point, that is 9 wt.%, additional PP-g-MA causes to increase MFI. With regard to composites with Cloisite20A, an optimal amount of compatibilizer is 6 wt.% and extra compatibilizer just leads to the increase in the melt flow without participating in intercalation or exfoliation. Intercalated centers in the form of physical knots (similar to crosslinking), as PP-g-MA rises, leads to the increase of the compounds' viscosity. An extremal dependence of viscosity is observed for exfoliated structures (uniform distribution of nanoparticles) with a minimum at a PP-g-MA content of 6 wt.%. For these structures, the contribution of low-viscosity PP-g-MA above 6 wt.% becomes noticeable.

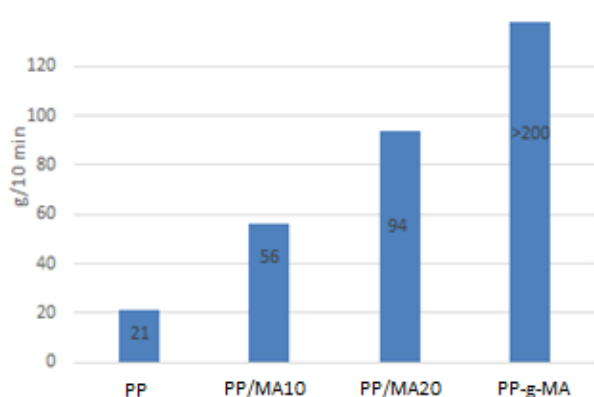


Figure 3. MFI of PP and PP-g-MA blends

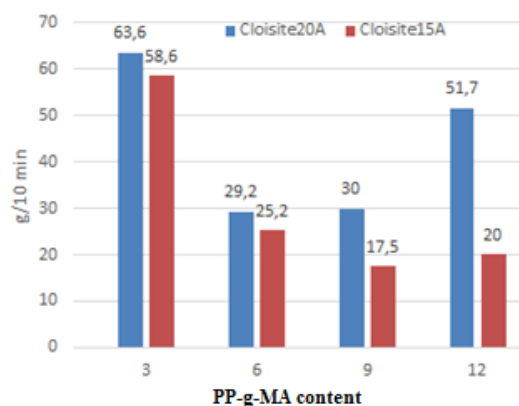


Figure 4. MFI of composites based on Cloisite15A and Cloisite20A

DSC and TGA measurements

DSC curves for PP and PP-g-MA blends show different oxidation behavior while the melting temperature of the samples is almost the same. Showing a melting point of 158.5°C, PP stands stable until 220 °C, and subsequent heating causes intensive oxidation. PP-g-MA with a melting point of 160.6 °C is immediately engaged in oxidation after melting. Their blends indicate thermal behavior corresponding to individual components. As PP-g-MA content increases in the blend, oxidation occurs in relatively lower temperatures (Figure 5). Figure 6 compares DSC curves of composites with Cloisite15A, reflecting differences only in oxidation behavior. In composites with 9 and 12 wt.%, although PP-g-MA leads to oxidation due to intercalation, engaging in oxidation is reduced. DSC curves of composites with Cloisite20A show distinction in both melting point and oxidation (Figure 7). 20A3, intercalated composite, has a melting point of 159.1 °C and gets involved in oxidation intensively after melting. However, when PP-g-MA content is increased by 6 wt.% the composite is stable to oxidation until 188 °C. Due to the penetration of PP-g-MA molecules into the interlayer space of filler, this exfoliated composite has a lower melting point temperature, which is 157.9 °C, in this case. Even though there is exfoliation, the subsequent addition of PP-g-MA again causes more sensitive oxidation behavior and increased melting points, in the compositions with 9 and 12 wt.% of Cloisite20A.

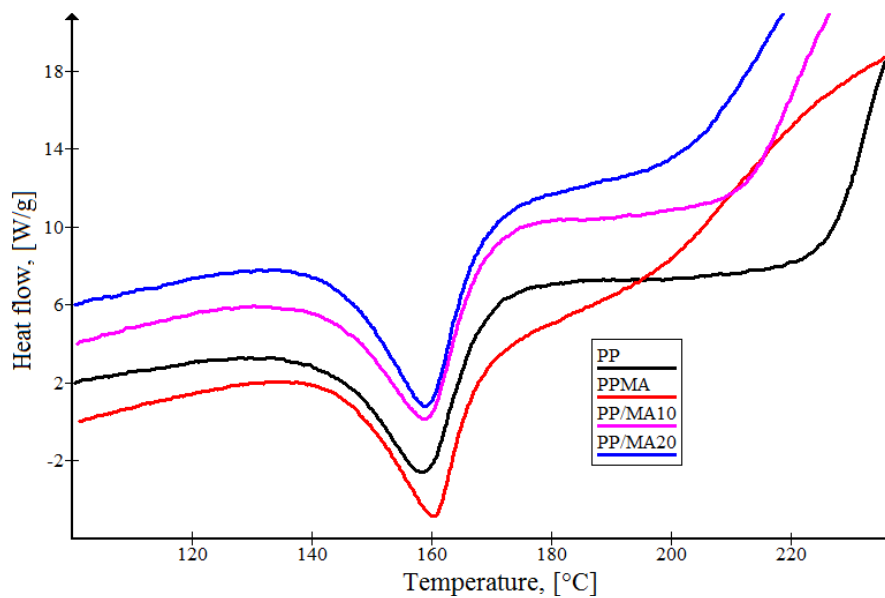


Figure 5. DSC curves of PP and PP-g-MA blends

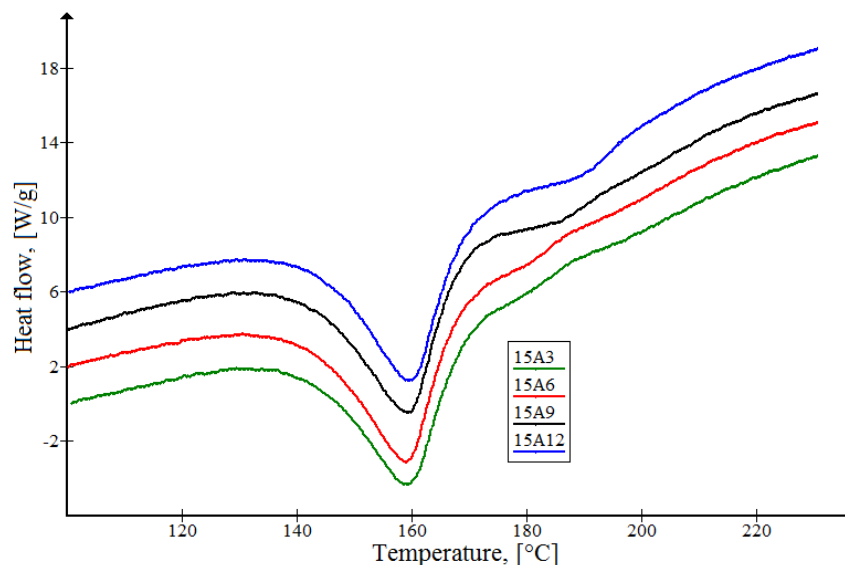


Figure 6. DSC curves of composites with Cloisite15A

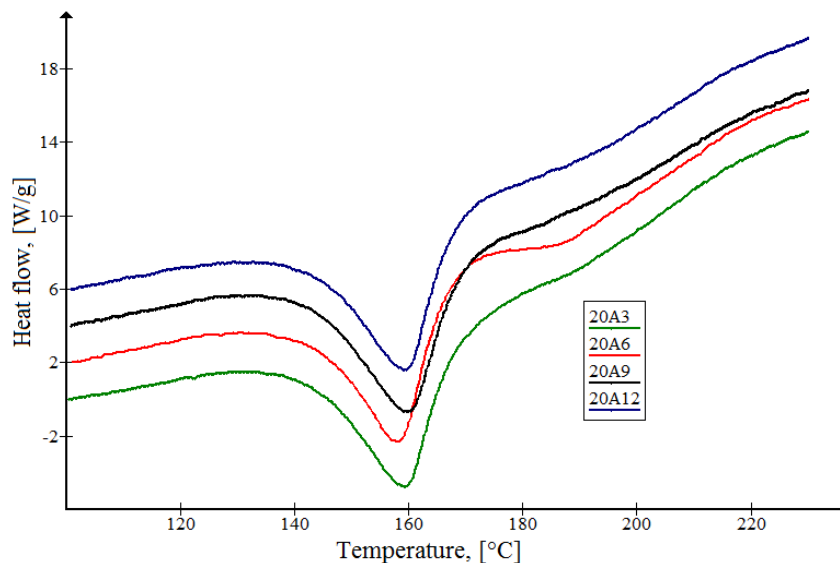


Figure 7. DSC curves of composites with Cloisite20A

Except for DSC, TGA analyses of obtained samples also were conducted. In Figure 8, PP starts mass loss at 237 °C (onset temperature of degradation) while in the case of PP-g-MA accounts for 256 °C. Furthermore, after starting degradation, PP engages in degradation more intensively than PP-g-MA. PP and PP-g-MA blends show different degradation mechanisms, as increases PP-g-MA content in the blends degradation curve of the blend tends to become similar to PP-g-MA. However, PP/MA10 and PP/MA20 blends start degradation in lower temperatures relative to PP. Actually, the onset temperature of degradation must have been between degradation temperatures of PP and PP-g-MA according to the rule of polymer additiveness. The reason for this is that PP-g-MA makes PP sensitive toward oxidation, due to its individual thermal behavior, during melt processing components, according to the DSC curves in Figure 5. PP-g-MA uptakes oxygen during melt processing and then this absorbed oxygen leads to degradation by generating free radical which causes PP/MA10 and PP/MA20 blends mass loss in relatively earlier temperatures [9]. With regard to TGA analysis of composites obtained with Cloisite15A and Cloisite20A, though PP shows superior thermal stability to oxidation among samples in DSC analysis, thermal degradation properties — mass loss — of PP are inferior to that of PP/clay nanocomposites (Figure 9). In PP/clay nanocomposites, clay acts as an excellent insulating barrier that slows the release of gas from decomposition, so the degradation temperature increases. In general, the presence of clay in the PP tends to the increased thermal stability of the polymer [29].

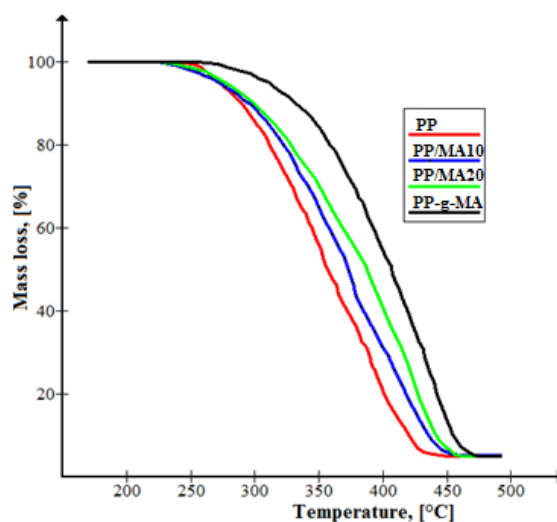


Figure 8. TGA of PP and PP-g-MA blends

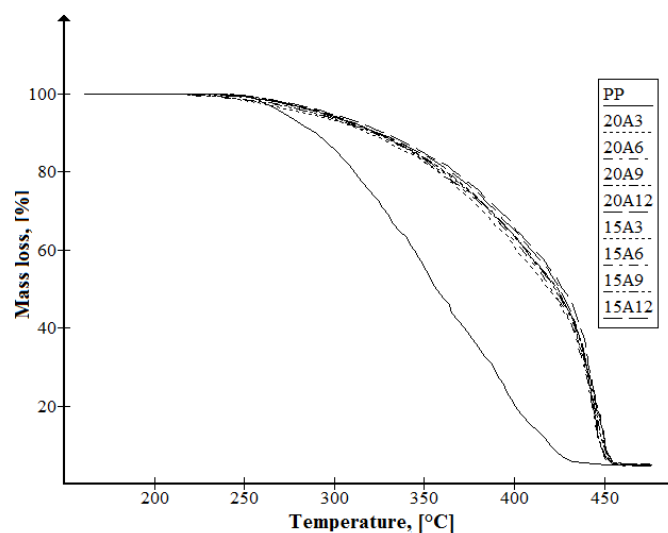


Figure 9. TGA of PP and PP/clay composites

Mechanical measurements

Tensile properties such as tensile module (E), yield stress (σ), and elongation at break (ϵ) have been studied. The results are given in Table 2. The neat PP possesses superior mechanical properties with the best E and σ , while PP-g-MA has good ϵ which is approximately five times more than neat PP. The addition of PP-g-MA to PP makes PP tougher that ϵ increases and reduces E and σ PP tends to become more brittle. In the compositions with Cloisite15A, as PP-g-MA increases, unlike PP/PP-g-MA blend, E and σ also increase; actually, filler content is constant. These phenomena occur due to the development of nano-dispersed clay particles through the matrix as can be seen from SAXS, shifting the peak in d_{001} to small angles. In the case of composites with Cloisite20A, a saturation of composite with PP-g-MA occurs when PP-g-MA content is 6 wt.% and further addition of compatibilizer leads mechanical properties to diminish by causing oxidation of composite in high temperature.

Table 2

Mechanical properties of obtained PP/clay composites

Sample names	E , [MPa]	σ , [MPa]	ϵ , [%]
PP	922±68	36.2±1.2	845±90
PP/MA10	918±54	36.5±1.2	738±93
PP/MA20	770±7	29.9±0.7	984±150
PP-g-MA	713±61	26.2±1.6	697±52
15A3	946±61	32.8±0.6	18.5±2
15A6	960±52	34.5±1.2	17.8±3.8
15A9	968±49	35.2±0.8	127±18
15A12	1008±41	35.3±1.1	102±29
20A3	1000±51	35.4±0.8	12.7±2
20A6	1087±19	37.6±0.3	52±7
20A9	1002±52	35.9±0.5	17.3±5
20A12	932±51	35.4±0.4	16.8±3

Conclusions

Studies have been carried out on the formation of nanocomposites of isotactic polypropylene with modified MMT (Cloisite15A, Cloisite20A), differing modifier densities in the interlayer space. To ensure the diffusion of PP into clays, PP-g-MA (2.5 wt.%) was employed as a compatibilizer, the amount of which a mixture with PP-g-MA varied within 3, 6, 9, and 12 wt.%. It was found that MMT with a high density of the modifier (Cloisite15A) promotes the formation of intercalated structures, while MMT with a low density of the modifier (Cloisite20A), predominantly exfoliated nanocomposites are formed. In the first case, an in-

crease in the content of PP-g-MA leads to an expansion of the interlayer space (from 30.6 to 39.5 Å). In composites with Cloisite20A, only 3 wt.% content of PP-g-MA shows the formation of mixed intercalated and exfoliated structures, while subsequent increasing compatibilizer content favors the formation of predominantly exfoliated structures. The observed structures are reflected in the viscosity parameter. Nanocomposites intercalated with an increase in less viscous PP-g-MA due to limitations associated with the intercalation of macromolecules in the interlayer space and the presence of a specific interaction with the modifier. The clay surface increases markedly (from 65 to 20 g/min), whereas the exfoliation of the structure passes through a minimum in the region between 6 and 9 % by weight of PP-g-MA. The formation of the nanocomposite is accompanied by a significant increase in thermal stability (50 % weight loss is observed at temperatures of 360 °C and 430 °C for polypropylene and nanocomposites based on it, respectively). An analysis of the mechanical properties of nanocomposites generally indicates an increase in the elastic modulus by 15–20 % (considering the presence of low-modulus PP-g-MA), and this effect is more pronounced for exfoliated structures, the yield strength practically does not change, and the elongation at break decreases very noticeably. Heat-resistance properties of intercalated and exfoliated nanocomposites (with a content of 9–12 wt.% and 6 wt.% PP-g-MA, respectively) with enhanced characteristics according to the tensile module and moderate deformability (more than 100 %) generate diverse practical and technological interest.

Acknowledgements

Authors of this work acknowledge JV Uz-Kor Gas Chemical LLC for kindly providing PP grades. For supplying with PP-g-MA JV UzAuto CEPLA LLC is gratefully acknowledged.

References

- 1 Gabr, M. H., Okumura, W., Ueda, H., Kuriyama, W., Uzawa, K., & Kimpara, I. (2015). Mechanical and thermal properties of carbon fiber/polypropylene composite filled with nano-clay. *Composites Part B: Engineering*, 69, 94–100. <https://doi.org/10.1016/j.compositesb.2014.09.033>
- 2 Dolgov, V. V., Ashurov, N. R., Sheveleva, E. E., & Khakberdiev, E. O. (2013). Strength-strain, barrier, thermal, and fire-resistance properties of nanocomposites based on linear polyethylene with montmorillonite. *Russian Journal of Applied Chemistry*, 86(12), 1885–1896. <https://doi.org/10.1134/S1070427213120148>
- 3 Villaluenga, J. P. G., Khayet, M., López-Manchado, M. A., Valentin, J. L., Seoane, B., & Mengual, J. I. (2007). Gas transport properties of polypropylene/clay composite membranes. *European polymer journal*, 43(4), 1132–1143. <https://doi.org/10.1016/j.eurpolymj.2007.01.018>
- 4 Kanny, K., Jawahar, P., & Moodley, V. K. (2008). Mechanical and tribological behavior of clay–polypropylene nanocomposites. *Journal of materials science*, 43(22), 7230–7238. <https://doi.org/10.1007/s10853-008-2938-x>
- 5 Lee, S. Y., Kang, I. A., Doh, G. H., Kim, W. J., Kim, J. S., Yoon, H. G., & Wu, Q. (2008). Thermal, mechanical and morphological properties of polypropylene/clay/wood flour nanocomposites. *Express Polymer Letters*, 2(2), 78–87. <https://doi.org/10.3144/expresspolymlett.2008.11>
- 6 Zhao, C., Qin, H., Gong, F., Feng, M., Zhang, S., & Yang, M. (2005). Mechanical, thermal and flammability properties of polyethylene/clay nanocomposites. *Polymer Degradation and Stability*, 87(1), 183–189. <https://doi.org/10.1016/j.polymdegradstab.2004.08.005>
- 7 Kato, M., Usuki, A., Hasegawa, N., Okamoto, H., & Kawasumi, M. (2011). Development and applications of polyolefin–and rubber–clay nanocomposites. *Polymer journal*, 43(7), 583–593. <https://doi.org/10.1038/pj.2011.44>
- 8 Hotta, S., & Paul, D. R. (2004). Nanocomposites formed from linear low density polyethylene and organoclays. *Polymer*, 45(22), 7639–7654. <https://doi.org/10.1016/j.polymer.2004.08.059>
- 9 Zdiri, K., Elamri, A., & Hamdaoui, M. (2017). Advances in thermal and mechanical behaviors of PP/clay nanocomposites. *Polymer-plastics technology and engineering*, 56(8), 824–840. <https://doi.org/10.1080/03602559.2016.1233282>
- 10 Cervantes-Uc, J. M., Cauich-Rodríguez, J. V., Vázquez-Torres, H., Garfias-Mesías, L. F., & Paul, D. R. (2007). Thermal degradation of commercially available organoclays studied by TGA–FTIR. *Thermochimica Acta*, 457(1–2), 92–102. <https://doi.org/10.1016/j.tca.2007.03.008>
- 11 Tessier, R., Lafranche, E., & Krawczak, P. (2012). Development of novel melt-compounded starch-grafted polypropylene/polypropylene-grafted maleic anhydride/organoclay ternary hybrids. *Express Polymer Letters*, 6(11). <https://doi.org/10.3144/expresspolymlett.2012.99>
- 12 Xie, S., Zhang, S., Wang, F., Liu, H., & Yang, M. (2005). Influence of annealing treatment on the heat distortion temperature of nylon-6/montmorillonite nanocomposites. *Polymer Engineering & Science*, 45(9), 1247–1253. <https://doi.org/10.1002/pen.20359>
- 13 Tang, Y., Hu, Y., Song, L., Zong, R., Gui, Z., Chen, Z., & Fan, W. (2003). Preparation and thermal stability of polypropylene/montmorillonite nanocomposites. *Polymer Degradation and Stability*, 82(1), 127–131. [https://doi.org/10.1016/S0141-3910\(03\)00173-3](https://doi.org/10.1016/S0141-3910(03)00173-3)

- 14 Qin, H., Zhang, S., Zhao, C., Hu, G., & Yang, M. (2005). Flame retardant mechanism of polymer/clay nanocomposites based on polypropylene. *Polymer*, 46(19), 8386–8395. <https://doi.org/10.1016/j.polymer.2005.07.019>
- 15 Duvall, J., Sellitti, C., Myers, C., Hiltner, A., & Baer, E. (1994). Interfacial effects produced by crystallization of polypropylene with polypropylene-g-maleic anhydride compatibilizers. *Journal of applied polymer science*, 52(2), 207–216. <https://doi.org/10.1002/app.1994.070520208>
- 16 Lai, S. M., Chen, W. C., & Zhu, X. S. (2009). Melt mixed compatibilized polypropylene/clay nanocomposites: Part 1—The effect of compatibilizers on optical transmittance and mechanical properties. *Composites Part A: Applied Science and Manufacturing*, 40(6–7), 754–765. <https://doi.org/10.1016/j.compositesa.2009.03.006>
- 17 Lai, S. M., Chen, W. C., & Zhu, X. S. (2011). Melt mixed compatibilized polypropylene/clay nanocomposites. II. Dispersion vs. thermal properties, optical transmittance, and fracture behaviors. *Journal of composite materials*, 45(25), 2613–2631. <https://doi.org/10.1016/j.compositesa.2009.03.006>
- 18 Durmuş, A., Woo, M., Kaşgöz, A., Macosko, C. W., & Tsapatsis, M. (2007). Intercalated linear low density polyethylene (LLDPE)/clay nanocomposites prepared with oxidized polyethylene as a new type compatibilizer: structural, mechanical and barrier properties. *European Polymer Journal*, 43(9), 3737–3749. <https://doi.org/10.1016/j.eurpolymj.2007.06.019>
- 19 Bagheri-Kazemabad, S., Fox, D., Chen, Y., Geever, L.M., Khavandi, A., Bagheri, R., Higginbotham, C.L., Zhang, H., & Chen, B. (2012). Morphology, rheology and mechanical properties of polypropylene/ethylene–octene copolymer/clay nanocomposites: Effects of the compatibilizer. *Composites Science and Technology*, 72(14), 1697–1704. <https://doi.org/10.1016/j.compscitech.2012.06.007>
- 20 Reichert, P., Nitz, H., Klinke, S., Brandsch, R., Thomann, R., & Mülhaupt, R. (2000). Poly (propylene)/organoclay nanocomposite formation: Influence of compatibilizer functionality and organoclay modification. *Macromolecular Materials and Engineering*, 275(1), 8–17. [https://doi.org/10.1002/\(SICI\)1439-2054\(20000201\)275:1%3C8::AID-MAME8%3E3.0.CO;2-6](https://doi.org/10.1002/(SICI)1439-2054(20000201)275:1%3C8::AID-MAME8%3E3.0.CO;2-6)
- 21 Lee, S.S., & Kim, J. (2004). Surface modification of clay and its effect on the intercalation behavior of the polymer/clay nanocomposites. *Journal of Polymer Science Part B: Polymer Physics*, 42(12), 2367–2372. <https://doi.org/10.1002/polb.20109>
- 22 Dong, Y., & Bhattacharyya, D. (2010). Dual role of maleated polypropylene in processing and material characterisation of polypropylene/clay nanocomposites. *Materials Science and Engineering: A*, 527(6), 1617–1622. <https://doi.org/10.1016/j.msea.2009.10.043>
- 23 Ginzburg, V.V., Singh, C., & Balazs, A.C. (2000). Theoretical phase diagrams of polymer/clay composites: the role of grafted organic modifiers. *Macromolecules*, 33(3), 1089–1099. <https://doi.org/10.1021/ma991324e>
- 24 Balazs, A.C., Singh, C., & Zhulina, E. (1998). Modeling the interactions between polymers and clay surfaces through self-consistent field theory. *Macromolecules*, 31(23), 8370–8381. <https://doi.org/10.1021/ma980727w>
- 25 Gabr, M.H., Okumura, W., Ueda, H., Kuriyama, W., Uzawa, K., & Kimpara, I. (2015). Mechanical and thermal properties of carbon fiber/polypropylene composite filled with nano-clay. *Composites Part B: Engineering*, 69, 94–100. <https://doi.org/10.1016/j.compositesb.2014.09.033>
- 26 Rao, G.R., Srikanth, I., & Reddy, K.L. (2021). Effect of organo-modified montmorillonite nanoclay on mechanical, thermal and ablation behavior of carbon fiber/phenolic resin composites. *Defence Technology*, 17(3), 812–820. <https://doi.org/10.1016/j.dt.2020.05.012>
- 27 Fasihnia, S.H., Peighambaroust, S.H., & Peighambaroust, S.J. (2018). Nanocomposite films containing organoclay nanoparticles as an antimicrobial (active) packaging for potential food application. *Journal of Food Processing and Preservation*, 42(2), e13488. <https://doi.org/10.1111/jfpp.13488>
- 28 Hong, C. H., Lee, Y. B., Bae, J. W., Jho, J. Y., Nam, B. U., & Hwang, T. W. (2005). Molecular weight effect of compatibilizer on mechanical properties in polypropylene/clay nanocomposites. *Journal of Industrial and Engineering Chemistry*, 11(2), 293–296.
- 29 Chiu, F. C., Lai, S. M., Chen, J. W., & Chu, P. H. (2004). Combined effects of clay modifications and compatibilizers on the formation and physical properties of melt-mixed polypropylene/clay nanocomposites. *Journal of Polymer Science Part B: Polymer Physics*, 42(22), 4139–4150. <https://doi.org/10.1002/polb.20271>

Қ.Н. Бердиназаров, Е.О. Хакбердиев, Н.Ф. Нормуродов, Н.Р. Ашуров

Cloisite15A және Cloisite20A изотактикалық полипропилен композиттерінің механикалық және жылулық қасиеттері

Мақалада малеин ангидридімен (PP-g-MA) егілген полипропилен құрамының Cloisite15A және Cloisite20A қабатаралық кеңістіктегі модификатордың тығыздығымен ерекшеленетін саздың екі түрі бар полипропилен (ПП) композицияларының термиялық және механикалық қасиеттеріне әсері зерттелген. ПП/саз композиттері 3, 6, 9 және 12 массалық % әртүрлі PP-g-MA құрамының қатысуымен балкытылып, араластырылған. Модификатордың жоғары тығыздығы бар Cloisite15A интеркалирленген құрылымдардың түзілуіне ықпал ететіні, ал модификатордың төмен тығыздығы бар Cloisite20A негізінен қабыршақтанған нанокөпозиттерді түзетіні анықталды. Бірінші жағдайда құрылым интеркаляциялануға бейім, сол уақытта Cloisite20A композиттері негізінен қабыршақтанған құрылымдардың пайда болуына ықпал етеді. Нанокөпозиттің қалыптасуы термиялық

турақтылықтың едәуір артуымен қатар жүреді (50 % салмақ жоғалту полипропилен және оның негізіндегі нанокөпозиттер үшін сәйкесінше 360 °С және 430 °С температурада байқалады). Нанокөпозиттердің механикалық қасиеттерін талдау, әдетте, серпімділік модулінің 15–20 %-ға артқанын көрсетеді (төмен модульді PP-g-MA болуын ескере отырып) және бұл әсер қабыршақтанған құрылымдар үшін айқындық, аққыштық шегінде кернеу іс жүзінде өзгермейді, ал сыну кезінде салыстырмалы ұзару айтарлықтай төмендейді.

Кілт сөздер: полипропилен, саз, көпозит, малеин ангидридті егілген полипропилен, интеркаляция, қабыршақтану, тотығу, монтмориллонит.

К.Н. Бердиназаров, Э.О. Хакбердиев, Н.Ф. Нормуродов, Н.Р. Ашуров

Механические и термические свойства изотактических полипропиленовых композитов с Cloisite15A и Cloisite20A

В статье изучено влияние содержания полипропилена, привитого малеиновым ангидридом (PP-g-MA), на термические и механические свойства композиций полипропилена (ПП) с двумя типами глин, различающихся плотностью модификатора в межслоевом пространстве, Cloisite15A и Cloisite20A. Композиты ПП/глина смешивались в расплаве в присутствии различного содержания PP-g-MA от 3, 6, 9 и 12 мас.%. Выявлено, что Cloisite15A с высокой плотностью модификатора способствует образованию интеркалированных структур, тогда как Cloisite20A с низкой плотностью модификатора формируют преимущественно эксфолированные нанокөпозиты. В первом случае структура имеет тенденцию к интеркаливанию, в то время как композиты с Cloisite20A способствуют образованию преимущественно эксфолированных структур. Формирование нанокөпозита сопровождается значительным усилением термостабильности (50 % потеря веса наблюдается при температурах 360 °С и 430 °С для полипропилена и нанокөпозитов на его основе, соответственно). Анализ механических свойств нанокөпозитов свидетельствует, в целом, об увеличении модуля упругости на 15–20 % (с учетом присутствия низкомолекулярного ППМА), причем этот эффект более выражен для эксфолированных структур, напряжение при пределе текучести практически не претерпевает изменений, а относительное удлинение при разрушении весьма заметно уменьшается.

Ключевые слова: полипропилен, глина, көпозит, полипропилен с привитым малеиновым ангидридом, интеркаляция, эксфолиация, окисление, монтмориллонит.

Information about authors*

Berdinazarov, Qodirbek Nuridin ugli (*corresponding author*) — PhD student, Uzbekistan Academy of Sciences, Institute of Polymer Chemistry and Physics, 7^{“b”}, str. A. Kadyri, 100128, Tashkent, Uzbekistan; e-mail: qodirberdinazarov@mail.ru; <https://orcid.org/0000-0001-8888-2359>;

Khakberdiev, Elshod Olmosovich — PhD, Uzbekistan Academy of Sciences, Institute of Polymer Chemistry and Physics, 7^{“b”}, str. A. Kadyri, 100128, Tashkent, Uzbekistan; e-mail: profhaqberdiyev@gmail.com; <https://orcid.org/0000-0002-7707-2219>;

Normurodov, Nurbek Fayzullo ugli — PhD student, Uzbekistan Academy of Sciences, Institute of Polymer Chemistry and Physics, 7^{“b”}, str. A. Kadyri, 100128, Tashkent, Uzbekistan; e-mail: nnf7nnf7@gmail.com; <https://orcid.org/0000-0002-9817-9066>;

Ashurov, Nigmat Rustamovich — Doctor of Science (Technical), Professor, Uzbekistan Academy of Sciences, Institute of Polymer Chemistry and Physics, 7^{“b”}, str. A. Kadyri, 100128, Tashkent, Uzbekistan; e-mail: nigmat.ashurov@gmail.com; <https://orcid.org/0000-0003-0765-5942>

*The author's name is presented in the order: *Last Name, First and Middle Names*